ABSTRACT

Title of Dissertation: APPLICATION OF ADVANCED STATISTICAL METHODS TO ASSESS ATMOSPHERIC AND SOIL POLLUTION MITIGATION AND POTENTIAL RISKS

Zijiang Yang, Doctor of Philosophy, 2020

Dissertation Directed by: Professor Alba Torrents
Department of Civil and Environmental Engineering,
University of Maryland

Dr. Cathleen J. Hapeman
Agricultural Research Service,
United States Department of Agriculture

In environmental engineering field studies, data analysis plays an important role when presenting data into useful information that can be used by engineers and policy makers. However, traditional and currently used approaches have significant limitations due to the nature of the field data, such as high temporal variability, high spatial variability, and high heterogeneity. Such uncertainty may be better handled with more realistic statistical models than traditional statistical models with normal approximation. Additionally, a more robust incorporation of heterogeneity and variability may help to modify environmental fate models to achieve more accurate predictions. Therefore, this dissertation applied some advanced data analysis techniques to four case studies.

First, reparameterization was applied to modify the Gaussian plume model to predict dispersion of air pollutant emission from a ground-level active-discharge releasing source. Cross-validation was applied for model selection. The results showed that predictive accuracy of the modified GPM was greatly improved compared with the original model.

Second, dispersion of particulate matter was accessed, and a dispersion correction factor was developed to enhance the performance of the regulatory air dispersion model (AERMOD) for low-level sources. Cross-validation was used for model comparison. The results showed that predictive accuracy of the corrected model was greatly improved.

Third, carbon amendments were applied to a historically contaminated field to investigate the

feasibility for mitigating bioaccumulation. The effect of carbon amendments on bioaccumulation were evaluated. The results showed some evidence of the mitigation effect of compost, and in the meanwhile, the need of a robust statistical method was highlighted due to great spatial variability.

Lastly, the Bayesian hierarchical model (BHM) was applied to the field measurement dataset to characterize pollutant concentrations and bioaccumulation. Cross-validation and information criteria were used to evaluate model performance between the BHM and traditional model. The results showed that the BHM was preferred for smaller predictive errors and ability to handle data with larger observational error.

These case studies demonstrate the capability of advanced statistical methods for dealing with different environmental research problems. Such statistical methods will be useful for model modification with more specific situations, for data analysis with limited sample size and/or great variability and observational error, for environmental and ecological risk assessment, for evaluation of environmental mitigation strategies, for simulation of real-time pollutant distribution and forecasting with integration of monitoring and modelling approaches, and for minimization of sample size to meet with the accuracy requirement and lower the cost. In conclusion, advanced statistical methods are useful tools for environmental research.

APPLICATION OF ADVANCED STATISTICAL METHODS TO ASSESS ATMOSPHERIC AND SOIL POLLUTION MITIGATION AND POTENTIAL RISKS

by

Zijiang Yang

Dissertation submitted to the Faculty of the Graduate School of the
University of Maryland, College Park, in partial fulfillment
of the requirements for the degree of
Doctor of Philosophy
2020

Advisory Committee:
Professor Alba Torrents, Chair
Dr. Cathleen J. Hapeman, Co-advisor, USDA
Professor Michael N. Evans, Dean's Representative
Dr. Scott G. Lynn, US EPA
Dr. Natasha Andrade

Preface

~~I never think~~ I would have a PhD degree. Although when I was in high school, I told everyone that my dream was to get a Nobel Prize in Chemistry, I did not know a PhD degree is necessary for a Nobel Prize in Chemistry (the only exception is Tanaka Kōichi). My dream did not come true, and it seems like it will not come true anyway. In undergraduate school, majoring in structural engineering, my plan was to get a master's degree in structural engineering and then level up my painting and design skills to become a structural designer who also understands architecture design, so that I communicate with architect better when working together. However, this plan failed when I came to the US, where changing a major is much easier than I thought. Thus, I turned into environmental engineering, which is a combination of chemistry and civil engineering. Because of interest and encouragement from my advisor, I decided to get a PhD degree.

Environmental science and engineering is fun. It is a combination of chemistry, biology, ecology, physics, and modelling, which are all interesting subjects to learn about. In addition, the objects include lithosphere, biosphere, hydrosphere and atmosphere, which are literally everything in our activity. Last but not least, the problems of air pollution, water pollution, soil pollution and solid waste are very related to our health and economy, which is also helpful in daily life. Thus, it is a pleasure to be an environmental scientist and engineer.

Due to the interdisciplinary nature of environmental science and engineering, my thesis also includes topics of different fields. From soil remediation to air pollution, from analytical measurement to statistical modelling, I learnt a lot from different people who are masters in different fields, and I really enjoy this experience. This thesis is a product of such experience, including four case studies of different subjects.

In **Chapter 2**, a widely used Gaussian plume model was modified to adapt to the conditions of low-level horizontally-releasing emission source of a typical poultry house. In this case study, a virtual releasing point behind the ventilation fan was proposed to compensate for the error of point source assumption of the original model. The distance between the virtual releasing point and corresponding fan is optimized by cross-validation to obtain the best performance of the model.

In **Chapter 3**, a regulatory recommended air dispersion model, AERMOD, was also modified to overcome its issue of overestimation of particulate matter concentration from low-altitude emission source of a typical cotton gin. In this case study, a dispersion correction factor was developed and cross-validated to ameliorate the original AERMOD prediction based on potential influential factors including geometrical relation between receptor and source and wind.

In **Chapter 4**, two different kinds of manure compost were applied to soil in a field plot to investigate the effectiveness of mitigating bioaccumulation of organic chlorine pesticides. In this case study, the functional relation between pollutant concentration in soil and concentration in earthworm was revisited, and bioaccumulation and relative change of bioaccumulation change with time was investigated. During the data analysis of this case study, some problems were found for traditional data analysis methods, and this is the direct cause of Chapter 5.

In **Chapter 5**, a Bayesian hierarchical model was applied to the bioaccumulation dataset. In this case study, the Bayesian hierarchical model and traditional model were compared in terms of different aspects, such as out-of-sample predictive accuracy and the functional relation between predictive accuracy and magnitude of observational errors. Then, the bioaccumulation dataset was revisited by applying the Bayesian hierarchical model.

However, this thesis cannot be done with the help with those “the many people” who are masters in different fields.

Therefore, I would like to thank all of them.

First, I would like to thank my committee members. Thank you for kindly being my committee members and helping with this dissertation. I would like to thank my advisor, Dr. Alba Torrents for supporting and providing the chances to get involved in such interesting projects, vegetative environmental buffer at poultry house, particulate matter from cotton gin, and remediation of DDT contaminated soil, trusting me to do the research I am interested in, and advice about organic chemistry, soil chemistry and environmental engineering. I would also like to thank my co-adviser, Dr. Cathleen Hapeman for suggestions on manuscript writing and formatting, PowerPoint and presentation

communicating, patients for finalizing every manuscript and submissions, and advice about chemistry, agriculture, and English academic writing. I would also like to thank Dr. Michael Evans for help, support, critical reviews and suggestions on data analysis, and advice about simulation, model validation, and translation of statistics and mathematics ideas. I would like to thank Dr. Lynn Scott for critical reviews with the thesis, manuscript, and help and suggestions with finding literature and regulatory related documentations, and advice about toxicology and ecological risk assessment. I would also like to thank Dr. Natasha Andrade for critical review and comments for the thesis, and advisory about soil and earthworm sampling, and bioaccumulations.

I would also like to thank my other co-authors with each of the individual projects. I would like to thank Dr. Qi Yao for help and advice about air pollutants, vegetative environmental buffers, and poultry houses. I would like to thank Dr. Michael Buser for help, critical review, and advice about air dispersion modelling, model sensitivity, and particulate matter sampling. I would like to thank Derek Whitelock for help, critical review, and advice about cotton ginning, AERMOD modelling, and going back and forth with revising the manuscript. I would like to thank Dr. Joseph Alfieri for help and advice about Gaussian plume modelling, Matlab coding, and model validation. I would like to thank Marya Anderson for help and advice about use of analytical instruments, calibration, and soil and earthworm sampling. I would like to thank Rebecca Plummer for help and advice about pesticide analysis, use and troubleshooting of GC-MS and ASE, and QA/QC. I would like to thank Taylor Lachance for help and advice about soil and earthworm sampling, processing and analyzing. Lastly, I would like to thank Euna Jeong for helping with soil and earthworm sample analysis.

序：

~~我从没想过自己会拿到博士学位。~~虽然高中时，同学录里「梦想」一栏，我都写的是诺贝尔化学奖，但诺贝尔化学奖的前提是要有博士学位（唯一の例外は田中耕一さん）这件事单纯无知的我并不知道。如今我的梦想还是没有实现，而且以后应该也实现不了，残念(>_<)。本科专业是土木工程，那时的计划是结构工程硕士学位搞定之后，去研究绘画和设计，成为建筑设计也厉害

的结构设计师哟。但是当我来到美国，这个计划失败了。因为在美国转专业这件事比想象的要容易很多，并且环境是化学和土木的结合。所以，我便开心地转去了环境工程系攻读硕士。后来，出于对环境专业的兴趣和导师的鼓励，就决定读博玩啦(๑˃̵ᴗ˂̵)。

我认为环境这门学科还是蛮有趣哒。她是化学，生物，生态，物理，统计和数学建模的结合，这些都是有意思的学科。此外，环境的研究对象包括岩石圈，生物圈，水圈和大气圈，这些在身边就随处可见。此外，大气污染，水污染，土壤污染和固体废物问题与我们的健康和经济超相关，这些知识对日常生活也有帮助的说。因此，成为一名环境科学家或工程师这件事应该不能说是一件不厉害的事情，对吧对吧？

正是因为环境跨学科性质，该论文被包含不同方向的课题。从土壤修复到大气污染，从化学分析到统计建模，我从不同领域的专家那里学到了很多东西。这种经历的话，我还是蛮喜欢呢。这篇毕业论文正是这里和那里讨论学习的产物，四个不同方向的案例研究包括在了其中。

在**第二章**中，广泛使用的高斯烟羽模型被进行了修改，让禽舍的水平低程排放排设定得到适应。在此案例研究中，排风扇后面的虚拟点源被提出，以让原始模型中点源假设和风扇面积不匹配的误差得到修正。此外，虚拟点源与相应排风扇之间的距离通过交叉验证得到优化，让模型的最佳性能变得能够得到。

在**第三章**中，美国国家环境保护局推荐的大气扩散模型 AERMOD 被进行了修改，让其对轧棉厂低程排放源颗粒物浓度过高预测的问题得到修正。在本案例研究中，扩散校正系数被提出，并通过交叉验证进行测评。扩散校正系数的话，是基于潜在的影响因素（包括接收点与污染源和风之间的几何关系）来改善来自 AERMOD 的初始预测。

在**第四章**中，两种不同类型的堆肥被应用于田间土壤中，以对堆肥减轻有机氯农药生物富集的有效性进行研究。在本案例研究中，土壤中污染物浓度与蚯蚓中污染物浓度之间的函数关系被重新审视，生物富集系数和相对生物富集系数随时间的变化也被进行了研究。在数据分析过程中，传统数据分析方法问题的存在被发现，这也是第五章的一个契机。

在**第五章**中，贝叶斯分层模型被应用于场地试验的生物富集系数据。在本案例研究中，贝叶斯分层模型和传统模型被比较，从不同层面，如样本外预测准确性以及预测准确性与观测误差之间的函数关系。此外，贝叶斯分层模型也被用来分析场地试验的生物富集系数据。

但是，没有这些不同领域的专家的帮助，这篇论文也不能得以完成的说。

所以如果不对在研究中给予帮助和支持过的大家表示感谢的话，是不行的呢。

首先，我要感谢我的毕业委员会成员。感谢大家愿意成为毕业委员会成员并对论文提供帮助。感谢导师环境工程系的阿尔巴·托伦茨（Alba Torrents）教授的支持和提供了参与如此有趣项目的机会，养鸡场的植物缓冲带，轧棉厂的颗粒物排放和有机农药污染土壤的修复，以及对我的信任，让我可以做我感兴趣的研究。此外，还提供了有机化学，土壤化学和环境工程相关的建议。感谢共同导师美国农业部水文与遥感实验室的凯瑟琳·哈普曼（Cathleen Hapeman）博士对论文撰写和排版，演示稿和学术报告的建议，对每篇论文的建议，以及有关化学，农业和学术写作的建议。感谢地质系的迈克尔·埃文斯（Michael Evans）教授对数据分析的帮助和支持，重要批判性评论，以及有关数值模拟，模型验证以及如何“翻译”统计和数学内容的建议。我要感谢美国国家环境保护局科学协调与政策办公室暴露-评估协调和政策司的林恩·斯科特（Lynn Scott）博士对论文进行的批判性评论，有关查找文献和法规相关文件的帮助和建议，以及有关毒理学和生态风险评估的建议。我还要感谢环境工程系的娜塔莎·安德拉德（Natasha Andrade）博士对论文的评论和建议，有关土壤和蚯蚓采样以及生物富集的建议和指导。

我还要感谢每个项目的合著者。感谢直系学姐姚琪对空气污染物，植物环境缓冲带和养鸡场相关问题的帮助和建议。我要感谢美国农业部国家项目办公室自然资源与可持续农业系统的迈克尔·布塞（Michael Buser）博士对空气扩散建模，模型敏感度和颗粒物采样的帮助，论文稿的评论和建议。感谢美国农业部西南棉花轧花研究实验室的德里克·怀特洛克（Derek Whitelock）在轧棉，AERMOD 建模以及修改论文方面的帮助，批判性评论和建议。感谢美国农业部水文与遥感实验室的约瑟夫·阿尔菲耶里（Joseph Alfieri）博士对有关高斯烟羽模型，Matlab 代码和模型验证的帮助和建议。感谢环境工程系实验室主任玛丽亚·安德森（Marya Anderson）在使用分析仪器，标准曲线以及土壤和蚯蚓采样方面的帮助和建议。感谢美国农业部水文与遥感实验室主任丽贝卡·普拉默（Rebecca Plummer）对农药分析，质量检查/质量控制，以及 GC-MS 和 ASE 的使用和故障排除提供的帮助和建议。感谢美国农业部水文与遥感实验室实验员泰勒·拉坎斯（Taylor Lachance）和实习生郑恩雅（나정은）在土壤和蚯蚓采样，处理和分析方面的帮助。

Dedication

－ オレのまちがっている青春ラブコメへ －

「その認識を改めなさい。最低限度の努力もしない人間には才能がある人を羨む資格はないわ。成功できない人間は成功者が積み上げた努力を想象できないから成功しないのよ」雪ノ下の言葉は辛辣だった。

-『やはり俺の青春ラブコメはまちがっている。』

－ To my wrong *seishun* romantic comedy －

“Please change that perception. A person who does not make the minimum effort is not qualified to envy a person who has talent. A person who is indolent is not able to imagine the effort that a successful person has made to reach that talent” Yukinoshita said in a harsh way.

- *My Youth Romantic Comedy Is Wrong, As I Expected*

Acknowledgements

First, I would like to thank my parents. Without their support, understanding and kindness, I cannot make it, from the idea of studying a broad, to preparation for TOELF, GRE tests, application and suggestions for living in another country to name a few.

Second, I would like to thank my advisor, Dr. Alba Torrents. Thanks for accepting my major changing petition and providing the chance to do experiments at USDA. In addition, I also learn from Alba about how to think as an engineer, and how to make research have a broader impact, which will continually have a positive impact on my life. Except for research, Alba so provides chances of teaching, which allows me to think as a teacher as well. I would also like to thank my co-advisor Dr. Cathleen Hapeman. I also learn a lot from Cathleen, especially how to think as a scientist, how to communicate scientific theories and findings, which again will have a long-lasting positive impact on my life. “A paper must be written by many people, because one person cannot do everything. That’s why we need cooperation”, which is my favorite sentence from Cathleen. I would also like to thank my independent study advisor Dr. Michael Evans. I also learn a lot from Mike, especially how to think as a statistician, how to make data analysis “invulnerable”, which makes me feel data analysis is fun, doing simulation is fun, and cross-validation is fun.

I would also like to thank my dearest senpai, Dr. Qi Yao, who provides suggestions on both academic and daily lives, and suggestions for delicious food. I would also like to thank my dōki and friend, Xuanzhao Wang (Victor) and (Dr.) Lingxi Kong, who are always sharing interesting scientific, history, sentiments topics, good restaurants, and good animes with me. In addition, I would like to thank for my dear roommates during these six years, (Dr.) Jing Nie (Crystal), Wenyu Guo (Raina), Dr. Heng Liu (Henry), Dr. Li Ma, Dr. Panpan Yao, Rui Lu, and (Dr.) Lei Lei, who made my daily life interesting and home-like.

I would like to thank my fairy kōhai, Jili Wang, who is always sharing interesting things and gossip with me, which makes my life not only filled with research and food. In addition, thanks for her help with

video editing and Adobe Premiere Pro, which make my life significantly different from my life in a parallel world without her ($p < 0.05$). I would like to thank my cute kōhai, Yuting Peng (Painting), who is always sharing delicious food with me in photos, which is cruel anyway, but occasionally she is warm like a fire in winter, where her inadvertent words can make me feel cured. I would like to thank my lovely kōhai, Caijuan Li (Shaly), who is always sharing sentimental or lifetime related thoughts, which makes me feel calm and at peace and conquer things that are hard to overcome.

I would like to thank the ones that I never met physically, but gave me significant sentimental support, my very precious nēchan, Ai-nē, my beloved imōto, Ageha Masuki-chan, and and my love-and-hate tomo, L-chan. I would also like to thank Motoko-chan, who is always reading and marking books, which encourages me a lot.

Finally, I would like to thank my dearest ex-girlfriend, Siru Yuan (Inés), who makes my life colorful and black-and-white. Although there are both positive effects and negative effects, the positive effects are significantly greater than negative effects ($p < 0.05$).

致谢：

首先，我要感谢我的父母。没有他们的支持和理解，我恐怕不能成功拿到博士学位。从提出留学这个想法，到支持我准备托福，GRE，到帮助规划学校申请，签证材料，美国生活等等。

其次，我要感谢我的导师阿尔巴·托伦茨教授。感谢让转专业的申请被接受，并提供了在美国农业部进行实验的机会。此外，我还向阿尔巴教授学习了作为一名工程师应该如何思考，以及如何使研究产生更深远的影响，这将一直对我的人生产生积极影响。除研究外，阿尔巴教授还提供了教学的机会，这也使我能有机会作为老师来思考。我还要感谢我的共同导师凯瑟琳·哈普曼博士。我从凯瑟琳也学到很多东西，尤其是作为科学家应该如何思考，如何交流科学理论和发现，这也将对我的人生产生积极影响。“论文必须由很多人写，因为一个人不能做任何事情。这就是我们需要合作的原因”，这是我最喜欢的一句话。我还要感谢我的独立研究导师迈克尔·埃文斯教授。我还从迈克尔那里学到了很多东西，尤其是作为一名统计学家应该如何思考，如何使数据分析“无懈可击”，这让我感到数据分析很有趣，数值模拟很有趣，交叉验证也很有趣。

我还要感谢我最亲爱的学姐姚琪博士，她提供了有关学术的建议，日常生活的建议，和有关好吃的料理的建议。我还要感谢我的同期和基友王宣昭同学和孔令溪(博士)，他们一直与我分享有趣的科学，历史，情感话题，好吃的餐厅和好看的番。此外，我还要感谢这六年来我亲爱的室友们，聂晶(博士)，郭闻郁同学，刘亨博士，马莉博士，姚盼盼博士，陆瑞同学和雷蕾(博士)，让我的日常生活有趣又像在国内一样。

我要感谢我的小仙女学妹王寄力同学，她总是和我分享有趣的事情和八卦，这使我的生活除了科研和吃饭之外不那么枯燥。此外，感谢她在视频编辑和 Adobe Premiere Pro 使用方面的教导和帮助，这使我与没有她存在的平行世界的我有显著差异。我要感谢我的可爱学妹彭玉婷同学，她老是给我发好吃的东西的照片。虽然这样做很残忍，但偶尔地，她像冬天的火一样温暖，不经意间的言语会让我感觉到治愈。我要感谢学妹李彩娟同学，她经常会分享与情感或人生有关的想法，和她聊天之后会觉得很安心。

実生活では会うことがない方たちも感謝する気がします。いつでも話を聞いて、私の世界の見方を変えた大好きな姉ちゃん，藍ねえであります。私に超応援しまして、愛らしい妹，アゲハマスキちゃんであります。及びいつも困らせるエルちゃん であります。最後に，素子ちゃんもありがどう，彼女はいつでも新しい本をマークしたり本を読んだりしますから。彼女みたい人間になりたいと思います。

最后，我要感谢我最最亲爱的前女友袁斯茹同学，她使我的生活变得丰富多彩。当然也有让生活变得黑白相间的时候。尽管好的和坏的影响都有，但总的来说还是好的更多吧…

Table of Contents

List of Figures

List of Tables

List of Notations

a_{ej}: shape parameter of hyperprior for within-plot variance for earthworm concentration

a_{sj}: shape parameter of hyperprior for within-plot variance for soil concentration

b_i: linear regression coefficient of the i-th variable

b_{ej}: scale parameter of hyperprior for within-plot variance for earthworm concentration

b_{sj}: scale parameter of hyperprior for within-plot variance for soil concentration

BAF: bioaccumulation factor

BAF_j: bioaccumulation factor of the j-th plot

$NBAF$: normalized bioaccumulation factor

$\Delta NBAF$: change in normalized bioaccumulation factor

C_0: initial concentration of contaminant in earthworm

$c_{Q1,s,f}$: model-predicted concentration of sampler s of a separate fan f

C: concentration of pollutant

C_{bg}: background concentration

C_{cp}: corrected model-predicted concentration

$C_{c,s}$: contribution from horizontal plume in CBL or SBL

C_d: concentration contributions of direct source

c_e: shape parameter of hyperprior for between plot variance for earthworm concentration

C_e: contaminant concentration in earthworm

C_e^*: equivalent contaminant concentration in soil

C_{ej}: contaminant concentration in earthworm of the j-th plot

C_{ij}: contaminant concentration of i-th sample and j-th plot

$\bar{C}_j$: concentration mean of j-th plot

C_o: hourly average observed concentration

$C_{obs,s}$: observed concentration of sampler s

C_p: hourly average predicted concentration / concentration contribution of penetrated source

C_{pi}: predicted concentration of the i-th hour

C_{pre-cv}: out-of-sample model predicted concentration

$C_{pred,s}$: model-predicted concentration of sampler s

$C_{\mathrm{Q1},s}$: model-predicted concentration of sampler s when $Q = 1$

C_{r}: concentration contribution of indirect source

C_{s}: contaminant concentration in soil

c_{s}: shape parameter of hyperprior for between plot variance for soil concentration

$C_{\mathrm{s}ij}$: contaminant concentration in soil of i-th sample and j-th plot

$C_{\mathrm{s}j}$: contaminant concentration in soil of the j-th plot

C_{T}: total concentration of contaminant at receptor location

$\sum C_{\mathrm{o}}$: cumulative particle concentration during sampling period

CV_j: coefficient of variation of the j-th plot

$\overline{CV}$: mean of CV_j

$\overline{CV}_{\mathrm{critical}}$: critical value of $\overline{CV}$

d: distance of receptor from emission source

d_{e}: scale parameter of hyperprior for between plot variance for earthworm concentration

d_s: the distance of a point from a 1:1 ratio line on a logarithmic scale for sampler s

d_{s}: scale parameter of hyperprior for between plot variance for soil concentration

D: data

e_{e}: reported standard uncertainties of contaminant concentration in earthworm

e_{s}: reported standard uncertainties of contaminant concentration in soil

E: mathematical expectation

$\hat{E}$: estimated mathematical expectation

f: fan number

f_{c}: dispersion correction factor

$f_{\mathrm{t}i}$: fraction of effective time of the i-th hour

F_s: ratio of model predictions over observations of sampler s

FIR: food ingestion rate

h: height of source or receptor

$h(x)$: an arbitrary function of x

H: effective height

HQ_{s}: hazard quotient calculated solely on soil concentration

HQ_{se}: hazard quotient calculated on soil and earthworm concentration of pollutant

j: index of plot

J: total number of the plots

k: runs of cross-validation

k: number of independent parameters

k_0: degradation rate of DDT in soil

k_1: uptake rate of contaminant

k_2: degradation rate of contaminant in earthworm

k_{m}: coefficient of M_{m} and M_{ez}

k_{xy}: mass transfer coefficient from phase-x to phase-y

k_x: degradation rate of DDT

$\mathcal{K}$: diffusion coefficient

L: distance of virtual point from source

L_{e}: length of earthworm

L_{opt}: optimal L

m_{s}: mean of the hyperprior distribution for the grand mean of soil concentration

m_{e}: mean of the hyperprior distribution for the grand mean of earthworm concentration

M_{ez}: mass of ez-compost

M_{c}: mass of compost

M_{hd}: mass of hd-compost

M_{m}: carrying capacity

M_s: concentration ratio of sampler s

MLP: multiplier for estimation of concentration of contaminant in biota

n: sample size

n_j: sample size of the j-th plot

N: total sample size

$N_{\overline{\log BAF}_j|\mathrm{T}i|tr}$: normalized log-transformed BAF

$NBAF_{\mathrm{T}i,tr}$: normalized BAF

P: population of microbials

$P(\cdot)$: probability density function

Ps: soil ingestion proportion of diet

Q: constant source strength

$Q(t)$: concentration of contaminant in earthworm

r^2: coefficient of determination

r_{c}: degradation rate of compost in terms of each unit of microbial population

r_{m}: intrinsic rate of growth

R_{p}: ratio of prediction to observation

$\hat{R}_{\mathrm{p}}$: estimation of R_{p}

R_s: ratio of difference of sampler s

R^2: coefficient of determination

$R_{\overline{\log BAF}_j|\mathrm{T}i|tr}$: change in normalized log-transformed BAF

s: sampler name

S: source strength

S_{CV}: standard deviation of CV_j

s_{e}^2: variance of the hyperprior distribution for the grand mean of earthworm concentration

s_{s}^2: variance of the hyperprior distribution for the grand mean of soil concentration

t: time

tr: treatment type

Ti: sampling period

TRV: toxicity reference value

$\sum T$: total sampling period

u: wind speed

$\bar{u}_i$: average wind speed of i-th domain

$\vec{u}$: wind velocity

$\vec{u}_{\mathrm{a}}$: ambient wind velocity

$\vec{u}_{\mathrm{f}}$: wind velocity of fan

$\vec{u}_{\Sigma}$: total wind velocity

$\boldsymbol{V}$**:** covariance matrix

$V_{\mathrm{s}j}$: variance of mean of log-transformed soil concentration

$V_{\mathrm{e}j}$: variance of mean of log-transformed earthworm concentration

w_*: convective velocity scale

x: downwind coordinates

$\vec{x}$: three-dimensional location

$\vec{x}_r$: location of receptor

Δx: size of each sub-domain

X: random variable / constant depend on initial condition

$\boldsymbol{X}$**:** spatially referenced nonrandom variables

y: crosswind coordinates

z: vertical coordinates

$\boldsymbol{z}$**:** observed concentration of soil contaminant

α: significance level

$\boldsymbol{\beta}$**:** parameters that relates $\boldsymbol{X}$ to $\boldsymbol{z}$

$\gamma(h)$: covariance function

$\delta(\cdot)$: Dirac delta function

$\boldsymbol{\eta}$**:** spatially correlated random effect

θ: deviation from wind direction / parameter matrix

θ: parameter of interest

$\hat{\theta}$: estimation of θ

$\hat{\theta}_{\text{Bayes}}$: posterior mean

θ_j: mean of j-th plot

$\hat{\theta}_j$: estimation of θ_j

$\hat{\theta}_{\text{mle}}$: maximum likelihood estimation of θ

θ_{sj}: group mean of log-transformed soil concentration

θ_{ej}: group mean of log-transformed earthworm concentration

$\pi(\theta)$: prior probability distribution of θ

$\pi(D|\theta)$: likelihood function of data, D, given different θ values

$\pi(\theta|D)$: posterior probability distribution of θ given data D

μ_s: mean of θ_{sj}

μ_e: mean of θ_{ej}

ξ: independent variable during variable transformation

ϵ_{ij}: error random variable of i-th sample and j-th plot

σ: standard deviation of wind direction

σ^2: variance

$\hat{\sigma}^2$: estimated variance

$\sigma_{\mathrm{e}j}^2$: group variance of log-transformed earthworm concentration

$\sigma_{\mathrm{s}j}^2$: group variance of log-transformed soil concentration

σ_y: standard deviation of distribution concentration in *y*-axis

σ_z: standard deviation of distribution concentration in *z*-axis

τ_{e}^2: variance of $\theta_{\mathrm{e}j}$

τ_{s}^2: variance of $\theta_{\mathrm{s}j}$

List of Abbreviations

2YC: 2-year compost

4MC: 4-month compost

AERMOD: American Meteorological Society/Environmental Protection Agency Regulatory Model

AIC: Akaike information criterion

AMS: American Meteorological Society

ANOVA: One-way analysis of variance

ARS: Agricultural Research Service

BAF: bioaccumulation factors

BHM: Bayesian hierarchal model

BIC: Bayesian information criterion

CBL: convective boundary layer

CFD model: computational fluid dynamic model

CI: credible interval/confident interval

CM: carbonaceous material

CO: carbon monoxide

CV: coefficient of variance

DCF: dispersion correction factor

DDT: dichlorodiphenyltrichloroethane

DDx: DDT and its metabolites

EXP: experiment

Eco-SSL: Ecological Soil Screening Level

EPA: Environmental Protection Agency

ERA: Ecological risk assessment

FAC2: fraction of predictions within a factor of two

FB: fractional bias

GDP: gross domestic product

GPM: Gaussian plume model

HDI: highest density interval

HQ: hazard quotient

ISC-3: Industrial Source Complex 3

LOQ: limit of quantitation

LOO-CV: leave-one-out cross-validation

MCMC: Markov chain Monte Carlo

MG: geometric mean

NAAQS: National Ambient Air Quality Standards

NAD: normalized absolute difference

NBAF: normalized bioaccumulation factor

NMSE: normalized mean square error

NO_2: nitrogen dioxide

OCP: organochlorine pesticide

O_3: ozone

Pb: lead

PDF: probability density function

PM: particulate matter

$PM_{2.5}$: PM with an aerodynamic equivalent diameter less than 2.5 μm

PM_{10}: PM with an aerodynamic equivalent diameter less than 10 μm

PRIME: Plume Rise Model Enhancement

PSD: particle size distribution

SBL: stable boundary layer

SI: supplementary information

SO_2: sulfur dioxide

TSP: total suspended particle

TP: pre-application sampling period

USDA: United States Department of Agriculture

US EPA: United States Environmental Protection Agency

VEB: vegetative environmental buffer

VG: geometric variance

Chapter 1 Introduction

The main purpose of environmental monitoring and environmental engineering field studies is to provide data to decision makers about the state of the environment, exposure and potential risks of the pollutant, and the efficiency of remediation technologies with the main purpose to minimize risks. Data analysis plays an important role when presenting data into useful information that can be used by engineers and policy makers. However, traditional and currently used approaches have significant limitations due to the nature of the field data, such as high temporal variability, high spatial variability, and high heterogeneity in the samples collected. Such uncertainties may be better handled with more realistic statistical models than traditional statistical models that are based on normal approximation. In addition, a more robust incorporation of heterogeneity and variability may help to modify environmental fate models to achieve more accurate prediction on pollutant behaviors. Thus, there is a need to incorporate better data analysis methods in environmental engineering. As more data analysis tools become available with development of fast computers and available software, this field is evolving, and there are an increasing number of studies focused on applying advanced data analysis approaches in environmental engineering. In here we are addressing some unique field case studies with a large dataset from a single study. In this chapter, I will present an introduction of the different methods that were utilized to address questions related to each study.

1. Advanced Statistical Methods

1.1 Monte Carlo simulation

Monte Carlo method refers to any simulation that involves random (Martinez and Martinez, 2007), and in statistics, Monte Carlo method is a powerful tool for integration. For example, for a

random variable X with probability density function (PDF) denoted as $f(X)$, the expectation of a function of X can be calculated by integration:

$$\mathrm{E}h(x) = \int h(x)f(x)\mathrm{d}x \qquad \text{Eqn. } 1-1$$

where $h(x)$ is a function of X, and $\mathrm{E}h(x)$ is the expectation of $h(x)$. Under the Monte Carlo method, $\mathrm{E}h(x)$ can be calculated by independent and identically distributed random sample X_1, $X_2 \ldots X_n$ obtained from $f(x)$:

$$\widehat{\mathrm{E}}h(x) = \frac{1}{n}\sum_{i=1}^{n} h(X_i) \qquad \text{Eqn. } 1-2$$

where n is the number of random samples. As $n \to \infty$, $\mathrm{E}h(x)$ can be approximated by $\widehat{\mathrm{E}}h(x)$. An example of Monte Carlo integration is shown in **Figure 1-1**, where $n = 4$ in this case.

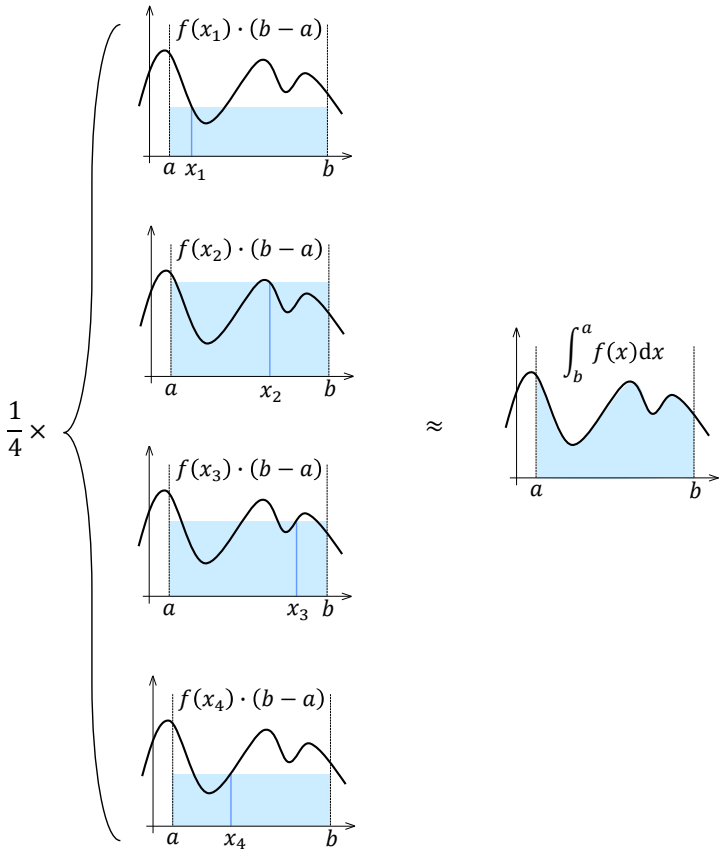

Figure 1-1 Demonstration of Monte Carlo integration. X_1, X_2, X_3 and X_4 are random draws from the distribution function $f(x)$. a and b are constant. In this case, $n = 4$.

Although Monte Carlo integration has a problem of slow convergence, it is still a powerful tool for two reasons. First, Monte Carlo integration is easier to conduct for high dimensional problems than quadrature methods, making the Monte Carlo method preferred for multivariable problems. In addition, quadrature methods get problematic if the transformation function $h(x)$ is not smooth, but Monte Carlo integration ignores smoothness and can be directly applied to any transformation functions (Martinez and Martinez, 2007). As a result, the Monte Carlo method is widely used in many fields, such as physics (Landau and Binder, 2014), chemistry (Nightingale and Umrigar, 1998), biology (Manly, 2006), engineering (Mordechai, 2011), finance (Glasserman, 2013), and etc. In the field of environmental and agricultural related studies, the Monte Carlo method is usually used for risk assessment problems (Hayes and Landis, 2004; Chow et al., 2005), and because of its increasingly usefulness, United States Environmental Protection Agency (US EPA) also proposed a guidance for conducting Monte Carlo simulation to handle uncertainties (Firestone et al., 1997).

1.2 Bayesian statistics

Different from classical Frequentist statistics, in the Bayesian framework, parameters are treated as random variables and can be described by probability distributions that can reflect knowledge and uncertainty about the parameters (Givens and Hoeting, 2013). A typical workflow of Bayesian framework is demonstrated in **Figure 1-2**.

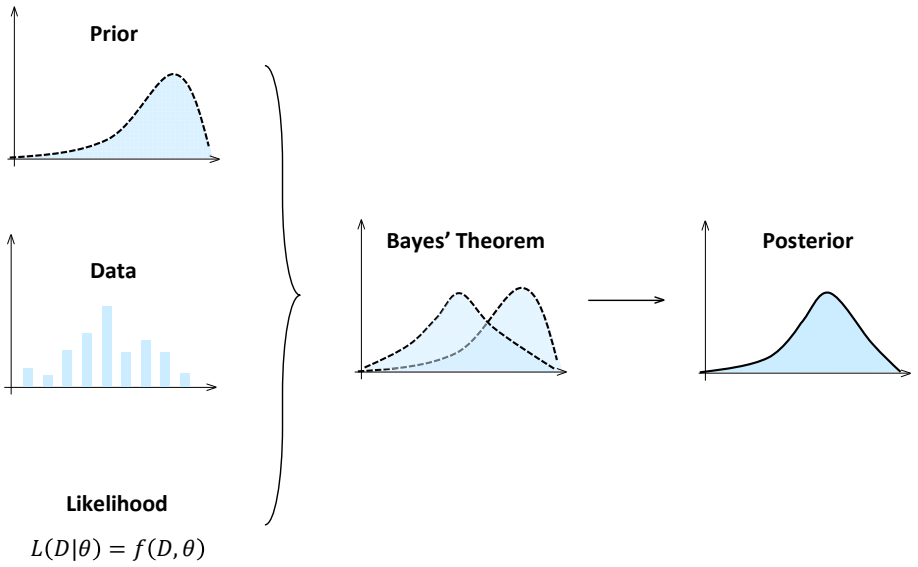

Figure 1-2 Paradigm of Bayesian framework. L refers to likelihood function, f refers to probability distribution function. D and θ are data and parameter, respectively.

All Bayesian frameworks are based on Bayes' theorem:

$$P(\theta|D) = \frac{P(\theta)P(D|\theta)}{P(D)} \qquad \text{Eqn. } 1-3$$

where θ refers to parameters, and D refers to the data. $P(\theta)$ is prior, which reflects the prior knowledge about the parameter. It may be based on previous studies, surveys, or personal beliefs (Gelman et al., 2013). $P(D|\theta)$ is the likelihood, which reflects the information of the data. $P(\theta|D)$ is the posterior distribution, which is the updated knowledge by the data information, and it shows that posterior distribution is a conditional distribution for the parameters given data. $P(D)$ is the marginal distribution, and $P(D) = \int P(\theta)P(D|\theta)\mathrm{d}\theta$. Since $P(D)$ is a constant, the posterior can also be expressed as being proportional to the product of prior and likelihood:

$$P(\theta|D) \propto P(\theta)P(D|\theta) \qquad \text{Eqn. } 1-4$$

When making inference based on posterior distribution, the interested quantities can be expressed as the posterior expectation of a function of the parameter, θ:

$$\mathrm{E}(h(\theta)|D) = \frac{\int h(\theta)P(\theta)P(D|\theta)\mathrm{d}\theta}{\int P(\theta)P(D|\theta)\mathrm{d}\theta} \qquad \text{Eqn. } 1-5$$

where $h(\theta)$ is a function of θ. **Eqn. 1-5** is difficult to obtain analytical solutions, and this is the reason why Bayesian inference was not widely used until 21st century. Nowadays, integrations in **Eqn. 1-5** are often done by Monte Carlo integration same as **Eqn. 1-1**, especially by Markov chain Monte Carlo (MCMC) methods (Gelman et al., 2013).

Bayesian statistical modelling has been widely applied in many fields, such as physics (Von Toussaint, 2011), chemistry (Okamoto, 2017), engineering (Lam et al., 2018), biometrics (Gonzalez-Rodriguez et al., 2005), finance (Hasan et al., 2018), psychometrics (Levy and Mislevy, 2016), and political science (Jackman, 2004). There are also increasing applications of Bayesian methods in the field of environment and agricultural related research (Cocchi et al., 2007; Goyal et al., 2005; Aelion et al., 2009; Azim et al., 2011; Banerjee et al., 2014; Billoir et al., 2008; Delignette et al., 2017; Tan et al., 2017; Øverjordet et al., 2018). In addition. Bayesian methods have been applied by US EPA as an alternative method for handling complex problems, such as multivariate exposure assessment problems (US EPA, 2005).

1.3 Predictive accuracy and model selection

Due to development of Monte Carlo methods and thereafter Bayesian statistics, many new models and approaches have become available, and determining the model with the best goodness of fit is not straight forward. Although a more complex model can always fit the data better, it may lead to the problems of overfitting. Overfitting refers to the situation that as the complexity of the model increases, the model may fail to fit the additional independent data (Wu and Shapiro, 2006) (**Figure 1-3**). One of the suggested ways to select the optimal complexity for a

model while accounting for overfitting is to evaluate predictive accuracy (Gelman et al., 2014). Therefore, predictive accuracy is an important standard for model selection.

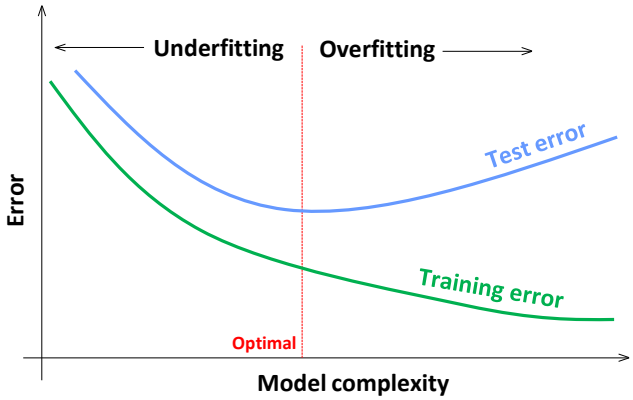

Figure 1-3 Demonstration of overfitting. This figure is reproduced from Wu and Shapiro, 2006.

There are several ways to measure predictive accuracy, such as Akaike information criterion (*AIC*), Bayesian information criterion (*BIC*), deviance information criterion (*DIC*), and cross-validation (Gelman et al., 2014). *AIC* is calculated by (Akaike, 1974):

$$AIC = -2\log p\left(D|\hat{\theta}_{\text{mle}}\right) + 2k \qquad \text{Eqn. } 1-6$$

where k refers to number of independent parameters; $\hat{\theta}_{\text{mle}}$ is maximum likelihood estimate of θ, which is the parameter of the model; D refers to observed data, and $\log p\left(D|\hat{\theta}_{\text{mle}}\right)$ is the log-likelihood function. *BIC* is an adjusted version of *AIC*, and *BIC* is calculated by (Schwarz, 1978):

$$BIC = -2\log p\left(D|\hat{\theta}\right) + 2k\log n \qquad \text{Eqn. } 1-7$$

where $\hat{\theta}$ is point estimate of parameter; n refers to the number of observations in D, or equivalently, sample size. *DIC* is a Bayesian version and also an adjusted version of *AIC*, and it is calculated by (Spiegelhalter et al., 2002):

$$DIC = -2\log p\left(D|\hat{\theta}_{\text{Bayes}}\right) + 2p_{\text{D}} \qquad \text{Eqn. } 1-8$$

where $\hat{\theta}_{\text{Bayes}}$ is the posterior mean, i.e., $\hat{\theta}_{\text{Bayes}} = \text{E}(\theta|D)$. p_{D} refers to effective number of parameters, and $p_{\text{D}} = 2\left(\log p\left(D|\hat{\theta}_{\text{Bayes}}\right) - \text{E}(\log p(D|\theta))\right)$.

Cross-validation is another method for evaluating predictive accuracy. Although cross-validation is more computationally intense, it is able to evaluate out-of-sample predictive accuracy (Gelman et al., 2014, Hooten and Hobbs, 2015). There are several ways of cross-validating a model, and a common way is *k*-fold cross-validation, where the dataset is divided into k sub-datasets. Then, one sub-dataset is retained for validation, and $k-1$ sub-datasets are used to calibrate the model. Such a process is executed *k*-times until each sub-dataset is validated, and then the results are used for evaluating predictive accuracy (**Figure 1-4**). If there are n observations in the data and $k = n$, then *k*-fold cross-validation becomes leave-one-out cross-validation (Molinaro et al., 2005).

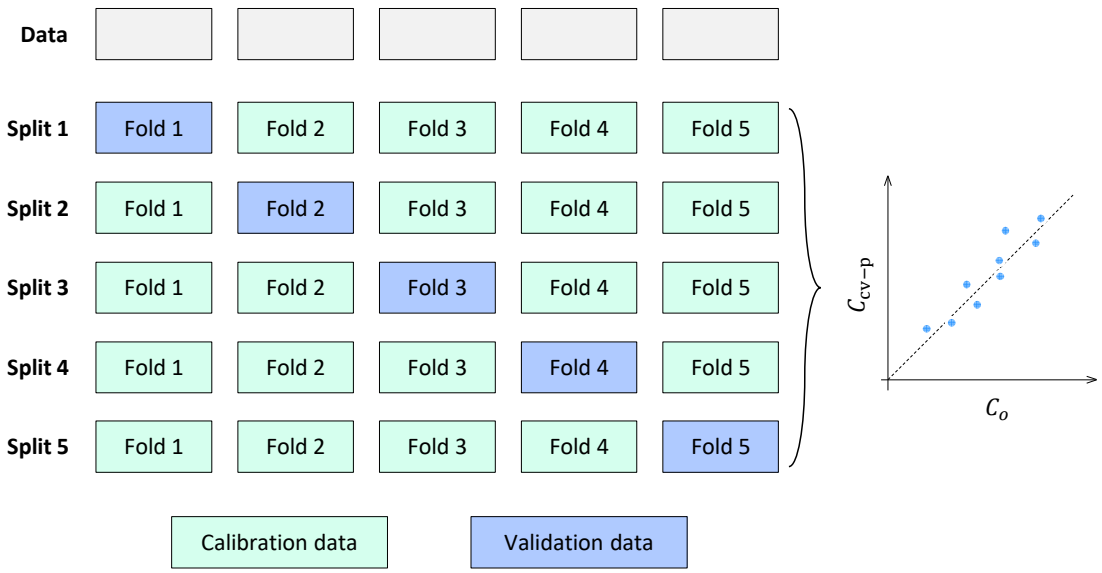

Figure 1-4 Paradigm of *k*-fold cross-validation. $k = 5$ is used as an example. $C_{\text{cv}-\text{p}}$ refers to the cross-validation model-prediction; C_{o} refers to observation.

2. Air Pollution and Dispersion Models

2.1 US agricultural industry

Agriculture, food, and related industries have a large contribution to the US economy and in 2017, these industries contributed 5.4% share (about $132.8 billion) of the US gross domestic product (GDP) (USDA ERS, 2020a). In addition, agriculture and its related industries provided 11% of US employment (about 22 million full and part time jobs) in 2018 (USDA ERS, 2020b), where meat, poultry and dairy related manufacturing contributed 38.1% of the total (USDA ERS, 2020c).

Since the mid of 1990's, broiler production has become the major meat production and consumption, reaching 42 billion pounds in 2018 (USDA ERS, 2019a), and it is still increasing (**Figure 1-5a**). The cotton industry is also an important sector of agriculture with production at 15 million bales per year (USDA ERS, 2019b). The US exports the most cotton in the world, about 70% of the overall production (**Figure 1-5b**).

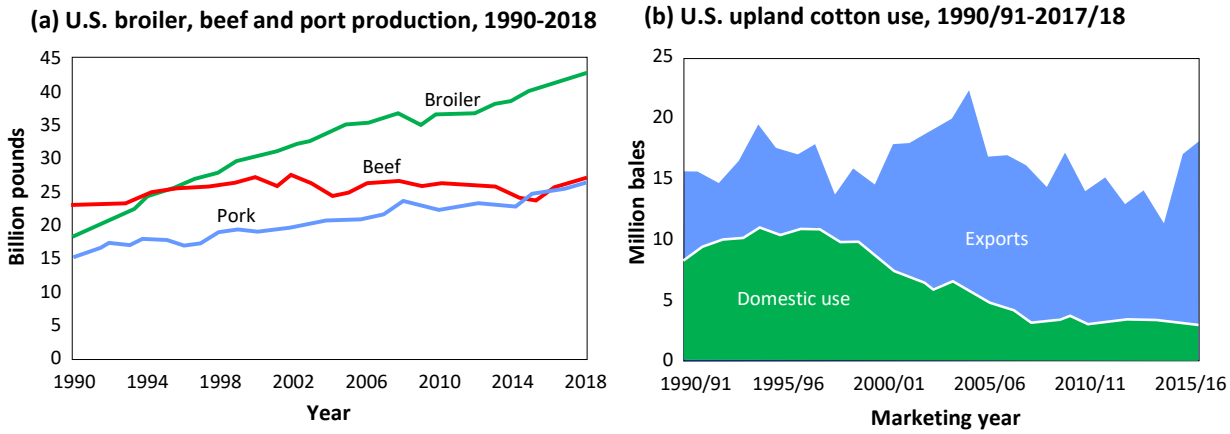

Figure 1-5 Broiler, beef and pork production and cotton use in U.S. Figures are reproduced from USDA ERS, 2019a and USDA ERS, 2019b.

2.2 Agriculture and air pollution

The expansion of agricultural industry has also resulted in air pollution problems. In the US, air pollutants are regulated by the National Ambient Air Quality Standards (NAAQSs), which

include carbon monoxide (CO), lead (Pb), nitrogen dioxide (NO_2), particulate matter (PM), ozone (O_3), and sulfur dioxide (SO_2) (US EPA, 2020a). These pollutants are regulated by US EPA due to their adverse effects on human health, the environment, and property damage (**Table 1-1**). Among these pollutants, the most abundant agricultural air pollutants related is particulate matter (Yang et al., 2020). The agriculturally-related sources of PM include poultry houses (Yao et al., 2018a), livestock (Cambra-López, et al., 2010), cotton gins (Whitelock et al., 2019), and straw burning (Cao et al., 2008). PM can lead to health problems, such as asthma attacks (Ding et al., 2017), chronic bronchitis (Löndahl et al., 2017), lung cancer (Sze-To et al., 2012), cardiovascular disease (Du et al., 2016), diabetes (Pearson et al., 2010), and premature death (Zeng et al., 2017). In addition, PM can reduce visibility (Davidson et al., 2005), damage buildings (Rabl, 1999) and plants (Grantz et al., 2003).

Table 1-1 National Ambient Air Quality Standard (NAAQS) Table. Primary standards provide public health protection, including protecting the health of "sensitive" populations such as asthmatics, children, and the elderly. Secondary standards provide public welfare protection, including protection against decreased visibility and damage to animals, crops, vegetation, and buildings (US EPA2020a).

Pollutant		Primary/Secondary	Averaging Time	Level	Form*
Carbon Monoxide (CO)		primary	8 hours 1 hour	9 ppm 35 ppm	A
Lead (Pb)		primary and secondary	Rolling 3-month average	0.15 μg/m^3	B
Nitrogen Dioxide (NO_2)		primary primary and secondary	1 hour 1 year	100 ppb 53 ppb	C D
Ozone (O_3)		primary and secondary	8 hours	0.070 ppm	E
Particle Pollution (PM)	$PM_{2.5}$	primary secondary primary and secondary	1 year 1 year 24 hours	12.0 μg/m^3 15.0 μg/m^3 35 μg/m^3	F F G
	PM_{10}	primary and secondary	24 hours	150 μg/m^3	H
Sulfur Dioxide (SO_2)		primary secondary	1 hour 3 hours	75 ppb 0.5 ppm	C A

*Form A: Not to be exceeded more than once per year;
B: Not to be exceeded;
C: 98th percentile of 1-hour daily maximum concentrations, averaged over 3 years;
D: Annual Mean;
E: Annual fourth-highest daily maximum 8-hour concentration, averaged over 3 years;
F: annual mean, averaged over 3 years;
G: 98th percentile, averaged over 3 years;
H: Not to be exceeded more than once per year on average over 3 years.

2.3 Air dispersion models

Air quality models are useful tools for assessing air pollution problems and can be used to evaluate the influence of new sources, to identify if the addition of the new sources will exceed air quality standards (US EPA, 2016), and to assist in the design of effective strategies to reduce the impact of the pollutant (Yang et al., 2020). In addition, air quality models can be applied inversely to calculate emission rates (Siefert et al., 2004; Siefert and Scudlark, 2008; Yao et al., 2018b) and to identify source contributions to air quality problems (Lushi and Stockie, 2010).

The three most commonly-used air quality model types are dispersion models, photochemical models, and receptor models (US EPA, 2016). Atmospheric dispersion models are focused on transport of contaminants in the atmosphere (Stockie, 2011), which can be described by the advection-diffusion equation.

The advection-diffusion equation is derived from mass conservation and assumes that the mass of the contaminant is conserved, i.e., no deposition or chemical reaction of the pollutant. The three-dimensional advection-diffusion equation can be expressed as (Stockie, 2011):

$$\frac{\partial C}{\partial t} + \nabla \cdot (C\vec{u}) - \nabla \cdot (\mathcal{K}\nabla C) = S \qquad \text{Eqn. } 1-9$$

where $C = C(\vec{x}, t)$ and it is the mass concentration of pollutant at location $\vec{x} = (x, y, z)$ and time t. $\vec{u}$ is wind velocity, and $C\vec{u}$ represents the flux of advection. $\mathcal{K}(\vec{x}) = \text{diag}(K_x, K_y, K_z)$ is the diffusion coefficient, and $\mathcal{K}\nabla C$ represents the flux of diffusion according to Fick's Law. $S = S(\vec{x}, t)$ and it is the source.

To obtain the close-form analytical solution of **Eqn. 1-9**, some assumptions are made to simplify the model. (1) The contaminant is assumed to be released at a constant emission rate

Q from a point source at $\vec{x} = (0,0,H)$, where H is the effective height above ground. Thus, the source term can be expressed as:

$$S(\vec{x}) = Q\delta(x)\delta(y)\delta(z-H) \qquad \text{Eqn. } 1-10$$

where $\delta(\cdot)$ is the Dirac delta function. (2) At time t, it is assumed that wind velocity is uniform in the modelling domain and has the same direction as positive *x*-axis, i.e., $\vec{u}(t) = (u(t),0,0)$, where u is the wind speed. (3) Wind speed is assumed to be sufficiently large so that diffusion in the *x*-direction is negligible compared with advection, i.e., $K_x\partial_x^2 C \approx 0$. (4) It is assumed that the time scale of interest is long enough so that within each time step, the wind velocity and other meteorological parameters are independent of time. Thus, the solution is steady-state. (5) It is assumed that the contaminant is reflected from the ground, i.e., no absorption or deposition when the pollutant reaches the ground surface.

Boundary conditions are necessary for solving the equation. It is assumed that as the concatenation approaches zero as we move infinitely far away from the source, and this is expressed as:

$$C(\infty,y,z) = 0 \qquad \text{Eqn. } 1-11$$

$$C(x,\pm\infty,z) = 0 \qquad \text{Eqn. } 1-12$$

$$C(x,y,\pm\infty) = 0 \qquad \text{Eqn. } 1-13$$

Since the wind velocity is in aligned with positive *x*-axis, there are no contaminants at $x < 0$. Thus, we have:

$$C(0,y,z) = 0 \qquad \text{Eqn. } 1-14$$

Finally, the contaminant cannot penetrate the ground surface, so flux at the ground surface is zero:

$$K_z\frac{\partial C}{\partial z}(x,y,0) = 0 \qquad \text{Eqn. } 1-15$$

Combining **Eqn. 1-9** to **Eqn. 1-15**, the advection-diffusion equation can be solved analytically, and the solution is called the *Gaussian plume*, which is expressed as:

$$C = \frac{Q}{2\pi\sigma_y\sigma_z u} \exp\left(\frac{-y^2}{2\sigma_y^2}\right)\left[\exp\left(\frac{-(z-H)^2}{2\sigma_z^2}\right) + \exp\left(\frac{-(z+H)^2}{2\sigma_z^2}\right)\right] \qquad \text{Eqn. } 1-16$$

where σ_y and σ_z are the standard deviation of the distribution concentration in y and z axis. $\sigma_y^2(x) = 2/u\int_0^x K_y(\xi)d\xi$, $\sigma_z^2(x) = 2/u\int_0^x K_z(\xi)d\xi$, where ξ is an independent variable during variable transformation. $K_y(\xi)$ and $K_z(\xi)$ are difficult to determined analytically for deriving expressions of σ_y and σ_z, so σ_y and σ_z are usually determined experimentally (Stockie, 2011). **Eqn. 1-16** is usually called as the Gaussian plume model (GPM) **(Figure 1-6)**, which is widely applied for air dispersion modelling (Asman et al., 2001; Arystanbekova, 2004; Siefert et al., 2004; Siefert and Scudlark, 2008; Hensen et al., 2009; Sutton et al., 2009; Lushi and Stockie, 2010; Yang et al., 2020).

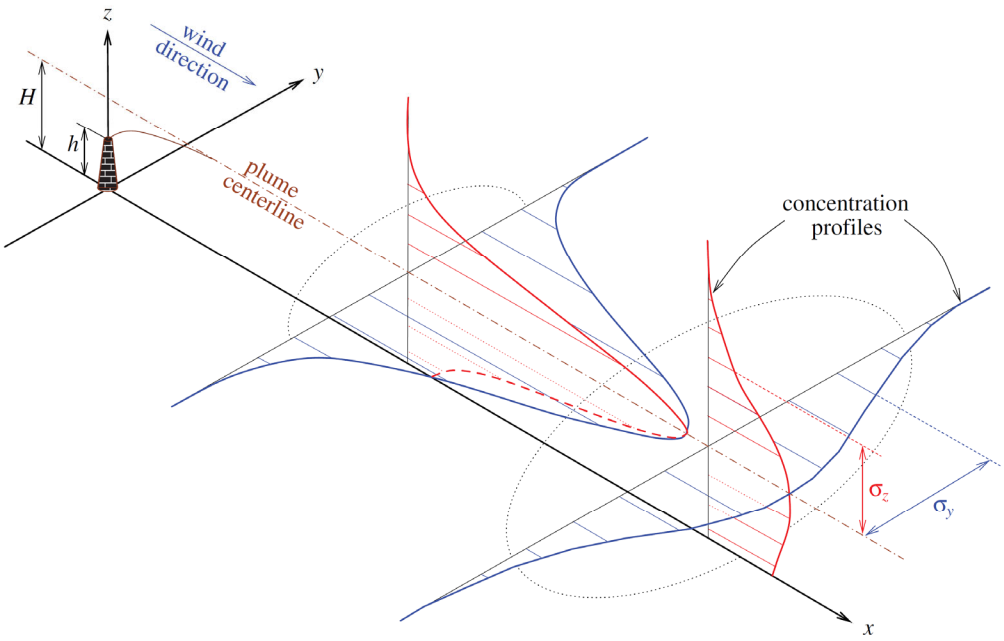

Figure 1-6 Demonstration of Gaussian plume model. H is the height of the source, h is the height of the stack. σ_y and σ_z are the standard deviation of the plume at y and z direction. Figure is adopted from Stockie, 2011.

Many regulatory air quality dispersion models are developed based on the GPM, such as American Meteorological Society/Environmental Protection Agency Regulatory Model (AERMOD), which is one of the US EPA preferred models (US EPA, 2020b). AERMOD is a steady-state model with multiple Gaussian plumes. The general form or AERMOD is (Cimorelli et al., 1998):

$$C_{\mathrm{T}}(\vec{x}_r) = fC_{\mathrm{c,s}}(\vec{x}_r) + (1-f)C_{\mathrm{c,s}}(\vec{x}_{\mathrm{p}}) \qquad \text{Eqn. } 1-17$$

where C_{T} is the total concentration of contaminant at receptor location $\vec{x}_r$. $\vec{x}_{\mathrm{p}}$ is the coordinates of receptors with terrain. f is the weighting factor. $C_{\mathrm{c,s}}$ is the contribution from horizontal plume in the convective boundary layer (CBL) or the stable boundary layer (SBL).

In SBL, the pollutant concentration (C_{s}) can be calculated based on a single Gaussian plume. However, in SBL, the concentration has three Gaussian plume components, which can be expressed as:

$$C_{\mathrm{c}}(\vec{x}_r) = C_{\mathrm{d}}(\vec{x}_r) + C_{\mathrm{r}}(\vec{x}_r) + C_{\mathrm{p}}(\vec{x}_r) \qquad \text{Eqn. } 1-18$$

where $C_{\mathrm{c}}(\vec{x}_r)$ is the total concentration of the contaminant at location $\vec{x}_r = (x_r, y_r, z_r)$ in CBL. C_{d}, C_{r} and C_{p} are the contributions from the direct source, indirect source, and penetrated source, respectively (**Figure 1-7**).

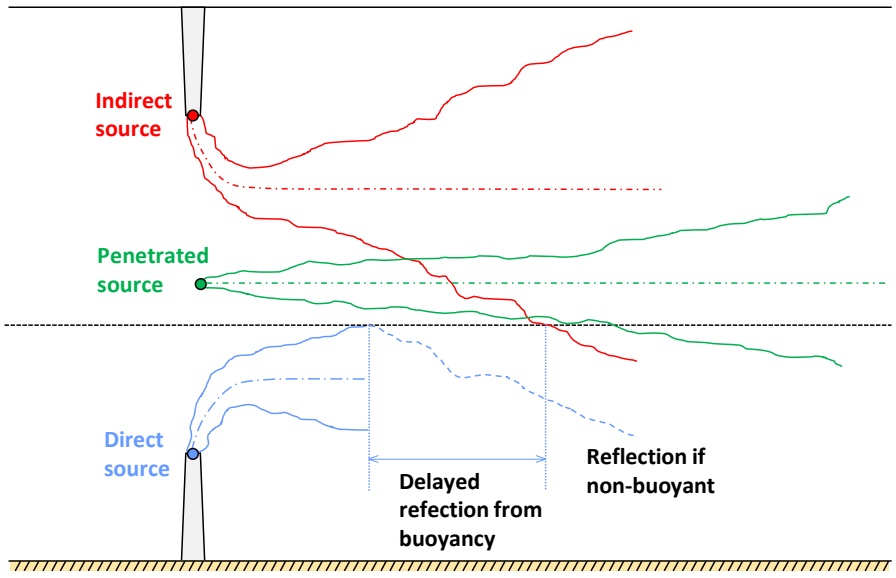

Figure 1-7 Demonstration of the three plumes of AERMOD in the convective boundary layer. The figure is reproduced from Cimorelli et al., 2005.

The source code of AERMOD is available online (US EPA, 2020b), and there are also commercially available AERMOD software packages with more interactive interphase (Lake Environmental, 2020; Breeze, 2020), which makes it widely applied for solving the environmental and agriculture related problems (Hadlocon et al., 2015; Bonifacio et al., 2013; Powell et al., 2006; Bairy, 2013).

2.4 Limitations of current air dispersion models

These dispersion models were originally designed for industrials stacks (Cimorelli et al., 1998; Kakosimos et al., 2011; Nagendra et al., 2012; Ma et al., 2013; Hadlocon et al., 2015), which may not be feasible for some specific situations of agricultural industry. For example, cotton gins are a source of PM, and PM is released through emission stacks. However, the stacks of cotton gins are much shorter than industrial stacks, which results in a near ground scenario and makes it more complex than usual condition of dispersion models. Previous studies have shown that regulation-recommended air dispersion models have a potential to overestimate concentration for

low-level sources by as much as a factor of 10 (Fritz, 2003; Zwicke, 1998). In addition, some poultry houses are usually equipped with exhaust tunnel fans, which generate a strong local wind, and this scenario violates the assumptions of the GPM for small spatial scale emissions.

Therefore, dispersion models require modification to address emissions fate from agricultural activities.

3. Soil Pollution and Remediation

3.1 Persistent organic pollutant

Organic chlorinated pesticides (OCPs) refer to a group of organic pesticides that have at least one covalently bonded atom of chlorine (**Figure 1-8**). Additional chlorine atom(s) can increase hydrophobicity and persistence and decrease volatility and water solubility. These properties increased the efficaciousness of OCPs and decreased their cost. OCPs have been used globally since the 1940s (Shi et al., 2005). However, their hydrophobicity and persistence also increase the tendency to accumulate in the food chain (Jensen, 2014; Walker et al., 1954; Darko and Acquaah, 2008; Darko et al., 2008; Bulut et al., 2011) to be toxic and have adverse health effects to humans and wildlife (Ratcliffe, 1970; Hua and Shan, 1996; Safe, 1992). Therefore, eight of the OCPs were banned globally according to Stockholm Convention on Persistent Organic Pollutants (Shi et al., 2005). In addition, the persistence and repeated applications of OCPs has resulted in highly-contaminated soils. These residues in the soil represent an exposure route and remain accessible to the food chain (Romijn et al., 1994; Feng et al., 2003; Tanabe et al., 1994; Bulut et al., 2011), which is a potential threat for the ecosystem and human health.

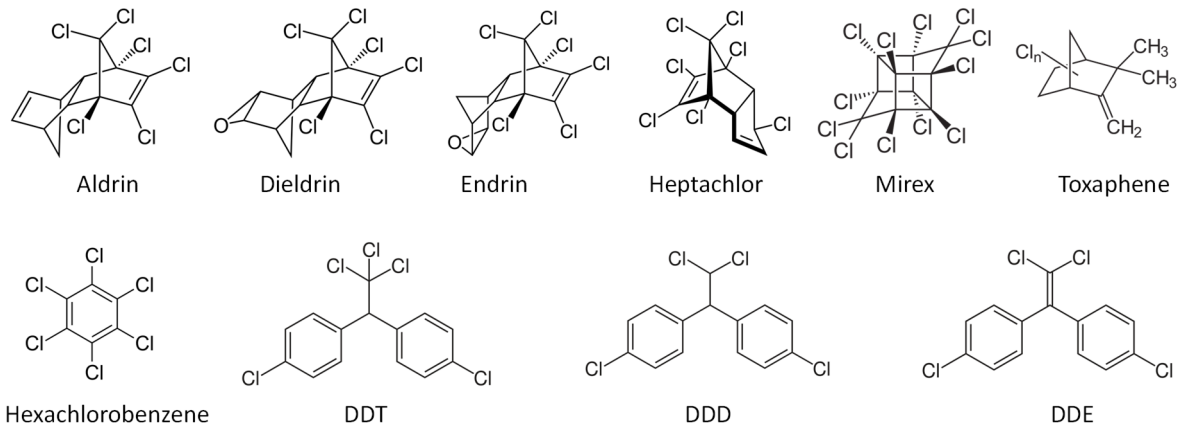

Figure 1-8 Chemical structure of OCPs, DDD and DDE

3.2 Ecological risk assessment

Ecological risk assessment (ERA) is a process proposed by United States Environmental Protection Agency (US EPA) to evaluate the likelihood that adverse ecological effects may occur or are occurring as a result of exposure to one or more stressors (US EPA, 1992). This assessment integrates the exposure and stressor response profiles for each species and part of the ecosystem (**Figure 1-9**) (US EPA, 1998a).

A commonly used approach for risk characterization is hazard quotient (*HQ*), which is defined as the ratio of an exposure concentration divided by a toxicological benchmark concentration. The risk is considered as unacceptable if $HQ > 1$, and because *HQ* is simple and quick to use, it provides an efficient and inexpensive means of identifying potential risk (Suter, 2016; US EPA, 1998a). Thus, *HQ* is widely used for risk characterization at screening level (US EPA, 1998a).

In the US, many historical agricultural sites are contaminated with dichlorodiphenyltrichloroethane (DDT), dieldrin, and other OCPs (US EPA, 2015; Centofanti et al., 2016). Although the level of contamination has decreased over time, many sites still contain OCP levels large enough to represent an ecological risk and require further characterization and

treatment. Therefore, a need exists to determine the best practices for the remediation of the historically contaminated sites.

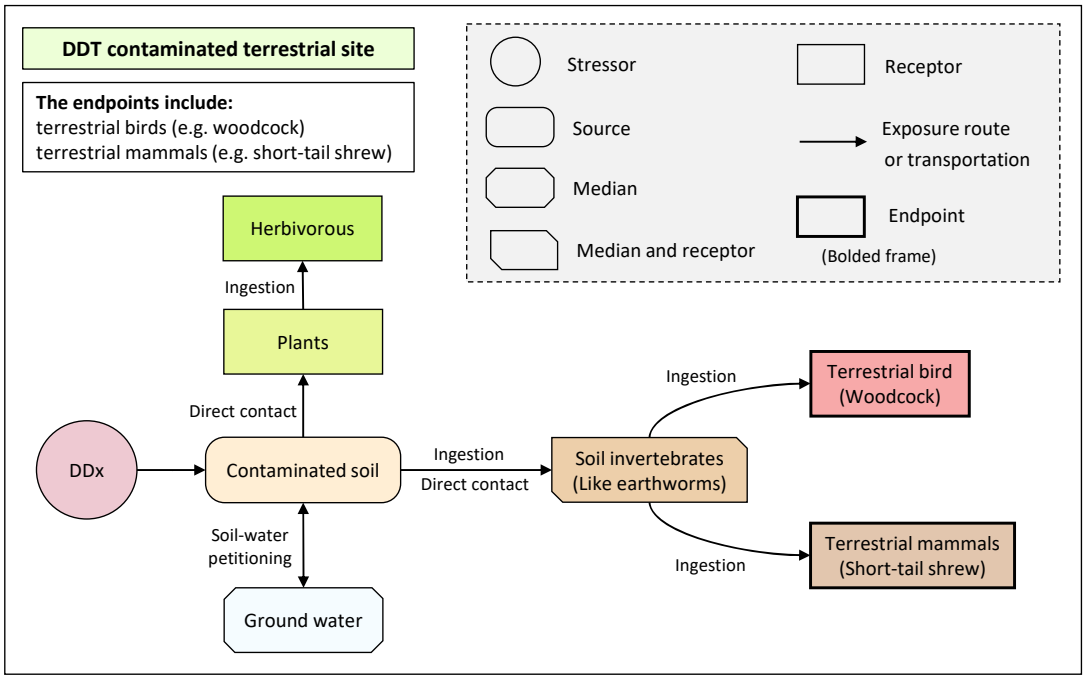

Figure 1-9 Conceptual site model of a terrestrial ecosystem

3.3 Soil remediation techniques

Currently applied soil remediation methods include physical remediation, chemical remediation, and bioremediation (Gaylord, 1998; FRTR, 2015; Megharaj et al., 2011; Atteia et al., 2013; Cunningham et al., 1995; Sudharshan et al., 2012). However, cleanup efficiency can decrease as the contaminants age within the soil matrix (Sudharshan et al., 2012). These treatments are also costly and time consuming (Hood, 2006; Gavrilescu, 2005). Thus, for a large historically contaminated area containing low levels, more feasible and economical remediation approaches are in need.

Bioavailability refers to the availability of contaminants to transfer from environmental abiotic media into a biological component of an ecosystem, and it is a critical parameter when

conducting an ecological risk assessment (Semple et al., 2013; US EPA, 1998a; Suter, 2006). Instead of removing the contaminants from the soil, reducing the bioavailability can decrease the overall ecological risk, i.e., less contaminants are transferred from soil into the food web of the ecosystem. Previous studies have shown that by adding carbonaceous materials into soil, e.g., activated charcoal (Hilber at al., 2009; Saito at al., 2011), activated carbon (Paul and Ghosh, 2011; Langlois at al., 2011), biochar (Yang at al., 2010), and dairy manure compost (Clostre at al., 2014), bioavailability of OCPs in soil can be effectively reduced. These materials can adsorb and/or absorb OCPs due to large surface area and/or hydrophobicity, leading to a reduced amount of OCPs transferred from soil into organisms (Cornelissen at al., 2005; Oen at al., 2012). However, these studies were mainly conducted in laboratories or greenhouses, where experimental conditions were well controlled. In addition, they are mainly short terms studies (e.g., up to 48 days for earthworms, up to 3 months for cucumbers), so the long-term effectiveness of this approach has not yet been investigated.

Because there is a the lack of field studies to assess the long-term effect of reducing ecological risk by increasing the soil carbon, a multi-phase project was initiated in 2010 to assess the bioavailability of the a historically contaminated site, aiming at finding effective and readily available carbonaceous material amendments to decreases bioavailability of the OCPs. A short-term lab experiment was conducted using the site soil which revealed that two dairy composts (**Figure 1-10**) were effective in reducing the bioavailability of OCPs (Centofanti et al., 2016). This study was followed by a longer-term investigation using the two dairy composts and seven plots which were randomly distributed in the contaminated site (Anderson et al., 2020). This study showed that spatial variability of soil and earthworm concentrations and bioavailability were considerable between subplots and within subplots, increasing uncertainty and making risk

assessment challenging. Thus, this study suggests that developing methods which are more robust for sites with large spatial variability is necessary, and more investigations are needed to evaluate the effectiveness of carbon amendments in field conditions.

Figure 1-10 Photo of diary compost. Photo credit Zijiang Yang.

3.4 Limitations of current data analysis methods

Considerable spatial variability of the contaminant has also been recognized by other studies (Tieyu et al., 2005; Zhang et al., 2011). High spatial variability often causes difficulties with sampling design (Lammel et al., 2011), specifically the spatial sampling layout and the sample size (US EPA, 1997; US EPA, 1999; US EPA, 2014). In addition, since spatial variability may be different at different spatial scales (Anderson et al., 2020), it is also an obstacle to extrapolating spatial data in the field, and further hinders the understanding of environmental fate of the contaminants.

When spatial variability is large, uncertainties may be underestimated. When investigating bioavailability, bioaccumulation factor (*BAF*) is usually used to quantify bioavailability, and it is defined as follows (Centofanti et al., 2016; Anderson et al., 2020):

$$BAF = \frac{C_{\mathrm{e}}}{C_{\mathrm{s}}} \qquad \text{Eqn. } 1-19$$

where C_e is concentration of contaminant of earthworms at equilibrium, and C_s is the concentration of contaminant of soil at equilibrium. This definition works well for experiments with homogenous soil and habitat-constrained earthworms, e.g., greenhouse pot studies, where heterogeneity of soil concentration and earthworm concentration are reasonably assumed to be negligible (Centofanti et al., 2016; Rich et al., 2015). In these studies, contaminant concentration in a pot were measured in triplicate, and means of soil and earthworm measurements were used in **Eqn. 1-19** as C_s and C_e, respectively (Centofanti et al., 2016; Rich et al., 2015). A point estimate of *BAF* (e.g., mean) was calculated for an individual pot, and the *BAF*'s of the individual pots were summarized for further statistical inference. However, when applied to heterogenous soils, i.e., soil with large variability, the use of **Eqn. 1-19** can be problematic. Spatial variability and small sample sizes may cause total variance and standard error estimates to be biased (Anderson et al., 2020), degrading the estimation of *BAF*. Thus, the traditional method leads to underestimation of variability in C_e and C_s, and therefore substantially increase uncertainty in the estimation of *BAF* (**Figure 1-11** and **Table 1-2**). This under-estimation of uncertainty can have a negative impact on further inference.

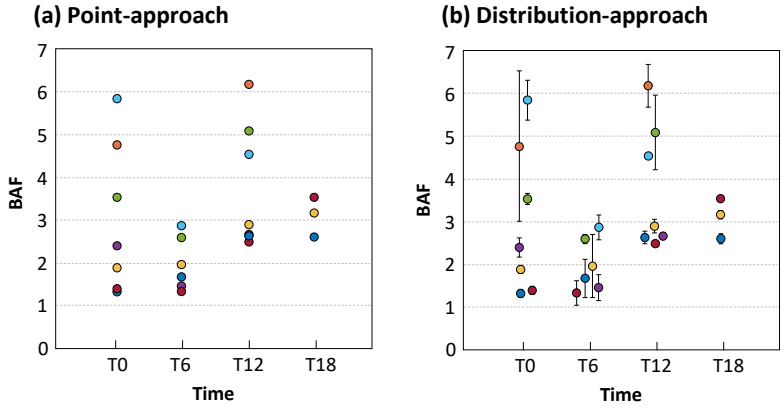

Figure 1-11 Plot of *BAF* at different time. Error bards refers to standard deviation

Table 1-2 Simulation results of Point-approach and Distribution-approach. Data were the same data from **Figure 1-11**. n = 50000 by Monte-Carlo simulation (Martinez and Martinez, 2015), results are expressed as mean ± std; Underestimation refers to relative difference in terms of std of point approach.

Time	T0	T6	T12	T18
Point approach	3.11±1.78	2.07±0.63	3.87±1.50	3.19±0.50
Distribution approach	3.11±1.93	2.07±0.77	3.87±1.55	3.19±0.51
Underestimation	8.5%	**22%**	3.9%	1.9%

Spatial variability may also case problems with ratio variables. When calculating *BAF*, pollutant concentration measurements were usually inexplicitly assumed to be independent and normally distributed when applying statistical analysis (Centofanti et al., 2016; Anderson et al., 2020; Rich et al., 2015), and sample mean is usually used to estimate population mean. However, ratio of two independent normal variables follows a mixed distribution of Cauchy distribution and a bimodal distribution (**Figure 1-12)** (Marsaglia, 1965; Marsaglia, 2006). Since the Cauchy distribution has no population mean or variance (Casella and Berger, 2002; Davison and Hinkley, 1997), a sample mean may be calculated but is not an appropriate measure of the underlying population (Press, 1969; Hayya et al., 1975). Although the delta method (Casella and Berger, 2002) and error propagation equations (Farrance and Frenkel, 2002) can be used to approximate the ratio of two independent normal variables such as *BAF* by a normal distribution, a critical constraint of these methods is that the denominator should be positive (Casella and Berger, 2002; Davison and Hinkley, 1997). Unfortunately, great spatial variability and misestimated sample statistics may permit the modelled denominator, C_s, to have small but non-negligible negative probability (**Figure 1-13a**), resulting in failure of delta methods and error propagation equations, and leading to incorrect inferences (see **Figure 1-13** for a numerical example).

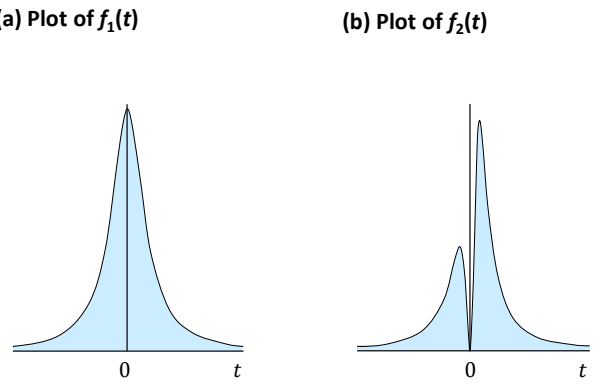

Figure 1-12 Plot of the two components $f_1(t)$ and $f_2(t)$ of a ratio variable of two normal variables, where $f_1(t)$ and $f_2(t)$ are the two components of the ratio variable t, and $t = (a + x) / (b + y)$. a and b are two nonnegative constants, and x and y are two independent standard normal variables. In addition, the following relations hold: $f(t) = pf_1(t) + (1-p)f_2(t)$ with $p = e^{-\frac{1}{2}(a^2+b^2)}$, $f_1(t) = \frac{1}{\pi(1+t^2)}$, and $f_2(t) = \frac{q\int_0^q e^{-\frac{1}{2}(a^2+b^2)}\mathrm{d}x}{\pi(1+t^2)\left(e^{\frac{1}{2}(a^2+b^2)}-1\right)}$ with $q = \frac{b+at}{\sqrt{1+t^2}}$ (Marsaglia, 1965; Marsaglia, 2006). Figure is reproduced from Marsaglia, 2006.

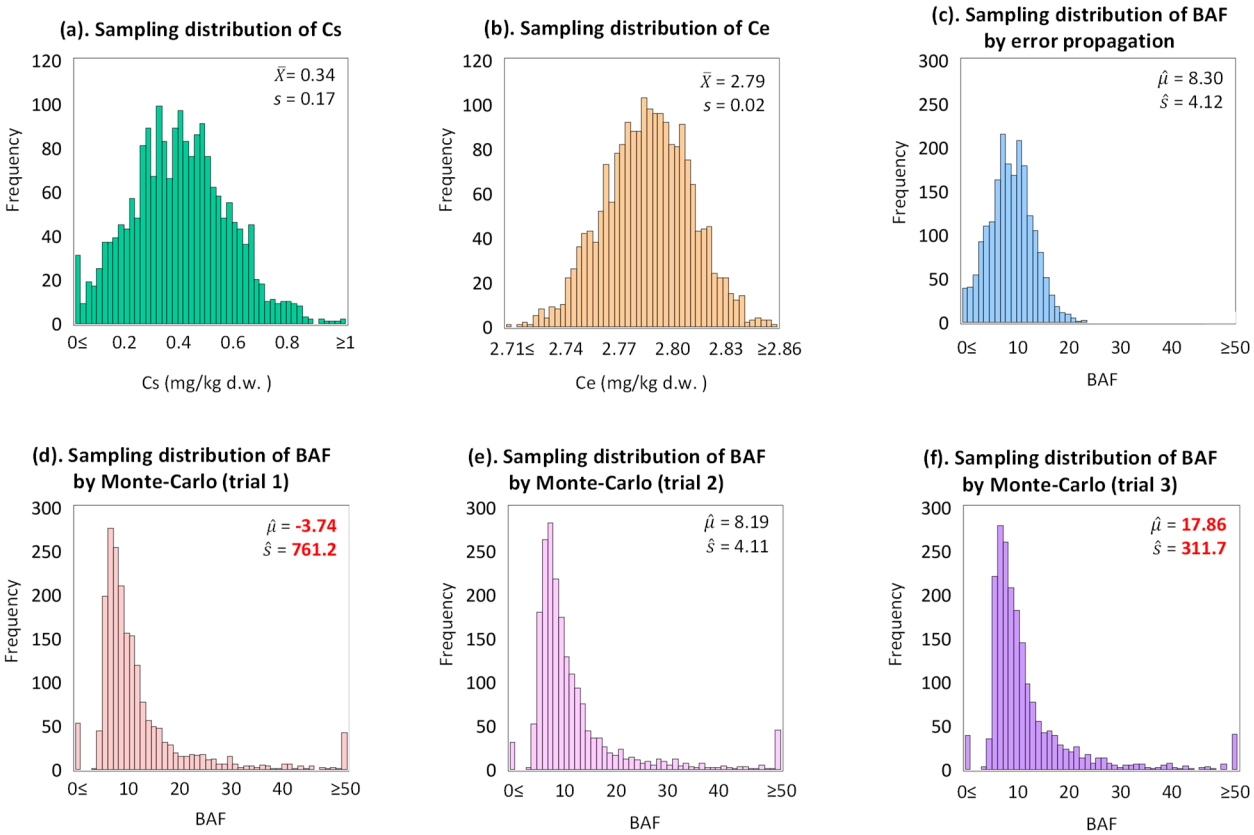

Figure 1-13 Difference between results from normal approximation and Monte Carlo simulation. The plots are based on data of the previous field plot study (Anderson et al., 2020). μ refers to sample mean, and s refers to sample standard deviation. Simulation runs n = 5000. Note the overflows and underflows in (d), (e) and (f), which reflect the great heavy tail. It shows that the *BAF* estimated by Monte-Carlo simulation is skewed and the estimated mean and standard deviation has a great variability among three independent trials (d), (e), (f), and reflecting lack of convergence.

In addition, extreme values and potential outliers are likely to come with large spatial variability. Due to the nature of small sample size in soil remediation experiment (Anderson et al., 2020), it is difficult to identify and determine the outliers.

In order to address the problems mentioned above, trunked normal distribution (Byon et al., 2008), log-normal transformation (Díez et al., 2007), and trunked log-normal transformation (Bowers et al., 1996) have been used in previous studies. However, these methods can only address the ratio variable problem to some extent; they are not able to overcome the problems of underestimation of uncertainties and extreme values. Thus, an approach that is capable of addressing all of those problems is needed.

Therefore, an approach that is capable to address all of those problems is in need.

4. Objectives

The main objective of this dissertation is to address the problems and limitations mentioned above, and these challenges are addressed into four cases-studies.

4.1 Modification of Gaussian plume model

Due to limitations of Gaussian plume model, the main goals of this case-study is to modify and to validate the Gaussian plume models for the following situations: pollutants that are released horizontally from the source; a spatial scale that is small, i.e., the sampling system is in close proximity to the exhaust tunnel fans; and a strong localized wind flow that is controlled by the tunnel fan and dominates the ambient wind conditions.

4.2 Development of dispersion correction factor

Due to the limitations of AERMOD, the main goals of this case-study are to characterize PM concentrations around a cotton gin, to evaluate the performance of EPA-recommended models for predicting PM concentrations, and to develop dispersion modeling correction factors for low-level sources.

4.3 Data analysis for field remediation plot study

Due to limitations of previous greenhouse soil remediation studies, the goal of this field case-study is to investigate bioaccumulation of DDx and dieldrin to native earthworms, analyze the effectiveness of CM amendments under real field conditions, and to evaluate the Eco-SSL risk assessment results using field data.

4.4 Application of Bayesian hierarchical model

Due to limitations of traditional statistical methods in soil remediation research, the main goal of this study is to apply of Bayesian hierarchical model to characterize soil concentration, earthworm concentration, *BAF* and their uncertainties, to compare the performance of the proposed model with traditional model, and to draw implications of the modelling results for evaluation of soil remediation techniques.

Chapter 2 Modification and Validation of the Gaussian Plume Model (GPM) to Predict Ammonia and Particulate Matter Dispersion

(This chapter has been published in *Atmospheric Pollution Research*)

Zijiang Yang[a], Qi Yao[a], Michael D. Buser[b], Joseph G. Alfieri[c], Hong Li[d], Alba Torrents[a], Laura L. McConnell[a], Peter M. Downey[c], and Cathleen J. Hapeman[c]

[a] *Department of Civil and Environmental Engineering, University of Maryland, 1173 Glenn L. Martin Hall, College Park, MD 20742, USA*

[b] *Biosystems and Agricultural Engineering Department, Oklahoma State University, 111 Ag Hall, Stillwater, OK 74078, USA*[†]

[c] *US Department of Agriculture, Agricultural Research Service, Henry A. Wallace Beltsville Agricultural Research Center,10300 Baltimore Avenue, Beltsville, MD 20705, USA*

[d] *Department of Animal and Food Sciences, University of Delaware, 237 Townsend Hall, Newark, DE 19716, USA*

Abstract

Estimating the transport of ammonia and particulate matter (PM) from ventilation tunnel fans of poultry houses is needed to develop effective mitigation strategies. However, field measurements are time-consuming and costly. Alternatively, air dispersion models can provide more

information under a variety of conditions. Therefore, this study was conducted to modify and to validate the Gaussian plume model to predict poultry house plumes. The most notable modification was the addition of a virtual, emission-releasing point behind the exhaust tunnel fan. The modified model was validated using previously-reported field measurements. The fraction of predictions within a factor of two (*FAC2*) for both ammonia and PM observations was greatly improved compared with original model. In addition, the model performance was not sensitive to different sampling scenarios. This new model can be applied to other experiments and will be useful in evaluating the effectiveness of mitigation strategies for air pollutant emissions.

1. Introduction

The United States is the largest broiler chicken producer in the world and exports nearly 20% of what is produced (National Chicken Council, 2019). The demand for poultry products is rising, and the poultry industry is responding by increasing the number of concentrated poultry farms. With such an expansion, there is increased concern about atmospheric emissions and the potential environmental risks and harm to public health that these emissions present (Donham et al., 2007, Aneja et al., 2008; Willis et al., 2017). The two most abundant air pollutants emitted from poultry houses are particulate matter (PM) and ammonia (Ritz et al., 2004; Pescatore et al., 2005; Cambra-López et al., 2011; Yao et al., 2018b).

PM can decrease visibility and be harmful to human health. Adverse health effects associated with PM include asthma attacks, chronic bronchitis, cancer, cardiovascular disease, diabetes, and premature death (Löndahl et al., 2007; World Health Organization, 2017). World-wide, an estimated 2.1 million people die annually due to $PM_{2.5}$ (PM with an aerodynamic equivalent diameter less

than 2.5 μm) (Kim et al., 2015). PM is also associated with negative effects on nearby ecosystems, such as abrasion, radiative heating, and photosynthesis reduction (Grantz et al., 2003). Ammonia emissions from animal production have been shown to change the pH in soil near the source due to increased nitrogen deposition (Stevens and Tilman, 2010; Jones et al., 2013). These effects can also decrease species diversity (Jones et al., 2013). In addition, ammonia can form $PM_{2.5}$ in the atmosphere (Behera et al., 2013).

Currently used technologies to control poultry house air emissions include dietary management (Carey et al., 2004) and litter amendments (Choi and Moore, 2008). Filter and bio-filters (Ullman et al., 2004), electrostatic precipitation (Chai et al., 2009), and acid scrubbers (Melse and Ogink, 2005) have been tested but are expensive and not feasible for many poultry houses. Vegetative environmental buffers (VEBs), which consist of a trees, shrubs, and grasses planted around the poultry-house ventilation fans, have been examined as low-cost mitigation strategy (Malone et al. 2006; USDA-NRCS, 2007). Recent simulation studies have shown that VEBs can remove up to 70% of the air emissions from poultry houses (Belt et al., 2015; Ro et al., 2018; Willis et al., 2017a, 2017b), but few studies have been conducted on-farm (Yao et al., 2018a). These types of studies require knowledge of the emission plumes and how environmental conditions can affect pollutant transport and collection of large data sets that can be time consuming and cost prohibitive.

Utilizing air dispersion models may expand the usefulness of the limited available field datasets, yet most of these models are not useful when applied to small-spatial scale and/or in systems with horizontally-releasing source(s). For example, the American Meteorological Society/Environmental Protection Agency Regulatory Model (AERMOD) is a commercially-available and widely-used model developed by the United States Environmental Protection

Agency (US EPA) and was originally designed to predict stack plumes for industrial applications (Cimorelli et al., 1998; Kakosimos et al., 2011; Nagendra et al., 2012; Ma et al., 2013; Hadlocon et al., 2015; US EPA, 2019). However, the underlying structure of AERMOD is not useful for investigating exhaust tunnel fans because the orientation for the horizontal point source option in AERMOD is always pointed in the downwind direction as opposed to an active discharge from a horizontally released source. Computational fluid dynamic (CFD) models are based on aerodynamics and fluid dynamics and can effectively handle the challenges of complex landscapes and sources (Anderson and Wendt, 1995; Endalew et al., 2010; Tominaga and Stathopoulos, 2013; Lee et al., 2013), but these models are computer-intensive and require considerable detailed input data (Riddle et al., 2004; Jeong et al., 2005) and are not useful for current study.

The Gaussian plume model (GPM) is relatively simple, requires much less data than CFD models, and is widely used to predict regular or instantaneous emissions (Asman et al., 2001; Arystanbekova, 2004; Siefert et al., 2004; Siefert and Scudlark, 2008; Hensen et al., 2009; Sutton et al., 2009; Lushi and Stockie, 2010). For example, the GPM was used to estimate the source strength of ammonia emissions and amount of deposition to the ecosystem surrounding a livestock farm (up to 1 km) (Asman et al., 2001), and an inverse GPM was modified to calculate the source strength of an actively-ventilated poultry house and to determine the ammonia emission factor (i.e., the amount of ammonia emitted per bird per day) (Siefert et al., 2004; Siefert and Scudlark, 2008; Hensen et al., 2009; Sutton et al., 2009). In these studies, the actual plume emitted from the animal facilities was not measured immediately next to the source, but this information is required to assess the effectiveness of any practices implemented to mitigate the pollutant plumes, particularly those very near the poultry house.

Therefore, we conducted a study to measure the ammonia and PM emission plumes released from a poultry house and to examine the factors influencing the plumes (Yao et al., 2018b).

Results of that study revealed that the plume direction was determined by the exhaust tunnel fans, not the ambient wind, that the particle size distribution did not change with distance in the plume, and that diffusion and dispersion of ammonia in the plumes was greater than PM under calmer atmospheric conditions. In the current study, we used the dataset of Yao et al., 2018b to modify and to validate a GPM that addresses the following system parameters: pollutants that are released horizontally from the source (the exhaust tunnel fans); a spatial scale that is small (2 – 47 m), i.e., the sampling system is in close proximity to the exhaust tunnel fans; and a strong localized wind flow that is controlled by the tunnel fan and dominates the ambient wind conditions. These modifications lay the foundation for additional air pollution mitigation studies from active horizontal sources.

2. Material and Methods

2.1 Sampling campaign

The sampling campaign was conducted at a typical two-house broiler farm in Delaware from 17 May to 25 May 2015 and has been previously described (Yao et al., 2018b). Briefly, each 122 m × 21 m house was vented using five, commonly used, 1.3-m tunnel fans on both sides of the house (Model 48319-215 from Chore-Time, Milford, IN). Three sampling arrays were deployed. The middle sampling array consisted of three 10-m sampling towers which were set up perpendicularly downwind of the middle fan at the following distances: tower 1 (T1) at 2 m, tower 2 (T2) at 23 m, and tower 3 (T3) at 47 m from the primary tunnel fan. Each tower was equipped with 4 sampling crossbars (1, 2, 3, and 4) at 2, 4.5, 7.25, and 10 m, respectively. Two additional arrays emanating from the middle fan with two samplers at 2 m above ground level were deployed on the either side and were in parallel with the poultry house; S1 and S2 were 4 m

from T2, and S3 and S4 were 8-m from T3 (**Figure 2-1, SI Figure 2-1 and SI Figure 2-2**). The influence of other buildings in the area is negligible. A background sampler location was also deployed approximately 70 m east of the tunnel fans and 2 m above ground level. In addition to PM and ammonia collection, the wind speed (using an anemometer) and other meteorological data were also obtained at each sampling point. No PM data were reported for T1-3 because the electronic controller for the sampler malfunctioned. Additional details regarding the site, data collection, and analysis methods are described elsewhere (Allen, 2005; Wanjura et al., 2005; Radiello, 2006; Yao et al., 2018b) and in the **Supplementary Information**. Of the ten experiments conducted, only eight were used in model development (see **Section 3.1**).

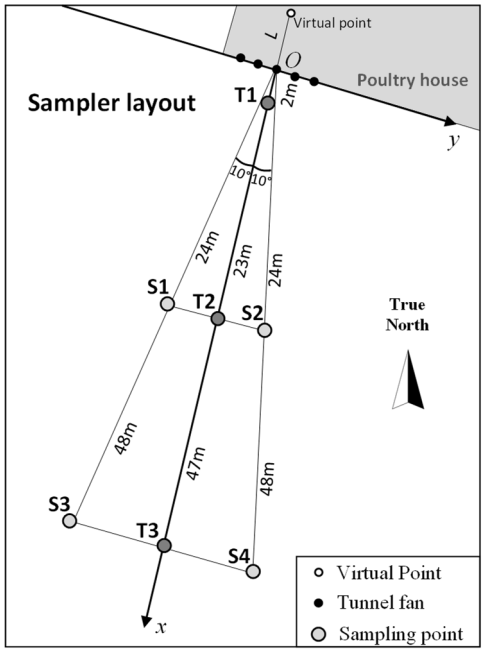

Figure 2-1 Sampler layout. The virtual point is only shown for the middle fan. *L* is the distance between virtual point and its corresponding fan. T1 was 2 m from the fan; S1, T2 and S2 were about 20 m from the fan; S3, T3 and S4 were about 47 m away from the fan. T1, T2 and T3 were equipped 4 sampler bars at 2 m (T*i*-1), 4.5 m (T*i*-2), 7.25 m (T*i*-3) and 10 m (T*i*-4), where *i* = 1,2,3. S1, S2, S3 and S4 samplers were 2 m in height. The positive *x*-axis direction was the direction of wind from the fan; the positive direction of *y*-axis eastly parallel to the side-wall of poultry house, and the middle fan (fan #3) was at the origin of the coordinate system. *L* was *x* to model the plume.

2.2 Gaussian plume model

The Gaussian plume model is a steady-state model that treats the turbulence in the atmosphere as stationary and homogeneous (Abdel-Rahman, 2008; Stockie, 2011). The plume concentration from a point source can be calculated using **Eqn. 2-1**:

$$C(x,y,z) = \frac{Q}{2\pi\sigma_y\sigma_z u} \exp\left(\frac{-y^2}{2{\sigma_y}^2}\right)\left[\exp\left(\frac{-(z-h)^2}{2{\sigma_z}^2}\right) + \exp\left(\frac{-(z+h)^2}{2{\sigma_z}^2}\right)\right] \quad \text{Eqn. } 2-1$$

where x, y, and z are the downwind, crosswind, and vertical coordinates (m), h is the release height from the ground (m), Q is source strength (g/s), u is wind speed (m/s), σ_y and σ_z are the standard deviation of the distribution concentration in y and z axis (m). For small distances, where x < 1000 m, σ_y and σ_z can be calculated from wind speed, u (m/s), distance from source, x (m), and the convective velocity scale, w_* (m/s), following the equations given by Venkatram (2015):

$$\sigma_y = \frac{0.6w_*}{u}x, \qquad \sigma_z = \frac{0.6w_*}{u}x \qquad \text{Eqn. } 2-2$$

The GPM assumes that (1) the pollutant concentration is normally distributed in the horizontal and vertical directions, (2) the wind speed and other meteorological data are uniform, (3) the source strength and position are constant, and (4) the wind speed is sufficiently large that diffusive transport can be neglected in the direction of the wind (Stockie, 2011; Hanna et al., 1982). It also assumes that mass is conserved which for this study assumed that no deposition occurred for either ammonia or PM, i.e., over such short distances, there is too little time for the air pollutants to settle out of the air. This has been verified previously in small spatial scale studies (Hensen et al., 2009; Nemitz et al., 2009, Yao et al., 2018b).

2.3 Model modifications and additional assumptions

Several modifications and additional assumptions were made to the standard GPM. (1) Virtual pollutant releasing points were assigned directly behind each tunnel fan. The distance between the fan and its corresponding virtual point was defined as L ($L > 0$). L increases the distance from the source and the sampler in terms of x (**Figure 2-1 and SI Figure 2-3**). (2) The height of the virtual point was equal to the distance from the center of the fan to the ground below it (1.2 m). (3) The direction of airflow produced by the fan was normal to the surface of the fan and was defined as *fan direction* **(Figure 2-1, SI Figure 2-3, and SI Figure 2-4)**. Over the short distance between the tunnel fans and the sampling points, the airflow produced by the ventilation tunnel fans overwhelmed the much weaker ambient winds (Yao et al., 2018b). Therefore, the direction of the airflow produced by the fans, 15 degrees from true north based on building geometry, was used for concentration calculations in the model instead of the ambient wind direction.

2.4 Concentration calculations

The source strength (Q) was not measured directly, therefore, air pollutant concentrations were calculated using an alternative approach. Q was estimated using one sample measured concentration from each field sampling experiment, which was chosen based on the following criteria: 1) this sample location is the most sensitive to the source strength; 2) this sample location is the most independent from the ambient environment; i.e., the sampling point that is the closest to the tunnel fans. This chosen sample point is referred as the *reference point* in this approach. In this concentration calculation, the reference point plays a similar role as the real-time monitored source strength to calculate pollutant concentrations at all other sampler locations. In the field experimental set-up, T1-1 sampler location was the closest to the tunnel

fan with the least influence from the ambient environment, (**Figure 2-1**), therefore, T1-1 was used as the reference point to estimated Q and other sample concentrations.

The air pollutant calculations can be also estimated by employing the ratio between sample concentration versus reference point concentration (**Eqn**. **2-4**), in which the calculation of Q was excluded. The model-predicted concentration of each sampler, s, ($C_{\mathrm{pred},s}$) was calculated by observed concentration of reference point (T1-1, $C_{\mathrm{obs,T1-1}}$) and background concentration (C_{bg}) as following:

$$C_{\mathrm{pred},s} = \left(C_{\mathrm{obs,T1-1}} - C_{\mathrm{bg}}\right) \cdot M_s + C_{\mathrm{bg}} \qquad \mathrm{Eqn.}\ 2-3$$

where M_s was the *concentration ratio* of sampler s and was described as:

$$M_s = \frac{C_{\mathrm{Q1},s}}{C_{\mathrm{Q1,T1-1}}} \qquad \mathrm{Eqn.}\ 2-4$$

where $C_{\mathrm{Q1},s}$ was the model-predicted concentration of sampler s when Q = 1. $C_{\mathrm{Q1,T1-1}}$ was the $C_{\mathrm{Q1},s}$ when s = T1-1 (reference point).

The concentration ratio, M_s, was independent from Q according to **Eqn. 2-1**, so M_s can be calculated by assigning Q as any positive value, and we assigned Q = 1 for calculation. $C_{\mathrm{Q1},s}$ was the superimposed concentration contributed by five fans, i.e., the superposition principle was applied for concentration calculation of multiple sources (Siefert et al., 2004; Lushi and Stockie, 2010; Stockie, 2011). Thus, $C_{\mathrm{Q1},s}$ was calculated as following:

$$C_{\mathrm{Q1},s} = \sum_{f=1}^{5} c_{\mathrm{Q1},s,f} \qquad \mathrm{Eqn.}\ 2-5$$

where $c_{\mathrm{Q1},s,f}$ was the model-predicted concentration of sampler s of a separate fan f (f = 1, 2, 3, 4, 5) when Q = 1 in **Eqn. 2-1**.

Wind speed and other meteorological parameters, e.g., temperature, relative humidity, atmospheric pressure and etc., were hourly averaged as the model input (**SI Table 2-1**). Matlab R2018a (The MathWorks, Inc. Natick, MA) was used for modelling computations and statistical analyses. Figure construction were carried out using Microsoft Excel.

2.5 Determination of optimal L (L_{opt}) and model validation

The optimal L (noted as L_{opt}) was determined based on the L that generated the maximum value of the fraction of predictions within a factor of two of observations (*FAC2*) for ammonia and for PM as described in **Section 2.6** (Chang and Hanna, 2004). Predicted concentrations at each sampling point, $C_{\mathrm{pred},s}$, were calculated by increasing L values from zero. Preliminary results showed that for L values greater than 35 m, model performance decreased. In addition, large L values are not physically feasible for the virtual point. Thus, determination of L_{opt} was based on L values ranging from 0 to 35.4 m increasing at an interval of 0.6 m, which was half of the height of the virtual point.

The modified GPM, i.e., GPM with L_{opt}, was validated by k-fold cross-validation and its predictive accuracy compared with the original GPM (Gelman et al., 2014; Hooten and Hobbs, 2015). Here k was set to 8, i.e., each subset of data contains data of one experiment. During cross-validation, seven of the eight experiments were used for L_{opt} calibration, and one of the eight experiments was held for validation. This process was executed eight times until each experiment was validated. After cross-validation, an L_{opt} was calculated using all of the eight experiments.

2.6 Model evaluation – performance

FAC2 was used to evaluate the performance of the model (Chang and Hanna, 2004) and were expressed as the following,

$$FAC2 = \text{fraction of data that satisfy: } 0.5 \leq \frac{C_{\text{pred},s}}{C_{\text{obs},s}} \leq 2.0 \qquad \text{Eqn. } 2-6$$

where $C_{\text{obs},s}$ is the observed concentration of sampler *s*. *FAC2* is a measure of total effect of systematic error and random error, and it is robust because it is not influenced by extreme values. A perfect model would have *FAC2* = 1. Using **Eqn. 2-6**, the larger *FAC2*, the closer the model predicted the observed field data; *FAC2* > 0.5 was considered acceptable (Chang and Hanna, 2004; Hanna et al., 2004). A *FAC2* was calculated for each *L* value with all samplers (*n* = 12 for ammonia, *n* = 11 for PM) in eight experiments (*n* = 8), i.e., *FAC2* is calculated using 96 points for ammonia and 88 points for PM.

Furthermore, for sampler *s*, the distance of a point from a 1:1 ratio line on a logarithmic scale was defined as d_s:

$$d_s = \frac{\log_{10}(C_{\text{pred},s}) - \log_{10}(C_{\text{obs},s})}{\sqrt{2}} \qquad \text{Eqn. } 2-7$$

d_s also served as a measure of model performance (Warton et al., 2006). If the model over-predicted the concentration ($C_{\text{pred},s} > C_{\text{obs},s}$), then $d_s > 0$, whereas if the model under-predicted the concentration ($C_{\text{pred},s} < C_{\text{obs},s}$), then $d_s < 0$ (**SI Figure 2-5**). The absolute value of d_s ($|d_s|$) represented the scatter; the smaller the magnitude of $|d_s|$, the closer the point was to 1:1 ratio line. The average of d_s and $|d_s|$ of each sampler of all experiments was noted as $\overline{d_s}$ and $\overline{|d_s|}$, respectively. $\overline{d_s}$ and $\overline{|d_s|}$ served as indicators of overall performance in terms of precision and accuracy, respectively. The factor F_s was the ratio of model predictions over observations: $F_s = C_{\text{pred},s}/C_{\text{obs},s}$, and therefore, the relationship between F_s and d_s was derived as: $F_s = 10^{\sqrt{2}\cdot d_s}$.

2.7 Model evaluation – sensitivity to meteorological inputs

During preliminary trials, meteorological data from all the anemometers and other meteorological equipment associated with each sampler location were used for calculating the hourly average wind speed and other meteorological data for model input (scenario A1 in **Table 2-1**). Model performance was acceptable using scenario A1.

Table 2-1 Summary of wind speed scenarios. Wind speed and other meteorological input of each sampler were used as inputs for each scenario. S1, S2, S3 and S4 (not shown) samplers were used in all scenarios.

		Samplers used											
Sampler		T1-1	T1-2	T1-3	T1-4	T2-1	T2-2	T2-3	T2-4	T3-1	T3-2	T3-3	T3-4
Height		2m	4.5m	7.25m	10m	2m	4.5m	7.25m	10m	2m	4.5m	7.25m	10m
Scenario	A1	√	√	√	√	√	√	√	√	√	√	√	√
	A2					√	√	√	√	√	√	√	√
	B1	√	√	√		√	√	√		√	√	√	
	B2					√	√	√		√	√	√	
	C1	√	√			√	√			√	√		
	C2					√	√			√	√		
	D1	√				√				√			
	D2					√				√			

However, this model could be employed using a different arrangement of samplers than was used in Yao et al. 2018b. Seven additional sampling arrangements for wind speed and other meteorological inputs were considered and are described in **Table 2-1 and SI Figure 2-6**. Scenarios A2, B2, C2, and D2 exclude the T1 samplers, the tower closest to the source. Scenario B1 and B2 do not include the 10-m height samplers, scenarios C1 and C2 do not include the 10-m or 7.25-m heights, and scenarios D1 and D2 only include the 2-m height samplers.

These scenarios were used to assess the sensitivity of the model to different meteorological inputs.

2.8 Model evaluation – sensitivity to *L* values

The model sensitivity to L values (0 to 35.4 m, 0.6 m increments) was also evaluated with the various scenarios. The condition based on scenario A1 with $L = L_{opt}$ was used as the *reference condition*. For each sampler s, the model-predicted concentrations of the reference condition were compared with the model-predicted concentrations of the other scenarios by calculating the *ratio of difference*, R_s, expressed as:

$$R_s = \frac{\left| C_{\text{pred},s,scenario,L} - C_{\text{pred},s,\text{A1},L_{\text{opt}}} \right|}{C_{\text{pred},s,\text{A1},L_{\text{opt}}}} \qquad \text{Eqn. } 2-8$$

where $C_{\text{pred},s,\text{A1},L_{\text{opt}}}$ was model-predicted concentration of sampler s under the reference condition (scenario A1 and L_{opt}) and $C_{\text{pred},s,scenario,L}$ was the model-predicted concentration of the same sampler s under another scenario or using another L value.

3. Results and Discussion

3.1 Summary of field experiments

The emission plume of a poultry house was measured at multiple heights and distances from the ventilation fans in a campaign of ten experiments, and results are summarized here (Yao et al., 2018b). The atmospheric pressure, relative humidity, and air density in the plume were similar to background observations for each experiment. However, small diurnal differences between the ambient temperatures and the plume temperatures were observed because the temperature inside the chicken house is controlled and relatively constant while the outside temperature varied from day to night.

The prevailing wind direction during the experiments was from a south-southwest direction, which was opposite to the exhaust direction of the tunnel fans. The wind speed and the

atmospheric instability are shown in **SI Table 2-2**. The average background wind speed measured at 2-m height was converted to wind speed at 10-m height, the standard height for surface wind speed (World Meteorological Organization, 2008). Atmospheric instability was classified according to Pasquill stability classes (National Oceanic and Atmospheric Administration, 2018). The results showed that the atmosphere during all the daytime experiments was unstable or neutral, while all the nighttime experiments were stable. In addition, the background surface wind speed during days 2 and 3 (wind speed was greater than 4 m/s) was much larger than on the other days. Although such great surface wind speed was uncommon in the study region (73.2% of days with wind speed smaller than 4 m/s) (**SI Figure 2-7**), these strong ambient winds significantly affected the plume shape (Yao et al., 2018b), which violated the assumption that the air flow from the fan overwhelmed the ambient wind. Thus, the data collected when on days with large ambient surface wind speeds were not used in the development and evaluation of the model discussed here.

3.2 Cross-validation results

The cross-sectional area of the ventilation fans was 1.33 m^2, therefore a virtual release point for each pollutant was assumed which was directly behind each tunnel fan at a distance, L (**Figure 2-1 and SI Figure 2-3**). L_{opt} was determined by varying the L values (0 to 35.4 m, 0.6 m increments) and evaluating *FAC2*. During cross-validation, seven out of eight experiments were used to calibrate L_{opt} based on *FAC2*. Then the calibrated L_{opt} was used as an input for the modified GPM to predict pollutant concentration of the eighth experiment as validation. This process was executed for each of the eight experiments. The *FAC2* versus L plots for each cross-validation showed a similar pattern (**SI Figure 2-8**), suggesting that the L_{opt} is a property of the

pollutant under the same experimental setup. The out-of-sample model-predicted concentration, $C_{\text{pred-cv}}$, versus observed concentration, C_{obs}, for ammonia and PM are shown in **Figure 2-2**.

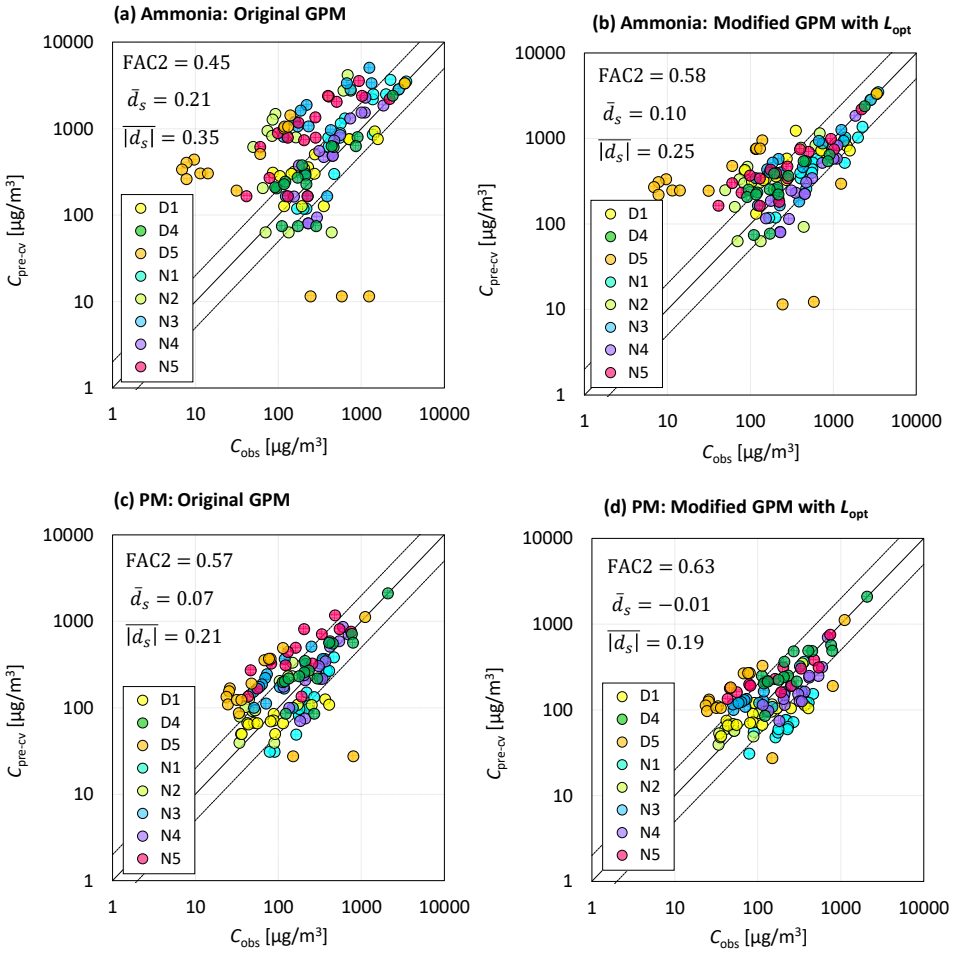

Figure 2-2 Plots of observed concentration (C_{obs}) vs. out-of-sample model-predicted concentration ($C_{\text{pred-cv}}$). Solid lines are a 1:1 ratio, and dashed lines are 1:0.5 and 1:2 ratio. N refers to nighttime experiment; D refers to daytime experiment. *FAC2*, $\overline{d_s}$ and $\overline{|d_s|}$ are defined in **Section 2.6**. Points inside the dashed-line region indicate that the prediction is acceptable.

The results showed that the data points in the modified GPM were more assembled around the 1:1 ratio line, indicating a better performance of modified GPM than original GPM. *FAC2* of ammonia of modified GPM was greater than *FAC2* of original GPM (0.45 for original GPM and 0.58 for modified GPM). The same performance was found for PM (0.57 for original GPM and 0.63 for modified GPM). In addition, $\overline{d_s}$ of modified GPM of both ammonia and PM were closer to zero than $\overline{d_s}$ of original GPM. Furthermore, $\overline{|d_s|}$ of modified GPM of both pollutants were

smaller than $\overline{|d_s|}$ of original GPM. These results demonstrated that modified GPM outperformed over original GPM for both pollutants. Therefore, the modified GPM can better predict pollutant concentrations than original GPM by assuming a virtual point behind the fan. Since cross-validation showed that modified GPM had better predictive accuracy than original GPM, the following analyses were based on applying modified GPM to all eight experiments.

3.3 Determining optimal L (L_{opt})

Based on the eight experiments, an overall L_{opt} was determined, and the *FAC2* results were plotted as a function of L (**Figure 2-3a and SI Figure 2-9a**). *FAC2* increased rapidly from 0 m to ~2 m and then plateaued until ~13 m when *FAC2* gradually decreased. Similar results can be found in **SI Animation**, which shows more points are moving towards the 1:1 line as L increases from 0 m to L_{opt}, followed by more points moving away from 1:1 line as L increased beyond L_{opt}. Clearly, by considering a virtual point behind the fan by the distance of L_{opt}, the model performance was greatly improved compared with the original model where L is 0 m.

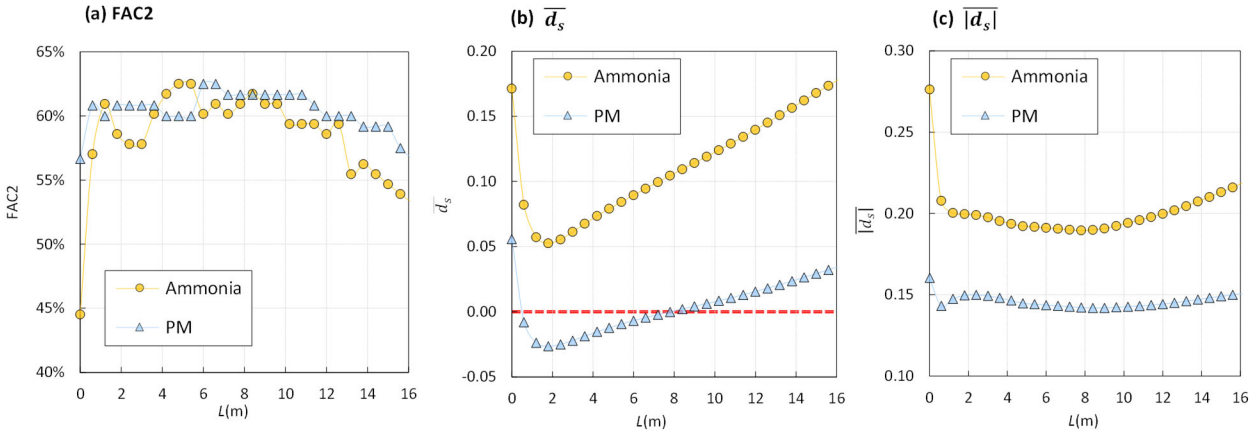

Figure 2-3 Plot of *FAC2* (a), $\overline{d_s}$ (b) and $\overline{|d_s|}$ (c) of ammonia and PM along different L values. For L values beyond 15 m, see extended x-axes in **SI Figure 2-9**.

This trend is consistent with the geometrical relationship between the plume and the fan (**Figure 2-4**). With increasing *L*, the cross-sectional area of the plume at the fan expanded up to the size of the fan (**Figure 2-4a**). When *L* increased further, the cross-section of the plume continued expanding and became larger than the size of the fan, giving rise to observed *FAC2* curve – sharp increase, plateau, gradual decrease. However, the *FAC2* curves of ammonia and PM differed somewhat. The L_{opt} value for ammonia was smaller than the L_{opt} value for PM. This is reflective of the observed concentration data where the diffusion of ammonia is larger than the diffusion of PM (Yao et al., 2018b), thus, a greater distance was required for the PM plume to expand to fan size from virtual point compared with PM (**Figure 2-4b**). For ammonia, the highest *FAC2* values ranged from *L* values between 3.6 m and 6 m. A value of 4.8 m was selected for L_{opt} of ammonia which afforded *FAC2* values of 0.63. For PM, the highest *FAC2* values ranged from *L* values between 6.0 m and ~11 m. A value of 6.6 m, which has the largest *FAC2*, was selected for L_{opt} of PM which afforded *FAC2* values of 0.63. Tunnel fan characteristics, such as motor power, blade shape and number, ventilation rate, and static pressure can potentially influence the shape of the plume and further influence the geometry and location of the virtual point, L_{opt}. Therefore, a new L_{opt} may be needed when using different fans.

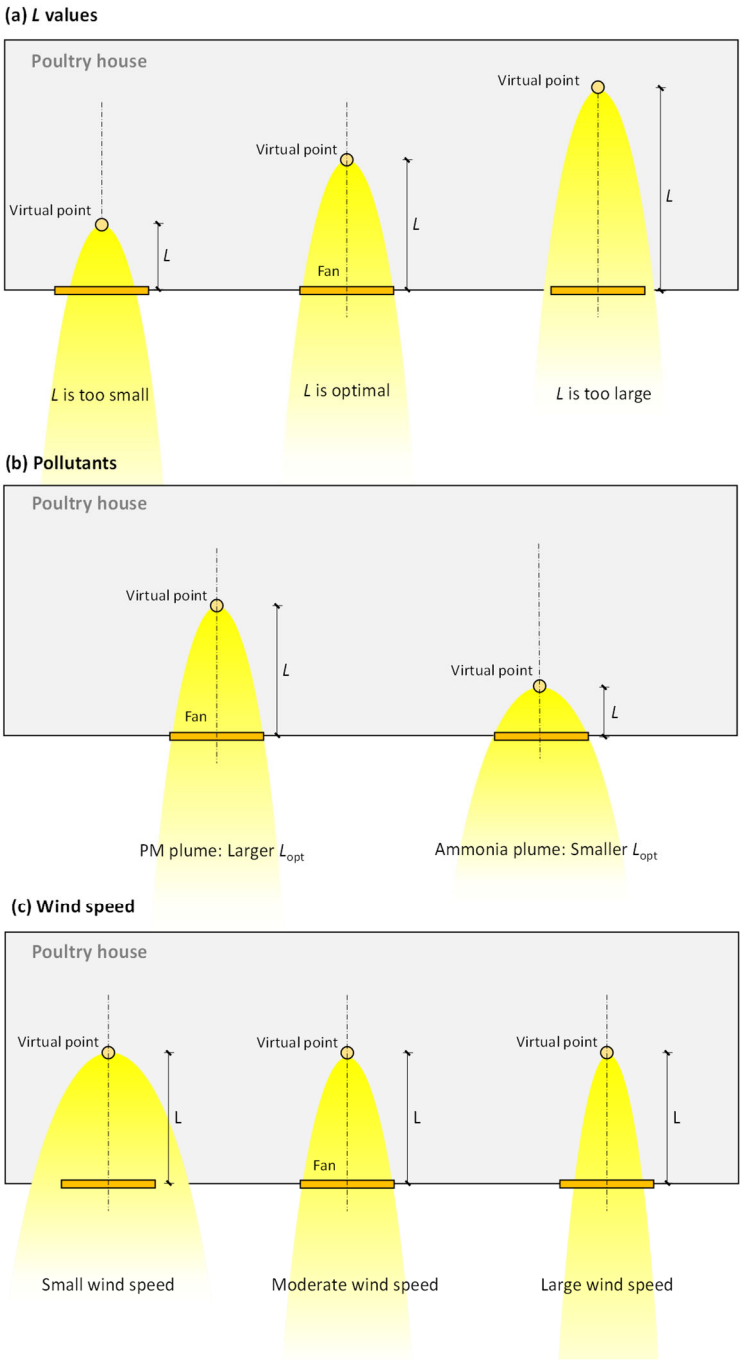

Figure 2-4 Plume changes as a function of (a) distance between fan and virtual point, L, (b) pollutants, and (c) wind speed of the fan.

3.4 Model predictions

Ammonia and PM concentrations throughout the plume were predicted for each experiment using the concentration observed at the reference point (T1-1) and L_{opt} = 4.8 m for ammonia and

L_{opt} = 6.6 m for PM (**SI Table 2-3 and SI Table 2-4**). Scatter plots of ammonia and PM predicted concentrations (C_{pred}) versus observed concentrations (C_{obs}) are shown in **Figure 2-5** with lines for 1:0.5, 1:1, and 1:2 ratios. Points that fall within between the dash-line regions are acceptable (**Eqn. 2-6**) (Chang and Hanna, 2004). Most points for ammonia and for PM fell within or very close to this region, although nearly all the day 5 points did not (**SI Figure 2-10 and SI Figure 2-11**). The lack of agreement on day 5 is probably due to the large on-site wind speed compared to the other days (**SI Table 2-2**).

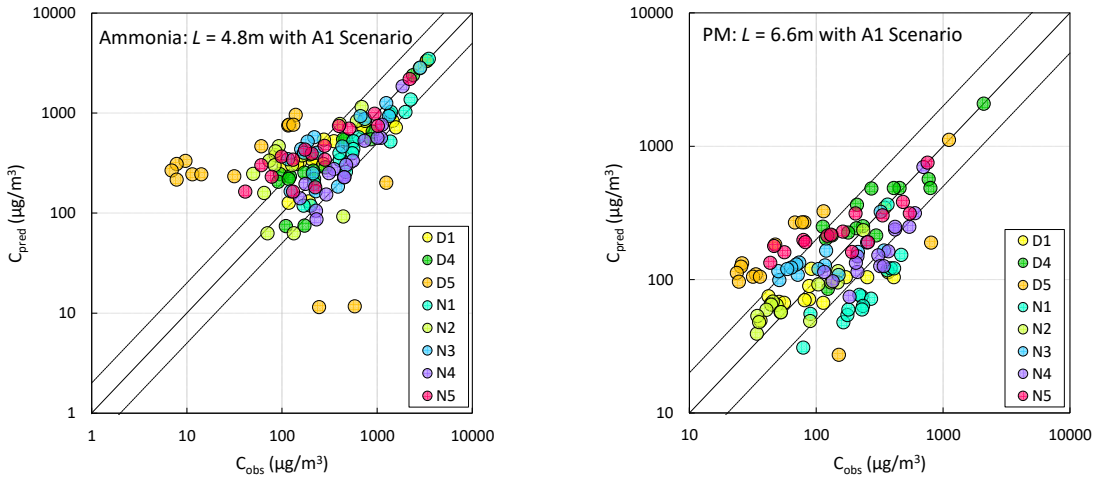

Figure 2-5 Plots of observed concentration (C_{obs}) vs. model-predicted concentration (C_{pred}) of (a) ammonia and (b) PM using L_{opt} = 4.8 or 6.6m for ammonia and PM, respectively. Solid lines are a 1:1 ratio, and dashed lines are 1:0.5 and 1:2 ratio. N refers to nighttime experiment; D refers to daytime experiment. Points inside the dashed-line region indicate that the prediction is acceptable. The two plots are not on the same scale.

3.5 Reflectivity

The above calculations included ground reflection. Reflectivity is related to the adsorptive properties of ammonia and PM to the ground surface and can range in value from 0 (no reflection) to 1.0 (full reflection) (Burkhardt et al., 2009). In this study, a grass-covered ground surface would most likely have a larger adsorption capability due to its higher surface area than bare ground. To examine this concept, the model was also evaluated ignoring the ground

reflection of ammonia and PM (noted as *non-reflection*) using the A1 scenario **(SI Table 2-5)**. Results showed that *FAC2* values including the reflection scenario were significantly larger than *FAC2* values of the non-reflection scenario ($p < 0.001$). Full reflection and non-reflection are two extreme situations, but in reality, some degree of adsorption most likely occurred when the pollutant reached the ground. However, better model performance was obtained with full reflection than non-reflection, suggesting that the reflectivity was more likely to be closer to one. Although non-reflection was expected to be important, the large wind speed from the tunnel fans appears to mitigate adsorption by reducing retention time.

3.6 Assessment of overall model performance

The overall model performance was quantified using $\overline{d_s}$ and $\overline{|d_s|}$ as a function of L (**Figure 2-4b** and **Figure 2-4c**). For both ammonia and PM, $\overline{d_s}$ decreased quickly as L increased up to ~2 m and then increased gradually with L. The overall extent of overestimation changed with L with a minimum occurring at ~2 m for both ammonia and PM; the concentration of ammonia was overpredicted along all L values up to 35.4 m, while the concentration of PM was underpredicted from 0.6 m to 8 m (**SI Figure 2-9b**). For ammonia, $\overline{|d_s|}$ decreased sharply from 0 m to 0.6 m, gradually decreased until ~8 m, and then slowly increased with L (**SI Figure 2-9c**). $\overline{|d_s|}$ for PM had the similar trend, except for the range between 0.6 m and 2 m. These data indicate that model predictions were the most accurate (closest to the 1:1 ratio line) for values of L less than 8 m. In addition, smaller $\overline{|d_s|}$ values of PM also suggested better model performance for PM than ammonia. All in all, the accuracy and precision of the model were greatly improved when using the virtual point L_{opt} compared with the original model where $L = 0$ m.

The better performance of model to predict PM concentration versus ammonia concentration is most likely due to the different properties of these two pollutants. The ammonia plume consists of small molecules where diffusion would be expected to have a larger effect on dispersion which would contribute to an increase in randomness, and thereby decrease the ability of the model to predict ammonia concentration (Yao et al., 2018b).

3.7 Assessment of model performance by sampler

The distance of a point from 1:1 ratio line on a logarithmic scale (d_s) was an indicator of model performance at the level of a single sampler. Box plot of d_s values of eight experiments of individual sampler is shown in **SI Figure 2-12**. Since T1-1 was the reference point for both ammonia and PM, the model-predicted concentration of T1-1 was always equal to the observed concentration ($C_{\mathrm{pred,T1-1}} = C_{\mathrm{obs,T1-1}}$), and thus, $d_{\mathrm{T1-1}}$ values were zero per **Eqn. 2-7**. Examining the ammonia samplers on tower 1 (T1), the mean values for d_s were close to zero indicating that the model predictions and observations were very close to each other. The model generally overpredicted the ammonia concentration of the T2 and T3 samplers as the mean values of d_s were all greater than zero. Moreover, the means of d_s at T2 and T3 increased with height, suggesting that concentration of higher samplers have a larger likelihood to be over-predicted. The mean values of d_s of the side samplers to the west of the tower array (S1 and S3) were larger than those to the east of the towers array (S2 and S4), i.e., $\bar{d}_{\mathrm{S1,NH_3}} > \bar{d}_{\mathrm{S2,NH_3}}$, $\bar{d}_{\mathrm{S3,NH_3}} > \bar{d}_{\mathrm{S4,NH_3}}$. This similar pattern of the side samplers could be due to eastly-orientated drift of the plume caused by ambient wind (Yao et al., 2018b).

The pattern of d_s values for PM concentration predictions of the T1, T2, and T3 samplers was similar to ammonia. However, the absolute mean values of d_s of PM for each sampler were

smaller than the absolute mean values of d_s of ammonia which again indicates that the model predictions for PM were more accurate than for ammonia. In addition, at T2, concentrations of 2-m-high and 4.5-m-high samplers were slightly under-predicted while concentrations of 7.25-m-high and 10-m-high samplers were slightly over-predicted. For S1, S2, S3 and S4 samplers, similarly, mean values of d_s of S1 and S3 were larger than mean values of d_s of S2 and S4, respectively ($\bar{d}_{\mathrm{S1,PM}} > \bar{d}_{\mathrm{S2,PM}}$, $\bar{d}_{\mathrm{S3,PM}} > \bar{d}_{\mathrm{S4,PM}}$).The average d_s values for all ammonia and PM samplers were $\bar{d}_{\mathrm{NH_3}}$ = 0.10 and $\bar{d}_{\mathrm{PM}}$ = -0.01, which gave to $\bar{F}_{\mathrm{NH_3}}$ = 1.38 and $\bar{F}_{\mathrm{PM}}$ = 0.98. Again, the model provided more accurate predictions for PM than ammonia.

3.8 Model sensitivity

Applying this model to other systems requires knowledge of the model sensitivity to different sampling regimes and changes in wind speed. Therefore, the model was used to predict the concentrations using different wind speed scenarios (A1 – D2) and *L* values (ammonia: *L* = 3.6 m to 6.6 m, PM: *L* = 5.4 m to 8.4 m), and the *FAC2* were then calculated. Results are shown in **SI Figure 2-13**. The *FAC2* values ranged from 0.58 to 0.63 for ammonia and from 0.60 to 0.63 for PM indicating that the model performance was always acceptable. The results indicated that the model was robust to the changes within the wind speed scenarios or *L* values.

The ratio of difference (R_s) was used to measure the sensitivity of the model functionality at each sampling point to changes in wind speed and to changes in *L* values. A series of R_s box plots for the eight ammonia and PM experiments is shown in **SI Figure 2-14** (note the different scales in the y-axis for each plot). In all the plots, $R_{\mathrm{T1-1}}$ = 0 because T1-1 is the reference point, and the model-predicted concentration of T1-1 is equal to the observed concentration ($C_{\mathrm{pred,T1-1}} = C_{\mathrm{obs,T1-1}}$). Examining the sensitivity of the model to wind speed changes **(SI**

Figure 2-14a and 2-14b) showed that the mean R_s values of the T1-2 sampler ($\bar{R}_{\mathrm{T1-2}}$) were significantly larger ($p < 0.001$) than the mean R_s values for other samplers for both ammonia and PM. For the samplers at T2, T3, S1, S2, S3, and S4, the mean R_s values were very small indicating that the model functionality was not very sensitive to wind speed at these sampling points.

For the limited changes in L values (ammonia: L = 3.6 m to 6.6 m, PM: L = 5.4 m to 8.4 m), R_s values (**SI Figure 2-14c and 2-14d**) were generally less than the R_s values for wind speed (**SI Figure 2-14a and 2-14b**). However, as with the wind speed changes, the mean R_s values of the T1-2 sampler ($\bar{R}_{\mathrm{T1-2}}$) were significantly larger ($p < 0.001$) than the mean R_s values for other samplers for both ammonia and PM and for the samplers at T2, T3, S1, S2, S3, and S4.

The large sensitivity for the T1-2 sampler is most likely due to its very close location to the fan (and the source), where a small change in the position (caused by L) or plume shape (caused by input wind speed) would lead to a large response in the $M_{\mathrm{T1-2}}$ value in Eq. (3) (**Figure 2-4a and 2-4c**). Although T1-2 samplers are the most sensitive, if L_{opt} is determined correctly, the model does provide accurate concentration predictions for this sampling point (**SI Figure 2-12**).

The performance and sensitivity of the model under an additional 47 scenarios were also evaluated for all ten experiments, and the results are provided in the **Supporting Information**. As shown above, the model did not perform well for the day 2 and day 3 experiments due to large ambient wind speeds. Model runs were also conducted using different background measurements which showed minimal effects on the model performance (see **Supplementary Information**).

4. Conclusion

The Gaussian plume model was originally designed for vertical stack plumes. Here, the GPM was adapted to consider the movement of ammonia and PM horizontally released (expelled by large fans) in close proximity to the ground-level. The point source was changed from the fan to a virtual point behind the fan (the addition of L_{opt}) which greatly improved the model performance especially for predicting concentrations of the samplers that were closer to the source. Model validation initially required a number of measurements of the pollutant concentration, but once the L_{opt} was determined and model was validated, only one measurement (i.e., the reference point) was needed to predict the concentrations at further distances and additional heights. In addition, the modified GPM did not perform well for the conditions with large ambient wind speeds (greater than 4 m/s). These strong ambient winds and increased turbulence affected the plume shape and violated the assumption that the wind speed of the fan overwhelmed the ambient wind. Thus, this model is best used to predict the emissions from similar animal houses and fans and during relatively low turbulence. It should also be useful in evaluating the effectiveness of mitigation strategies for air pollutant emissions from animal houses where creating control experiments is difficult. Future studies include quantifying the influence of fan characteristics on L_{opt}. Temperature could also be an accurate indicator to show how model works (Grimmond et al., 2010), thus, mass balance and energy balance could be combined to improve the predictions further. These future endeavors combined with this study will allow the global agricultural community to address the challenges of mitigating the atmospheric emissions from animal production.

Chapter 3 Assessment of Particulate Matter Concentration from Low-altitude Emission Source and Improved AERMOD Prediction of Particulate Matter Dispersion

(This chapter is submitted to *Environmental Pollution*)

Zijiang Yang [a], Derek P. Whitelock [b], Michael D. Buser [c], Michael N. Evans [d,e], Cathleen J. Hapeman [f], Alba Torrents [a]

[a] *Department of Civil and Environmental Engineering, University of Maryland College Park, 1173 Glenn L. Martin Hall, College Park, Maryland 20742, USA*

[b] *United States Department of Agriculture, Agricultural Research Service, Southwestern Cotton Ginning Research Laboratory, PO Box 578, Mesilla Park, New Mexico 88047, USA*

[c] *United States Department of Agriculture, Agricultural Research Service, Office of National Programs, 5601 Sunnyside Ave (GWCC 4–2282), Beltsville, Maryland 20705, USA.*

[d] *Department of Geology, University of Maryland College Park, 1212B Chemistry Building, College Park, Maryland 20742, USA*

[e] *Earth System Science Interdisciplinary Center, 1120 Geology Building, University of Maryland, College Park, Maryland 20742, USA*

[f] *United States Department of Agriculture, Agricultural Research Service, Henry A. Wallace Beltsville Agricultural Research Center, 10300 Baltimore Avenue, Beltsville, Maryland 20705, USA*

Abstract

Due to lack of scientifically sound information about PM emissions and dispersion from low-altitude emission sources, and the tendency toward overestimation by regulatory recommended models, field samples of $PM_{2.5}$, PM_{10}, and TSP were collected during 11 sets of experiments at a typical cotton gin. The concentration and dispersion of the air pollutants were assessed, and the regulatory recommended model (AERMOD) was modified and validated. Pollutant concentrations were negatively correlated with height ($p < 0.05$), distance from source ($p < 0.05$) and standard deviation of wind direction ($p < 0.001$), and positively correlated with average wind speed ($p < 0.001$). In addition, pollutant concentrations were overestimated by AERMOD by factors of 64.7, 6.97 and 7.44 on average for $PM_{2.5}$, PM_{10}, and TSP, and thus dispersion correction factors were developed. Cross-validation results showed that predictive accuracy was greatly improved by applying AERMOD coupled with dispersion correction factors, and the average overprediction factors decreased to 3.75, 1.52 and 1.44 for $PM_{2.5}$, PM_{10} and TSP, respectively. These data and observations will be useful in developing and evaluating dispersion models for low-altitude emission sources. Dispersion correction factors are recommended for regulatory and practical use, and similar approaches can be extended in other pollution detection, remediation, exposure and risk assessment studies.

1. Introduction

The United States plays an important role in the global cotton market, where more than 20 million bales of cotton were produced in 2017, representing over 7 billion dollars in total value (USDA ERS, 2019). Most cotton in the United States is grown within 17 states in the southern U.S. from Virginia to California. After harvest, the cotton fiber must be separated from the seed

(ginned) at a cotton gin to produce a saleable product. Material is conveyed between the cotton gin processes predominantly using pneumatic conveying systems. Each of these systems exhausts air to the environment through air pollution abatement devices which reduce the amount of particulate matter (PM) that a cotton gin emits to the atmosphere (Whitelock et al., 2019).

Ambient PM can also come from a variety of other sources, such as roads (Brugge et al., 2007), industrial activities (Rodrıguez et al., 2004), construction sites (Zhan et al., 2015), mining operations (Gautam et al., 2016), and animal feeding operations (Yao et al., 2018b). Depending on its size and source, PM can lead to a variety of adverse effects to human beings, such as asthma attacks, chronic bronchitis, cancer, cardiovascular disease, diabetes, etc. (Löndahl et al., 2007; World Health Organization, 2018), and can pose more danger to human health than other common ground-level air pollutants, such as ozone and carbon monoxide (Kim et al., 2015). For these reasons PM with an aerodynamic diameter less than or equal to 10 μm (PM_{10}) and PM with an aerodynamic diameter less than or equal to 2.5 μm ($PM_{2.5}$) are regulated as ambient air pollutants (US EPA, 2018). In 2006 and 2012, the United States Environmental Protection Agency (US EPA) twice revised the National Ambient Air Quality Standards (NAAQS) for PM (Federal Register, 2006; Federal Register, 2013). Most notably, the maximum allowable 24-hour average $PM_{2.5}$ concentration was decreased from 65 $\mu g/m^3$ to 35 $\mu g/m^3$. As a result, all cotton gins in the United States were affected.

The primary issue for the US cotton ginning industry is a lack of scientifically-sound information about heterogeneous PM emissions from low-altitude sources (Buser et al., 2009). In addition, regulation-recommended air dispersion models have a potential to overestimate the concentration for low-altitude emission sources by as much as a factor of 10 (Fritz, 2003; Zwicke,

1998), making it difficult for cotton gins to meet the new standards where modeling is used to determine property-line concentrations. In addition to cotton gins, other low-altitude emission sources may also face the same issue, such as animal operations (Dai et al., 2020), food and agricultural product processing facilities (Venkataraman et al., 2018), and domestic combustion (Piwowar and Maciej, 2019).

Therefore, a sampling campaign was conducted to collect PM emissions and associated meteorological data to provide a robust data set for assessment and modelling of PM concentrations and dispersion. This study includes the following: (1) assessment of PM concentrations and dispersion (2) evaluation of the performance of EPA-recommended models for predicting PM concentrations; and (3) development of dispersion modeling correction factors for low-altitude emission sources.

2. Material and Methods

2.1 Sampling Campaign

A sampling campaign was conducted in the Mid-South of the U.S. from September 20 to 29, 2010 at a typical cotton gin with stack heights that ranged from about 9 to 12 m. Ten sampling periods (experiments) of ca. 10 hrs were conducted each day while the gin was operating from 07:00 to 17:00 and are noted as EXP01 – EXP10. A test run was also carried out on September 13 from 11:00 to 24:00 (EXP00). The summary of the experiment time periods is shown in **SI Table 3-1**. Preliminary calculations did not show significant differences between the test run and the other experiments, so EXP00 was included in the analysis.

The cotton gin was surrounded by a sampling array consisting of samplers located on three concentric circles 60, 120, and 180 m from the main cyclone bank at 30° intervals shown in

Figure 3-1. Some samplers were moved or not installed due to site restriction (e.g., buildings and roads). The middle ring samplers were installed on towers at heights of 1, 2, 3, 4.5, 7.25, and 10 m, while only 2-m samplers were deployed on the inner and outer rings. Samplers were designated with a letter for the ring ("I" for inner, "O" for outer, and "T" for middle towers) and a number for the bearing from North (1 for 0° or North, 2 for 30°, and so forth). An additional indicator for sampler height on the tower was also added (e.g., T01-1 for tower 01 at 0° and sampler at the first level or 1-m height and T07-5 for tower 07 at 180° and sampler at the fifth level or 7.25-m high, etc.).

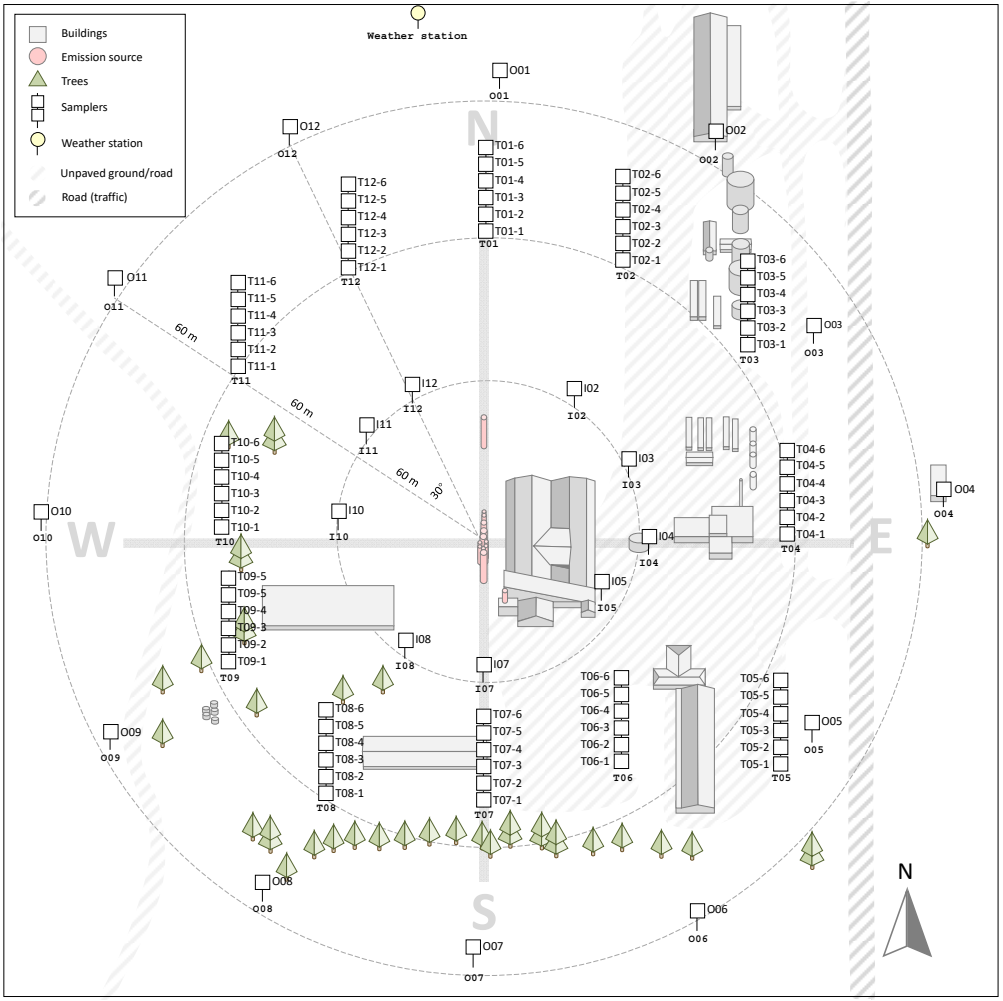

Figure 3-1 Layout of ambient sampler sites. O refers to outer samplers; T to middle sampling towers; and I to inner samplers. Inner samplers, middle towers, and outer samplers were about 60 m, 120 m, and 180 m from the source, respectively. Middle towers were equipped with 6 samplers at 1, 2, 3, 4.5, 7.25 and 10-m heights. Outer and inner samplers were deployed at 2 m.

2.2 Meteorological data

An onsite weather station was located approximately 200 m North of the cotton gin. Onsite meteorological data were collected using a Hobo H21-001 weather station datalogger with compatible sensors (Onset Computer Corporation, Bourne, MA): 1) S-THA temperature and relative humidity sensor at 2-m height; 2) S-TMB-M002 temperature sensors at 1, 3, 4.5, 7.25 and 10-m height; 3) S-BPA-CM10 barometric pressure sensor; 4) S-WCA-M003 wind speed and direction smart sensor; 5) S-LIB-M003 silicon pyranometer solar radiation sensors, one facing upward and one facing downward, for net radiation. Data were collected every 5 min. Surface hourly meteorological data was from a station at Blytheville, AR (Station ID 53869) and upper air meteorological data was from the North Little Rock station (Station ID 3952).

2.3 Particulate matter measurements and analysis

Particulate matter concentration and particle size distribution were determined based on previous work (Buser et al., 2007a, b, c; Buser et al., 2009). Briefly, total suspended particle (TSP) samples were collected on Teflon filters using low-volume (16.7 Lpm) TSP sampler inlets. After collection, filters were preserved and delivered for analysis. The mass percent of $PM_{2.5}$ and PM_{10} of each TSP sample was determined by particle size distribution (PSD) analysis (Beckman Coulter L230 laser diffraction system with software version 3.29, Beckman Coulter Inc., Miami, FL). $PM_{2.5}$ and PM_{10} concentrations were calculated by multiplying the determined percentage by the corresponding TSP concentration.

In cases where the PM concentrations were very low, and insufficient PM was collected on the filter to derive a PSD, the corresponding $PM_{2.5}$ and PM_{10} concentrations could not be obtained. These data were noted as N/A, treated as non-detects, and removed from further analyses.

The concentration measurements were cumulative concentrations over the whole sampling period. To eliminate the influence of time, an hourly average concentration was calculated by:

$$C_o = \frac{\sum C_o}{\sum T} \cdot 60 \qquad \text{Eqn. } 3-1$$

where C_o refers to the hourly average observed concentration ($\mu g/m^3$); $\sum C_o$ is the cumulative particle concentration during the sampling period ($\mu g/m^3$); $\sum T$ is the total sampling period (min).

Outliers can bias the summary statistics and have a significant impact on the results, so to eliminate their effects, potential outliers were identified for potential removal from further analyses using the following procedure. The data were log-transformed since concentration data of air pollutants usually appear to be skewed and log-normally distributed (Ott, 1990). Rosner's statistical outlier test was applied to identify the statistical outliers at $\alpha = 0.05$ significance level (US EPA, 2000a). Finally, scientific judgement was applied to determine whether or not to remove a statistical outlier.

2.4 AERMOD and air dispersion modelling

American Meteorological Society/Environmental Protection Agency Regulatory Model (AERMOD) is a Gaussian plume model-based steady-state air dispersion model developed by the American Meteorological Society (AMS)/ EPA Regulatory Model Improvement Committee (US EPA, 2004). As a replacement of Industrial Source Complex 3 (ISC-3), AERMOD is recommended by US EPA as a regulatory model (US EPA, 2019). and it is widely used in many fields due to its performance, convenience, and availability (Hadlocon et al., 2015; Gibson et al., 2013; Chen et al., 2009).

Here AERMOD View modelling package (version 9.7.0, Lakes Environmental, Waterloo, Ontario) was used to run AERMOD. Onsite measured meteorological data were averaged hourly and pre-treated by AERMET View (Lake Environmental, Waterloo, Ontario). Emission rate (ER) and PSD were based on stack sampling of the thirteen point sources adopted from previous cotton gin emission study publications and using PSD methodology described above and summarized in **SI Table 3-2** (Boykin et al., 2013a, b; Buser et al., 2013a, b, c; Whitelock et al., 2013a, b, c). PSD was assumed to be log-normal to derive mass fractions, and density was set as 2.65 g/cm^3 (Buser et al., 2013b).

AERMOD View was used to predict the hourly-averaged pollutant concentration of each receptor (details of model configuration see **SI Table 3-3**). Then, weighted hourly average of the whole sampling period was calculated by:

$$C_{\mathrm{p}} = \frac{\sum_{i=1}^{n} f_{\mathrm{t}i} \cdot C_{\mathrm{p}i}}{\sum_{i=1}^{n} f_{\mathrm{t}i}} \qquad \mathrm{Eqn.}\ 3-2$$

where C_{p} refers to the hourly-average predicted concentration (μg/m^3); n refers to the total hours of the sampling period; $C_{\mathrm{p}i}$ refers to the predicted concentration of the i-th hour; and f_{ti} is the *fraction of effective time* of the i-th hour. The values of f_{ti} for each run are summarized in **SI Table 3-4**.

2.5 Dispersion correction factor modelling and validation

A dispersion correction factor is modeled as a multiplier to correct the original AERMOD predicted concentrations:

$$C_{\mathrm{cp}} = f_{\mathrm{c}} \cdot C_{\mathrm{p}} \qquad \mathrm{Eqn.}\ 3-3$$

where C_{cp} is the corrected model-predicted concentration of the air pollutant (μg/m^3), and C_{p} is the original model-predicted concentration (μg/m^3). f_{c} is the *dispersion correction factor*. The

value of f_c can be calculated by the *ratio of prediction to observation* (noted as R_p), which is defined as the ratio of model-predicted concentration over observed concentration:

$$R_p = \frac{C_p}{C_o} \qquad \text{Eqn. } 3-4$$

where R_p is a measure of the extent of over/under prediction. $R_p > 1$ indicates overestimation and $R_p < 1$ indicates underestimation. Based on **Eqn. 3-4**, if R_p can be estimated, i.e., the extent of over/under prediction can be estimated, then the estimated R_p can be used to calculate f_c:

$$f_c = \frac{1}{\hat{R}_p} \qquad \text{Eqn. } 3-5$$

where $\hat{R}_p$ is the estimate of R_p.

Potential predictors of R_p were investigated, and a model was built to estimate R_p. Based on correlation analyses, potential variables that may be used for R_p estimation were used as predictors, and stepwise ordinary least square regression was applied to determine the variables. A model was constructed using log-transformed R_p, and results were back transformed into the linear scale to calculate R_p. The generalized statistical model for R_p is as follows:

$$R_p = \exp(b_0 + b_1 h + b_2 d + b_3 u + b_4 \sigma + b_5 \theta) \qquad \text{Eqn. } 3-6$$

where b_i (i = 0,1,2,3,4,5) refer to the regression coefficients. If b_i was not significantly different from zero (α = 0.05), then the corresponding variable was not included in the model. Variable h is height of receptor (m); d is the distance of receptor from emission source (m); u is the ambient wind speed (m/s); σ is the standard deviation of wind direction (deg); and θ is the *deviation from wind direction* (deg) (Venkatram et al., 2004), defined as the absolute difference between the direction of the wind velocity and the direction from the source to the receptor, $0 \leqslant \theta \leqslant 180$ (deg).

The developed dispersion correction factors were coupled with AERMOD to create a new model, and then validated by *k*-fold cross-validation to evaluate out-of-sample predictive accuracy, and compared with the original model (Gelman et al., 2014; Hooten and Hobbs, 2015). Since there were 11 independent observations, *k* was set to 11, i.e., each subset of data contains data from one experiment, and the set of 11 out-of-sample predictions of f_c may be evaluated for precision and accuracy, as described below.

2.6 Model performance evaluation

Model evaluation was based on the statistics proposed by previous air quality modelling literature (Hanna and Chang, 2012) below:

(1) Fractional bias (FB): $FB = \dfrac{\bar{C}_\mathrm{o} - \bar{C}_\mathrm{p}}{0.5 \cdot (\bar{C}_\mathrm{o} + \bar{C}_\mathrm{p})}$ Eqn. 3 − 7

(2) Geometric mean (MG): $MG = \exp\left(\overline{\ln C_\mathrm{o}} - \overline{\ln C_\mathrm{p}}\right)$ Eqn. 3 − 8

(3) Normalized mean square error ($NMSE$): $NMSE = \dfrac{\overline{(C_\mathrm{o} - C_\mathrm{p})^2}}{\bar{C}_\mathrm{o} \cdot \bar{C}_\mathrm{p}}$ Eqn. 3 − 9

(4) Geometric variance (VG): $VG = \exp\left[\overline{(\ln C_\mathrm{o} - \ln C_\mathrm{p})^2}\right]$ Eqn. 3 − 10

(5) Normalized absolute difference (NAD): $NAD = \dfrac{\overline{|C_\mathrm{o} - C_\mathrm{p}|}}{\bar{C}_\mathrm{o} + \bar{C}_\mathrm{p}}$ Eqn. 3 − 11

(6) Fraction of predictions within a factor of two of observations ($FAC2$):

$$FAC2 = \text{fraction of data that satisfy: } 0.5 \leq \frac{C_\mathrm{p}}{C_\mathrm{o}} \leq 2.0 \qquad \text{Eqn. } 3 - 12$$

where the "overbar" refers to the average over the data set. *Fractional bias* (*FB*) and *geometric mean* (*MG*) are measures of systematic bias, and the difference is that *FB* is based on the linear scale while *MB* is on the log-scale. A perfect model would have *FB* = 1 and *MB* = 1. *Normalized*

mean square error (*NMSE*) and *geometric variance* (*VG*) are measures of scatter and can reflect systematic and random errors. Again, the difference is that *NMSE* is based on the linear scale while *VG* is on the log-scale. A perfect model would have *NMSE* = 0 and *VG* = 0. *Normalized absolute difference* (*NAD*) is a measure of normalized difference between prediction and observation. *NAD* is between 0 and 1, and a perfect model would have *NAD* = 0. *Fraction of predictions within a factor of two of observations* (*FAC2*) is a measure of the total effect of systematic and random error, and it is the most robust measure because it is not influenced by extreme values. A perfect model would have *FAC2* = 1.

In terms of acceptance criteria for an aerosol dispersion model, previous literature suggested that $|FB| \lesssim 0.30$, $NMSE \lesssim 3$, $FAC2 \gtrsim 0.5$, $NAD \lesssim 0.30$ (Hanna and Chang, 2012). These criteria were used in the current study to evaluate the performance of the model. However, it should be noted that these proposed acceptance criteria are somewhat arbitrary (Hanna and Chang, 2012). Thus, these criteria were used as a standard for discussion, not as an absolute test for accepting or rejecting the model.

2.7 Model sensitivity evaluation

Prior to estimation and cross-validation of f_c and estimation of evaluation statistics, outliers were identified and removed from the data set to meet statistical assumptions (US EPA, 2000a; Ott, 1990). However, for future applications it may not be possible to identify outliers due to smaller sample sizes or a different sampler layout. Therefore, an evaluation of model sensitivity to outliers was conducted. The sensitivity analysis included two parts. First, the effect of outliers on variable selection and estimation of parameters for the empirical equation of R_p (**Eqn. 3-5**) was evaluated by comparing selected variables and regression coefficients with and without the

outliers. Second, the sensitivity of the combined model, i.e., AERMOD coupled with the dispersion correction factor model was evaluated by comparing model performance by cross-validation with and without the outliers.

3. Results and Discussion

3.1 Meteorological conditions

A summary of the meteorological conditions of the 11 sampling experiments are shown in **SI Table 3-5**; pressure, relative humidity, and temperature were similar among each experiment. Wind roses for each experiment are shown in **SI Figure 3-1.** Average wind speed was different among experiments and ranged from 1.00 m/s for EXP00 up to 4.67 m/s for EXP04. The mean and standard deviation of wind direction were calculated by Yamartino method (Yamartino, 1984; US EPA, 2000b). Average wind direction showed a large difference among experiments, indicating that wind could come from any direction on the site and that any direction could be the downwind direction.

3.2 PM Concentration Measurements

The observed PM concentrations from each experiment are shown in **SI Fig 3-2**, and summary statistics are presented in **SI Table 3-6**. The results show that the average observed concentration varied among experiments, which was the result of different meteorological conditions and PM emissions variability (Whitelock et al., 2013c). Samplers that had statistical outliers detected are summarized in **SI Table 3-7**, and the outliers were classified into low-outliers and high-outliers (Cousineau and Chartier, 2010). The table shows that outliers were much more likely to appear on the lower samplers (1-m and 2-m heights) suggesting influence of ground activities. The possible sources that may contribute to high-outliers include movement of

cotton modules (**SI Figure 3-3a**); pneumatic cottonseed loading (**SI Figure 3-3b**); and PM resuspension from road and unpaved ground by traffic and wind (**SI Figure 3-3c, d, e**). In addition, rice straw burning in distant fields (**SI Figure 3-3f**) may also have led to large concentrations at outer samplers (i.e., O09 and O10). On the other hand, the possible sinks that can lower PM concentrations include vegetation (**SI Figure 3-3g**) and water spraying in the industrial area (**SI Figure 3-3h**) (Adrizal et al., 2008; Azarov et al., 2017). All these activities are not part of atmospheric dispersion, and thus all the statistical outliers were removed from further analysis.

Typical spatial distribution of observed concentrations for $PM_{2.5}$, PM_{10}, and TSP are shown in **Figure 3-2**, where the greatest observed concentrations occurred in the downwind direction from the source. Initial analysis revealed that the spread of the spatial distribution appeared to be positively correlated to the spread of wind direction (**SI Figure 3-2**), i.e., particles were more concentrated in one direction if the wind direction was relatively constant.

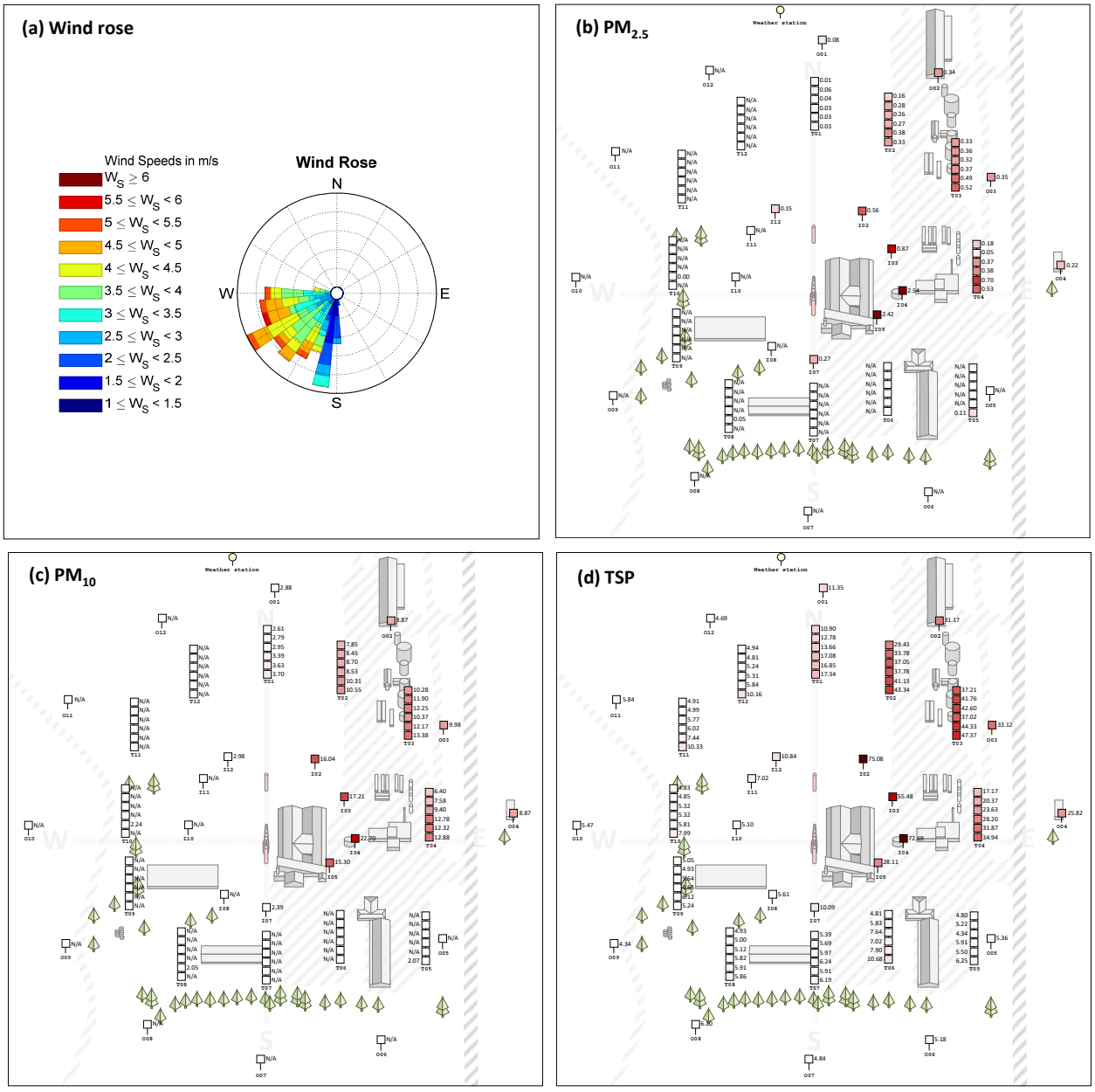

Figure 3-2 Hourly average concentration distribution (μg/m^3) of (b) $PM_{2.5}$, (c) PM_{10} and (d) TSP for EXP03. N/A means that insufficient particles were on the filter to derive a particle size distribution. For **Figure 3-2b – 2d**, the darker the shade, the higher the concentration.

3.3 PM concentration as a function of height, distance and wind

PM concentration changes as a function of height, distance, wind speed, deviation from wind direction, and standard deviation of wind direction were investigated. Pearson correlation coefficients were calculated and are presented in **SI Table 3-8** and in corresponding scatter plots

SI Figure 3-4. A negative correlation for $PM_{2.5}$, PM_{10}, and TSP concentration with height ($p < 0.001$ for $PM_{2.5}$, $p < 0.05$ for PM_{10} and TSP) was observed, i.e., lower concentrations were more likely to occur in the higher samplers. In addition, the concentration of $PM_{2.5}$, PM_{10}, and TSP showed a significant negative correlation with distance from source ($p < 0.05$ for $PM_{2.5}$ and PM_{10}, $p < 0.001$ for TSP). This was most likely due to dispersion and deposition of the particles as the particles moved from the source.

A significant positive correlation was found between $PM_{2.5}$, PM_{10}, and TSP concentrations and average ambient wind speed ($p < 0.001$). However, such positive correlation does not meet with theoretical expectation where lower wind speeds generally correspond to lower dispersion and more deposition and lead to a higher concentration of pollutants near the source (Lu and Fang, 2002). Thus, the observed positive correlation is probably due to particles from the surroundings, especially the bare ground and road being entrained or resuspended by the increasing wind speed and contributing particles to the total PM concentrations (Elminir, 2005; Pérez et al., 2010; Nowak et al., 2013; Gehrig and Buchmann, 2003).

A negative correlation was found between PM_{10} and TSP concentrations and the deviation from wind direction ($p < 0.001$); this pattern is consistent with the spatial distribution of the concentrations (**SI Figure 3-2**). A lack of correlation of deviation from wind direction with $PM_{2.5}$ was probably caused by the larger dispersion coefficient due to its smaller size (Ounis and Ahmadi, 1990), making such a pattern insignificant. Finally, a significant negative correlation was found between the standard deviation of wind direction and particle concentrations for all sizes of pollutants ($p < 0.001$), indicating that concentration of the pollutants was more likely to decrease as wind direction become more variable during the sampling period. This is consistent

in that a multidirectional wind causes greater mixing and stronger dilution which contributes to lower concentrations (Flagan and Seinfeld, 2012).

3.4 PM size distribution as a function of height and distance

Particulate size distribution changes as function of height and distance were investigated because the effects on human health vary with PM size (**SI Table 3-8**, **SI Figure 3-5**) (Brown et al., 2013). Both the percent of $PM_{2.5}$ and the percent of PM_{10} showed a significant decrease with height ($p < 0.05$), i.e., lower heights had more mass percent of $PM_{2.5}$ and PM_{10}. But this is contradictory to prior observations and theory where heavier particles deposit faster than small particles leading to differential deposition of the particles and a decreased percentage of smaller particles at lower heights (Yao et al., 2018b; Flagan and Seifeld, 2012). Our observations here may be due to the effects of the downdraft on the low-altitude sources where smaller particles are more easily pulled by the downward wind flow and/or the contribution of entrained or resuspended particles from the ground as discussed above.

The percent of PM_{10} were positively correlated with distance from the emission source ($p < 0.001$). This expected positive correlation is easily explained in that heavier particles settle quickly during dry deposition resulting in an increase in the mass percentage of smaller particles especially for a longer distance from the source (~180 m). The percent of $PM_{2.5}$ was also expected to have a positive correlation, however a lack of correlation of the percent of $PM_{2.5}$ and distance from the emission source could be due to interference from other sources or resuspension from the surroundings (Elminir, 2005; Pérez et al., 2010; Nowak et al., 2013; Gehrig and Buchmann, 2003).

3.5 Performance of AERMOD

AERMOD was used to predict the concentration of $PM_{2.5}$, PM_{10}, and TSP at all the sampling sites for each experiment. Spatial distributions of the model-predicted concentrations were consistent with observed concentrations (**SI Figure 3-2**). However, scatter plots of the observed concentrations (C_o) versus model-predicted concentrations (C_p) show that the model consistently over predicted the concentrations (**Figure 3-3a, c, e**; **SI Figure 3-6**, **SI Table 3-9**). *FAC2* values of the overall performance were only 0.14, 0.26, and 0.24 for $PM_{2.5}$, PM_{10}, and TSP, respectively, which are substantially smaller than the acceptable value of 0.50 (Hanna and Chang, 2012). |*FB*|, *NMSE*, and *NAD* values also deviated from acceptance criteria. In addition, the R_p values for each sampling site in each experiment and for the overall experiment were calculated **(SI Table 3-10)**. The results showed that concentrations were over-predicted by factors of 64.07, 6.97, and 7.44 on average for $PM_{2.5}$, PM_{10}, and TSP, respectively. Clearly, pollutant concentrations were over-predicted by AERMOD for such low-altitude emission sources, and a dispersion correction factor is needed.

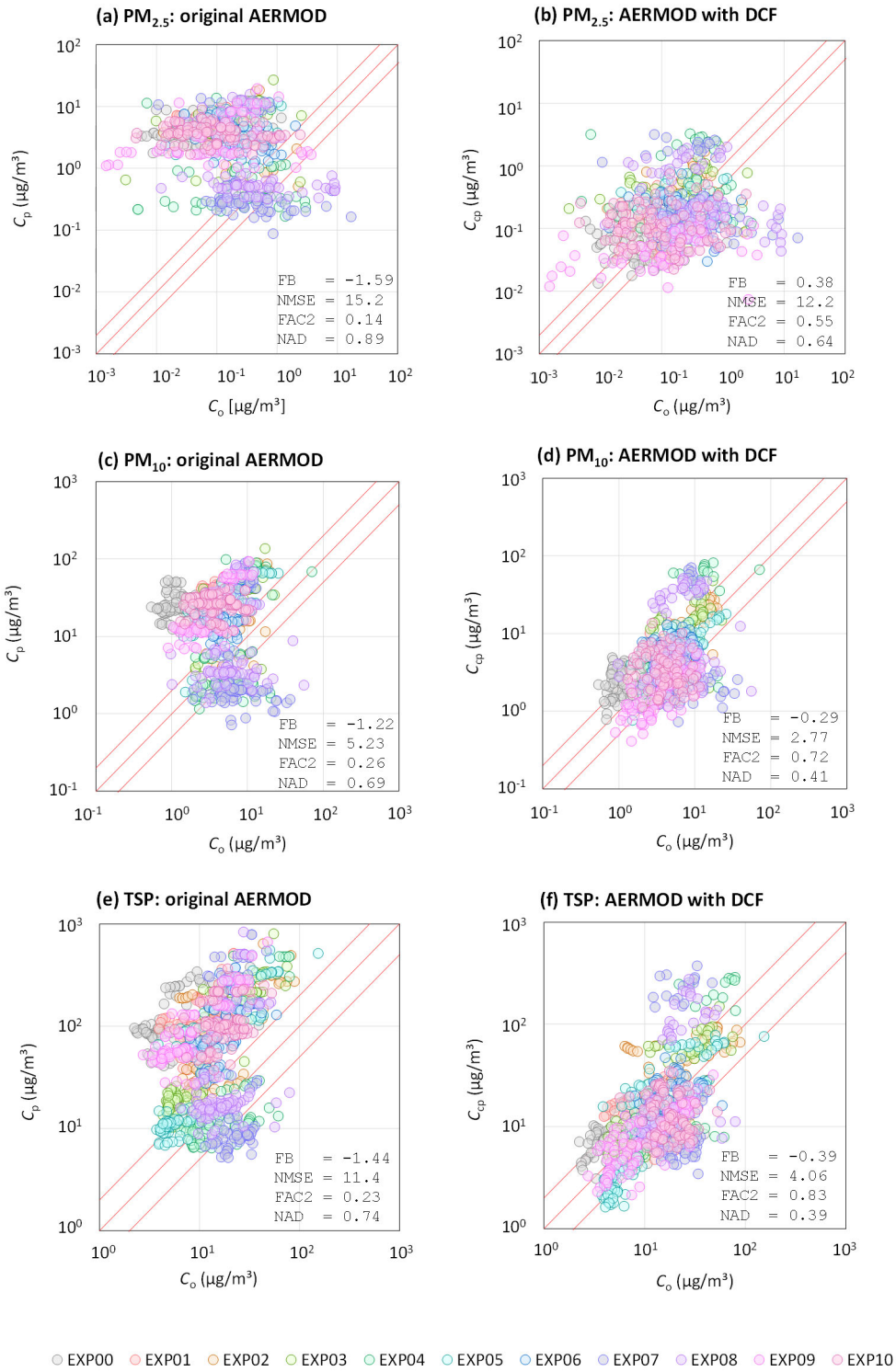

Figure 3-3 Scatter plot of observed concentration (C_o) versus original AERMOD model-predicted concentration (C_p) and observed concentration versus out-of-sample corrected model-predicted concentration (C_{cp}). Solid lines refer to 1:1 ratio and dotted lines refer to 1:2 and 1:0.5 ratios. *DCF* refers to dispersion correction factor; *FB* = fraction bias; *NMSE* = normalized mean square error; *FAC2* = fraction of predictions within a factor of two of observations; *NAD* = normalized absolute difference.

The unsatisfactory performance of the model in consistent with previous findings (Fritz, 2003; Zwicke, 1998). AERMOD was designed for industrial situations with tall stacks and long distances of up to 3000 m from emission source to sampling locations (Perry et al., 2005). In addition, gaseous pollutant datasets were used in the first model validations (Cimorelli et al., 2005; Perry et al., 2005). Although AERMOD has options for dry (particle) deposition within its simulation process, cotton gin emissions contain particles from sticks, leaves, hulls, and leaf materials which are not uncommon but are different from idealized silica particles in terms of shape and density (Buser et al., 2013d). These differences can lead to different aerodynamic behaviors in the atmosphere. The stacks of cotton gins are much shorter than typical industrial stacks, where the wind and dispersion are less apt to be influenced by interactions with the ground surface. AERMOD does not fully consider the expected complicated interactions between the wind and the ground in predicting the emission fate of the short, cotton gin stacks.

Since wind is an important factor to the transport of particles from the source, the correlation between model performance measures (*FB*, *MG*, *NMSE*, *VG*, *NAD*, and *FAC2*) and wind characteristics, namely average wind speed and the standard deviation of wind direction, were investigated further (**SI Table 3-11**). Wind speed was positively correlated significantly with *FB*, *MG*, and *FAC2* for PM_{10} and TSP and with *MG* and *FAC2* for $PM_{2.5}$. Such correlations suggest that systematic error decreased with increasing wind speed, i.e., the model performed better at greater wind speeds. AERMOD is a Gaussian plume-based model and assumes that if wind speed is sufficiently large then diffusive transport can be neglected in the wind direction (Stockie, 2011). However, if wind speed is small, this assumption does not hold introducing systematic errors. Another AERMOD assumption is that wind direction is constant, i.e., model performance

improves if wind direction is relatively constant (Stockie, 2011). Thus, systematic errors will also increase as the standard deviation of wind direction becomes larger.

3.6 Ratio of prediction to observation (R_p) as a function of height, distance and wind

Several strategies, log transformation of data and use of correction factors, were considered to improve the predictive capability of AERMOD for cotton gin emissions. This was carried out by using R_p to examine the possible factors that may lead to over-prediction or under-prediction. Since the probability distribution of R_p was positively skewed (**SI Figure 3-7**), log-transformation was applied to standardize the skewed data to approach a normal distribution. Pearson correlation calculations were performed between the possible factors and the log-transformed R_p (**SI Table 3-12** and **SI Figure 3-8**). Log-transformed R_p was positively correlated with height for $PM_{2.5}$ and PM_{10} ($p < 0.05$), but not for TSP. On the other hand, the extent of over-prediction decreased for TSP with increasing distance from the source as a negative correlation was observed between log-transformed R_p and distance from the source, but was significant only for TSP ($p < 0.001$).

Linear correlations were found between log-transformed R_p and wind speed, deviation from wind direction, and standard deviation of wind direction ($p < 0.001$). The result showed that as wind speed increased, the extent of over-prediction decreased, meaning that over-prediction was more severe for low wind conditions. Again, low wind speeds violate one of the Gaussian model assumptions which can result in unacceptable simulations. The negative correlation between log-transformed R_p and deviation from wind direction suggests that concentrations for samplers in the downwind direction from the source were more severely overestimated than other samplers, and as the angle difference increases, the extent of overestimation decreased. Such a phenomenon was also observed by previous air dispersion studies (Venkatram et al., 2004; Isakov

et al., 2004), and it was probably related to errors introduced by the Plume Rise Model Enhancement (PRIME) building downwash algorithm in AERMOD (Petersen et al., 2017). Furthermore, a significant correlation was found between log-transformed R_p and standard deviation of wind direction, i.e., overestimation is more severe when multidirectional wind occurs during a sampling period. This is again likely due to the assumption of the Gaussian plume model that wind direction is constant in the modelling domain.

3.7 Dispersion correction factor and model validation

Stepwise ordinary least square regression showed that log-transformed R_p of $PM_{2.5}$, PM_{10} and TSP could be estimated by the following equations:

$$PM_{2.5}: R_p = \exp(b_0 + b_1 h + b_4 \sigma + b_5 \theta) \qquad \text{Eqn. } 3-13$$

$$PM_{10}: R_p = \exp(b_0 + b_1 h + b_4 \sigma + b_5 \theta) \qquad \text{Eqn. } 3-14$$

$$TSP: R_p = \exp(b_0 + b_1 h + b_2 d + b_4 \sigma + b_5 \theta) \qquad \text{Eqn. } 3-15$$

where the b_i are estimated separately for each pollutant. The dispersion correction factor, f_c, was then used with the original AERMOD prediction, C_p, to calculate a corrected prediction, C_{cp}, by **Eqn. 3-3** and **Eqn. 3-5**. The dispersion correction factor together with AERMOD was considered as a new model, and this new model was validated by 11-fold cross-validation as described in **Section 2.5**. (**Figure 3-3b, d, f;** for results from an individual experiment, see **SI Figure 3-9**).

Scatter plots of the out-of-sample corrected predicted concentration, C_{cp}, versus the observed concentrations (**Figure 3-3b, d, f**) showed that the data points were more grouped and closer to a 1:1 ratio line than the original AERMOD prediction (**Figure 3-3a, c, e**), indicating that the correction factor improved model performance. Additionally, the average R_p decreased from 64.07 to 3.75, from 6.97 to 1.52, and from 7.44 to 1.44, for $PM_{2.5}$, PM_{10}, and TSP, respectively,

suggesting that on average the overprediction was mitigated significantly. The correction factor greatly improved the 90th percentile of the R_p values, decreasing from 159.4 to 7.30, from 15.40 to 3.39, and from 17.6 to 2.67, for $PM_{2.5}$, PM_{10}, and TSP, respectively.

The summary performance statistics of the corrected model (**SI Table 3-13**) were greatly improved over those of the original model (**SI Table 3-9**). The |*FB*| values decreased significantly for all pollutants, suggesting that model bias was greatly mitigated. Although only |*FB*| of PM_{10} was smaller than 0.30, the acceptance criterion, values of |*FB*| of $PM_{2.5}$ and TSP were closer to 0.30 (0.38 and 0.39 for $PM_{2.5}$ and TSP, respectively) than with the original model. *NMSE* was also reduced for all pollutants, indicating that prediction accuracy was improved. The *NMSE* of PM_{10} was smaller than 3.0, satisfying the acceptance criterion, and the *NMSE* of TSP was much closer to 3.0 than in the original AERMOD prediction (4.06 versus 11.4). However, for $PM_{2.5}$, the *NMSE* was still much greater than 3.0, but it reduced from an original 15.2 to 12.2. The *NAD* decreased for all pollutants; *NAD* values of PM_{10} and TSP were closer to the proposed acceptance criterion, 0.30 (0.41 for PM_{10} and 0.39 for TSP), while *NAD* of $PM_{2.5}$ reduced from 0.89 to 0.64. The overall *FAC2* values increased from 0.14 to 0.55 for $PM_{2.5}$, from 0.26 to 0.72 for PM_{10}, and from 0.24 to 0.83 for TSP, substantially above the acceptance critical value of 0.50 and close to the ideal of 1.0. Similar improvements occurred for most individual experiments (**SI Table 3-9** and **SI Table 3-13)**. Although performance of the new model did not completely satisfy the proposed acceptance criteria, prediction accuracy was greatly improved. In summary, cross-validation showed that the developed dispersion correction factor model coupled with AERMOD outperformed the original AERMOD. This suggests that the dispersion correction factors should be used with AERMOD for small scale and low-altitude situations.

The regression coefficients calculated for **Eqn. 3-13, Eqn. 3-14** and **Eqn. 3-15** based on all 11 experiments are listed in **SI Table 3-14**. These empirical equations can be used to estimate R_p and to calculate f_c. In addition, for situations without 5-min wind direction data, an alternative regression was conducted by excluding standard deviation of wind direction, and regression results are also listed in **SI Table 3-14**.

3.8 Sensitivity to the outliers

The dispersion correction factor model was evaluated with and without statistical outliers to evaluate the sensitivity to the log-normal assumption of observed concentration data. The selected predictors for estimating R_p were the same for $PM_{2.5}$, PM_{10}, and TSP, and the regression coefficients were indistinguishable within uncertainty **(SI Table 3-14)**. This result suggests that the dispersion correction factor models and the derived empirical equations were not sensitive to outliers. Then, dispersion correction factor models of $PM_{2.5}$, PM_{10}, and TSP were used to estimate out-of-sample R_p, calculate f_c and C_{cp} by 11-fold cross-validation. Results showed that there were negligible differences in the summary statistics between the corrected model with and without outliers (**SI Tables 3-13** and **SI Tables 3-15**). Therefore, we conclude that the results are robust with respect to outliers.

3.9 Application of dispersion correction factor

The developed dispersion correction factor was applied for prediction of $PM_{2.5}$, PM_{10}, and TSP concentration and risk assessment of the current cotton gin by using available onsite meteorological data measured during experiment from September 12-31, 2010. Model configuration and model inputs were the same as previously (**SI Table 3-2** and **SI Table 3-3**).

Maximum 24-hour average concentration was calculated by AERMOD based on 101× 101 × 5 m uniform Cartesian grids with 1.8 m height (i.e., 10201 receptors in total). Ginning facilities were assumed to run 24 hours a day to reflect the worst-case scenario. Then, dispersion correction factors were calculated based on **Table 3-1** and **Eqn. 3-5** for each of the pollutants and applied using **Eqn. 3-3** to the original AERMOD output to determine the corrected AERMOD prediction. The risk quotient (*RQ*), which is defined as the ratio of exposure to the regulatory standard, was calculated using 35 μg/m^3, 150 μg/m^3, and 260 μg/m^3 for the regulatory standards of $PM_{2.5}$, PM_{10}, and TSP, respectively (US EPA, 2018).

Original and corrected AERMOD predict concentrations of the pollutants are shown in **Figure 3-4**, histogram and descriptive statistical summary of pollutant concentrations of the 10201 receptors are shown in **SI Figure 3-10**, and the corresponding *RQ* are shown in **SI Figure 3-11**. $PM_{2.5}$ and PM_{10} concentrations in the simulation domain of both original AERMOD predictions and corrected predictions were smaller than regulatory permitted levels. The corrected pollutant concentrations around the ginning facilities were effectively lowered from the original AERMOD prediction, which was reflected by the smaller yellowish area on the map (**Figure 3-4a, b, c, d**). The average 24-hr average concentration of $PM_{2.5}$ in the simulation domain was 5.53 μg/m^3 for the original AERMOD prediction and 0.81 μg/m^3 for the corrected prediction. The average 24-hr average concentration of PM_{10} was 32.2 μg/m^3 for the original AERMOD prediction and 17.8 μg/m^3 for the corrected prediction.

TSP concentrations of some locations exceeded the regulatory standards, giving *RQ* a greater than 1 value (**SI Figure 3-11e, f**). However, the area of corrected model that exceeds regulatory standards was much smaller than the violation area of the original model (**SI Figure 3-4e, 4f**). The average original prediction in the domain was 313 μg/m^3 with 46% of the receptors

exceeding regulatory standards while the average corrected prediction was 140 μg/m^3 with 14% of the receptors exceeding regulatory standards. The maximum 24-hr average concentration was based on the assumption that cotton gins operate 24 hours a day, which resulted in overestimation for the real scenario. Thus, actual operation times are needed for more accurate estimation.

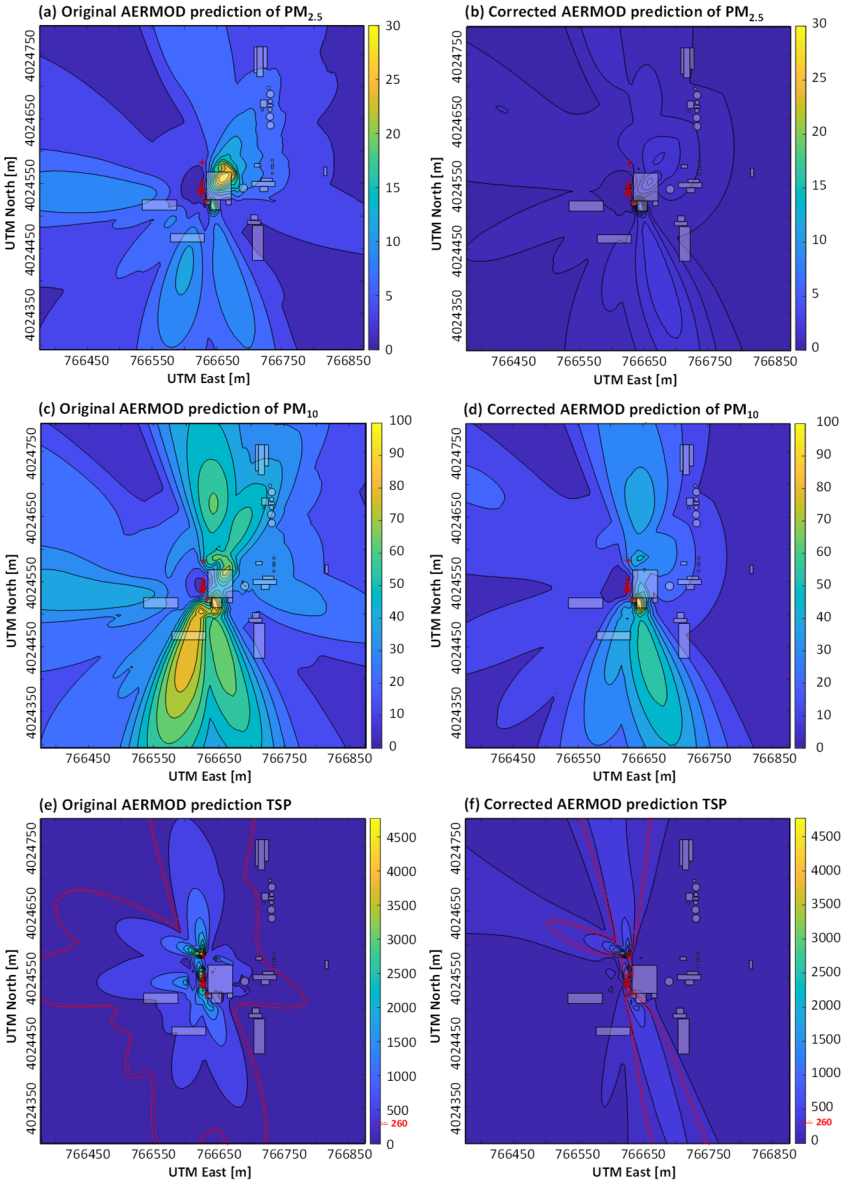

Figure 3-4 Spatial distribution of maximum of 24-hour average PM concentration of AERMOD original prediction and corrected AERMOD prediction for $PM_{2.5}$ **(a, b)**, PM_{10} **(c, d)**, and TSP **(e, f)**. Unit is μg/m^3. ⊕ refers to emission source. □ and ○ refer to buildings. Red solid line refers to the boundary that exceeds regulatory standard, and dashed line indicates the higher concentration side. For map details see **Figure 3-1**. Note that plots of each pollutant are on the same scale.

3.10 Limitations of current study

There are some limitations with the current study. First, the background concentration was not measured. However, due to multidirectional wind during sampling periods and spatial heterogeneity of the concentration, it was difficult to have a single on-site background measurement. The influence of the background concentration was taken into account when calibrating dispersion correction factors. Second, other possible variables may also influence on the dispersion correction factors, such as the influence of stacks, roads (traffic), buildings and production activities, and thus these factors may need further consideration. In addition, this model was established using experimental data limited to 10 m height and 180 m distance from source, but the performance of the dispersion correction factor outside this spatial domain could be different. Therefore, careful evaluations are needed when applying the dispersion correction factor model with data outside the domain.

4. Conclusion

Field samples of $PM_{2.5}$, PM_{10}, and TSP from low-altitude emission source were collected during 11 experiments at a typical cotton ginning facility. The concentrations and dispersion of the air pollutants were assessed. The regulatory recommended model was modified and validated based on the field dataset. height, distance from source, wind and geometry between wind direction and location of source and receptor are the significant factors influencing pollutant concentrations. In addition, pollutant concentrations were overestimated by AERMOD, and thus dispersion correction factors were developed. Cross-validation results showed that predictive accuracy was greatly improved by applying AERMOD coupled with dispersion correction

factors. Empirical equations to calculate dispersion correction factors were derived and are recommended for regulatory and practical use of AERMOD under similar conditions. The same approach may be useful for developing and evaluating dispersion models for other low-altitude emission sources of particulate matters, such as animal operations (Dai et al., 2020), food and agricultural product processing facilities (Venkataraman et al., 2018), and domestic combustion (Piwowar and Maciej, 2019).

Chapter 4 Evaluation of the Effects of Carbonaceous Material Amendments on the Bioavailability of Organochlorine Pesticide Residues in Soil Under Field Conditions

(This chapter is under preparation for *Environmental Pollution*)

Marya O. Anderson [a], Zijiang Yang [a], Cathleen J. Hapeman [b], Laura L. McConnell [a], Carrie Green [b], Dana Jackson [b], Michael N. Evans [c d], Alba Torrents [a]

[a] *Department of Civil and Environmental Engineering, University of Maryland College Park, 1173 Glenn L. Martin Hall, College Park, Maryland 20742, USA*

[b] *United States Department of Agriculture, Agricultural Research Service, 10300 Baltimore Avenue, Beltsville, Maryland 20705, USA*

[c] *Department of Geology, University of Maryland College Park, 1212B Chemistry Building, College Park, Maryland 20742, USA*

[d] *Earth System Science Interdisciplinary Center, 1120 Geology Building, University of Maryland, College Park, Maryland, USA*

Abstract

Reducing the bioavailability of persistent organic contaminants in soil by incorporating carbonaceous material (CM) has been investigated and confirmed by numerous laboratory studies. However, the efficacy under more complex field conditions has not been explored. Therefore, we conducted an 18-month, small-scale plot experiment to investigate the ability of two CMs, a compost aged 2-years and a compost aged 4 months, to reduce the bioavailability of

the organochlorine pesticide (OCP), including dichlorodiphenyltrichloroethane (DDT) and its metabolites (together as DDx) and dieldrin under field conditions. Soil and earthworms were collected, contaminant concentrations were measured, and bioaccumulation factors (BAF) were calculated for 28 subplots at multiple timepoints. Experimental results show great spatial variability of bioaccumulation in the field and show a decrease in the uptake and bioaccumulation of the OCPs with increasing soil concentration. These two findings expose the limitation of the fixed BAF value used in the current risk assessment of OCP contaminated soil sites. Additionally, bioaccumulation time series results show some evidence that CM amendments may reduce bioaccumulation over time. However, due to large spatial and temporal variability, such effectiveness was not statistically significant, and long-term data is required to confirm such effect. This field experiment demonstrates the necessity of developing more robust risk assessment methods, particularly for sites with high concentrations and large spatial variability, as well as the hazards of extrapolating results from the laboratory to the field.

1. Introduction

Organochlorine pesticides (OCPs), such as dichlorodiphenyltrichloroethane (DDT) and dieldrin, are among the first synthetic insecticides developed; they were widely used and have become legacy contaminants in the terrestrial environment. Despite their discontinued use globally, the persistence of these compounds and their widespread historical use has left numerous sites with elevated soil concentrations which require remediation. These compounds are not readily biodegradable, have long half-lives in soil of up to 15 years and 7 years for DDT and dieldrin, respectively, and are highly toxic, particularly to ecological receptors (US EPA, 2007a, 2007b). The potential of enhanced degradation of DDT and dieldrin has been investigated.

The majority of recent research has been focused on the potential of fungi, co-cultures of microbes and fungi, or enhanced microbial activity with addition of co-substrates (Matsumoto et al., 2009; Ortíz et al., 2013; Purnomo et al., 2017; Sariwati et al., 2017). However, these bioremediation methods are expensive, time consuming, and their effectiveness is uncertain in field application (Mansouri et al., 2017), therefore alternative remediation techniques may show greater promise.

In the United States (US), the US Environmental Protection Agency (US EPA) regulates the remediation of these sites, with their primary goal being risk reduction. The importance of bioavailability has been recognized during site assessment, as there is ample evidence showing that total concentration is not the only factor governing risk (Alexander, 2000; Reid et al., 2000). The US EPA Ecological Soil Screening Levels (Eco-SSLs), used to evaluate contaminated soil sites, recognizes this by including a bioavailability parameter (US EPA, 2007a, 2007b). This parameter is a fixed value for each OCP and is assigned as the mean value of an extensive evaluation of experimentally determined bioaccumulation factor (*BAF*) values (US EPA, 2007c). However, it has been well established that the bioavailability of persistent organic pollutants (POPs) like OCPs change over time, and are greatly affected by soil characteristics (Alexander, 2000; Reid et al., 2000). The Eco-SSL calculations do not take any variations in bioavailability into account.

When an Eco-SSL evaluation deems an OCP contaminated site high risk, the EPA requires remediation. Traditional remediation techniques involve significant cost and effort, so alternative techniques for remediation which focus on the reduction of OCP bioavailability have been increasingly explored. These techniques include the use of carbonaceous materials (CMs) as amendments for OCP contaminated soils (Hilber et al., 2009; Langlois et al., 2011; Morillo and

Villaverde, 2017; Paul and Ghosh, 2011; Saito et al., 2011; Yang et al., 2010). Various research has shown that CMs have a positive role in environmental mitigation of POP contaminated sites. There are two ways to use CMs as amendments, either to promote biodegradation of OCPs by microorganisms, where CMs provide nutrients and a carbon source, and/or to sequester the OCPs in the carbonaceous material, making them unavailable to the food chain. The promotion of biodegradation is a challenge for DDT, its metabolites, and dieldrin, due to their resistance to biodegradation. Therefore, it is more feasible to evaluate the immobilization of the OCPs, in an effort to provide significant bioavailability reduction and mitigate potential ecological risks. OCP immobilization has been studied a significant amount in controlled small-scale studies (Langlois et al., 2011; Morillo and Villaverde, 2017; Paul and Ghosh, 2011; Saito et al., 2011; Yang et al., 2010), and while this technique looks promising, there is a need for investigations under larger and more realistic conditions. The small-scale studies do not evaluate many important factors that affect bioavailability under real world conditions, including the significance of contaminant aging on bioavailability (Alexander, 2000; Morrison et al., 2000), and the variation in OCP uptake between different earthworm species (Kelsey et al., 2005). In real world applications, these important factors cannot be controlled, i.e. small-scale studies may not accurately evaluate the real-world potential use of these amendments. Thus, there is a significant need for studies of OCP bioavailability to native earthworm species under field conditions.

The research presented here is part of multi-phase investigation of OCP bioavailability of the site's soil, which aims to find effective and readily available CM amendments for immobilization of OCPs. The first phase was a growth chamber experiment used to evaluate the effectiveness of four inexpensive and readily available carbon amendments (Centofanti et al., 2016). Significant reduction in bioavailability was observed for 4,4'-DDT, 4,4'-DDE and dieldrin

in soil amended with several of the carbonaceous materials, including the two dairy composts used in this experiment, and one biosolids compost. Additionally, there was a significant difference in the effectiveness between two application rates.

Here we discuss the second phase, which involves a small-scale field experiment. The goals of this experiment were to investigate bioaccumulation of DDx and dieldrin to native earthworms, analyze the effectiveness of CM amendments under real field conditions, and to evaluate the Eco-SSL risk assessment results using field data.

2. Material and Methods

2.1 Site description

The historically contaminated site used for this experiment is a former orchard located at the US Department of Agriculture, Henry A. Wallace Beltsville Agricultural Research Center in Beltsville, MD, USA. More extensive site information on historical pesticide applications, and the soil profile, is provided elsewhere (Centofanti et al., 2016). While a more highly contaminated area of 0.55 ha was excavated and removed from the site, an area of approximately 9 ha of less elevated OCP concentrations remains in place, designated as the “site”.

2.2 Experimental design

During experimental set up, seven plots were established on the site at randomly determined locations, and assigned labels A-G (**Figure 4-1**). The plots were oriented with the long edge of the plot perpendicular to the contour line of the elevation. Each plot was divided into four subplots, and each subplot was randomly assigned a treatment. The four subplot treatments consisted of three forms of amendments and a control.

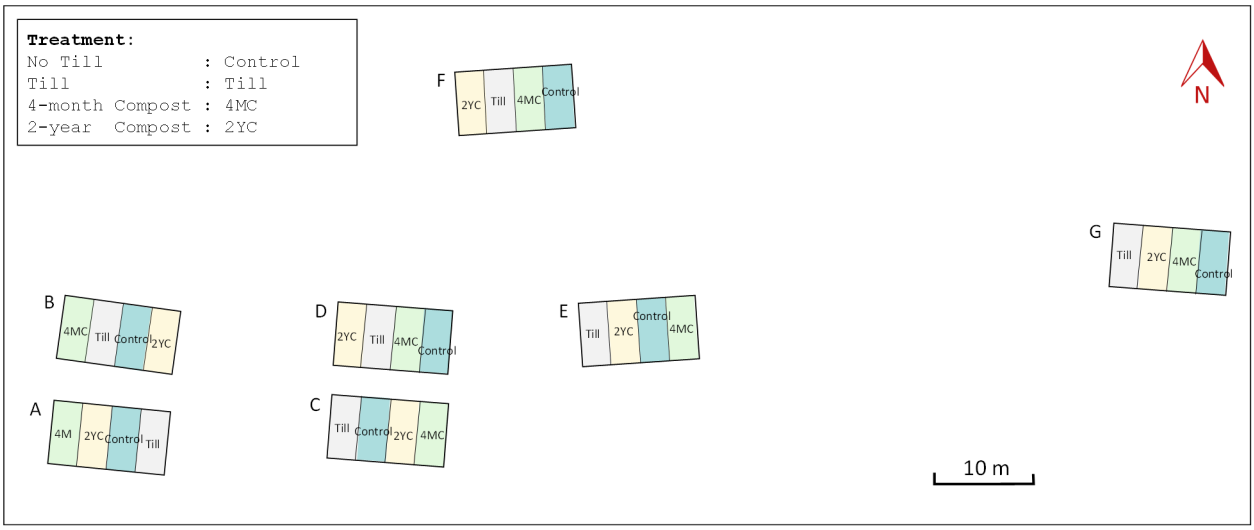

Figure 4-1 Locations and index of the 7 plots on the site, with each subplot shown, and treatment assignments specified. Each subplot is physically separated by silt fence to prevent earthworm migration.

The control for this experiment was a subplot left completely undisturbed, noted as "Control". Because it was hypothesized that the tilling action used when applying CM may affect the bioavailability, tillage was considered an amendment, and designated as "Till". The remaining treatments were two CMs applied at the same application rate of 224 dry t/ha. The first CM, a dairy compost that had been aged for 2 years, was chosen due to its best performance in the initial phase growth chamber experiment (Centofanti et al., 2016). The second CM was a "fresh" dairy compost, aged for 4 months before application. This compost was not as successful at reducing the bioavailability of 4,4'-DDE and dieldrin as a biosolids compost during the growth chamber experiment, however it was chosen for two reasons. First, it is more readily available and less expensive than the biosolids compost, which is increasingly important as the scale of a contaminated site increases. Secondly, it makes a direct comparison between two dairy composts possible, where changes in performance based on the pre-application compost aging could be evaluated. This could provide additional information on long-term effectiveness. The two compost amendments are designated as "2YC" for the 2-year compost and "4MC" for the 4-month compost.

Due to high heterogeneity of soil concentrations, the plot dimensions were designed to make them large enough for amendment application and to reliably collect the required number of earthworms for analysis, but small enough to minimize the variability within each subplot, helping to reduce the number of uncontrolled factors.

To ensure successful long-term evaluation of bioavailability, each subplot needed to retain their native earthworms throughout the experiment. This was accomplished by surrounding each subplot with silt fence, a material that prohibits earthworms from traveling through but allows natural soil moisture movement. By placing the silt fence at least 30.5 cm above and below the surface, the likelihood of earthworms being able to move between or out of treatment areas would be minimal (Gish and Hughes, 1982).

The 7.3 m × 12.2 m plots were established over a three-day period in the spring of 2013. Each plot was sectioned into four-3.0 m wide subplots. Compost amendments were spread over assigned application areas using a 2.4 m wide skid steer loader. In each plot, the three amendment subplots were tilled using a 2.4 m wide tractor pulled rotary tiller. A border was dug, at least 30 cm deep, around all subplot sampling areas using a skid steer trencher. A silt fence of 91 cm height was placed into the trench, to a depth of 30-60 cm deep, which ensured at least 30 cm below and above the surface of the plot. Wooden stakes were used to support the fence, the trenches were backfilled, the subplots leveled using hand tools, and all plots were seeded with orchard grass.

2.3 Sampling and analysis

All plots were sampled three times, and a fourth sampling event was carried out on the three most highly contaminated plots. The first sampling event occurred approximately six months

before plot establishment, before any soil disturbance. This pre-application sampling period is noted as TP. The tillage during plot establishment is expected to disturb and possibly damage the earthworm population, so the first post-application sampling was done approximately 6 months after application, noted as T6, to give the population time to recover. The third sampling was done at approximately 12 months after application, noted as T12, and the fourth, limited sampling event, was at approximately 18 months post-application, noted as T18. Exact sampling times were dependent on earthworm availability, which was affected by temperature and rainfall, and are listed in **SI Table 4-1**.

Soil and earthworms were collected by hand for pesticide analysis during each sampling event by digging up multiple soil portions across the sampling area of each subplot using shovels. The soil was broken apart by hand and sieved to 4mm on site. Any earthworms found in the soil were removed and placed in glass sampling jars. The soil was transferred to 19-L plastic buckets for later processing. Once sampling was complete, subplot composite soil samples were mixed as thoroughly as possible within the buckets. Two 0.47-L glass jars were filled with soil taken from throughout the bucket and stored at -20 °C until processing and analyses. All earthworms from each subplot were combined into a composite sample, rinsed with DI water to remove any affixed soil particles and stored, non-depurated, at -20°C until lyophilization. Lyophilized composite earthworm samples were ground to produce a homogenous sample.

Contaminant quantification was achieved following an extraction and analysis methodology described in Centofanti et al., 2016. The limit of quantitation (LOQ) for each of the analytes was 0.80 µg/g based on a 2-g sample for the pre-application soil samples, and 0.40 µg/g for all other soil and earthworm samples. In soil, average sand spike recovery of analytes was 85.9 ± 22.6% (n = 38), extraction surrogate recoveries for samples and spikes averaged 89.4 ± 23.8% (n =

326); duplicate samples resulted in an average percent difference of 7.3 ± 5.7% (n = 165) for all analytes. In earthworms, average spike recovery was 86.8 ± 41.4% (n = 23), extraction surrogate recoveries averaged 76.6 ± 18.3% (n = 278), and duplicate samples resulted in an average percent difference of 12.0 ± 10.5% (n = 96) for all compounds. Additional analyses carried out on soil samples included moisture content, pH and total organic carbon content. The lipid content of the earthworm samples was determined during the extraction process, also described in Centofanti et al., 2016.

2.4 Bioaccumulation factor

When evaluating bioavailability, it is common to look at the bioaccumulation factor (*BAF*) rather than soil and earthworm concentrations separately. The *BAF* normalizes the earthworm concentration to the soil concentrations, making comparisons across samples and plots possible. In this experiment, *BAF* is defined as the ratio of contaminant concentration in earthworms to contaminant concentration in soil. Thus, for a particular treatment, *BAF* was calculated:

$$BAF_j = \frac{C_{ej}}{C_{sj}} \qquad \text{Eqn. } 4-1$$

where BAF_j is the *BAF* of the j-th plot (j = A, B, C, D, E, F, G), C_{sj} and C_{ej} are the concentrations of contaminant in soil and earthworms (μg/g d.w.) of the j-th plot, respectively.

2.5 Normalization and the net effect of treatment

Within each subplot there was a significant variability seen for pollutant concentration in both soil and earthworms, resulting in large *BAF* variability. The *BAFs* were normalized to pre-application results in an effort to allow for direct comparison of the effect of different treatments. *Normalized BAF*, noted as *NBAF*, were calculated as follows:

$$NBAF_{\mathrm{T}i,tr} = \frac{BAF_{j,\mathrm{T}i,tr}}{BAF_{j,\mathrm{TP},tr}} \qquad \text{Eqn. } 4-2$$

where $NBAF_{j,\mathrm{T}i,tr}$ is the *NBAF* of the *j*-th plot (*j* = A, B, C, D, E, F, G) at sampling period T*i* (T*i* = TP, T6, T12, T18), and *tr* refers to treatment type (*tr* = "Control", "Till", "4MC" and "2YC"). $BAF_{j,\mathrm{TP},tr}$ is the *BAF* of the same *j*-th plot at time TP of the same treatment *tr*.

In order to investigate the effect of the amendments, net effect was evaluated by calculating *NBAF* differences between two treatments. First, any potential effect due to tillage was investigated by calculating the change in normalized bioaccumulation factor (Δ*NBAF*); the difference between "Till" and "Control":

$$\Delta NBAF_{\mathrm{T}i,\mathrm{Till}} = NBAF_{\mathrm{T}i,\mathrm{Till}} - NBAF_{\mathrm{T}i,\mathrm{Control}} \quad \text{Eqn. } 4-3$$

where $\Delta NBAF_{\mathrm{T}i,\mathrm{Till}}$ is the change of *NBAF* at time T*i*, for the tillage treatment. The net effect of each compost was then calculated as the difference between "4MC" or "2YC" and "Till". Those corresponding Δ*NBA*F's were calculated as follows:

$$\Delta NBAF_{\mathrm{T}i,4\mathrm{MC}} = NBAF_{\mathrm{T}i,4\mathrm{MC}} - NBAF_{\mathrm{T}i,\mathrm{Till}} \qquad \text{Eqn. } 4-4$$

$$\Delta NBAF_{\mathrm{T}i,2\mathrm{YC}} = NBAF_{\mathrm{T}i,2\mathrm{YC}} - NBAF_{\mathrm{T}i,\mathrm{Till}} \qquad \text{Eqn. } 4-5$$

where $\Delta NBAF_{\mathrm{T}i,4\mathrm{MC}}$ and $\Delta NBAF_{\mathrm{T}i,2\mathrm{YC}}$ refer to the change of *NBAF* at T*i* in terms of the effect of 4-month compost and 2-year compost, respectively.

2.6 Hazard quotient calculations

The US EPA Eco-SSL evaluation gives a safe limit for each contaminant, using a value called the hazard quotient (*HQ*) to assess a site's risk to specific organisms (US EPA, 2007a, 2007b). When a soil concentration equals the Eco-SSL value, the site is considered safe, and the *HQ* is equal to 1. The *HQ* is calculated using a referenced mean *BAF* (presented below as *MLP*),

determined by the US EPA (US EPA, 2007c). The *HQ* calculated in this manner, based solely on a site's soil concentration, is given as:

$$HQ_{\mathrm{s}} = FIR \cdot (C_{\mathrm{s}} \cdot Ps + C_{\mathrm{s}} \cdot MLP) \cdot \frac{1}{TRV} \qquad \text{Eqn. } 4-6$$

where *FIR* is food ingestion rate, *Ps* is soil ingestion proportion of diet, *MLP* is the multiplier for estimation of concentration of contaminant in biota based on soil concentration, and *TRV* is the toxicity reference value. In this study, the values for each parameter were taken from Eco-SSL documents for DDT and dieldrin (US EPA, 2007a, 2007b) and are summarized in **SI Table 4-2**. **Eqn. 4-6** is the current calculation of *HQ*, used for ecological risk assessment, which we denote as HQ_{s}, and refer to as the *traditional HQ*.

In situations where the biota concentrations are known, *HQ* can be calculated using both soil and biota concentrations. In this study, earthworms are expected to be the main food source for the woodcock and short-tail shrew (US EPA, 2007a, 2007b; DNP, 2020). Thus, the concentration of contaminants in earthworms can be directly used as the biota concentration, and the *HQ* for those organisms can be calculated as follows:

$$HQ_{\mathrm{se}} = FIR \cdot (C_{\mathrm{s}} \cdot Ps + C_{\mathrm{e}}) \cdot \frac{1}{TRV} \qquad \text{Eqn. } 4-7$$

where HQ_{se} is referred to as the *adjusted HQ*. This value offers a more accurate evaluation of the potential ecological risks of a particular site, because the experimentally determined biota concentration is taken into account rather than an estimated value.

2.7 Statistical analysis

To carry out statistical analysis on the experimental data, results that were below the detection limit were assigned a concentration of half the value of the detection limit (Yao et al., 2018b). Mean, standard deviation, coefficient of variance (*CV*), regression analysis and plots

were done by Microsoft Excel (2016) and GraphPad Prism 6.07 (GraphPad Software, Inc. La Jolla, CA). Variability was evaluated using the *coefficient of variance* (*CV*), which is the normalized standard deviation by mean, allowing cross comparison among plots. Hypothesis testing on *NBAF* and Δ*NBAF* was performed by bootstrapping sampling of uncertainties, and evaluation of results with significance level $\alpha = 0.05$ (Martinez and Martinez, 2015); for more details see **Supplementary Information**. Matlab R2019b was used to conduct Monte Carlo simulation (The MathWorks, Inc. Natick, MA). The goodness of fit is evaluated by adjusted R^2, Akaike information criterion (*AIC*) and Bayesian information criterion (*BIC*) (Akaike, 1974; Schwarz, 1978).

3. Results and Discussion

3.1 C_e as a function of C_s

Results for soil and earthworm concentrations and *BAF*'s for DDx and dieldrin are shown in **SI Table 4-3** and **SI Table 4-4**. These results were evaluated for correlation between values. To exclude the influence of any amendment on the correlations, the data was divided into two groups: an *unamended* group and an *amended* group. The data for soil and earthworm concentrations for the *unamended* group includes all data from TP (pre-application), and all "Control" subplot data from T6, T12, and T18. The *amended* group includes data from all amended subplots, "Till", "2YC" and "4MC", for T6, T12 and T18.

Scatter plots for C_s vs C_e of DDx are shown in **Figure 2a** and **2b**. Several models of the C_e and C_s relationship were fitted to the dataset of each group, including linear and nonlinear relations (Sample et al., 1999; Kelsey et al., 2005; Luo and Deng, 2018; Sparks, 2003), and the results are presented in **SI Table 4-5**. While all of the tested models are significant ($p < 0.05$), results

suggest that nonlinear relations between C_e and C_s have better fit than the linear response between C_e and C_s described by **Eqn. 4-1** for both the *unamended* and *amended* groups. Among the nonlinear models, the regression model of $C_e = k\ln(C_s) + b$ was found to have the best performance for larger adjusted R^2 and smaller *AIC* and *BIC* values in most of the cases. This result suggests that as soil concentration increases, uptake and bioaccumulation of contaminants decreases, a phenomenon which has been observed in previous studies (Sample et al., 1999; Pagnanelli et al., 2000; Kelsey et al., 2005; Vermeulen et al., 2010; Gaylor et al., 2013). The mechanism of such decrease probably related to increased metabolism or excretion rate when toxicity increased at higher soil concentration (Sample et al., 1999). In addition, increased toxicity leads to higher mortality (Fordham, 1985), and the individuals with lower uptake and bioaccumulation of OCPs are more likely to survive, which resulted in lowered accumulation at higher soil concentration. The experimental results for dieldrin show smaller but significant regression of C_e on C_s and greater random error than for DDx **(Figure 4-2c** and **4-2d)**.

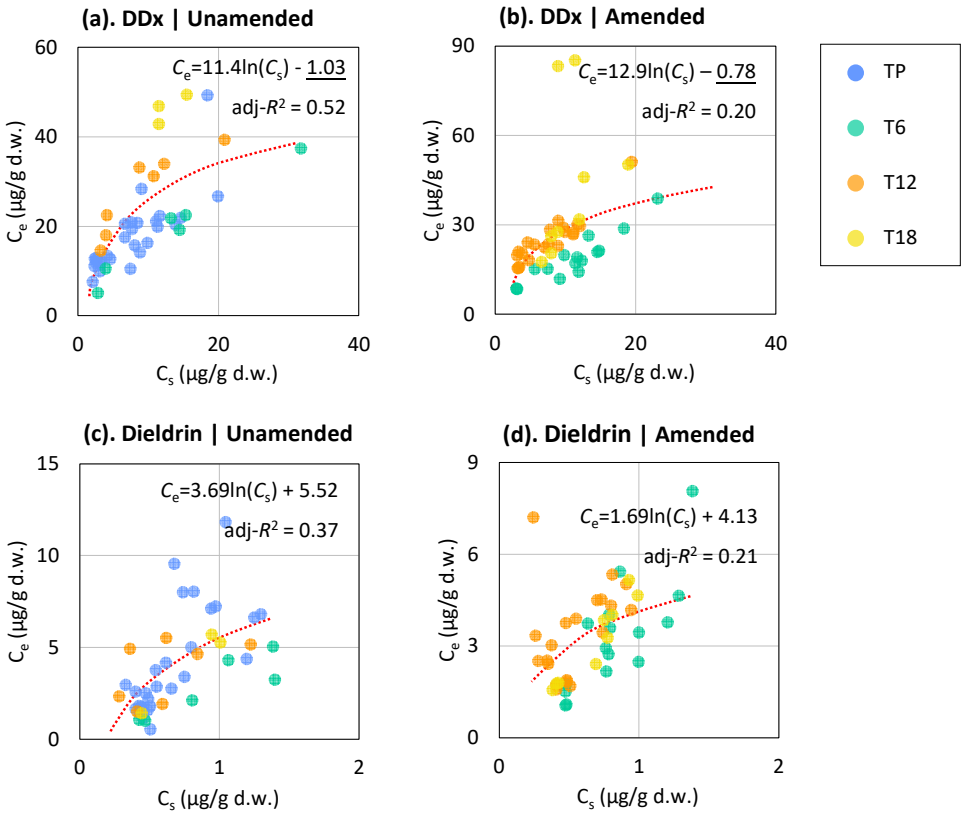

Figure 4-2 Scatter plots of C_s, C_e for DDx and dieldrin. Dotted lines are hypothetical nonlinear relation by using all points: $C_e = k\ln(C_s) + b$, where k and b are regression coefficients, and the underlined value refers to insignificant difference from zero ($p < 0.05$). More details on regression are presented in **SI Table 4-5**. adj-R^2 is the adjusted coefficient of determination.

These results suggest an inaccuracy in the HQ_s calculation, which assumes linearity between C_s and C_e (**Eqn. 4-6**); $C_e = MLP \cdot C_s$). The assumed linear relationship between C_e and C_s may result in overestimation of risk at high C_s values. To remedy this, we would suggest using a correction factor in the HQ_s equation, which takes the decreasing BAF as soil concentration increases into account. However, because there is very little difference in the fit of the various nonlinear models of the C_e and C_s relationship, further investigation is needed to more confidently define the relationship.

3.2 Spatial variability

The site used in this study has experienced multiple historical sampling events, which have shown high spatial variability of OCP concentrations. During this experiment, the pre-application sampling event (TP), carried out before any disturbance of the field due to amendment application, provides a unique data set for assessing the spatial variability of bioaccumulation in aged soil. Variability of C_e, C_s and *BAF*, was found to be considerable between subplots (**SI Tables 4-3** and **SI Table 4-4**). The *BAF*s for DDx and dieldrin at TP are shown in **Figure 4-3**. The variability in *BAF* is large for DDx across the entire site, ranging from 1.34 to 5.34 with *CV* = 0.42 (**Figure 4-3a)**, and is even larger for dieldrin, ranging from 1.09 to 14.58 with *CV* = 0.51 (**Figure 4-3b)**. In addition to the variability across the site, there is also high variability within plots, even though the largest distance between subplots is only 5.5 m. Within plots, the variation of the *BAF* is largest for DDx in plot D, where the values range from 1.47 to 3.14 with *CV* = 0.40 and largest for dieldrin in plot A, with values that vary from 3.66 to 11.33 given *CV* = 0.48. There are even some individual subplots with high *BAF* variability. For example, *BAF* of DDx at TP for "4MC" in plot B has a *BAF* of 1.90 ± 0.44 given *CV* = 0.23 and the *BAF* of dieldrin at TP for "4MC" in plot B has *BAF* of 7.57 ± 3.46 given *CV* = 0.46.

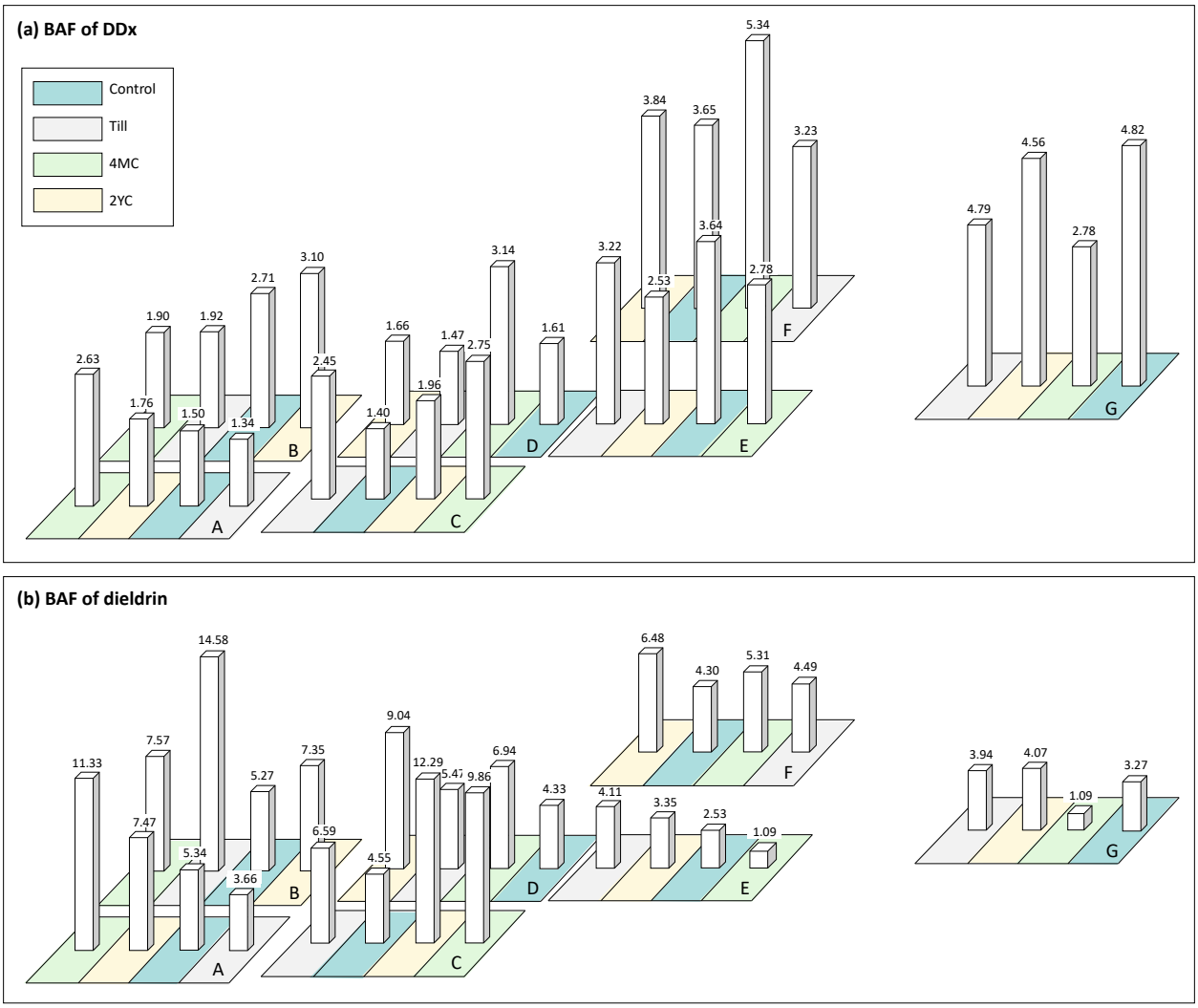

Figure 4-3 Spatial distribution of *BAF* of DDx (a) and dieldrin (b) at TP (pre-application of compost). Height of bars are proportional to the *BAF* value. Spatial scale is not in proportional to real scale. Different colors refer to treatments that were assigned to the subplot. But since this is at TP, none of the subplot had received treatment yet.

The high spatial variability seen in this experiment makes the evaluation of ecological risk a challenge, particularly in two significant ways. First, as the input argument(s) for calculating *HQ* (**Eqn. 4-6** and **Eqn. 4-7**), the variability of the concentrations result in large uncertainty for the *HQ*, which reduces precision and reliability. Second, *BAF* is not constant across plots, so that assuming a grand mean *BAF* produces locally biased *HQ* values, and consequently may result in incorrect inferences when recommending a plan of action.

The high spatial variability seen in this experiment makes the evaluation of ecological risk a challenge. First, as the input argument(s) for calculating *HQ* (**Eqn. 4-6** and **Eqn. 4-7**), the concentration variability results in a large uncertainty for the *HQ*, which reduces precision and reliability. Second, *BAF* is not constant across plots, so that assuming a grand mean *BAF* produces locally biased *HQ* values, and consequently may result in incorrect inferences when recommending a plan of action.

3.3 Bioaccumulation change over time

Normalized bioaccumulation factors (*NBAF*) of DDx and dieldrin over time are shown in **SI Figure 4-1** and **SI Figure 4-2** (for *NBAF* of each individual subplot see **SI Figure 4-3** and **SI Figure 4-4**). The large standard deviation seen in **SI Figure 4-3** and **SI Figure 4-4** displays the large variability of bioaccumulation in the field among different subplots, which is consistent with the conclusions of the spatial variability analyses.

Theoretically, the control subplots (Control) received no amendment, so are at equilibrium, and bioaccumulation should not change. Instead, the data shows significant changes in the Control subplots' DDx *NBAF*s. From TP to T6 there was one plot which showed a significant *NBAF* decrease, and then significant *NBAF* increases were seen in four plots from T6 to T12 and all three plots sampled at T18. The overall variability seen in Control *NBAF*s is likely due to spatial variability of the contaminants and temporal variability of certain environmental factors that can influence bioaccumulation, such as temperature and rainfall (Gish and Hughes, 1982; Beyer and Gale, 2013).

With the Control subplots showing changes in *NBAF* with time, it is not surprising that the DDx *NBAF*s for all of the amendments also show changes over time. However, the amendments showed a greater variation in *NBAF* trends over time. For example, the tilled but no compost

added treatment (Till), shows significant *NBAF* decreases for three plots from TP to T6, and then significant increases in 2 plots from T6 to T12 and 1 plot from T12 to T18. Again, these different behaviors among subplots is most likely explained by spatial variability.

The *NBAF*s of dieldrin show similar trends as DDx, with the exception of plot E which showed a dramatic increase of *NBAF* between TP and T12. Additionally, from T12 to T18 no significant increase was seen in any of plots sampled.

Overall, there was a general pattern for both DDx and dieldrin from TP to T12 for all treatments, where the *NBAF*s show a V-shaped or J-shape pattern. This shape indicates a potential reduction from TP to T6, however, not all of the reductions were significant. These results make it difficult to derive any impact the compost amendments may have had. This is not unexpected, as normalization does not reduce variability of the data, only re-scales it. This means that the data is dominated by the high concentration variabilities on the site. Therefore, we suggest that a better understanding of the change of bioaccumulation requires a higher number of samples. Additionally, further collection events after T18 would provide insight into the changes in bioaccumulation, and whether they were influenced by any of the treatments.

3.4 Effect of amendment

Change in *NBAF* (Δ*NBAF*) was used as an additional technique to evaluate the effect of treatments, regardless of any temporal trends. First, the net effect of tillage was evaluated by taking the *NBAF* of "Till" minus *NBAF* of "Control". To evaluate the effect from each compost, any effect from tilling had to be excluded, so Δ*NBAF*s were calculated by taking the *NBAF* of the compost ("4MC" or "2YC") minus the *NBAF* of "Till". Results of the different amendment's Δ*NBAF*s are shown in **Figure 4-4**. Details of each subplot can be found in **SI Figure 4-5** and **SI Figure 4-6**.

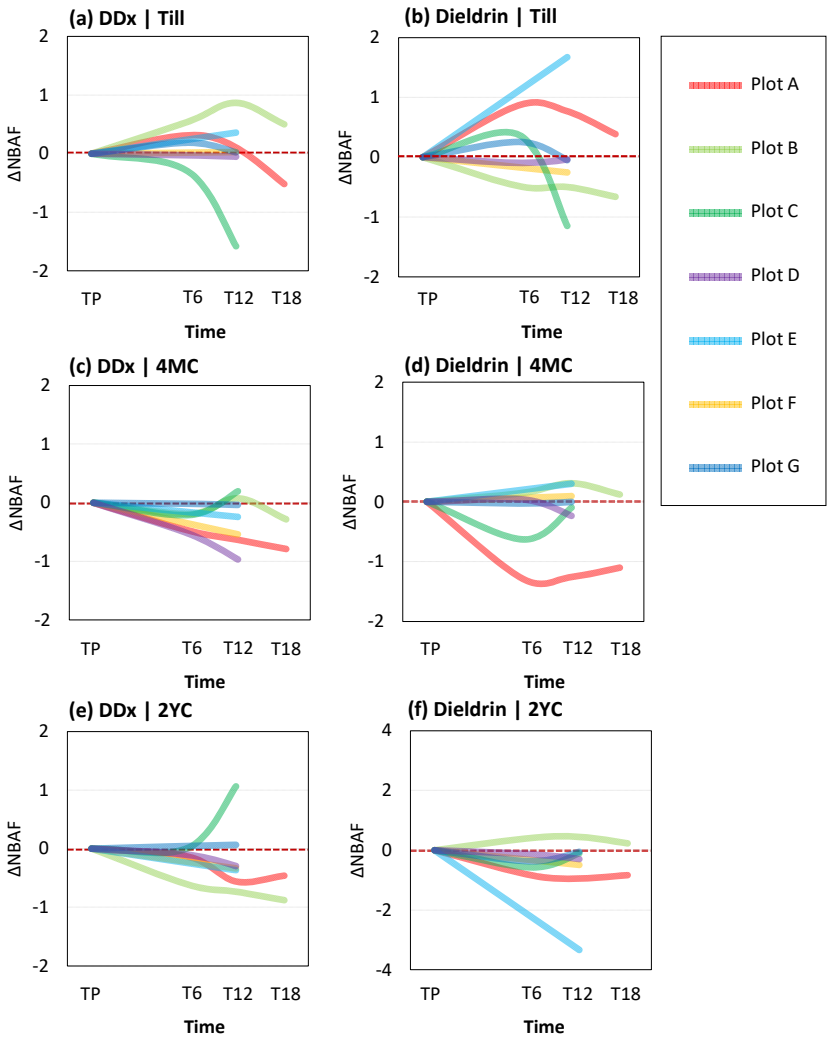

Figure 4-4 Change of normalized bioaccumulation factor (Δ*NBAF*) change with time. Each curve refers to the central tendency of Δ*NBAF*. For more details of the uncertainty, see **SI Figure 4-5** and **SI Figure 4-6**.

For DDx, Δ*NBAF*'s show mixed responses for all amendments. The Till treatment results show reduced bioaccumulation in 2 plots, increased bioaccumulation in 2 plots, and no significant effect for 3 plots (**Figure 4-4a**). The 4MC treatment results show reduced bioaccumulation in 4 plots, no significant effect in 2 plots and a small increase in 1 plot (**Figure 4-4c**). The 2YC treatment subplots also show 4 plots with reduced bioaccumulation, and an additional plot demonstrates a reduced effect, but the difference is not significant. There was an increased bioaccumulation in 2 plots (**Figure 4-4e**). In general, the results show some evidence

that composting may reduce bioaccumulation, as over half of the plots show reduction, but a mitigation effect is difficult to confirm.

The Δ*NBAF*s for dieldrin have the similar pattern to the DDx Δ*NBAF*'s. For the Till subplots, 3 show reduced bioaccumulation, 2 show an increase in bioaccumulation, and 2 show no significant effect. For 4MC subplots, bioaccumulation was significantly reduced in 2 plots, and significantly increased in 1 plot. There was no significant effect seen in 3 plots, however, one of those plots shows reduced effect at T6. The 2YC subplots show 4 plots with reduced bioaccumulation, and 1 plot with an increase in bioaccumulation. Again, the remediation effect of composting is hard to confirm with this data. While there is some evidence that composting may reduce bioaccumulation, collecting data after T18 could help confirm any such effect.

3.5 Hazard quotient

As previously mentioned, the calculation of the *HQ* for a particular compound is meant to incorporate the concentration of the contaminant in biota (i.e. earthworm) along with the concentration in the media (i.e., soil). Most often, biota concentrations are not available, and are estimated using the soil concentration times a multiplier (*MPL*), which functions as a constant *BAF* value (**Eqn. 4-6** and **Eqn. 4-7)**. However, it was found that the experimentally determined *BAF*'s on the site, for both contaminants, were lower than the *MPL* values used to calculate HQ_s in **SI Table 4-2**. The traditional *HQ* calculations result in significantly inaccurate risk estimation for this site due to the observed effect increasing soil concentrations have on bioavailability, and the extensive variability of contaminant concentrations in the aged soil.

The adjusted *HQ* presented here (HQ_{se}) provides a more accurate assessment of risk, as it corrects for a number of the faults in the HQ_s calculation. The significance of this difference can

be seen when comparing the traditional and adjusted *HQ* values using TP (pre-application) data, for the receptors short-tailed shrew and woodcock. The resulting scatter plots of HQ_{se} vs HQ_s are shown in **Figure 4-5** and highlight the differences in implied risk between the traditional *HQ* calculations (*y*-axis) and the adjusted *HQ*, calculated using the experimental *BAF* values (*x*-axis). Values above the 1:1 dotted line represent instances when the traditional *HQ* gives an overestimation of risk. All of the data points, for both contaminants in both receptors, plot above this line. The site evaluated here is known to have a high ecological risk, and it is not a surprise that the *HQ*'s are nowhere near the risk target of 1. However, the extent and variability of overestimation highlights how inaccurate and imprecise the traditional *HQ* evaluation can be for a real historically contaminated site.

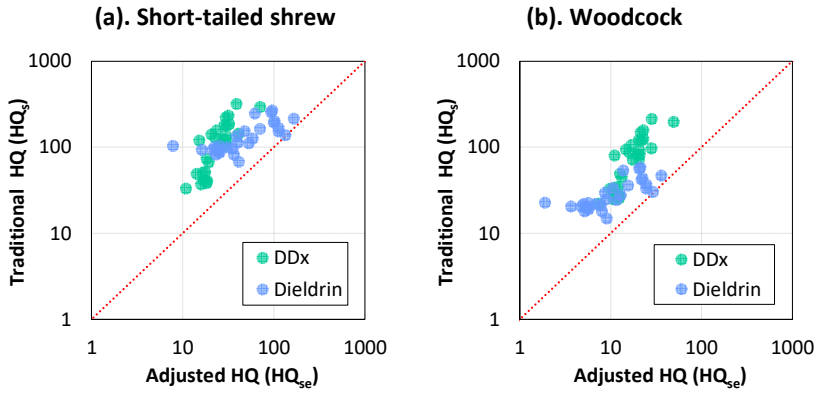

Figure 4-5 Plot of traditional *HQ* (HQ_s) vs adjusted HQ (HQ_{se}) of DDx and dieldrin based on data at TP (pre-application). Dotted lines are 1:1 ratio, and axis is under log-scale. All of the *HQ*'s are greater than 1, revealing that remediation is needed.

The risk overestimation shown in **Figure 4-5** illustrates the need for improvement in the evaluation of risk of contaminated soil. The extent of overestimation indicates that the *HQ* is much more dependent on earthworm concentrations vs soil concentrations. Using the variable values from the Eco-SSL documents (**SI Table 4-2**), mathematical derivation of **Eqn. 4-6** and **Eqn. 4-7** shows that when $C_e \gg 0.03C_s$ and $C_e \gg 0.16C_s$ (for shrew and woodcock respectively), HQ_{se} can be accurately calculated using only C_e (details of derivation see **Supplementary**

Information). In other words, the earthworm concentration is the key contributor to the HQ_{se} for all samples in this study. Therefore, for the site studied in this experiment, the risk to higher trophic ecological receptors can be determined exclusively from earthworm concentrations. This is different from the most common risk assessment practice, which only samples for and uses soil concentrations. While earthworms are more difficult to collect than soil, it is clear that they provide a significantly more accurate representation of the risk on this type of site. Thus, it is suggested that if the constraining factor when performing a risk assessment is the ability of testing only one media, or sample set, the earthworm is the better medium for risk assessment compared with soil.

3.6 Limitations of current study

There are a number of limitations with the current study. First, there were some uncontrollable environmental variables that may influence the physiology of earthworms and further OCP uptake and bioaccumulation, such as temperature (Muijs and Jonker, 2009), soil moisture (Cortez, 1998) etc. However, these uncontrollable variables were taken into account by spatial and temporal variability. Second, vertical movement of earthworm (Lavelle, 1998), vertical distribution of earthworm species (Fierer, 2019) and vertical spatial distribution of contaminant (Liu et al., 2015) could make 15-cm depth soil and earthworm sampling unrepresentative for the whole ecosystem. However, as the main purpose is to evaluate potential risks of OCPs to indigenous animals, soil and earthworm samples from such depth are representative of what would be available to the local food chain. Another limitation was the integrity of the silt fence. There is significant potential for damage, which could allow earthworms movement between the subplots. During sampling, it was observed that the silt fence

was progressively affected by vegetative growth, sampling techniques, and weathering, with each passing sampling event. Thus, an evaluation of the silt fence performance over time is recommended for future work. Finally, any effects the sampling procedure had on earthworm populations and OCP concentrations cannot be evaluated but may have the potential to be significant.

4. Conclusions

A field plot study was conducted on a historically contaminated site, with two types of CM added to the contaminated soil. Soil and earthworm samples were collected from 28 subplots during four sampling events and used to evaluate the bioaccumulation of DDx and dieldrin to native earthworms. The effectiveness of the CM amendments at reducing bioavailability was assessed, and ecological risks to indigenous animals was calculated. Results of OCP soil and earthworm concentrations show that uptake and bioaccumulation of the OCPs decreased as soil concentration increases and that there was great spatial variability of bioaccumulation in the field. These two findings reveal the shortcomings of the current risk assessment process for OCP contaminated soil sites, which uses a fixed *BAF* value. In addition, time series of bioaccumulation show some evidence that CM amendments may reduce bioaccumulation over time. However, due to large spatial and temporal variability, such effectiveness was not statistically significant. Thus, long-term data is required to confirm such effects. Overall, these experimental observations demonstrate the necessity of developing more robust risk assessment methods, particularly for sites with high concentrations and large spatial variability, as well as the hazards of extrapolating results from the laboratory to the field.

Chapter 5 Estimation of Space-time Patterns of Contaminant Bioaccumulation Using Bayesian Hierarchical Modeling

(This chapter is under preparation for *Environmental Pollution*)

Zijiang Yang[a], Michael N. Evans[b,c], Cathleen J. Hapeman[d], Marya O. Anderson[a], Scott G. Lynn[e], Taylor LaChance[d], Rebecca E. Plummer[d], Dana Jackson[d], Laura L. McConnell[a], Alba Torrents[a]

[a] *Department of Civil and Environmental Engineering, University of Maryland College Park, 1173 Glenn L. Martin Hall, College Park, Maryland 20742, USA*

[b] *Department of Geology, University of Maryland College Park, 1212B Chemistry Building, College Park, Maryland 20742, USA*

[c] *Earth System Science Interdisciplinary Center, 1120 Geology Building, University of Maryland, College Park, Maryland, USA*

[d] *United States Department of Agriculture, Agricultural Research Service, 10300 Baltimore Avenue, Beltsville, Maryland 20705, USA*

[e] *U.S. Environmental Protection Agency, William Jefferson Clinton Building, 1200 Pennsylvania Ave. NW, Washington, DC 20460, USA*

Abstract

To assess the sensitivity of interpretation to spatial heterogeneity and observational uncertainties, we applied Bayesian hierarchical modeling (BHM) to the re-analysis of DDT, metabolite (DDx) and dieldrin concentrations in soils and earthworms across spatiotemporally resolved field study. Predictive accuracy of the model was quantified by normalized mean

standard error (*NMSE*) through cross-validation, Akaike information criterion (*AIC*) and Bayesian information criterion (*BIC*); in parallel, results were compared to those obtained from ANOVA modeling. We found no difference in skill for 9 of 16 tests; improved skill for the BHM in 6/16 of the tests, and improved skill for the ANOVA model in 1/16 of the tests. These results suggest the BHM is the preferred model when observational uncertainty is large and when information among groups is highly variable. Implications of remediation techniques were drawn from the posterior distributions of the BHM, and suggest that there are some evidence that treatment with compost improves DDx and dieldrin remediation in soils and reduces bioaccumulation, but longer-term observations are necessary to test this hypothesis.

1. Introduction

Field study is an important component for environmental research, and it is used to confirm the effectiveness of the new techniques under real conditions, such soil remediation studies (Kołtowski et al., 2016; Oleszczuk et al., 2019). However, field data often has great spatial variability and other uncertainty issues, making it difficult to reproduce the results from the lab study to the field study (Centofanti et al., 2016; Anderson et al., 2020). Considerable spatial variability of the contaminant has also been recognized by other studies (Tieyu et al., 2005; Zhang et al., 2006). High spatial variability often causes difficulties with sampling design (Lammel et al., 2011), specifically the spatial sampling layout and the sample size (US EPA, 1997; US EPA, 1999; US EPA, 2014). In addition, since spatial variability may be different at different spatial scales (Anderson et al., 2020), it is also an obstacle to extrapolating spatial data in the field, and further hinders the understanding of environmental fate of the contaminants.

When spatial variability is large, uncertainties may be underestimated. When investigating

bioavailability, bioaccumulation factor (*BAF*) is usually used to quantify bioavailability, and it is defined as follows (Centofanti et al., 2016; Anderson et al., 2020):

$$BAF = \frac{C_e}{C_s} \qquad \text{Eqn. } 5-1$$

where C_e is concentration of contaminant of earthworms at equilibrium, and C_s is the concentration of contaminant of soil at equilibrium. This definition works well for experiments with homogenous soil and habitat-constrained earthworms, e.g., greenhouse pot studies, where heterogeneity of soil concentration and earthworm concentration are reasonably assumed to be negligible (Centofanti et al., 2016; Rich et al., 2015). In these studies, contaminant concentration in a pot were measured in triplicate, and means of soil and earthworm measurements were used in **Eqn. 5-1** as C_s and C_e, respectively (Centofanti et al., 2016; Rich et al., 2015). A point estimate of *BAF* (e.g., mean) was calculated for an individual pot, and the *BAF*'s of the individual pots were summarized for further statistical inference. However, when applied to heterogenous soils, i.e., soil with large variability, the use of **Eqn. 5-1** can be problematic. Spatial variability and small sample sizes may cause total variance and standard error estimates to be biased (Anderson et al., 2020), degrading the estimation of *BAF*. Thus, the traditional method leads to underestimation of variability in C_e and C_s, and therefore substantially increase uncertainty in the estimation of *BAF* (**SI Figure 5-1** and **SI Table 5-1**). This under-estimation of uncertainty can have a negative impact on further inference.

Spatial variability may also case problems with ratio variables. When calculating *BAF*, pollutant concentration measurements were usually inexplicitly assumed to be independent and normally distributed when applying statistical analysis (Centofanti et al., 2016; Anderson et al., 2020; Rich et al., 2015), and sample mean is usually used to estimate population mean. However, ratio of two independent normal variables follows a mixed distribution of Cauchy distribution

and a bimodal distribution (**SI Figure 5-2)** (Marsaglia, 1965; Marsaglia, 2006). Since the Cauchy distribution has no population mean or variance (Casella and Berger, 2002; Davison and Hinkley, 1997), a sample mean may be calculated but is not an appropriate measure of the underlying population (Press, 1969; Hayya et al., 1975). Although the delta method (Casella and Berger, 2002) and error propagation equations (Farrance and Frenkel, 2002) can be used to approximate the ratio of two independent normal variables such as *BAF* by a normal distribution, a critical constraint of these methods is that the denominator should be positive (Casella and Berger, 2002; Davison and Hinkley, 1997). Unfortunately, great spatial variability and misestimated sample statistics may permit the modelled denominator, C_s, to have small but non-negligible negative probability (**SI Figure 5-3a**), resulting in failure of delta methods and error propagation equations, and leading to incorrect inferences (see **SI Figure 5-3** for a numerical example).

In addition, extreme values and potential outliers are likely to come with large spatial variability. Due to the nature of small sample size in soil remediation experiment (Anderson et al., 2020), it is difficult to identify and determine the outliers.

In order to address the problems mentioned above, trunked normal distribution (Byon et al., 2008), log-normal transformation (Díez et al., 2007), and trunked log-normal transformation (Bowers et al., 1996) have been used in previous studies. However, these methods can only address the ratio variable problem to some extent; they are not able to overcome the problems of underestimation of uncertainties and extreme values. Thus, an approach that is capable of addressing all of those problems is needed.

Bayesian hierarchical modelling (BHM) is one approach. Bayesian statistical modelling has been increasingly applied in the field of environment and agricultural related research (Cocchi et al., 2007; Goyal et al., 2005; Aelion et al., 2009; Azim et al., 2011; Banerjee et al., 2014; Billoir et al., 2008; Delignette et al., 2017; Tan et al., 2017; Øverjordet et al., 2018). BHM can address uncertainty

issues by allowing uncertainty of C_s and C_e to propagate through its hierarchical structure (Gelman et al, 2013). In addition, extreme value uncertainties can be addressed under BHM framework, by assigning different weights to extreme values and outliers, using information from other groups (Gelman and Hill, 2006). As a result, outliers are not removed or retained, but simply assigned a smaller weight, and thereby provide some information. Ratio variables may also be addressed by applying BHM coupled to log-transformation of original variables. In addition, other prior knowledge, such as previous studies, surveys, or personal beliefs, can be explicitly added into the inferential process through the Bayesian framework (Gelman et al., 2013).

The main objective of the present study is to investigate the suitability of BHM for the estimation of ratio variables under the circumstances of large spatial variability. The goals of current study include: (1) apply BHM to characterize soil concentration, earthworm concentration, *BAF* and their uncertainties; (2) compare the performance of the proposed model with traditional model; (3) draw implications of the modelling results for evaluation of soil remediation techniques.

2. Material and Methods

2.1 Site description

The historically contaminated site used for this experiment is a former orchard located at the United States Department of Agriculture (USDA), Henry A. Wallace Beltsville Agricultural Research Center in Beltsville, MD, USA, where DDT were continuously applied in the site from 1940s to 1972 (US EPA, 2015). Dieldrin has also been found in this site although specific records of its usage were not found (US EPA, 1998b). This area was preliminarily assessed and under site investigation at 1986 (US EPA, 2017; US EPA, 2018b), and in 1994, this area was listed as a

Superfund site under the Comprehensive Environmental Response, Compensation, and Liability Act (CERCLA) (USDA, 2018). In 2007, a bioavailability study was conducted in this area followed by an ecological risk assessment using Eco-SSL for DDT and dieldrin (USDA, 2009). This area was then identified as contaminated, and 0.55 ha of the highest contaminated soil was removed from the site, leaving about 9 ha remaining area, and the remaining area has lower levels of contamination (USDA, 2009; US EPA, 2017).

2.2 Experimental design

Seven plots were randomly established in the field to conduct experiments. Locations and geometry of the seven plots are shown in **Figure 5-1**. Compost that had been aged for 2 years, and the compost that had been aged for 4 months, were applied to random quadrate subplots of each of the 7 plots. Each plot was divided into four subplots by silt fence to ensure native earthworms are kept within the corresponding treatments (Anderson et al., 2020) **(SI Figure 5-4)**, and four treatments were randomly assigned within each plot, including: (1) a control, where the soil was left undisturbed, noted as "No Till", (2) treatment with tilling, where the soil was tilled but no compost was applied noted as "Till" (3) treatment with tilling and dairy compost that had been aged for 2 years, noted as "2YC" and (4) treatment with tilling and dairy compost that had been aged for 4 months, noted as "4MC".

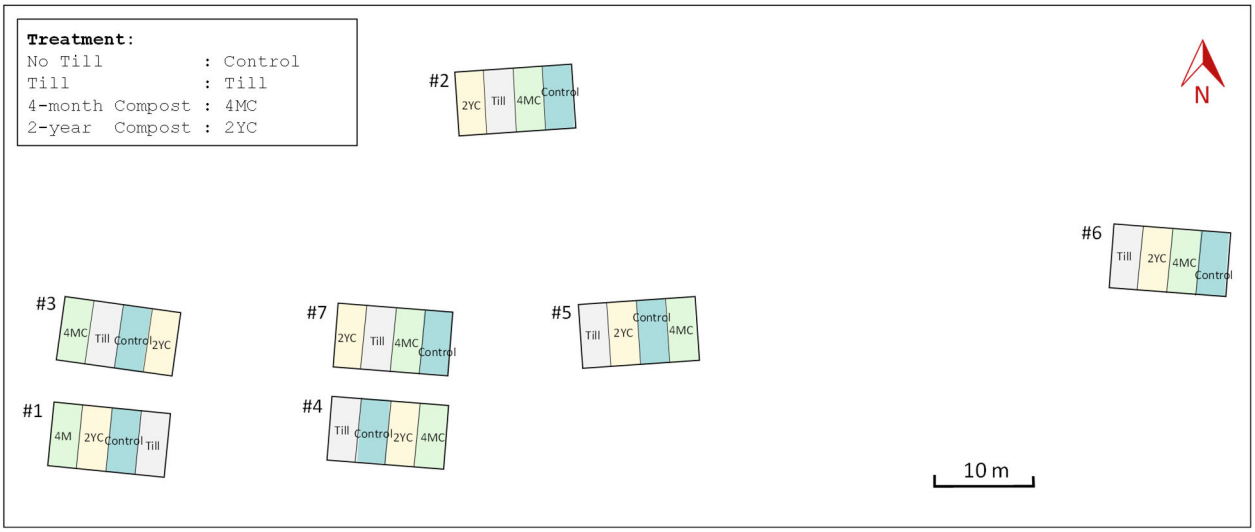

Figure 5-1 Locations of plots and subplots treatment assignments. There are 7 plots in the field, and each plot was divided into 4 subplots with each subplot randomly receiving one of the four different treatments. Each sub-plot was physically separated by silt web to prevent earthworm migration.

2.3 Soil and earthworm sampling and measurement

Soil and earthworm samples of each subplot ($n = 4 \times 7 = 28$) were collected at three different time points, while for the fourth sampling time point, samples were only collected at the three plots with greatest concentration (plot #1, #3 and #7, thus $n = 4 \times 3 = 12$) at the fourth sampling period. During the first sampling period, samples for each subplot were taken from the undisturbed soil before the plots were established, noted as TP (Dec. 2012). The second sampling was done at 6 months after establishment of silt fence and applying tilling and compost treatment, noted as T6 (Nov. 2013). The third sampling period was about 12 months after application of compost, noted as T12 (May 2014). The fourth samples were done at about 18 months after application, noted as T18 (Nov. 2014).

Analytical measurement of DDT and its metabolites (together as DDx) and dieldrin in soil and earthworm samples follows an extraction and analysis methodology elsewhere (Centofanti et al., 2016). The detection limit (DL) was 0.8 µg/g for soil samples at TP, and 0.4 µg/g for soil and earthworm samples for the rest. In the following data analyses, the value below DL is assigned to

half of DL value (Shoari and Dubé, 2018).

2.4 Traditional data analysis approach

The analysis of variance (ANOVA) is one of the most used statistical techniques for multiple comparison, focusing on analyzing variance in means (Casella and Berger et al., 2002). Previous study used *one-way ANOVA model* (in the following texts, we briefly call it as ANOVA model) based multiple comparison approaches for soil and earthworm concentration analysis (Anderson et al., 2020). In terms of the experimental dataset, ANOVA model can be expressed as follows:

$$C_{ij} = \theta_j + \epsilon_{ij} \qquad \text{Eqn. } 5-2$$

where i refers to index of sample, and $i = 1,2 \ldots n_j$. n_j is the sample size of j-th plot. j refers to index of plot, and $j = 1,2 \ldots J$. J is the total number of plots, and in current study, n_j = 3 and J = 7. C_{ij} refers to either soil or earthworm concentration of i-th sample in j-th plot; θ_j is j-th group mean and ϵ_{ij} is the corresponding error random variable. ANOVA model assumes that ϵ_{ij} are independent and follows a normal distribution with mean equal to zero and non-infinite variance, i.e. $\mathrm{E}\epsilon_{ij} = 0, \mathrm{Var}\epsilon_{ij} = \sigma^2 < \infty$ (Casella and Berger et al., 2002). Thus, this model can also be expressed in an alternative form:

$$C_{ij} \sim N(\theta_j, \sigma^2) \qquad \text{Eqn. } 5-3$$

In **Eqn. 5-3**, σ^2 can be estimated by pooled variance of each plot:

$$\hat{\sigma}^2 = \frac{1}{N-J}\sum_{j=1}^{J}\sum_{i=1}^{n_j}\left(C_{ij} - \bar{C}_j\right)^2 \qquad \text{Eqn. } 5-4$$

where N is the total sample size; $\bar{C}_j$ is the concentration mean of j-th plot, and it is also the estimate of θ_j:

$$\hat{\theta}_j = \bar{C_j} = \frac{1}{n_j}\sum_{i=1}^{n_j} C_{ij} \qquad \text{Eqn. } 5-5$$

2.5 Bayesian hierarchical modelling and assumptions

Based on previous studies, contaminant concentrations in soil and earthworm were usually positively skewed and thus log-transformed to remove skewness for further data analysis and modeling (Gish, 1970; Gish and Hughes, 1982; Cocchi et al., 2007; Goyal et al., 2005; Aelion et al., 2009; Azim et al., 2011; Banerjee et al., 2014; Arhonditsis et al., 2007; Kim et al., 2011; Zhang et al., 2011; Tao et al., 2008; Niazi et al., 2011; Saito and Goovaerts et al., 2000; Esmen and Hammad, 1977). In addition, by assuming log-normal distribution, contaminant concentration as a random variable is ensured to be positive, which addresses the discontinuity issue. Therefore, it was assumed that contaminant concentrations in soil and earthworm were log-normally distributed.

For each treatment or control at a certain sampling period, a hierarchical structure of analysis of soil concentration was developed to predict the posterior probability distribution of soil concentrations, shown as follows:

$$\log C_{s_{ij}} \sim N\left(\theta_{sj}, \sigma_{sj}^2\right) \qquad \text{Eqn. } 5-6$$

$$\theta_{sj} \sim N(\mu_s, \tau_s^2) \qquad \text{Eqn. } 5-7$$

$$\mu_s \sim N(m_s, s_s^2) \qquad \text{Eqn. } 5-8$$

$$\sigma_{sj}^2 \sim IG\left(a_{sj}, b_{sj}\right) \qquad \text{Eqn. } 5-9$$

$$\tau_s^2 \sim IG(c_s, d_s) \qquad \text{Eqn. } 5-10$$

where $C_{s_{ij}}$ is contaminant concentration in soil, i refers to the i-th sample and j refers to the j-th

plot. θ_{sj} is the group mean of $\log C_{sij}$, i.e. average log-transformed soil concentration of the j-th plot, and σ_{sj}^2 is the group-specific variance of $\log C_{s_{ij}}$. For θ_{sj}, it was assumed that the group means, θ_{sj}'s, were independent and follows a normal distribution with mean, μ_s, and variance, τ_s^2. The hyperprior distribution for the grand mean was assumed to be normal distribution with mean, m_s, and variance, s_s^2. Without prior knowledge, the vague hyperprior is used, i.e. $m_s = 0$ and $s_s^2 = 10000$ (Qian et al., 2004). The hyperprior for within-plot variance and between-plot variance are inverse-gamma distributions with parameters a_{sj} and b_{sj}, c_s and d_s, respectively. Again, without prior knowledge, the vague hyperprior is used, i.e. $a_{sj} = b_{sj} = c_s = d_s = 0.001$ (Qian et al., 2004).

In terms of earthworm concentration of contaminant at a certain sampling period, for each treatment or control, we assumed that earthworm concentration follows the same hierarchical structure, which can be expressed as:

$$\log C_{e_{ij}} \sim N\left(\theta_{ej}, \sigma_{ej}^2\right) \qquad \text{Eqn. } 5-11$$

$$\theta_{ej} \sim N(\mu_e, \tau_e^2) \qquad \text{Eqn. } 5-12$$

$$\mu_e \sim N(m_e, s_e^2) \qquad \text{Eqn. } 5-13$$

$$\sigma_{ej}^2 \sim IG\left(a_{ej}, b_{ej}\right) \qquad \text{Eqn. } 5-14$$

$$\tau_e^2 \sim IG(c_e, d_e) \qquad \text{Eqn. } 5-15$$

where C_{eij} is earthworm concentration of contaminant, i refers to the i-th sample and j refers to the j-th plot. θ_{ej} is the mean of $\log C_{eij}$, and σ_{ej}^2 is the group-specific variance of $\log C_{eij}$. θ_{ej} follow a normal distribution with mean μ_e and variance τ_e^2. Again, vague hyperprior distributions were used for all the hyperparameters as the same to soil's.

2.6 Parameter estimation for Bayesian hierarchical model

Parameter estimation of the model was conducted under Bayesian framework, which has been widely used in many fields (Gelman and Hill, 2006; Cocchi et al., 2007; Goyal et al., 2005; Aelion et al., 2009; Azim et al., 2011; Banerjee et al., 2014; Billoir et al., 2008; Delignette et al., 2017; Tan et al., 2017; Øverjordet et al., 2018). It treats each parameter as a random variable, and thus allows to combine prior information in the model applications and explicitly handle the uncertainty of parameter (Azim et al., 2011; Arhonditsis et al., 2007; Kim et al, 2011). Parameters in the model can be estimated under Bayesian framework:

$$\pi(\theta|D) = \frac{\pi(\theta) \cdot \pi(D|\theta)}{\int_{\theta} \pi(\theta) \cdot \pi(D|\theta) \mathrm{d}\theta} \qquad \text{Eqn. } 5-16$$

where θ is the parameter of interest and D is the observed data, i.e., soil and earthworm concentrations. $\pi(\theta)$ refers to the *prior probability distribution* of θ, which represents the prior knowledge. $\pi(D|\theta)$ is the likelihood function of data given different θ values. $\pi(\theta|D)$ is the *posterior probability distribution*, which represents the beliefs on θ after obtaining data, D. Markov Chain Monte Carlo (MCMC) simulation is a general numerical methodology for model fitting and parameter estimation for high dimensional problems (Andrieu et al., 2003), and it has been widely applied in environmental field especially under Bayesian framework (Goyal et al., 2005; Azim et al., 2011; Kim et al., 2011; Øverjordet et al., 2018; Andrieu et al., 2003; Stow et el., 2004; Görlitz et al., 2011; Hong and Gurian , 2011; Rieckermann et al., 2011; Loos et al.. 2012; Weijs et al., 2013; Oldenkamp et al., 2015). In current research, Gibbs sampler was used for generating posterior distribution, details of Gibbs sampler see **Supplementary Information**.

2.7 Model validation and performance evaluation

There is no general consensus on model validation and comparison, but the most commonly sought model characteristic on model selection is predictive ability (Hooten and Hobbs, 2015). Predictive ability of a model can be evaluated by cross-validation (Link and Sauer, 2016), and thus both traditional model and BHM were validated by leave-one-out cross-validation (LOO-CV) to evaluate out-of-sample predictive accuracy (Gelman et al., 2014; Hooten and Hobbs, 2015).

Due to the fact that parameters of the models are different by contaminant, sampling time, treatment and medium, dataset was divided into sub-datasets, i.e., one sub-dataset included the concentration data of a given contaminant (DDx, dieldrin), sampling period (TP, T6, T12, T18), treatment ("No Till", "Till", "2YC", "4MC") and medium (soil, earthworm), and LOO-CV was conducted to each sub-dataset. Therefore, for a given contaminant and given medium combination (e.g. DDx concentration in soil), there were 4 × 4 = 16 sub-datasets (four sampling times and four treatments), and each sub-datasets contained 3 × 7 = 21 concentration data (three measurements in each subplot and seven (sub)plots), regardless of missing data.

Squared error is the most widely used scoring function to evaluate point estimate (Gneiting, 2011), and thus, the predictive accuracy was quantified by *normalized mean standard error* (*NMSE*), which is defined as follows:

$$NMSE = \frac{\overline{\left(C_{\mathrm{o}} - C_{\mathrm{p}}\right)^2}}{\bar{C}_{\mathrm{o}} \cdot \bar{C}_{\mathrm{p}}} \qquad \text{Eqn. } 5-16$$

where C_{o} refers to observed concentration of the contaminant (mg/kg); C_{p} refers to model-predicted concentration of the contaminant (μg/g); "overbar" refers to the average over data set. For a given sub-dataset, *NMSE* was calculated. On the other hand, *NMSE* is a squared variable, which is not supposed to be normally distributed, but follows a Chi-square distribution. In order

to eliminate the potential skewness for further statistical analysis, the square root of *NMSE* was also calculated for each sub-dataset, noted as $\sqrt{NMSE}$.

Akaike information criterion (*AIC*) and Bayesian information criterion (*BIC*) were also calculated based on each sub-dataset (Gelman et al., 2014). Akaike information criterion is calculated by (Akaike, 1974):

$$AIC = -2\log p\left(D|\hat{\theta}_{\text{mle}}\right) + 2k \qquad \text{Eqn. } 5-17$$

where k refers to number of independent parameters; $\hat{\theta}_{\text{mle}}$ is maximum likelihood estimate of θ, which is the parameter of the model; D refers to observed data, and $\log p\left(D|\hat{\theta}_{\text{mle}}\right)$ is the log-likelihood function. Bayesian information criterion (BIC) is calculated by (Schwarz, 1978):

$$BIC = -2\log p\left(D|\hat{\theta}\right) + 2k\log n \qquad \text{Eqn. } 5-18$$

where $\hat{\theta}$ is point estimate of parameter; n refers to the number of observations in D, or equivalently, sample size.

2.8 Descriptive statistics of data properties

The properties of the dataset may influence the goodness of fit and predictive accuracy of the models. Therefore, the relation between properties of the dataset and model performance was investigated. Since large observational uncertainty of data may lead to bias of estimation and further may further bias the model prediction, observational uncertainty was considered as an important factor of parameter estimation and model performance. A good descriptive statistic of observational uncertainty was standard deviation, but the concentration data had large spatial variability. Therefore, normalized standard deviation, i.e., coefficient of variation (*CV*), was a better measure. After preliminary trials, *average coefficient of variation* and *standard deviation*

of coefficient of variation showed a significant linear relation with model performance, and thus the correlations were further investigated.

For a certain treatment (No Till, Till, 2YC, 4MC) at a certain sampling time (TP, T6, T12, T18), *CV* of the *j*-th plot is defined as:

$$CV_j = \frac{\sigma_j}{\mu_j} \qquad \text{Eqn. } 5-19$$

where μ_j and σ_j are the mean and standard deviation of the *j*-th subplot (*j* = 1,2,3,4,5,6,7). Then, the average CV_j's of the seven plots was calculated, which represents the average relative observational error of the dataset. The average *CV*, noted as $\overline{CV}$, is calculated by:

$$\overline{CV} = \frac{1}{J}\sum_{j=1}^{J} CV_j \qquad \text{Eqn. } 5-20$$

where *J* is the total number of subplots, and $J = 7$ for current experiment. On the other hand, standard deviation of *CV* represented the uncertainty of the uncertainty, noted as S_{CV}, is the standard deviation of the CV_j values.

2.9 Calculation of bioaccumulation

Bioaccumulation factor (*BAF*) of the *j*-th plot can be calculated by contaminant concentrations in soil (C_{sj}) and contaminant concentration in earthworm (C_{ej}) of the same plot (Anderson et al., 2020):

$$BAF_j = \frac{C_{ej}}{C_{sj}} \qquad \text{Eqn. } 5-21$$

where BAF_j refers to bioaccumulation factor of the *j*-the plot. Then, natural logarithm can be taken for both sides, then we have:

$$\log BAF_j = \log \frac{C_{ej}}{C_{sj}}$$

$$\Rightarrow \log BAF_j = \log C_{ej} - \log C_{sj} \qquad \text{Eqn. } 5-22$$

Then, we define $\overline{\log BAF_j}$ as mean of $\log BAF_j$, and it can be calculated by following:

$$\overline{\log BAF_j} = \overline{\log C_{ej}} - \overline{\log C_{sj}} \qquad \text{Eqn. } 5-23$$

where $\overline{\log C_{sj}}$ and $\overline{\log C_{ej}}$ are means of log-transformed C_{ej} and C_{sj}. Based on assumptions of BHM, $\overline{\log C_{sj}}$ is estimated by $\bar{\theta}_{sj}$, and $\overline{\log C_{ej}}$ is estimated by $\bar{\theta}_{ej}$, where the conditional distribution of $\bar{\theta}_{sj}$ and $\bar{\theta}_{ej}$ can be expressed as:

$$\bar{\theta}_{sj} \sim N(\theta_{sj}, V_{sj}) \qquad \text{Eqn. } 5-24$$

$$\bar{\theta}_{ej} \sim N(\theta_{ej}, V_{ej}) \qquad \text{Eqn. } 5-25$$

In **Eqn. 5-24** and **Eqn. 5-25**, V_{sj} and V_{ej} are variance of $\bar{\theta}_{sj}$ and $\bar{\theta}_{ej}$, and they can be calculated by $V_{sj} = 1/\left(\frac{1}{\tau_s^2} + \frac{n_{sj}}{\sigma_{sj}^2}\right)$ and $V_{ej} = 1/\left(\frac{1}{\tau_e^2} + \frac{n_{ej}}{\sigma_{ej}^2}\right)$. n_{sj} and n_{ej} are the soil and earthworm sample size of the *j*-th plot.

Therefore, $\overline{\log BAF_j}$ is calculated by posterior samples of θ_{sj}, θ_{ej}, τ_s^2, τ_e^2, σ_{sj}^2, σ_{ej}^2 and known constant n_{sj} and n_{ej}:

$$\overline{\log BAF_j} \sim N(\theta_{ej} - \theta_{sj}, V_{ej} + V_{sj}) \qquad \text{Eqn. } 5-26$$

In current study, the $\overline{\log BAF_j}$ was used to quantify bioaccumulation.

2.10 Effectiveness of compost remediation

Due to the fact that only plot #1, #3 and #7 have samples over the four sampling periods, we proposed that combing all the seven plots to evaluate effectiveness of compost may introduce bias. Thus, only plot #1, #3 and #7 were used for further analysis after applying BHM for

parameter estimation.

In order to directly compare the effect of different treatments, normalization was applied to log-transformed *BAF*. Bioaccumulation at pre-application (TP) was used as a *reference*, and bioaccumulation at other sampling time points were normalized by the reference. Normalized log-transformed *BAF* was calculated by:

$$N_{\overline{\log BAF}_j,\mathrm{T}i,tr} = \frac{\overline{\log BAF}_{j,\mathrm{T}i,tr}}{\overline{\log BAF}_{j,\mathrm{TP},tr}} \qquad \text{Eqn. } 5-27$$

where $N_{\overline{\log BAF}_j,\mathrm{T}i,tr}$ is normalized log-transformed *BAF* of the *j*-th plot (*j* = 1, 3, 7) at time point T*i* (*i* = P, 6, 12, 18) and *tr* refers to treatment type (tr = "No Till", "Till", "2YC" and "4MC"). $\overline{\log BAF}_{j,\mathrm{T}i,tr}$ is the mean of $\log BAF_j$ of the *j*-th plot (*j* = 1, 3, 7) at time point T*i* (*i* = P, 6, 12, 18) and *tr* refers to treatment type. $\overline{\log BAF}_{j,\mathrm{TP},tr}$ refers to the corresponding *reference*.

The net effect of treatments was also investigated by calculating difference between a treatment and a control (Anderson et al., 2020). In previous study, net effect of compost was calculated by treatment minus control till. This calculation assumed that effects of tillage and compost are addictive. However, the effects may not be addictive, and the total effect of tilling and compost is better evaluated together. Therefore, net effects of tillage and different kinds of composts were evaluated by followings:

$$\Delta_{\overline{\log BAF}_j,\mathrm{T}i,\mathrm{Till}} = N_{\overline{\log BAF}_j,\mathrm{T}i,\mathrm{Till}} - N_{\overline{\log BAF}_j,\mathrm{T}i,\mathrm{NoTill}} \qquad \text{Eqn. } 5-28$$

$$\Delta_{\overline{\log BAF}_j,\mathrm{T}i,\mathrm{2YC}} = N_{\overline{\log BAF}_j,\mathrm{T}i,\mathrm{2YC}} - N_{\overline{\log BAF}_j,\mathrm{T}i,\mathrm{NoTill}} \qquad \text{Eqn. } 5-29$$

$$\Delta_{\overline{\log BAF}_j,\mathrm{T}i,\mathrm{4MC}} = N_{\overline{\log BAF}_j,\mathrm{T}i,\mathrm{4MC}} - N_{\overline{\log BAF}_j,\mathrm{T}i,\mathrm{NoTill}} \qquad \text{Eqn. } 5-30$$

where $\Delta_{\overline{\log BAF}_j,\mathrm{T}i,\mathrm{Till}}$, $\Delta_{\overline{\log BAF}_j|\mathrm{T}i|\mathrm{2YC}}$ and $\Delta_{\overline{\log BAF}_j,\mathrm{T}i,\mathrm{4MC}}$ refer to the change in log-transformed *BAF* of the *j*-th plot at Ti in terms of tillage, 2-year compost and 4-month compost.

2.11 Statistics and data analysis

Normal approximation was performed by assuming samples are representative of the true distribution. Median of posterior distribution was used as a point estimate of a parameter, and the 95% *highest density interval* (HDI) were calculated as 95% *credible interval* (95% CI) (Chen et al., 2012). Comparison of two variables was based on Student's *t*-test at significance level of $p < 0.05$, and if two variables were from Bayesian models, then comparison was calculated based on 95% CI (Kruschke, 2013). Mean, median, variance, standard deviation, coefficient of variance, and linear regression and Pearson correlation coefficient were calculated by Microsoft Excel (2016) and Matlab R2019b (The MathWorks, Inc. Natick, MA). Model fitting and predictions were encoded in Matlab. Plots were done in Microsoft Excel and Matlab.

3. Results and Discussion

3.1 MCMC simulation and model sensitivity

Data of each subplot was summarized in **SI Table 5-2** and **SI Table 5-3**. During simulations, 150000 runs were used for parameter estimation, and convergence was checked by trace plot, cumulative running mean and autocorrelation. After burn-in and thinning, there are 20000 posterior samples of each parameter. The diagnosis plots of μ_e of Till at T6 as an example are shown in **SI Figure 5-5**. The sensitivity of BHM to priors were also investigated, and the results showed that BHM was not sensitive to priors (**SI Figure 5-6**, for more details see **Supplementary Information**).

3.2 Comparison between BHM and traditional approach

The out-of-sample model-predicted concentration of DDx and dieldrin were calculated by both models, and model-predicted concentration versus observed concentration are show in **Figure 5-2**. Then, the model performance statistics between two models was also calculated, and the results are summarized in **SI Table 5-4**.

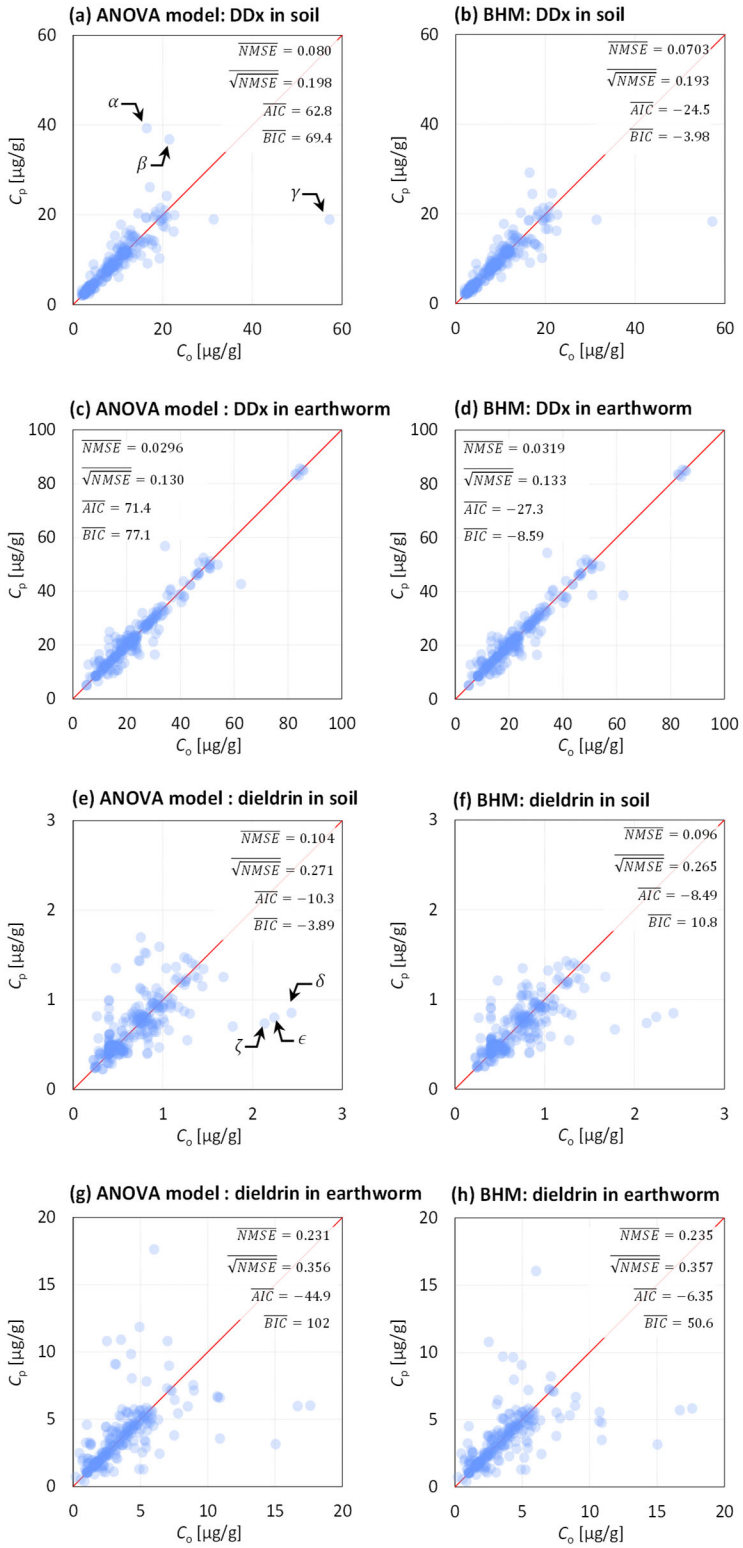

Figure 5-2 Scatter plot of observed concentration of C_o versus out-of-sample model-predicted concentration of C_o refers to observation and C_p refers to out-of-sample prediction. Solid lines refer to 1:1 ratio. *NMSE* refers to normalized mean square error. *AIC* and *BIC* refer to average Akaike information criterion and Bayesian information criterion. Over bar refers to average over the 16 sub-datasets. respectively. α, β, γ, δ, ε and ζ are the labelled points discussed in **Section 3.2**.

For DDx concentration in soil, both $NMSE$ and $\sqrt{NMSE}$ were relative smaller for the BHM, but the difference was not significant. On the other hand, *AIC* and *BIC* of the BHM were significantly smaller ($p < 0.001$), indicating a better fit by the BHM. Such a difference was mainly due to different ways of handling information by two models. The traditional model only utilized data information within group (subplot), while BHM also utilized data information from other groups (subplots) through its hierarchical structure. The most typical example were the two points labelled as α and β in **Figure 5-2a and 5-2b**, which corresponded to DDx concentration in soil of the subplot treated by "No Till" at T6 in plot #3 (**SI Table 5-5**). The three observed concentration of the subplot were α_{obs} = 21.48 (μg/g), β_{obs} = 16.45 (μg/g), and the third one was 57.22 (μg/g) (labelled as γ in **Figure 5-2a, SI Table 5-5**). During LOO-CV, the BHM predicted concentration for α and β (α_{BHM} = 24.26 (μg/g), β_{BHM} = 29.21 (μg/g)) were closer to observation than ANOVA model predicted concentration of α and β (α_{ANOVA} = 36.83 (μg/g), β_{ANOBA} = 39.35 (μg/g)). Although the third observation of 57.22 (μg/g) could raise the predictions during LOO-CV, observed concentrations from other plots were low (average concentration of other plots is 8.90 (μg/g)), which lowered the predicted concentration of α and β by the BHM. Furthermore, for the third observed concentration in the subplot, 57.22 (μg/g), it was much larger than any other observations, which substantially increased the standard deviation and lowered the accuracy. Consequently, during LOO-CV, the BHM assigned less weight to information from its own plot but more weight to information from other plots, which lowered the predicted concentration of α and β. As a result, these two predictions of BHM were closer to observations than the ANOVA model.

On the other hand, both models had poor out-of-sample prediction on γ (γ_{obs} = 57.22 (μg/g), γ_{ANOVA} = 18.96 (μg/g), γ_{BHM} = 18.34 (μg/g)) in **Figure 5-2a and 2b**. This was due to systematic

error of both models, i.e., both models could hardly predict extremely large or small values. Based on the data (**SI Table 5-5**), it was unlikely to have a measurement to be as large as 57.22 (μg/g), and thus both models were unable to have good prediction on γ. In summary, although both models had systematic error, relative smaller *NMSE* and $\sqrt{NMSE}$ and significant smaller *AIC* and *BIC* of BHM suggested that BHM was the preferred model for DDx concentration in soil.

For dieldrin concentration in soil, both *NMSE* and $\sqrt{NMSE}$ were relative smaller for the BHM, but the difference was not significant. *AIC* of the ANOVA model was smaller but not significant while *BIC* of the ANOVA model was significantly smaller ($p = 0.002$), suggesting that the ANOVA model would better be the preferred model. The insignificance of *AIC* and significance of *BIC* values were due to internal difference of the two information criterions, where *BIC* had an additional term $\log n$ in **Eqn. 5-18**. This term made *BIC* lean towards a preferred model with a smaller number of parameters, i.e., simpler model, when there were more than eight observations (Schwarz, 1978). In current study, each sub-dataset had about 21 concentration data, and thus ANOVA model was identified for its less parameters. Additionally, similar to DDx, both plots also had several points due to systematic errors, which, for example, were labelled as δ, ε and ζ in **Figure 5-2e**. All of them corresponded to much greater concentrations not only within subplots but also among other subplots (**SI Table 5-4**). In summary, although three out of four statistics showed no significant difference, the ANOVA model was determined as the preferred model.

In terms of DDx and dieldrin concentrations in earthworm, *NMSE* and $\sqrt{NMSE}$ values were not significantly different between two models (**Figure 5-2c, 2d, 2e, 2f** and **SI Table 5-4**). On

the other hand, *AIC* and *BIC* values of the BHM were significantly smaller, respectively ($p < 0.01$), which suggested that the BHM was the preferred model.

In general, 9/16 of the tests showed no preference, 6/16 of the tests indicated preference of the BHM, and 1/16 of the tests suggested the ANOVA model. Therefore, the BHM was determined as the preferred model for data analysis.

3.3 Relation between data properties and model performance

The relation between data properties and statistics of model performance (i.e., *NMSE*, $\sqrt{NMSE}$, *AIC* and *BIC*) was investigated, and preliminary trials showed that both $\overline{CV}$ and S_{CV} had significant correlation with model performance. However, $\overline{CV}$ and S_{CV} were found highly correlated (**SI Figure 5-7** and **Supplementary Information** a for possible explanation). Thus, linear regression was applied only between $\overline{CV}$ (as explanatory variable) and the statistics of model performance (as the response).

As discussed in **Section 2.8**, $\overline{CV}$ represents the average relative observational error of the dataset, slope of the regression line refers to the change of normalized predictive accuracy of the model in response to increased observational uncertainty of the data. Intercept of the regression line refers to predictive accuracy value when observational uncertainty equals to zero, i.e., $\overline{CV} = 0$. However, for a dataset, it is impossible to have measurements with perfect precision and zero standard deviation. Thus, intercept is interpreted as the limiting predictive accuracy of the model as observations become perfectly precise.

By putting two regression lines of the BHM and the ANOVA model together in one plot, the possible geometric relations between two regression lines have three typical types (**Figure 5-3a, 3b, 3c**). For type I (**Figure 5-3a**), where regression line of model A is consistently above than

regression line of model B, it suggests that the predictive accuracy of model B is consistently better than model A. For example, *BIC* of DDx concentration in soil of the two models showed such relation (**Figure 5-4a**), where the regression lines of the ANOVA model were consistently above the regression lines of the BHM, indicating smaller predictive errors from the BHM. For type II (**Figure 5-3b**), where two regression lines intersect, the corresponding $\overline{CV}$ value was defined as the critical value of $\overline{CV}$ (noted as $\overline{CV}_{\text{critical}}$). Type II suggests that the predictive accuracy of model B is better when $\overline{CV} < \overline{CV}_{\text{critical}}$, and predictive accuracy of model A is better when $\overline{CV} > \overline{CV}_{\text{critical}}$, meaning that each model has its own advantage depending on amplitude of the observational uncertainty. For example, *AIC* of dieldrin concentration in soil of the two models showed such relation (**Figure 5-4b**). As $\overline{CV}$ > 0.17, *AIC* of the BHM was smaller while as $\overline{CV}$ < 0.17, *AIC* of the ANOVA model was smaller, indicating the ANOVA model appears to have relative smaller predictive error for data with smaller observational uncertainty while the BHM appeared to have relative smaller predictive error for data with greater observational uncertainty. For type III (**Figure 5-3c**), the two regression lines are overlapped, suggesting no difference between two models. For example, $\sqrt{NMSE}$ of dieldrin concentration in earthworm of the two models showed such relation (**Figure 5-4c**), where regression lines of the two models were indistinguishable.

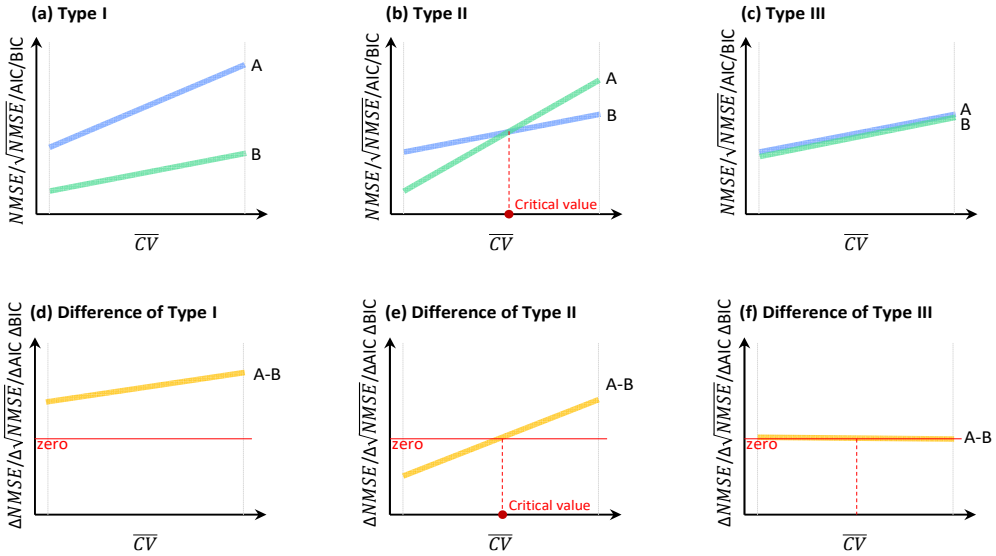

Figure 5-3 Demonstration of three types of relation and difference between two regression curves. Model A and model B refers to two models. Differences of $NMSE$, $\sqrt{NMSE}$, AIC and BIC between two models were calculated by model A minus model B:$\Delta NMSE = NMSE_{\mathrm{A}} - NMSE_{\mathrm{B}}$; $\Delta\sqrt{NMSE} = \sqrt{NMSE}_{\mathrm{A}} - \sqrt{NMSE}_{\mathrm{B}}$; $\Delta AIC = AIC_{\mathrm{A}} - AIC_{\mathrm{B}}$; $\Delta BIC = BIC_{\mathrm{A}} - BIC_{\mathrm{B}}$, where subscript refers to the model. According to the definitions of these statistics, if the difference is negative, then model A has better predictive accuracy; if the difference is positive, then model B has better predictive accuracy.

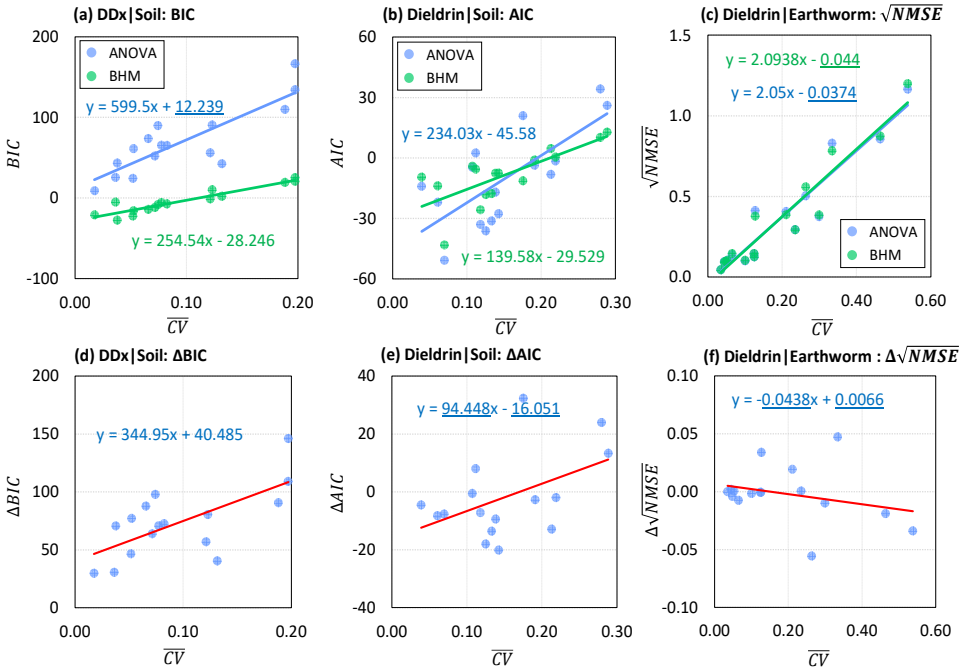

Figure 5-4 Typical data corresponding to the three types in **Figure 5-3**. Differences of $\sqrt{NMSE}$, AIC and BIC between two models were calculated by "ANOVA" minus "BHM":$\Delta\sqrt{NMSE} = \sqrt{NMSE}_{\mathrm{ANOVA}} - \sqrt{NMSE}_{\mathrm{BHM}}$; $\Delta AIC = AIC_{\mathrm{ANOVA}} - AIC_{\mathrm{BHM}}$; $\Delta BIC = BIC_{\mathrm{ANOVA}} - BIC_{\mathrm{BHM}}$, where subscript refers to the model. Regression coefficient with underline refers to not significantly different from zero at α = 0.05. According to the definitions of these statistics, if the difference is negative, then ANOVA model has better predictive accuracy; if the difference is positive, then BHM has better predictive accuracy.

However, due to that fact that two regression lines of statistics of performance were calculated by the same dataset, the parameters of the regression lines were non-independent. Therefore, pair-wise differences of *NMSE*, $\sqrt{NMSE}$, *AIC* and *BIC* were also calculated. The difference was defined as the statistics of the ANOVA model minus the corresponding statistics of the BHM model. The relations between $\overline{CV}$ and the differences were investigated by linear regression (**Figure 5-3d, 3e 3f**). Here, slope refers to the change of normalized predictive accuracy difference in response to increase of average relative data variation and variability. Intercept refers to the limiting predictive accuracy difference between two models as the experimental data gets perfectly precise. If slope is not significantly different from zero, then the intercept can be interpreted as the difference between two models over all range of $\overline{CV}$, and such difference does not change with data precision. In addition, if the regression line is above zero, then model B has better predictive accuracy; if the line is below zero, then model A has better predictive accuracy.

For the difference of Type I relation (**Figure 5-3d**, **Figure 5-4d**)**,** where the slope and intercept were both significantly greater than zero, suggested that the advantage of the BHM over the ANOVA model increased with increased observational uncertainty of the data. For the difference in corresponding to Type II relation (**Figure 5-3e**, **Figure 5-4e**)**,** where the regression line went across zero at $\overline{CV} \approx 0.17$, suggested that the ANOVA model was preferred for $\overline{CV} < 0.17$ and the BHM was better for $\overline{CV} > 0.17$. However, none of the regression parameters of ΔAIC was significantly different from zero, indicating that such preference was not significant based on current data set. For the difference in corresponding to Type III relation (**Figure 5-3f**, **Figure 5-4f)**, where the slope and intercept were close to zero, showed that the performance of the two models are almost identical.

A comprehensive discussion of the whole dataset (**SI Figure 5-8 to SI Figure 5-15**) is in **Supplementary Information**. Based on the discussion, it was found that model performance decreased with observational uncertainties, and in general, both models had advantages and disadvantages. The ANOVA model was simple and easy to use while the BHM, by using information across all replicates within a treatment, was more robust to data with high observational uncertainty. In this current study, the contaminant data had great spatial variability and therefore the BHM was used for further data analysis.

A comprehensive discussion on the whole dataset (**SI Figure 5-8 to SI Figure 5-15**) is in **Supplementary Information**. Based on the discussion, it was found model performance decreased with observational uncertainties, and in general, both models had advantages and disadvantages. The ANOVA model was simple and easy to use while the BHM, by using information across all replicates within a treatment, was more robust to data with high observational uncertainty. In this current study, the contaminant data had great spatial variability and therefore the BHM was used for further data analysis.

3.4 Bioaccumulation change with time

Although there were seven plots in total, only three of the seven plots with four sampling periods were used for remediation analysis to eliminate bias. Normalized log-transformed *BAF* ($N_{\overline{\log BAF}}$) change with time was calculated and analyzed shown in **Figure 5-5** (for individual plot see **SI Figure 5-16** and **SI Figure 5-17**).

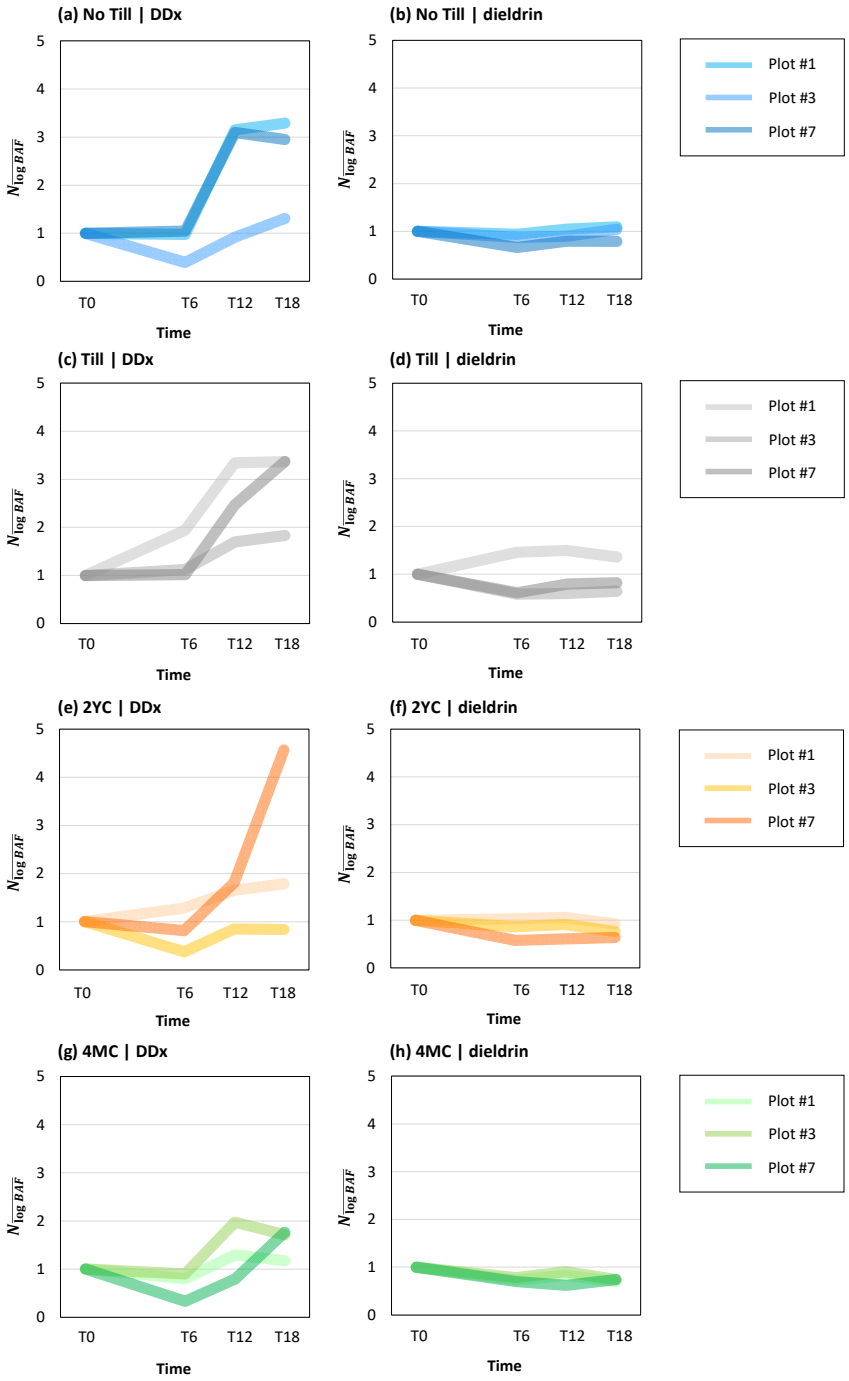

Figure 5-5 Normalized log-transformed *BAF* change with time. $N_{\overline{\log BAF}}$ refers to Normalized log-transformed BAF. Details of each plot see **SI Figure 5-16, SI Figure 5-17**.

For bioaccumulation of DDx of controls, theoretically it was expected that bioaccumulation did not have significant change over time due to equilibrium. However, plot #1 and #7 had

significant increase of bioaccumulation between T6 and T12. This was probably due to spatial variability (Anderson et al., 2020) and disturbance from environment, such as rainfall, temperature and etc (Gish and Hughes, 1982; Beyer and Gale, 2013). In addition, this could also be due to establishment of silt fence, where soil was disturbed during this process even if there were no treatment applied. For plots treated with tillage, bioaccumulation of DDx appeared to increase, but only significant for plot #3. This could also be due to spatial variability and disturbance of environment. However, if putting together with control "No Till", it could possibly be explained by disturbance of soil, where soil was aerated during establishment of silt fence and tillage. Thus, aeration could be the possible reason for increased bioaccumulation, but further confirmation was needed by evaluating more data. In addition, bioaccumulation of DDx of the plots that were treated by 2YC and 4MC showed less extent of increase, except for a rapid rise of 2YC treated plot #7. Again, such significant increase was most likely due to spatial variability and disturbance from environment.

Bioaccumulation of dieldrin showed less extent of fluctuation than bioaccumulation of DDx (note that all *y*-axis in **Figure 5-5** has the same range). Neither for control nor treatment, no significant difference was identified among dieldrin data.

Overall, bioaccumulation of DDx has greater temporal variability than bioaccumulation of dieldrin. This could probably due to the fact that uptake of DDx is more sensitive to disturbance of soil, but to our knowledge, no literature about sensitivity of uptakes of DDx or dieldrin was found. Thus, future work could investigate the sensitivity of uptake and bioaccumulation process among different organic pollutants.

3.5 Net effect of composting

Change in normalized log-transformed *BAF* performed as an additional way to evaluate the net effect of treatments. Different from previous study (Anderson et al., 2020), the effects of tillage and CM amendments were not assumed to be additional, i.e., the total effect applying a CM amendment to soil was not simply the addition of net effect of tillage and net effect of amendments. Additionally, applying an amendment was naturally coupled with tillage. Thus, the net effect of applying composting was directly calculated by the difference between treatment minus control (i.e., no till). Change in normalized log-transformed BAF ($\Delta_{\overline{\log BAF}}$) change with time was calculated and analyzed shown in **Figure5- 6** (for individual plot see **SI Figure 5-18** and **SI Figure 5-19**).

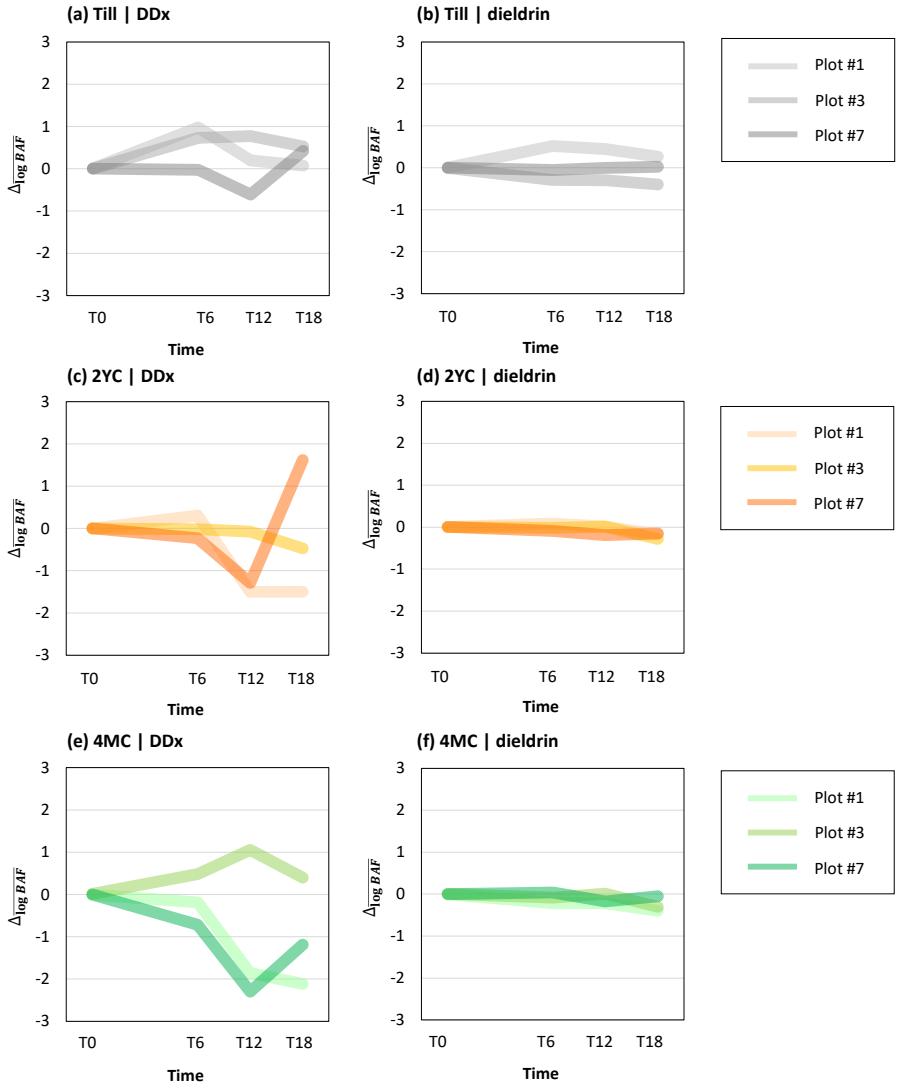

Figure 5-6 Change in log-transformed *BAF* change with time. $\Delta_{\overline{\log BAF}}$ refers to change in log-transformed BAF. Details of each plot see **SI Figure 5-18 and SI Figure 5-19**.

In terms of DDx, for plots treated with tillage, only $\Delta_{\overline{\log BAF}}$ of plot #3 at T12 had significant increase, which suggested that the change of bioaccumulation over time was less likely due to aeration of soil, but influence of environment. For 2YC treatment, bioaccumulation of DDx showed mixed effects. Plot #1 showed significant reduction of BAF, plot #3 showed no significant effect, and plot #7 showed significant reduction followed by a significant rise. For 4MC treatment, bioaccumulation of DDx also showed mixed effects. Plot #1 and #7 showed significant reduction while plot #3 showed increase at T12 but dropped back at T18.

For dieldrin, no significant effect for tillage, but there were some significant reductions for compost treatment, such as reduction at T12 of plot #7 for 2YC and reduction at T18 of plot #1 for 4MC.

In general, net effect on bioaccumulation change over time of dieldrin had smaller fluctuation than DDx. There were some evidence showing reduction potential by compost, but long-term data were needed to confirm its effectiveness.

4. Conclusion

Field study is an important step for soil remediation studies. However, field data often has great variability, which makes data analysis problematic. Here, the BHM was applied to a previous field plot study dataset to characterize contaminant concentration in soil, earthworm and bioaccumulation, and compared with traditional one-way ANOVA model. Validation results showed that the BHM outperformed traditional ANOVA model and was determined as the preferred model for data analysis due smaller predictive accuracy. The smaller predictive accuracy of the BHM is due to its ability to utilize data information among groups (subplots) through its hierarchical structure and increased predictive accuracy while the traditional model only utilizes data information within group (subplot). In addition, predictive accuracy of both models appeared to decrease with increased observational uncertainty, but the BHM was more robust and had greater predictive accuracy for data with high observational uncertainty. A greater temporal variability of bioaccumulation of DDx over dieldrin was found. Inferential results showed that there were some evidence showing reduction potential by the compost, but long-term data are needed to confirm its effectiveness. The developed BHM is recommended for other environmental studies that has similar hieratical structure and large variability.

Chapter 6 Conclusions

In this dissertation, advanced statistical methods were applied to solve problems in the environmental research.

In the first case study (**Chapter 2**), reparameterization was applied to modify Gaussian plume model (GPM) to predict dispersion of air pollutant emission from a ground-level active-discharge releasing source. Cross-validation was applied for model selection and comparison between original GPM and the new model by the data of a field poultry house emission experiment. The results showed that predictive accuracy of the modified GPM was greatly improved compared with original model, and the new model can be applied to other experiments and will be useful in evaluating the effectiveness of mitigation strategies for air pollutant emissions.

In the second case study (**Chapter 3**), dispersion of particulate matter (PM) from cotton gins was characterized, and a dispersion correction factor was developed by stepwise ordinary least square regression to enhance the performance of the regulatory air dispersion model (AERMOD) for low-level sources. Cross-validation was used for model comparison between AERMOD and enhanced AERMOD by field measurements. The results showed that predictive accuracy of the corrected model was greatly improved. Additionally, empirical equations for estimating dispersion correction factor was derived and recommended for practical and regulatory use.

In the third case study (**Chapter 4**), carbon amendments were applied to a historically contaminated field to investigate the feasibility for mitigating bioaccumulation under field conditions. Based on field measurements, the effect of carbon amendments on bioaccumulation and change of bioaccumulation over time were quantified and evaluated by parametric Bootstrapping method. The results showed that there were some evidences of the mitigation

effect of compost. However, due to great spatial variability of the concentrations, more data are needed to confirm the remediation effect. These experimental observations also demonstrate the necessity of developing more robust risk assessment methods, particularly for sites with high concentrations and large spatial variability, as well as the hazards of extrapolating results from the laboratory to the field.

In the last case study (**Chapter 5**), the Bayesian hierarchical model (BHM) was applied to the field measurement dataset to characterize pollutant concentrations and bioaccumulation. Cross-validation and information criteria were used to evaluate and compare predictive accuracy between the BHM and conventional one-way ANOVA model. Results suggested that the BHM is the preferred model when observational uncertainty is large and when information among groups is highly variable. Implications of remediation techniques were drawn from the posterior distributions of the BHM, and suggested that there are some evidence that treatment with compost improves DDx and dieldrin remediation in soils and reduces bioaccumulation, but longer-term observations were necessary to test this hypothesis. The developed BHM is recommended for other environmental studies that has similar hieratical structure and large variability.

These case studies demonstrate the capability of advanced statistical methods for dealing with different environmental research problems. Such statistical methods will be useful for model modification with more specific situations, for data analysis with limited sample size and/or great variability, for environmental and ecological risk assessment, for evaluation of environmental mitigation strategies, and for simulation of real-time pollutant distribution and forecasting, and for minimization of sample size to meet with the accuracy requirement and lower the cost. In conclusion, advanced statistical methods are useful tools for environmental research.

Chapter 7 Future Work

As demonstrated in the dissertation, the advanced statistical tools can be used for modification of models to better fit with specific situations by reparameterization or correction factor, for data analysis with limited sample size and great variability by applying models with complex structure, for environmental and ecological risk assessment by more explicitly handling uncertainties. In addition, these tools can also be coupled with site monitoring and modelling to simulate real-time pollutant distribution and forecast by integration of monitoring and modelling approaches, and to minimize necessary sample size to meet with the accuracy requirement and lower the cost. In this chapter, future works are presented based on the four case studies.

1 Further Modification of Gaussian Plume Model

1.1 Ununiform wind field of fan

In current study wind speed was assumed to be uniform in the modelling domain. However, since wind speed is not uniform near fan (Ozono et al., 2007), and assuming uniform wind speed leads to incorrect turbulence estimation and introduces errors for small spatial scale situation (**Figure 7-1a**). Thus, to eliminate such error, the modelling domain can be divided into sub-domains (**Figure 7-1b and 7-1c**).

In each sub-domain, the wind speed is assumed to be uniform, and the average wind speed in the sub-domains can be measured experimentally. Then, GPM can be applied multiple times to predict pollutant concentrations. Furthermore, if the size of each sub-domain, Δx, approaches to zero, i.e., $\Delta x \to 0$, then, the average wind speeds in each sub-domain, $\bar{u}_1, \bar{u}_2, \dots, \bar{u}_i, \dots$, become wind speed profile of the fan (**Figure 7-1d**). Since wind profile of a fan is determined by the fan itself, $u(x)$ can be measured experimentally and used for other experiments.

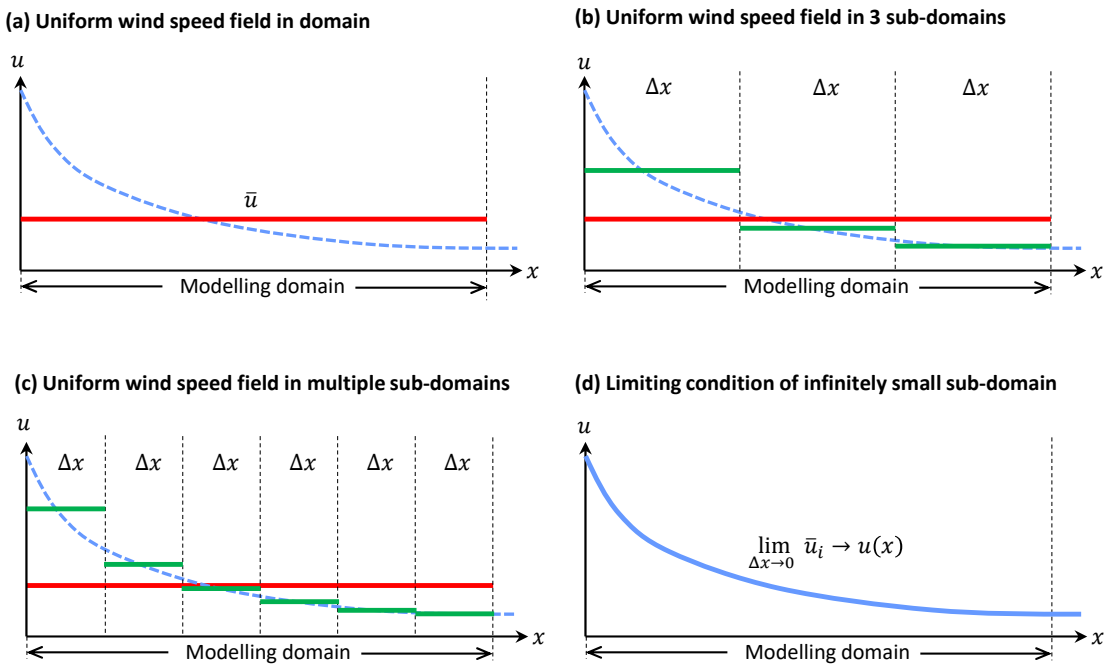

Figure 7-1 Demonstration of sub-domain. u refers to wind speed, x refers to distance from source (fan). Δx refers to the size of sub-domain, and $\bar{u}_i$ refers to the average wind speed in the i-th sub-domain. $u(x)$ is the wind speed profile of the fan

1.2 Influence of ambient wind

Previous study shows that ambient wind could change the direction of the plume from the fan (Yao et al., 2018b), and such influence introduces errors to Gaussian plume model (GPM) (**Figure 7-2**). However, such effect was not considered in current study. Therefore, it is necessary to take into account for the influence of ambient wind.

The wind field in the modelling domain can be described by:

$$\vec{u}_{\Sigma}(x, y, z, t) = \vec{u}_{\mathrm{f}}(x, y, z) + \vec{u}_{\mathrm{a}}(t) \qquad \text{Eqn. } 7-1$$

where $\vec{u}_{\Sigma}(x, y, z, t)$ is the total wind velocity, which is a function of space (x, y, z) and time (t). It is the combination of wind generated by fan and ambient wind. $\vec{u}_{\Sigma}(x, y, z)$ is the fan wind velocity. Given a certain fan, $\vec{u}_{\Sigma}$ is a function of space and can be measured experimentally. $\vec{u}_{\mathrm{a}}$ is the ambient wind velocity, and since ambient wind field can be assumed to be uniform in the domain, it is the function of time and can be monitored on site.

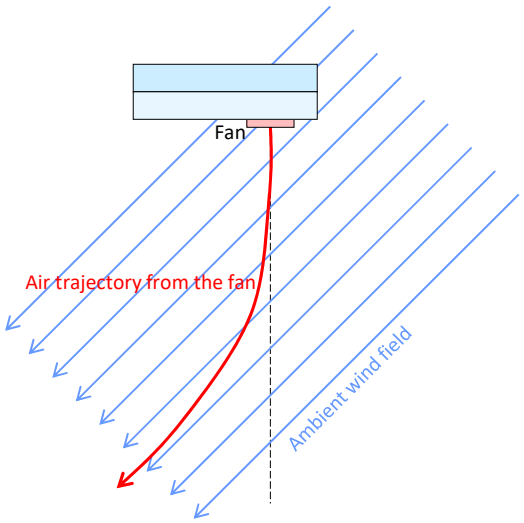

Figure 7-2 Demonstration of wind velocity combination

Thus, future work can be focused on establishment of wind profile of the fans and development of correction factors for GPM by considering ununiform wind speed and influence of ambient wind.

2 Further Validation of Dispersion Correction Factor

2.1 Extension to more gin facilities

In current study, dispersion correction factor (DCF) was developed and validated by data of one gin facility. However, if applied for other gins or low-altitude emission facilities, due to different layout of buildings, topography and environment, regression coefficients, b_i in **Eqn. 3-13, Eqn. 3-14 and Eqn. 3-15** may be different. Therefore, more data from other gin facilities is necessary for further validation of this approach.

By having data from more facilities, b_i also be modelled by Bayesian hierarchical model (BHM):

$$b_{ij} \sim N\left(\theta_{ij}, \sigma_{ij}^2\right) \qquad \text{Eqn. } 7-2$$

$$\theta_{ij} \sim N(\mu_i, \tau_i^2) \qquad \text{Eqn. } 7-3$$

where b_{ij} refers to regression coefficient of the *i*-th predictor and *j*-th gin, which is assumed to follow a normal distribution with θ_{ij} and σ_{ij}^2 as the mean and variance. θ_{ij} also follows a normal distribution with μ_i and τ_i^2, which represent the grand mean and variance of the *i*-th predictor. These parameters can be estimated under Bayesian framework.

In addition, once the parameter has been estimated, the relation between θ_{ij} and σ_{ij}^2 and characteristics of the *j*-th facility can be investigated. The characteristics of a low-altitude emission facility include facility layout (such as building height, shape, density etc.), source (stack parameters) and environment (such as terrain, climate etc.), and these predictors can be used for estimating b_i's when applying the model for a new gin facility.

2.2 Extension to infinite space

Dispersion correction factor (DCF) was developed and validated based on the data of sampling array with up to 10-m height and 180-m distance samplers. However, when applying this approach for receptors outside such spatial range, the problem of extrapolation occurs.

According to **Eqn. 3-6**, as the height (h) gets large, the dispersion correction factor (f_c) will be:

$$\lim_{h\to\infty} f_c = \frac{1}{\exp(b_1 h)}, b_1 \neq 0 \qquad \text{Eqn. } 7-4$$

$$b_1 > 0 \Rightarrow \lim_{h\to\infty} f_c = 0 \qquad \text{Eqn. } 7-5$$

$$b_1 < 0 \Rightarrow \lim_{h\to\infty} f_c = \infty \qquad \text{Eqn. } 7-6$$

Such limiting condition performs in the same way for the distance from source (d):

$$\lim_{d\to\infty} f_{\mathrm{c}} = \frac{1}{\exp(b_2 d)}, b_2 \neq 0 \qquad \text{Eqn. } 7-7$$

$$b_2 > 0 \Rightarrow \lim_{d\to\infty} f_{\mathrm{c}} = 0 \qquad \text{Eqn. } 7-8$$

$$b_2 < 0 \Rightarrow \lim_{d\to\infty} f_{\mathrm{c}} = \infty \qquad \text{Eqn. } 7-9$$

These limiting situations result in unrealistic model-predicted concentrations. However, this issue can be solved by making the dispersion correction factor satisfy the following condition:

$$\lim_{d,h\to\infty} C_{\mathrm{cp}} = C_{\mathrm{p}} \qquad \text{Eqn. } 7-10$$

$$\Rightarrow \lim_{d,h\to\infty} f_{\mathrm{c}} \cdot C_{\mathrm{p}} = C_{\mathrm{p}} \qquad \text{Eqn. } 7-11$$

$$\Rightarrow \lim_{d,h\to\infty} f_{\mathrm{c}} = \lim_{d,h\to\infty} \frac{1}{R_{\mathrm{p}}} = 1 \qquad \text{Eqn. } 7-12$$

$$\Rightarrow \lim_{d,h\to\infty} R_{\mathrm{p}} = 1 \qquad \text{Eqn. } 7-13$$

Thus, the prediction function for R_{p} should satisfy restrictions of **Eqn. 7-13**. Here, one form of R_{p} can be proposed:

$$R_{\mathrm{p}} = \exp\left(\frac{b_1 h + b_2 d}{b_0 + b_1 h + b_2 d + b_3 u + b_4 \sigma + b_5 \theta}\right) \qquad \text{Eqn. } 7-14$$

3 Analysis and Modelling for Long-term Remediation Data

3.1 Parallel normalization for time series

When analyzing soil remediation data, T1 data is used for normalization (**Figure 7-3a, 7-3b**). However, data at T1 may have errors (**Figure 7-3c**), which may distort the pattern of normalized data (**Figure 7-3d)**. Therefore, to minimize such error, it is necessary to develop the method for normalization by applying all data instead of using the data at T1 only.

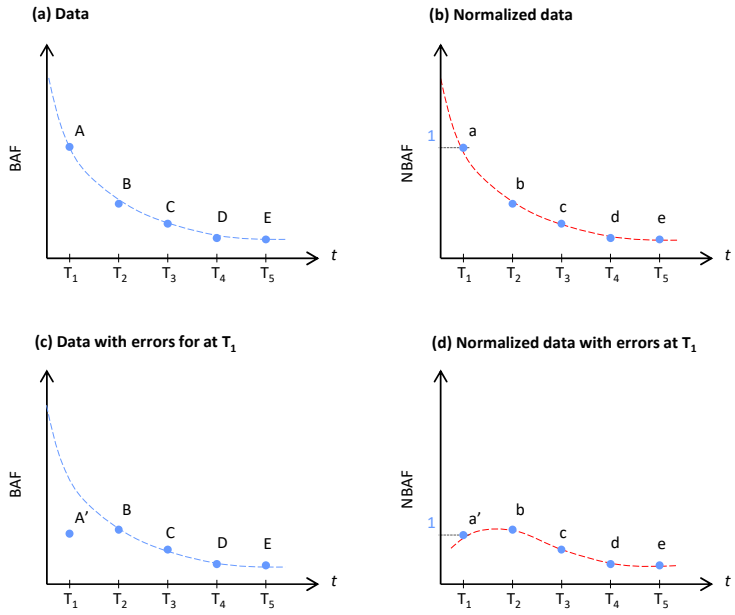

Figure 7-3 Demonstration of normalization errors. Dashed lines in (a) and (c) refer to the true trend, and dashed lines in (b) and (d) refer to the fitted trend by data.

3.2 Compost degradation modelling

Compost degrades with time (Agassi et al., 1998), and the degradation of compost may have significant influence on the soil system and influence bioaccumulation of organic pollutants. However, such degradation effects are not considered in current studies. Thus, it is necessary to take into account for degradation of the composts.

Here, we assume that compost consists two part, including a part that is easy to degrade, called *ez-compost* and a part that is hard to degrade, called *hd-compost*. Only ez-compost can be degraded while hd-compost is stable in terms of time scale of years. Based on the assumptions above, the mass of ez-compost can be expressed as following:

$$M_{\mathrm{c}}(t) = M_{\mathrm{hd}} + M_{\mathrm{ez}}(t) \qquad \text{Eqn. } 7-15$$

where M_{c} is the mass of compost, M_{hd} is the mass of hd-compost, which is a constant, M_{ez} is the mass of ez-compost, and t refers to time.

In addition, degradation of ez-compost is assumed to be caused by microbials only (Agassi et al., 1998), and the degradation rate is in proportional to the microbial population. Thus, we have:

$$\frac{\mathrm{d}M_{\mathrm{ez}}}{\mathrm{d}t} = -r_{\mathrm{c}} \cdot P \qquad \text{Eqn. } 7-16$$

where r_{c} is the degradation rate of compost in terms of each unit of microbial population, and P is population of microbials that can degradate compost. Then, it is assumed the population growth of microbials follows logistic growth model (Thompson and Stewart, 2002; Begon et al., 2006):

$$\frac{\mathrm{d}P}{\mathrm{d}t} = r_{\mathrm{m}}(M_{\mathrm{m}} - P)P \qquad \text{Eqn. } 7-17$$

where r_{m} is the intrinsic rate of growth; M_{m} is the *carrying capacity* for microbials that can degrade compost. Furthermore, we assume that carrying capacity is in proportional to the mass of ez-compost (Begon et al., 2006), which can provide food and habitat for the microbials:

$$M_{\mathrm{m}} = k_{\mathrm{m}} \cdot M_{\mathrm{ez}} \qquad \text{Eqn. } 7-18$$

where k_{m} is the coefficient of M_{m} and M_{ez}.

Combine **Eqn.7-15, 7-16, 7-17** and **7-18**, we have an ordinary deferential equation (ODE) system:

$$\begin{cases} \dfrac{\mathrm{d}P}{\mathrm{d}t} = r_{\mathrm{m}}(k_{\mathrm{m}}M_{\mathrm{ez}} - P)P \\ \dfrac{\mathrm{d}M_{\mathrm{ez}}}{\mathrm{d}t} = -r_{\mathrm{c}} \cdot P \end{cases} \qquad \text{Eqn. } 7-19$$

In **Eqn. 7-19**, if r_{m}, k_{m} and r_{c} are positive, the phase portrait can be obtained and the time series of P and M_{ez} can be derived as shown in **Figure 7-4** (Thompson and Stewart, 2002).

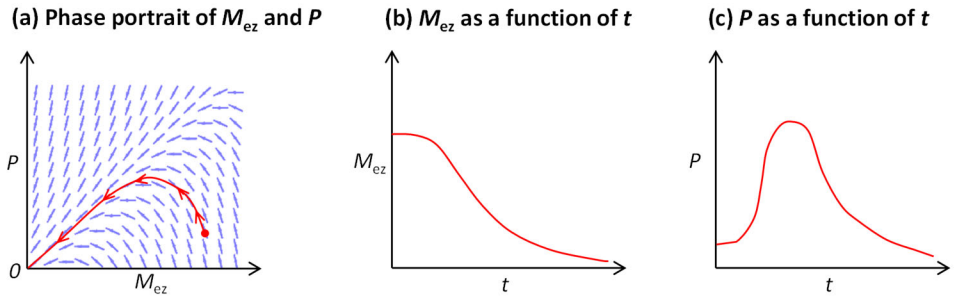

Figure 7-4 Demonstration of solution of the ODE system. P refers to population of microbials; M_{ez} is the mass of ez-compost; t refers to time.

3.3 Phase-transfer modelling

As long as the compost is added to the soil, it performs as a new phase. In addition, contaminants can transport among different phases in the time scale of years. However, such phase-transfer is not considered in current studies. Thus, a phase-transfer model can be proposed to model such process and mitigate the errors.

We assume that the medium of organic pollutants has three phases, including soil, earthworm and compost. In addition, the phase-transfer kinetics are assumed following the diagram shown in **Figure 7-5** (Schnoor, 1996), where k_{xy} refers to the mass transfer coefficient from phase-x to phase-y (x, y = soil (s), earthworm (e), compost (c)), k_x refers to degradation of DDT, and we assume the degradation rate is identical in all phases. Combining all of the assumptions mentioned above and mass balance, a phase-transfer model is proposed:

$$\begin{cases} \dfrac{\mathrm{d}C_\mathrm{s}}{\mathrm{d}t} = -(k_\mathrm{sc} + k_\mathrm{se} + k_\mathrm{d})C_\mathrm{s} + k_\mathrm{es}C_\mathrm{e} + k_\mathrm{cs}C_\mathrm{c} \\ \dfrac{\mathrm{d}C_\mathrm{e}}{\mathrm{d}t} = k_\mathrm{se}C_\mathrm{s} - (k_\mathrm{es} + k_\mathrm{ec} + k_\mathrm{d})C_\mathrm{e} + k_\mathrm{ce}C_\mathrm{c} \\ \dfrac{\mathrm{d}C_\mathrm{c}}{\mathrm{d}t} = k_\mathrm{sc}C_\mathrm{s} + k_\mathrm{ec}C_\mathrm{e} - (k_\mathrm{cs} + k_\mathrm{ce} + k_\mathrm{d})C_\mathrm{c} \end{cases} \qquad \text{Eqn. } 7-20$$

where C_s is the concentration of DDT in soil, C_e is the concentration of DDT in earthworm, C_c is the concentration of DDT in compost, and t refers to time. This is a first-order linear ODE system.

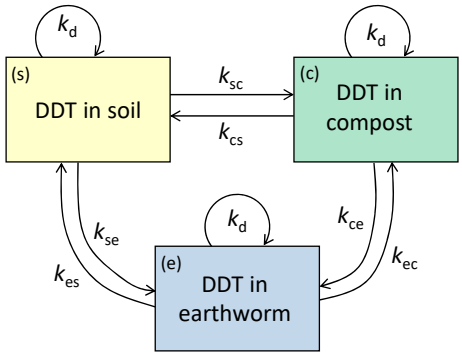

Figure 7-5 Mass transfer of DDT in soil, compost and earthworm. k_{xy} refers to the mass transfer coefficient from phase-x to phase-y (x, y = soil (s), earthworm (e), compost (c)), k_x refers to degradation of DDT; k_d is the degradation rate of DDT.

3.4 Soil contaminant fate dynamic model

As ez-compost degrades, the absorbed DDT will be released to the environment and become available again to earthworms. Thus, understanding of such dynamic process is important to access the effect of composting.

Contaminant concentration in compost can be described by:

$$C_{\mathrm{c}}(t) = \frac{m_{\mathrm{c}}(t)}{M_{\mathrm{c}}(t)} = \frac{m_{\mathrm{c}}(t)}{M_{\mathrm{hd}} + M_{\mathrm{ez}}(t)} \qquad \text{Eqn. } 7-21$$

where m_{c} is the mass of contaminant in compost. The concentration changes with time can be expressed by differentiating C_{c} with respect to t:

$$\frac{\mathrm{d}C_{\mathrm{c}}}{\mathrm{d}t} = \frac{m'_{\mathrm{c}}(M_{\mathrm{hd}} + M_{\mathrm{ez}}) - m_{\mathrm{c}}M'_{\mathrm{ez}}}{\left(M_{\mathrm{hd}} + M_{\mathrm{ez}}(t)\right)^2} = \frac{m'_{\mathrm{c}}(M_{\mathrm{hd}} + M_{\mathrm{ez}}) + m_{\mathrm{c}} \cdot r_{\mathrm{c}}P}{\left(M_{\mathrm{hd}} + M_{\mathrm{ez}}(t)\right)^2} \qquad \text{Eqn. } 7-22$$

Based on mass balance, the concentration of DDT in soil can also be calculated. By combining phase transfer, compost degradation and microbial population equations, the contaminants in compost degradation system can be derived. By assuming the degradation of DDT is negligible (Beyer and Gale, 2013), the hypothetical solution of the compost degradation system is presented in **Figure 7-6**. The details of each phase are in **Figure 7-7**.

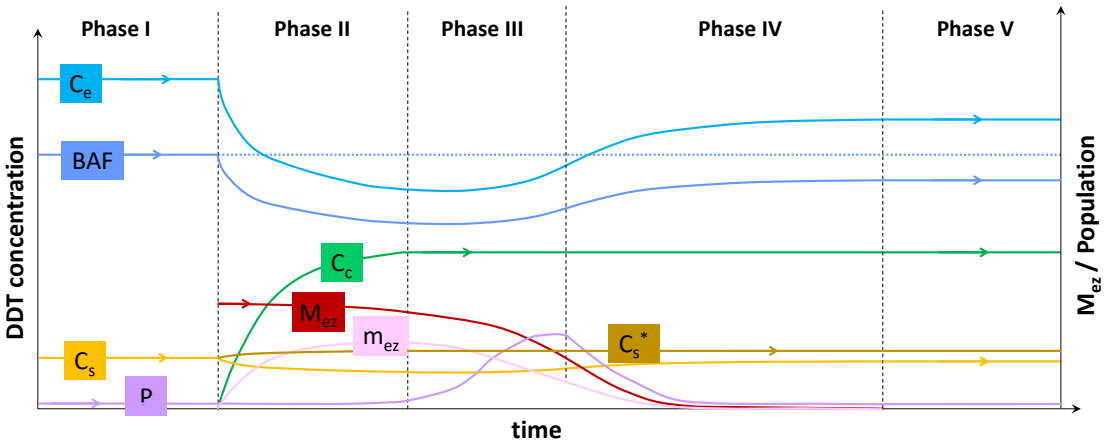

Figure 7-6 Demonstration of hypothetical solution of the compost degradation system C_e, C_c and C_s is contaminant concentration in earthworm, compost, indigenous soil, respectively. C_s^* is the contaminant concentration in the new soil that consists of compost and indigenous soil. *BAF* refers to bioaccumulation factor. M_{ez} and m_{ez} are the mass of ez-compost and mass of contaminants in ez-compost, respectively. P refers to the population of microbials. Details of each phase is described in **Figure 7-7**.

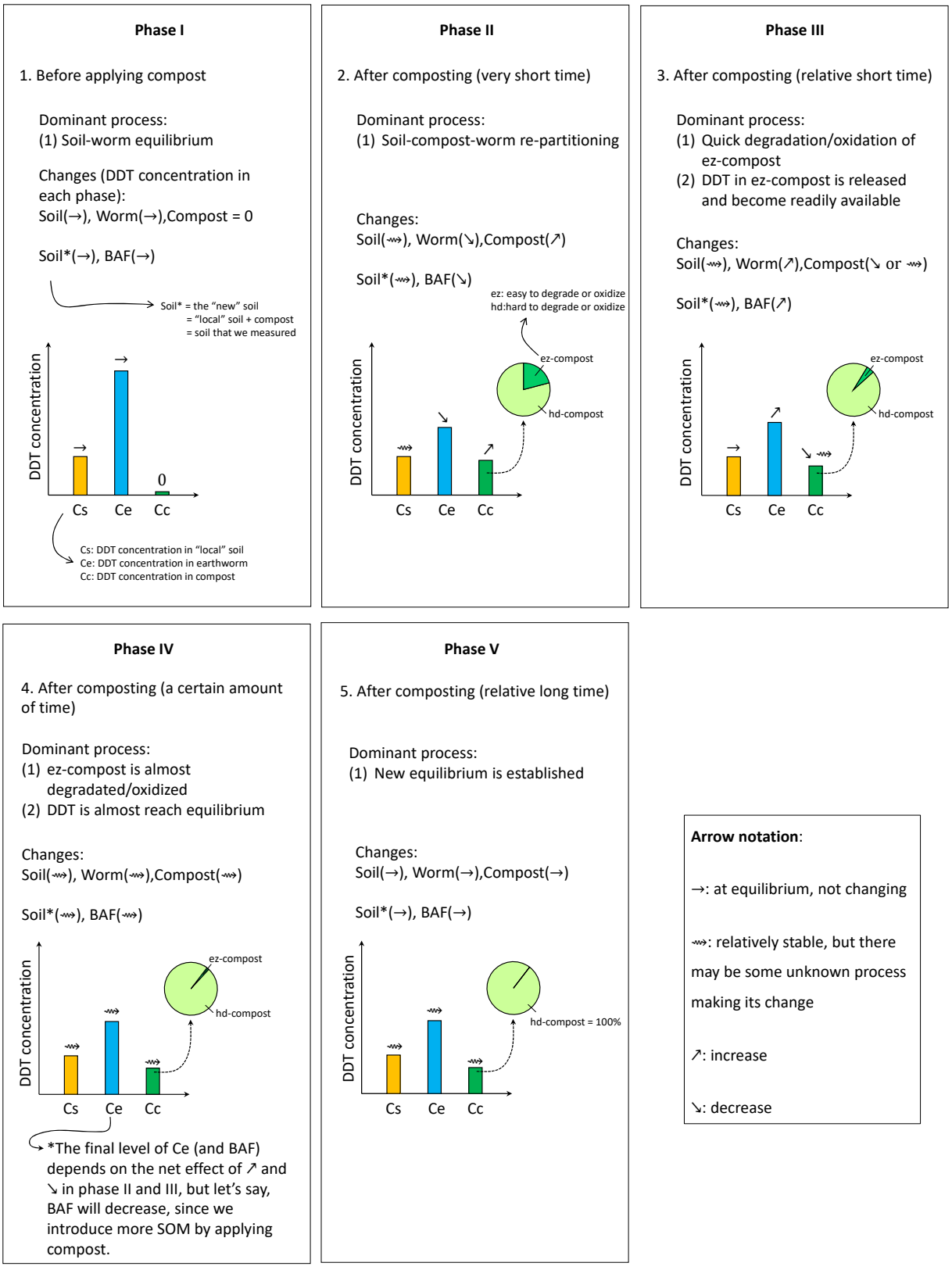

Figure 7-7 Details of each phases in **Figure 7-6**

4 Full Spatial Scale of Remediation Study

4.1 Spatial remediation experiment

Field plot study is a step from lab to real application (Kołtowski et al., 2016; Oleszczuk et al., 2019), but a full-scale spatial remediation study is needed to demonstrate the effectiveness of compost to mitigate bioaccumulation of soil organic pollutants. Thus, a field study was conducted in 2015 on a 1.2-ha field historical orchard where DDT was heavily applied. The soil was amended with compost to decrease DDT bioavailability, with ten control pots of soil (no compost) placed in a nearby filed. Soil and earthworms were collected at sampling points (n = 53) using a 15-m × 15-m grid (**Figure 7-8**) before compost was applied in every spring and fall after application until now (2020). Each sampling point consists of 3 sub-sampling points which are 1 m from the central point (**Figure 7-9**).

Figure 7-8 Sampling layout and sampling points of spatial sampling

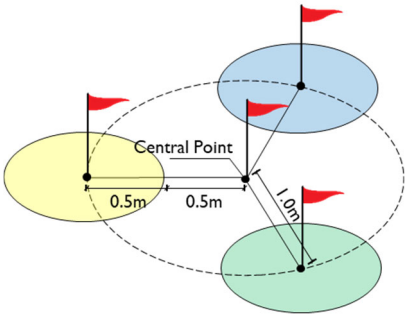

Figure 7-9 Sub-sampling points

4.2 Earthworm size recognition

Previous study indicated that animal size is an important factor of accumulation of persistent organic pollutant in animals (McLeese et al., 1980). However, the influence of size on the uptake of contaminant in earthworms was not investigated yet. Thus, the relation between length of bioaccumulation can be investigated to better estimate bioaccumulation in the field.

Earthworms were collected by hand, and then transferred on a grid paper to obtain photos. For some of the sampling points with plenty of earthworms, the collected earthworms were separated into two groups: long group (earthworm length, $L_e > 5.5$ cm) and short group ($L_e < 5.5$ cm), by comparing the length of earthworms with a 5.5-cm-long ruler. 5.5 cm was determined by previous data showing that the average length of earthworms in the field was about 5.5 cm. Afterwards, the earthworms were washed, freeze dried, and ground. Photos were processed to identify the length and number of earthworms at each sampling point. The length identification method was validated by using thread with known length ($n = 6 \times 20 = 120$) (**Figure 7-10**).

The validation test is as following. First, each photo was imported into Adobe Photoshop CC 2018 (Adobe, Inc. San Jose, CA), and perspective wrap was applied to correct the distortion of camera lens. Then central lines of the earthworms were defined manually by Microsoft PowerPoint (2016), saved as binary bitmap image, and processed by Matlab 2018b (The

MathWorks, Inc. Natick, MA) to calculate the length of the lines. Finally, the length of earthworms and count of earthworms at each sampling points were obtained (**Figure 7-11**). Once the contaminant concentration in soil is measure, the relation between length of earthworms and bioaccumulation factor is investigated.

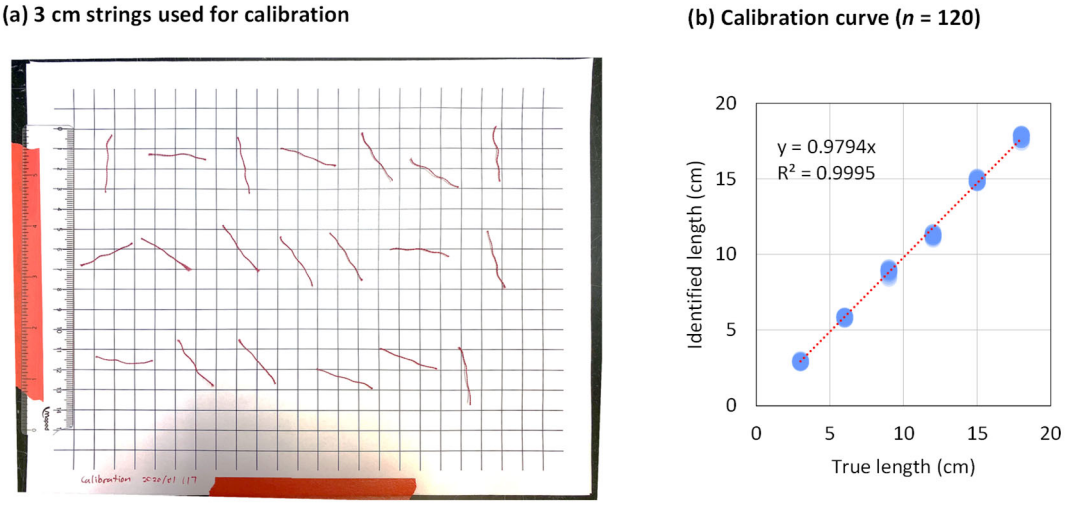

Figure 7-10 Validation of earthworm length recognition

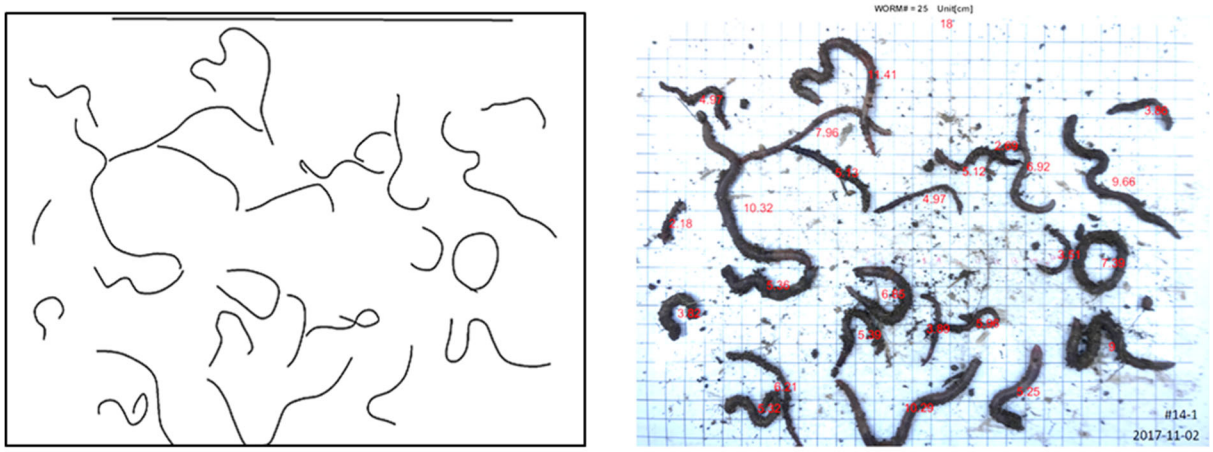

Figure 7-11 Processed earthworm photo

4.3 Spatial statistical analysis

The spatial distribution of organic pollutants is an important information for soil management and ecological risk assessment, and there are some studies investigating spatial distribution of such organic pollutants (Rice and Shigaev, 1997; Tao et al., 2008; Zhang et al., 2011). However, these

studies are large scale studies with scale of kilometers, and the small spatial scale distribution and characterization is lacking. Thus, characterization of distribution of scale of about several meters is necessary, and the layout of current full-scale study is of such spatial scale.

A linear mix model (also known as ordinary Kriging) can be used for geostatistical analysis of contaminant concentration in soil (Webster and Oliver, 2007; Niazi et al., 2011):

$$\boldsymbol{z} = \boldsymbol{X\beta} + \boldsymbol{\eta} \qquad \text{Eqn. } 7-23$$

$$\boldsymbol{\eta} \sim N(0, \boldsymbol{V}) \qquad \text{Eqn. } 7-24$$

$$V_{ij} = \sigma^2 - \gamma(\boldsymbol{h}) \qquad \text{Eqn. } 7-25$$

where $\boldsymbol{z}$ is observed concentration of soil contaminant. $\boldsymbol{X}$ is spatially referenced nonrandom variables. $\boldsymbol{\beta}$ is the parameters that relates $\boldsymbol{X}$ to $\boldsymbol{z}$. $\boldsymbol{\eta}$ is spatially correlated random effect. $\boldsymbol{V}$ is covariance matrix, and σ^2 is the variance of random effect. $\boldsymbol{h}$ is the spatial distance between *i*-th and *j*-th observations. $\gamma(h)$ is covariance function, defined as:

$$\gamma(h) = \frac{1}{2} Var[Z(\boldsymbol{X}) - Z(\boldsymbol{X} + \boldsymbol{h})] \qquad \text{Eqn. } 7-26$$

where $Z(\boldsymbol{X})$ is the measured value at $\boldsymbol{X}$. $Z(\boldsymbol{X} + \boldsymbol{h})$ is the measured value at $\boldsymbol{X} + \boldsymbol{h}$. Two forms of variogram are considered, *spherical model* and *exponential model*.

Concentration of contaminant at an unsampled location can be predicted based on observations and locations (Webster and Oliver, 2007). Prediction of unsampled location is based on ordinary Kriging and BHM coupled with different data transformation approaches. Performance of the model is validated and evaluated by leave-one-out-cross-validation using observed data.

The quality of prediction was evaluated by mean error (*ME*), mean square error (*MSE*) and mean square deviation ratio (MSDR) through leave-one-out cross-validation (Webster and Oliver, 2007):

$$ME = \frac{1}{N}\sum_{i=1}^{N}[\hat{z}(\boldsymbol{x}_i) - z(\boldsymbol{x}_i)] \qquad \text{Eqn. } 7-27$$

$$MSE = \frac{1}{N}\sum_{i=1}^{N}[\hat{z}(\boldsymbol{x}_i) - z(\boldsymbol{x}_i)]^2 \qquad \text{Eqn. } 7-28$$

$$MSDR = \frac{1}{N}\sum_{i=1}^{N}\frac{[\hat{z}(\boldsymbol{x}_i) - z(\boldsymbol{x}_i)]^2}{\hat{\sigma}^2(\boldsymbol{x}_i)} \qquad \text{Eqn. } 7-29$$

where N is the number of data values; $z(\boldsymbol{x}_i)$ is the true value at $\boldsymbol{x}_i$; $\hat{Z}(\boldsymbol{x}_i)$ is the estimated value at at $\boldsymbol{x}_i$; $\hat{\sigma}^2(\boldsymbol{x}_i)$ is the estimated variance.

Random samples can be generated by the model with the estimated parameter, and the random samples are analyzed for determination of minimal sample size to accurately characterize contaminant concentration in the field. In addition, space-time patterns can be evaluated by using data from multiple sampling times.

5 Stochastic Dynamic Modelling of Bioaccumulation

For a single earthworm, due to its movement (Capowiez et al., 2001) and great spatial variability of contaminants in the field (Anderson et al., 2020), the equilibrium of contaminant between soil and earthworm may not be reached (Šmídová and Hofman, et al., 2014). In other words, the contaminant concentration of an earthworm changes with time as the earthworm moves from one spot to another spot. However, this phenomenon has not been investigated, and such phenomenal may improve the accuracy of prediction of bioaccumulation of organic pollutants between soil and earthworm in field. Thus, in order to more accurately model bioaccumulation of earthworms in the field condition, a stochastic dynamic model can be developed.

5.1 Uptake kinetic model

It can be assumed that uptake is in proportional to concentration gradient between earthworm and soil, and degradation is the first order reaction. Therefore, the concentration of organic contaminant in earthworm can be expressed as:

$$\frac{dQ(t)}{dt} = k_1\left(C_s(t) - C_e^*(t)\right) - k_2 Q(t) \qquad \text{Eqn. } 7-30$$

where, $Q(t)$ is the concentration of contaminant in earthworm; t is the time, and $C_s(t)$ is the concentration of contaminant in soil (Widianarko and VanStraalen, 1996), and thus we have:

$$C_s(t) = C_0 \cdot e^{-k_0 t} \qquad \text{Eqn. } 7-31$$

where C_0 is the initial concentration; k_0 is the degradation rate of DDT in soil; k_1 is the uptake rate of contaminant; k_2 is the degradation rate of contaminant in earthworm, and $C_e^*(t)$ is the equivalent contaminant concentration in soil, and there is:

$$C_e^*(t) = \frac{Q(t)}{BAF} \qquad \text{Eqn. } 7-32$$

where BAF is the bio-accumulation factor, and at equilibrium, we have:

$$BAF = \frac{C_s}{C_e} \qquad \text{Eqn. } 7-33$$

This model can be simplified by additional assumptions. (1) Since contaminant of interest, such as DDT, is persistent, degradation rate is assumed to be zero; (2) Amount of contaminant exchanged between soil and earthworm is negligible for soil, so contaminant uptake by earthworm does not change soil concentration. Thus, the model can be simplified as following,

$$\frac{dQ(t)}{dt} = k_1\left(C_s - \frac{Q(t)}{BAF}\right) \qquad \text{Eqn. } 7-34$$

$$\Rightarrow\ Q(t) = C_s \cdot BAF - X \cdot e^{-\frac{k_1}{BAF}\cdot t} \qquad \text{Eqn. } 7-35$$

where X is a constant and depends on initial condition.

If $Q(0) = 0$, then, the solution is

$$Q(t) = C_s \cdot BAF - C_s \cdot BAF \cdot e^{-\frac{k_1}{BAF} \cdot t} \qquad \text{Eqn. } 7-36$$

Let Q_f be the final earthworm concentration of the previous state. If $Q(0) = Q_f$, then the solution would be,

$$Q(t) = C_s \cdot BAF + (Q_f - C_s \cdot BAF) \cdot e^{-\frac{k_1}{BAF} \cdot t} \quad \text{Eqn. } 7-37$$

Eqn. 7-37 indicates that if $Q_f < C_s \cdot BAF$, then $dQ(t)/dt > 0$, and earthworm will uptake contaminant from soil; if $Q_f > C_s \cdot BAF$, then $dQ(t)/dt < 0$, and earthworm will release contaminant into soil. Additionally, the concentration of earthworms given time t depends on (1) BAF, (2) k_1 and (3) C_s.

5.2 Earthworm random walk model

It can be assumed that the area of the field is divided into $i \times j$ cells, and in each cell, soil concentration is uniform across the space, noted as $\boldsymbol{C} = C_{ij}$ (**Figure 7-12)**.

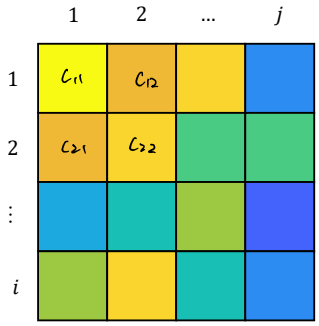

$$\Rightarrow \quad \boldsymbol{C} = C_{ij} = \begin{bmatrix} C_{11} & \cdots & C_{1j} \\ \vdots & \ddots & \vdots \\ C_{i1} & \cdots & C_{ij} \end{bmatrix}_{i \times j}$$

Figure 7-12 Demonstration of ***C*** matrix

In addition, it can be assumed that the time period for an earthworm to stay in a cell is t, and t is smaller than the time needed to reach equilibrium (i.e. $t < T_{\text{equilibrium}}$), and thus the earthworm randomly moves to an adjacent cell or stay in the same cell. The probability of each decision is equal, thus, we have

$$P(A \to B_k) = P(A \to A) = \frac{1}{k+1} \qquad \text{Eqn. } 7-38$$

where $P(A \to B_k)$ refers to the probability of an earthworm moves from cell A to cell B_k (k = 1,2,3,4 or k = 1,2,3 or k = 1,2) (**Figure 7-13**), $P(A \to B_k)$ is the probability of an earthworm stays in the same cell.

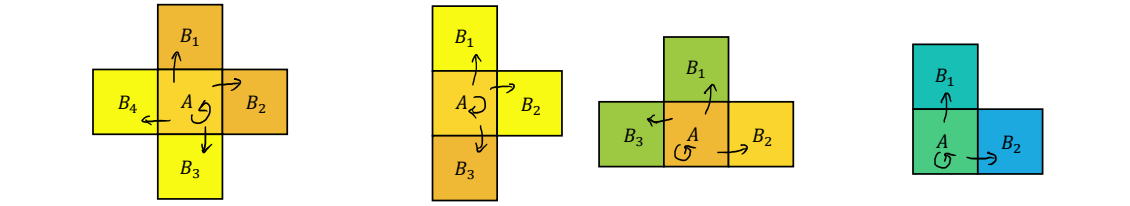

Transfer probability:

$P(A \to B_k) = P(A \to A) = \frac{1}{5}$ $P(A \to B_k) = P(A \to A) = \frac{1}{4}$ $P(A \to B_k) = P(A \to A) = \frac{1}{3}$

Figure 7-13 Demonstration of earthworm transfer rules

5.3 Stochastic dynamic model

It can be assumed that at initial time, clean earthworms are randomly distributed in the contaminated site, with initial concentration $Q(0) = 0$. Each earthworm stays in the cell for a period, t. Afterwards, each earthworm will stay or leave to another adjacent cell with equal probability. Then, this process becomes a stochastic dynamic system. Let total time equals to T, and thus $T = \sum t_i$. This dynamic process can be expressed as following.

In the first cell, $Q(0) = 0$, thus we have

$$Q(t) = C_1 \cdot BAF - C_1 \cdot BAF \cdot e^{-\frac{k_1}{BAF} \cdot t} \qquad \text{Eqn. } 7-39$$

where t_1 is the duration for earthworm staying in the first cell, C_1 is the contaminant concentration of soil in the first cell. After t_1, and $T = t_1$, contaminant concentration in the earthworm is Q_{f1}, and we have

$$Q_{f1} = Q(t_1) = C_1 \cdot BAF - C_1 \cdot BAF \cdot e^{-\frac{k_1}{BAF} \cdot t_1} \qquad \text{Eqn. } 7-40$$

In the second cell, $Q(0) = Q_{f1}$, thus we have

$$Q(t) = C_2 \cdot BAF + (Q_{f1} - C_2 \cdot BAF) \cdot e^{-\frac{k_1}{BAF} \cdot t} \qquad \text{Eqn. } 7-41$$

After t_2, and $T = t_1 + t_2$, DDT concentration in the earthworm is Q_{f1}, and we have

$$Q_{f2} = Q(t_2) = C_2 \cdot BAF + (Q_{f1} - C_2 \cdot BAF) \cdot e^{-\frac{k_1}{BAF} \cdot t_2} \qquad \text{Eqn. } 7-42$$

Similarly, in the ith cell, $Q(0) = Q_{f(i-1)}$, thus we have

$$Q(t) = C_i \cdot BAF + \left(Q_{f(i-1)} - C_i \cdot BAF\right) \cdot e^{-\frac{k_1}{BAF} \cdot t} \qquad \text{Eqn. } 7-43$$

After t_i, and $T = \sum_{i=1}^{i} t_i$, DDT concentration in the earthworm is Q_{fi}, and we have

$$Q_{fi} = Q(t_i) = C_i \cdot BAF + \left(Q_{f(i-1)} - C_i \cdot BAF\right) \cdot e^{-\frac{k_1}{BAF} \cdot t_i} \qquad \text{Eqn. } 7-44$$

Thus, the final contaminant concentration in earthworm can be calculated by using soil concentration, BAF, uptake rate of contaminant (k_1) and the time of earthworms staying in an area. t, BAF, k_1 can be assumed as constant or variables following a given distribution. The values can be summarized from the previous lab studies. Simulation of a single earthworm when there are two cells are shown in **Figure 7-14** (Capowiez et al., 2001; Šmídová and Hofman, 2014). This model can be also reversely used for calculating BAF probabilistically by using field observations.

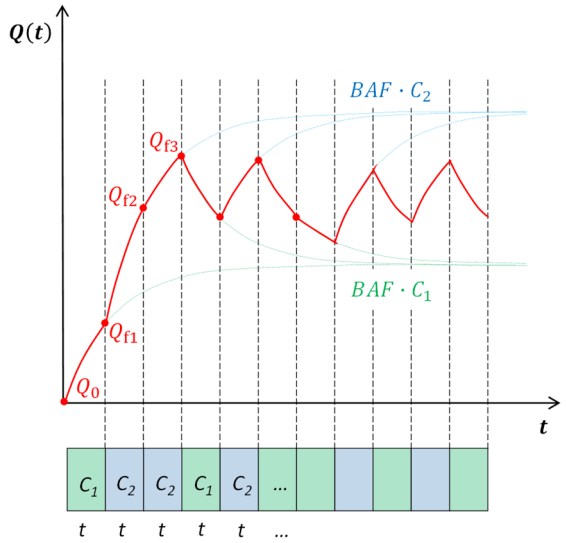

Figure 7-14 Demonstrative solution of the stochastic dynamic model when there are two cells.

Appendices A: SI of Chapter 2

Sampling Campaign and Sample Analysis

We conducted a study to measure the ammonia and PM emission plumes released from a poultry house and to examine the factors influencing the plumes (Yao et al., 2018b). The sampling campaign was conducted at a typical two-house broiler farm in Delaware from 17 May to 25 May 2015. Each 122 m × 21 m house contained approximately 28,000 broilers at 7-weeks of age. Each flock was raised for 60 days with a 10-day inactive time between flocks. Mechanical ventilation of the broiler house was accomplished by the five 48-inch tunnel fans on both sides of the house. The terrain was relatively flat and covered in mowed grass making it suitable for GPM application. Influence of other pollutant sources was minimal.

Details of sampler layout and sample collection and analysis are described elsewhere (Yao et al., 2018b). In brief, the positions of each sampler were obtained in Universal Transverse Mercator (UTM) coordinate system, and GPM receptors were defined to align directly with the actual pollutant sampling points (**SI Figure 2-1 and SI Figure 2-2**). UTM coordinates were transformed into coordinate system shown in **Figure 2-1**, where the positive *x*-axis direction was the direction of wind from the fan, the positive direction of *y*-axis easterly parallel to the side-wall of the poultry house, the *z*-axis was the height above ground, and the origin of the coordinate system was the projection of the central point of middle fan on the ground.

The middle sampling array consisted of three 10-m sampling towers which were deployed perpendicularly downwind of the primary fan at the following distances: tower 1 (T1) at 2 m, tower 2 (T2) at 23 m, and tower 3 (T3) at 47 m from the primary tunnel fan. Each tower was equipped with 4 sampling crossbars (1, 2, 3, and 4) at 2, 4.5, 7.25, and 10 m, respectively. Two additional arrays with two samplers at 2 m above ground level were deployed on the either side and were in parallel with the poultry house; S1 and S2 were 4 m from T2, and S3 and S4 were 8-m from T3 (**Figure 2-1**). A background sampler, S5, was located 70 m east of the tunnel fans. No PM data were reported for T1-3 because the electronic control device for the sampler malfunctioned. Passive diffusive samplers (Radiello™, Sigma-Aldrich Co. LLC., Darmstadt, Germany) were used to measure the time-averaged ammonia concentrations (Radiello, 2006). PM samples were collected using Teflon™ filters coupled with low-volume sampler heads designed and manufactured by Texas A&M / USDA-ARS (Wanjura et al., 2005) and analyzed by in environmental chambers by USDA-ARS Air Quality Lab (Lubbock, TX). Results are shown in **SI Table 2-3**.

Meteorological recording devices were installed at each of the sampling points to record the weather conditions during the sampling period: atmospheric pressure was recorded by a 15 pisa board mount pressure sensor (TE Connectivity Corporation, Berwyn, PA), and relative humidity was recorded by a HTM2500LF humidity sensor (TE Connectivity Corporation, Berwyn, PA). Wind speed and wind direction data were recorded using a 034 B wind sensor (Met One Instruments, Inc. Grats Pass, OR). Ambient meteorological measurements were recorded by a HOBO U30 Station 3.0.0 (Onset Computer Corporation, Bourne, MA). Additional meteorological parameters for the model, including density of water vapor, sensible heat flux, and friction velocity, were derived from the observational data (Allen, 2005). Meteorological input was calculated as hourly averages of the on-site observation at each sampling point.

SI Figure 2-1. Sampler setup for sampling campaign to measure poultry house emission plume. S = single sampler, T = 10 m tower with 4 sampling points. Satellite image was obtained from https://nrcs.app.box.com/v/naip.

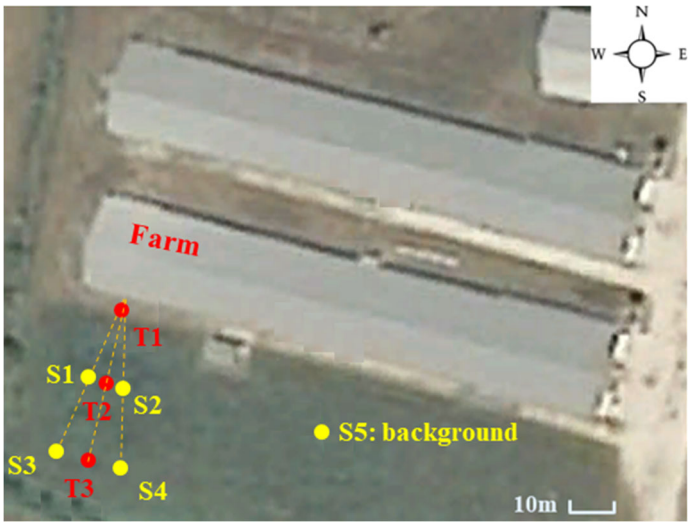

SI Figure 2-2. Fan number and house number (H) of the poultry farm. Satellite image was obtained from https://nrcs.app.box.com/v/naip.

SI Figure 2-3. Geometry of L, virtual points, and fan direction. The poultry house was equipped with five tunnel fans, and a virtual point assigned behind each fan. Fan direction was the same as the positive direction of the x-axis. The distance between the centers of each adjacent fan was 1.8 m, and the diameter of each fan was 1.3 m. When calculating the plume concentrations, the virtual points become the origin of the coordinate system, while the direction of x-axis and y-axis did not change.

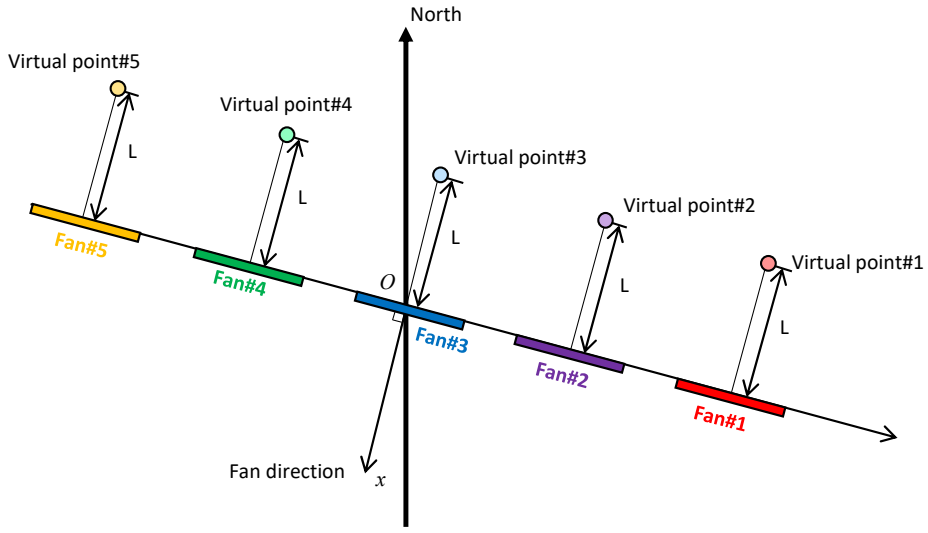

SI Figure 2-4. Fan geometry. The diameter of each fan was 1.3 m; the height of fan center was 1.2 m.

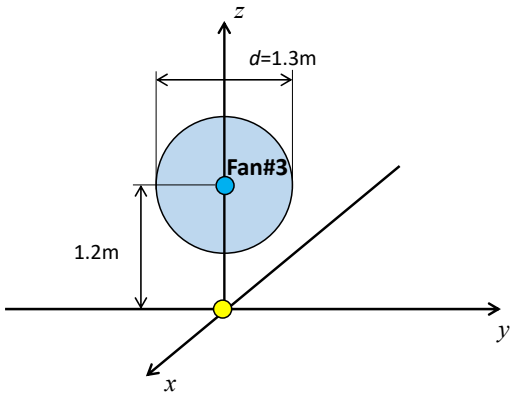

SI Figure 2-5. Illustration of *d*. The solid line is the 1:1 ratio line of $\log_{10}(C_{\text{pred},s})$ as a function of $\log_{10}(C_{\text{obs},s})$, where $C_{\text{pred},s}$ is the model-predicted concentration at sampler s, and $C_{\text{obs},s}$ is the observed concentration at sampler *s*.

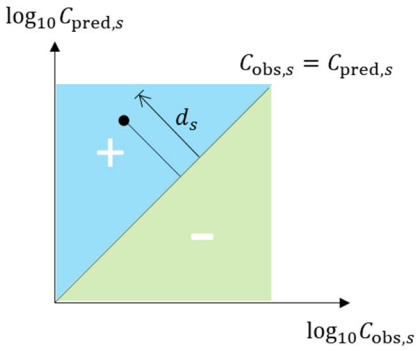

SI Figure 2-6. Diagram of sampler locations used in each wind speed scenario (WSS). The solid filled points refer to the sampling points where the meteorological data were used as the meteorological input for the model. (meteorological data of S1, S2, S3 and S4 were also used for meteorological input for all the scenarios, but not shown here.)

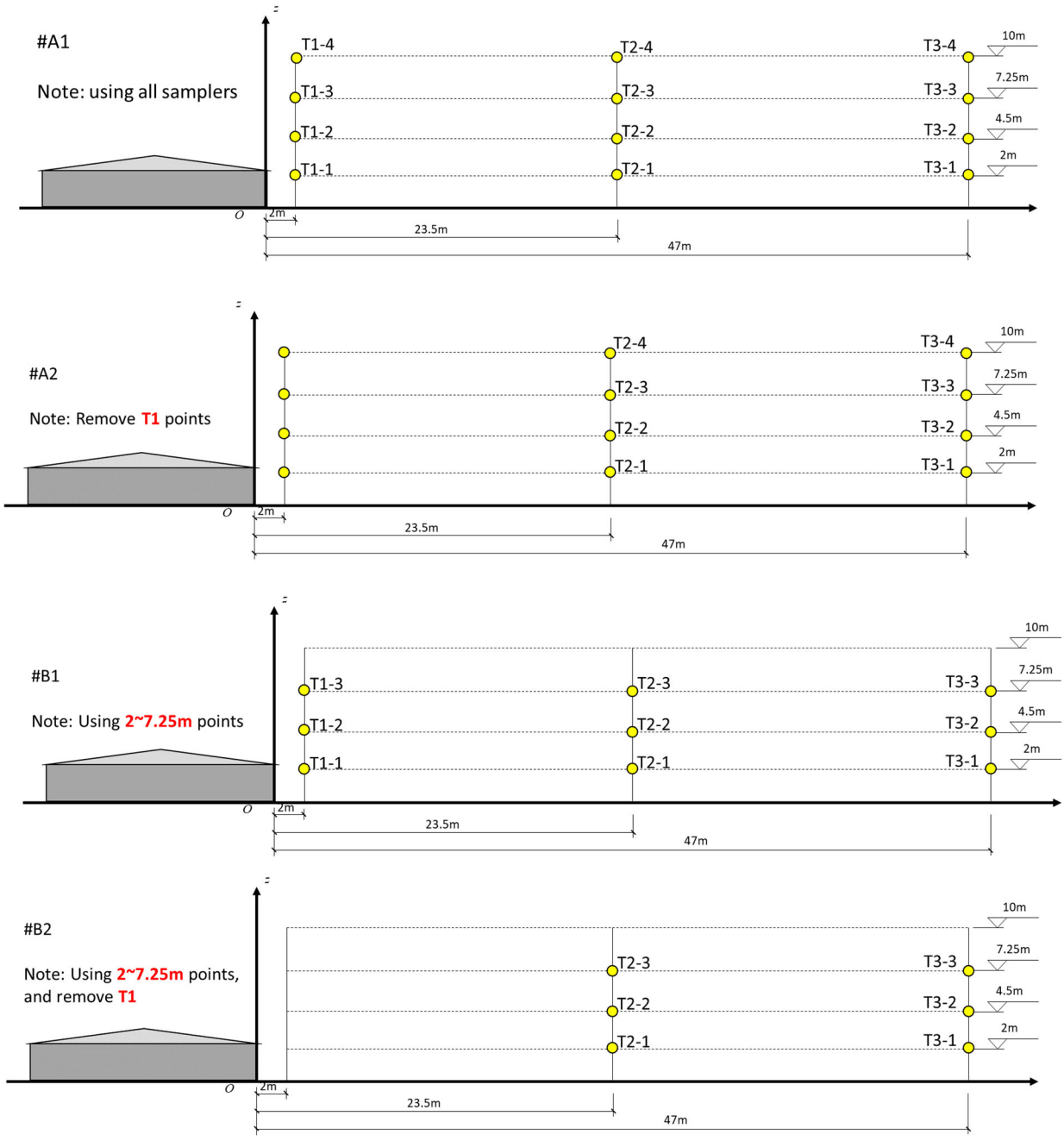

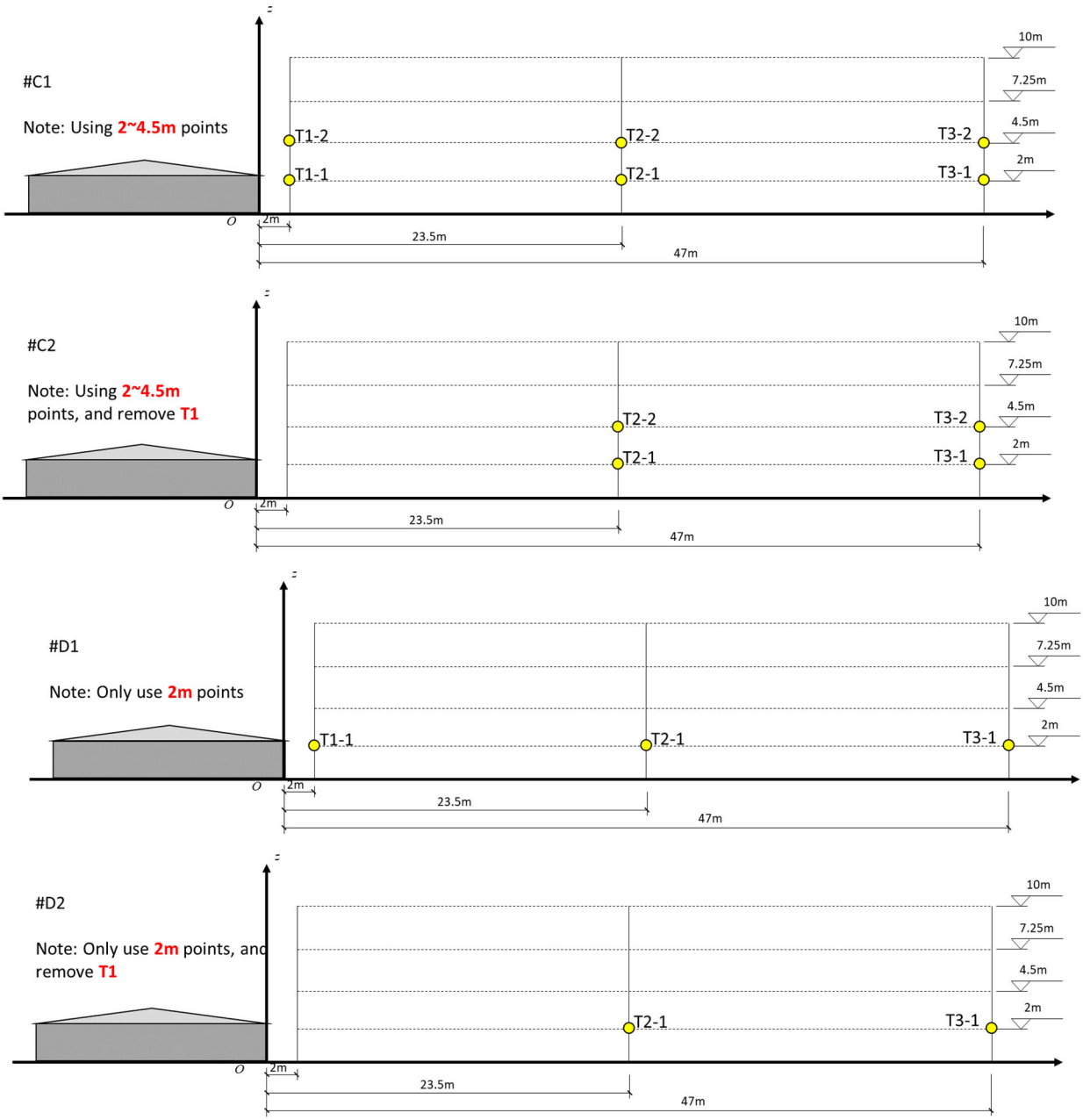
#C1
Note: Using 2~4.5m points
T1-2
T1-1
T2-2
T2-1
T3-2
T3-1
10m
7.25m
4.5m
2m
O
2m
23.5m
47m
#C2
Note: Using 2~4.5m points, and remove T1
T2-2
T2-1
T3-2
T3-1
10m
7.25m
4.5m
2m
O
2m
23.5m
47m
#D1
Note: Only use 2m points
T1-1
T2-1
T3-1
10m
7.25m
4.5m
2m
O
2m
23.5m
47m
#D2
Note: Only use 2m points, and remove T1
T2-1
T3-1
10m
7.25m
4.5m
2m
O
2m
23.5m
47m

SI Table 2-1. Meteorological measurement of each sampler. See Excel spreadsheet file.

SI Table 2-2 Average instability parameter and background wind speed of the five daytime (D1 - D5) and the five nighttime (N1 - N5) experiments. Ambient wind speed was from the background anemometer, the on-site wind speed was from the sampling champions. u refers to wind speed.

Experiment	Ambient			On-site		
	u at 2m [m/s]	*u* at 10m [m/s]	Pasquill stability	*u* at 6m [m/s]*	*u* at 10m [m/s]	Pasquill stability
D1	1.42	2.18	A-B	1.78	2.01	A-B
D2	4.06	6.24	D	4.05	4.57	B-C
D3	2.96	4.55	B-C	3.34	3.77	B-C
D4	1.74	2.67	B	2.09	2.36	B
D5	1.69	2.60	B	2.94	3.31	B-C
N1	0.27	0.41	E	1.13	1.27	E
N2	0.59	0.91	E	1.59	1.79	E
N3	1.44	2.21	E	1.98	2.23	E
N4	0.96	1.47	E	1.57	1.77	E
N5	1.18	1.81	E	1.63	1.84	E

*6-m height was the average height of 2m, 4.5m, 7.25m and 10m .
Conversion is based on the equation (World Meteorological Organization, 2008):

$$u_2 = u_1 \cdot \frac{\ln\left(\frac{h_2}{z_0}\right)}{\ln\left(\frac{h_1}{z_0}\right)}$$

where the reference speed u_1 is measured at the reference height h_1. u_2 is the wind speed at height h_2. z_0 is the roughness length. For current experiment, z_0 = 0.1 m (World Meteorological Organization, 2008).

Pasquill stability:
A: Extremely unstable conditions
B: Moderately unstable conditions
C: Slightly unstable conditions
D: Neutral conditions
E: Slightly stable conditions
F: Moderately stable conditions

SI Figure 2-7 Average daily surface wind speed of year 2015 from Salisbury Reginal Airport, which is the nearest weather station to the experimental site. The probability that wind speed is smaller than 4 m/s is 73.2%.

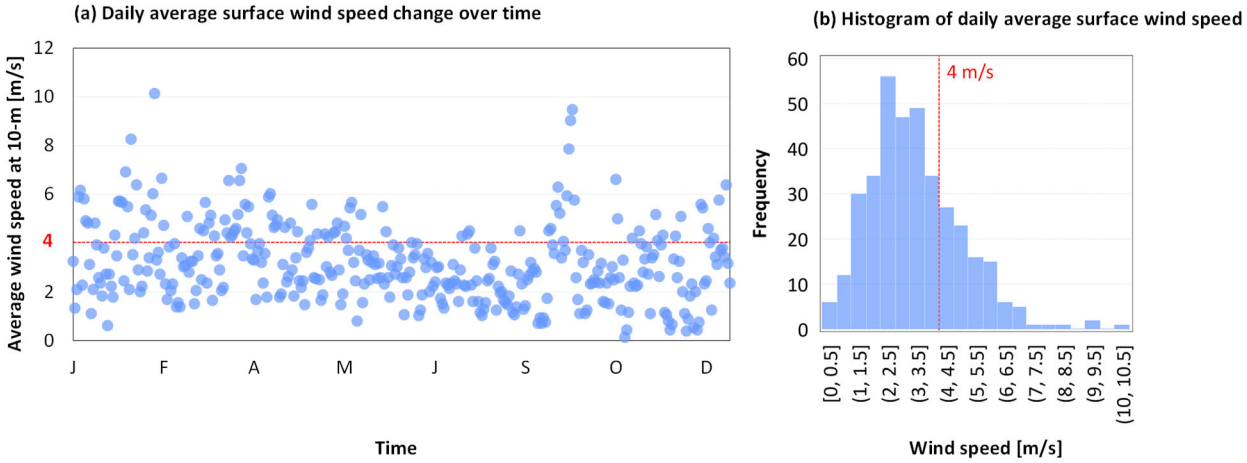

SI Figure 2-8 Plot of FAC2 of the eight cross validation calculation along different L values. Each line refers to the calculation without that experiment. L_{opt}'s of ammonia are 8.4, 5.4, 5.4, 4.8, 4.8, 4.8, 1.2, 4.8 [m] for D1 – N5, respectively; L_{opt}'s of for PM are 6.6, 6.6, 6.6, 6.6, 6.6, 6.6, 6.6, 6.6 [m] for D1 – N5, respectively.

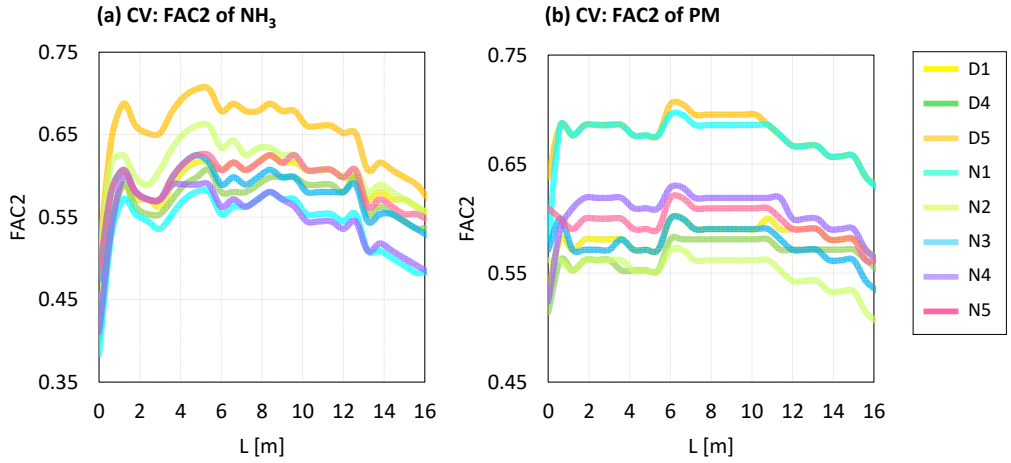

SI Figure 2-9 Plot of FAC2 based on the eight experiments of ammonia and PM along different L values. The x-axes in these plots are an extension of x-axes shown in **Figure 2-3**.

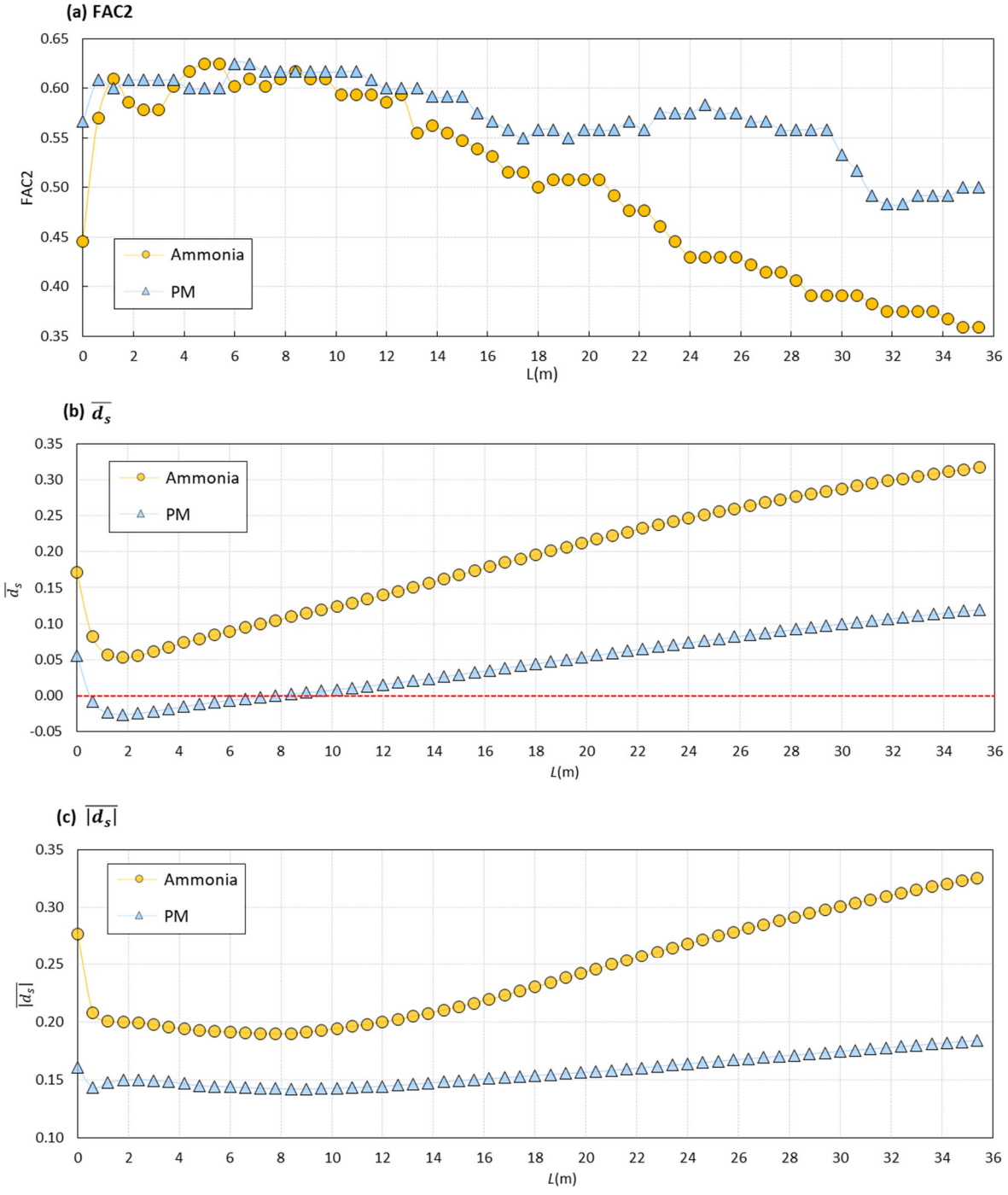

SI Figure 2-10 Individual plots of C_{obs} versus C_{pred} of ammonia. L = 4.8m. C_{obs} is the model-predicted concentration; C_{pred} is the observed concentration. Solid lines are a 1:1 ratio, and dashed lines are 1:0.5 and 1:2 ratio. N refers to nighttime experiment; D refers to daytime experiment.

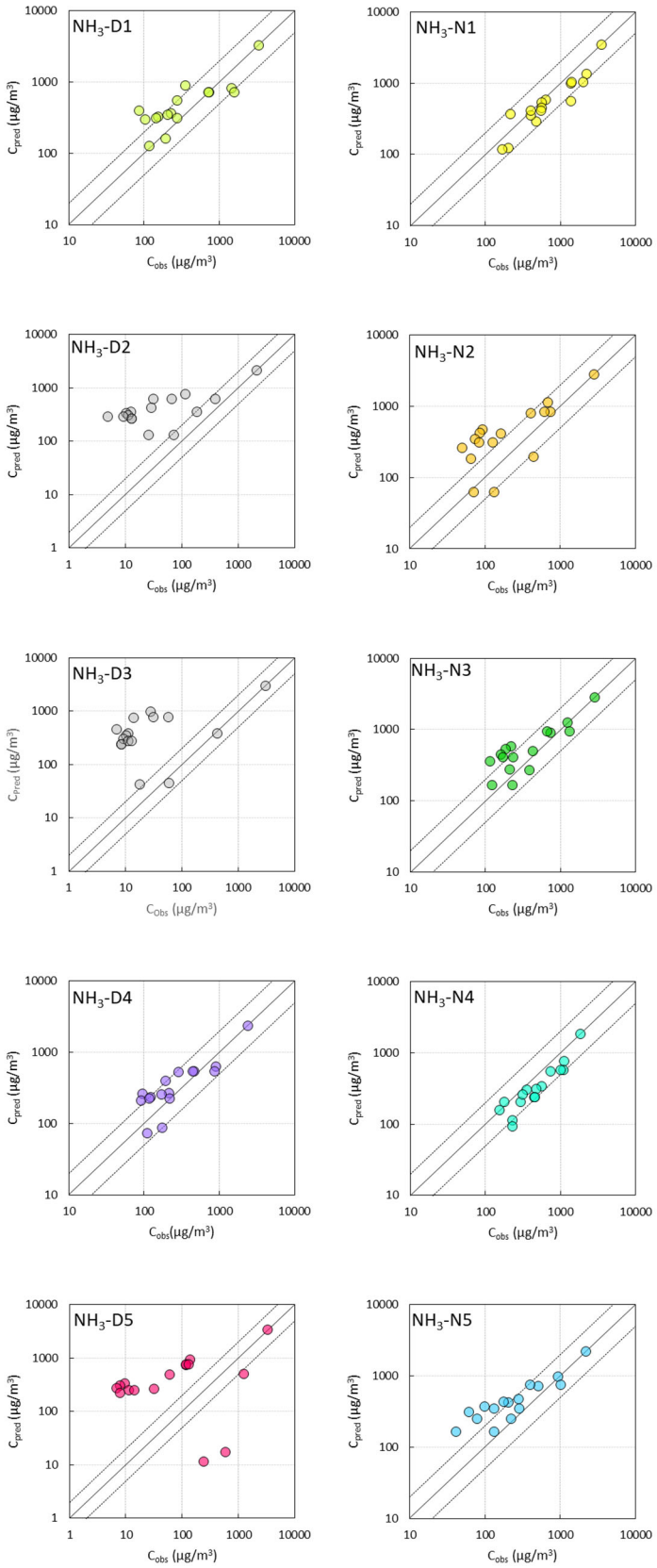

SI Figure 2-11. Individual plot of C_{obs} versus C_{pred} of PM. L = 6.6m. C_{obs} is the model-predicted concentration; C_{pred} is the observed concentration. Solid lines are a 1:1 ratio, and dashed lines are 1:0.5 and 1:2 ratio. N refers to nighttime experiment; D refers to daytime experiment.

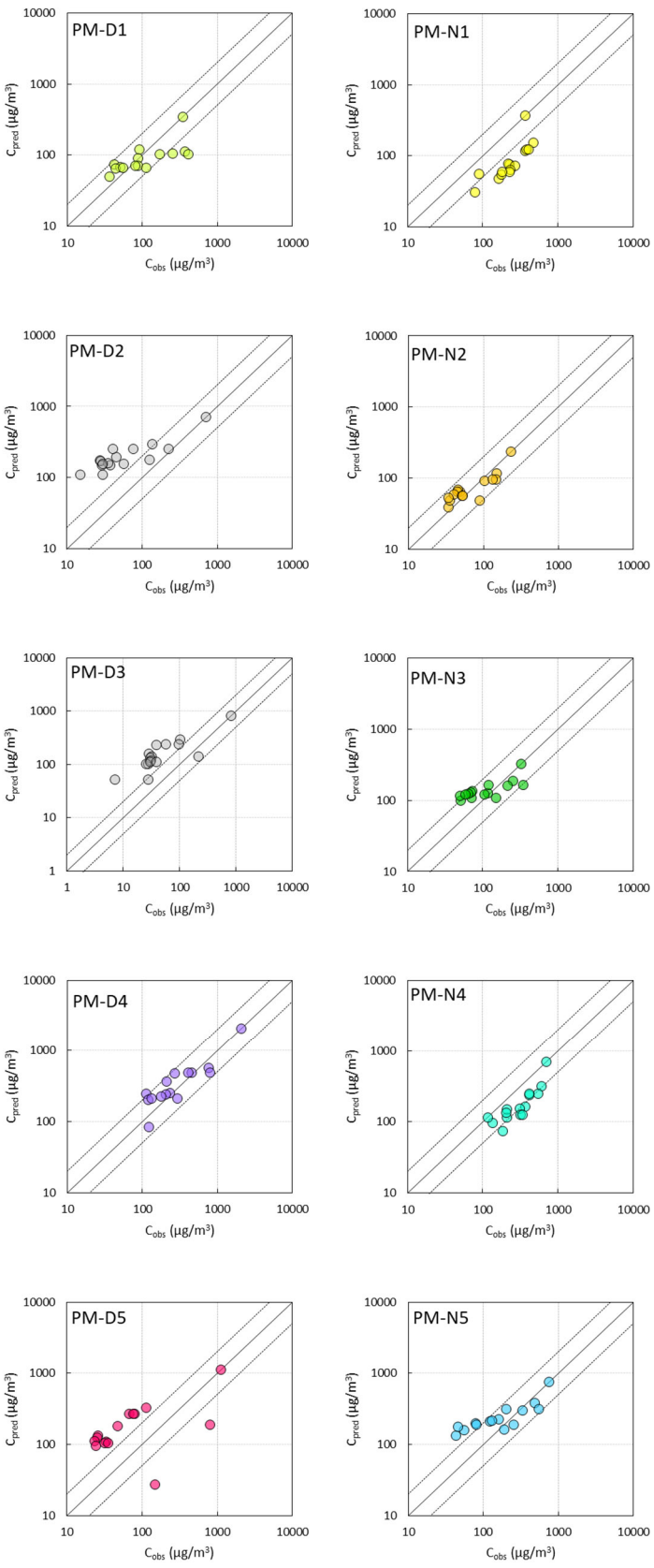

SI Table 2-3 Observed concentrations of ammonia and PM (unit: μg/m^3). No PM data were reported for T1-3 because the electronic control device for the sampler malfunctioned.

NH_3										
Sampler	**D1**	**D2**	**D3**	**D4**	**D5**	**N1**	**N2**	**N3**	**N4**	**N5**
T1-1	3310	2140	3020	2400	3340	3490	2800	2840	1850	2200
T1-2	352	185	429	286	1250	217	440	388	292	224
T1-3	192	72	60	173	582	201	133	124	228	131
T1-4	118	26	18	110	245	169	70	227	230	41
T2-1	1450	117	28	900	139	2250	687	1250	1120	939
T2-2	726	67	14	465	117	1370	407	742	737	508
T2-3	276	29	7	194	61	1370	163	430	352	205
T2-4	86	13	9	95	32	471	65	211	155	78
T3-1	228	13	11	212	10	637	92	219	556	280
T3-2	205	10	10	171	8	563	85	186	473	175
T3-3	154	11	9	122	7	560	74	159	312	99
T3-4	104	13	9	91	8	404	50	116	177	61
S1	712	32	32	439	119	1990	747	669	1100	397
S2	1580	395	58	862	132	1400	613	1330	1010	1020
S3	144	9	11	118	12	550	128	171	449	131
S4	273	5	13	218	14	401	84	232	453	283
Background	127	130	42	74	12	118	63	165	80	164

PM										
Sampler	**D1**	**D2**	**D3**	**D4**	**D5**	**N1**	**N2**	**N3**	**N4**	**N5**
T1-1	347	706	823	2090	1120	364	234	323	700	754
T1-2	92	125	213	272	804	90	90	150	211	191
T1-3										
T1-4	36	30	28	123	151	79	34	51	183	43
T2-1	368	137	103	769	114	468	149	251	599	482
T2-2	253	75	39	454	68	364	104	213	418	334
T2-3	88	46	28	210	48	228	49	117	211	122
T2-4	42	38	27	113	33	164	36	71	135	56
T3-1	88	28	32	234	26	219	45	73	370	163
T3-2	81	28	30	206	26	270	44	70	308	130
T3-3	51	35	31	178	24	234	40	64	205	79
T3-4	44	29	25	119	25	177	34	50	116	46
S1	171	40	57	409	81	386	147	120	541	205
S2	408	224	96	794	77	410	131	342	418	546
S3	56	30	30	133	32	229	52	59	320	82
S4	114	57	39	296	36	179	53	104	341	256
Background	49	110	52	85	27	31	39	99	70	134

SI Table 2-4. Model-predicted concentrations (unit: μg/m^3) for eight experiments (D2 and D3 excluded). For ammonia, L_{opt} = 4.8 m; for PM, L_{opt} = 6.6 m; R = reflection; NR = non-reflection. PM concentration at T1-3 was not predicted because the sampler malfunctioned and data were not reported.

Experiment	Sampler	NH_3-R	NH_3-NR	PM-R	PM-NR	Experiment	Sampler	NH_3-R	NH_3-NR	PM-R	PM-NR
D1	T1-1	3310	3310	347	347	N2	T1-1	2800	2800	234	234
	T1-2	523	577	121	136		T1-2	92	93	49	49
	T1-3	131	131				T1-3	63	63		
	T1-4	127	127	49	49		T1-4	63	63	39	39
	T2-1	833	558	114	94		T2-1	1159	687	116	85
	T2-2	718	511	104	89		T2-2	779	532	92	74
	T2-3	543	415	90	80		T2-3	377	293	65	58
	T2-4	376	309	75	70		T2-4	159	139	48	46
	T3-1	358	263	71	64		T3-1	465	275	68	55
	T3-2	346	258	70	63		T3-2	415	257	65	54
	T3-3	323	247	68	62		T3-3	334	220	59	51
	T3-4	295	232	66	61		T3-4	247	175	53	48
	S1	718	488	104	87		S1	836	506	95	72
	S2	718	488	104	87		S2	835	506	95	72
	S3	309	234	67	61		S3	300	188	57	49
	S4	309	234	67	61		S4	300	188	57	49
D4	T1-1	2390	2390	2090	2090	N3	T1-1	2840	2840	323	323
	T1-2	287	309	481	559		T1-2	184	184	108	109
	T1-3	75	75				T1-3	165	165		
	T1-4	74	74	85	85		T1-4	165	165	99	99
	T2-1	650	416	567	405		T2-1	1260	794	190	153
	T2-2	542	373	486	369		T2-2	872	631	161	140
	T2-3	385	287	364	296		T2-3	462	385	128	120
	T2-4	245	199	249	216		T2-4	249	232	109	107
	T3-1	265	183	252	192		T3-1	574	380	134	118
	T3-2	253	179	242	188		T3-2	521	361	130	117
	T3-3	232	168	225	178		T3-3	435	322	123	114
	T3-4	205	154	202	165		T3-4	345	275	116	110
	S1	545	353	487	352		S1	934	607	165	138
	S2	545	353	487	352		S2	934	607	165	138
	S3	220	157	214	168		S3	400	289	120	111
	S4	220	157	214	168		S4	400	289	120	111

Experiment	Sampler	NH_3-R	NH_3-NR	PM-R	PM-NR	Experiment	Sampler	NH_3-R	NH_3-NR	PM-R	PM-NR
D5	T1-1	3340	3340	1116	1116	N4	T1-1	1850	1850	700	700
	T1-2	201	214	190	216		T1-2	153	134	114	109
	T1-3	12	12				T1-3	105	99		
	T1-4	12	12	27	27		T1-4	86	85	74	73
	T2-1	957	557	326	217		T2-1	764	481	315	217
	T2-2	752	476	267	192		T2-2	529	380	238	183
	T2-3	466	321	183	142		T2-3	276	226	150	130
	T2-4	234	174	110	92		T2-4	140	128	97	92
	T3-1	332	187	132	91		T3-1	334	216	163	122
	T3-2	309	179	125	89		T3-2	302	205	152	117
	T3-3	267	160	112	82		T3-3	250	181	134	109
	T3-4	217	134	97	73		T3-4	195	151	114	98
	S1	762	444	269	181		S1	566	364	248	176
	S2	762	444	269	181		S2	566	364	248	176
	S3	244	139	105	75		S3	229	160	126	101
	S4	244	139	105	75		S4	229	160	126	101
N1	T1-1	3490	3490	364	364	N5	T1-1	2200	2200	754	754
	T1-2	198	200	55	57		T1-2	181	181	161	162
	T1-3	119	119				T1-3	164	164		
	T1-4	118	118	31	31		T1-4	164	164	134	134
	T2-1	137	840	153	105		T2-1	984	636	382	280
	T2-2	968	673	117	89		T2-2	698	515	303	247
	T2-3	519	407	75	64		T2-3	393	332	213	193
	T2-4	258	225	48	44		T2-4	231	217	160	155
	T3-1	574	361	77	57		T3-1	469	325	228	186
	T3-2	521	343	72	55		T3-2	430	311	217	181
	T3-3	434	302	63	51		T3-3	367	282	198	173
	T3-4	340	253	54	46		T3-4	301	247	178	162
	S1	1020	641	122	86		S1	744	497	313	240
	S2	1020	641	122	86		S2	744	497	313	240
	S3	397	267	60	47		S3	342	257	190	165
	S4	397	267	60	47		S4	342	257	190	165

SI Table 2-5 *FAC2* for ammonia and PM for *L* values using scenario A1. R = reflection, NR = non-reflection.

L (m)	NH_3-R	PM-R	NH_3-NR	PM-NR	*L* (m)	NH_3-R	PM-R	NH_3-NR	PM-NR
0.0	0.45	0.57	0.52	0.56	18.0	0.5	0.56	0.51	0.53
0.6	0.57	0.61	0.59	0.59	18.6	0.51	0.56	0.52	0.53
1.2	0.61	0.6	0.56	0.58	19.2	0.51	0.55	0.49	0.54
1.8	0.59	0.61	0.55	0.58	19.8	0.51	0.56	0.48	0.54
2.4	0.58	0.61	0.55	0.57	20.4	0.51	0.56	0.48	0.56
3.0	0.58	0.61	0.56	0.57	21.0	0.49	0.56	0.47	0.56
3.6	0.6	0.61	0.58	0.58	21.6	0.48	0.57	0.46	0.55
4.2	0.62	0.6	0.55	0.58	22.2	0.48	0.56	0.46	0.56
4.8	0.63	0.6	0.55	0.58	22.8	0.46	0.58	0.45	0.56
5.4	0.63	0.6	0.55	0.58	23.4	0.45	0.58	0.45	0.56
6.0	0.6	0.63	0.58	0.6	24.0	0.43	0.58	0.45	0.55
6.6	0.61	0.63	0.57	0.59	24.6	0.43	0.58	0.45	0.53
7.2	0.6	0.62	0.59	0.59	25.2	0.43	0.58	0.44	0.53
7.8	0.61	0.62	0.59	0.58	25.8	0.43	0.58	0.43	0.53
8.4	0.62	0.62	0.6	0.58	26.4	0.42	0.57	0.41	0.53
9.0	0.61	0.62	0.59	0.58	27.0	0.41	0.57	0.41	0.55
9.6	0.61	0.62	0.59	0.59	27.6	0.41	0.56	0.41	0.54
10.2	0.59	0.62	0.56	0.59	28.2	0.41	0.56	0.41	0.53
10.8	0.59	0.62	0.55	0.59	28.8	0.39	0.56	0.41	0.53
11.4	0.59	0.61	0.55	0.59	29.4	0.39	0.56	0.41	0.53
12.0	0.59	0.6	0.53	0.59	30.0	0.39	0.53	0.39	0.53
12.6	0.59	0.6	0.52	0.59	30.6	0.39	0.52	0.39	0.53
13.2	0.55	0.6	0.51	0.59	31.2	0.38	0.49	0.38	0.51
13.8	0.56	0.59	0.5	0.58	31.8	0.38	0.48	0.38	0.5
14.4	0.55	0.59	0.5	0.56	32.4	0.38	0.48	0.36	0.5
15.0	0.55	0.59	0.49	0.58	33.0	0.38	0.49	0.36	0.49
15.6	0.54	0.58	0.49	0.57	33.6	0.38	0.49	0.36	0.48
16.2	0.53	0.57	0.51	0.56	34.2	0.37	0.49	0.36	0.48
16.8	0.52	0.56	0.5	0.56	34.8	0.36	0.5	0.36	0.5
17.4	0.52	0.55	0.5	0.55	35.4	0.36	0.5	0.36	0.5

SI Figure 2-12. Box plot of d_s of 8 experiments of individual sampler of ammonia (a) and PM (b). The two plots do not have the same y-axis. For each sampler, the point represents the mean, the line the median, the boxes 25% to 75%, and the bars the range of values. No PM data were reported for T1-3 because the electronic control device for the sampler malfunctioned.

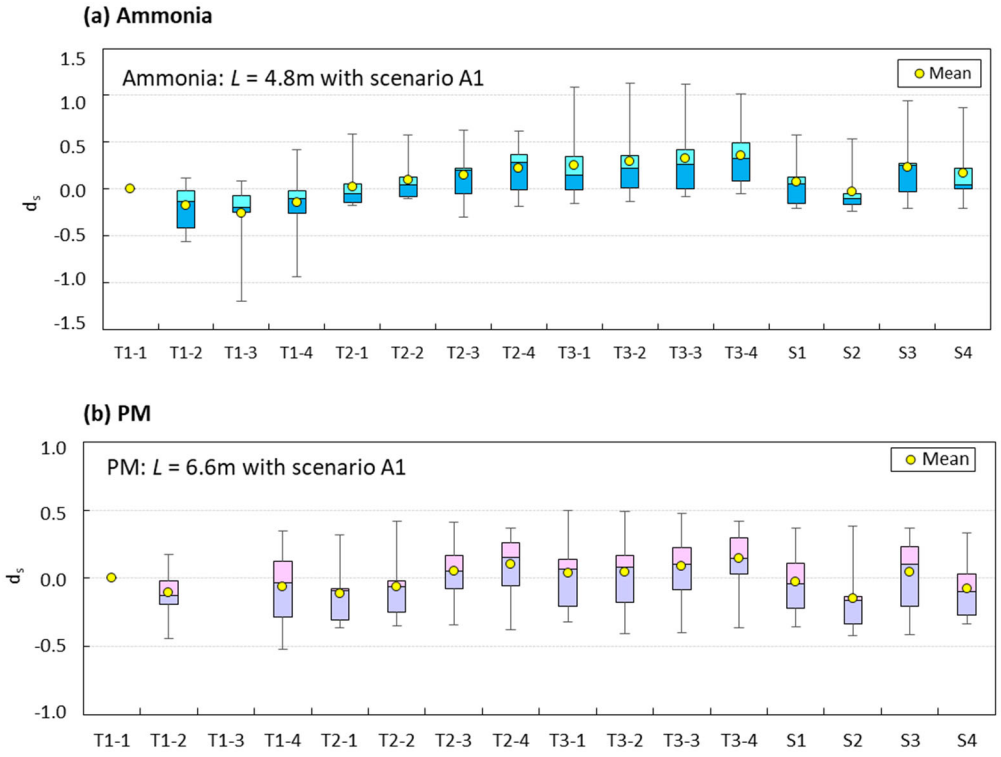

SI Figure 2-13. FAC2 values for different L values and wind speed scenario combinations of ammonia (a) and PM (b) discussed in the manuscript. Different wind speed scenarios are shown in **Figure 2-1**. L refers to the distance between the virtual point and the fan. Color indicates the relative magnitude of FAC2: red refers to smaller values, green refers to greater values. All FAC2 are above 0.5.

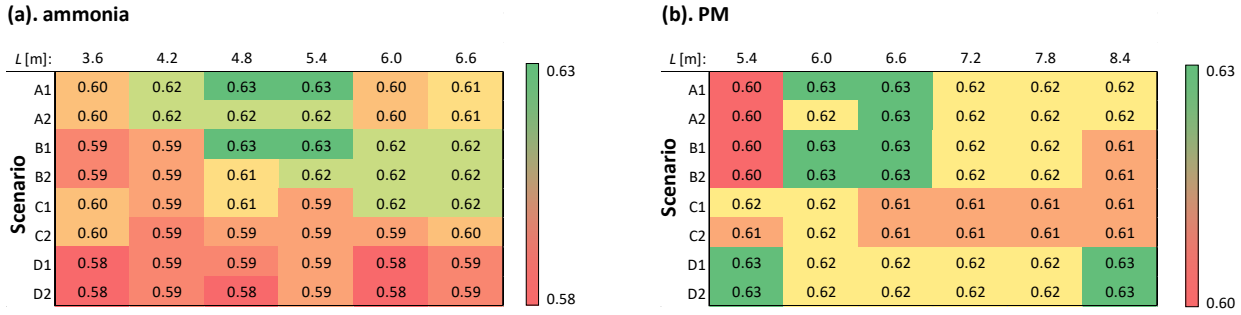

SI Figure 2-14 Box plot of ratio of difference (R_s). Box plot of ratio of difference (R_s) of individual samplers of ammonia (NH_3) and PM. Each plot two *y*-axes. The left *y*-axis corresponds is used for T1-1, T1-2 and T1-3 samplers (orange and red boxes), while right *y*-axis is used for the remaining samplers (peach and pink boxes). (a) model sensitivity for NH_3 predictions under different wind speed scenarios using L = 4.8 m; (b) model sensitivity for PM predictions under different wind speed scenarios using L = 6.6 m; (c) model sensitivity for NH_3 predictions under different L values by using A1 scenario; (d) sensitivity for PM predictions under different L values by using A1 scenario. For each sampler, the point represents the mean, the line the median, the boxes 25% to 75%, and the bars the range of values. No PM data were reported for T1-3 because the electronic control device for the sampler malfunctioned.

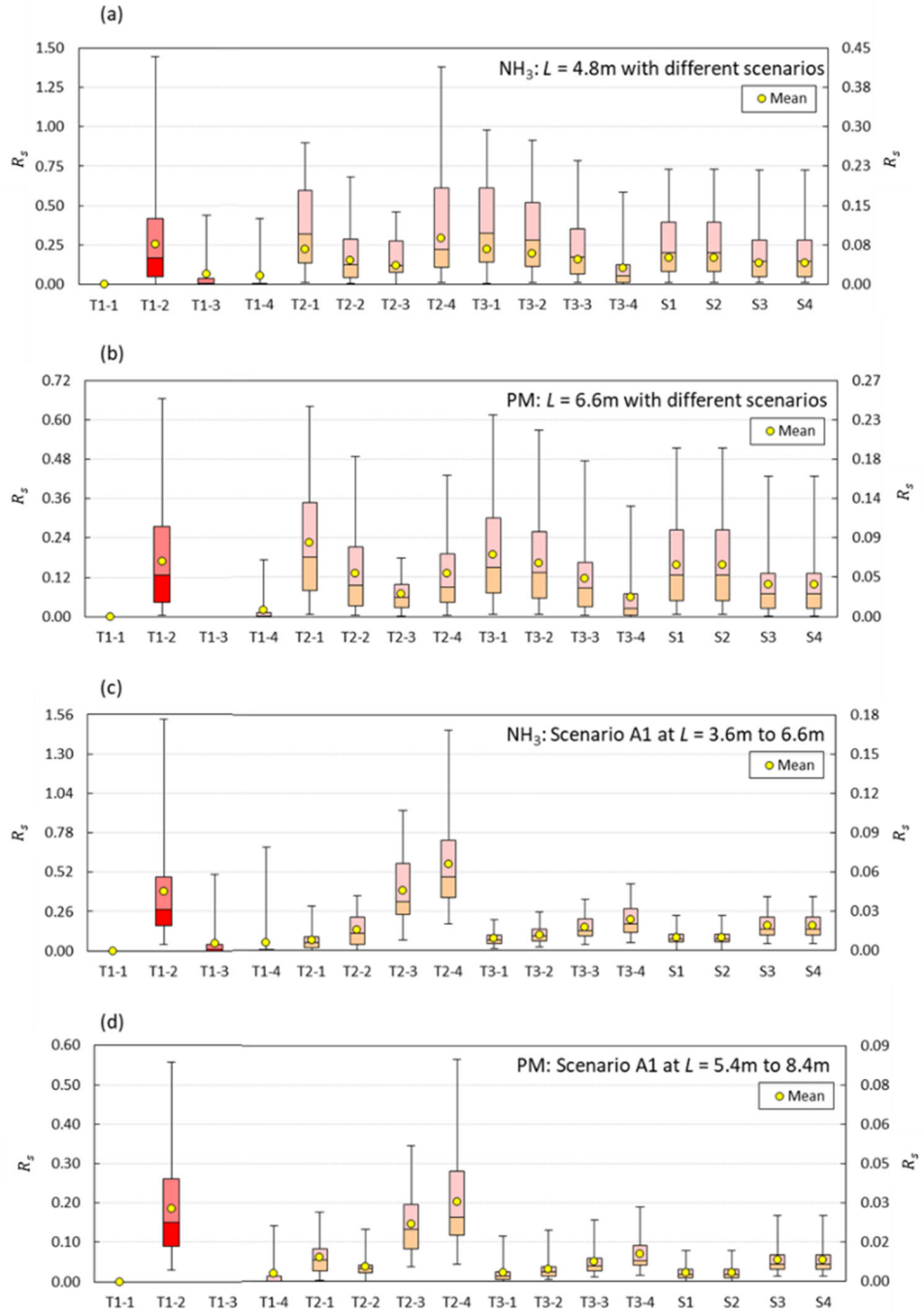

Evaluation of the Model Using Additional Scenarios

To provide more insight into the model, the performance and sensitivity of the model were evaluated using different combinations of background values, experiments, sampling points, and meteorological data inputs. For the background scenarios (BGSs), the source for the C_{bg} term in Eqn. 2 was different. C_{bg} was equal to: (1) the observed background concentration (*bg method*); (2) the minimum on-site observed concentration (*MIN method*); and (3) zero (*bg=0 method*). The experiment scenarios (EXSs) considered different combinations of the ten experiments: (1) all 10 experiments were used in model; (2) experiments D2 and D3 were removed; and (3) experiments D2, D3, and D5 were removed. The sampler scenarios (SPSs) examined different combinations of samplers: (1) all samplers were used; (2) the T1-3 and T1-4 samplers were removed; (3) the T1-2, T1-3, and T1-4 samplers were removed. In the WSSs, the meteorological inputs for the model were based on different sampling point combinations as shown in **Figure 2-1**.

SI Figure 2-15 and **SI Figure 2-16** show the values of *FAC2* to BGSs. **SI Figure 2-15** indicates that *MIN method* provided better performance than *bg method* and *bg=0 method*. This may be due to some of samplers were spatially out of the plume, such as T1-3 and T1-4, where observed concentrations were similar to background concentrations. Although *MIN method* was better, using the observed background is a more general approach, especially for experimental design where all the samplers are spatially inside the plume. The sensitivity of *L* to BGSs is shown in **SI Figure 2-16**. For ammonia, L_{opt} is not sensitive to *bg method*, *MIN method*, and *bg=0 method*, since around L_{opt} = 4.8 m, the *FAC2* values are always greater than 0.5 and do not vary greatly. In addition, the drift of optimal *L* of MIN method is smaller than the drift of *bg=0 method*. For PM, optimal *L* is not sensitive between *bg method* and *MIN method* although a small drift exists. However, L_{opt} of ammonia of *bg=0 method* is different from *bg method* and *MIN method* as the L_{opt} values of *bg=0 method* are much smaller, and most of the *FAC2* values are smaller than 0.5, which is considered as unacceptable. L_{opt} was also reasonable using *MIN method*, but not for *bg=0 method* for PM.

SI Figure 2-17 and **SI Figure 2-18** show the values of *FAC2* to EXSs. The model does not perform well for experiments D2, D3, and D5. D2 and D3 had larger average background wind speed and smaller present calm. D5 also had very small value of percent calm. Therefore, one of the limitations of this model is that it is does not perform well when the on-site wind speed is too large (> 3 m/s). This model performs better when under stable atmospheric conditions. demonstrates the sensitivity of optimal *L* to EXS. Removing D2, D3, and D5 would slightly change the value of L_{opt}. L_{opt} became smaller for ammonia **(SI Figure 2-18a)** while L_{opt} became larger for PM **(SI Figure 2-18b)**, but within the range of 1.2m to 10.8m, the *FAC2* values are always greater than 0.5. Therefore, *L* was not sensitive to EXS.

SI Figure 2-19 and **SI Figure 2-20** show the values of *FAC2* to SPSs. Since among each of the five sub-groups, the differences of *FAC2* values is minor indicating that little difference exists in model performance between using all samplers, eliminating T1-3 and T1-4, or eliminating T1-2, T1-3 and T1-4. However, L_{opt} is affected by the removal of T1-2 as an obvious decrease in *FAC2* for ammonia and PM is observed. A possible explanation is to consider the distance of the towers from the source. T1 was 2 m away from the fan, while T2 was 23 m away from the fan. If the T1 samplers were removed, the changes in the fan size and L_{opt} was would be smaller than distance

between samplers and fan (23 m for T2 and 47 m for T3), and therefore assuming fan as a point source generated less error. Therefore, assumptions of virtual point and optimal *L* are more suitable for situations when samplers were close to the fan. In other words, the plume had negligible contribution to T1-3 and T1-4, and this result indicates that this model was able to deal with samplers that were spatially "out of the plume", like T1-3 and T1-4 in this case.

SI Figure 2-21 and **SI Figure 2-22** show demonstrates the sensitivity of *FAC2* to WSS. It indicates that performance of the model and L_{opt} were not sensitive to WSS for ammonia and PM.

Legend Figures and Tables of Additional Scenarios. In the following figures and tables, A1, A2, B1, B2, C1, C2, D1 and D2 are noted as A1-2, A2-2, B1-2, B2-2, C1-2, C2-2, D1-2 and D2-2, respectively. Details of condition scenario are shown in SI Table 6. The results were organized in several groups for comparison.

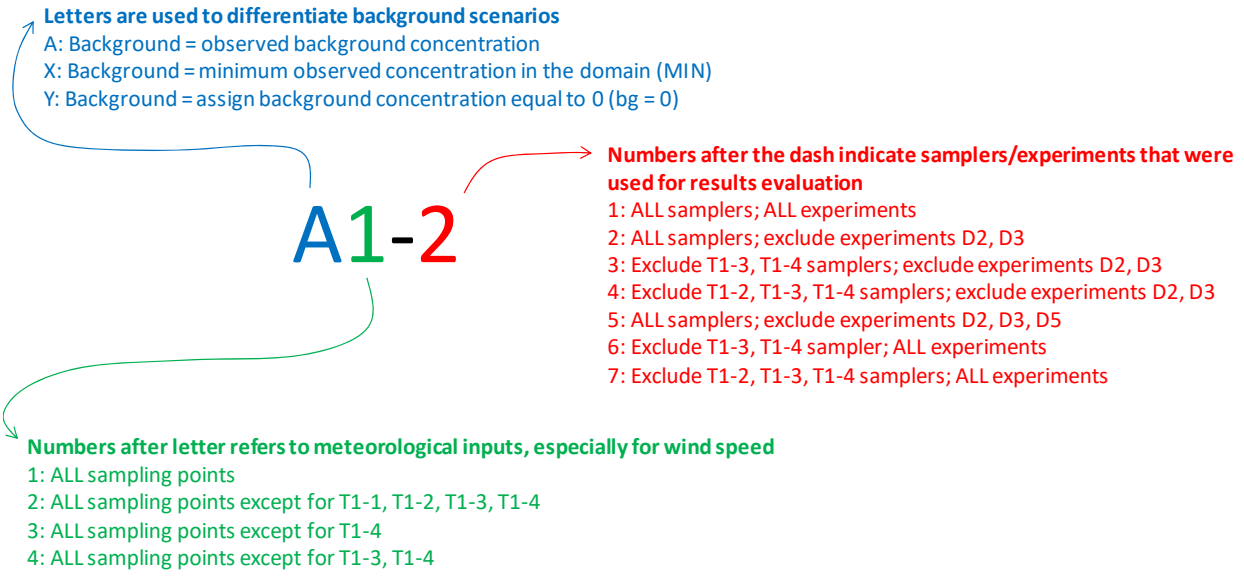

SI Figure 2-15 *FAC2* values for BGS versus changes in *L* for ammonia (A) and PM (B). L refers to the distance between virtual point and fan. The values inside each cell are *FAC2*. The color scale compares values *within a column* where red are greater *FAC2* values, and green are smaller values. Then the rows are compared.

(A)

Trend of FAC2 of NH3

L[m]	0.0	0.6	1.2	1.8	2.4	3.0	3.6	4.2	4.8	5.4	6.0	6.6	7.2	7.8	8.4	9.0	9.6	10.2	10.8	11.4	12.0
A1-1	0.39	0.49	0.53	0.51	0.50	0.50	0.52	0.53	0.54	0.54	0.53	0.53	0.52	0.53	0.53	0.52	0.52	0.50	0.49	0.49	0.49
A1-2	0.45	0.57	0.61	0.59	0.58	0.58	0.60	0.62	0.63	0.63	0.60	0.61	0.60	0.61	0.62	0.61	0.61	0.59	0.59	0.59	0.59
A1-3	0.43	0.57	0.62	0.59	0.58	0.58	0.61	0.63	0.63	0.63	0.61	0.61	0.60	0.61	0.61	0.60	0.59	0.58	0.58	0.58	0.57
A1-5	0.44	0.60	0.64	0.62	0.61	0.60	0.62	0.63	0.63	0.63	0.61	0.61	0.61	0.61	0.61	0.60	0.60	0.59	0.59	0.59	0.59
A1-6	0.50	0.64	0.69	0.66	0.65	0.65	0.68	0.70	0.71	0.71	0.68	0.69	0.68	0.68	0.69	0.68	0.68	0.66	0.66	0.66	0.65
A2-1	0.38	0.49	0.53	0.52	0.51	0.52	0.52	0.53	0.53	0.54	0.53	0.53	0.52	0.52	0.52	0.51	0.50	0.49	0.48	0.48	0.49
A2-2	0.44	0.57	0.62	0.60	0.59	0.60	0.60	0.62	0.62	0.62	0.60	0.61	0.60	0.60	0.60	0.60	0.59	0.58	0.58	0.58	0.59
A2-3	0.42	0.57	0.63	0.61	0.59	0.61	0.61	0.63	0.63	0.63	0.61	0.61	0.60	0.60	0.60	0.59	0.57	0.57	0.57	0.57	0.57
A2-5	0.43	0.60	0.65	0.63	0.62	0.63	0.62	0.63	0.63	0.63	0.61	0.61	0.60	0.60	0.60	0.59	0.58	0.58	0.58	0.58	0.59
A2-6	0.49	0.64	0.70	0.68	0.66	0.68	0.68	0.70	0.70	0.70	0.68	0.69	0.68	0.67	0.67	0.67	0.65	0.64	0.64	0.64	0.65
X1-1	0.38	0.53	0.56	0.57	0.57	0.57	0.56	0.55	0.55	0.55	0.56	0.57	0.56	0.56	0.56	0.54	0.54	0.53	0.53	0.54	0.53
X1-2	0.45	0.63	0.67	0.68	0.68	0.68	0.67	0.66	0.66	0.65	0.65	0.66	0.66	0.66	0.66	0.64	0.63	0.63	0.63	0.63	0.63
X1-3	0.42	0.62	0.67	0.68	0.68	0.68	0.67	0.65	0.65	0.64	0.63	0.65	0.64	0.65	0.65	0.63	0.62	0.62	0.61	0.62	0.60
X1-5	0.43	0.64	0.70	0.71	0.71	0.71	0.68	0.66	0.66	0.65	0.65	0.65	0.65	0.65	0.65	0.63	0.62	0.62	0.62	0.63	0.63
X1-6	0.51	0.71	0.76	0.77	0.77	0.77	0.76	0.74	0.74	0.73	0.73	0.75	0.74	0.74	0.74	0.71	0.71	0.71	0.70	0.71	0.70
X2-1	0.37	0.51	0.56	0.56	0.57	0.56	0.57	0.56	0.54	0.55	0.56	0.57	0.56	0.57	0.56	0.54	0.54	0.53	0.53	0.54	0.54
X2-2	0.45	0.60	0.66	0.67	0.68	0.67	0.68	0.66	0.65	0.65	0.65	0.66	0.65	0.66	0.66	0.63	0.63	0.63	0.63	0.63	0.63
X2-3	0.41	0.59	0.66	0.67	0.68	0.67	0.68	0.66	0.64	0.64	0.63	0.65	0.63	0.65	0.64	0.62	0.62	0.62	0.61	0.62	0.61
X2-5	0.42	0.62	0.69	0.70	0.71	0.70	0.69	0.67	0.65	0.65	0.65	0.65	0.65	0.65	0.64	0.62	0.62	0.62	0.62	0.63	0.63
X2-6	0.50	0.68	0.75	0.76	0.77	0.76	0.77	0.75	0.73	0.73	0.73	0.75	0.73	0.74	0.73	0.71	0.71	0.71	0.70	0.71	0.71
Y1-1	0.36	0.43	0.46	0.46	0.46	0.46	0.48	0.48	0.48	0.49	0.49	0.49	0.49	0.49	0.49	0.50	0.52	0.52	0.52	0.49	0.50
Y1-2	0.43	0.51	0.55	0.55	0.55	0.55	0.57	0.57	0.58	0.58	0.58	0.57	0.57	0.59	0.59	0.59	0.61	0.61	0.61	0.59	0.59
Y1-3	0.49	0.58	0.63	0.63	0.63	0.63	0.65	0.65	0.66	0.66	0.66	0.65	0.65	0.67	0.66	0.66	0.68	0.68	0.68	0.66	0.65
Y1-5	0.53	0.63	0.67	0.67	0.67	0.67	0.69	0.68	0.69	0.68	0.68	0.68	0.66	0.66	0.66	0.66	0.68	0.68	0.68	0.67	0.66
Y1-6	0.48	0.57	0.62	0.62	0.62	0.62	0.64	0.64	0.65	0.65	0.65	0.64	0.64	0.65	0.65	0.65	0.68	0.68	0.68	0.65	0.66
Y2-1	0.36	0.42	0.47	0.45	0.46	0.46	0.47	0.48	0.48	0.49	0.50	0.48	0.49	0.50	0.50	0.51	0.51	0.51	0.51	0.49	0.49
Y2-2	0.43	0.50	0.56	0.54	0.55	0.55	0.56	0.57	0.57	0.58	0.59	0.56	0.57	0.59	0.59	0.59	0.60	0.60	0.60	0.58	0.58
Y2-3	0.49	0.57	0.64	0.62	0.63	0.63	0.64	0.65	0.65	0.66	0.67	0.64	0.65	0.67	0.67	0.67	0.67	0.67	0.67	0.65	0.64
Y2-5	0.53	0.62	0.69	0.66	0.67	0.68	0.69	0.69	0.68	0.68	0.69	0.67	0.67	0.66	0.67	0.67	0.67	0.67	0.67	0.66	0.65
Y2-6	0.48	0.56	0.63	0.61	0.62	0.63	0.63	0.64	0.64	0.65	0.66	0.63	0.64	0.65	0.66	0.66	0.67	0.67	0.67	0.64	0.64

(B)

Trend of FAC2 of PM

L[m]	0.0	0.6	1.2	1.8	2.4	3.0	3.6	4.2	4.8	5.4	6.0	6.6	7.2	7.8	8.4	9.0	9.6	10.2	10.8	11.4	12.0
A1-1	0.49	0.52	0.51	0.52	0.52	0.52	0.52	0.51	0.51	0.51	0.54	0.54	0.53	0.53	0.53	0.53	0.53	0.53	0.53	0.52	0.51
A1-2	0.57	0.61	0.60	0.61	0.61	0.61	0.61	0.60	0.60	0.60	0.63	0.63	0.62	0.62	0.62	0.62	0.62	0.62	0.62	0.61	0.60
A1-3	0.57	0.62	0.61	0.62	0.62	0.62	0.62	0.61	0.61	0.61	0.63	0.63	0.63	0.63	0.63	0.63	0.63	0.63	0.63	0.62	0.61
A1-5	0.59	0.63	0.63	0.63	0.63	0.63	0.63	0.62	0.62	0.62	0.62	0.62	0.62	0.62	0.62	0.62	0.62	0.62	0.62	0.61	0.60
A1-6	0.64	0.69	0.68	0.69	0.69	0.69	0.69	0.68	0.68	0.68	0.70	0.70	0.70	0.70	0.70	0.70	0.70	0.70	0.69	0.68	0.67
A2-1	0.48	0.51	0.52	0.52	0.52	0.52	0.52	0.51	0.51	0.51	0.53	0.54	0.53	0.53	0.53	0.53	0.53	0.52	0.52	0.52	0.51
A2-2	0.56	0.60	0.61	0.61	0.61	0.61	0.61	0.60	0.60	0.60	0.62	0.63	0.62	0.62	0.62	0.62	0.62	0.61	0.61	0.61	0.59
A2-3	0.56	0.61	0.62	0.62	0.62	0.62	0.62	0.61	0.61	0.61	0.63	0.63	0.63	0.63	0.63	0.63	0.63	0.62	0.62	0.62	0.60
A2-5	0.58	0.63	0.63	0.63	0.63	0.63	0.63	0.62	0.62	0.62	0.62	0.62	0.62	0.62	0.62	0.62	0.62	0.61	0.61	0.61	0.59
A2-6	0.63	0.68	0.69	0.69	0.69	0.69	0.69	0.68	0.68	0.68	0.70	0.70	0.70	0.70	0.70	0.70	0.70	0.69	0.68	0.68	0.66
X1-1	0.56	0.64	0.62	0.61	0.61	0.61	0.63	0.63	0.63	0.64	0.63	0.64	0.64	0.64	0.65	0.65	0.65	0.65	0.65	0.64	0.63
X1-2	0.64	0.73	0.71	0.70	0.69	0.70	0.72	0.72	0.72	0.73	0.72	0.72	0.72	0.73	0.73	0.73	0.73	0.73	0.74	0.73	0.73
X1-3	0.63	0.72	0.70	0.69	0.68	0.69	0.71	0.71	0.71	0.71	0.71	0.71	0.71	0.71	0.72	0.72	0.72	0.72	0.73	0.72	0.71
X1-5	0.65	0.76	0.73	0.72	0.71	0.71	0.72	0.72	0.72	0.73	0.72	0.72	0.72	0.72	0.72	0.72	0.72	0.72	0.72	0.72	0.71
X1-6	0.72	0.83	0.80	0.79	0.78	0.79	0.81	0.81	0.81	0.82	0.81	0.81	0.81	0.82	0.83	0.83	0.83	0.83	0.83	0.82	0.81
X2-1	0.55	0.64	0.63	0.62	0.61	0.62	0.63	0.63	0.63	0.64	0.63	0.64	0.64	0.64	0.65	0.65	0.65	0.65	0.65	0.64	0.63
X2-2	0.63	0.73	0.71	0.71	0.70	0.71	0.72	0.72	0.72	0.73	0.72	0.72	0.72	0.73	0.73	0.73	0.73	0.73	0.74	0.73	0.73
X2-3	0.61	0.72	0.70	0.70	0.69	0.70	0.71	0.71	0.71	0.71	0.71	0.71	0.71	0.71	0.72	0.72	0.72	0.72	0.73	0.72	0.71
X2-5	0.63	0.76	0.73	0.73	0.72	0.72	0.72	0.72	0.72	0.73	0.72	0.72	0.72	0.72	0.72	0.72	0.72	0.72	0.72	0.72	0.71
X2-6	0.70	0.83	0.80	0.80	0.79	0.80	0.81	0.81	0.81	0.82	0.81	0.81	0.81	0.82	0.83	0.83	0.83	0.83	0.83	0.82	0.81
Y1-1	0.40	0.44	0.37	0.36	0.36	0.35	0.36	0.35	0.36	0.37	0.37	0.39	0.39	0.39	0.39	0.39	0.40	0.42	0.45	0.43	0.43
Y1-2	0.45	0.44	0.34	0.33	0.33	0.33	0.33	0.34	0.36	0.37	0.38	0.38	0.38	0.38	0.39	0.39	0.40	0.43	0.46	0.44	0.45
Y1-3	0.48	0.47	0.37	0.36	0.36	0.35	0.36	0.37	0.38	0.39	0.40	0.41	0.41	0.41	0.42	0.42	0.43	0.46	0.49	0.47	0.48
Y1-5	0.52	0.51	0.39	0.38	0.38	0.38	0.38	0.39	0.40	0.40	0.41	0.42	0.42	0.43	0.43	0.42	0.42	0.45	0.47	0.45	0.45
Y1-6	0.50	0.48	0.36	0.35	0.35	0.35	0.36	0.38	0.40	0.41	0.42	0.43	0.43	0.43	0.44	0.44	0.45	0.48	0.50	0.49	0.50
Y2-1	0.38	0.45	0.40	0.37	0.35	0.35	0.37	0.36	0.36	0.37	0.38	0.38	0.39	0.39	0.39	0.39	0.40	0.42	0.45	0.43	0.43
Y2-2	0.43	0.46	0.37	0.34	0.33	0.33	0.34	0.35	0.36	0.37	0.38	0.38	0.38	0.38	0.39	0.39	0.40	0.43	0.46	0.45	0.46
Y2-3	0.46	0.49	0.39	0.37	0.35	0.35	0.37	0.38	0.38	0.39	0.41	0.41	0.41	0.41	0.42	0.42	0.43	0.46	0.49	0.48	0.49
Y2-5	0.49	0.53	0.42	0.39	0.38	0.38	0.39	0.40	0.40	0.40	0.42	0.42	0.42	0.43	0.43	0.43	0.42	0.45	0.47	0.46	0.46
Y2-6	0.47	0.50	0.39	0.36	0.35	0.35	0.37	0.39	0.40	0.41	0.43	0.43	0.43	0.43	0.44	0.44	0.45	0.48	0.50	0.50	0.50

SI Figure 2-16. *FAC2* values for BGS versus changes in *L* for ammonia (A) and PM (B). *L* refers to the distance between virtual point and fan. The values inside each cell are *FAC2*. The color scale compares values *within a row* where red are greater *FAC2* values, and green are smaller values. Then the columns are compared.

(A)

Trend of optimal L of NH3

L[m]	0.0	0.6	1.2	1.8	2.4	3.0	3.6	4.2	4.8	5.4	6.0	6.6	7.2	7.8	8.4	9.0	9.6	10.2	10.8	11.4	12.0
A1-1	0.39	0.49	0.53	0.51	0.50	0.50	0.52	0.53	0.54	0.54	0.53	0.53	0.52	0.53	0.53	0.52	0.52	0.50	0.49	0.49	0.49
A1-2	0.45	0.57	0.61	0.59	0.58	0.58	0.60	0.62	0.63	0.63	0.60	0.61	0.60	0.61	0.62	0.61	0.61	0.59	0.59	0.59	0.59
A1-3	0.43	0.57	0.62	0.59	0.58	0.58	0.61	0.63	0.63	0.63	0.61	0.61	0.60	0.61	0.61	0.60	0.59	0.58	0.58	0.58	0.57
A1-5	0.44	0.60	0.64	0.62	0.61	0.60	0.62	0.63	0.63	0.63	0.61	0.61	0.61	0.61	0.61	0.60	0.60	0.59	0.59	0.59	0.59
A1-6	0.50	0.64	0.69	0.66	0.65	0.65	0.68	0.70	0.71	0.71	0.68	0.69	0.68	0.68	0.69	0.68	0.68	0.66	0.66	0.66	0.65
A2-1	0.38	0.49	0.53	0.52	0.51	0.52	0.52	0.53	0.53	0.54	0.53	0.53	0.52	0.52	0.52	0.51	0.50	0.49	0.48	0.48	0.49
A2-2	0.44	0.57	0.62	0.60	0.59	0.60	0.60	0.62	0.62	0.62	0.60	0.61	0.60	0.60	0.60	0.60	0.59	0.58	0.58	0.58	0.59
A2-3	0.42	0.57	0.63	0.61	0.59	0.61	0.61	0.63	0.63	0.63	0.61	0.61	0.60	0.60	0.60	0.59	0.57	0.57	0.57	0.57	0.57
A2-5	0.43	0.60	0.65	0.63	0.62	0.63	0.62	0.63	0.63	0.63	0.61	0.61	0.60	0.60	0.60	0.59	0.58	0.58	0.58	0.58	0.59
A2-6	0.49	0.64	0.70	0.68	0.66	0.68	0.68	0.70	0.70	0.70	0.68	0.69	0.68	0.67	0.67	0.67	0.65	0.64	0.64	0.64	0.65
X1-1	0.38	0.53	0.56	0.57	0.57	0.57	0.56	0.55	0.55	0.55	0.56	0.57	0.56	0.56	0.56	0.54	0.54	0.53	0.53	0.54	0.53
X1-2	0.45	0.63	0.67	0.68	0.68	0.68	0.67	0.66	0.66	0.65	0.65	0.66	0.66	0.66	0.66	0.64	0.63	0.63	0.63	0.63	0.63
X1-3	0.42	0.62	0.67	0.68	0.68	0.68	0.67	0.65	0.65	0.64	0.63	0.65	0.64	0.65	0.65	0.63	0.62	0.62	0.61	0.62	0.60
X1-5	0.43	0.64	0.70	0.71	0.71	0.71	0.68	0.66	0.66	0.65	0.65	0.65	0.65	0.65	0.65	0.63	0.62	0.62	0.62	0.63	0.63
X1-6	0.51	0.71	0.76	0.77	0.77	0.77	0.76	0.74	0.74	0.73	0.73	0.75	0.74	0.74	0.74	0.71	0.71	0.71	0.70	0.71	0.70
X2-1	0.37	0.51	0.56	0.56	0.57	0.56	0.57	0.56	0.54	0.55	0.56	0.57	0.56	0.57	0.56	0.54	0.54	0.53	0.53	0.54	0.54
X2-2	0.45	0.60	0.66	0.67	0.68	0.67	0.68	0.66	0.65	0.65	0.65	0.66	0.65	0.66	0.66	0.63	0.63	0.63	0.63	0.63	0.63
X2-3	0.41	0.59	0.66	0.67	0.68	0.67	0.68	0.66	0.64	0.64	0.63	0.65	0.63	0.65	0.64	0.62	0.62	0.62	0.61	0.62	0.61
X2-5	0.42	0.62	0.69	0.70	0.71	0.70	0.69	0.67	0.65	0.65	0.65	0.65	0.65	0.65	0.64	0.62	0.62	0.62	0.62	0.63	0.63
X2-6	0.50	0.68	0.75	0.76	0.77	0.76	0.77	0.75	0.73	0.73	0.73	0.75	0.73	0.74	0.73	0.71	0.71	0.71	0.70	0.71	0.71
Y1-1	0.36	0.43	0.46	0.46	0.46	0.46	0.48	0.48	0.48	0.49	0.49	0.49	0.49	0.49	0.49	0.50	0.52	0.52	0.52	0.49	0.50
Y1-2	0.43	0.51	0.55	0.55	0.55	0.55	0.57	0.57	0.58	0.58	0.58	0.57	0.57	0.59	0.59	0.59	0.61	0.61	0.61	0.59	0.59
Y1-3	0.49	0.58	0.63	0.63	0.63	0.63	0.65	0.65	0.66	0.66	0.66	0.65	0.65	0.67	0.66	0.66	0.68	0.68	0.68	0.66	0.65
Y1-5	0.53	0.63	0.67	0.67	0.67	0.67	0.69	0.68	0.69	0.68	0.68	0.68	0.66	0.66	0.66	0.66	0.68	0.68	0.68	0.67	0.66
Y1-6	0.48	0.57	0.62	0.62	0.62	0.62	0.64	0.64	0.65	0.65	0.65	0.64	0.64	0.65	0.65	0.65	0.68	0.68	0.68	0.65	0.66
Y2-1	0.36	0.42	0.47	0.45	0.46	0.46	0.47	0.48	0.48	0.49	0.50	0.48	0.49	0.50	0.50	0.51	0.51	0.51	0.51	0.49	0.49
Y2-2	0.43	0.50	0.56	0.54	0.55	0.55	0.56	0.57	0.57	0.58	0.59	0.56	0.57	0.59	0.59	0.59	0.60	0.60	0.60	0.58	0.58
Y2-3	0.49	0.57	0.64	0.62	0.63	0.63	0.64	0.65	0.65	0.66	0.67	0.64	0.65	0.67	0.67	0.67	0.67	0.67	0.67	0.65	0.64
Y2-5	0.53	0.62	0.69	0.66	0.67	0.68	0.69	0.69	0.68	0.68	0.69	0.67	0.67	0.66	0.67	0.67	0.67	0.67	0.67	0.66	0.65
Y2-6	0.48	0.56	0.63	0.61	0.62	0.63	0.63	0.64	0.64	0.65	0.66	0.63	0.64	0.65	0.66	0.66	0.67	0.67	0.67	0.64	0.64

(B)

Trend of optimal L of PM

L[m]	0.0	0.6	1.2	1.8	2.4	3.0	3.6	4.2	4.8	5.4	6.0	6.6	7.2	7.8	8.4	9.0	9.6	10.2	10.8	11.4	12.0
A1-1	0.49	0.52	0.51	0.52	0.52	0.52	0.52	0.51	0.51	0.51	0.54	0.54	0.53	0.53	0.53	0.53	0.53	0.53	0.53	0.52	0.51
A1-2	0.57	0.61	0.60	0.61	0.61	0.61	0.61	0.60	0.60	0.60	0.63	0.63	0.62	0.62	0.62	0.62	0.62	0.62	0.62	0.61	0.60
A1-3	0.57	0.62	0.61	0.62	0.62	0.62	0.62	0.61	0.61	0.61	0.63	0.63	0.63	0.63	0.63	0.63	0.63	0.63	0.63	0.62	0.61
A1-5	0.59	0.63	0.63	0.63	0.63	0.63	0.63	0.62	0.62	0.62	0.62	0.62	0.62	0.62	0.62	0.62	0.62	0.62	0.62	0.61	0.60
A1-6	0.64	0.69	0.68	0.69	0.69	0.69	0.69	0.68	0.68	0.68	0.70	0.70	0.70	0.70	0.70	0.70	0.70	0.70	0.69	0.68	0.67
A2-1	0.48	0.51	0.52	0.52	0.52	0.52	0.52	0.51	0.51	0.51	0.53	0.54	0.53	0.53	0.53	0.53	0.53	0.52	0.52	0.52	0.51
A2-2	0.56	0.60	0.61	0.61	0.61	0.61	0.61	0.60	0.60	0.60	0.62	0.63	0.62	0.62	0.62	0.62	0.62	0.61	0.61	0.61	0.59
A2-3	0.56	0.61	0.62	0.62	0.62	0.62	0.62	0.61	0.61	0.61	0.63	0.63	0.63	0.63	0.63	0.63	0.63	0.62	0.62	0.62	0.60
A2-5	0.58	0.63	0.63	0.63	0.63	0.63	0.63	0.62	0.62	0.62	0.62	0.62	0.62	0.62	0.62	0.62	0.62	0.61	0.61	0.61	0.59
A2-6	0.63	0.68	0.69	0.69	0.69	0.69	0.69	0.68	0.68	0.68	0.70	0.70	0.70	0.70	0.70	0.70	0.70	0.69	0.68	0.68	0.66
X1-1	0.56	0.64	0.62	0.61	0.61	0.61	0.63	0.63	0.63	0.64	0.63	0.64	0.64	0.64	0.65	0.65	0.65	0.65	0.65	0.64	0.63
X1-2	0.64	0.73	0.71	0.70	0.69	0.70	0.72	0.72	0.72	0.73	0.72	0.72	0.72	0.73	0.73	0.73	0.73	0.73	0.74	0.73	0.73
X1-3	0.63	0.72	0.70	0.69	0.68	0.69	0.71	0.71	0.71	0.71	0.71	0.71	0.71	0.71	0.72	0.72	0.72	0.72	0.73	0.72	0.71
X1-5	0.65	0.76	0.73	0.72	0.71	0.71	0.72	0.72	0.72	0.73	0.72	0.72	0.72	0.72	0.72	0.72	0.72	0.72	0.72	0.72	0.71
X1-6	0.72	0.83	0.80	0.79	0.78	0.79	0.81	0.81	0.81	0.82	0.81	0.81	0.81	0.82	0.83	0.83	0.83	0.83	0.83	0.82	0.81
X2-1	0.55	0.64	0.63	0.62	0.61	0.62	0.63	0.63	0.63	0.64	0.63	0.64	0.64	0.64	0.65	0.65	0.65	0.65	0.65	0.64	0.63
X2-2	0.63	0.73	0.71	0.71	0.70	0.71	0.72	0.72	0.72	0.73	0.72	0.72	0.72	0.73	0.73	0.73	0.73	0.73	0.74	0.73	0.73
X2-3	0.61	0.72	0.70	0.70	0.69	0.70	0.71	0.71	0.71	0.71	0.71	0.71	0.71	0.71	0.72	0.72	0.72	0.72	0.73	0.72	0.71
X2-5	0.63	0.76	0.73	0.73	0.72	0.72	0.72	0.72	0.72	0.73	0.72	0.72	0.72	0.72	0.72	0.72	0.72	0.72	0.72	0.72	0.71
X2-6	0.70	0.83	0.80	0.80	0.79	0.80	0.81	0.81	0.81	0.82	0.81	0.81	0.81	0.82	0.83	0.83	0.83	0.83	0.83	0.82	0.81
Y1-1	0.40	0.44	0.37	0.36	0.36	0.35	0.36	0.35	0.36	0.37	0.37	0.39	0.39	0.39	0.39	0.39	0.40	0.42	0.45	0.43	0.43
Y1-2	0.45	0.44	0.34	0.33	0.33	0.33	0.33	0.34	0.36	0.37	0.38	0.38	0.38	0.38	0.39	0.39	0.40	0.43	0.46	0.44	0.45
Y1-3	0.48	0.47	0.37	0.36	0.36	0.35	0.36	0.37	0.38	0.39	0.40	0.41	0.41	0.41	0.42	0.42	0.43	0.46	0.49	0.47	0.48
Y1-5	0.52	0.51	0.39	0.38	0.38	0.38	0.38	0.39	0.40	0.40	0.41	0.42	0.42	0.43	0.43	0.42	0.42	0.45	0.47	0.45	0.45
Y1-6	0.50	0.48	0.36	0.35	0.35	0.35	0.36	0.38	0.40	0.41	0.42	0.43	0.43	0.43	0.44	0.44	0.45	0.48	0.50	0.49	0.50
Y2-1	0.38	0.45	0.40	0.37	0.35	0.35	0.37	0.36	0.36	0.37	0.38	0.38	0.39	0.39	0.39	0.39	0.40	0.42	0.45	0.43	0.43
Y2-2	0.43	0.46	0.37	0.34	0.33	0.33	0.34	0.35	0.36	0.37	0.38	0.38	0.38	0.38	0.39	0.39	0.40	0.43	0.46	0.45	0.46
Y2-3	0.46	0.49	0.39	0.37	0.35	0.35	0.37	0.38	0.38	0.39	0.41	0.41	0.41	0.41	0.42	0.42	0.43	0.46	0.49	0.48	0.49
Y2-5	0.49	0.53	0.42	0.39	0.38	0.38	0.39	0.40	0.40	0.40	0.42	0.42	0.42	0.43	0.43	0.43	0.42	0.45	0.47	0.46	0.46
Y2-6	0.47	0.50	0.39	0.36	0.35	0.35	0.37	0.39	0.40	0.41	0.43	0.43	0.43	0.43	0.44	0.44	0.45	0.48	0.50	0.50	0.50

SI Figure 2-17. *FAC2* values for EXS versus changes in *L* for ammonia (A) and PM (B). *L* refers to the distance between virtual point and fan. The values inside each cell are *FAC2*. The color scale compares values *within a column* where red are greater *FAC2* values, and green are smaller values. Then the rows are compared.

(A)

Trend of FAC2 of NH3

L[m]	0.0	0.6	1.2	1.8	2.4	3.0	3.6	4.2	4.8	5.4	6.0	6.6	7.2	7.8	8.4	9.0	9.6	10.2	10.8	11.4	12.0
A1-1	0.39	0.49	0.53	0.51	0.50	0.50	0.52	0.53	0.54	0.54	0.53	0.53	0.52	0.53	0.53	0.52	0.52	0.50	0.49	0.49	0.49
A1-2	0.45	0.57	0.61	0.59	0.58	0.58	0.60	0.62	0.63	0.63	0.60	0.61	0.60	0.61	0.62	0.61	0.61	0.59	0.59	0.59	0.59
A1-5	0.50	0.64	0.69	0.66	0.65	0.65	0.68	0.70	0.71	0.71	0.68	0.69	0.68	0.68	0.69	0.68	0.68	0.66	0.66	0.66	0.65
A2-1	0.38	0.49	0.53	0.52	0.51	0.52	0.52	0.53	0.53	0.54	0.53	0.53	0.52	0.52	0.52	0.51	0.50	0.49	0.48	0.48	0.49
A2-2	0.44	0.57	0.62	0.60	0.59	0.60	0.60	0.62	0.62	0.62	0.60	0.61	0.60	0.60	0.60	0.60	0.59	0.58	0.58	0.58	0.59
A2-5	0.49	0.64	0.70	0.68	0.66	0.68	0.68	0.70	0.70	0.70	0.68	0.69	0.68	0.67	0.67	0.67	0.65	0.64	0.64	0.64	0.65
A4-1	0.41	0.50	0.53	0.51	0.50	0.50	0.51	0.53	0.54	0.55	0.53	0.53	0.53	0.53	0.53	0.53	0.51	0.50	0.49	0.49	0.49
A4-2	0.48	0.58	0.61	0.59	0.58	0.58	0.59	0.62	0.63	0.63	0.61	0.61	0.61	0.61	0.62	0.62	0.60	0.59	0.59	0.59	0.59
A4-5	0.54	0.65	0.69	0.67	0.65	0.65	0.67	0.70	0.71	0.71	0.69	0.69	0.68	0.68	0.69	0.69	0.67	0.66	0.66	0.66	0.65
X1-1	0.38	0.53	0.56	0.57	0.57	0.57	0.56	0.55	0.55	0.55	0.56	0.57	0.56	0.56	0.56	0.54	0.54	0.53	0.53	0.54	0.53
X1-2	0.45	0.63	0.67	0.68	0.68	0.68	0.67	0.66	0.66	0.65	0.65	0.66	0.66	0.66	0.66	0.64	0.63	0.63	0.63	0.63	0.63
X1-5	0.51	0.71	0.76	0.77	0.77	0.77	0.76	0.74	0.74	0.73	0.73	0.75	0.74	0.74	0.74	0.71	0.71	0.71	0.70	0.71	0.70
X2-1	0.37	0.51	0.56	0.56	0.57	0.56	0.57	0.56	0.54	0.55	0.56	0.57	0.56	0.57	0.56	0.54	0.54	0.53	0.53	0.54	0.54
X2-2	0.45	0.60	0.66	0.67	0.68	0.67	0.68	0.66	0.65	0.65	0.65	0.66	0.65	0.66	0.66	0.63	0.63	0.63	0.63	0.63	0.63
X2-5	0.50	0.68	0.75	0.76	0.77	0.76	0.77	0.75	0.73	0.73	0.73	0.75	0.73	0.74	0.73	0.71	0.71	0.71	0.70	0.71	0.71

(B)

Trend of FAC2 of PM

L[m]	0.0	0.6	1.2	1.8	2.4	3.0	3.6	4.2	4.8	5.4	6.0	6.6	7.2	7.8	8.4	9.0	9.6	10.2	10.8	11.4	12.0
A1-1	0.49	0.52	0.51	0.52	0.52	0.52	0.52	0.51	0.51	0.51	0.54	0.54	0.53	0.53	0.53	0.53	0.53	0.53	0.53	0.52	0.51
A1-2	0.57	0.61	0.60	0.61	0.61	0.61	0.61	0.60	0.60	0.60	0.63	0.63	0.62	0.62	0.62	0.62	0.62	0.62	0.62	0.61	0.60
A1-5	0.64	0.69	0.68	0.69	0.69	0.69	0.69	0.68	0.68	0.68	0.70	0.70	0.70	0.70	0.70	0.70	0.70	0.70	0.69	0.68	0.67
A2-1	0.48	0.51	0.52	0.52	0.52	0.52	0.52	0.51	0.51	0.51	0.53	0.54	0.53	0.53	0.53	0.53	0.53	0.52	0.52	0.52	0.51
A2-2	0.56	0.60	0.61	0.61	0.61	0.61	0.61	0.60	0.60	0.60	0.62	0.63	0.62	0.62	0.62	0.62	0.62	0.61	0.61	0.61	0.59
A2-5	0.63	0.68	0.69	0.69	0.69	0.69	0.69	0.68	0.68	0.68	0.70	0.70	0.70	0.70	0.70	0.70	0.70	0.69	0.68	0.68	0.66
A4-1	0.49	0.52	0.51	0.52	0.52	0.52	0.52	0.51	0.51	0.51	0.54	0.54	0.53	0.53	0.53	0.53	0.53	0.52	0.52	0.52	0.51
A4-2	0.58	0.61	0.60	0.61	0.61	0.61	0.61	0.60	0.60	0.60	0.63	0.63	0.62	0.62	0.62	0.62	0.62	0.61	0.61	0.61	0.59
A4-5	0.65	0.69	0.68	0.69	0.69	0.69	0.69	0.68	0.68	0.68	0.70	0.70	0.70	0.70	0.70	0.70	0.70	0.69	0.68	0.68	0.66
X1-1	0.56	0.64	0.62	0.61	0.61	0.61	0.63	0.63	0.63	0.64	0.63	0.64	0.64	0.64	0.65	0.65	0.65	0.65	0.65	0.64	0.63
X1-2	0.64	0.73	0.71	0.70	0.69	0.70	0.72	0.72	0.72	0.73	0.72	0.72	0.72	0.73	0.73	0.73	0.73	0.73	0.74	0.73	0.73
X1-5	0.72	0.83	0.80	0.79	0.78	0.79	0.81	0.81	0.81	0.82	0.81	0.81	0.81	0.82	0.83	0.83	0.83	0.83	0.83	0.82	0.81
X2-1	0.55	0.64	0.63	0.62	0.61	0.62	0.63	0.63	0.63	0.64	0.63	0.64	0.64	0.64	0.65	0.65	0.65	0.65	0.65	0.64	0.63
X2-2	0.63	0.73	0.71	0.71	0.70	0.71	0.72	0.72	0.72	0.73	0.72	0.72	0.72	0.73	0.73	0.73	0.73	0.73	0.74	0.73	0.73
X2-5	0.70	0.83	0.80	0.80	0.79	0.80	0.81	0.81	0.81	0.82	0.81	0.81	0.81	0.82	0.83	0.83	0.83	0.83	0.83	0.82	0.81

SI Figure 2-18. *FAC2* values for EXS versus changes in *L* for ammonia (A) and PM (B). *L* refers to the distance between virtual point and fan. The values inside each cell are *FAC2*. The color scale compares values *within a row* where red are greater *FAC2* values, and green are smaller values. Then the columns are compared.

(A)

Trend of optimal L of NH3

L[m]	0.0	0.6	1.2	1.8	2.4	3.0	3.6	4.2	4.8	5.4	6.0	6.6	7.2	7.8	8.4	9.0	9.6	10.2	10.8	11.4	12.0
A1-1	0.39	0.49	0.53	0.51	0.50	0.50	0.52	0.53	0.54	0.54	0.53	0.53	0.52	0.53	0.53	0.52	0.52	0.50	0.49	0.49	0.49
A1-2	0.45	0.57	0.61	0.59	0.58	0.58	0.60	0.62	0.63	0.63	0.60	0.61	0.60	0.61	0.62	0.61	0.61	0.59	0.59	0.59	0.59
A1-5	0.50	0.64	0.69	0.66	0.65	0.65	0.68	0.70	0.71	0.71	0.68	0.69	0.68	0.68	0.69	0.68	0.68	0.66	0.66	0.66	0.65
A2-1	0.38	0.49	0.53	0.52	0.51	0.52	0.52	0.53	0.53	0.54	0.53	0.53	0.52	0.52	0.52	0.51	0.50	0.49	0.48	0.48	0.49
A2-2	0.44	0.57	0.62	0.60	0.59	0.60	0.60	0.62	0.62	0.62	0.60	0.61	0.60	0.60	0.60	0.60	0.59	0.58	0.58	0.58	0.59
A2-5	0.49	0.64	0.70	0.68	0.66	0.68	0.68	0.70	0.70	0.70	0.68	0.69	0.68	0.67	0.67	0.67	0.65	0.64	0.64	0.64	0.65
A4-1	0.41	0.50	0.53	0.51	0.50	0.50	0.51	0.53	0.54	0.55	0.53	0.53	0.53	0.53	0.53	0.53	0.51	0.50	0.49	0.49	0.49
A4-2	0.48	0.58	0.61	0.59	0.58	0.58	0.59	0.62	0.63	0.63	0.61	0.61	0.61	0.61	0.62	0.62	0.60	0.59	0.59	0.59	0.59
A4-5	0.54	0.65	0.69	0.67	0.65	0.65	0.67	0.70	0.71	0.71	0.69	0.69	0.68	0.68	0.69	0.69	0.67	0.66	0.66	0.66	0.65
X1-1	0.38	0.53	0.56	0.57	0.57	0.57	0.56	0.55	0.55	0.55	0.56	0.57	0.56	0.56	0.56	0.54	0.54	0.53	0.53	0.54	0.53
X1-2	0.45	0.63	0.67	0.68	0.68	0.68	0.67	0.66	0.66	0.65	0.65	0.66	0.66	0.66	0.66	0.64	0.63	0.63	0.63	0.63	0.63
X1-5	0.51	0.71	0.76	0.77	0.77	0.77	0.76	0.74	0.74	0.73	0.73	0.75	0.74	0.74	0.74	0.71	0.71	0.71	0.70	0.71	0.70
X2-1	0.37	0.51	0.56	0.56	0.57	0.56	0.57	0.56	0.54	0.55	0.56	0.57	0.56	0.57	0.56	0.54	0.54	0.53	0.53	0.54	0.54
X2-2	0.45	0.60	0.66	0.67	0.68	0.67	0.68	0.66	0.65	0.65	0.65	0.66	0.65	0.66	0.66	0.63	0.63	0.63	0.63	0.63	0.63
X2-5	0.50	0.68	0.75	0.76	0.77	0.76	0.77	0.75	0.73	0.73	0.73	0.75	0.73	0.74	0.73	0.71	0.71	0.71	0.70	0.71	0.71

(B)

Trend of optimal L of PM

L[m]	0.0	0.6	1.2	1.8	2.4	3.0	3.6	4.2	4.8	5.4	6.0	6.6	7.2	7.8	8.4	9.0	9.6	10.2	10.8	11.4	12.0
A1-1	0.49	0.52	0.51	0.52	0.52	0.52	0.52	0.51	0.51	0.51	0.54	0.54	0.53	0.53	0.53	0.53	0.53	0.53	0.53	0.52	0.51
A1-2	0.57	0.61	0.60	0.61	0.61	0.61	0.61	0.60	0.60	0.60	0.63	0.63	0.62	0.62	0.62	0.62	0.62	0.62	0.62	0.61	0.60
A1-5	0.64	0.69	0.68	0.69	0.69	0.69	0.69	0.68	0.68	0.68	0.70	0.70	0.70	0.70	0.70	0.70	0.70	0.70	0.69	0.68	0.67
A2-1	0.48	0.51	0.52	0.52	0.52	0.52	0.52	0.51	0.51	0.51	0.53	0.54	0.53	0.53	0.53	0.53	0.53	0.52	0.52	0.52	0.51
A2-2	0.56	0.60	0.61	0.61	0.61	0.61	0.61	0.60	0.60	0.60	0.62	0.63	0.62	0.62	0.62	0.62	0.62	0.61	0.61	0.61	0.59
A2-5	0.63	0.68	0.69	0.69	0.69	0.69	0.69	0.68	0.68	0.68	0.70	0.70	0.70	0.70	0.70	0.70	0.70	0.69	0.68	0.68	0.66
A4-1	0.49	0.52	0.51	0.52	0.52	0.52	0.52	0.51	0.51	0.51	0.54	0.54	0.53	0.53	0.53	0.53	0.53	0.52	0.52	0.52	0.51
A4-2	0.58	0.61	0.60	0.61	0.61	0.61	0.61	0.60	0.60	0.60	0.63	0.63	0.62	0.62	0.62	0.62	0.62	0.61	0.61	0.61	0.59
A4-5	0.65	0.69	0.68	0.69	0.69	0.69	0.69	0.68	0.68	0.68	0.70	0.70	0.70	0.70	0.70	0.70	0.70	0.69	0.68	0.68	0.66
X1-1	0.56	0.64	0.62	0.61	0.61	0.61	0.63	0.63	0.63	0.64	0.63	0.64	0.64	0.64	0.65	0.65	0.65	0.65	0.65	0.64	0.63
X1-2	0.64	0.73	0.71	0.70	0.69	0.70	0.72	0.72	0.72	0.73	0.72	0.72	0.72	0.73	0.73	0.73	0.73	0.73	0.74	0.73	0.73
X1-5	0.72	0.83	0.80	0.79	0.78	0.79	0.81	0.81	0.81	0.82	0.81	0.81	0.81	0.82	0.83	0.83	0.83	0.83	0.83	0.82	0.81
X2-1	0.55	0.64	0.63	0.62	0.61	0.62	0.63	0.63	0.63	0.64	0.63	0.64	0.64	0.64	0.65	0.65	0.65	0.65	0.65	0.64	0.63
X2-2	0.63	0.73	0.71	0.71	0.70	0.71	0.72	0.72	0.72	0.73	0.72	0.72	0.72	0.73	0.73	0.73	0.73	0.73	0.74	0.73	0.73
X2-5	0.70	0.83	0.80	0.80	0.79	0.80	0.81	0.81	0.81	0.82	0.81	0.81	0.81	0.82	0.83	0.83	0.83	0.83	0.83	0.82	0.81

SI Figure 2-19. *FAC2* values for SPS versus changes in *L* for ammonia (A) and PM (B). *L* refers to the distance between virtual point and fan. The values inside each cell are *FAC2*. The color scale compares values *within a column* where red are greater *FAC2* values, and green are smaller values. Then the rows are compared.

(A)

Trend of FAC2 of NH3

L[m]	0.0	0.6	1.2	1.8	2.4	3.0	3.6	4.2	4.8	5.4	6.0	6.6	7.2	7.8	8.4	9.0	9.6	10.2	10.8	11.4	12.0
A1-2	0.45	0.57	0.61	0.59	0.58	0.58	0.60	0.62	0.63	0.63	0.60	0.61	0.60	0.61	0.62	0.61	0.61	0.59	0.59	0.59	0.59
A1-3	0.43	0.57	0.62	0.59	0.58	0.58	0.61	0.63	0.63	0.63	0.61	0.61	0.60	0.61	0.61	0.60	0.59	0.58	0.58	0.58	0.57
A1-4	0.44	0.60	0.64	0.62	0.61	0.60	0.62	0.63	0.63	0.63	0.61	0.61	0.61	0.61	0.61	0.60	0.60	0.59	0.59	0.59	0.59
A2-2	0.44	0.57	0.62	0.60	0.59	0.60	0.60	0.62	0.62	0.62	0.60	0.61	0.60	0.60	0.60	0.60	0.59	0.58	0.58	0.58	0.59
A2-3	0.42	0.57	0.63	0.61	0.59	0.61	0.61	0.63	0.63	0.63	0.61	0.61	0.60	0.60	0.60	0.59	0.57	0.57	0.57	0.57	0.57
A2-4	0.43	0.60	0.65	0.63	0.62	0.63	0.62	0.63	0.63	0.63	0.61	0.61	0.60	0.60	0.60	0.59	0.58	0.58	0.58	0.58	0.59
A4-2	0.48	0.58	0.61	0.59	0.58	0.58	0.59	0.62	0.63	0.63	0.61	0.61	0.61	0.61	0.62	0.62	0.60	0.59	0.59	0.59	0.59
A4-3	0.46	0.58	0.62	0.60	0.58	0.58	0.60	0.63	0.63	0.64	0.62	0.61	0.61	0.61	0.61	0.61	0.59	0.58	0.58	0.58	0.57
A4-4	0.48	0.61	0.64	0.63	0.61	0.60	0.61	0.63	0.63	0.63	0.62	0.61	0.61	0.61	0.61	0.61	0.60	0.59	0.59	0.59	0.59
X1-2	0.45	0.63	0.67	0.68	0.68	0.68	0.67	0.66	0.66	0.65	0.65	0.66	0.66	0.66	0.66	0.64	0.63	0.63	0.63	0.63	0.63
X1-3	0.42	0.62	0.67	0.68	0.68	0.68	0.67	0.65	0.65	0.64	0.63	0.65	0.64	0.65	0.65	0.63	0.62	0.62	0.61	0.62	0.60
X1-4	0.43	0.64	0.70	0.71	0.71	0.71	0.68	0.66	0.66	0.65	0.65	0.65	0.65	0.65	0.65	0.63	0.62	0.62	0.62	0.63	0.63
X2-2	0.45	0.60	0.66	0.67	0.68	0.67	0.68	0.66	0.65	0.65	0.65	0.66	0.65	0.66	0.66	0.63	0.63	0.63	0.63	0.63	0.63
X2-3	0.41	0.59	0.66	0.67	0.68	0.67	0.68	0.66	0.64	0.64	0.63	0.65	0.63	0.65	0.64	0.62	0.62	0.62	0.61	0.62	0.61
X2-4	0.42	0.62	0.69	0.70	0.71	0.70	0.69	0.67	0.65	0.65	0.65	0.65	0.65	0.65	0.64	0.62	0.62	0.62	0.62	0.63	0.63

(B)

Trend of FAC2 of PM

L[m]	0.0	0.6	1.2	1.8	2.4	3.0	3.6	4.2	4.8	5.4	6.0	6.6	7.2	7.8	8.4	9.0	9.6	10.2	10.8	11.4	12.0
A1-2	0.57	0.61	0.60	0.61	0.61	0.61	0.61	0.60	0.60	0.60	0.63	0.63	0.62	0.62	0.62	0.62	0.62	0.62	0.62	0.61	0.60
A1-3	0.57	0.62	0.61	0.62	0.62	0.62	0.62	0.61	0.61	0.61	0.63	0.63	0.63	0.63	0.63	0.63	0.63	0.63	0.63	0.62	0.61
A1-4	0.59	0.63	0.63	0.63	0.63	0.63	0.63	0.62	0.62	0.62	0.62	0.62	0.62	0.62	0.62	0.62	0.62	0.62	0.62	0.61	0.60
A2-2	0.56	0.60	0.61	0.61	0.61	0.61	0.61	0.60	0.60	0.60	0.62	0.63	0.62	0.62	0.62	0.62	0.62	0.61	0.61	0.61	0.59
A2-3	0.56	0.61	0.62	0.62	0.62	0.62	0.62	0.61	0.61	0.61	0.63	0.63	0.63	0.63	0.63	0.63	0.63	0.62	0.62	0.62	0.60
A2-4	0.58	0.63	0.63	0.63	0.63	0.63	0.63	0.62	0.62	0.62	0.62	0.62	0.62	0.62	0.62	0.62	0.62	0.61	0.61	0.61	0.59
A4-2	0.58	0.61	0.60	0.61	0.61	0.61	0.61	0.60	0.60	0.60	0.63	0.63	0.62	0.62	0.62	0.62	0.62	0.61	0.61	0.61	0.59
A4-3	0.58	0.62	0.61	0.62	0.62	0.62	0.62	0.61	0.61	0.61	0.63	0.63	0.63	0.63	0.63	0.63	0.63	0.62	0.62	0.62	0.60
A4-4	0.60	0.63	0.63	0.63	0.63	0.63	0.63	0.62	0.62	0.62	0.62	0.62	0.62	0.62	0.62	0.62	0.62	0.62	0.61	0.61	0.59
X1-2	0.64	0.73	0.71	0.70	0.69	0.70	0.72	0.72	0.72	0.73	0.72	0.72	0.72	0.73	0.73	0.73	0.73	0.73	0.74	0.73	0.73
X1-3	0.63	0.72	0.70	0.69	0.68	0.69	0.71	0.71	0.71	0.71	0.71	0.71	0.71	0.71	0.72	0.72	0.72	0.72	0.73	0.72	0.71
X1-4	0.65	0.76	0.73	0.72	0.71	0.71	0.72	0.72	0.72	0.73	0.72	0.72	0.72	0.72	0.72	0.72	0.72	0.72	0.72	0.72	0.71
X2-2	0.63	0.73	0.71	0.71	0.70	0.71	0.72	0.72	0.72	0.73	0.72	0.72	0.72	0.73	0.73	0.73	0.73	0.73	0.74	0.73	0.73
X2-3	0.61	0.72	0.70	0.70	0.69	0.70	0.71	0.71	0.71	0.71	0.71	0.71	0.71	0.71	0.72	0.72	0.72	0.72	0.73	0.72	0.71
X2-4	0.63	0.76	0.73	0.73	0.72	0.72	0.72	0.72	0.72	0.73	0.72	0.72	0.72	0.72	0.72	0.72	0.72	0.72	0.72	0.72	0.71

SI Figure 2-20. *FAC2* values for SPS versus changes in *L* for ammonia (A) and PM (B). *L* refers to the distance between virtual point and fan. The values inside each cell are *FAC2*. The color scale compares values *within a row* where red are greater *FAC2* values, and green are smaller values. Then the columns are compared.

(A)

Trend of optimal L of NH3

L[m]	0.0	0.6	1.2	1.8	2.4	3.0	3.6	4.2	4.8	5.4	6.0	6.6	7.2	7.8	8.4	9.0	9.6	10.2	10.8	11.4	12.0
A1-2	0.45	0.57	0.61	0.59	0.58	0.58	0.60	0.62	0.63	0.63	0.60	0.61	0.60	0.61	0.62	0.61	0.61	0.59	0.59	0.59	0.59
A1-3	0.43	0.57	0.62	0.59	0.58	0.58	0.61	0.63	0.63	0.63	0.61	0.61	0.60	0.61	0.61	0.60	0.59	0.58	0.58	0.58	0.57
A1-4	0.44	0.60	0.64	0.62	0.61	0.60	0.62	0.63	0.63	0.63	0.61	0.61	0.61	0.61	0.61	0.60	0.60	0.59	0.59	0.59	0.59
A2-2	0.44	0.57	0.62	0.60	0.59	0.60	0.60	0.62	0.62	0.62	0.60	0.61	0.60	0.60	0.60	0.60	0.59	0.58	0.58	0.58	0.59
A2-3	0.42	0.57	0.63	0.61	0.59	0.61	0.61	0.63	0.63	0.63	0.61	0.61	0.60	0.60	0.60	0.59	0.57	0.57	0.57	0.57	0.57
A2-4	0.43	0.60	0.65	0.63	0.62	0.63	0.62	0.63	0.63	0.63	0.61	0.61	0.60	0.60	0.60	0.59	0.58	0.58	0.58	0.58	0.59
A4-2	0.48	0.58	0.61	0.59	0.58	0.58	0.59	0.62	0.63	0.63	0.61	0.61	0.61	0.61	0.62	0.62	0.60	0.59	0.59	0.59	0.59
A4-3	0.46	0.58	0.62	0.60	0.58	0.58	0.60	0.63	0.63	0.64	0.62	0.61	0.61	0.61	0.61	0.61	0.59	0.58	0.58	0.58	0.57
A4-4	0.48	0.61	0.64	0.63	0.61	0.60	0.61	0.63	0.63	0.63	0.62	0.61	0.61	0.61	0.61	0.61	0.60	0.59	0.59	0.59	0.59
X1-2	0.45	0.63	0.67	0.68	0.68	0.68	0.67	0.66	0.66	0.65	0.65	0.66	0.66	0.66	0.66	0.64	0.63	0.63	0.63	0.63	0.63
X1-3	0.42	0.62	0.67	0.68	0.68	0.68	0.67	0.65	0.65	0.64	0.63	0.65	0.64	0.65	0.65	0.63	0.62	0.62	0.61	0.62	0.60
X1-4	0.43	0.64	0.70	0.71	0.71	0.71	0.68	0.66	0.66	0.65	0.65	0.65	0.65	0.65	0.65	0.63	0.62	0.62	0.62	0.63	0.63
X2-2	0.45	0.60	0.66	0.67	0.68	0.67	0.68	0.66	0.65	0.65	0.65	0.66	0.65	0.66	0.66	0.63	0.63	0.63	0.63	0.63	0.63
X2-3	0.41	0.59	0.66	0.67	0.68	0.67	0.68	0.66	0.64	0.64	0.63	0.65	0.63	0.65	0.64	0.62	0.62	0.62	0.61	0.62	0.61
X2-4	0.42	0.62	0.69	0.70	0.71	0.70	0.69	0.67	0.65	0.65	0.65	0.65	0.65	0.65	0.64	0.62	0.62	0.62	0.62	0.63	0.63

(b)

Trend of optimal L of PM

L[m]	0.0	0.6	1.2	1.8	2.4	3.0	3.6	4.2	4.8	5.4	6.0	6.6	7.2	7.8	8.4	9.0	9.6	10.2	10.8	11.4	12.0
A1-2	0.57	0.61	0.60	0.61	0.61	0.61	0.61	0.60	0.60	0.60	0.63	0.63	0.62	0.62	0.62	0.62	0.62	0.62	0.62	0.61	0.60
A1-3	0.57	0.62	0.61	0.62	0.62	0.62	0.62	0.61	0.61	0.61	0.63	0.63	0.63	0.63	0.63	0.63	0.63	0.63	0.63	0.62	0.61
A1-4	0.59	0.63	0.63	0.63	0.63	0.63	0.63	0.62	0.62	0.62	0.62	0.62	0.62	0.62	0.62	0.62	0.62	0.62	0.62	0.61	0.60
A2-2	0.56	0.60	0.61	0.61	0.61	0.61	0.61	0.60	0.60	0.60	0.62	0.63	0.62	0.62	0.62	0.62	0.62	0.61	0.61	0.61	0.59
A2-3	0.56	0.61	0.62	0.62	0.62	0.62	0.62	0.61	0.61	0.61	0.63	0.63	0.63	0.63	0.63	0.63	0.63	0.62	0.62	0.62	0.60
A2-4	0.58	0.63	0.63	0.63	0.63	0.63	0.63	0.62	0.62	0.62	0.62	0.62	0.62	0.62	0.62	0.62	0.62	0.61	0.61	0.61	0.59
A4-2	0.58	0.61	0.60	0.61	0.61	0.61	0.61	0.60	0.60	0.60	0.63	0.63	0.62	0.62	0.62	0.62	0.62	0.61	0.61	0.61	0.59
A4-3	0.58	0.62	0.61	0.62	0.62	0.62	0.62	0.61	0.61	0.61	0.63	0.63	0.63	0.63	0.63	0.63	0.63	0.62	0.62	0.62	0.60
A4-4	0.60	0.63	0.63	0.63	0.63	0.63	0.63	0.62	0.62	0.62	0.62	0.62	0.62	0.62	0.62	0.62	0.62	0.62	0.61	0.61	0.59
X1-2	0.64	0.73	0.71	0.70	0.69	0.70	0.72	0.72	0.72	0.73	0.72	0.72	0.72	0.73	0.73	0.73	0.73	0.73	0.74	0.73	0.73
X1-3	0.63	0.72	0.70	0.69	0.68	0.69	0.71	0.71	0.71	0.71	0.71	0.71	0.71	0.71	0.72	0.72	0.72	0.72	0.73	0.72	0.71
X1-4	0.65	0.76	0.73	0.72	0.71	0.71	0.72	0.72	0.72	0.73	0.72	0.72	0.72	0.72	0.72	0.72	0.72	0.72	0.72	0.72	0.71
X2-2	0.63	0.73	0.71	0.71	0.70	0.71	0.72	0.72	0.72	0.73	0.72	0.72	0.72	0.73	0.73	0.73	0.73	0.73	0.74	0.73	0.73
X2-3	0.61	0.72	0.70	0.70	0.69	0.70	0.71	0.71	0.71	0.71	0.71	0.71	0.71	0.71	0.72	0.72	0.72	0.72	0.73	0.72	0.71
X2-4	0.63	0.76	0.73	0.73	0.72	0.72	0.72	0.72	0.72	0.73	0.72	0.72	0.72	0.72	0.72	0.72	0.72	0.72	0.72	0.72	0.71

SI Figure 2-21. *FAC2* values for WSS versus changes in *L* for ammonia (A) and PM (B). *L* refers to the distance between virtual point and fan. The values inside each cell are *FAC2*. The color scale compares values *within a column* where red are greater *FAC2* values, and green are smaller values. Then the rows are compared.

(A)

Trend of FAC2 of NH3

L[m]	0.0	0.6	1.2	1.8	2.4	3.0	3.6	4.2	4.8	5.4	6.0	6.6	7.2	7.8	8.4	9.0	9.6	10.2	10.8	11.4	12.0
A1-2	0.45	0.57	0.61	0.59	0.58	0.58	0.60	0.62	0.63	0.63	0.60	0.61	0.60	0.61	0.62	0.61	0.61	0.59	0.59	0.59	0.59
A2-2	0.44	0.57	0.62	0.60	0.59	0.60	0.60	0.62	0.62	0.62	0.60	0.61	0.60	0.60	0.60	0.60	0.59	0.58	0.58	0.58	0.59
B1-2	0.52	0.59	0.61	0.59	0.57	0.59	0.59	0.59	0.63	0.63	0.62	0.62	0.61	0.61	0.62	0.61	0.61	0.60	0.59	0.59	0.59
B2-2	0.52	0.59	0.61	0.59	0.57	0.59	0.59	0.59	0.63	0.63	0.62	0.62	0.61	0.61	0.62	0.61	0.61	0.60	0.59	0.59	0.59
C1-2	0.55	0.61	0.59	0.58	0.59	0.60	0.60	0.59	0.61	0.59	0.62	0.62	0.62	0.59	0.59	0.59	0.59	0.58	0.59	0.56	0.55
C2-2	0.54	0.61	0.59	0.59	0.59	0.60	0.60	0.59	0.59	0.59	0.59	0.60	0.61	0.60	0.59	0.59	0.59	0.58	0.58	0.56	0.55
D1-2	0.57	0.57	0.58	0.58	0.59	0.59	0.58	0.59	0.59	0.59	0.58	0.59	0.58	0.57	0.54	0.53	0.55	0.53	0.53	0.53	0.52
D2-2	0.57	0.57	0.58	0.58	0.59	0.59	0.58	0.59	0.59	0.59	0.58	0.59	0.58	0.57	0.54	0.53	0.55	0.53	0.53	0.53	0.52

(B)

Trend of FAC2 of PM

L[m]	0.0	0.6	1.2	1.8	2.4	3.0	3.6	4.2	4.8	5.4	6.0	6.6	7.2	7.8	8.4	9.0	9.6	10.2	10.8	11.4	12.0
A1-2	0.57	0.61	0.60	0.61	0.61	0.61	0.61	0.60	0.60	0.60	0.63	0.63	0.62	0.62	0.62	0.62	0.62	0.62	0.62	0.61	0.60
A2-2	0.56	0.60	0.61	0.61	0.61	0.61	0.61	0.60	0.60	0.60	0.62	0.63	0.62	0.62	0.62	0.62	0.62	0.61	0.61	0.61	0.59
B1-2	0.59	0.62	0.60	0.61	0.60	0.61	0.61	0.60	0.60	0.60	0.63	0.63	0.62	0.62	0.61	0.61	0.61	0.61	0.61	0.61	0.60
B2-2	0.59	0.62	0.60	0.61	0.60	0.61	0.61	0.60	0.60	0.60	0.63	0.63	0.62	0.62	0.61	0.61	0.61	0.61	0.61	0.61	0.60
C1-2	0.61	0.60	0.60	0.59	0.60	0.60	0.60	0.60	0.60	0.62	0.62	0.61	0.61	0.61	0.61	0.62	0.61	0.61	0.61	0.60	0.60
C2-2	0.59	0.61	0.60	0.60	0.60	0.60	0.60	0.60	0.60	0.61	0.62	0.61	0.61	0.61	0.61	0.61	0.61	0.61	0.61	0.60	0.60
D1-2	0.61	0.59	0.58	0.59	0.59	0.60	0.60	0.60	0.62	0.63	0.62	0.62	0.62	0.62	0.63	0.62	0.62	0.62	0.60	0.60	0.60
D2-2	0.61	0.59	0.58	0.59	0.59	0.60	0.60	0.60	0.62	0.63	0.62	0.62	0.62	0.62	0.63	0.62	0.62	0.62	0.60	0.60	0.60

SI Figure 2-22. *FAC2* values for WSS versus changes in *L* for ammonia (A) and PM (B). *L* refers to the distance between virtual point and fan. The values inside each cell are *FAC2*. The color scale compares values *within a row* where red are greater *FAC2* values, and green are smaller values. Then the columns are compared.

(A)

Trend of optimal L of NH3

L[m]	0.0	0.6	1.2	1.8	2.4	3.0	3.6	4.2	4.8	5.4	6.0	6.6	7.2	7.8	8.4	9.0	9.6	10.2	10.8	11.4	12.0
A1-2	0.45	0.57	0.61	0.59	0.58	0.58	0.60	0.62	0.63	0.63	0.60	0.61	0.60	0.61	0.62	0.61	0.61	0.59	0.59	0.59	0.59
A2-2	0.44	0.57	0.62	0.60	0.59	0.60	0.60	0.62	0.62	0.62	0.60	0.61	0.60	0.60	0.60	0.60	0.59	0.58	0.58	0.58	0.59
B1-2	0.52	0.59	0.61	0.59	0.57	0.59	0.59	0.59	0.63	0.63	0.62	0.62	0.61	0.61	0.62	0.61	0.61	0.60	0.59	0.59	0.59
B2-2	0.52	0.59	0.61	0.59	0.57	0.59	0.59	0.59	0.63	0.63	0.62	0.62	0.61	0.61	0.62	0.61	0.61	0.60	0.59	0.59	0.59
C1-2	0.55	0.61	0.59	0.58	0.59	0.60	0.60	0.59	0.61	0.59	0.62	0.62	0.62	0.59	0.59	0.59	0.59	0.58	0.59	0.56	0.55
C2-2	0.54	0.61	0.59	0.59	0.59	0.60	0.60	0.59	0.59	0.59	0.59	0.60	0.61	0.60	0.59	0.59	0.59	0.58	0.58	0.56	0.55
D1-2	0.57	0.57	0.58	0.58	0.59	0.59	0.58	0.59	0.59	0.59	0.58	0.59	0.58	0.57	0.54	0.53	0.55	0.53	0.53	0.53	0.52
D2-2	0.57	0.57	0.58	0.58	0.59	0.59	0.58	0.59	0.59	0.59	0.58	0.59	0.58	0.57	0.54	0.53	0.55	0.53	0.53	0.53	0.52

(B)

Trend of optimal L of PM

L[m]	0.0	0.6	1.2	1.8	2.4	3.0	3.6	4.2	4.8	5.4	6.0	6.6	7.2	7.8	8.4	9.0	9.6	10.2	10.8	11.4	12.0
A1-2	0.57	0.61	0.60	0.61	0.61	0.61	0.61	0.60	0.60	0.60	0.63	0.63	0.62	0.62	0.62	0.62	0.62	0.62	0.62	0.61	0.60
A2-2	0.56	0.60	0.61	0.61	0.61	0.61	0.61	0.60	0.60	0.60	0.62	0.63	0.62	0.62	0.62	0.62	0.62	0.61	0.61	0.61	0.59
B1-2	0.59	0.62	0.60	0.61	0.60	0.61	0.61	0.60	0.60	0.60	0.63	0.63	0.62	0.62	0.61	0.61	0.61	0.61	0.61	0.61	0.60
B2-2	0.59	0.62	0.60	0.61	0.60	0.61	0.61	0.60	0.60	0.60	0.63	0.63	0.62	0.62	0.61	0.61	0.61	0.61	0.61	0.61	0.60
C1-2	0.61	0.60	0.60	0.59	0.60	0.60	0.60	0.60	0.60	0.62	0.62	0.61	0.61	0.61	0.61	0.62	0.61	0.61	0.61	0.60	0.60
C2-2	0.59	0.61	0.60	0.60	0.60	0.60	0.60	0.60	0.60	0.61	0.62	0.61	0.61	0.61	0.61	0.61	0.61	0.61	0.61	0.60	0.60
D1-2	0.61	0.59	0.58	0.59	0.59	0.60	0.60	0.60	0.62	0.63	0.62	0.62	0.62	0.62	0.63	0.62	0.62	0.62	0.60	0.60	0.60
D2-2	0.61	0.59	0.58	0.59	0.59	0.60	0.60	0.60	0.62	0.63	0.62	0.62	0.62	0.62	0.63	0.62	0.62	0.62	0.60	0.60	0.60

SI Table 2-6 Details of scenarios. X = this sampler/experiment was used in this condition.

See Excel spreadsheet file.

SI Animation. Changes in *FAC2* as *L* increases from 0 to 12 m. Link: https://youtu.be/sD-Kl22gC0M

Appendices B: SI of Chapter 3

SI Table 3-1 Summary of experimental sampling time periods.

	EXP00	EXP01	EXP02	EXP03	EXP04	EXP05	EXP06	EXP07	EXP08	EXP09	EXP10
Date	13-Sep	20-Sep	21-Sep	22-Sep	23-Sep	24-Sep	25-Sep	26-Sep	27-Sep	28-Sep	29-Sep
Start	11:00	7:00	7:00	7:00	7:00	7:00	7:00	7:00	7:00	7:00	7:00
End	24:00	17:00	16:30	17:00	17:00	17:00	16:30	16:30	16:30	18:30	16:00
Total Time (hr)	13	10	9.5	10	10	10	9.5	9.5	9.5	11.5	9

SI Table 3-2 Parameters for emission sources for PM2.5, PM10, and TSP calculation. ER refers to emission rate.

ID	Description	Height	Diameter	Exit Velocity	Emission Rate			Reference
		(m)	(m)	(m/s)	$PM_{2.5}$ (g/s)	PM_{10} (g/s)	TSP (g/s)	
STCK1	Combined Mote	18.6	1.04	11.4	0.13	0.60	1.70	Boykin et al., 2013a
STCK2	Battery Condenser	16.7	1.30	7.4	0.01	0.05	0.16	Whitelock et al., 2013a
STCK3	Overflow	12.4	0.61	10.2	0.00	0.02	0.06	Buser et al., 2013a
STCK4	Mote Trash	12.4	0.61	9.0	0.01	0.04	0.12	Buser et al., 2013b
STCK5A	Combo Lint Cleaner-1	9.40	0.66	10.8	0.06	0.52	1.67	Buser et al., 2013c
STCK5B	Combo Lint Cleaner-1	9.40	0.66	10. 8	0.01	0.09	0.28	Buser et al., 2013c
STCK6A	Combo Lint Cleaner-2	11.5	0.66	10.8	0.01	0.09	0.28	Buser et al., 2013c
STCK6B	Combo Lint Cleaner-2	11.5	0.66	10.8	0.01	0.09	0.28	Buser et al., 2013c
STCK7		11.8	1.04	0.00	0.00	0.00	0.00	*Not used*
STCK8	Combo Lint Cleaner-3	14.7	0.97	10.8	0.02	0.17	0.56	Buser et al., 2013c
STCK9	2nd Stage SCC	14.8	1.04	9.6	0.04	0.27	0.74	Boykin et al., 2013b
STCK10	1st Stage SCC	14.8	1.04	11.8	0.12	0.72	1.85	Whitelock et al., 2013b
STCK11	Huller Fan	12.1	0.61	10.2	0.01	0.06	0.15	*Unpublished data*
STCK12	Master Trash	15.0	1.22	3.5	0.02	0.53	2.99	Whitelock et al., 2013c

SI Table 3-3 Model configuration options for AERMET and AERMOD.

	Options	Selections	Note
		AERMET	
Onsite	Onsite data - Include Onsite Data?	Yes	
Upper Air	Upper Air Data - Mode	Standard AERMET	
	Substitute missing onsite data by NWS data	Selected	
	Adjust surface friction velocity	Selected	
Sectors	Randomize wind direction	Yes	
	Apply missing cloud cover substitution	All Hours	
	Apply missing ambient temperature substitution	All Hours	
		AERMOD	
	Regulatory options	Default	
Control	Depletion Options	Dry depletion	Particulate matters have dry depletion
	Dispersion coefficient	Rural	Experimental site is in rural area
	Source type	Point	Other parameters can be found in **SI Table 2**
Source	Building downwash	Selected	
	Particulates	Selected - Method 1	Default method
	background concentrations	None of them are selected	Background concentration was not measured
	Flagpole receptors	Yes - 2 m	
Receptor	Terrain height options	Elevated	
	Receptor elevation/hill heights	Using the AERMAP receptor output file	
Meteorology	Wind speed categories	Default values	

SI Table 3-4 Summary of experimental time and fraction of effective time.

	Fraction of effective time f_{ti}																
Hour:	**7**	**8**	**9**	**10**	**11**	**12**	**13**	**14**	**15**	**16**	**17**	**18**	**19**	**20**	**21**	**22**	**23**
EXP00					1	1	1	1	1	1	1	1	1	1	1	1	1
EXP01	1	1	1	1	1	1	1	1	1	1							
EXP02	1	1	1	1	1	1	1	1	1	0.5*							
EXP03	1	1	1	1	1	1	1	1	1	1							
EXP04	1	1	1	1	1	1	1	1	1	1							
EXP05	1	1	1	1	1	1	1	1	1	1							
EXP06	1	1	1	1	1	1	1	1	1	0.5							
EXP07	1	1	1	1	1	1	1	1	1	0.5							
EXP08	1	1	1	1	1	1	1	1	1	0.5							
EXP09	1	1	1	1	1	1	1	1	1	1	1	0.5					
EXP10	1	1	1	1	1	1	1	1	1								

*0.5 refers to the ending time is ~16:30

SI Table 3-5 Summary statistics of meteorological parameters. Data are expressed as mean ± std. Mean and standard deviation of wind direction are calculated by Yamartino method (Yamartino, 1984; US EPA, 2000b).

	Pressure (Pa)	**Relative Humidity (%)**	**Temperature (℃)**	**Wind Speed (m/s)**	**Wind Direction (degrees from N)**
EXP00	10093 ± 13	45.4 ± 20.4	26.8 ± 4.2	1.00 ± 0.68	190 ± 63
EXP01	10080 ± 13	46.1 ± 25.0	30.3 ± 5.38	1.31 ± 0.69	70 ± 54
EXP02	10057 ± 10	43.0 ± 17.2	31.1 ± 5.20	3.15 ± 1.25	211 ± 30
EXP03	10089 ± 9	44.9 ± 13.8	30.4 ± 4.33	3.44 ± 1.03	229 ± 29
EXP04	10089 ± 16	44.6 ± 18.0	30.5 ± 4.14	4.67 ± 1.60	191 ± 11
EXP05	10091 ± 5	58.9 ± 5.8	27.1 ± 1.58	3.94 ± 1.18	263 ± 34
EXP06	10098 ± 17	49.3 ± 22.6	22.7 ± 4.40	1.62 ± 0.82	45 ± 39
EXP07	10059 ± 7	64.8 ± 13.2	18.2 ± 2.63	4.39 ± 1.86	14 ± 10
EXP08	10043 ± 9	50.8 ± 17.1	19.0 ± 4.22	3.72 ± 0.98	0.0 ± 17
EXP09	10000 ± 13	49.8 ± 21.5	20.3 ± 4.99	1.54 ± 0.86	257 ± 58
EXP10	10013 ± 12	46.1 ± 24.5	22.0 ± 5.17	1.28 ± 0.71	59 ± 48

SI Figure 3-1 On-site wind roses of the experiments

(a). EXP00

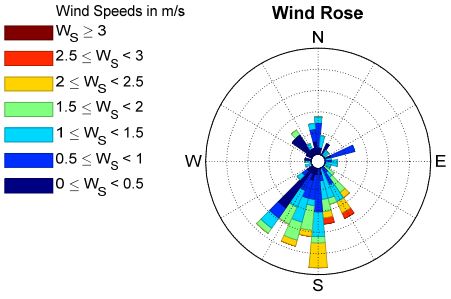

(b). EXP01

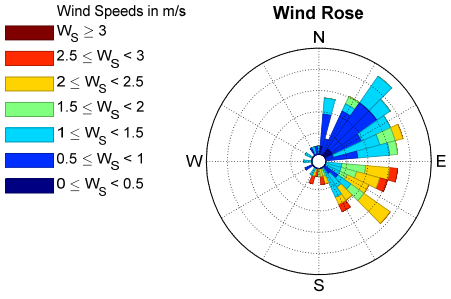

(c). EXP02

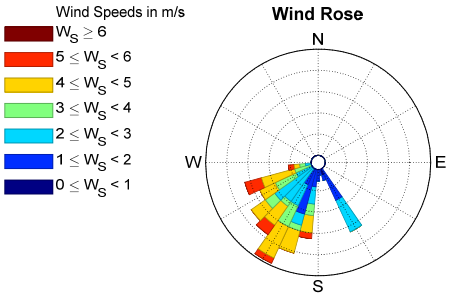

(d). EXP03

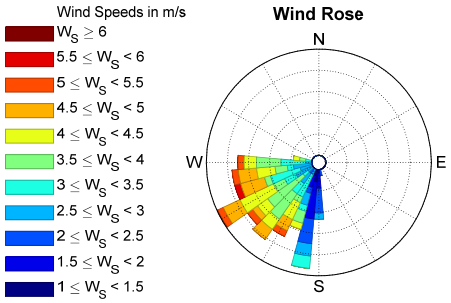

(e). EXP04

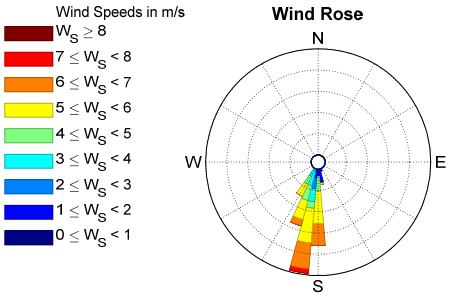

(f). EXP05

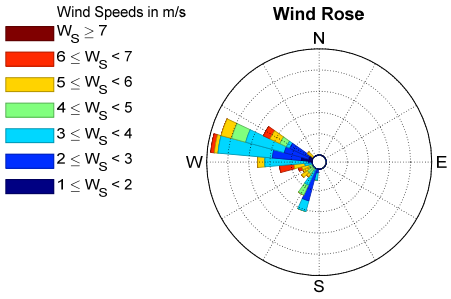

(g). EXP06

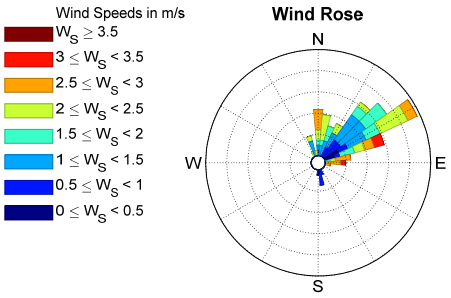

(h). EXP07

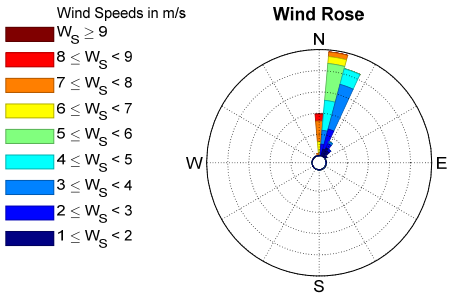

(i). EXP08

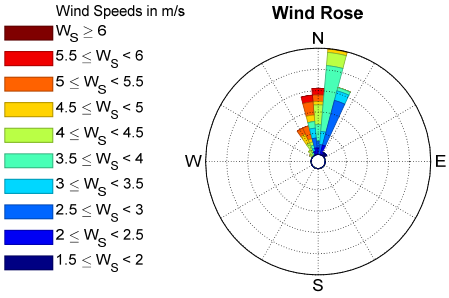

(j). EXP09

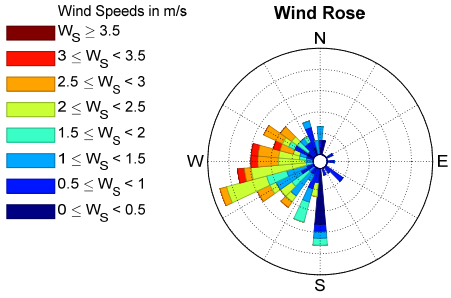

(k). EXP010

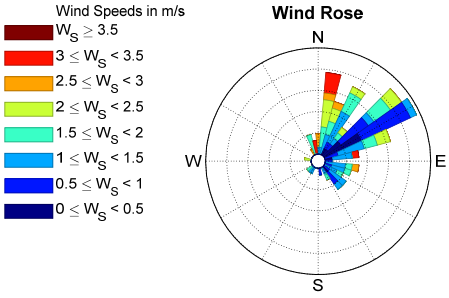

SI Figure 3-2 Spatial distribution of observed concentration, model predicted concentration, and R_p (ratio of model-predicted to observed concentration) values. Unit of C_o and C_p is μg/m^3, and R_p is unitless. High-outliers are labelled in yellow arrow; low-outliers are labelled in green arrow.

(a). $PM_{2.5}$ - EXP00

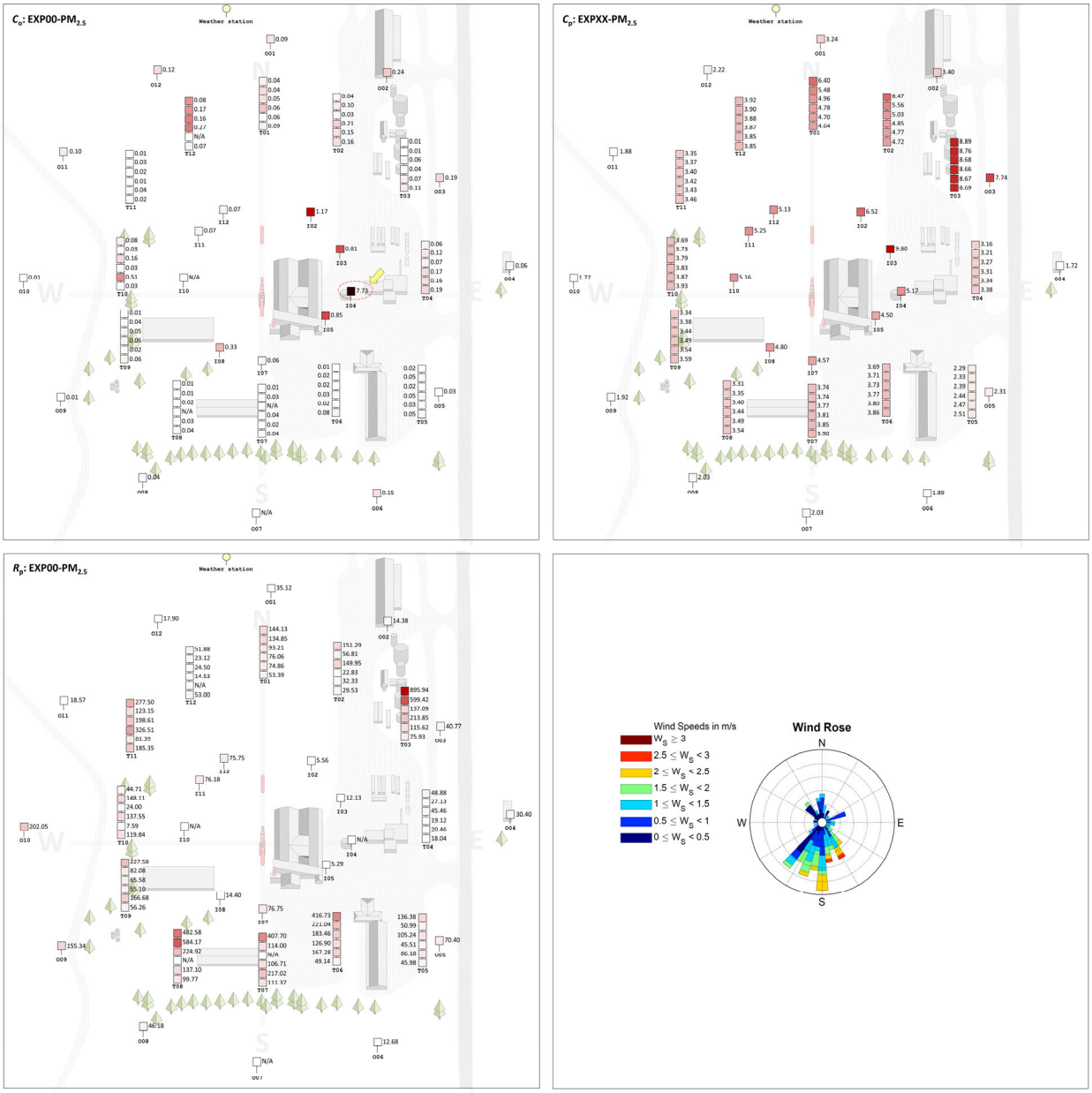

(b). $PM_{2.5}$ - EXP01

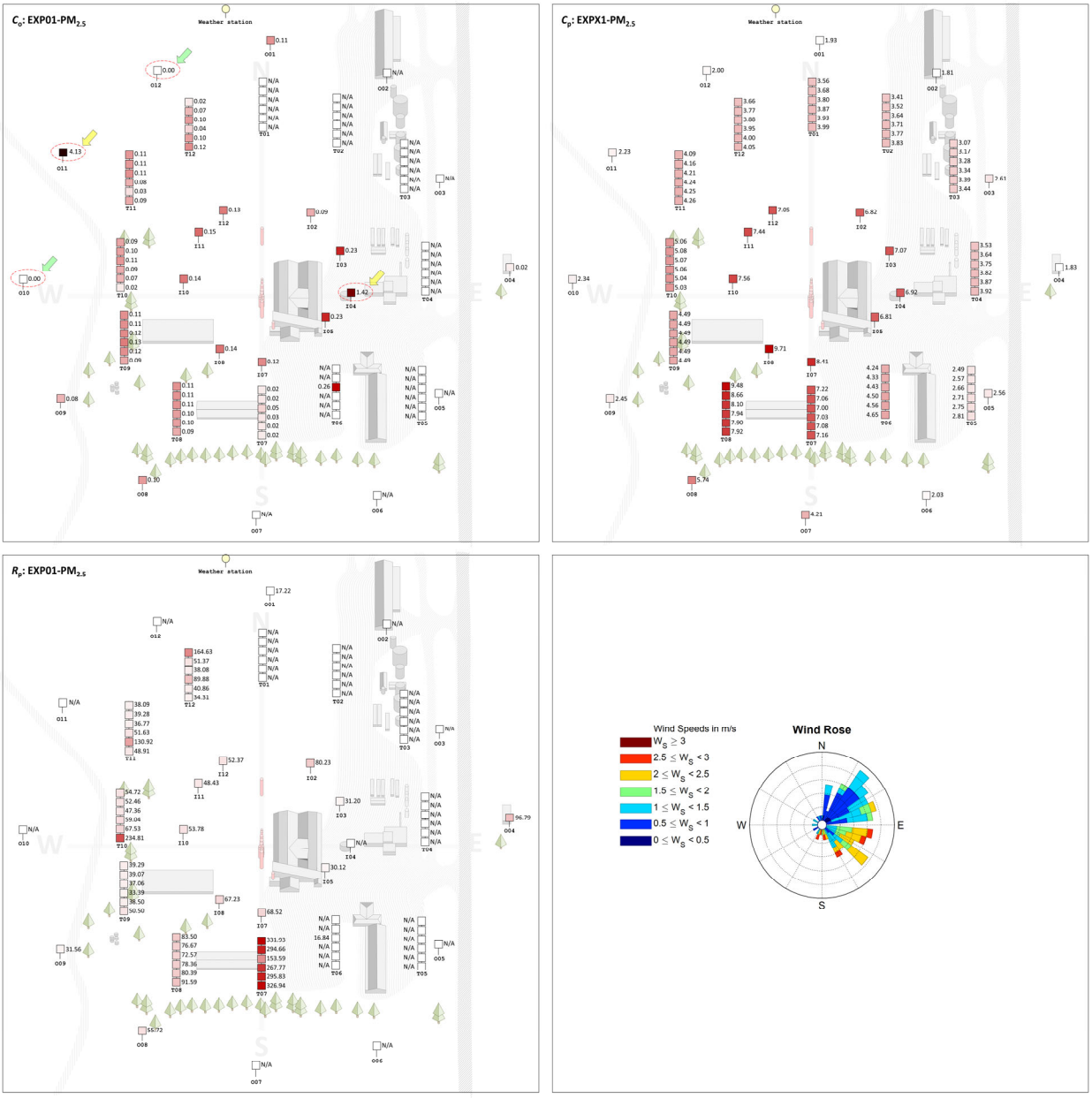
C_0: EXP01-$PM_{2.5}$
C_p: EXPX1-$PM_{2.5}$
R_p: EXP01-$PM_{2.5}$
Weather station
Wind Speeds in m/s
$W_S \geq 3$
$2.5 \leq W_S < 3$
$2 \leq W_S < 2.5$
$1.5 \leq W_S < 2$
$1 \leq W_S < 1.5$
$0.5 \leq W_S < 1$
$0 \leq W_S < 0.5$
Wind Rose
N
E
S
W

(c). $PM_{2.5}$ - EXP02

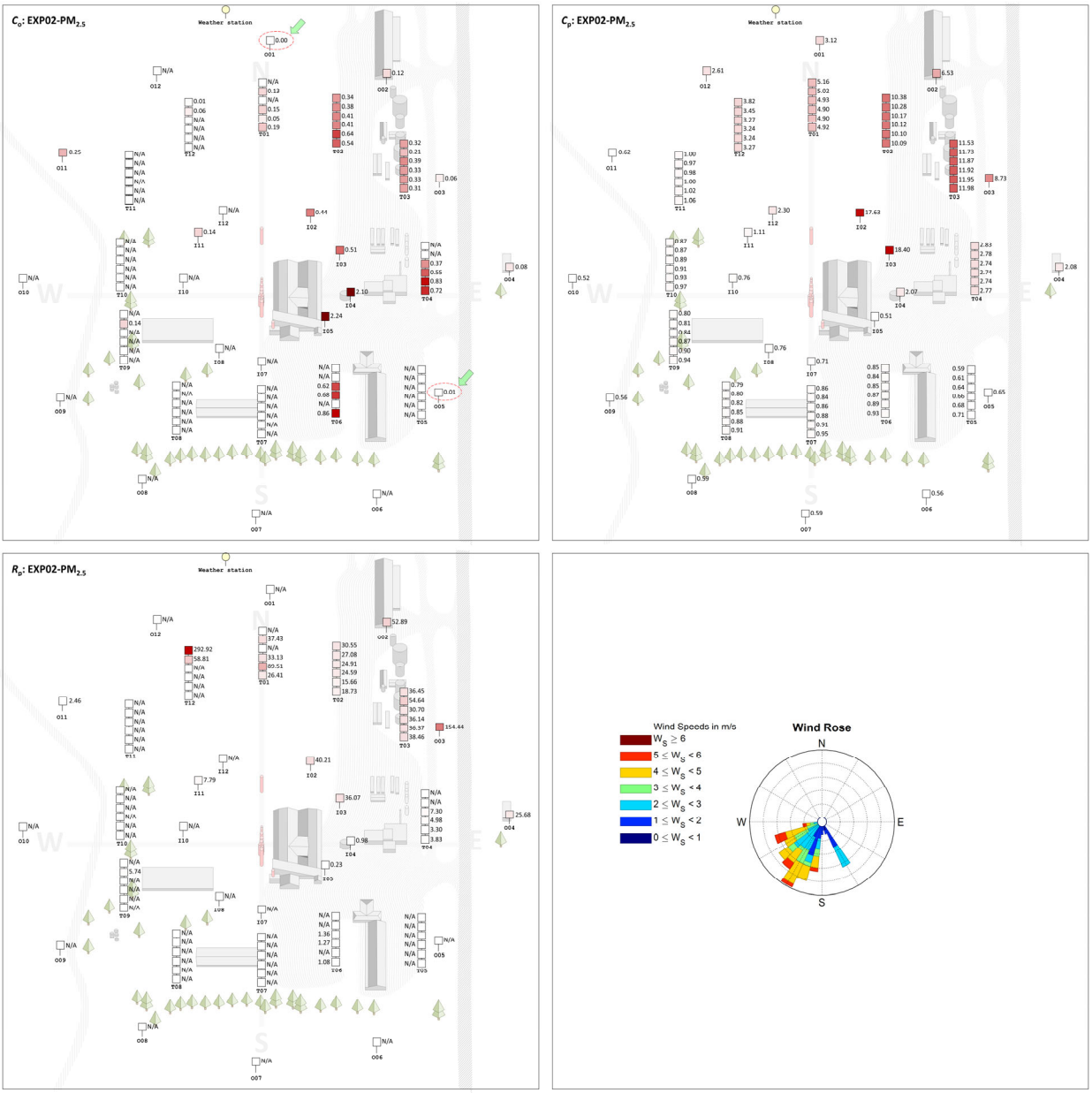
C_o: EXP02-$PM_{2.5}$
Weather station
C_p: EXP02-$PM_{2.5}$
Weather station
R_p: EXP02-$PM_{2.5}$
Weather station
Wind Speeds in m/s
$W_S \geq 6$
$5 \leq W_S < 6$
$4 \leq W_S < 5$
$3 \leq W_S < 4$
$2 \leq W_S < 3$
$1 \leq W_S < 2$
$0 \leq W_S < 1$
Wind Rose
N
W
E
S

(d). $PM_{2.5}$ - EXP03

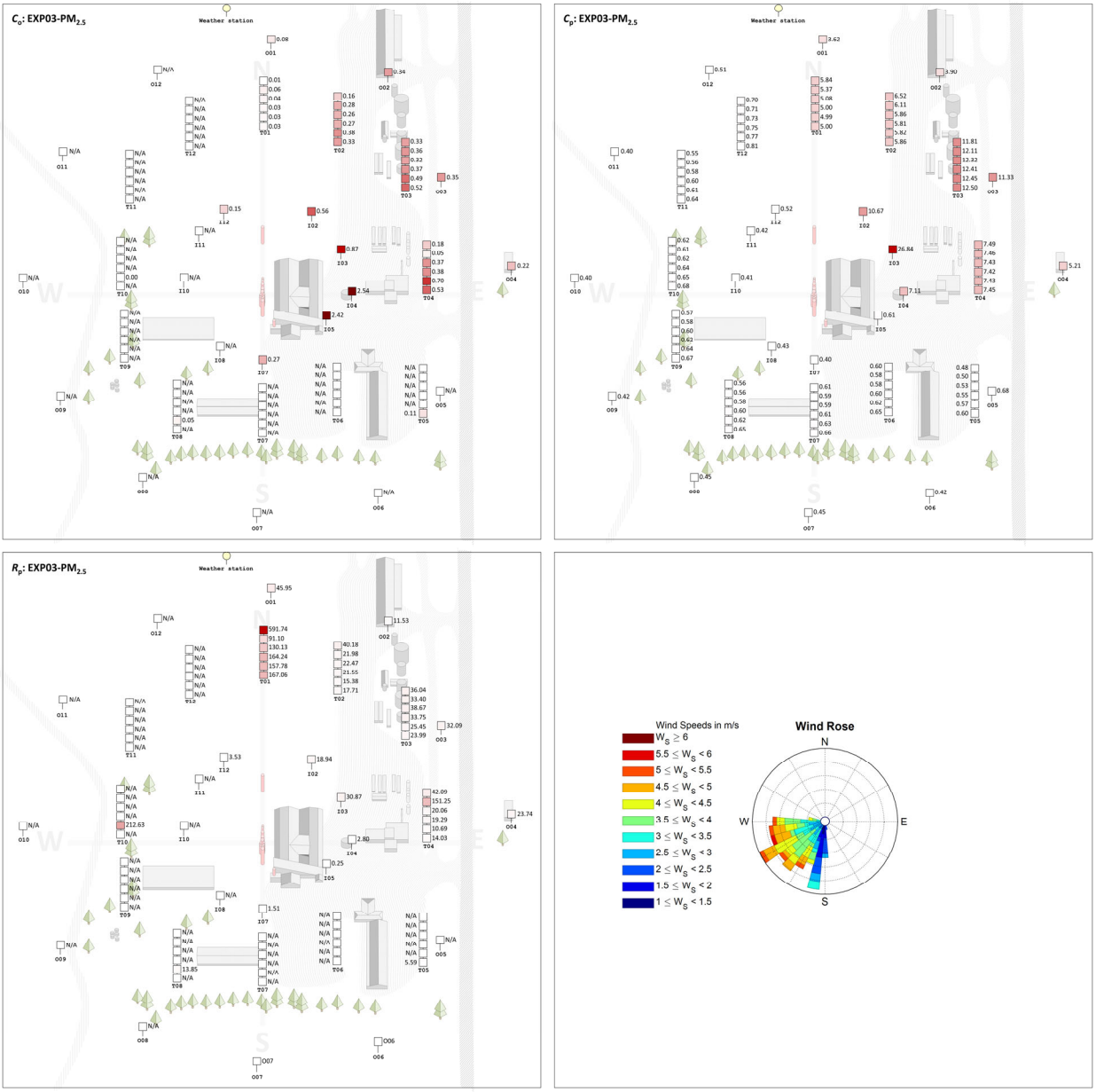
C_o: EXP03-$PM_{2.5}$
C_p: EXP03-$PM_{2.5}$
R_p: EXP03-$PM_{2.5}$
Weather station
Wind Speeds in m/s
$W_S \geq 6$
$5.5 \leq W_S < 6$
$5 \leq W_S < 5.5$
$4.5 \leq W_S < 4.5$
$4 \leq W_S < 4.5$
$3.5 \leq W_S < 4$
$3 \leq W_S < 3.5$
$2.5 \leq W_S < 3$
$2 \leq W_S < 2.5$
$1.5 \leq W_S < 2$
$1 \leq W_S < 1.5$
Wind Rose
N
E
S
W

(e). $PM_{2.5}$ - EXP04

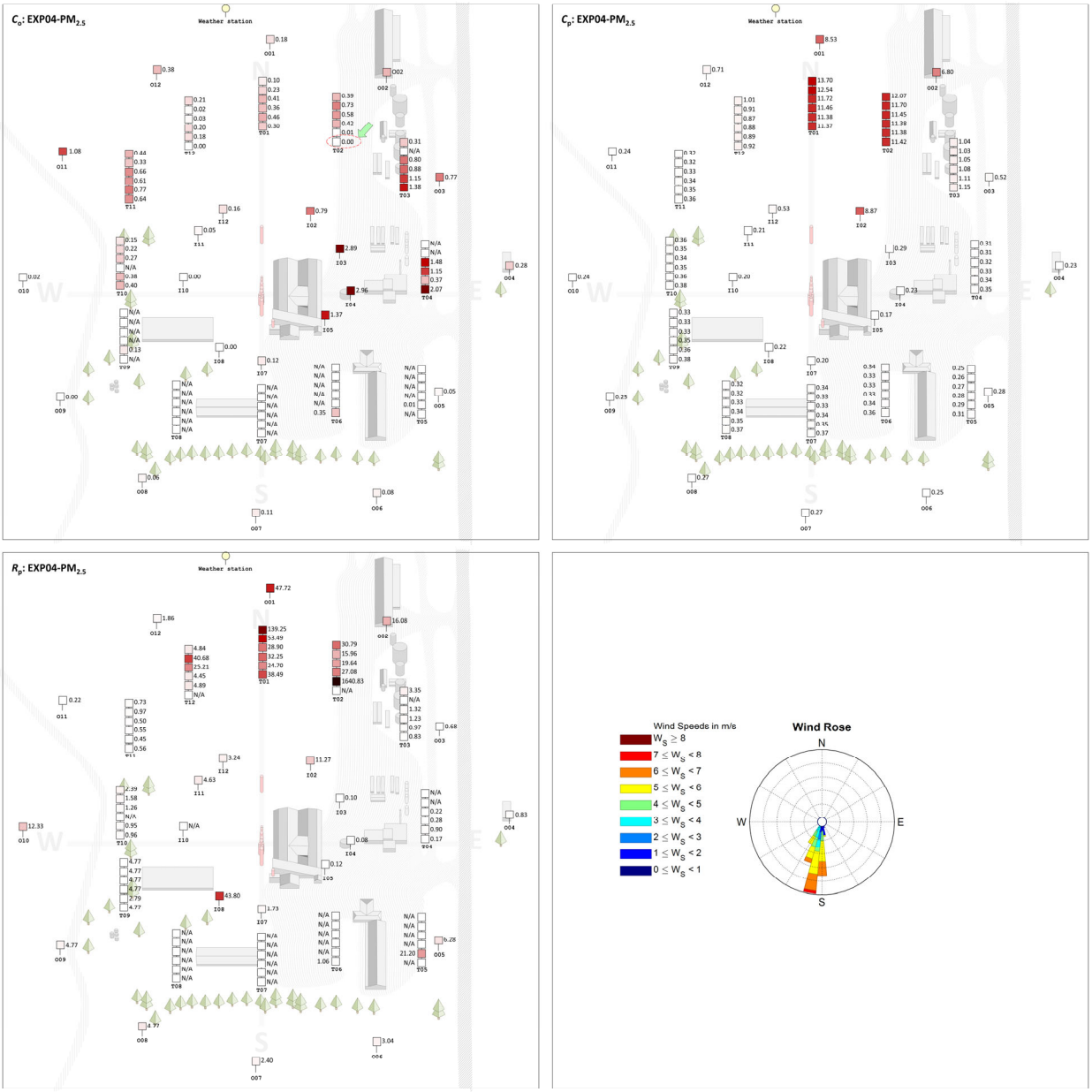
C_o: EXP04-$PM_{2.5}$
C_p: EXP04-$PM_{2.5}$
R_p: EXP04-$PM_{2.5}$
Weather station
Wind Speeds in m/s
$W_s \geq 8$
$7 \leq W_s < 8$
$6 \leq W_s < 7$
$5 \leq W_s < 6$
$4 \leq W_s < 5$
$3 \leq W_s < 4$
$2 \leq W_s < 3$
$1 \leq W_s < 2$
$0 \leq W_s < 1$
Wind Rose
N
W
E
S

(f). $PM_{2.5}$ - EXP05

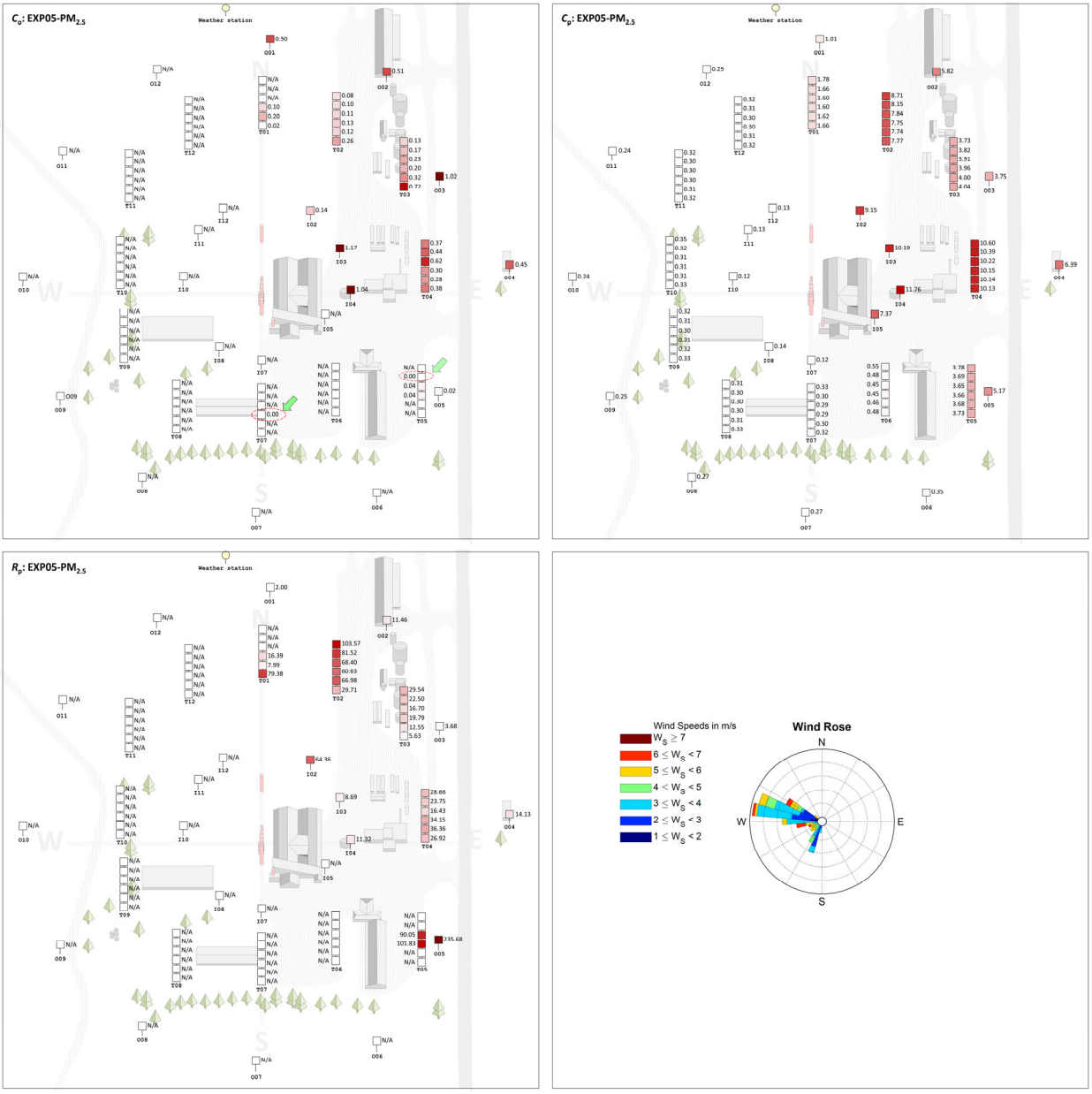
C_o: EXP05-$PM_{2.5}$
C_p: EXP05-$PM_{2.5}$
R_p: EXP05-$PM_{2.5}$
Weather station
Wind Speeds in m/s
$W_S \geq 7$
$6 \leq W_S < 7$
$5 \leq W_S < 6$
$4 \leq W_S < 5$
$3 \leq W_S < 4$
$2 \leq W_S < 3$
$1 \leq W_S < 2$
Wind Rose
N
E
S
W

(g). $PM_{2.5}$ - EXP06

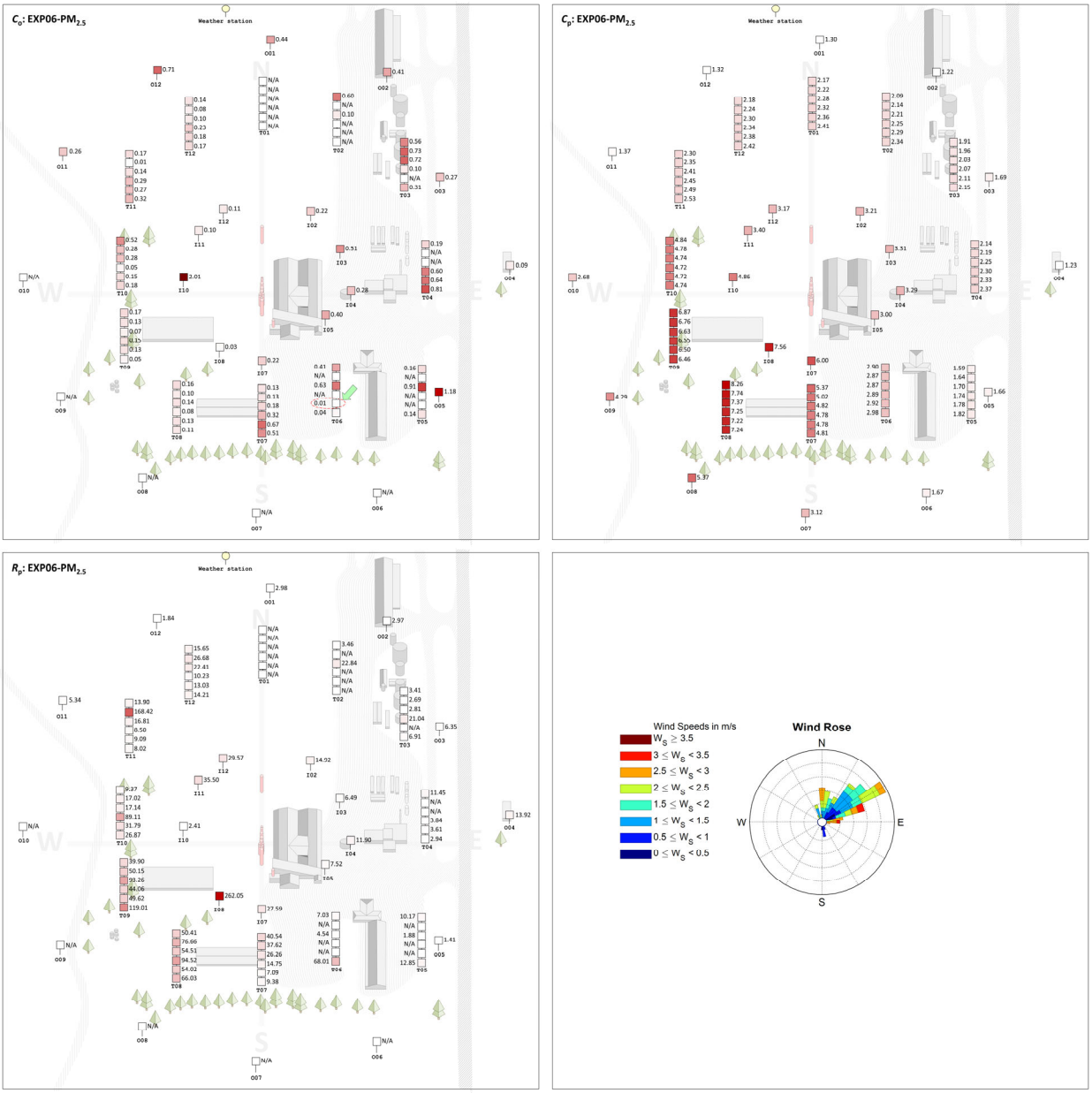
C_0: EXP06-$PM_{2.5}$
C_p: EXP06-$PM_{2.5}$
R_p: EXP06-$PM_{2.5}$
Weather station
Wind Speeds in m/s
$W_s \geq 3.5$
$3 \leq W_s < 3.5$
$2.5 \leq W_s < 3$
$2 \leq W_s < 2.5$
$1.5 \leq W_s < 2$
$1 \leq W_s < 1.5$
$0.5 \leq W_s < 1$
$0 \leq W_s < 0.5$
Wind Rose
N
E
S
W

(h). $PM_{2.5}$ - EXP07

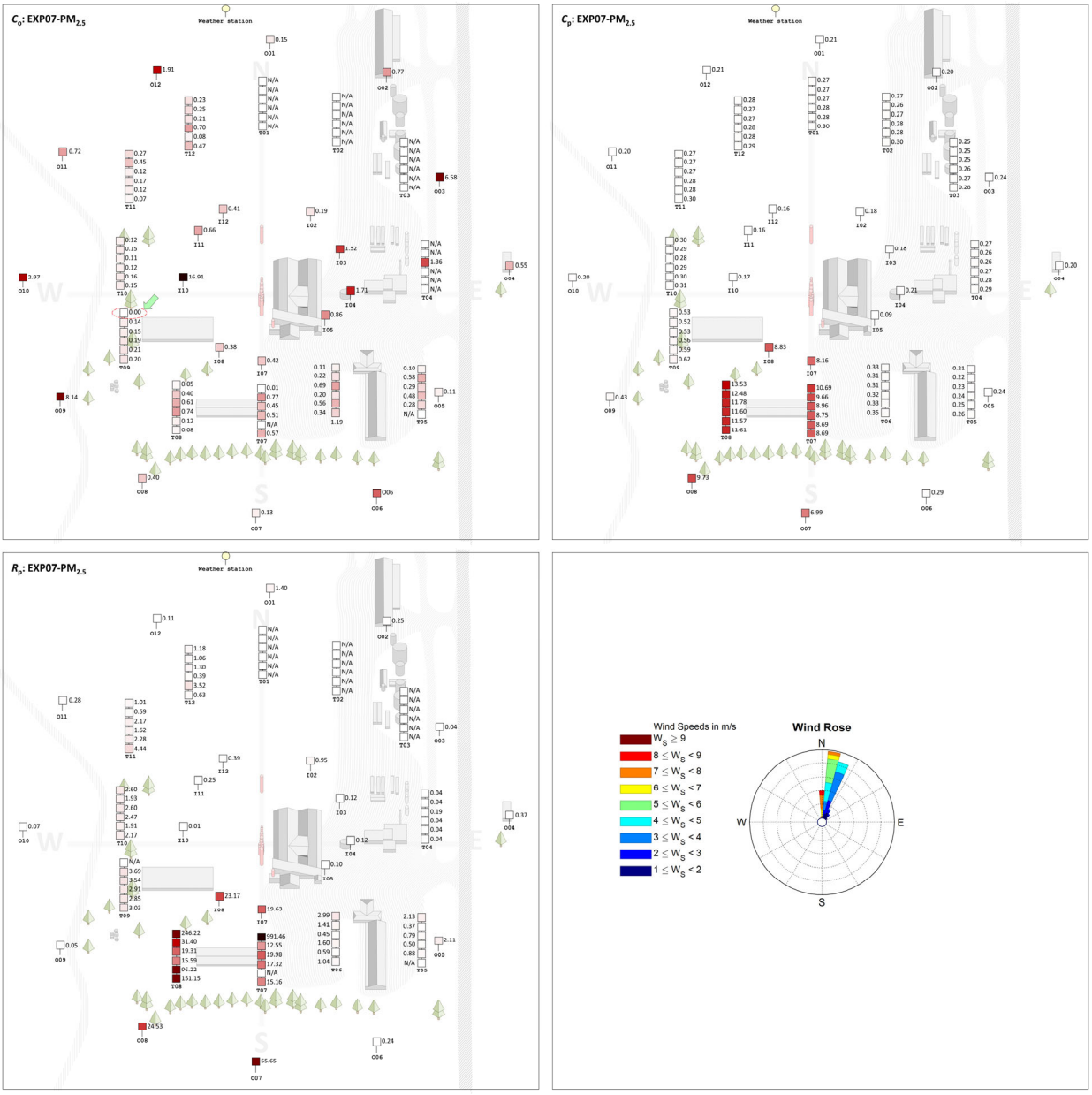
C_0: EXP07-$PM_{2.5}$
C_p: EXP07-$PM_{2.5}$
R_p: EXP07-$PM_{2.5}$
Weather station
Wind Speeds in m/s
$W_s \geq 9$
$8 \leq W_s < 9$
$7 \leq W_s < 8$
$6 \leq W_s < 7$
$5 \leq W_s < 6$
$4 \leq W_s < 5$
$3 \leq W_s < 4$
$2 \leq W_s < 3$
$1 \leq W_s < 2$
Wind Rose
N
E
S
W

(i). $PM_{2.5}$ - EXP08

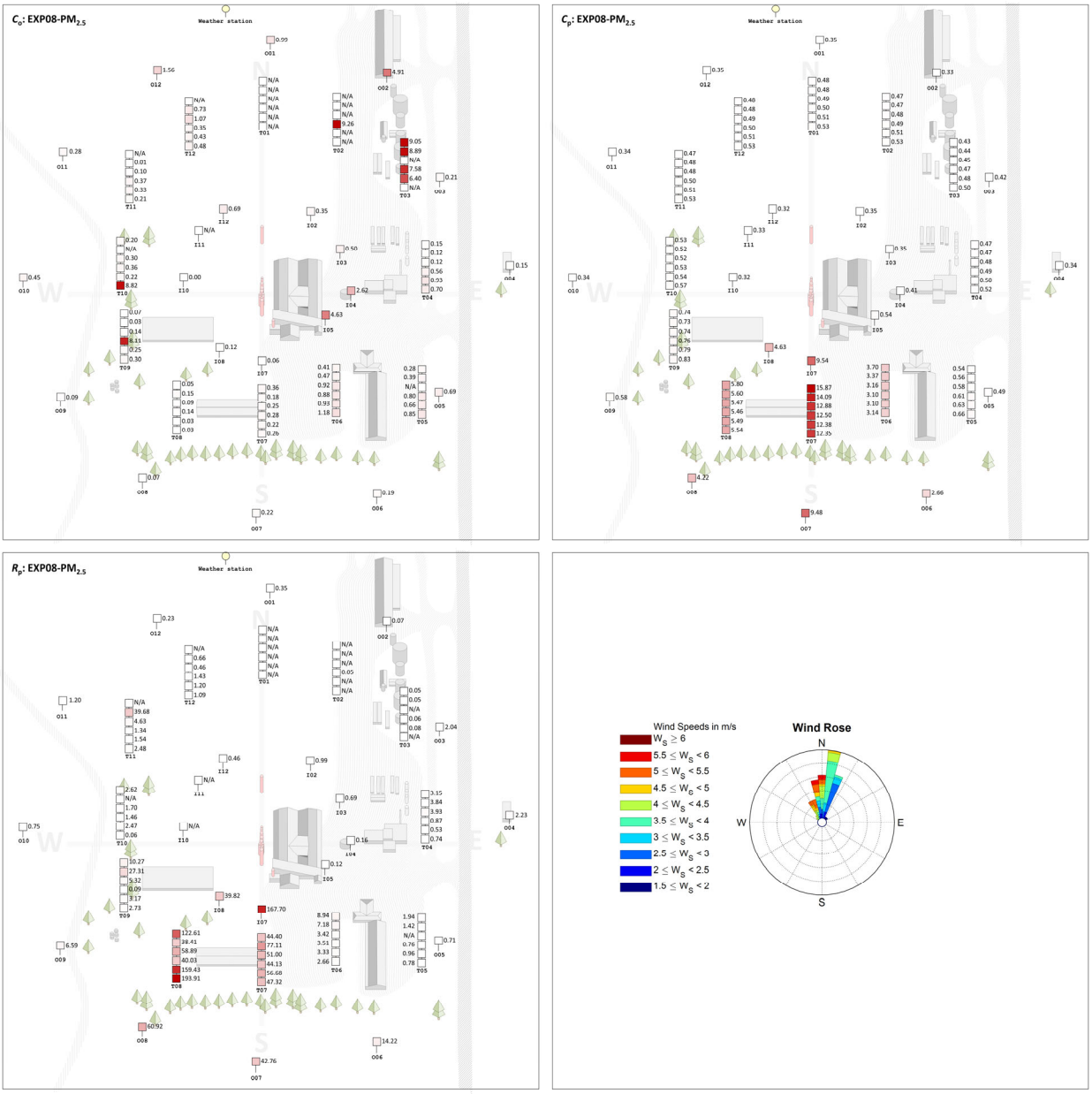
C_o: EXP08-$PM_{2.5}$
C_p: EXP08-$PM_{2.5}$
R_p: EXP08-$PM_{2.5}$
Weather station
Wind Speeds in m/s
$W_S \geq 6$
$5.5 \leq W_S < 6$
$5 \leq W_S < 5.5$
$4.5 \leq W_S < 5$
$4 \leq W_S < 4.5$
$3.5 \leq W_S < 4$
$3 \leq W_S < 3.5$
$2.5 \leq W_S < 3$
$2 \leq W_S < 2.5$
$1.5 \leq W_S < 2$
Wind Rose
N
E
S
W

(j). $PM_{2.5}$ - EXP09

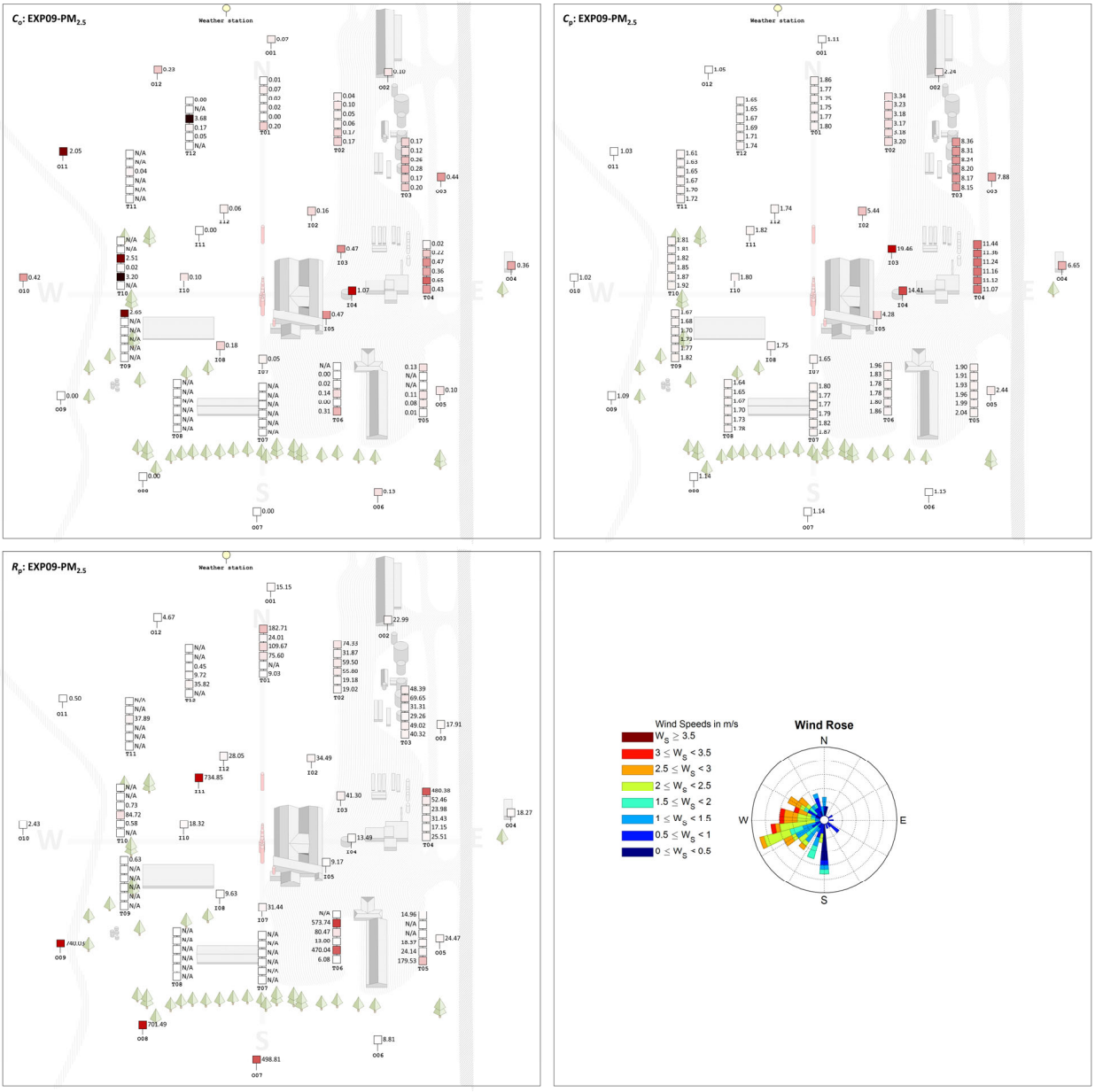
C_o: EXP09-$PM_{2.5}$
Weather station
C_p: EXP09-$PM_{2.5}$
Weather station
R_p: EXP09-$PM_{2.5}$
Weather station
Wind Speeds in m/s
$W_S \geq 3.5$
$3 \leq W_S < 3.5$
$2.5 \leq W_S < 3$
$2 \leq W_S < 2.5$
$1.5 \leq W_S < 2$
$1 \leq W_S < 1.5$
$0.5 \leq W_S < 1$
$0 \leq W_S < 0.5$
Wind Rose
N
W
E
S

(k). $PM_{2.5}$ – EXP10

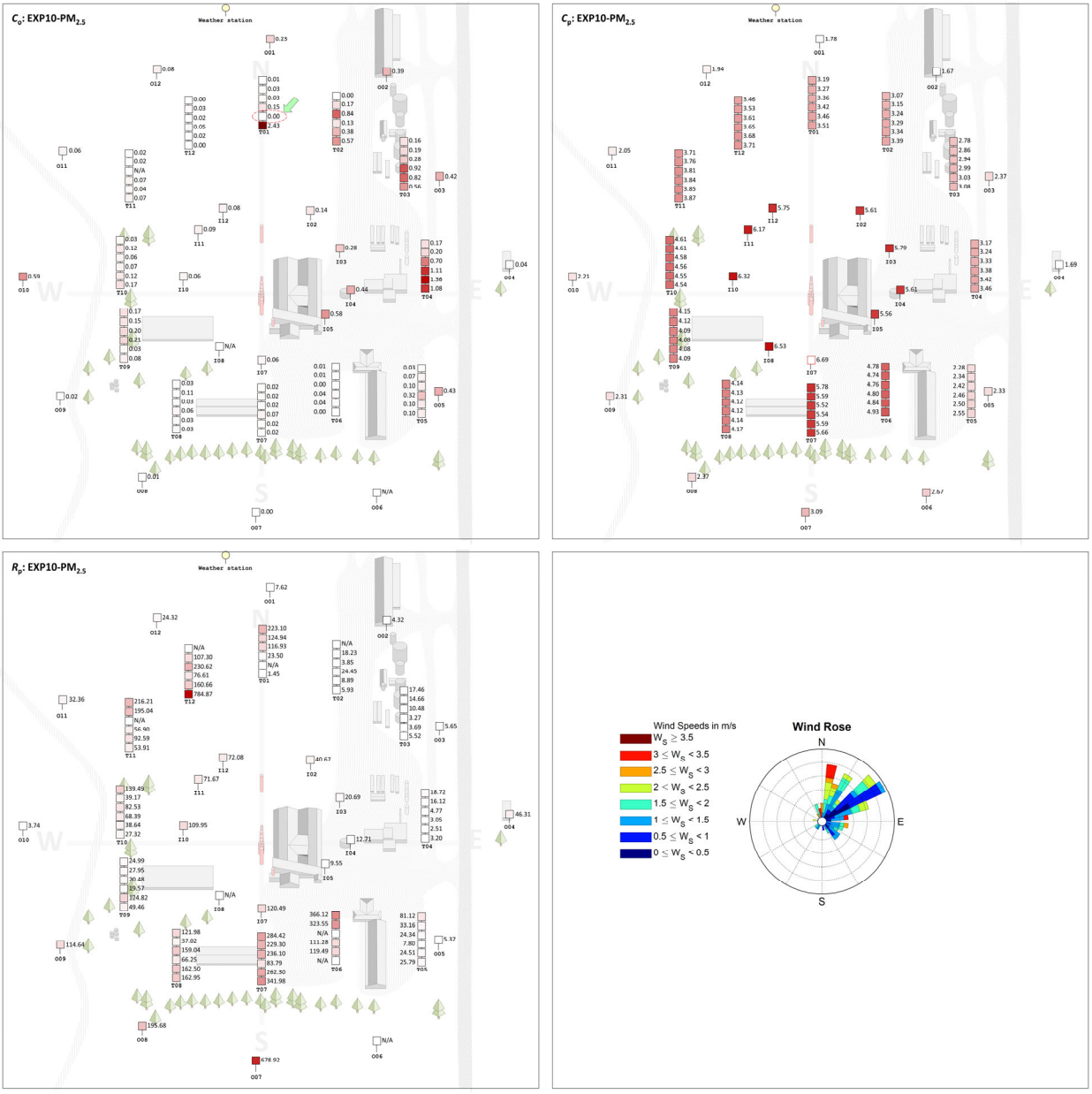
C_o: EXP10-$PM_{2.5}$
C_p: EXP10-$PM_{2.5}$
R_p: EXP10-$PM_{2.5}$
Weather station
Wind Speeds in m/s
$W_S \geq 3.5$
$3 \leq W_S < 3.5$
$2.5 \leq W_S < 3$
$2 < W_S < 2.5$
$1.5 \leq W_S < 2$
$1 \leq W_S < 1.5$
$0.5 \leq W_S < 1$
$0 \leq W_S < 0.5$
Wind Rose
N
E
S
W

(I). PM_{10} - EXP00

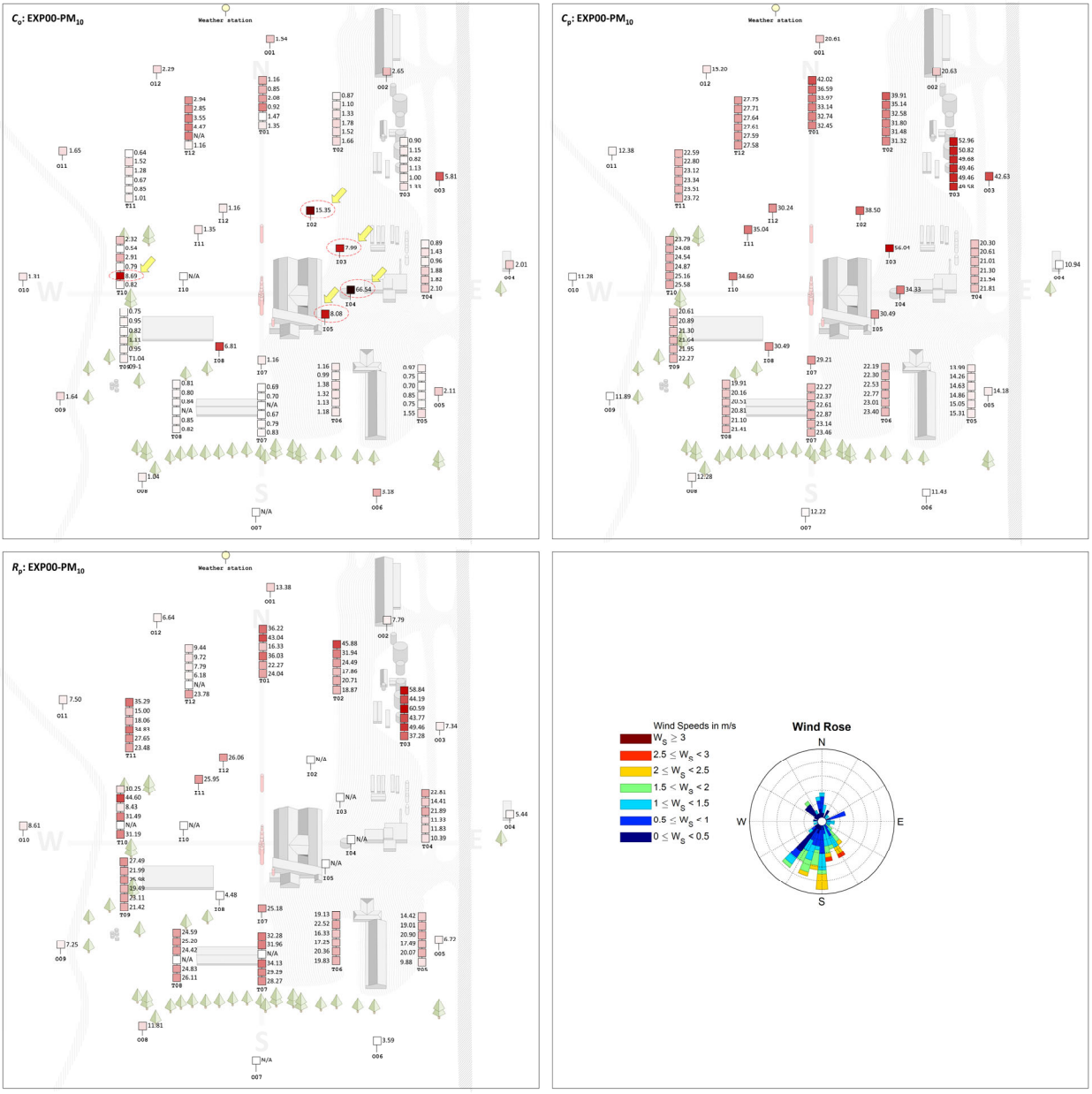
C_o: EXP00-PM_{10}
C_p: EXP00-PM_{10}
R_p: EXP00-PM_{10}
Weather station
Wind Speeds in m/s
$W_S \geq 3$
$2.5 \leq W_S < 3$
$2 \leq W_S < 2.5$
$1.5 \leq W_S < 2$
$1 \leq W_S < 1.5$
$0.5 \leq W_S < 1$
$0 \leq W_S < 0.5$
Wind Rose
N
E
S
W

(m). PM_{10} - EXP01

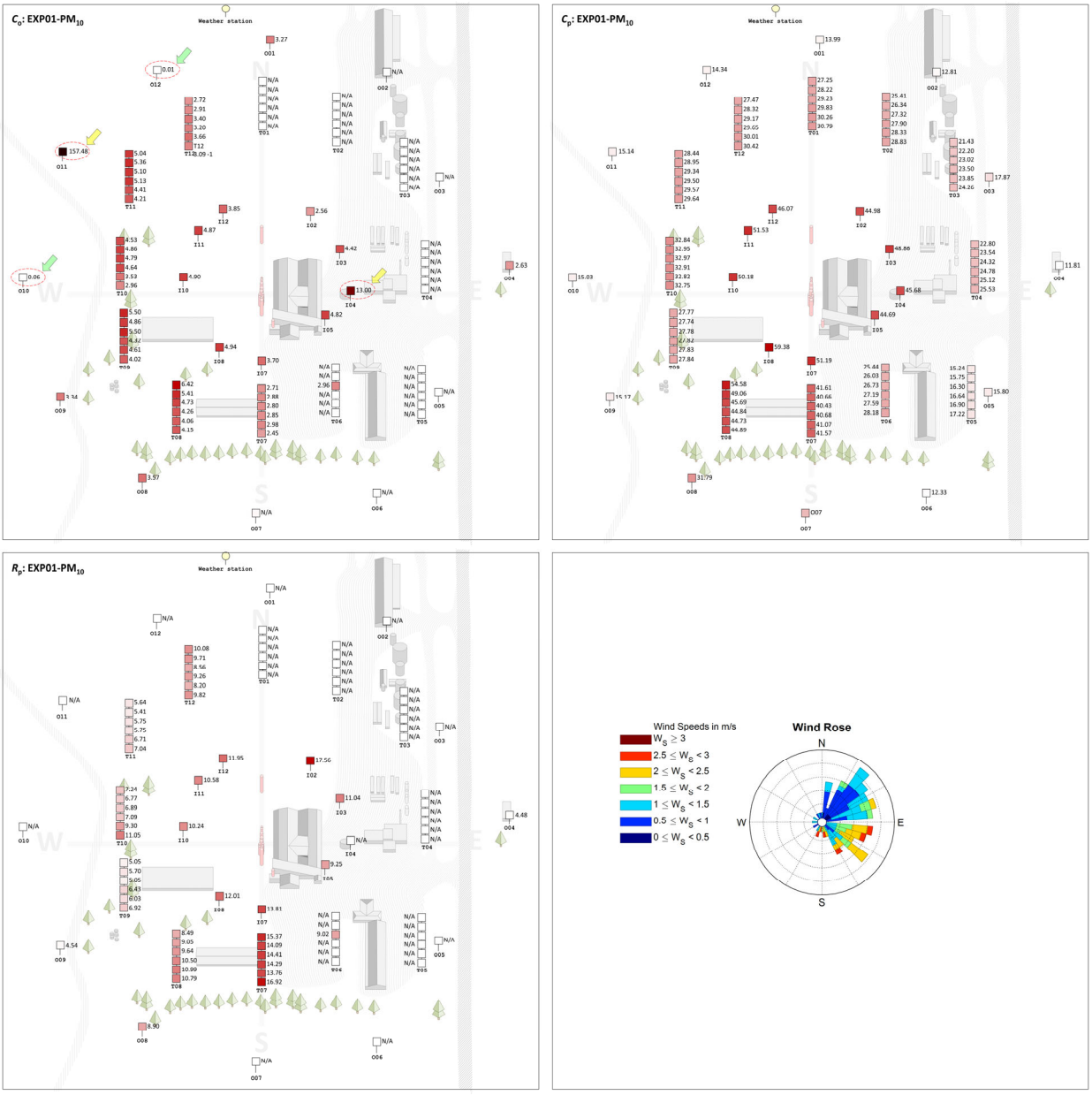
C_0: EXP01-PM_{10}
C_p: EXP01-PM_{10}
R_p: EXP01-PM_{10}
Weather station
Wind Speeds in m/s
$W_S \geq 3$
$2.5 \leq W_S < 3$
$2 \leq W_S < 2.5$
$1.5 \leq W_S < 2$
$1 \leq W_S < 1.5$
$0.5 \leq W_S < 1$
$0 \leq W_S < 0.5$
Wind Rose
N
E
S
W

(n). PM_{10} - EXP02

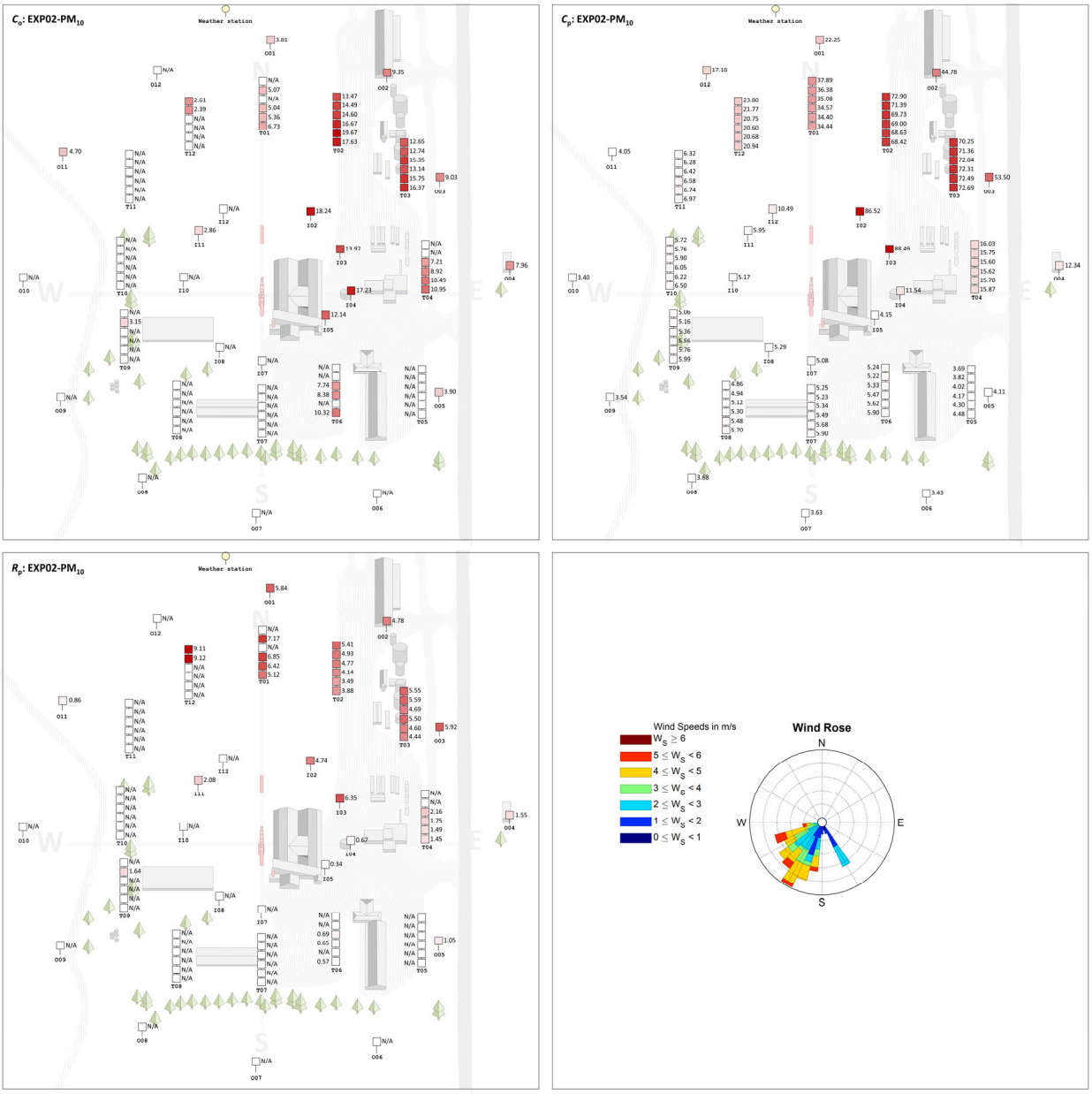
C_o: EXP02-PM_{10}
C_p: EXP02-PM_{10}
R_p: EXP02-PM_{10}
Weather station
Wind Speeds in m/s
$W_S \geq 6$
$5 \leq W_S < 6$
$4 \leq W_S < 5$
$3 \leq W_S < 4$
$2 \leq W_S < 3$
$1 \leq W_S < 2$
$0 \leq W_S < 1$
Wind Rose
N
E
S
W

(o). PM_{10} - EXP03

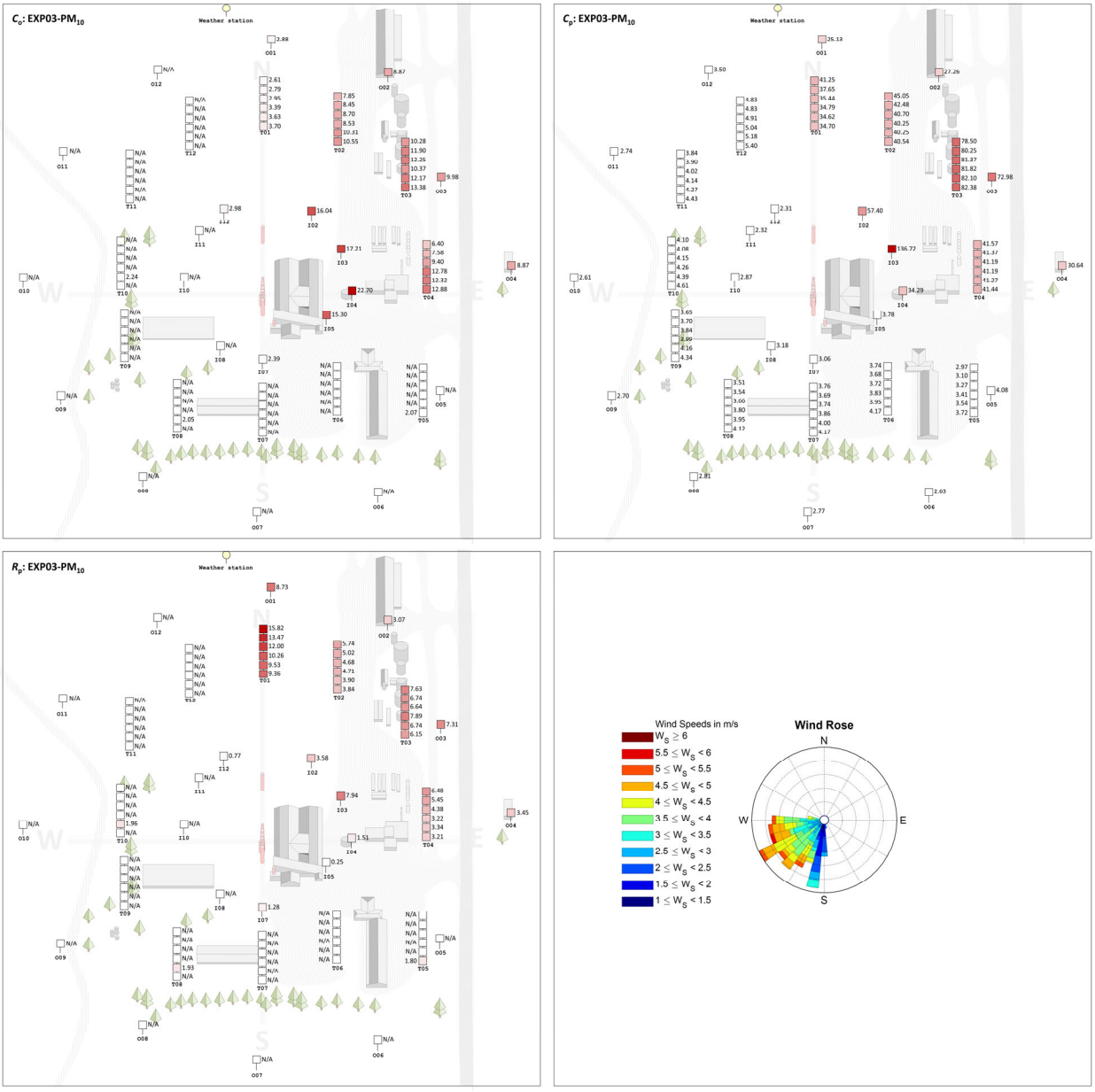
C_o: EXP03-PM10
C_p: EXP03-PM10
R_p: EXP03-PM10
Weather station
Wind Speeds in m/s
$W_S \geq 6$
$5.5 \leq W_S < 6$
$5 \leq W_S < 5.5$
$4.5 \leq W_S < 5$
$4 \leq W_S < 4.5$
$3.5 \leq W_S < 4$
$3 \leq W_S < 3.5$
$2.5 \leq W_S < 3$
$2 \leq W_S < 2.5$
$1.5 \leq W_S < 1.5$
$1 \leq W_S < 1.5$
Wind Rose
N
E
S
W

(p). PM_{10} - EXP04

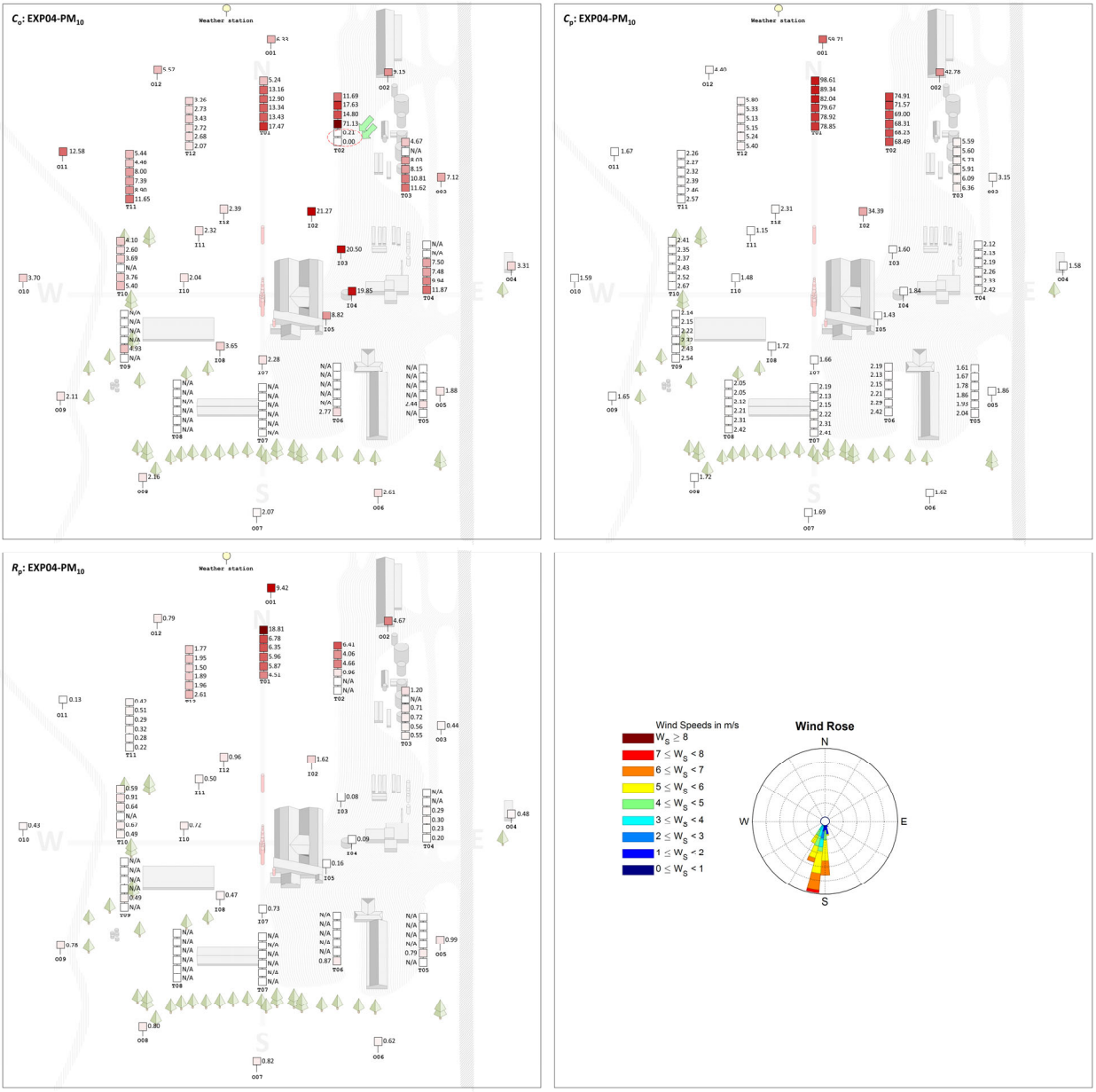
C_o: EXP04-PM_{10}
C_p: EXP04-PM_{10}
R_p: EXP04-PM_{10}
Weather station
Wind Speeds in m/s
$W_S \geq 8$
$7 \leq W_S < 8$
$6 \leq W_S < 7$
$5 \leq W_S < 6$
$4 \leq W_S < 5$
$3 \leq W_S < 4$
$2 \leq W_S < 3$
$1 \leq W_S < 2$
$0 \leq W_S < 1$
Wind Rose
N
E
S
W

(q). PM_{10} - EXP05

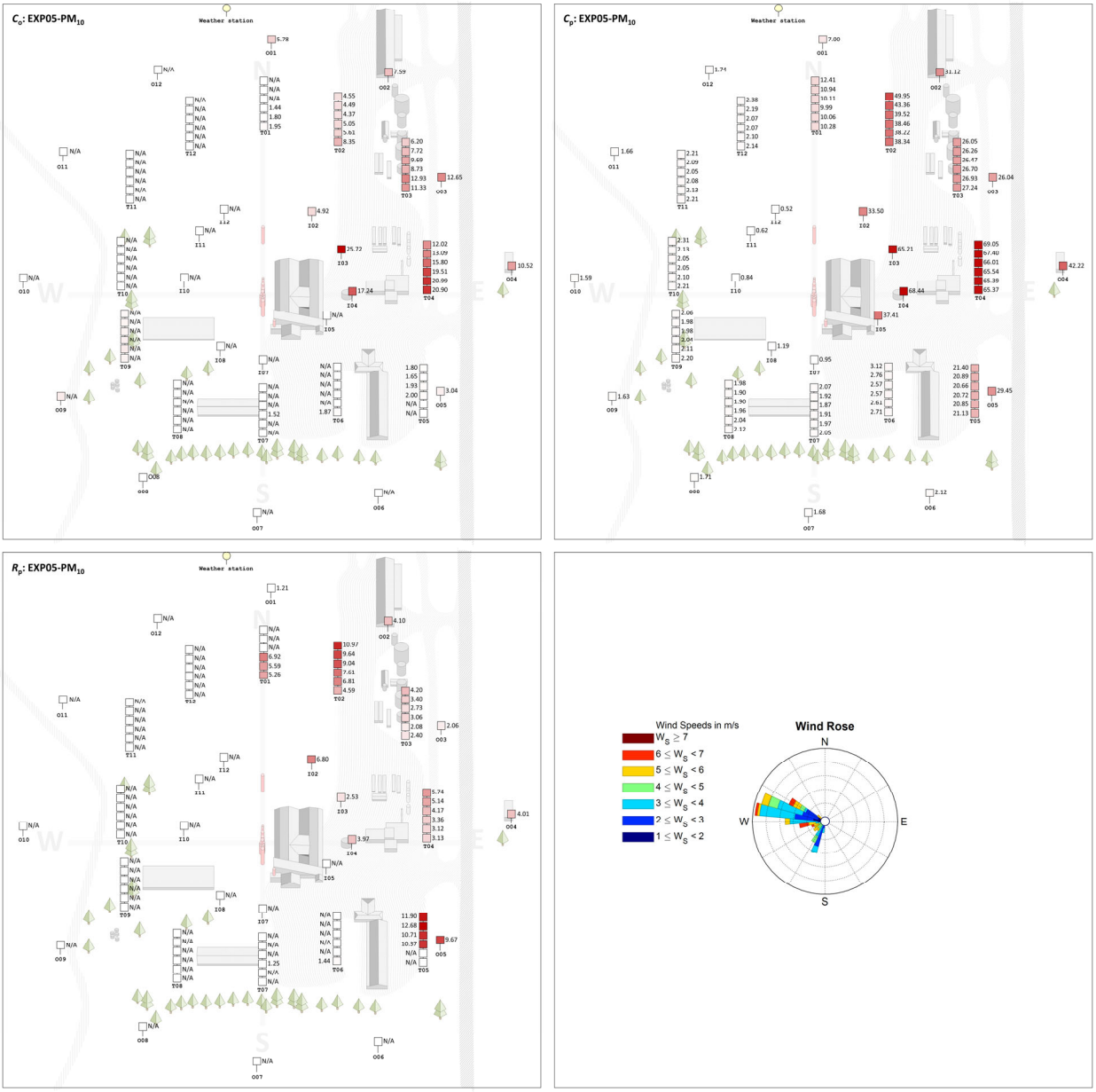
C_o: EXP05-PM_{10}
C_p: EXP05-PM_{10}
R_p: EXP05-PM_{10}
Weather station
Wind Speeds in m/s
$W_S \geq 7$
$6 \leq W_S < 7$
$5 \leq W_S < 6$
$4 \leq W_S < 5$
$3 \leq W_S < 4$
$2 \leq W_S < 3$
$1 \leq W_S < 2$
Wind Rose
N
E
S
W

(r). PM_{10} - EXP06

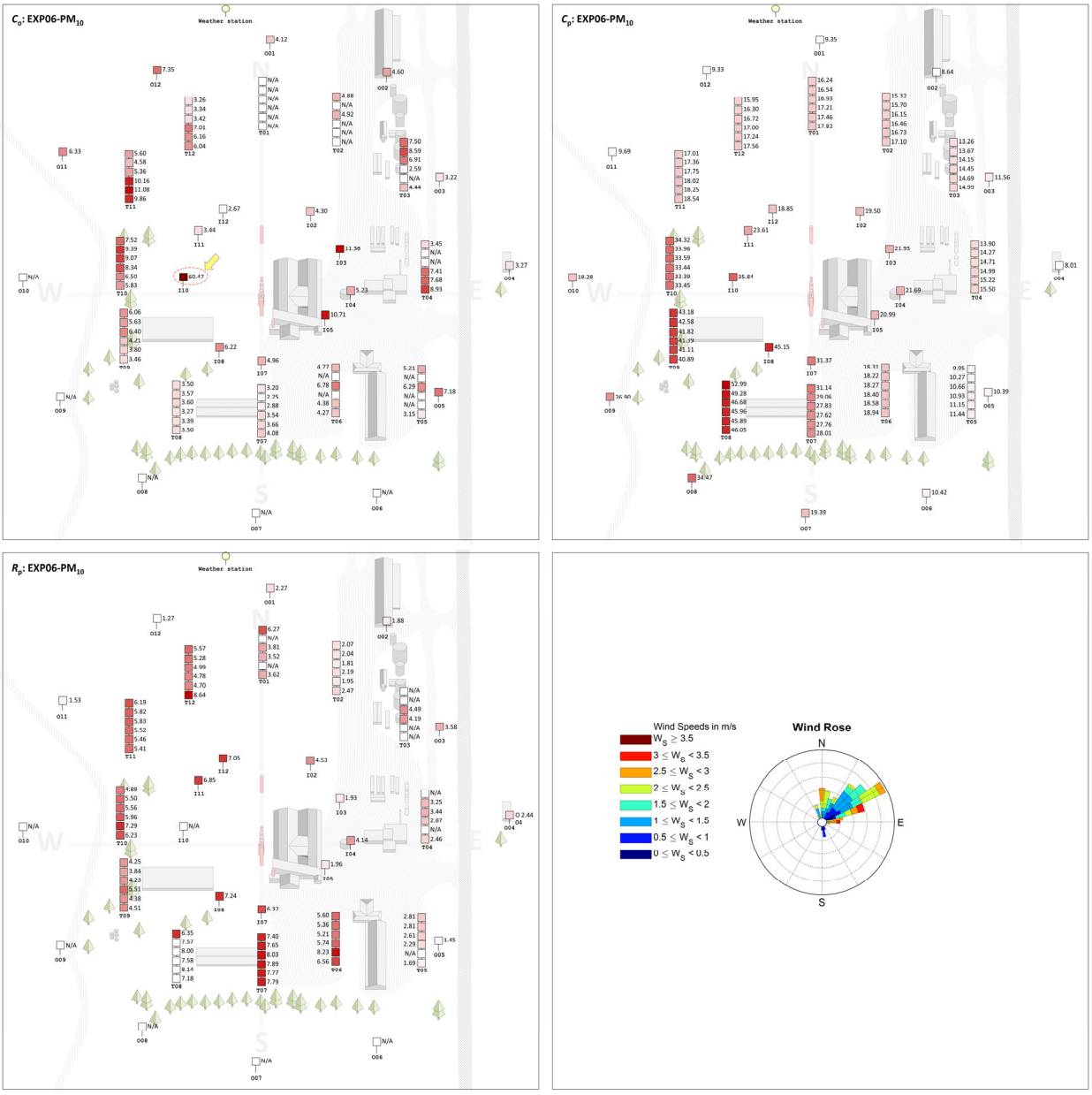
C_0: EXP06-PM_{10}
C_p: EXP06-PM_{10}
R_p: EXP06-PM_{10}
Weather station
Wind Speeds in m/s
$W_S \geq 3.5$
$3 \leq W_S < 3.5$
$2.5 \leq W_S < 3$
$2 \leq W_S < 2.5$
$1.5 \leq W_S < 2$
$1 \leq W_S < 1.5$
$0.5 \leq W_S < 1$
$0 \leq W_S < 0.5$
Wind Rose
N
E
S
W

(s). PM_{10} - EXP07

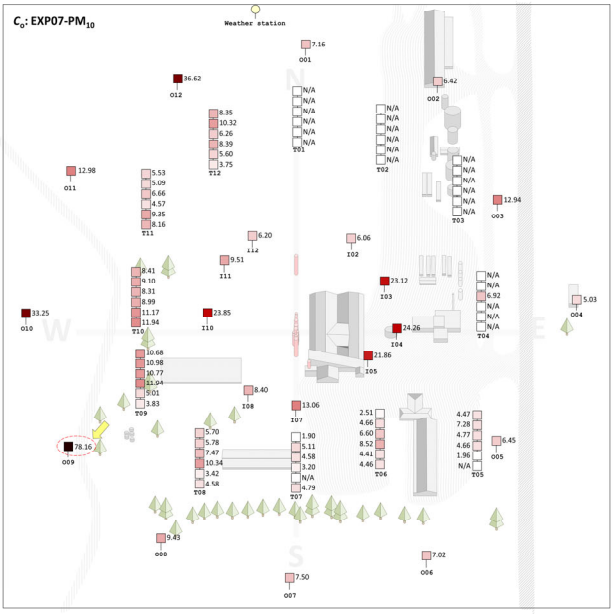
C_o: EXP07-PM_{10}
Weather station

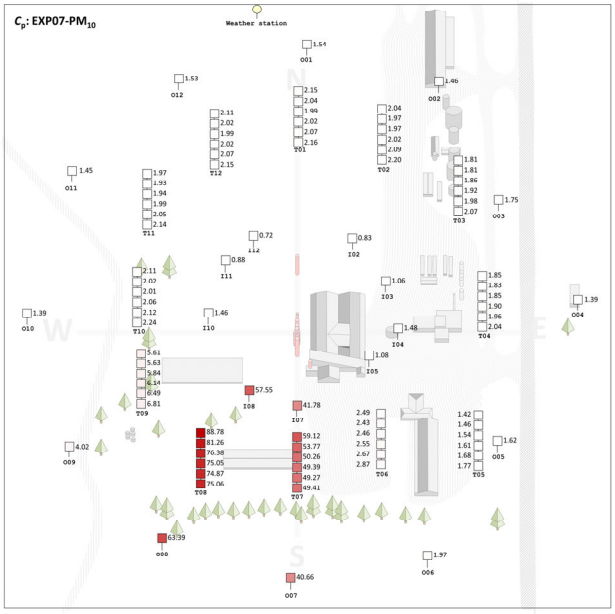
C_p: EXP07-PM_{10}
Weather station

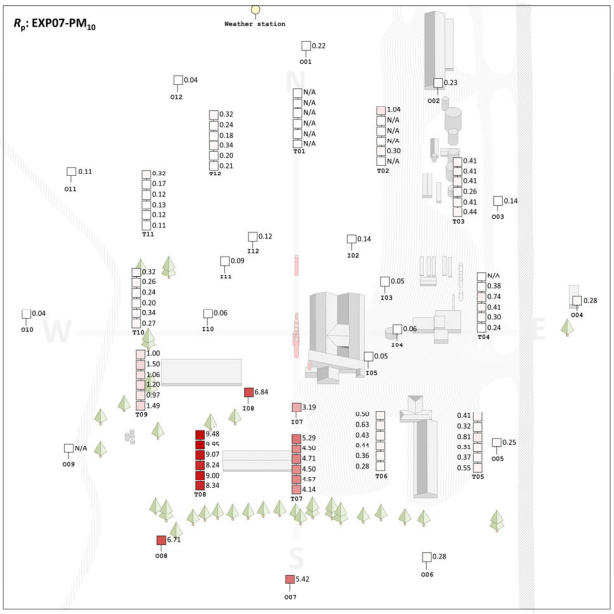
R_p: EXP07-PM_{10}
Weather station

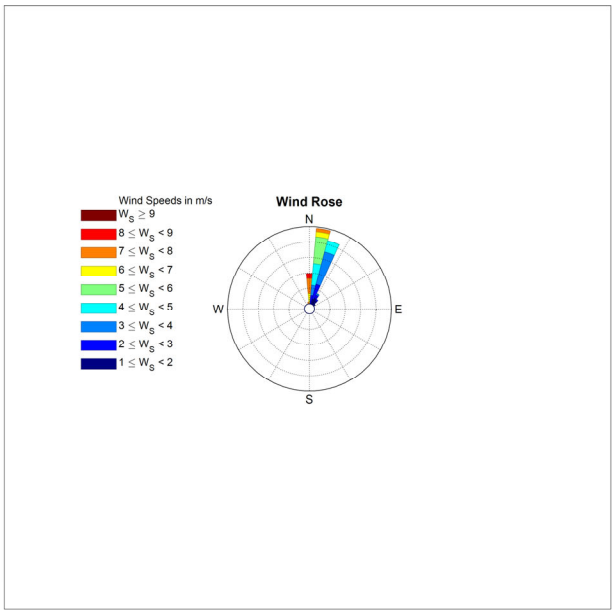
Wind Speeds in m/s
$W_S \geq 9$
$8 \leq W_S < 9$
$7 \leq W_S < 8$
$6 \leq W_S < 7$
$5 \leq W_S < 6$
$4 \leq W_S < 5$
$3 \leq W_S < 4$
$2 \leq W_S < 3$
$1 \leq W_S < 2$
Wind Rose
N
E
S
W

(t). PM_{10} - EXP08

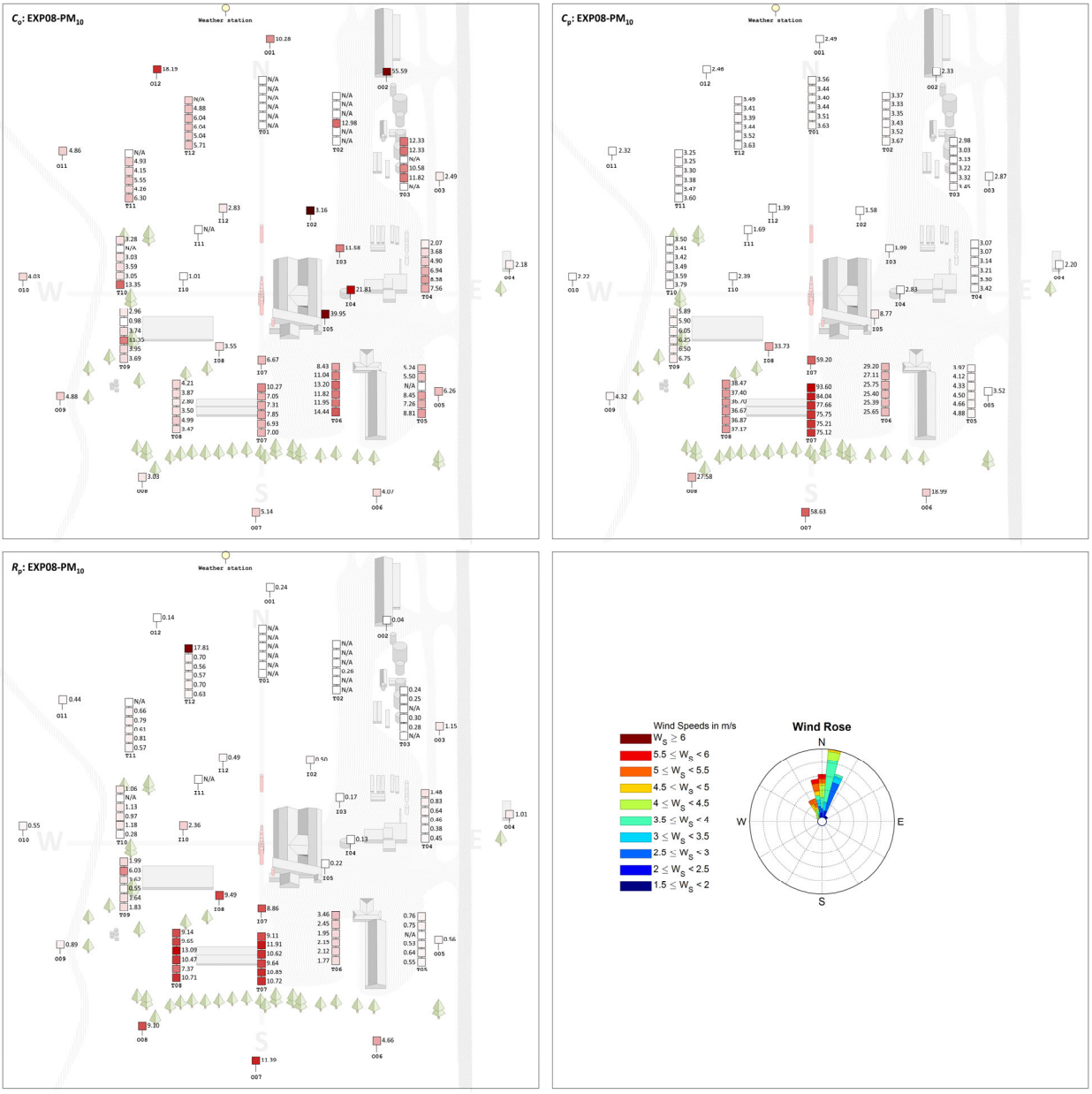
C_o: EXP08-PM_{10}
C_p: EXP08-PM_{10}
R_p: EXP08-PM_{10}
Weather station
Wind Speeds in m/s
$W_S \geq 6$
$5.5 \leq W_S < 6$
$5 \leq W_S < 5.5$
$4.5 < W_S < 5$
$4 < W_S < 4.5$
$3.5 \leq W_S < 4$
$3 \leq W_S < 3.5$
$2.5 \leq W_S < 3$
$2 \leq W_S < 2.5$
$1.5 \leq W_S < 2$
Wind Rose
N
E
S
W

(u). PM_{10} - EXP09

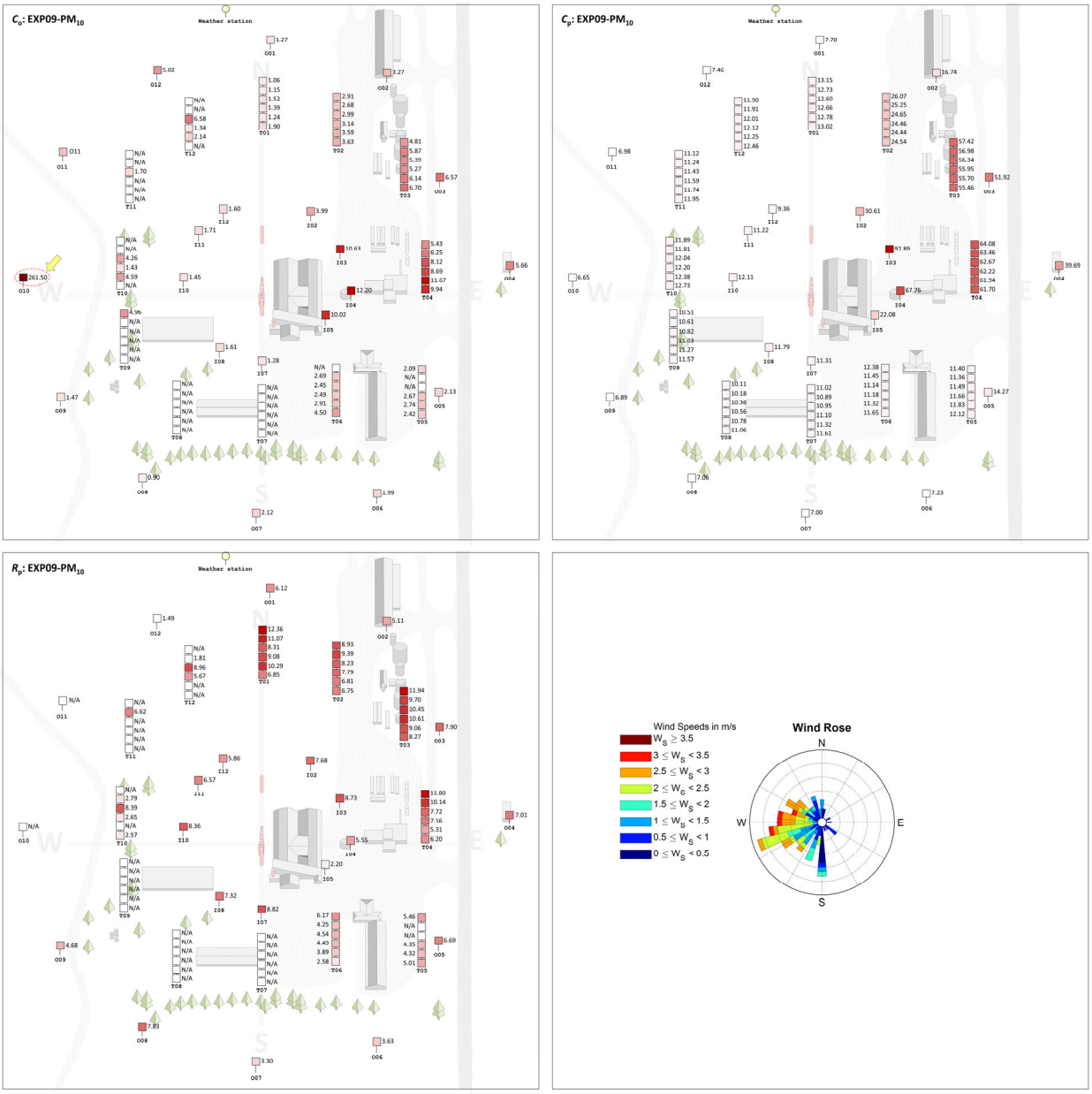
C_c: EXP09-PM_{10}
C_p: EXP09-PM_{10}
R_p: EXP09-PM_{10}
Weather station
Wind Speeds in m/s
$W_S \geq 3.5$
$3 \leq W_S < 3.5$
$2.5 \leq W_S < 3$
$2 \leq W_S < 2.5$
$1.5 \leq W_S < 1.5$
$1 \leq W_S < 1.5$
$0.5 \leq W_S < 1$
$0 \leq W_S < 0.5$
Wind Rose
N
E
S
W

(v). PM_{10} – EXP10

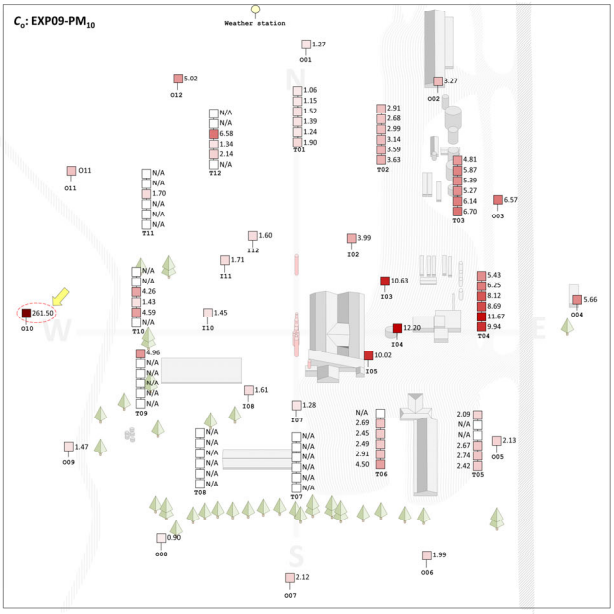
C_o: EXP09-PM_{10}
Weather station

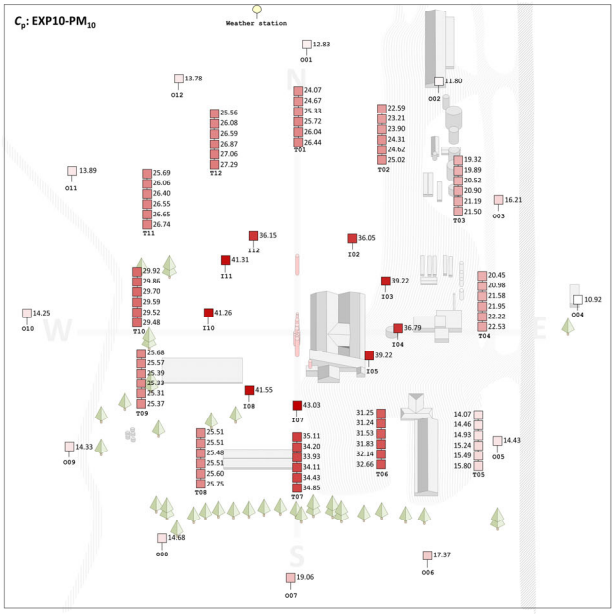
C_p: EXP10-PM_{10}
Weather station

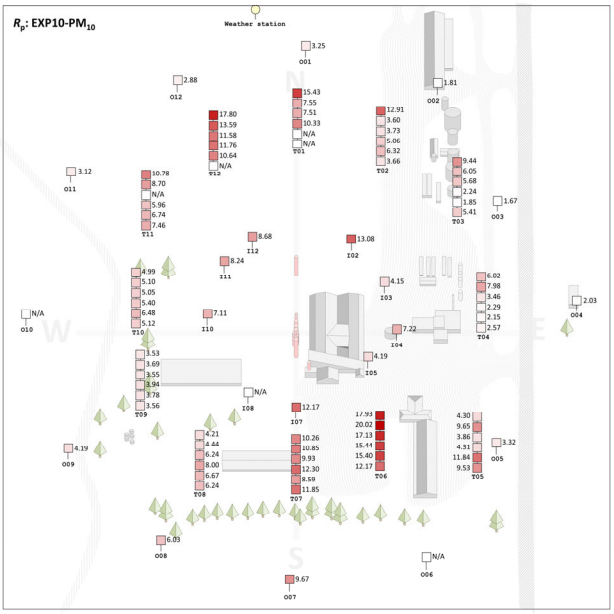
R_p: EXP10-PM_{10}
Weather station

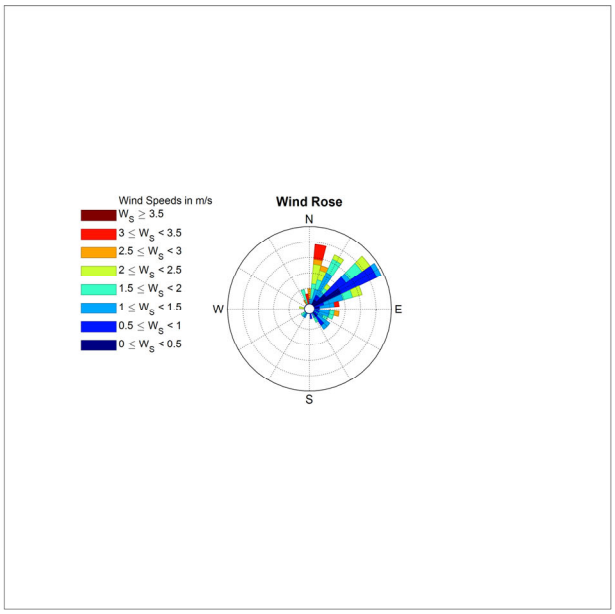
Wind Speeds in m/s
$W_S \geq 3.5$
$3 \leq W_S < 3.5$
$2.5 \leq W_S < 3$
$2 \leq W_S < 2.5$
$1.5 \leq W_S < 2$
$1 \leq W_S < 1.5$
$0.5 \leq W_S < 1$
$0 \leq W_S < 0.5$
Wind Rose
N
W
E
S

(w). TSP – EXP00

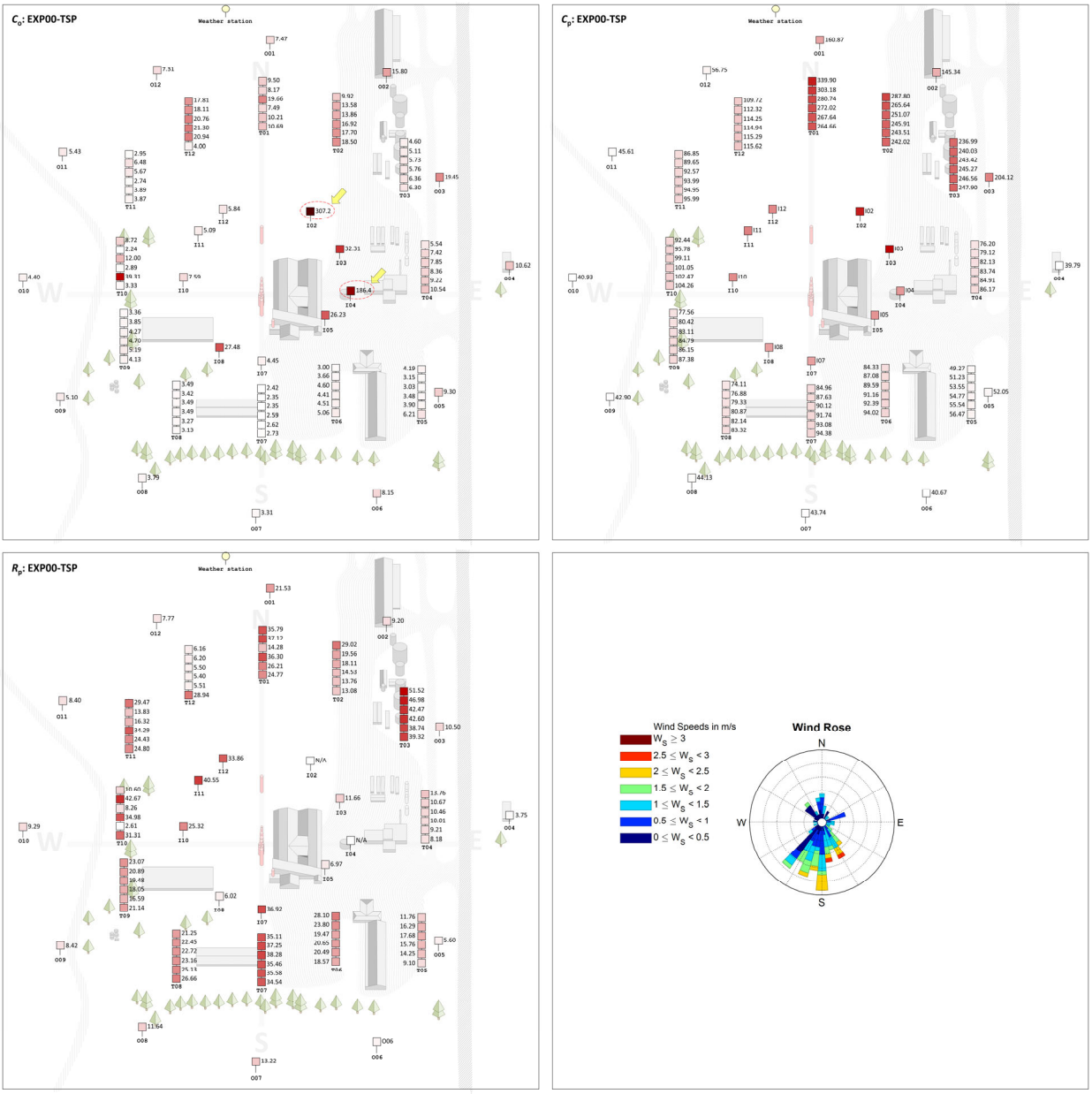
C_0: EXP00-TSP
C_p: EXP00-TSP
R_p: EXP00-TSP
Weather station
Wind Speeds in m/s
$W_S \geq 3$
$2.5 \leq W_S < 3$
$2 \leq W_S < 2.5$
$1.5 \leq W_S < 2$
$1 \leq W_S < 1.5$
$0.5 \leq W_S < 1$
$0 \leq W_S < 0.5$
Wind Rose
N
E
S
W

(x). TSP – EXP01

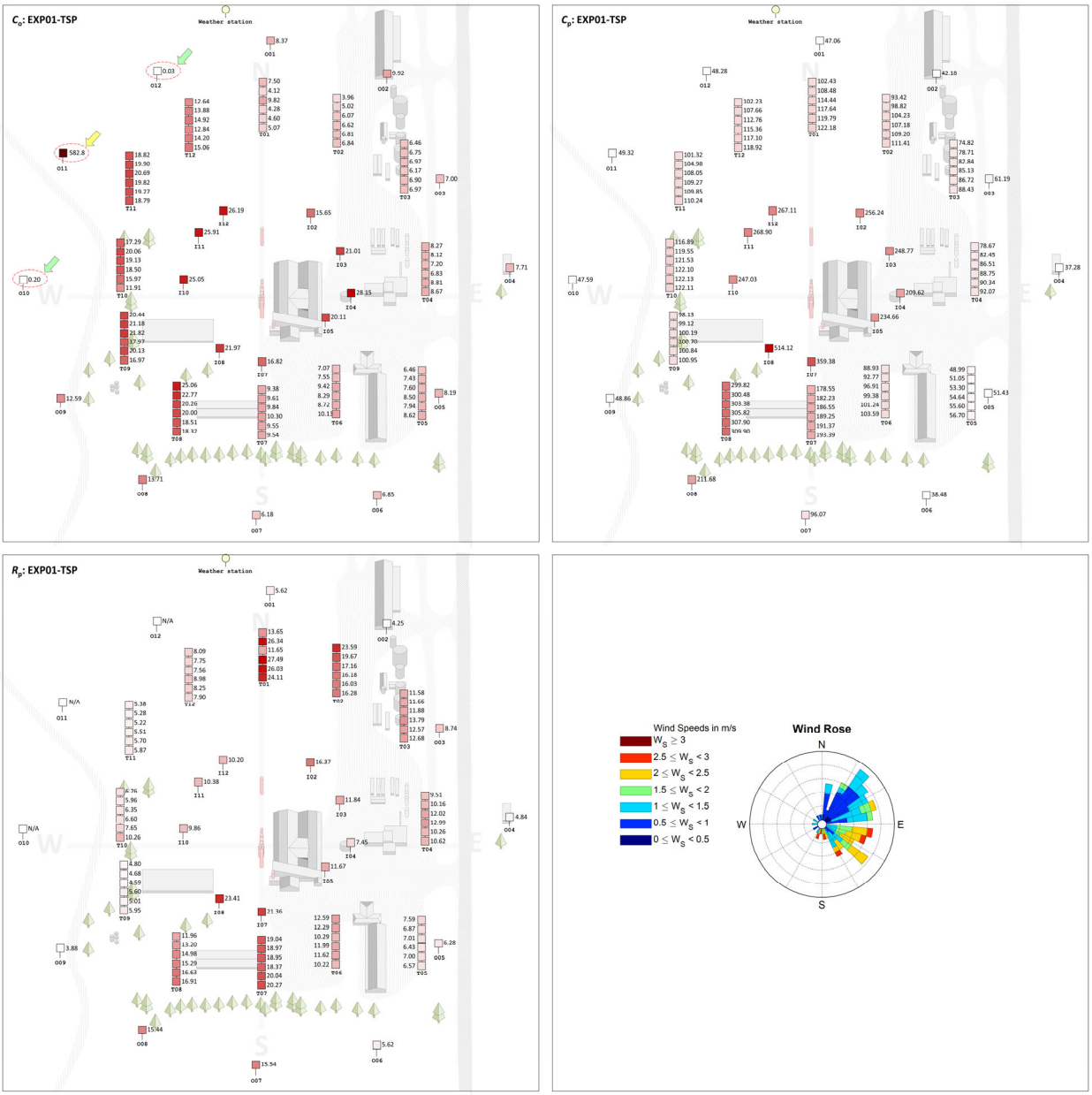
C_o: EXP01-TSP
C_p: EXP01-TSP
R_p: EXP01-TSP
Weather station
Wind Speeds in m/s
$W_S \geq 3$
$2.5 \leq W_S < 3$
$2 \leq W_S < 2.5$
$1.5 \leq W_S < 2$
$1 \leq W_S < 1.5$
$0.5 \leq W_S < 1$
$0 \leq W_S < 0.5$
Wind Rose
N
S
W
E

(y). TSP – EXP02

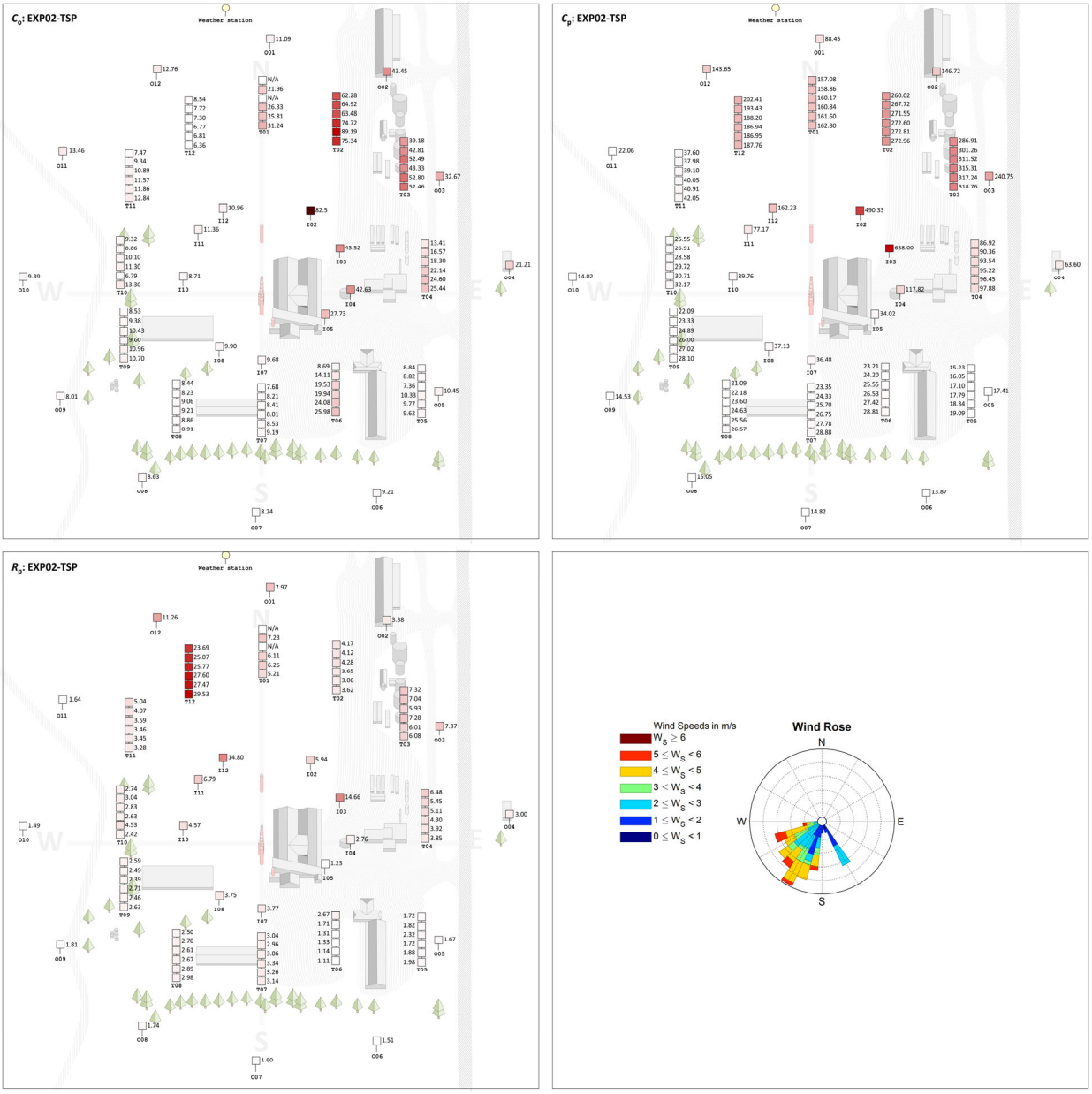
C_0: EXP02-TSP
C_p: EXP02-TSP
R_p: EXP02-TSP
Weather station
Wind Speeds in m/s
$W_S \geq 6$
$5 \leq W_S < 6$
$4 \leq W_S < 5$
$3 \leq W_S < 4$
$2 \leq W_S < 3$
$1 \leq W_S < 2$
$0 \leq W_S < 1$
Wind Rose
N
E
S
W

(z). TSP – EXP03

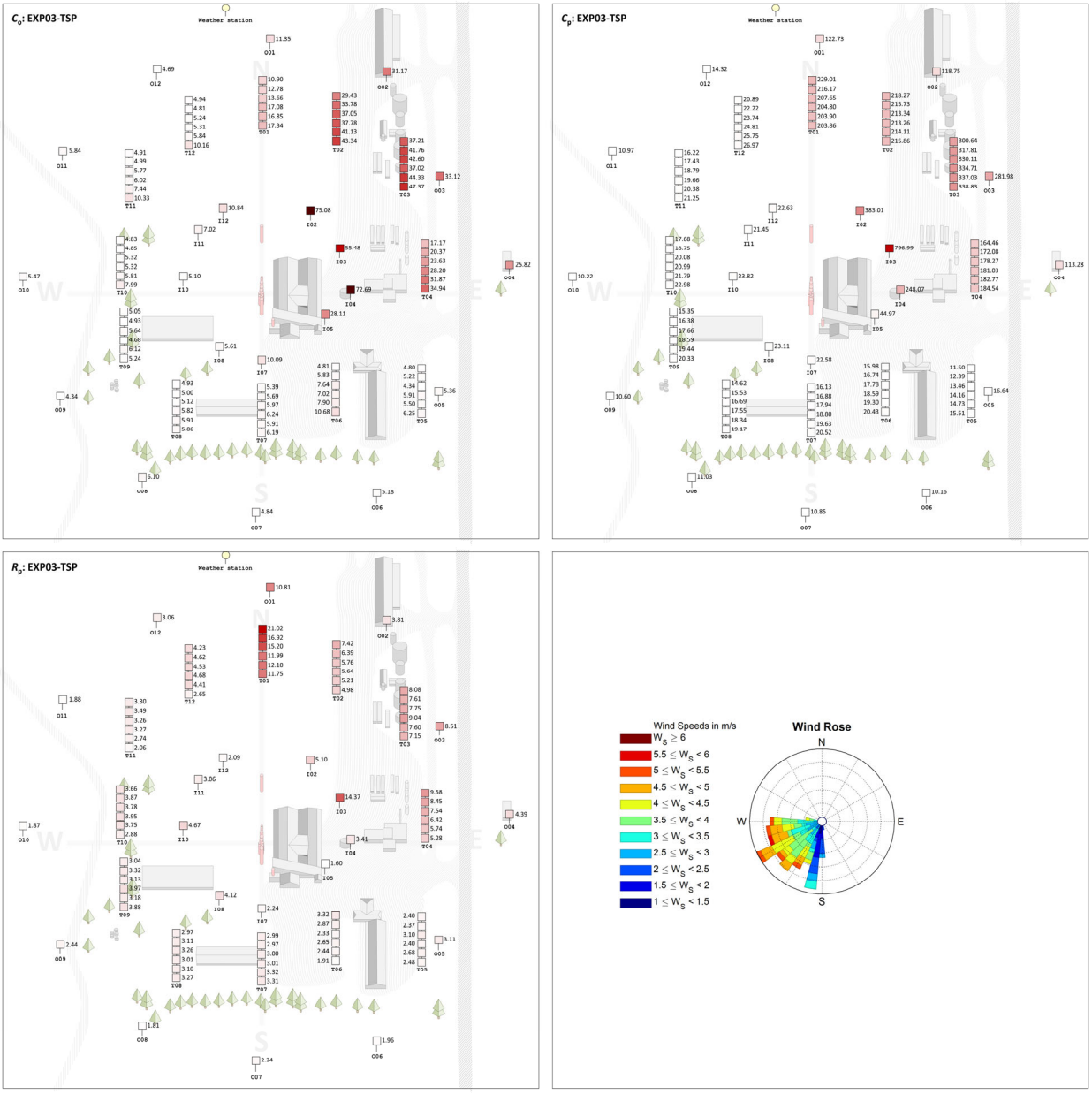
C_0: EXP03-TSP
C_p: EXP03-TSP
R_p: EXP03-TSP
Weather station
Wind Speeds in m/s
$W_S \geq 6$
$5.5 \leq W_S < 6$
$5 \leq W_S < 5.5$
$4.5 < W_S < 5$
$4 < W_S < 4.5$
$3.5 \leq W_S < 4$
$3 \leq W_S < 3.5$
$2.5 \leq W_S < 3$
$2 \leq W_S < 2.5$
$1.5 \leq W_S < 2$
$1 \leq W_S < 1.5$
Wind Rose
N
E
S
W

(aa). TSP – EXP04

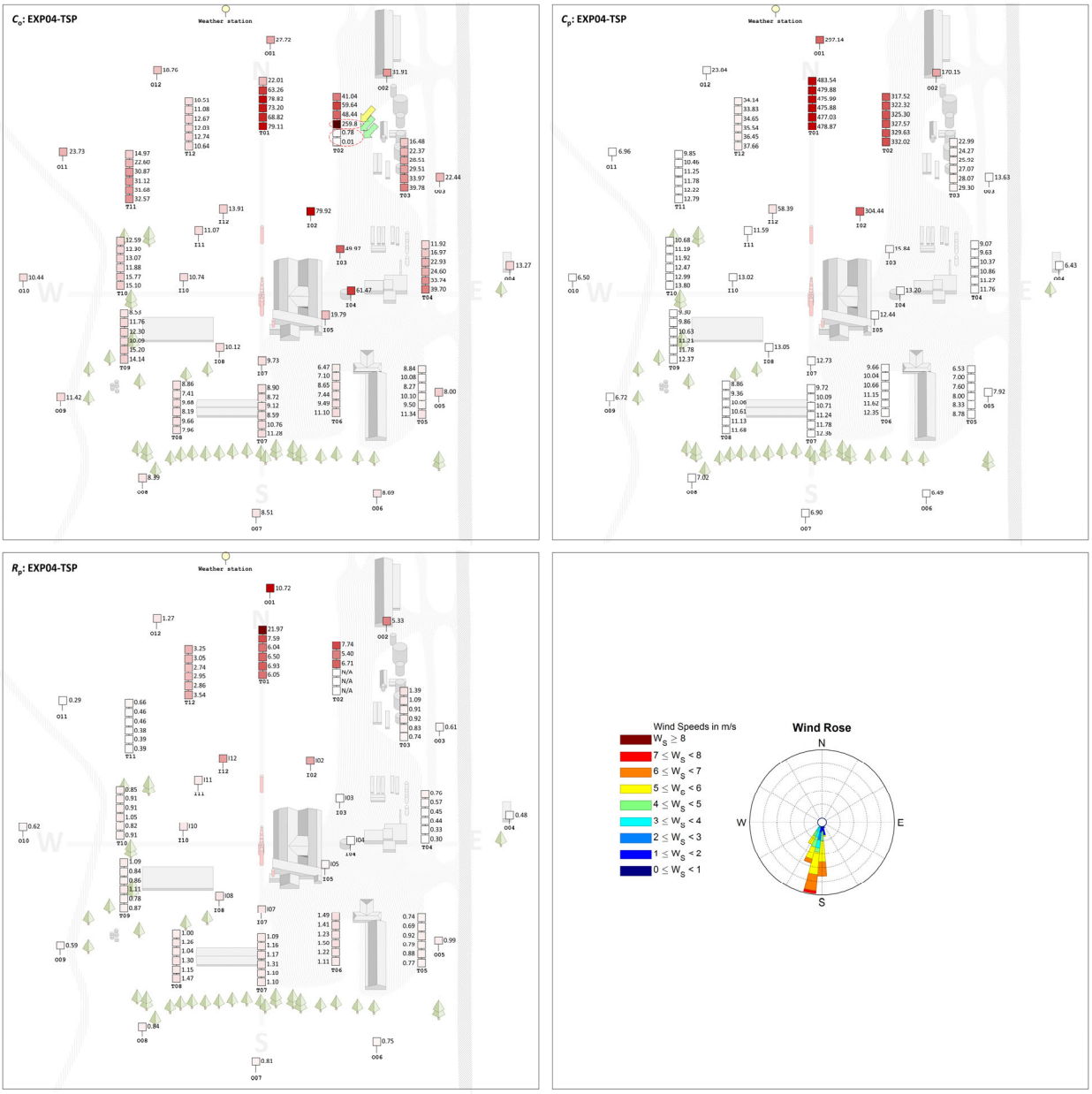
C_o: EXP04-TSP
C_p: EXP04-TSP
R_p: EXP04-TSP
Weather station
Wind Speeds in m/s
$W_S \geq 8$
$7 \leq W_S < 8$
$6 \leq W_S < 7$
$5 \leq W_S < 6$
$4 \leq W_S < 5$
$3 \leq W_S < 4$
$2 \leq W_S < 3$
$1 \leq W_S < 2$
$0 \leq W_S < 1$
Wind Rose
N
E
S
W

(ab). TSP – EXP05

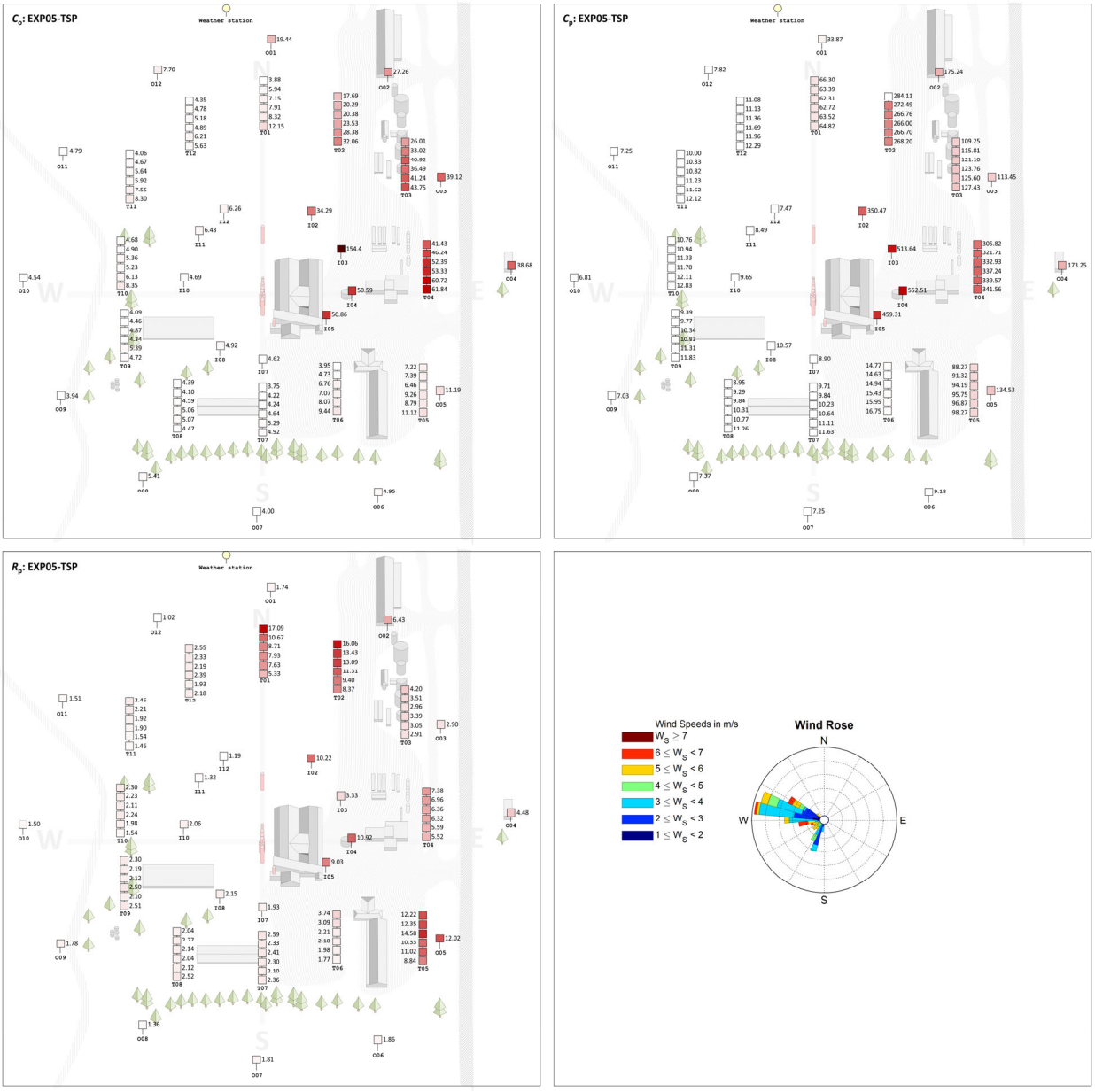
C_o: EXP05-TSP
C_p: EXP05-TSP
R_p: EXP05-TSP
Weather station
Wind Speeds in m/s
$W_S \geq 7$
$6 \leq W_S < 7$
$5 \leq W_S < 6$
$4 \leq W_S < 5$
$3 \leq W_S < 4$
$2 \leq W_S < 3$
$1 \leq W_S < 2$
Wind Rose
N
E
S
W

(ac). TSP – EXP06

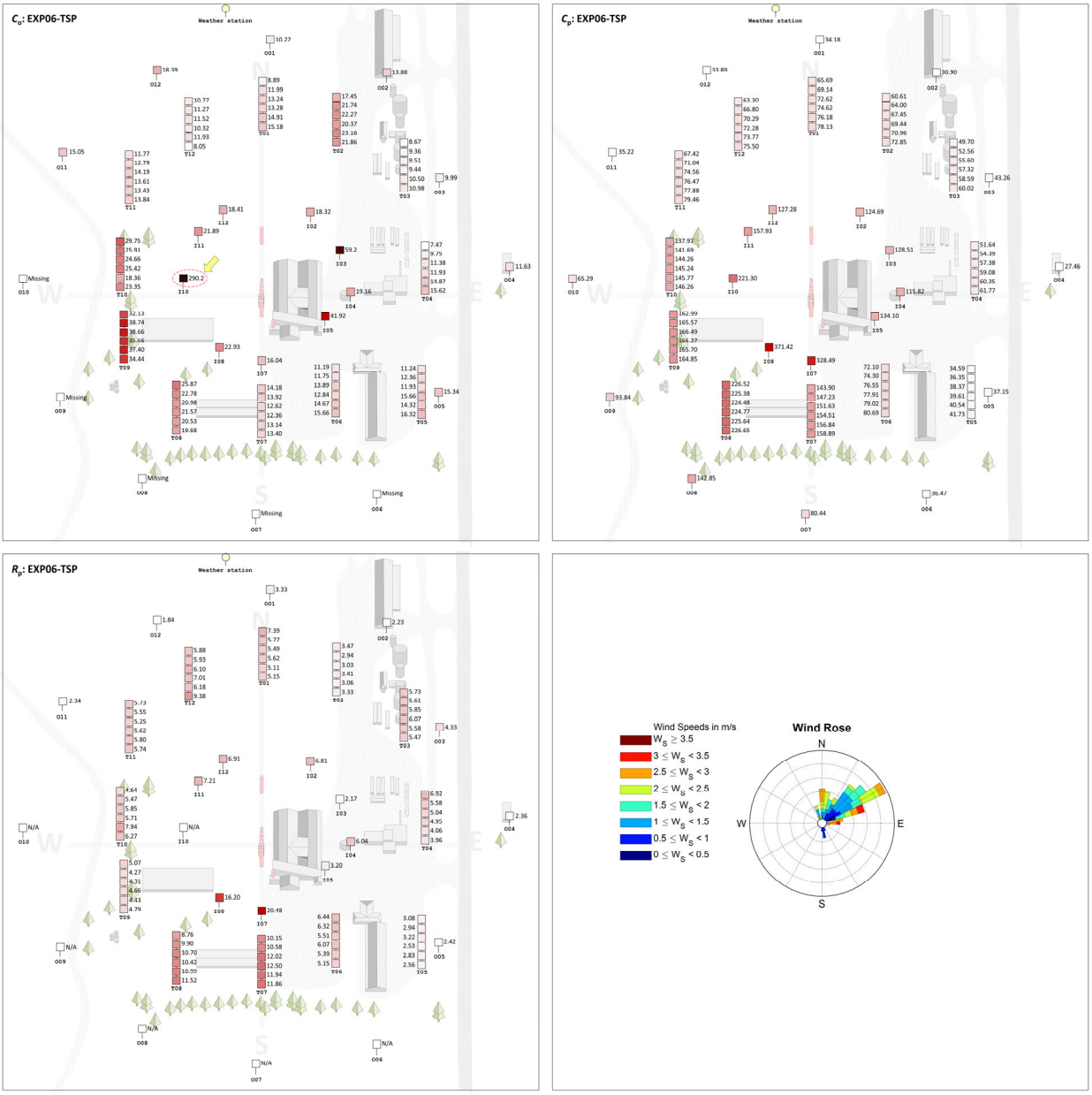
C_o: EXP06-TSP
C_p: EXP06-TSP
R_p: EXP06-TSP
Weather station
Wind Speeds in m/s
$W_S \geq 3.5$
$3 \leq W_S < 3.5$
$2.5 \leq W_S < 3$
$2 \leq W_S < 2.5$
$1.5 \leq W_S < 2$
$1 \leq W_S < 1.5$
$0.5 \leq W_S < 1$
$0 \leq W_S < 0.5$
Wind Rose
N
S
W
E

(ad). TSP – EXP07

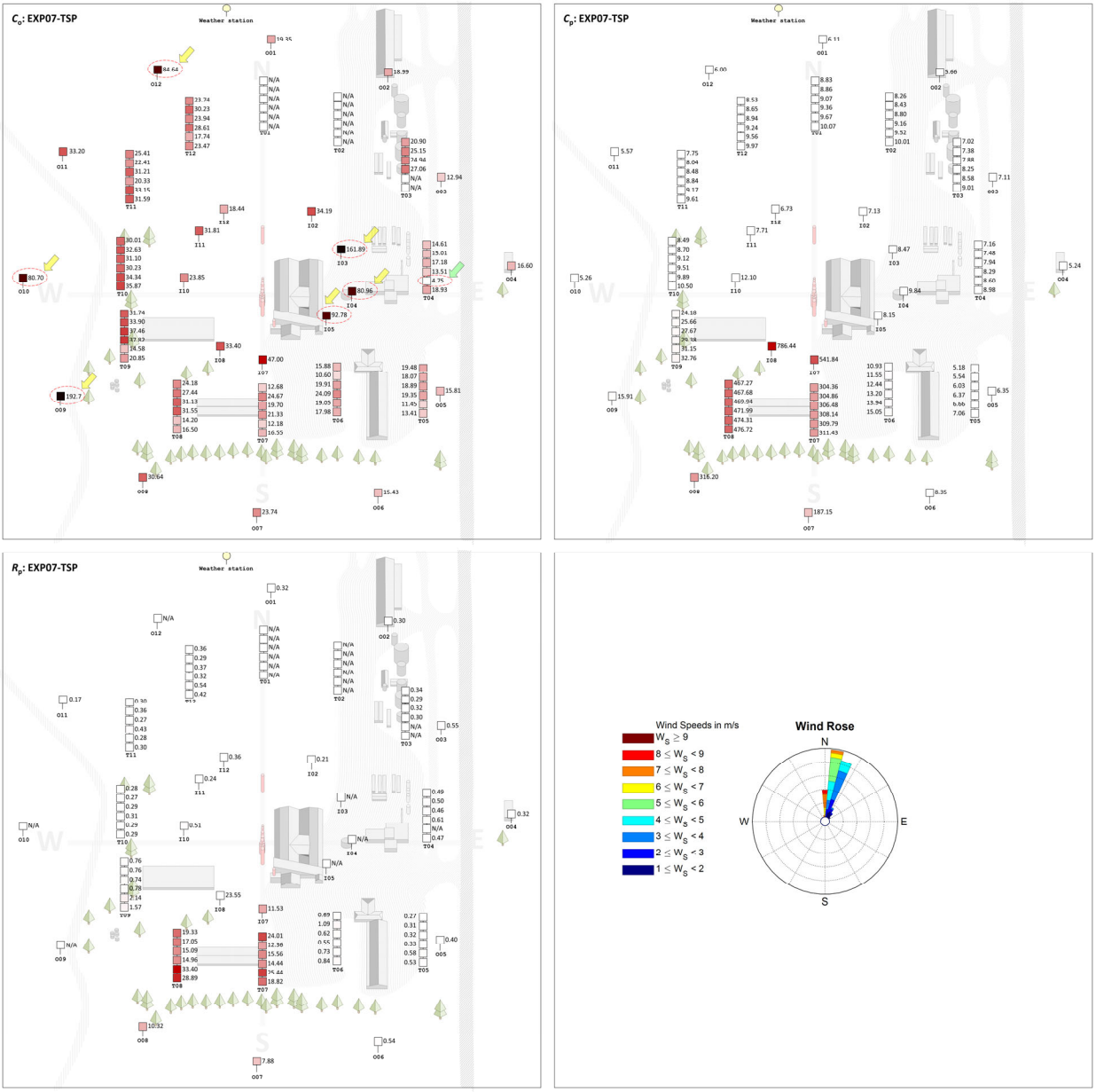
C_o: EXP07-TSP
C_p: EXP07-TSP
R_p: EXP07-TSP
Weather station
Wind Speeds in m/s
$W_S \geq 9$
$8 \leq W_S < 9$
$7 \leq W_S < 8$
$6 \leq W_S < 7$
$5 \leq W_S < 6$
$4 \leq W_S < 5$
$3 \leq W_S < 4$
$2 \leq W_S < 3$
$1 \leq W_S < 2$
Wind Rose
N
E
S
W

(ae). TSP – EXP08

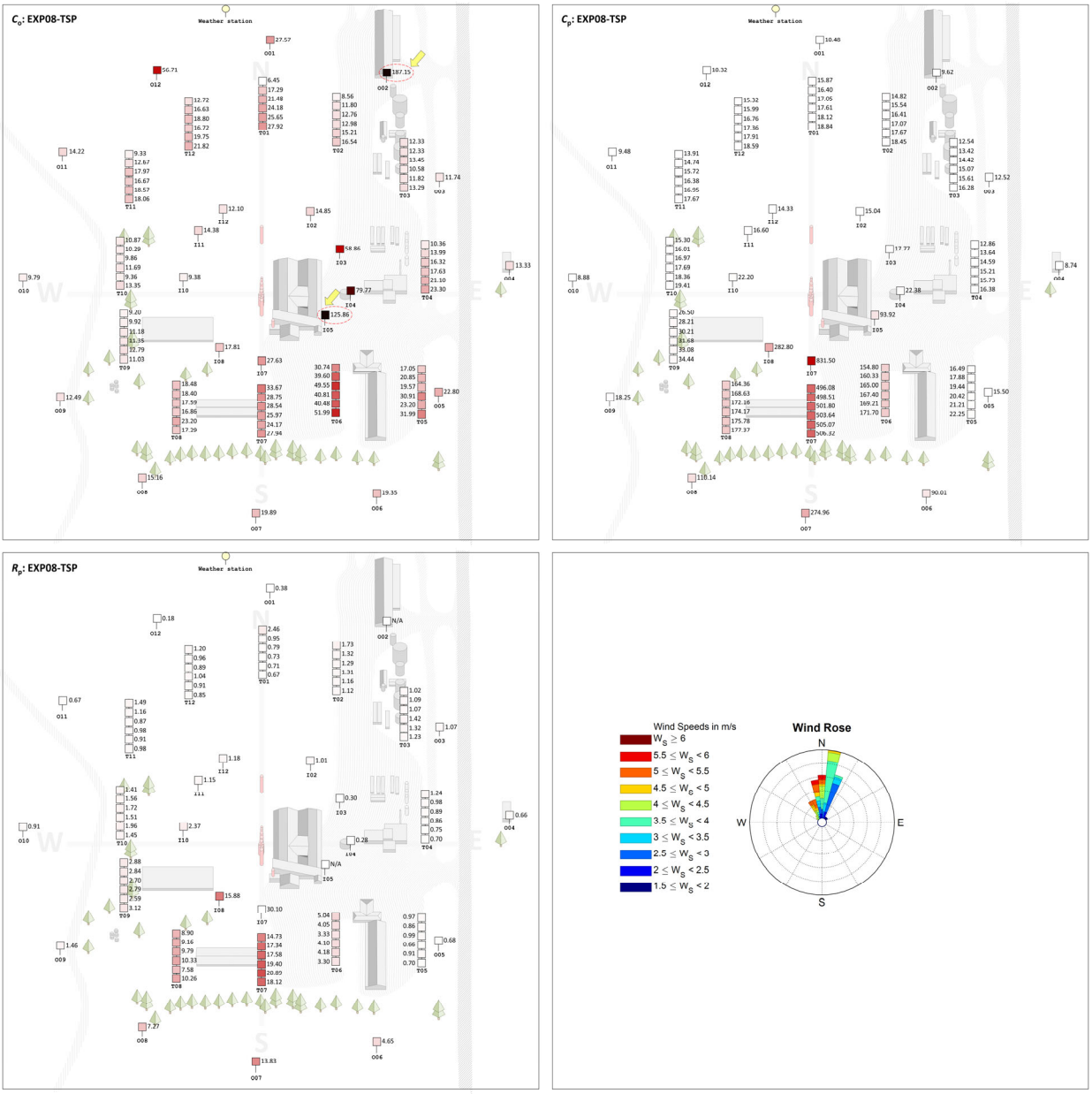
C_0: EXP08-TSP
C_p: EXP08-TSP
R_p: EXP08-TSP
Weather station
Wind Speeds in m/s
$W_S \geq 6$
$5.5 \leq W_S < 6$
$5 \leq W_S < 5.5$
$4.5 \leq W_S < 5$
$4 \leq W_S < 4.5$
$3.5 \leq W_S < 4$
$3 \leq W_S < 3.5$
$2.5 \leq W_S < 3$
$2 \leq W_S < 2.5$
$1.5 \leq W_S < 2$
Wind Rose
N
E
S
W

(af). TSP – EXP09

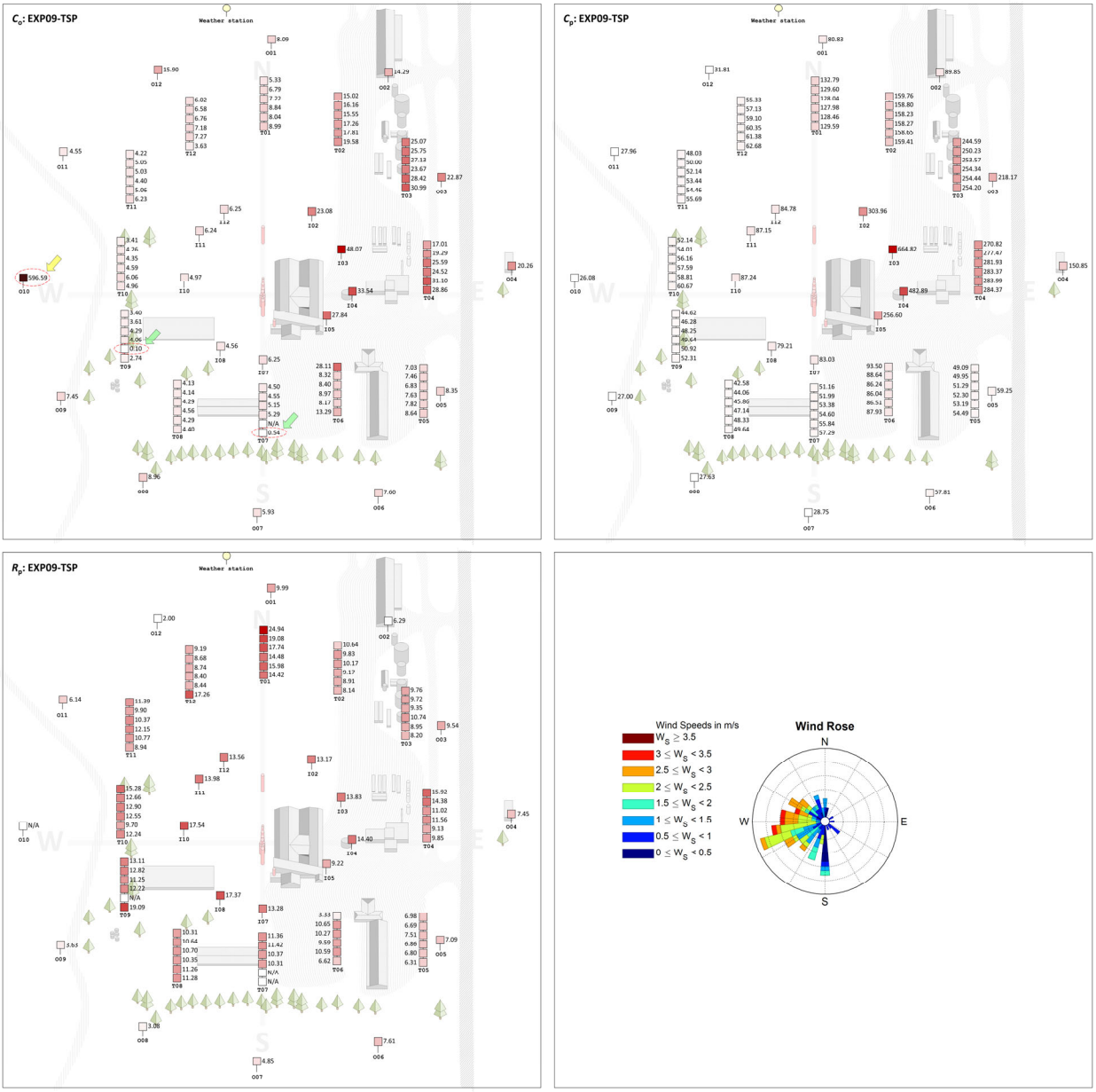
C_o: EXP09-TSP
C_p: EXP09-TSP
R_p: EXP09-TSP
Weather station
Wind Speeds in m/s
$W_S \geq 3.5$
$3 \leq W_S < 3.5$
$2.5 \leq W_S < 3$
$2 \leq W_S < 2.5$
$1.5 \leq W_S < 2$
$1 \leq W_S < 1.5$
$0.5 \leq W_S < 1$
$0 \leq W_S < 0.5$
Wind Rose
N
S
W
E

(ag). TSP – EXP10

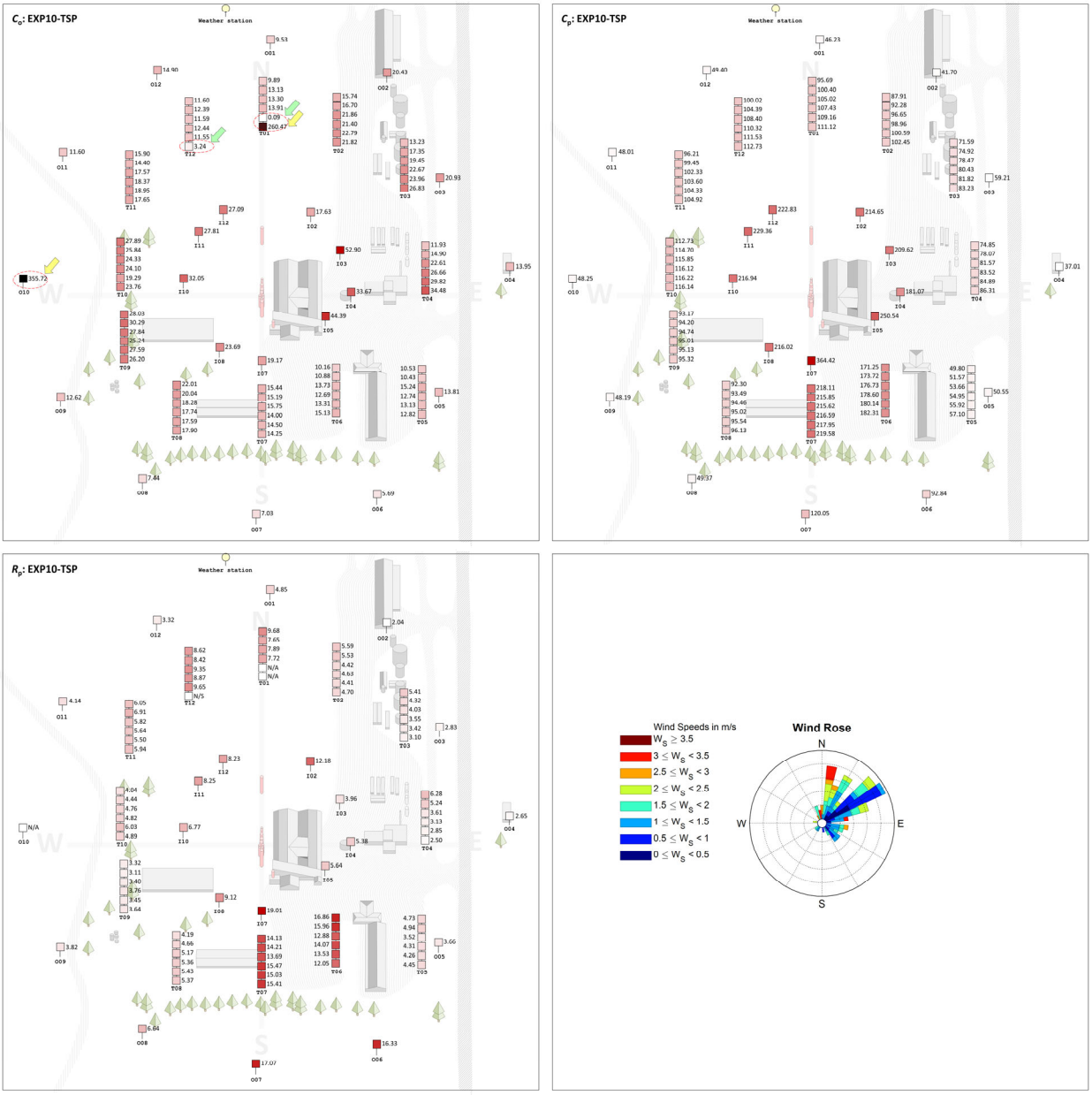
C_o: EXP10-TSP
C_p: EXP10-TSP
R_p: EXP10-TSP
Weather station
Wind Speeds in m/s
$W_S \geq 3.5$
$3 \leq W_S < 3.5$
$2.5 \leq W_S < 3$
$2 \leq W_S < 2.5$
$1.5 \leq W_S < 1.5$
$1 \leq W_S < 1$
$0.5 \leq W_S < 1$
$0 \leq W_S < 0.5$
Wind Rose
N
W
E
S

SI Table 3-6 Statistical summary of pollutant concentrations with and without statistical outliers. Data are expressed as mean ± std. (a) PM2.5, (b) PM10 and (c) TSP. N/A refers to situation that no sufficient data available to derive particle size distribution.

(a) $PM_{2.5}$ concentration

	N/A percentage of total	w/o Statistical Outliers ($\mu g/m^3$)			w/ Statistical Outliers ($\mu g/m^3$)		
EXP00	5%	0.10	±	0.18	0.19	±	0.83
EXP01	43%	0.10	±	0.05	0.19	±	0.58
EXP02	60%	0.46	±	0.49	0.43	±	0.48
EXP03	60%	0.39	±	0.55	0.39	±	0.55
EXP04	37%	0.54	±	0.62	0.53	±	0.62
EXP05	65%	0.33	±	0.31	0.31	±	0.31
EXP06	25%	0.32	±	0.32	0.31	±	0.32
EXP07	27%	0.91	±	2.37	0.90	±	2.35
EXP08	20%	1.29	±	2.44	1.29	±	2.44
EXP09	34%	0.39	±	0.77	0.39	±	0.77
EXP10	8%	0.23	±	0.37	0.22	±	0.37

(b) PM_{10} concentration

	N/A percentage of total	w/o Statistical Outliers ($\mu g/m^3$)			w/ Statistical Outliers ($\mu g/m^3$)		
EXP00	5%	1.47	±	1.05	2.59	±	7.23
EXP01	43%	4.04	±	0.99	6.96	±	21.2
EXP02	60%	10.28	±	5.09	10.3	±	5.09
EXP03	60%	8.62	±	5.03	8.62	±	5.03
EXP04	33%	8.42	±	9.75	8.15	±	9.70
EXP05	62%	8.43	±	6.59	8.43	±	6.59
EXP06	15%	5.22	±	2.30	5.92	±	6.63
EXP07	12%	9.20	±	6.31	10.0	±	9.87
EXP08	19%	7.84	±	7.89	7.84	±	7.89
EXP09	33%	3.94	±	2.83	8.10	±	32.8
EXP10	3%	4.47	±	2.35	5.97	±	11.7

(c) TSP concentration

	N/A percentage of total	w/o Statistical Outliers ($\mu g/m^3$)			w/ Statistical Outliers ($\mu g/m^3$)		
EXP00	0%	8.30	±	7.17	13.4	±	36.6
EXP01	0%	12.7	±	6.38	18.6	±	59.5
EXP02	2%	20.6	±	19.4	20.6	±	19.4
EXP03	0%	15.2	±	15.8	15.2	±	15.8
EXP04	0%	21.3	±	18.5	23.4	±	30.9
EXP05	0%	16.0	±	21.4	16.0	±	21.4
EXP06	5%	17.6	±	8.89	20.7	±	30.4
EXP07	15%	23.6	±	7.84	30.3	±	28.6
EXP08	0%	20.3	±	12.3	23.2	±	23.7
EXP09	1%	11.4	±	9.28	17.6	±	61.7
EXP10	0%	18.8	±	7.91	24.7	±	43.6

SI Table 3-7 Samplers that have statistical outliers. Small outliers refer to statistical outliers that are at lower end; large outliers are statistical outliers that are at higher end. (a) PM2.5, (b) PM10 and (c) TSP. O refers to samplers in the outlier ring (~180 m from source); I refers to samplers in the inner ring (~ 60 m from source); T refers to sampler tower, which is in the middle ring (~ 120 m from source). Samplers on map are shown in Figure 1 in manuscript, and details are shown in **Section 3.1** in manuscript.

(a) $PM_{2.5}$ outliers

	Low-outliers		High-outliers	
EXP00			I04	
EXP01	O10	O12	I04	O11
EXP02	O01	O05		
EXP03				
EXP04	T02-1			
EXP05	T05-5	T07-3		
EXP06	T06-2			
EXP07	T09-6			
EXP08				
EXP09				
EXP10	T01-2			

(b) PM_{10} outliers

	Low-outliers		High-outliers				
EXP00			I02	I03	I04	I05	T10-2
EXP01	O10	O12	I04	O11			
EXP02							
EXP03							
EXP04	T02-1	T02-2					
EXP05							
EXP06			I10				
EXP07			O09				
EXP08							
EXP09			O10				
EXP10	T01-2	T12-1	O10	T01-1			

(c) TSP outliers

	Low-outliers		High-outliers					
EXP00			I02	I04				
EXP01	O10	O12	O11					
EXP02								
EXP03								
EXP04	T02-1	T02-2	T02-3					
EXP05								
EXP06			I10					
EXP07	T04-2		I03	I04	I05	O09	O10	O12
EXP08			I05	O02				
EXP09	T09-2	T07-1	O10					
EXP10	T01-2	T12-1	O10	T01-1				

SI Figure 3-3 Possible emission source rather than emission stack. Photos were provided author.

(a) Inner 12, Tower 12, Outer 12 – module truck unloading module

(b) Cottonseed loaded (blown) into truck

(c) Outer 2 looking back at gin with Tower 2 & Inner 2 in background

(d) Inner 12, Tower 12, Outer 12 – Module truck unloading module

(e) Looking NW – Outer 9 and Outer 10 – field road used very little by farmer

(f) Burning rice straw in distance field (facing SE). Possible source of background PM

(g) Outer 9 looking back at gin

(h) Module truck (facing North) backing into gin with Inner 5 on right

SI Table 3-8 Pearson correlation coefficients between log-transformed concentrations and potential influential factors and between mass percent PM and height and distance. Concentration and percentage data were log-transformed before applying correlation analysis. h is heigh (m); d is distance from source (m); u is the ambient wind speed (m/s); σ is the standard deviation of wind direction (deg); θ is the deviation from wind direction (deg), defined as the difference between the wind direction and the from the source to the direction of wind velocity and the direction of source to the receptor. Notations: $^{*}p < 0.05$; $^{**}p < 0.001$.

	Concentration			**Percent**	
	$PM_{2.5}$	PM_{10}	TSP	$\%PM_{2.5}$	$\%PM_{10}$
h	-0.17^{**}	-0.12^{*}	-0.12^{*}	-0.15^{*}	-0.09^{*}
d	-0.13^{*}	-0.13^{*}	-0.26^{**}	-0.01	0.22^{**}
u	0.41^{**}	0.51^{**}	0.22^{**}	\	\
θ	-0.03	-0.23^{**}	-0.34^{**}	\	\
σ	-0.44^{**}	-0.56^{**}	-0.35^{**}	\	\

SI Figure 3-4 Scatter plot of log-transformed observed concentration versus height, distance, average ambient wind speed and deviation from wind direction. h is heigh; d is distance from source; u is the ambient wind speed; σ is the standard deviation of wind direction; θ is the deviation from wind direction, defined as the difference between the wind direction and the from the source to the direction of wind velocity and the direction of source to the receptor. The solid red lines are the linear regression to show the trend.

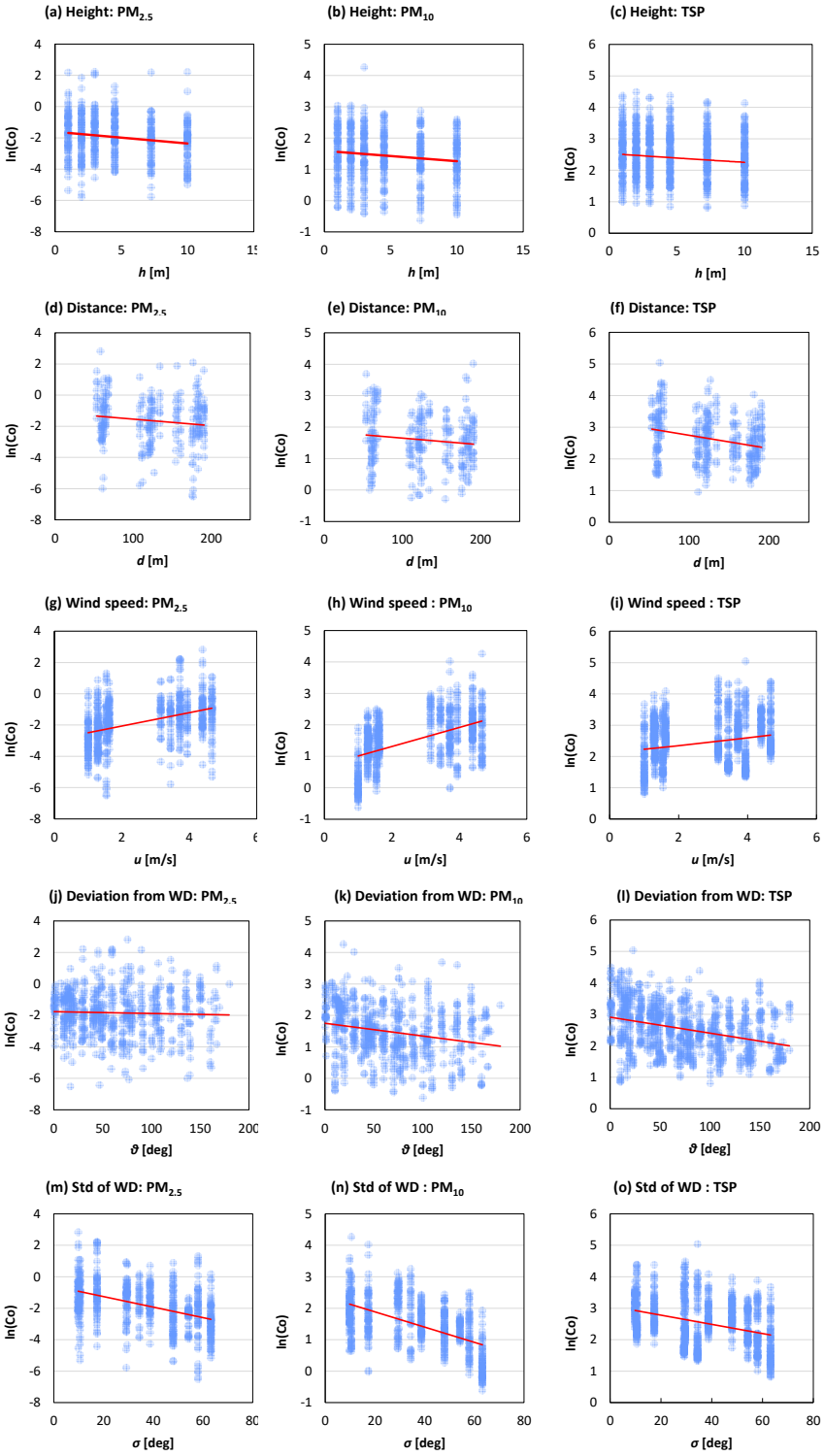

SI Figure 3-5 Scatter plot of log-transformed percent of PM versus height and distance. *h* is heigh; *d* is distance from source; *u* is the ambient wind speed. The solid red lines are the linear regression to show the trend.

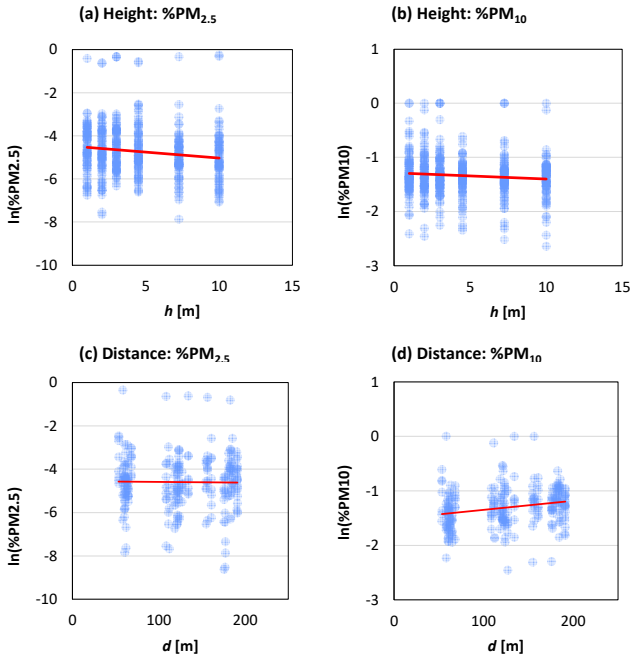

SI Figure 3-6 Scatter plot of observed concentration (C_o) versus model-predicted concentration (C_p) of each experiment. Solid lines refer to 1:1 ratio.

(a). $PM_{2.5}$

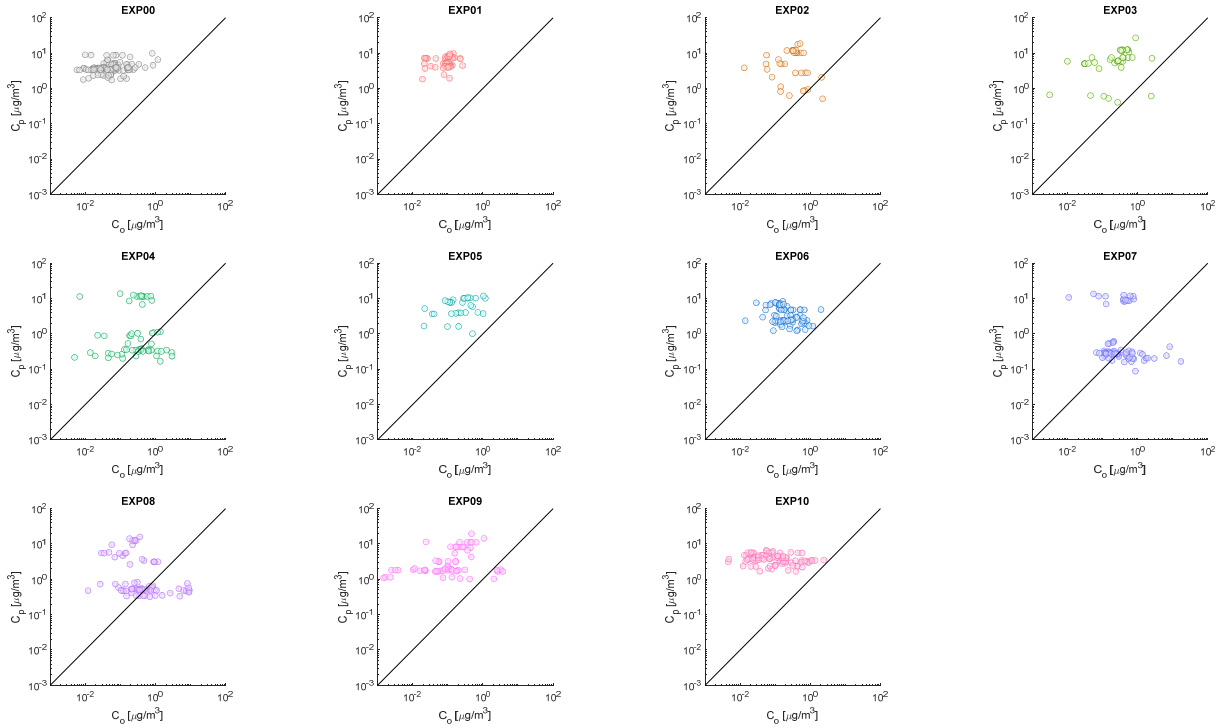

(b). PM_{10}

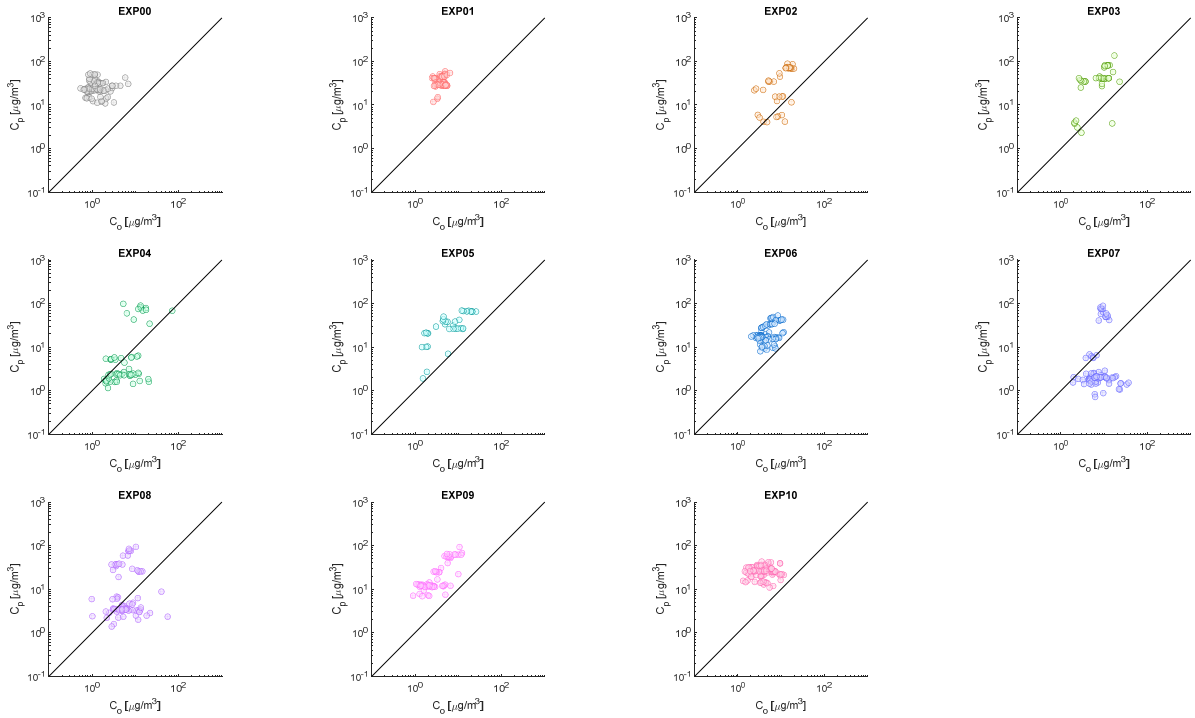
EXP00
EXP01
EXP02
EXP03
EXP04
EXP05
EXP06
EXP07
EXP08
EXP09
EXP10
C_p [μg/m³]
C_o [μg/m³]

(c). TSP

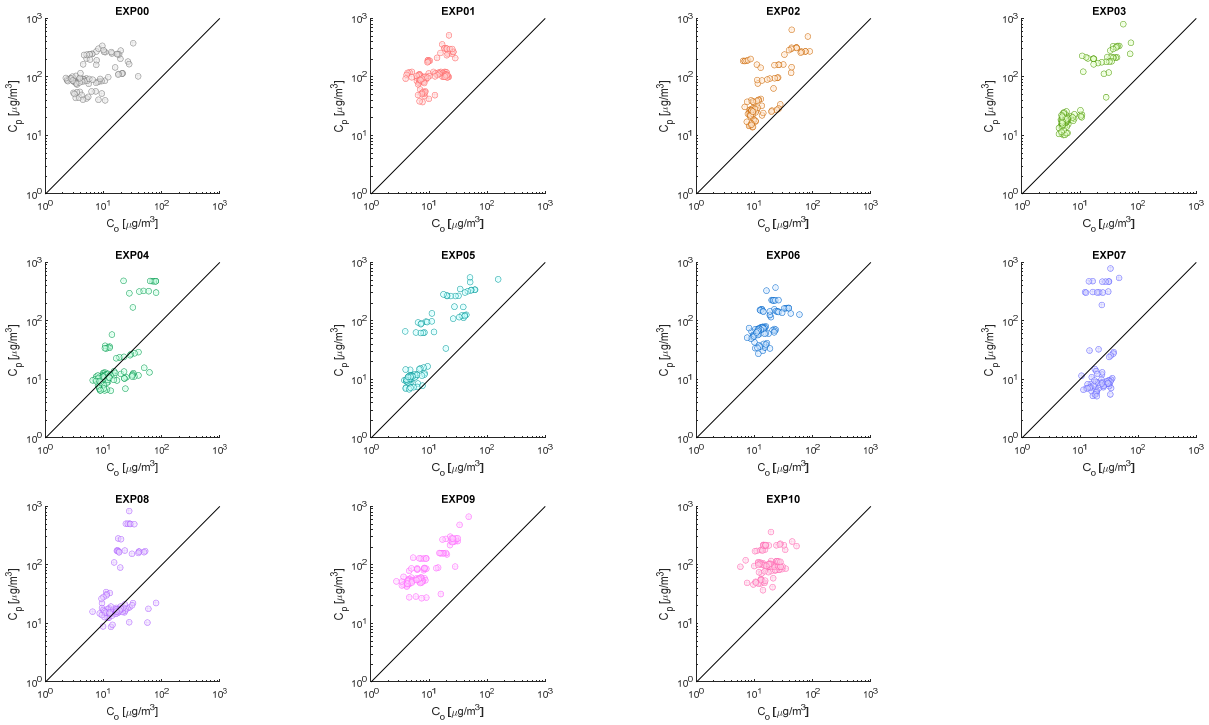
EXP00
EXP01
EXP02
EXP03
EXP04
EXP05
EXP06
EXP07
EXP08
EXP09
EXP10
C_p [μg/m³]
C_o [μg/m³]

SI Table 3-9 Summary performance statistics of original AERMOD model. *N* refers to sample size; *FB* refers to fractional bias; *MG* refers to geometric mean *NMSE* refers to normalized mean standard error; *VG* refers to geometric variance; *NAD* refers to normalized absolute difference; *FAC2* is fraction of predictions within a factor of two of observations.

(a). $PM_{2.5}$

STATS	*N*	*FB*	*MG*	*NMSE*	*VG*	*NAD*	*FAC2*
EXP00	87	-1.90	0.01	44.5	3.10×10^8	0.95	0.00
EXP01	49	-1.93	0.02	62.6	6.44×10^7	0.97	0.00
EXP02	35	-1.74	0.07	21.3	1.78×10^4	0.89	0.14
EXP03	37	-1.79	0.04	24.7	3.12×10^5	0.91	0.05
EXP04	58	-1.39	0.30	17.5	226	0.82	0.40
EXP05	31	-1.80	0.04	22.1	1.23×10^5	0.90	0.00
EXP06	69	-1.69	0.07	13.6	6.40×10^3	0.84	0.04
EXP07	67	-0.93	0.56	12.4	139	0.86	0.40
EXP08	74	-0.66	0.37	8.01	348	0.82	0.34
EXP09	61	-1.66	0.04	19.2	1.15×10^6	0.87	0.08
EXP10	85	-1.77	0.03	16.8	6.80×10^6	0.89	0.01
All	653	-1.59	0.07	15.2	1.18×10^5	0.89	0.14

(b). PM_{10}

STATS	*N*	*FB*	*MG*	*NMSE*	*VG*	*NAD*	*FAC2*
EXP00	83	-1.78	0.05	18.0	8.59×10^3	0.89	0.00
EXP01	49	-1.59	0.12	7.62	119	0.80	0.00
EXP02	37	-1.17	0.34	3.72	7	0.61	0.32
EXP03	37	-1.34	0.23	5.00	18	0.68	0.19
EXP04	60	-0.71	1.13	5.25	4	0.56	0.73
EXP05	35	-1.23	0.22	3.24	15	0.61	0.09
EXP06	78	-1.26	0.23	3.65	11	0.63	0.12
EXP07	81	-0.41	1.98	5.11	13	0.68	0.58
EXP08	75	-0.72	0.81	5.35	7	0.64	0.64
EXP09	61	-1.47	0.16	8.48	34	0.74	0.03
EXP10	86	-1.40	0.16	4.38	40	0.70	0.03
All	682	-1.22	0.30	5.23	34	0.69	0.26

(c). TSP

STATS	*N*	*FB*	*MG*	*NMSE*	*VG*	*NAD*	*FAC2*
EXP00	91	-1.76	0.06	19.4	5210	0.88	0.00
EXP01	90	-1.65	0.10	12.5	287	0.83	0.00
EXP02	91	-1.33	0.26	8.31	10	0.67	0.20
EXP03	93	-1.44	0.24	13.6	10	0.72	0.06
EXP04	90	-1.00	0.83	11.6	2	0.59	0.79
EXP05	93	-1.40	0.29	12.3	8	0.70	0.22
EXP06	87	-1.42	0.19	6.18	21	0.71	0.01
EXP07	72	-1.23	1.04	15.8	13	0.78	0.75
EXP08	91	-1.24	0.54	15.1	5	0.67	0.65
EXP09	89	-1.64	0.10	15.5	236	0.82	0.00
EXP10	89	-1.44	0.17	5.91	32	0.72	0.00
All	976	-1.44	0.23	11.4	32	0.74	0.23

SI Table 3-10 Summary statistics of ratio of prediction (Rp). STD = standard deviation; GM = geometric mean, GSD = geometric standard deviation.

(a). $PM_{2.5}$

	R_p - $PM_{2.5}$			
	Mean	**STD**	***GM***	***GSD***
EXP00	124	145	73.0	2.93
EXP01	88.2	83.4	65.3	2.07
EXP02	36.1	53.8	15.0	4.90
EXP03	62.0	105	25.9	4.31
EXP04	40.3	215	3.29	7.53
EXP05	42.9	47.1	26.0	2.93
EXP06	30.0	42.2	15.0	3.33
EXP07	27.0	125	1.78	8.68
EXP08	19.4	39.3	2.69	9.22
EXP09	99.8	189	27.7	5.61
EXP10	95.7	131	39.9	4.38
Overall	**64.1**	**131**	**15.2**	**7.90**

(b). PM_{10}

	R_p - PM_{10}			
	Mean	**STD**	***GM***	***GSD***
EXP00	22.5	12.3	19.0	1.85
EXP01	9.21	3.36	8.63	1.44
EXP02	3.93	2.45	2.93	2.44
EXP03	5.67	3.58	4.40	2.30
EXP04	1.90	3.04	0.89	3.27
EXP05	5.48	3.30	4.53	1.91
EXP06	4.81	2.08	4.30	1.66
EXP07	1.59	2.65	0.51	4.33
EXP08	2.98	3.92	1.23	3.93
EXP09	6.78	2.69	6.15	1.62
EXP10	7.38	4.30	6.22	1.83
Overall	**6.97**	**8.11**	**3.39**	**4.19**

(c). TSP

	R_p - TSP			
	Mean	**STD**	***GM***	***GSD***
EXP00	21.0	12.0	17.3	1.95
EXP01	11.6	5.80	10.3	1.65
EXP02	5.39	6.18	3.80	2.11
EXP03	4.89	3.54	4.09	1.75
EXP04	2.00	2.95	1.20	2.47
EXP05	4.63	3.97	3.44	2.09
EXP06	6.06	3.20	5.39	1.62
EXP07	4.44	8.14	0.96	5.02
EXP08	3.77	5.63	1.85	3.00
EXP09	10.7	3.76	10.0	1.49
EXP10	6.92	4.18	5.94	1.71
Overall	**7.44**	**7.81**	**4.27**	**3.20**

SI Table 3-11 Pearson correlation coefficients between summary statistics for model performance and wind parameters. u is the ambient wind speed; σ is the standard deviation of wind direction. *FB* refers to fractional bias; *MG* refers to geometric mean *NMSE* refers to normalized mean standard error; *VG* refers to geometric variance; *NAD* refers to normalized absolute difference; *FAC2* is fraction of predictions within a factor of two of observations. Notations: $^{*}p < 0.05$; $^{**}p < 0.001$.

		FB	***MG***	***NMSE***	***VG***	***NAD***	***FAC2***
$PM_{2.5}$	u	0.59	0.69^{*}	-0.51	-0.49	-0.55	0.75^{*}
	σ	-0.72^{*}	-0.8^{*}	0.61^{*}	0.56	0.70^{*}	-0.84^{*}
PM_{10}	u	0.84^{*}	0.71^{*}	-0.51	-0.51	-0.73^{*}	0.82^{*}
	σ	-0.94^{**}	-0.8^{*}	0.6	0.6	0.77^{*}	-0.91^{**}
TSP	u	0.85^{**}	0.82^{*}	0.1	0.1	-0.66^{*}	0.84^{*}
	σ	-0.94^{**}	-0.89^{**}	0.08	0.08	0.73^{*}	-0.88^{**}

SI Figure 3-7 Histogram of R_p (ratio of model-predicted to observed concentration) of the 11 experiments of each pollutant.

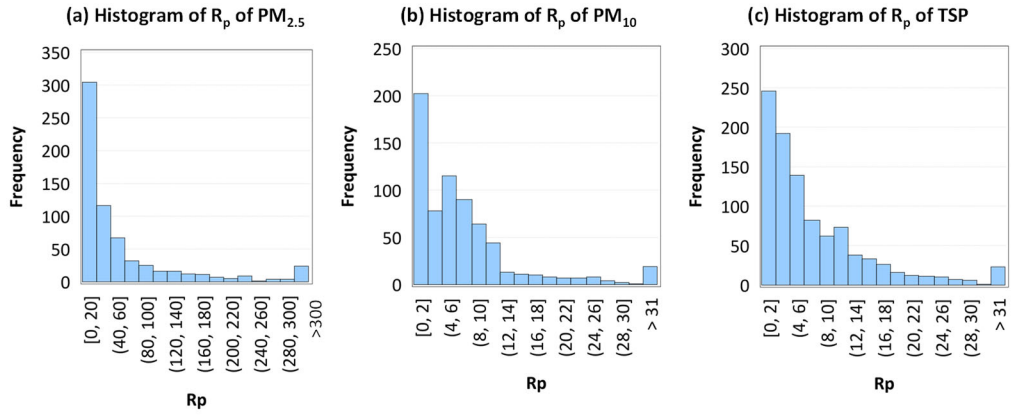

SI Table 3-12 Pearson correlation coefficients between log-transformed R_p and potential influential factors. h is heigh; d is distance from source; u is the ambient wind speed; σ is the standard deviation of wind direction; θ is the deviation from wind direction, defined as the difference between the wind direction and the from the source to the direction of wind velocity and the direction of source to the receptor. Notations: $^{*}p < 0.05$; $^{**}p < 0.001$.

	R_p		
	$PM_{2.5}$	**PM_{10}**	**TSP**
h	0.15^{*}	0.12^{*}	0.03
d	-0.02	-0.05	-0.19^{**}
u	-0.54^{**}	-0.69^{**}	-0.66^{**}
θ	-0.28^{**}	-0.26^{**}	-0.25^{**}
σ	0.59^{**}	0.74^{**}	0.71^{**}

SI Figure 3-8 Scatter plot of log-transformed R_p (ratio of model-predicted to observed concentration) of $PM_{2.5}$, PM_{10}, and TSP versus height, distance from source and deviation from wind direction. h is heigh; d is distance from source; u is the ambient wind speed; σ is the standard deviation of wind direction; θ is the deviation from wind direction, defined as the difference between the wind direction and the from the source to the direction of wind velocity and the direction of source to the receptor. The solid red lines are the linear regression just to show the linear trend.

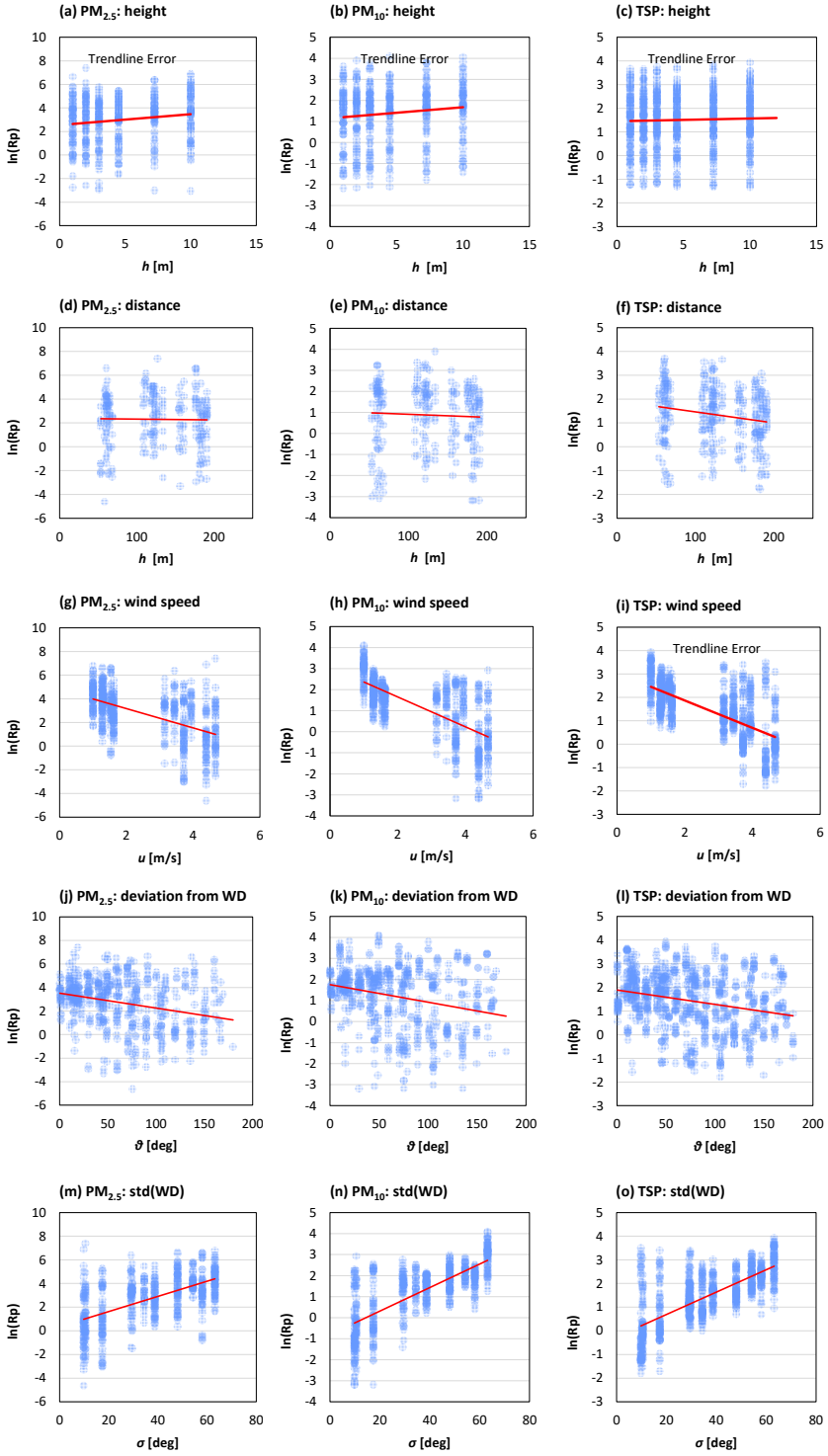

SI Figure 3-9 Scatter plot of observed concentration (C_o) versus out-of-sample corrected model-predicted concentration (C_{cp}) of each experiment. (a) $PM_{2.5}$; (b) PM_{10} and (c) TSP. Solid lines refer to 1:1 ratio.

(a). PM2.5

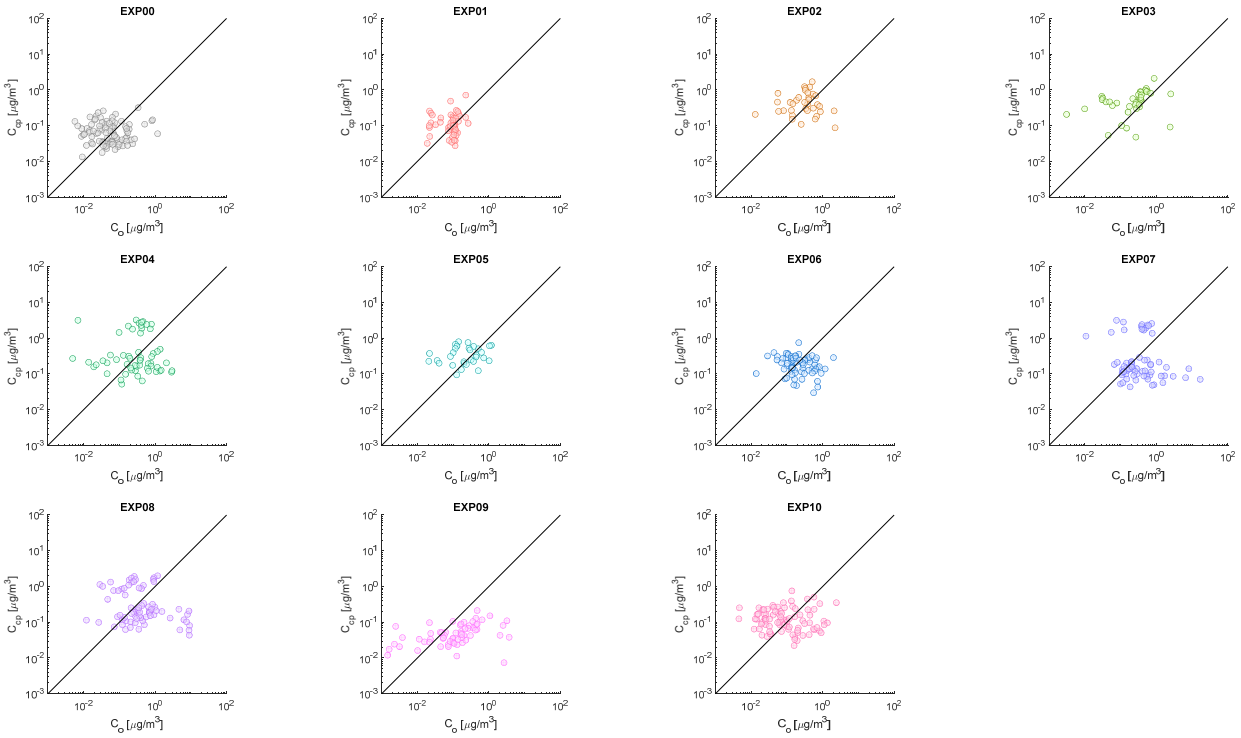

(b). PM_{10}

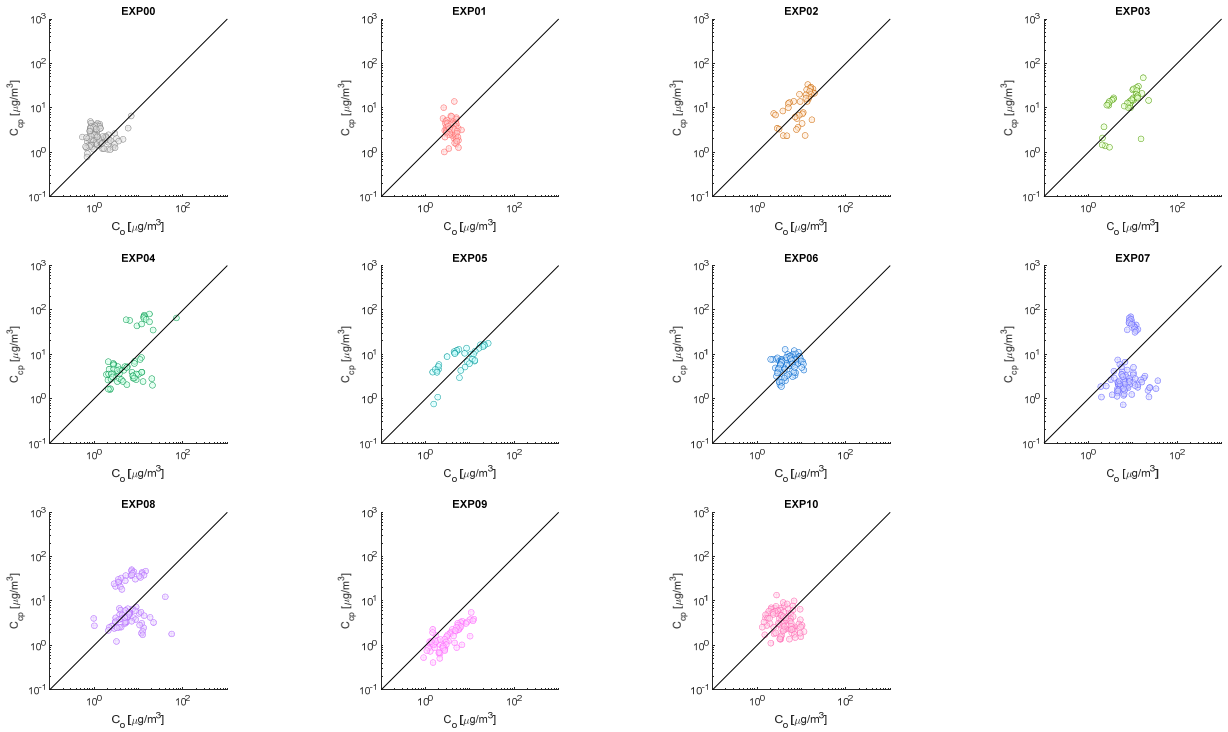
EXP00
EXP01
EXP02
EXP03
EXP04
EXP05
EXP06
EXP07
EXP08
EXP09
EXP10
C_cp [μg/m³]
C_o [μg/m³]

(c). TSP

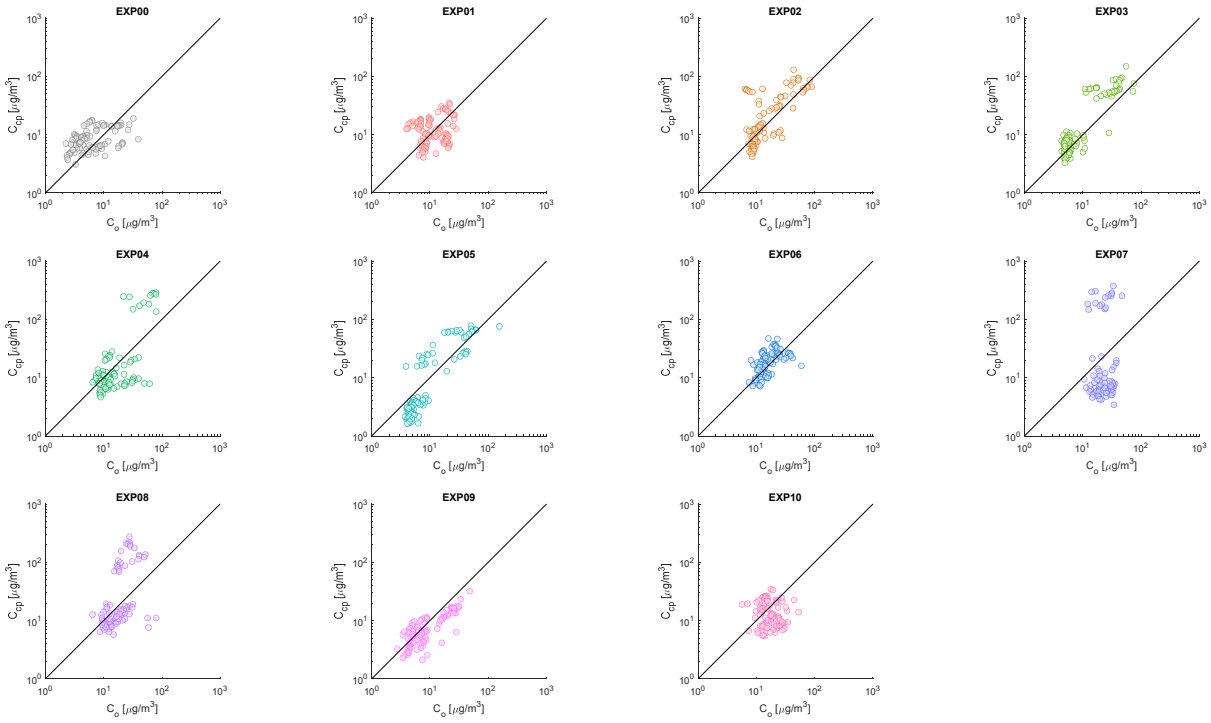
EXP00
EXP01
EXP02
EXP03
EXP04
EXP05
EXP06
EXP07
EXP08
EXP09
EXP10
C_cp [μg/m³]
C_o [μg/m³]

SI Table 3-13 Summary performance statistics of out-of-sample corrected AERMOD model. *N* refers to sample size; *FB* refers to fractional bias; *MG* refers to geometric mean; *NMSE* refers to normalized mean standard error; *VG* refers to geometric variance; *NAD* refers to normalized absolute difference; *FAC2* is fraction of predictions within a factor of two of observations.

(a). $PM_{2.5}$

STATS	*N*	*FB*	*MG*	*NMSE*	*VG*	*NAD*	*FAC2*
EXP00	87	0.27	0.83	4.06	5	0.52	0.54
EXP01	49	-0.33	0.76	1.10	2	0.34	0.71
EXP02	35	-0.10	0.73	1.83	5	0.46	0.51
EXP03	37	-0.34	0.45	1.74	13	0.42	0.54
EXP04	58	-0.28	0.83	3.87	30	0.67	0.43
EXP05	31	-0.13	0.65	0.90	4	0.37	0.65
EXP06	69	0.43	1.24	2.11	4	0.47	0.70
EXP07	67	0.48	1.54	13.5	43	0.76	0.52
EXP08	74	0.91	1.48	12.0	68	0.77	0.51
EXP09	61	1.51	2.35	32.0	31	0.78	0.57
EXP10	85	0.41	0.79	4.32	12	0.58	0.41
All	653	0.38	1.02	12.2	13	0.64	0.55

(b). PM_{10}

STATS	*N*	*FB*	*MG*	*NMSE*	*VG*	*NAD*	*FAC2*
EXP00	83	-0.47	0.58	0.76	2	0.34	0.58
EXP01	49	0.08	1.21	0.45	2	0.24	0.94
EXP02	37	-0.24	0.88	0.37	2	0.24	0.76
EXP03	37	-0.54	0.61	0.75	2	0.33	0.65
EXP04	60	-0.64	0.89	3.70	3	0.49	0.68
EXP05	35	-0.06	0.81	0.25	2	0.22	0.60
EXP06	78	-0.18	0.84	0.29	1	0.22	0.88
EXP07	81	-0.22	1.86	3.70	8	0.62	0.59
EXP08	75	-0.53	0.82	3.01	5	0.55	0.59
EXP09	61	0.78	2.14	1.33	2	0.40	0.95
EXP10	86	0.11	1.13	0.71	2	0.33	0.78
All	682	-0.29	1.01	2.77	2	0.41	0.72

(c). TSP

STATS	*N*	*FB*	*MG*	*NMSE*	*VG*	*NAD*	*FAC2*
EXP00	91	-0.08	0.77	0.61	2	0.29	0.76
EXP01	90	-0.03	0.97	0.40	2	0.26	0.80
EXP02	91	-0.33	0.84	0.76	2	0.26	0.87
EXP03	93	-0.54	0.73	1.23	1	0.30	0.82
EXP04	90	-0.60	1.08	5.03	2	0.48	0.83
EXP05	93	-0.17	1.16	0.80	2	0.26	0.80
EXP06	87	-0.11	0.90	0.28	1	0.19	0.92
EXP07	72	-0.85	1.40	7.80	10	0.71	0.69
EXP08	91	-0.72	0.88	4.43	3	0.52	0.71
EXP09	89	0.31	1.26	0.38	1	0.21	1.00
EXP10	89	0.30	1.41	0.54	2	0.30	0.96
All	976	-0.39	1.00	4.06	2	0.39	0.83

SI Table 3-14 Regression coefficients and regression statistics of predicting R_p (ratio of model-predicted to observed concentration) of $PM_{2.5}$, PM_{10} and TSP. $R_p = \exp(b_0 + b_1 h + b_2 d + b_3 u + b_4 \sigma + b_5 \theta)$. h = height (m), d = distance from source (m), u = wind speed (m/s), σ = standard deviation of wind direction (deg), θ = deviation from wind direction (deg). Regression coefficients are expressed as mean ± standard error. *RMSE* = square root of mean standard error; *adj_r2* = adjusted coefficient of determination; *AIC* = Akaike information criterion; *BIC* = Bayesian information criterion.

(a). Without statistical outliers

	b0	b1	b2	b3	b4	b5	RMSE	adj_r2	AIC	BIC
$PM_{2.5}$	0.695±0.182	0.110±0.021			0.062±0.003	-0.011±0.001	1.560	0.430	2438	2456
PM_{10}	-0.534±0.099	0.063±0.012			0.055±0.002	-0.007±0.001	0.885	0.618	1772	1790
TSP	0.656±0.129	0.021±0.008	-0.005±0.001		0.046±0.001	-0.005±0.001	0.762	0.569	2245	2270
Alternative										
$PM_{2.5}$	5.095±0.186	0.106±0.022		-0.795±0.046		-0.012±0.001	1.620	0.383	2491	2509
PM_{10}	3.366±0.109	0.060±0.013		-0.706±0.027		-0.008±0.001	0.954	0.556	1876	1894
TSP	3.867±0.136	0.020±0.009	-0.005±0.001	-0.571±0.020		-0.005±0.001	0.821	0.500	2391	2415

(b). With statistical outliers

	b0	b1	b2	b3	b4	b5	RMSE	adj_r2	AIC	BIC
$PM_{2.5}$	0.832±0.195	0.106±0.023			0.061±0.003	-0.011±0.001	1.690	0.378	2592	2610
PM_{10}	-0.398±0.122	0.060±0.014			0.052±0.002	-0.008±0.001	1.100	0.495	2121	2139
TSP	0.644±0.158	0.022±0.010	-0.005±0.001		0.046±0.002	-0.005±0.001	0.965	0.458	2775	2800
Alternative										
$PM_{2.5}$	5.097±0.198	0.102±0.024		-0.767±0.049		-0.012±0.002	1.750	0.334	2638	2656
PM_{10}	3.338±0.129	0.057±0.015		-0.677±0.031		-0.009±0.001	1.150	0.447	2186	2204
TSP	3.851±0.164	0.012±0.011	-0.005±0.001	-0.571±0.024		-0.005±0.001	1.020	0.399	2878	2903

SI Table 3-15 Summary statistics of out-of-sample corrected AERMOD model performance with outliers in calibration datasets. *N* refers to sample size; *FB* refers to fractional bias; *MG* refers to geometric mean; *NMSE* refers to normalized mean standard error; *VG* refers to geometric variance; *NAD* refers to normalized absolute difference; *FAC2* is fraction of predictions within a factor of two of observations.

(a). $PM_{2.5}$

STATS	*N*	*FB*	*MG*	*NMSE*	*VG*	*NAD*	*FAC2*
EXP00	87	0.33	0.87	4.29	5	0.53	0.54
EXP01	49	-0.31	0.78	1.07	2	0.33	0.71
EXP02	35	-0.04	0.78	1.85	5	0.46	0.51
EXP03	37	-0.27	0.48	1.74	12	0.40	0.57
EXP04	58	-0.21	0.89	3.79	30	0.66	0.43
EXP05	31	-0.07	0.68	0.91	4	0.38	0.65
EXP06	69	0.48	1.30	2.23	4	0.47	0.68
EXP07	67	0.59	1.75	14.9	49	0.76	0.52
EXP08	74	1.00	1.66	13.4	76	0.77	0.51
EXP09	61	1.51	2.40	32.8	32	0.78	0.57
EXP10	85	0.43	0.81	4.42	13	0.59	0.41
All	653	0.46	1.08	13.0	13	0.64	0.55

(b). PM_{10}

STATS	*N*	*FB*	*MG*	*NMSE*	*VG*	*NAD*	*FAC2*
EXP00	83	-0.51	0.56	0.83	2	0.35	0.55
EXP01	49	0.03	1.16	0.49	2	0.25	0.94
EXP02	37	-0.20	0.92	0.32	2	0.23	0.78
EXP03	37	-0.50	0.63	0.66	2	0.31	0.65
EXP04	60	-0.64	0.89	3.68	3	0.49	0.68
EXP05	35	-0.03	0.83	0.27	2	0.23	0.60
EXP06	78	-0.18	0.83	0.30	1	0.23	0.87
EXP07	81	-0.08	2.08	3.20	9	0.61	0.59
EXP08	75	-0.48	0.86	2.81	4	0.54	0.59
EXP09	61	0.75	2.05	1.23	2	0.38	0.95
EXP10	86	0.07	1.10	0.76	2	0.34	0.73
All	682	-0.25	1.02	2.52	2	0.41	0.72

(c). TSP

STATS	*N*	*FB*	*MG*	*NMSE*	*VG*	*NAD*	*FAC2*
EXP00	91	-0.06	0.78	0.62	2	0.29	0.75
EXP01	90	-0.05	0.95	0.42	2	0.27	0.77
EXP02	91	-0.32	0.83	0.76	2	0.26	0.87
EXP03	93	-0.53	0.73	1.19	1	0.30	0.83
EXP04	90	-0.67	0.99	5.62	2	0.49	0.81
EXP05	93	-0.16	1.15	0.79	2	0.26	0.80
EXP06	87	-0.12	0.89	0.28	1	0.19	0.93
EXP07	72	-0.78	1.47	7.07	10	0.70	0.65
EXP08	91	-0.72	0.87	4.29	2	0.52	0.70
EXP09	89	0.30	1.25	0.36	1	0.21	1.00
EXP10	89	0.28	1.40	0.55	2	0.30	0.93
All	976	-0.38	1.00	3.92	2	0.39	0.82

SI Figure 3-10 Histogram and summary statistics of predicted concentrations of the 10201 simulation receptors. Min and max refer to the minimum and maximum values, mean refers to the average concentration. %Exceed refers to the number of receptors that have concentration exceeds the regulatory standards.

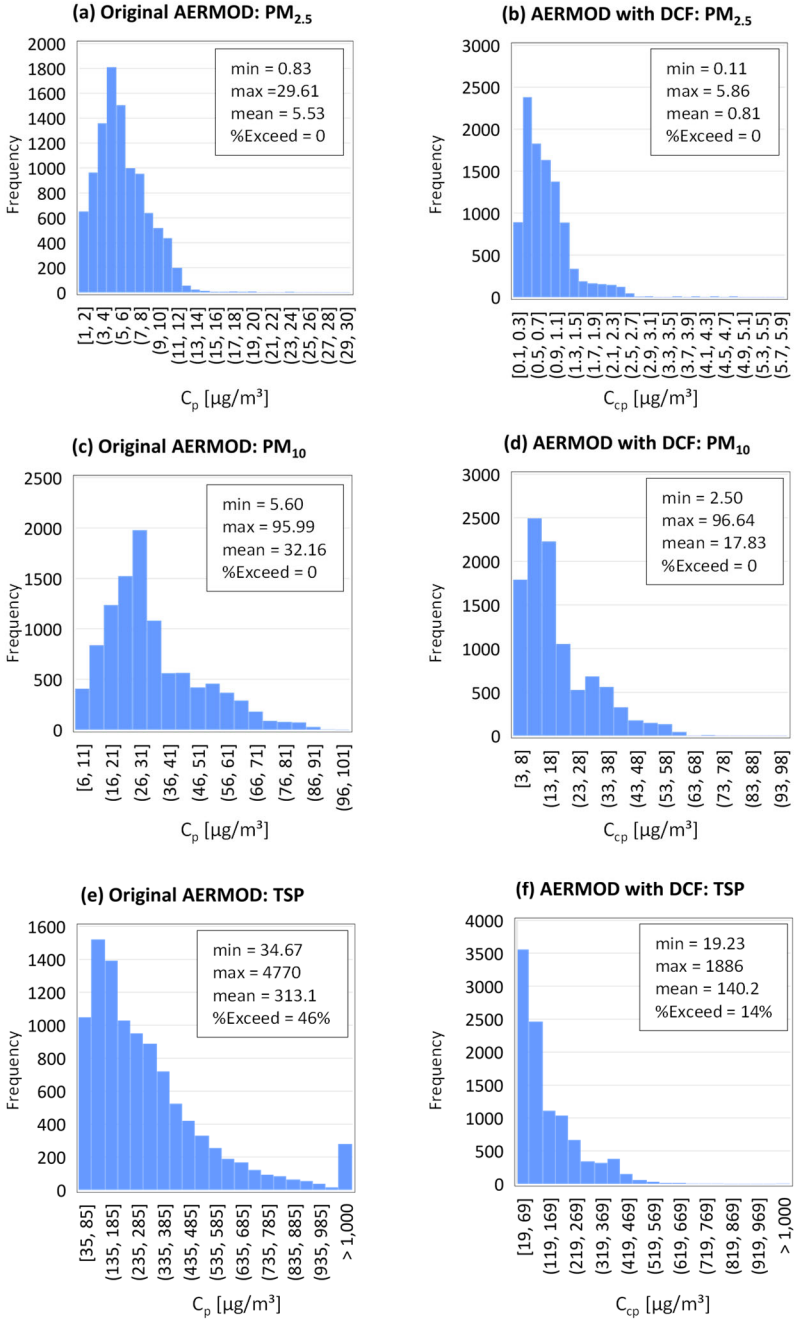

SI Figure 3-11 Spatial distribution of risk quotient (RQ). ⊕ refers to emission source. □ and ○ refer to buildings. Red solid line refers to the boundary that exceeds regulatory standard, and dashed line indicates the higher RQ side. Details of the map see **Figure 3-1** in manuscript.

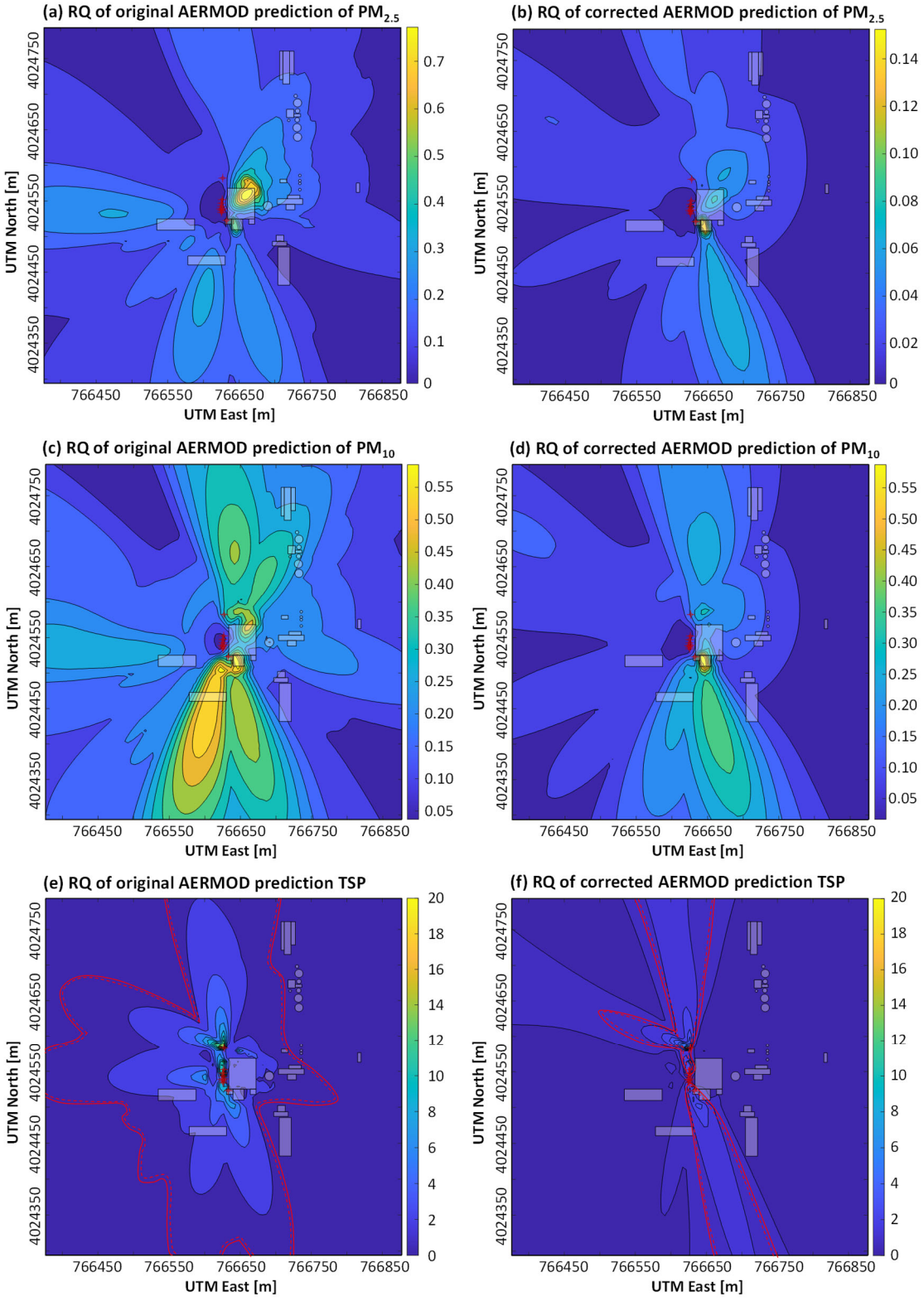

Appendices C: SI of Chapter 4

SI Table 4-1 Exact sampling times

Sampling Time	Date	Notation
Pre-application: 1	Dec. 2012	TP
2	Nov. 2013	T6
3	May. 2014	T12
4	Nov. 2014	T18

SI Table 4-2 Values for each parameter were taken from Ecological Soil Screening Level documents for DDT and dieldrin (US EPA, 2007a, 2007b, 2007c)

		FIR	Ps	TRV	MLP
DDT	Woodcock	0.214	0.164	0.227	11.2
	Short-tailed shrew	0.209	0.03	0.147	11.2
Dieldrin	Woodcock	0.214	0.164	0.0709	14.7
	Short-tailed shrew	0.209	0.03	0.015	14.7

* FIR is food ingestion rate, Ps is soil ingestion proportion of diet, MLP is the multiplier for estimation of concentration of contaminant in biota by soil concentration, and TRV is the toxicity reference value.

SI Table 4-3 Summaries of soil concentration, earthworm concentration and *BAF* of DDx.
Blanks refer to data not available. Data are expressed as mean±std (μg/g d.w.) for C_s and C_e.

Control

	Plot	TP			T6			T12			T18		
C_s	A	14.60	±	1.14	15.32	±	2.20	12.25	±	1.62	11.48	±	0.73
	B	18.39	±	3.37	31.72	±	22.23	20.86	±	1.60	15.46	±	4.11
	C	7.45	±	0.10	14.46	±	1.73	8.72	±	0.24			
	D	8.80	±	0.37	13.23	±	0.92	10.75	±	0.62	11.50	±	0.40
	E	3.16	±	0.16	3.90	±	0.69	3.95	±	0.02			
	F	3.06	±	0.11	3.70	±	0.55	4.11	±	0.60			
	G	2.31	±	0.27	2.79	±	0.06	3.20	±	0.04			
C_e	A	21.84	±	2.45	22.49	±	1.84	33.92	±	1.14	42.83	±	1.47
	B	49.28	±	14.22	37.40	±	2.66	39.33	±	2.63	49.41	±	2.15
	C	10.47	±	4.08	19.14	±	2.86	33.12	±	1.30			
	D	14.14	±	0.15	21.78	±	1.42	31.17	±	0.21	46.83	±	0.19
	E	11.47	±	3.32	10.53	±	0.28	18.01	±	0.04			
	F	9.90	±	0.68				22.48	±	0.11			
	G	11.10	±	0.03	5.11	±	0.06	14.52	±	0.11			
BAF	A	1.50	±	0.12	1.48	±	0.14	2.79	±	0.23	3.74	±	0.16
	B	2.71	±	0.54	1.51	±	31.90	1.89	±	0.11	3.28	±	0.55
	C	1.40	±	0.32	1.33	±	0.15	3.80	±	0.10			
	D	1.61	±	0.04	1.65	±	0.09	2.90	±	0.10	4.07	±	0.08
	E	3.64	±	0.62	2.73	±	0.29	4.56	±	0.02			
	F	3.23	±	0.15				5.52	±	0.47			
	G	11.10	±	0.03	5.11	±	0.06	14.52	±	0.11			

Till

	Plot	TP			T6			T12			T18		
C_s	A	19.93	±	1.36	23.14	±	7.41	19.45	±	0.94	18.94	±	0.83
	B	11.64	±	0.36	13.33	±	5.26	9.72	±	0.55	7.99	±	0.23
	C	8.47	±	0.43	18.36	±	3.54	9.98	±	0.26			
	D	13.88	±	1.04	14.57	±	3.56	11.74	±	0.23	12.65	±	0.00
	E	4.16	±	0.23	5.66	±	0.26	4.65	±	0.06			
	F	2.07	±	0.12	3.37	±	0.47	3.34	±	0.32			
	G	2.57	±	0.08	3.12	±	0.13	3.44	±	0.02			
C_e	A	26.71	±	1.32	38.91	±	2.57	51.20	±	2.61	50.21	±	0.95
	B	22.29	±	0.94	26.47	±	3.88	29.15	±	0.51	26.20	±	0.42
	C	20.77	±	2.19	28.86	±	4.32	27.63	±	0.15			
	D	20.38	±	0.65	20.97	±	0.59	30.30	±	0.44	46.02	±	0.42
	E	13.37	±	0.40	15.23	±	0.00	24.14	±	4.95			
	F	7.54	±	1.68				21.05	±	0.22			
	G	12.34	±	0.51	8.49	±	0.09	15.94	±	0.17			
BAF	A	1.34	±	0.07	1.75	±	0.38	2.63	±	0.11	2.65	±	0.07
	B	1.92	±	0.06	2.11	±	0.80	3.00	±	0.10	3.28	±	0.06
	C	2.45	±	0.17	1.59	±	0.25	2.77	±	0.04			
	D	1.47	±	0.07	1.47	±	0.22	2.58	±	0.04			
	E	3.22	±	0.12				5.20	±	0.62			
	F	3.65	±	0.48				6.32	±	0.35			
	G	12.34	±	0.51	8.49	±	0.09	15.94	±	0.17			

2YC

	Plot	TP			T6			T12			T18		
C_s	A	11.34	±	0.97	9.85	±	1.77	12.07	±	0.97	12.01	±	0.07
	B	6.66	±	0.77	11.42	±	1.73	8.95	±	0.70	7.97	±	0.28
	C	8.06	±	0.93	9.22	±	0.47	5.59	±	1.51			
	D	9.85	±	1.21	12.35	±	2.48	11.12	±	0.35	8.94	±	0.10
	E	7.67	±	0.39	8.53	±	0.62	7.11	±	0.32			
	F	3.20	±	0.03	4.11	±	0.73	3.83	±	0.25			
	G	2.58	±	0.11	3.07	±	0.08	3.31	±	0.02			
C_e	A	19.85	±	2.79	19.91	±	3.10	29.68	±	0.29	31.94	±	1.27
	B	20.55	±	2.77	17.18	±	0.93	23.04	±	0.20	20.57	±	4.35
	C	15.74	±	1.78	11.87	±	3.41	23.44	±	0.53			
	D	16.24	±	4.05	18.07	±	0.50	26.87	±	0.14	83.34	±	0.66
	E	19.38	±	3.94				22.36	±	0.28			
	F	12.27	±	3.14				20.50	±	0.05			
	G	11.76	±	0.03	8.58	±	0.28	15.56	±	0.21			
BAF	A	1.76	±	0.19	2.05	±	0.29	2.46	±	0.12	2.66	±	0.06
	B	3.10	±	0.32	1.52	±	0.14	2.58	±	0.12	2.58	±	0.32
	C	1.96	±	0.18	1.29	±	0.22	4.30	±	0.73			
	D	1.66	±	0.32	1.48	±	0.18	2.42	±	0.04	9.32	±	0.07
	E	2.53	±	0.31				3.15	±	0.09			
	F	3.84	±	0.57				5.36	±	0.20			
	G	11.76	±	0.03	8.58	±	0.28	15.56	±	0.21			

4MC

	Plot	TP			T6			T12			T18		
C_s	A	6.67	±	0.32	7.50	±	2.83	9.00	±	1.08	8.93	±	1.26
	B	11.12	±	0.23	11.67	±	4.31	7.58	±	0.75	6.60	±	1.49
	C	7.59	±	0.14	11.90	±	0.56	7.81	±	0.20			
	D	9.03	±	0.42	14.81	±	2.49	11.10	±	0.19	11.38	±	0.33
	E	4.58	±	0.05	5.36	±	0.27	4.80	±	0.23			
	F	2.39	±	0.09	2.85	±	0.81	3.15	±	0.54			
	G	2.53	±	0.46	3.07	±	0.06	3.24	±	0.06			
C_e	A	17.54	±	1.52	15.34	±	1.77	31.36	±	1.42	27.71	±	0.38
	B	21.14	±	8.54	19.22	±	5.73	23.55	±	0.42	17.58	±	0.25
	C	20.88	±	0.36	14.34	±	4.19	28.42	±	1.26			
	D	28.38	±	0.01	21.38	±	1.40	27.46	±	0.54	85.26	±	0.72
	E	12.70	±	3.36				18.26	±	0.26			
	F	12.77	±	3.68				19.82	±	0.18			
	G	12.91	±	0.07	8.70	±	0.17	15.52	±	0.18			
BAF	A	2.63	±	0.18	2.16	±	0.68	3.50	±	0.26	3.12	±	0.26
	B	1.90	±	0.44	1.73	±	0.66	3.12	±	0.18	2.71	±	0.37
	C	2.75	±	0.04	1.21	±	0.21	3.64	±	0.11			
	D	3.14	±	0.08	1.46	±	0.16	2.47	±	0.04	7.49	±	0.13
	E	2.78	±	0.43				3.81	±	0.11			
	F	5.34	±	0.90				6.35	±	0.65			
	G	12.91	±	0.07	8.70	±	0.17	15.52	±	0.18			

SI Table 4-4 Summaries of soil concentration, earthworm concentration and *BAF* of dieldrin. Blanks refer to data not available. Data are expressed as mean±std (μg/g d.w.) for C_s and C_e.

Control

	Plot	Tb			T6			T12			T18		
C_s	A	1.25	±	0.16	1.06	±	0.54	0.84	±	0.13	0.94	±	0.04
	B	1.30	±	0.11	1.38	±	0.75	1.22	±	0.04	1.01	±	0.19
	C	0.75	±	0.03	1.40	±	0.20	0.62	±	0.06			
	D	0.66	±	0.18	0.80	±	0.12	0.59	±	0.02	0.44	±	0.02
	E	0.45	±	0.04	0.43	±	0.06	0.36	±	0.07			
	F	0.49	±	0.02	0.40	±	0.00	0.28	±	0.05			
	G	0.49	±	0.07	0.47	±	0.06	0.41	±	0.00			
C_e	A	6.62	±	1.18	4.30	±	0.43	4.64	±	0.09	5.70	±	0.20
	B	6.82	±	1.78	5.04	±	1.76	5.17	±	0.42	5.26	±	0.07
	C	3.41	±	1.74	3.25	±	0.39	5.52	±	0.24			
	D	2.76	±	0.38	2.12	±	0.02	1.92	±	0.00	1.42	±	0.05
	E	1.14	±	0.32	1.06	±	0.04	4.93	±	0.45			
	F	2.19	±	0.17				2.34	±	0.11			
	G	1.58	±	0.03	1.01	±	0.00	1.51	±	0.03			
BAF	A	5.34	±	0.79	4.58	±	34.85	5.55	±	0.51	6.05	±	0.19
	B	5.27	±	0.83	4.09	±	74.60	4.23	±	0.22	5.29	±	0.59
	C	4.55	±	1.35	2.34	±	0.25	8.96	±	0.64			
	D	4.33	±	0.88	2.66	±	0.23	3.25	±	0.07	3.21	±	0.11
	E	2.53	±	0.42	2.51	±	0.20	13.91	±	1.84			
	F	4.49	±	0.23				8.46	±	1.15			
	G	1.58	±	0.03	1.01	±	0.00	1.51	±	0.03			

Till

	Plot	Tb			T6			T12			T18		
C_s	A	1.20	±	0.04	0.86	±	0.11	0.81	±	0.08	0.93	±	0.03
	B	0.67	±	0.20	1.28	±	0.68	0.94	±	0.05	0.81	±	0.02
	C	0.80	±	0.29	1.38	±	0.05	0.80	±	0.03			
	D	0.55	±	0.20	0.77	±	0.08	0.48	±	0.00	0.41	±	0.00
	E	0.40	±	0.00	0.47	±	0.06	0.24	±	0.00			
	F	0.42	±	0.03	0.40	±	0.00	0.35	±	0.05			
	G	0.44	±	0.06	0.48	±	0.04	0.41	±	0.00			
C_e	A	4.37	±	0.92	5.43	±	0.64	5.33	±	0.58	5.15	±	0.29
	B	9.55	±	5.12	4.64	±	0.80	4.17	±	0.03	4.02	±	0.07
	C	5.01	±	0.80	8.06	±	0.92	4.31	±	0.15			
	D	2.86	±	0.06	2.16	±	0.02	1.88	±	0.03	1.77	±	0.31
	E	1.64	±	0.64	1.05	±	0.00	7.20	±	0.15			
	F	1.82	±	0.96				2.41	±	0.13			
	G	1.72	±	0.05	1.74	±	0.92	1.74	±	0.07			
BAF	A	3.66	±	0.55	6.32	±	0.65	6.62	±	0.57	5.56	±	0.22
	B	14.58	±	5.30	4.21	±	36.16	4.43	±	0.13	4.97	±	0.09
	C	6.59	±	1.78	5.83	±	0.49	5.40	±	0.17			
	D	5.47	±	1.39	2.83	±	0.17	3.90	±	0.04			
	E	4.11	±	0.92				29.48	±	0.40			
	F	4.30	±	1.32				7.00	±	0.83			
	G	1.72	±	0.05	1.74	±	0.92	1.74	±	0.07			

2YC

	Plot	Tb			T6			T12			T18		
C_s	A	0.97	±	0.11	0.63	±	0.28	0.70	±	0.09	0.75	±	0.02
	B	0.54	±	0.20	0.79	±	0.07	0.91	±	0.04	0.78	±	0.03
	C	0.74	±	0.24	1.00	±	0.23	0.48	±	0.14			
	D	0.33	±	0.04	0.78	±	0.09	0.48	±	0.01	0.38	±	0.03
	E	0.45	±	0.08	0.47	±	0.05	0.26	±	0.01			
	F	0.40	±	0.00	0.40	±	0.00	0.34	±	0.05			
	G	0.44	±	0.06	0.48	±	0.05	0.41	±	0.00			
C_e	A	7.24	±	3.67	3.73	±	1.19	4.49	±	0.02	3.84	±	0.02
	B	3.78	±	1.88	4.02	±	0.99	5.02	±	0.68	3.27	±	0.39
	C	8.00	±	2.71	3.44	±	0.85	3.74	±	0.18			
	D	2.96	±	0.18	2.73	±	0.06	1.83	±	0.03	1.56	±	0.28
	E	1.50	±	0.64				3.33	±	0.35			
	F	2.59	±	1.87				2.52	±	0.10			
	G	1.78	±	0.03	1.08	±	0.02	1.70	±	0.04			
BAF	A	7.47	±	2.73	6.67	±	81.37	6.46	±	0.51	5.14	±	0.09
	B	7.35	±	2.94	5.13	±	0.78	5.54	±	0.46	4.22	±	0.31
	C	11.29	±	7.33	3.50	±	0.70	8.11	±	1.54			
	D	9.04	±	0.71	3.51	±	0.26	3.78	±	0.04	4.12	±	0.46
	E	3.35	±	0.89				12.87	±	0.82			
	F	6.48	±	2.69				7.40	±	0.75			
	G	1.78	±	0.03	1.08	±	0.02	1.70	±	0.04			

4MC

	Plot	Tb			T6			T12			T18		
C_s	A	1.04	±	0.06	0.79	±	0.36	0.73	±	0.13	0.99	±	0.09
	B	0.94	±	0.05	1.20	±	0.66	0.74	±	0.05	0.69	±	0.09
	C	0.82	±	0.03	1.00	±	0.18	0.55	±	0.06			
	D	0.62	±	0.16	0.76	±	0.09	0.51	±	0.01	0.42	±	0.02
	E	0.51	±	0.08	0.48	±	0.09	0.37	±	0.05			
	F	0.47	±	0.04	0.40	±	0.00	0.28	±	0.05			
	G	0.50	±	0.07	0.47	±	0.07	0.41	±	0.00			
C_e	A	11.82	±	5.80	3.59	±	0.35	4.51	±	0.40	4.65	±	0.08
	B	7.12	±	5.60	3.77	±	0.56	3.44	±	0.05	2.41	±	0.21
	C	8.04	±	3.91	2.48	±	1.08	3.89	±	0.27			
	D	4.18	±	0.18	2.93	±	0.28	1.69	±	0.02	1.80	±	0.36
	E	0.54	±	0.27				3.02	±	0.03			
	F	2.51	±	1.70				2.50	±	0.11			
	G	1.79	±	0.03	1.51	±	0.63	1.58	±	0.02			
BAF	A	11.33	±	3.97	4.93	±	4.74	6.24	±	0.73	4.71	±	0.25
	B	7.57	±	3.46	3.31	±	94.68	4.66	±	0.18	3.51	±	0.33
	C	9.86	±	2.79	2.52	±	0.70	7.11	±	0.52			
	D	6.94	±	1.18	3.87	±	0.37	3.32	±	0.04	4.25	±	0.50
	E	1.09	±	0.33				8.14	±	0.66			
	F	5.31	±	2.10				9.16	±	1.30			
	G	1.79	±	0.03	1.51	±	0.63	1.58	±	0.02			

SI Table 4-5 Regression coefficients and regression statistics of predicting C_e by C_s. *SE* refers to standard error. R^2 is the coefficient of determination, and adj-R^2 is the adjusted R^2. *RMSE* is the root-mean-square error. *AIC* and *BIC* refer to Akaike information criterion and Bayesian information criterion, respectively. In addition, results of C_e as a function of C_s are not sensitive within a standard error with including and excluding data below detection limit.

Model	*k*			*b*			Statistics						Note
	Estimate	*SE*	*p*-value	Estimate	*SE*	*p*-value	R^2	adj-R^2	*RMSE*	*AIC*	*BIC*	*p*-value	
DDx: untreated													
$C_e = kC_s$	2.03	0.13	< 0.001	\	\	\	0.25	0.25	9.76	325	327	< 0.001	A
$C_e = k \ln C_s + b$	11.43	1.65	< 0.001	-1.03	3.45	0.766	0.53	0.52	7.81	306	309	< 0.001	B
$C_e = e^{k \ln C_s + b}$	0.54	0.08	< 0.001	1.94	0.21	< 0.001	0.54	0.53	7.78	305	308	< 0.001	C
$C_e = C_s e^{kC_s + b}$	-0.04	0.01	< 0.001	1.30	0.12	< 0.001	0.53	0.52	7.81	305	309	< 0.001	D
$C_e = kbC_s/(1 + kC_s)$	0.09	0.03	0.017	54.39	11.26	< 0.001	0.54	0.53	7.74	304	308	< 0.001	E
$C_e = kC_s^{1/b}$	6.93	1.48	< 0.001	1.85	0.29	< 0.001	0.54	0.53	7.78	305	308	< 0.001	F
DDx: treated													
$C_e = kC_s$	2.54	0.21	< 0.001	\	\	\	0.07	0.07	15.10	380	382	< 0.001	A
$C_e = k \ln C_s + b$	12.92	3.72	0.001	-0.78	8.06	0.923	0.22	0.20	14.10	373	377	0.001	B
$C_e = e^{k \ln C_s + b}$	0.51	0.16	0.003	2.17	0.39	< 0.001	0.21	0.20	14.10	373	377	< 0.001	C
$C_e = C_s e^{kC_s + b}$	-0.05	0.02	0.009	1.54	0.21	< 0.001	0.21	0.19	14.10	374	377	< 0.001	D
$C_e = kbC_s/(1 + kC_s)$	0.11	0.08	0.168	55.11	18.55	0.005	0.21	0.20	14.10	373	377	< 0.001	E
$C_e = kC_s^{1/b}$	8.76	3.39	0.013	1.97	0.62	0.003	0.21	0.20	14.10	373	377	< 0.001	F
Dieldrin: untreated													
$C_e = kC_s$	5.40	0.41	< 0.001	\	\	\	0.34	0.34	2.08	189	191	< 0.001	A
$C_e = k \ln C_s + b$	3.69	0.72	< 0.001	5.52	0.44	< 0.001	0.39	0.37	2.03	186	190	< 0.001	B
$C_e = e^{k \ln C_s + b}$	0.82	0.19	< 0.001	1.67	0.08	< 0.001	0.36	0.34	2.08	189	192	< 0.001	C
$C_e = C_s e^{kC_s + b}$	-0.31	0.23	0.186	1.98	0.22	< 0.001	0.37	0.36	2.05	188	191	< 0.001	D
$C_e = kbC_s/(1 + kC_s)$	0.35	0.39	0.376	20.62	17.69	0.250	0.37	0.35	2.06	188	191	< 0.001	E
$C_e = kC_s^{1/b}$	5.30	0.43	< 0.001	1.22	0.28	< 0.001	0.36	0.34	2.08	189	192	< 0.001	F
Dieldrin: treated													
$C_e = kC_s$	4.70	0.28	< 0.001	\	\	\	0.23	0.23	1.35	158	160	< 0.001	A
$C_e = k \ln C_s + b$	1.69	0.48	0.001	4.13	0.31	< 0.001	0.22	0.21	1.37	159	163	0.001	B
$C_e = e^{k \ln C_s + b}$	0.67	0.15	< 0.001	1.48	0.07	< 0.001	0.29	0.27	1.32	155	159	< 0.001	C
$C_e = C_s e^{kC_s + b}$	-0.30	0.22	0.171	1.81	0.19	< 0.001	0.26	0.24	1.34	157	161	< 0.001	D
$C_e = kbC_s/(1 + kC_s)$	0.49	0.42	0.244	13.51	8.26	0.109	0.27	0.25	1.34	157	160	< 0.001	E
$C_e = kC_s^{1/b}$	4.38	0.31	< 0.001	1.48	0.33	< 0.001	0.29	0.27	1.32	155	161	< 0.001	F

Note:

A: Linear relation between C_s and C_e described by **Eqn. 4-1** in the manuscript

B: Nonlinear relation between C_s and C_e assuming a linear relation between log-transformed C_s and C_e

C: Nonlinear relation between C_s and C_e derived from a linear relation between log-transformed C_s and log-transformed C_e : $\ln C_e = k \ln C_s + b$ (Sample et al., 1999)

D: Nonlinear relation between C_s and C_e proposed by Kelsey et al., 2005

E: Nonlinear relation between C_s and C_e analogized from Langmuir isotherm model (Luo and Deng, 2018), where *k* is a parameter related to uptake rate, and *b* is a parameter related to uptake capacity

F: Nonlinear relation between C_s and C_e analogized from Freundlich isotherm model (Sparks, 2003), where *k* is a parameter related to distribution, and *b* is a correlation factor

SI Figure 4-1 *NBAF* of DDx change over time. Details of each plot are shown in **SI Figure 4-3**.

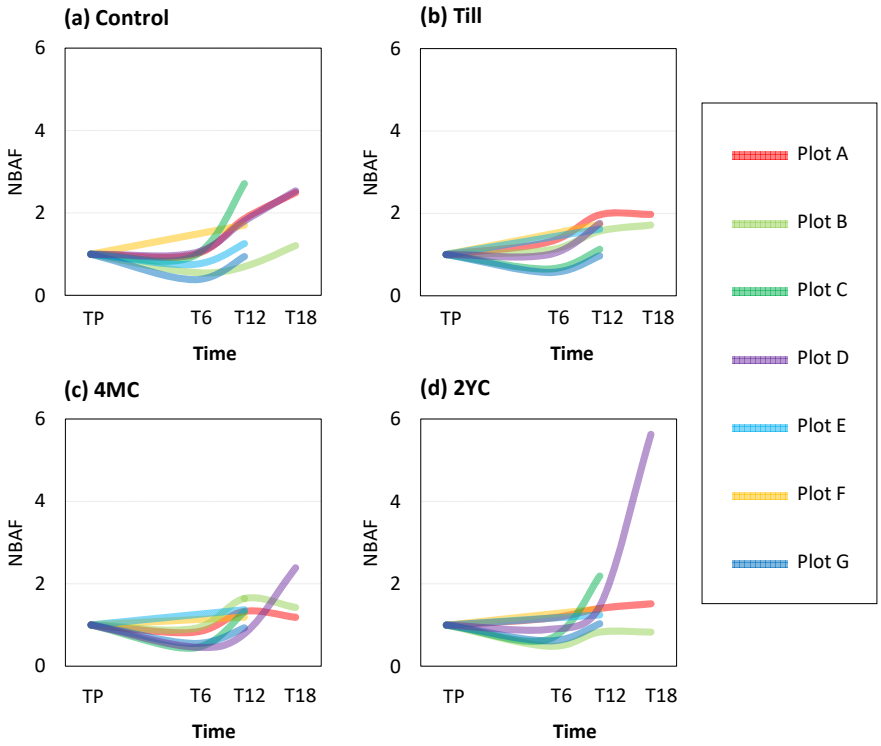

SI Figure 4-2 *NBAF* of dieldrin change over time. Details of each plot are shown in **SI Figure 4-4**.

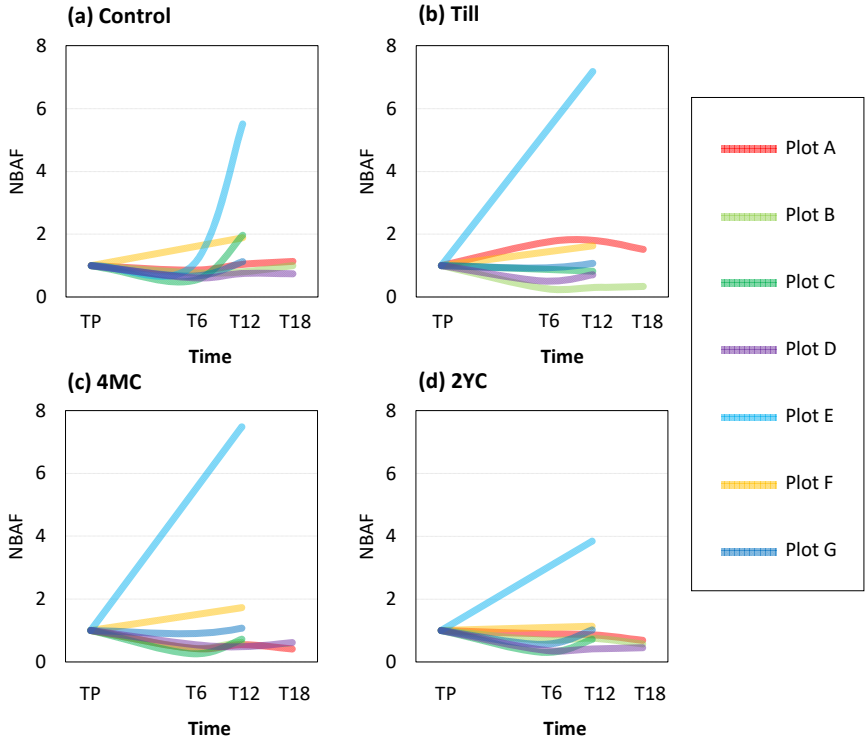

SI Figure 4-3 Plots of normalized *BAF* (*NBAF*) of DDx. Error bar refers to standard deviation. Different letters refer to statistical difference ($p < 0.05$)

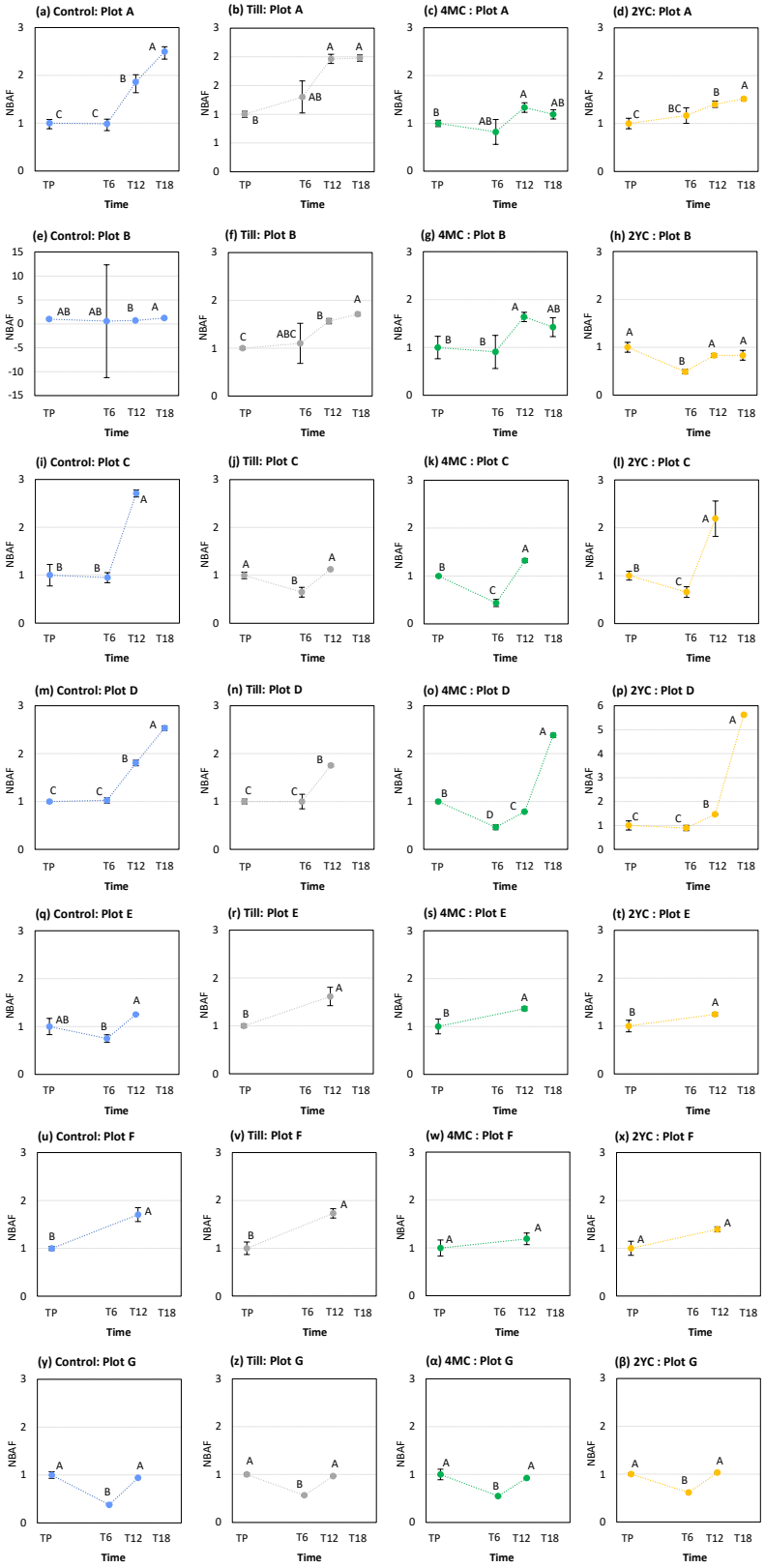

SI Figure 4-4 Plots of normalized *BAF* (*NBAF*) of dieldrin. Error bar refers to standard deviation. Different letters refer to statistical difference ($p < 0.05$).

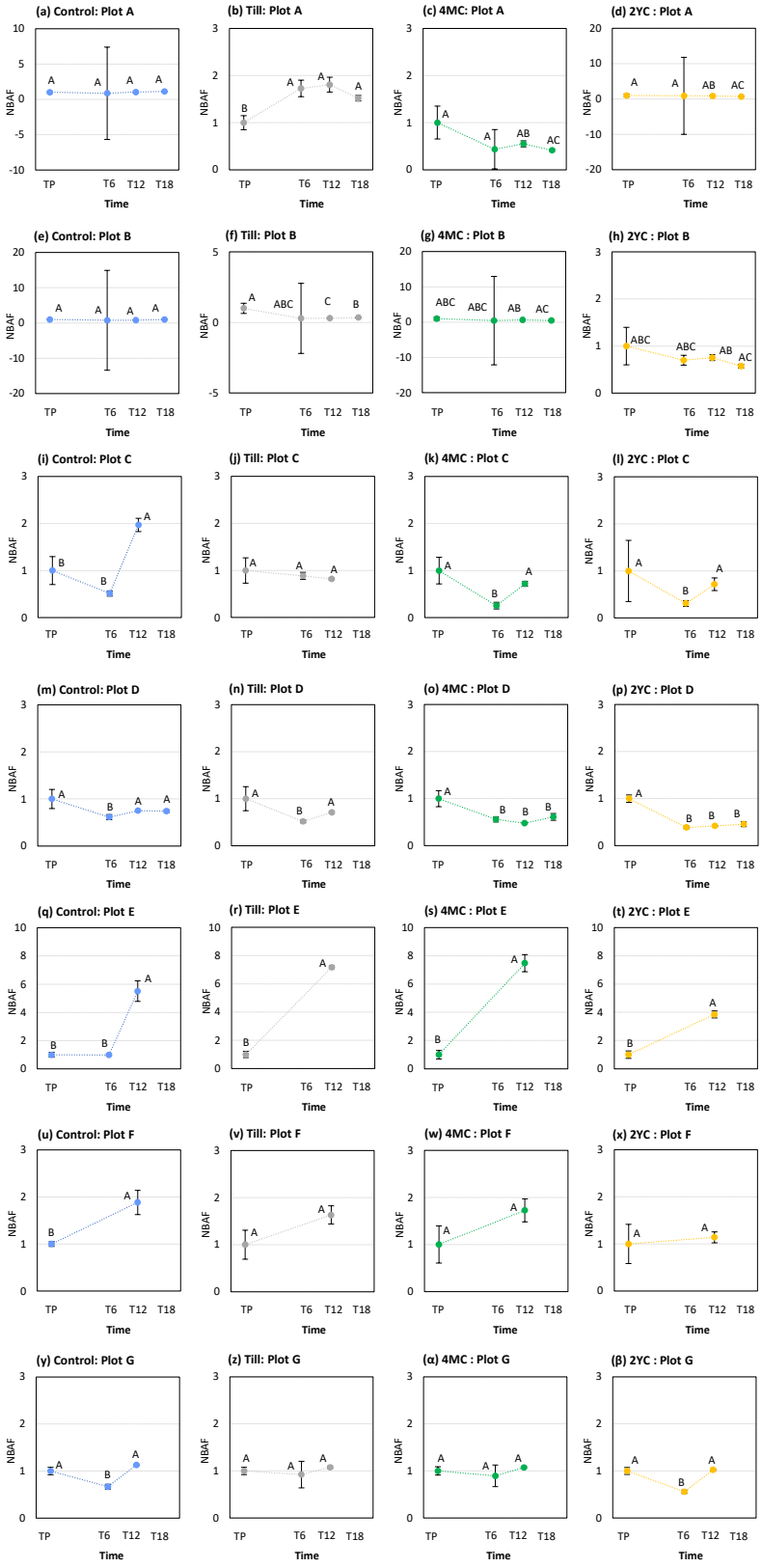

SI Figure 4-5 Plots of change of *NBAF* (Δ*NBAF*) of DDx. Error bar refers to standard error. N refers to no significant difference, I refers to significant increase, and R refers to significant reduce ($p < 0.05$).

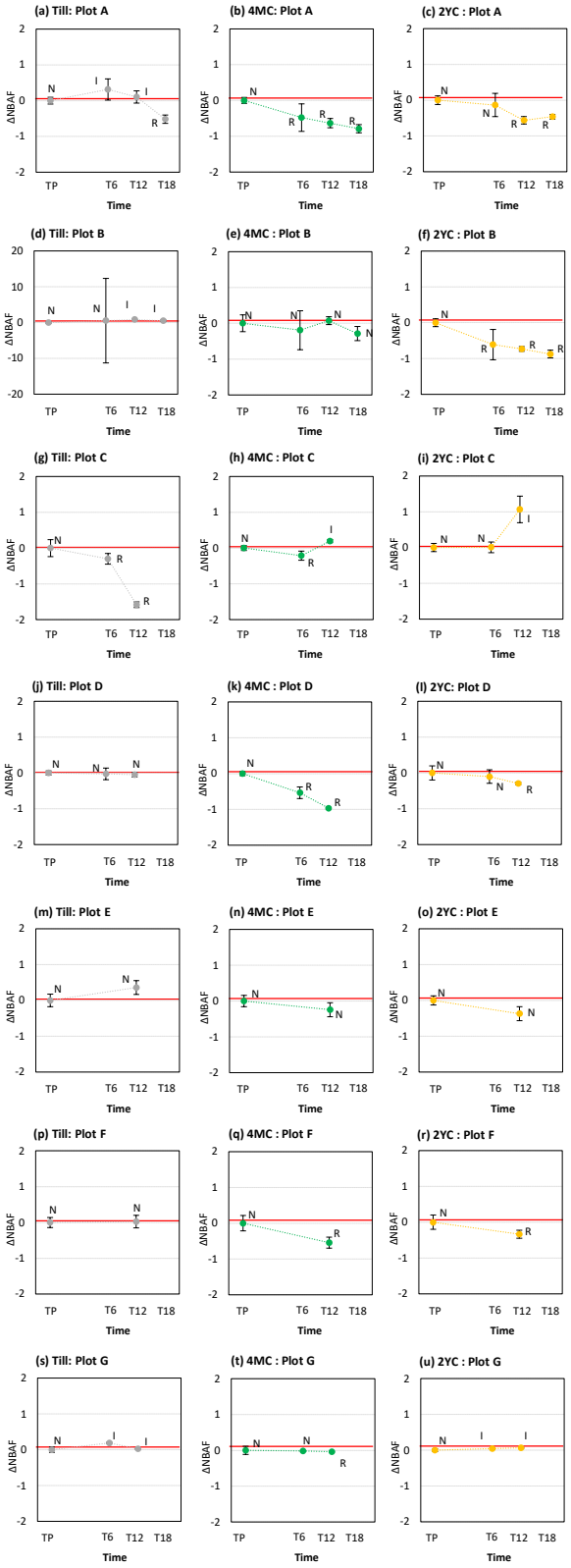

SI Figure 4-6 Plots of change of *NBAF* (Δ*NBAF*) of dieldrin. Error bar refers to standard error. N refers to no significant difference, I refers to significant increase, and R refers to significant reduce ($p < 0.05$).

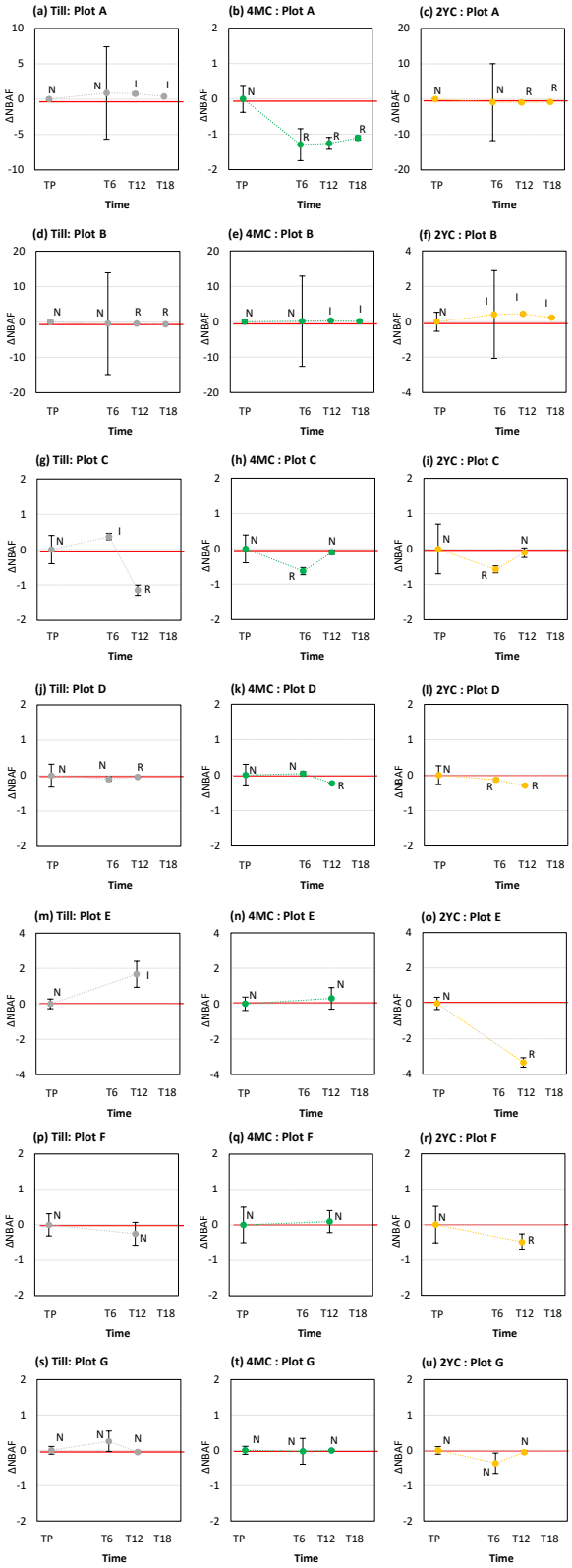

Monte Carlo simulation for BAF

Definitions and theories

It was assumed that concentration of the pollutant in soil and in earthworm of each subplot follows a normal distribution, respectively, and it can be expressed as follows:

$$C_{sij,\mathrm{T}i,tr} \sim N\left(\theta_{sj,\mathrm{T}i,tr}, \sigma^2_{sj,\mathrm{T}i,tr}\right)$$

$$C_{eij,\mathrm{T}i,tr} \sim N\left(\theta_{ej,\mathrm{T}i,tr}, \sigma^2_{ej,\mathrm{T}i,tr}\right)$$

where $C_{sij,\mathrm{T}i,tr}$ refers to pollutant concentration in soil of the *i*-th sample in the *j*-th plot of sampling period T*i* under treatment *tr*, $\theta_{sj,\mathrm{T}i,tr}$ refers to the population mean of $C_{sij,\mathrm{T}i,tr}$ of the *j*-the plot of sampling period T*i* under treatment *tr*, and $\sigma^2_{sj,\mathrm{T}i,tr}$ refers to the population variance of $C_{sij,\mathrm{T}i,tr}$ of the *j*-the plot of sampling period T*i* under treatment *tr*. $C_{eij,\mathrm{T}i,tr}$ refers to pollutant concentration in earthworm of the *i*-th sample in the *j*-th plot of sampling period T*i* under treatment *tr*, and $\theta_{ej,\mathrm{T}i,tr}$ and $\sigma^2_{ej,\mathrm{T}i,tr}$ are the corresponding population mean and population variance.

Bioaccumulation factor (*BAF*) is defined as the ratio of pollutant concentration in earthworm over pollutant concentration in soil. Conventionally, *BAF* was calculated by sample means of the pollutant concentration in soil and earthworm:

$$BAF_{j,\mathrm{T}i,tr} = \frac{\bar{C}_{ej,\mathrm{T}i,tr}}{\bar{C}_{sj,\mathrm{T}i,tr}}$$

where $BAF_{j,\mathrm{T}i,tr}$ is the bioaccumulation factor of the *j*-th plot of sampling period T*i* under treatment *tr*. $\bar{C}_{ej,\mathrm{T}i,tr}$ and $\bar{C}_{sj,\mathrm{T}i,tr}$ are the sample means of pollutant concentration in soil and earthworm of *j*-th plot of sampling period T*i* under treatment *tr*.

Normalized bioaccumulation factor (*NBAF*) is defined as the rescaled *BAF*, and the rescale factor is the corresponding *BAF* at TP. Thus, *NBAF* can be calculated:

$$NBAF_{j,\mathrm{T}i,tr} = \frac{BAF_{j,\mathrm{T}i,tr}}{BAF_{j,\mathrm{TP},tr}}$$

where $NBAF_{j,\mathrm{T}i,tr}$ is the normalized bioaccumulation factor of the *j*-th plot of sampling period T*i* under treatment *tr*.

Change of *NBAF* (*ΔNBAF*) is defined as the net effect of a treatment. For the net effect of till, it can be calculated by *NBAF* of till minus *NBAF* of control:

$$\Delta NBAF_{j,\mathrm{T}i,\mathrm{till}} = NBAF_{j,\mathrm{T}i,\mathrm{till}} - NBAF_{j,\mathrm{T}i,\mathrm{control}}$$

where $\Delta NBAF_{j,\mathrm{T}i,\mathrm{till}}$ refers to change of *NBAF* of the *j*-th plot of sampling period T*i* under treatment of till.

Similarly, the net effect of 4-month compost (4MC) and 2-year compost (2YC) can be calculated by:

$$\Delta NBAF_{j,\mathrm{T}i,4\mathrm{MC}} = NBAF_{j,\mathrm{T}i,4\mathrm{MC}} - NBAF_{j,\mathrm{T}i,\mathrm{till}}$$

$$\Delta NBAF_{j,\mathrm{T}i,2\mathrm{YC}} = NBAF_{j,\mathrm{T}i,2\mathrm{YC}} - NBAF_{j,\mathrm{T}i,\mathrm{till}}$$

where $\Delta NBAF_{j,\mathrm{T}i,4\mathrm{MC}}$ and $\Delta NBAF_{j,\mathrm{T}i,2\mathrm{YC}}$ are change of *NBAF* of the *j*-th plot of sampling period T*i* under treatment of 4-month compost and 2-year compost, respectively.

Generating random samples

Step 1: Estimate $\theta_{sj,\mathrm{T}i,tr}$, $\sigma_{sj,\mathrm{T}i,tr}$, $\theta_{ej,\mathrm{T}i,tr}$, and $\sigma_{ej,\mathrm{T}i,tr}$. The corresponding estimations are noted as $\hat{\theta}_{sj,\mathrm{T}i,tr}$, $\hat{\sigma}_{sj,\mathrm{T}i,tr}$, $\hat{\theta}_{ej,\mathrm{T}i,tr}$, and $\hat{\sigma}_{ej,\mathrm{T}i,tr}$.
Step 2: Draw $n_{sj,\mathrm{T}i,tr}$ and $n_{ej,\mathrm{T}i,tr}$ random samples from $N(\hat{\theta}_{sj,\mathrm{T}i,tr}, \hat{\sigma}^2_{sj,\mathrm{T}i,tr})$ and $N(\hat{\theta}_{ej,\mathrm{T}i,tr}, \hat{\sigma}^2_{ej,\mathrm{T}i,tr})$. $n_{sj|\mathrm{T}i|tr}$ and $n_{ej,\mathrm{T}i,tr}$ are the sample size of the *j*-th plot of sampling period T*i* under treatment of *tr*:
Step 3: Calculate $\bar{C}_{sj,\mathrm{T}i,tr}$ and $\bar{C}_{ej,\mathrm{T}i,tr}$ of the random samples.
Step 4: Repeat step 2 and step 3 for *n* times, then we have:

$$\overline{\boldsymbol{C}}_{sij,\mathrm{T}i,tr} = \begin{bmatrix} \bar{C}_{sj,\mathrm{T}i,tr,1} \\ \bar{C}_{sj,\mathrm{T}i,tr,2} \\ \vdots \\ \bar{C}_{sj,\mathrm{T}i,tr,n} \end{bmatrix}_{n\times 1}$$

$$\overline{\boldsymbol{C}}_{ej,\mathrm{T}i,tr} = \begin{bmatrix} \bar{C}_{ej,\mathrm{T}i,tr,1} \\ \bar{C}_{ej,\mathrm{T}i,tr,2} \\ \vdots \\ \bar{C}_{ej,\mathrm{T}i,tr,n} \end{bmatrix}_{n\times 1}$$

where $\overline{\boldsymbol{C}}_{sj,\mathrm{T}i,tr}$ is the sample mean matrix of pollutant concentration in soil of the *j*-th plot of sampling period T*i* under treatment *tr*, and where $\overline{\boldsymbol{C}}_{ej,\mathrm{T}i,tr}$ is the sample mean matrix of pollutant concentration in earthworm of the *j*-th plot of sampling period T*i* under treatment *tr*. They are $n \times 1$ matrix.
Step 5: Calculate *BAF* matrix by:

$$\boldsymbol{BAF}_{j,\mathrm{T}i,tr} = \overline{\boldsymbol{C}}_{sij,\mathrm{T}i,tr} \oslash \overline{\boldsymbol{C}}_{ej,\mathrm{T}i,tr} = \begin{bmatrix} \bar{C}_{sj,\mathrm{T}i,tr,1}/\bar{C}_{ej,\mathrm{T}i,tr,1} \\ \bar{C}_{sj,\mathrm{T}i,tr,2}/\bar{C}_{ej,\mathrm{T}i,tr,2} \\ \vdots \\ \bar{C}_{sj,\mathrm{T}i,tr,n}/\bar{C}_{ej,\mathrm{T}i,tr,n} \end{bmatrix} = \begin{bmatrix} BAF_{j,\mathrm{T}i,tr,1} \\ BAF_{j,\mathrm{T}i,tr,2} \\ \vdots \\ BAF_{j,\mathrm{T}i,tr,n} \end{bmatrix}_{n\times 1}$$

where $\boldsymbol{BAF}_{j|\mathrm{T}i|tr}$ is the BAF matrix of the *j*-th plot of sampling period T*i* under treatment *tr*.
Step 6: Calculate *NBAF* matrix by:

$$\boldsymbol{NBAF}_{j,\mathrm{T}i,tr} = \frac{\boldsymbol{BAF}_{j,\mathrm{T}i,tr}}{\overline{BAF}_{j,\mathrm{T}i,tr}} = \begin{bmatrix} BAF_{j,\mathrm{T}i,tr,1}/\overline{BAF}_{j,\mathrm{T}i,tr} \\ BAF_{j,\mathrm{T}i,tr,2}/\overline{BAF}_{j,\mathrm{T}i,tr} \\ \vdots \\ BAF_{j,\mathrm{T}i,tr,n}/\overline{BAF}_{j,\mathrm{T}i,tr} \end{bmatrix} = \begin{bmatrix} NBAF_{j,\mathrm{T}i,tr,1} \\ NBAF_{j,\mathrm{T}i,tr,2} \\ \vdots \\ NBAF_{j,\mathrm{T}i,tr,n} \end{bmatrix}_{n\times 1}$$

where $\overline{BAF}_{j|\mathrm{TP}|tr}$ is the mean of the elements in $\boldsymbol{BAF}_{j,\mathrm{T}i,tr}$.
Step 7: Calculate $\Delta NBAF$ matrices:

$$\Delta\boldsymbol{NBAF}_{j,\mathrm{T}i,\mathrm{till}} = \boldsymbol{NBAF}_{j,\mathrm{T}i,\mathrm{till}} - \boldsymbol{NBAF}_{j,\mathrm{T}i,\mathrm{control}}$$

$$\Delta\boldsymbol{NBAF}_{j,\mathrm{T}i,4\mathrm{MC}} = \boldsymbol{NBAF}_{j,\mathrm{T}i,4\mathrm{MC}} - \boldsymbol{NBAF}_{j,\mathrm{T}i,\mathrm{till}}$$
$$\Delta\boldsymbol{NBAF}_{j,\mathrm{T}i,2\mathrm{YC}} = \boldsymbol{NBAF}_{j,\mathrm{T}i,2\mathrm{YC}} - \boldsymbol{NBAF}_{j,\mathrm{T}i,\mathrm{till}}$$

Difference between NBAF of two sampling time periods

Critical value approach was used to develop the algorithm (Martinez and Martinez, 2015).

Step 1: Calculate difference matrix:

$$\boldsymbol{D} = \boldsymbol{NBAF}_{j,\mathrm{t}1,tr} - \boldsymbol{NBAF}_{j,\mathrm{t}2,tr}$$

where t1 and t2 refers to two different time periods, and $\mathrm{t}1 \neq \mathrm{t}2$.

Step 2: Calculate quantiles of the elements in $\boldsymbol{D}$. $\hat{q}_{\frac{\alpha}{2}}$ and $\hat{q}_{1-\frac{\alpha}{2}}$ are the α/2-th quantile and 1-α/2-th quantile of the elements in $\boldsymbol{D}$. α is the significant level.

Step 3: If $0 \notin \left[\hat{q}_{\frac{\alpha}{2}}, \hat{q}_{1-\frac{\alpha}{2}}\right]$, then the hypothesis that $\boldsymbol{NBAF}_{j,\mathrm{t}1,tr} = \boldsymbol{NBAF}_{j,\mathrm{t}2,tr}$ is rejected at significant level of α;

If $0 \in \left[\hat{q}_{\frac{\alpha}{2}}, \hat{q}_{1-\frac{\alpha}{2}}\right]$, then the hypothesis that $\boldsymbol{NBAF}_{j,\mathrm{t}1,tr} = \boldsymbol{NBAF}_{j,\mathrm{t}2,tr}$ is not rejected at significant level of α.

Algorithm – difference between ΔNBAF and zero

Critical value approach was used to develop the algorithm (Martinez and Martinez, 2015).

Step 1: Calculate quantiles of the elements in $\Delta\boldsymbol{NBAF}_{j,\mathrm{T}i,tr}$. $\hat{q}_{\frac{\alpha}{2}}$ and $\hat{q}_{1-\frac{\alpha}{2}}$ are the α/2-th quantile and 1-α/2-th quantile of the elements in $\Delta\boldsymbol{NBAF}_{j,\mathrm{T}i,tr}$. α is the significant level.

Step 2: If $0 \notin \left[\hat{q}_{\frac{\alpha}{2}}, \hat{q}_{1-\frac{\alpha}{2}}\right]$, then the hypothesis that $\Delta\boldsymbol{NBAF}_{j,\mathrm{T}i,tr} = 0$ is rejected at significant level of α; If $0 \in \left[\hat{q}_{\frac{\alpha}{2}}, \hat{q}_{1-\frac{\alpha}{2}}\right]$, then the hypothesis that $\Delta\boldsymbol{NBAF}_{j,\mathrm{T}i,tr} = 0$ is not rejected at significant level of α.

Relation between C_e and C_s

To calculate HQ, we have **Eqn. 7** in the manuscript:

$$HQ_{\mathrm{se}} = FIR \cdot (C_{\mathrm{s}} \cdot Ps + C_{\mathrm{e}}) \cdot \frac{1}{TRV}$$

where $Ps = 0.164(\mathrm{woodcock}), Ps = 0.03(\mathrm{shrew})$ according to **SI Table 2,** then we have,

$$HQ_{\mathrm{woodcock}} = FIR \cdot (C_{\mathrm{s}} \cdot 0.164 + C_{\mathrm{e}}) \cdot \frac{1}{TRV}$$

$$HQ_{\mathrm{shrew}} = FIR \cdot (C_{\mathrm{s}} \cdot 0.03 + C_{\mathrm{e}}) \cdot \frac{1}{TRV}$$

Define HQ' as the HQ with $C_s = 0$, then we have,

$$HQ'_{\mathrm{bird}} = FIR \cdot (0 + C_{worm}) \cdot \frac{1}{TRV}$$

$$HQ'_{\mathrm{shrew}} = FIR \cdot (0 + C_{worm}) \cdot \frac{1}{TRV}$$

Thus, the ratio of HQ and HQ' in terms of woodcock can be obtained,

$$\frac{HQ_{\mathrm{woodcock}}}{HQ'_{\mathrm{woodcock}}} = \frac{FIR \cdot (C_{\mathrm{s}} \cdot 0.164 + C_{\mathrm{e}}) \cdot \frac{1}{TRV}}{FIR \cdot (0 + C_{\mathrm{e}}) \cdot \frac{1}{TRV}} = \frac{C_{\mathrm{e}} + 0.164C_{\mathrm{s}}}{C_{\mathrm{e}}}$$

Thus, if $C_{\mathrm{e}} \gg 0.164C_{\mathrm{s}}$, then $HQ_{\mathrm{bird}} = HQ'_{\mathrm{bird}}$.

Similarly, the ratio of HQ and HQ' in terms of shrew can be obtained,

$$\frac{HQ_{\mathrm{shrew}}}{HQ'_{\mathrm{shrew}}} = \frac{FIR \cdot (C_{\mathrm{s}} \cdot 0.03 + C_{\mathrm{e}}) \cdot \frac{1}{TRV}}{FIR \cdot (0 + C_{\mathrm{e}}) \cdot \frac{1}{TRV}} = \frac{C_{\mathrm{e}} + 0.03C_{\mathrm{s}}}{C_{\mathrm{e}}}$$

Thus, if $C_{\mathrm{e}} \gg 0.03C_{\mathrm{s}}$, then $HQ_{\mathrm{shrew}} = HQ'_{\mathrm{shrew}}$.

Appendices D: SI of Chapter 5

SI Figure 5-1 Plot of BAF at different time point. The plots are based on data of the previous field plot study (Anderson et al., 2020). BAF derived by Eqn. 5-1 in the manuscript of each subplot (n = 7 for T0 and T12, n =6 for T6, and n = 3 for T18) was shown in (a). For plot (b), each point represents BAF same as in (a), and error bars refer to standard deviation derived from the corresponding Ce and Cs by error propagation equation (Farrance and Frenkel, 2002). The first approach is defined as point-approach, and the second approach is defined as distribution-approach. TP, T6, T12 and T18 refer to pre-application of compost, and 6, 12 and 18 months after application of compost.

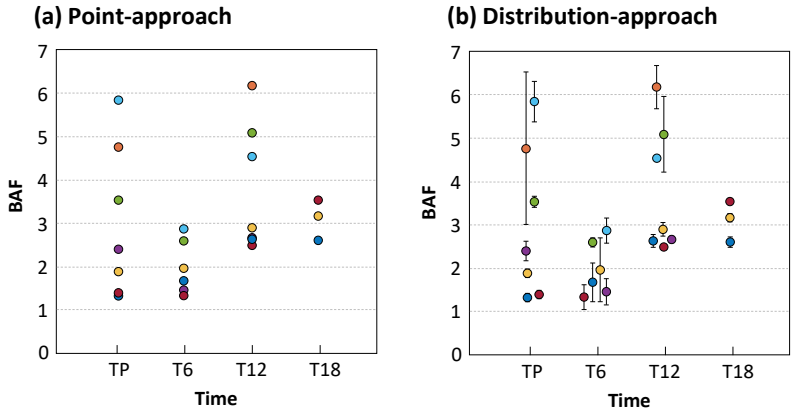

SI Table 5-1 Simulation results of Point-approach and Distribution-approach. Data were the same data from **SI Figure 1**. n = 50000 by Monte-Carlo simulation (Martinez and Martinez, 2015), results are expressed as mean ± std; Underestimation is calculated by standard deviation approach over distribution approach, and it refers to relative difference in terms of std of point approach

Time	T0	T6	T12	T18
Point approach	3.11±1.78	2.07±**0.63**	3.87±1.50	3.19±0.50
Distribution approach	3.11±1.93	2.07±**0.77**	3.87±1.55	3.19±0.51
Underestimation	8.50%	**22%**	3.90%	1.90%

SI Figure 5-2 Plot of the two components $f_1(t)$ and $f_2(t)$
where $f_1(t)$ and $f_2(t)$ are the two components of the ratio variable t, and $t = (a + x) / (b + y)$. a and b are two nonnegative constants, and x and y are two independent standard normal variables. In addition, the following relations hold: $f(t) = pf_1(t) + (1-p)f_2(t)$ with $p = e^{-\frac{1}{2}(a^2+b^2)}$, $f_1(t) = \frac{1}{\pi(1+t^2)}$, and $f_2(t) = \frac{q\int_0^q e^{-\frac{1}{2}(a^2+b^2)}dx}{\pi(1+t^2)\left(e^{\frac{1}{2}(a^2+b^2)}-1\right)}$ with $q = \frac{b+at}{\sqrt{1+t^2}}$ (Marsaglia, 1965; Marsaglia, 2006). Figure reproduced from Marsaglia, 2006.

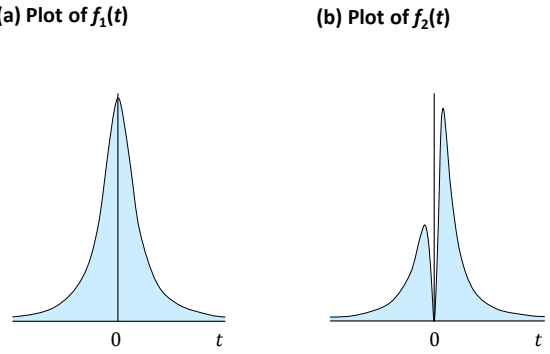

SI Figure 5-3 Difference between results from normal approximation and Monte-Carlo simulation
The plots are based on data of the previous field plot study (Anderson et al., 2020). μ refers to sample mean, and s refers to sample standard deviation. Simulation runs n = 5000. Note the overflows and underflows in (d), (e) and (f), which reflect the great heavy tail. It shows that the *BAF* estimated by Monte-Carlo simulation is skewed and the estimated mean and standard deviation has a great variability among three independent trials (d), (e), (f), and reflecting lack of convergence

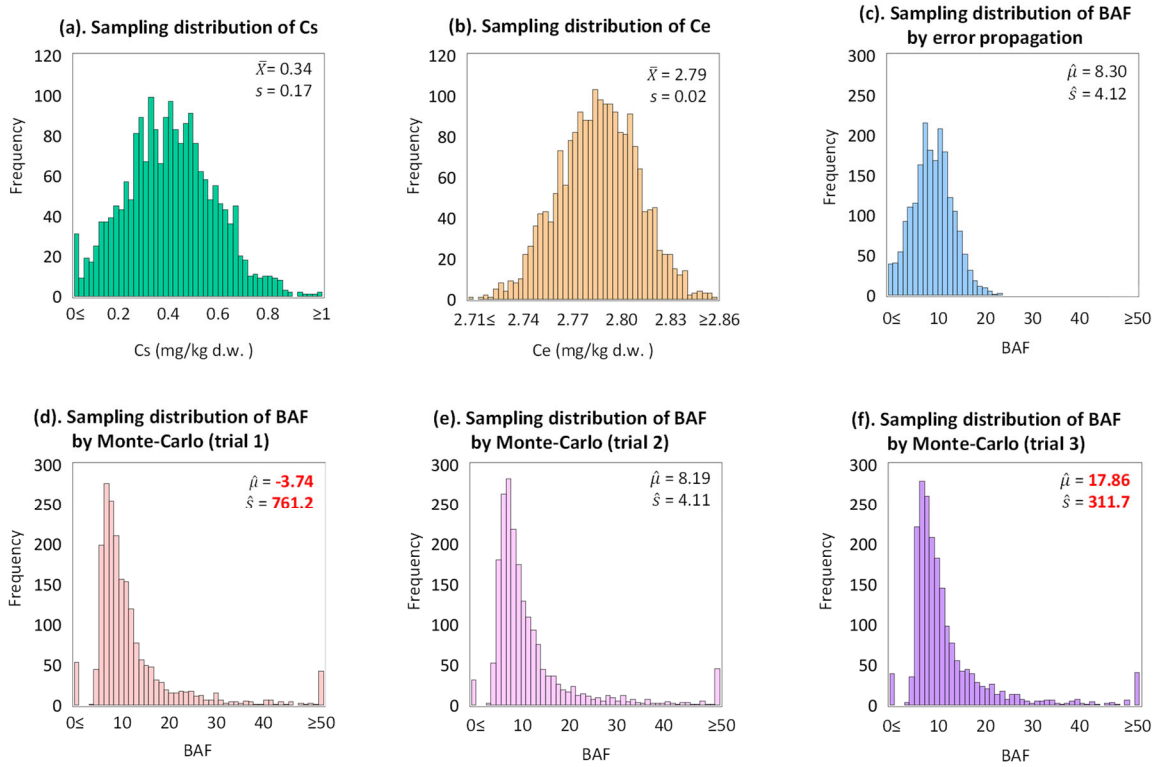

SI Figure 5-4 Photo of subplots in a plot

Gibbs Sampler

In current research, Gibbs sampler was used for this model. Since soil and earthworm concentrations follows the same hierarchical structure, subscript of s and e are ignored without confusion. The joint posterior distribution of parameters of interest is as following:

$$p(\mu, \tau^2, \theta_j, \sigma_j^2 | \log C_{ij}) \propto p(\log C_{ij} | \theta_j, \sigma_j^2) p(\theta_j | \mu, \tau^2) p(\mu | m, s^2) p(\tau^2 | a, b) p(\sigma_j^2 | c_j, d_j)$$

In the equation above, $p(\log C_{ij} | \theta_j, \sigma_j^2)$ is the likelihood function, and the likelihood is:

$$p(\log C_{ij} | \theta_j, \sigma_j^2) \propto \prod_{j=1}^{J} \prod_{i=1}^{n_j} \frac{1}{\sqrt{\sigma_j^2}} \exp\left\{ -\frac{(\log C_{ij} - \theta_j)^2}{2\sigma_j^2} \right\}$$

where J is the number of plots; n_j is the sampler size of the j-th plot. For θ_j, the distribution is also normal and thus we have:

$$p(\theta_j | \mu, \tau^2) \propto \prod_{J=1}^{J} \frac{1}{\sqrt{\tau^2}} \exp\left\{ -\frac{(\theta_j - \mu)^2}{2\tau^2} \right\}$$

The remaining terms are hyperprior distributions, and we have:

$$p(\mu | m, s^2) \propto \frac{1}{\sqrt{s^2}} \exp\left\{ -\frac{(\mu - m)^2}{2s^2} \right\}$$

$$p(\tau^2 | a, b) \propto \frac{1}{(\tau^2)^{a+1}} \exp\left\{ -\frac{b}{\tau^2} \right\}$$

$$p(\sigma_j^2 | c_j, d_j) \propto \frac{1}{(\sigma_j^2)^{c_j+1}} \exp\left\{ -\frac{d_j}{\sigma_j^2} \right\}$$

Then, the conditional distribution can be derived for each parameter. The conditional posterior distribution of μ is:

$$p(\mu | \cdot) \propto p(\theta_j | \mu, \tau^2) p(\mu) \propto \left(\prod_{J=1}^{J} \frac{1}{\sqrt{\tau^2}} \exp\left\{ -\frac{(\theta_j - \mu)^2}{2\tau^2} \right\} \right) \cdot \frac{1}{\sqrt{s^2}} \exp\left\{ -\frac{(\mu - m)^2}{2s^2} \right\}$$

$$\Rightarrow p(\mu | \cdot) \propto N\left(\frac{\frac{1}{s^2} m + \frac{1}{\tau^2} \sum_{j=1}^{J} \theta_j}{\frac{1}{s^2} + \frac{J}{\tau^2}}, \frac{1}{\frac{1}{s^2} + \frac{J}{\tau^2}} \right)$$

The conditional posterior distribution of each θ_j (i.e. j is fixed) is:

$$p(\theta_j | \cdot) \propto p(\log C_{ij} | \theta_j, \sigma_j^2) p(\theta_j | \mu, \tau^2) \propto \left(\prod_{i=1}^{n_j} \frac{1}{\sqrt{\sigma_j^2}} \exp\left\{ -\frac{(\log C_{ij} - \theta_j)^2}{2\sigma_j^2} \right\} \right) \cdot \left(\frac{1}{\sqrt{\tau^2}} \exp\left\{ -\frac{(\theta_j - \mu)^2}{2\tau^2} \right\} \right)$$

$$\Rightarrow p(\theta_j | \cdot) \propto N\left(\frac{\frac{1}{\sigma_j^2} \sum_{i=1}^{n_j} \log C_{ij} + \frac{1}{\tau^2} \mu}{\frac{n_j}{\sigma_j^2} + \frac{1}{\tau^2}}, \frac{1}{\frac{n_j}{\sigma_j^2} + \frac{1}{\tau^2}} \right)$$

The conditional posterior distribution of each σ_j^2 is:

$$p(\sigma_j^2|\cdot) \propto p(\log C_{ij}|\theta_j,\sigma_j^2)p(\sigma_j^2|c_j,d_j) \propto \left(\prod_{i=1}^{n_j}\frac{1}{\sqrt{\sigma_j^2}}\exp\left\{-\frac{(\log C_{ij}-\theta_j)^2}{2\sigma_j^2}\right\}\right)\cdot\frac{1}{(\sigma_j^2)^{c_j+1}}\exp\left\{-\frac{d_j}{\sigma_j^2}\right\}$$

$$\Rightarrow\ p(\sigma_j^2|\cdot) \propto IG\left(\frac{n_j}{2}+c_j,\frac{\sum_{i=1}^{n_j}(\log C_{ij}-\theta_j)^2}{2}+d_j\right)$$

The conditional posterior distribution of τ^2 is:

$$p(\tau^2|\cdot) \propto p(\theta_j|\mu,\tau^2)p(\tau^2|a,b) \propto \left(\prod_{J=1}^{J}\frac{1}{\sqrt{\tau^2}}\exp\left\{-\frac{(\theta_j-\mu)^2}{2\tau^2}\right\}\right)\cdot\frac{1}{(\tau^2)^{a+1}}\exp\left\{-\frac{b}{\tau^2}\right\}$$

$$\Rightarrow\ p(\tau^2|\cdot) \propto IG\left(\frac{J}{2}+a,\frac{\sum_{j=1}^{J}(\theta_j-\mu)^2}{2}+b\right)$$

The corresponding MCMC Matlab function is:

```
function [post_table] =
MCMC(logdat,para_n,para_r,para_t,para_m,para_s2,para_a,para_b,para_cj,para_dj)
% This is for MCMC calculation for hierarchical data
% It can handle missing data and nj = 1
% --------- INPUT ----------
% logdat       ~ structured data, column = group | dat is table format
% para_n       ~ number of simulations
% para_r       ~ burn-in
% para_t       ~ thinning
% para_m       ~ prior for mean of group mean
% para_s2      ~ prior for variance of group mean
% para.a       ~ prior for shape parameter of tau2
% para.b       ~ prior for scale parameter of tau2
% para.cj      ~ prior for shape parameter of sigmaj2
% para.dj      ~ prior for scale parameter of sigmaj2
% ---------- OUTPUT ---------
% post_table    ~ postertior samples of variable of interest
% post_mu       ~ grand mean
% post_tau2     ~ between group variance
% post_thetaj   ~ group mean
% post_sigma2j  ~ within group variance
% post_Vj       ~ variance of group means
% Extract data dimention information (n~sample size; j~group size)
[Jj,J,~,nj]= GroupInfo(logdat);
% Empty data matrix
theta_j   = nan(para_n,Jj);
sigma2_j  = nan(para_n,Jj);
mu        = nan(para_n,1);
tau2      = nan(para_n,1);
V_j       = nan(para_n,Jj); % variance of theta_j

% Initiation parameter
% (1) Group mean of #j
yij           = table2array(logdat);
y_bar         = nanmean(yij);
njs           = nj; % for sigma2_j correction. if nj = 1, then sigma2 = Inf
njs(njs==1)   = 0;
theta_j(1,:)  = y_bar + rand([1,Jj]);
```

```
sigma2_j(1,:) = nanvar(table2array(logdat));
sigma2_j(sigma2_j==0) = Inf;
mu(1)         = nanmean(theta_j(1,:));
tau2(1)       = nanvar(theta_j(1,:));
V_j(1,:)      = 1 ./ (1./tau2(1) + nj./sigma2_j(1,:));

% Gibbs sampler
for i = 2:1:para_n
    % Group mean of #i
    V_j(i,:)       = 1 ./ (1./tau2(i-1) + nj./ sigma2_j(i-1,:));
    thetahat_j     = (mu(i-1)/tau2(i-1) + nj./sigma2_j(i-1,:).* y_bar) ./ (1./tau2(i-1) +
nj./sigma2_j(i-1,:));
    theta_j(i,:)   = normrnd(thetahat_j,sqrt(V_j(i,:)));

    % Grand mean
    muhat          = (nanmean(theta_j(i,:))*J/tau2(i-1) + para_m/para_s2) / (1/para_s2 +
J/tau2(i-1));
    muV            = 1 / (1/para_s2 + J/tau2(i-1));
    mu(i)          = normrnd(muhat,sqrt(muV));

    % Within group variance
    clear shape scale
    shape          = nj ./ 2 + para_cj;
    scale          = 1./ (nansum((yij - theta_j(i,:)).^2)./2 + para_dj);
    sigma2_j(i,:)  = 1 ./ gamrnd(shape,scale);

    % Between group variance
    clear shape scale
    shape          = J/2 + para_a;
    scale          = 1 / nansum((theta_j(i,:) - mu(i)).^2)/2 + para_b;
    tau2(i)        = 1 ./ gamrnd(shape,scale);
end

%% Data processing
% Burn-in
mu(1:para_r)         = [];
theta_j(1:para_r,:)  = [];
sigma2_j(1:para_r,:) = [];
tau2(1:para_r)       = [];
V_j(1:para_r,:)      = [];

% Thinning
if para_t == 0 || para_t == 1
    disp('no thinning');
    post_mu         = mu;
    post_tau2       = tau2;
    post_thetaj     = theta_j;
    post_sigma2j    = sigma2_j;
    post_Vj         = V_j;
else
    post_mu         = mu(1:para_t:end);
    post_tau2       = tau2(1:para_t:end);
    post_thetaj     = theta_j(1:para_t:end,:);
    post_sigma2j    = sigma2_j(1:para_t:end,:);
    post_Vj         = V_j(1:para_t:end,:);
end

%% Tablize
theta_str = 'theta';
sigma_str = 'sigma2';
V_str     = 'V';
```

```
for k = 1:1:Jj
    thetaj{k}  = sprintf('%s_%d',theta_str,k);
    sigma2j{k} = sprintf('%s_%d',sigma_str,k);
    V{k}       = sprintf('%s_%d',V_str,k);
end
VarName = [{'mu'},{'tau2'},thetaj,sigma2j,V];

post_table =
array2table([post_mu,post_tau2,post_thetaj,post_sigma2j,post_Vj],'VariableNames',VarName);

end
```

SI Table 5-2 Observed DDx concentration
Unite: (μg/g d.w.)

(a). No Till

No Till								
		Plot1	Plot2	Plot3	Plot4	Plot5	Plot6	Plot7
Soil	T0	15.77	3.09	14.52	7.41	3.30	2.00	8.45
	T0	13.49	3.16	20.62	7.38	2.99	2.47	9.18
	T0	14.54	2.94	20.05	7.56	3.19	2.47	8.76
	T6	16.88	3.97	21.48 (α)	15.90	3.56	2.85	13.14
	T6	16.26	4.07	16.45 (β)	12.54	4.70	2.72	12.35
	T6	12.81	3.07	57.22 (γ)	14.93	3.46	2.81	14.18
	T12	14.00	4.79	19.46	8.86	3.96	3.23	11.46
	T12	10.80	3.72	22.61	8.44	3.92	3.22	10.42
	T12	11.94	3.80	20.52	8.85	3.96	3.15	10.37
	T18	12.29		18.07				11.08
	T18	10.86		10.72				11.86
	T18	11.30		17.58				11.55
Worm	T0	20.11	10.01	34.26	12.56	15.15	11.14	14.25
	T0	23.57	9.18	51.04	13.08	8.70	11.08	14.04
	T0		10.52	62.53	5.76	10.57	11.09	
	T6	20.36		35.10	19.50	10.79	5.14	22.78
	T6	23.51		36.79	21.80	10.23	5.03	20.78
	T6	23.59		40.32	16.12	10.57	5.14	
	T12	35.22	22.58	36.38	33.51	18.03	14.39	31.41
	T12	33.51	22.51	40.19	31.67	18.05	14.60	31.09
	T12	33.05	22.36	41.43	34.17	17.96	14.58	31.01
	T18	43.72		50.89				47.04
	T18	43.65		50.39				46.66
	T18	41.13		46.94				46.79

(b). Till

Till								
		Plot1	Plot2	Plot3	Plot4	Plot5	Plot6	Plot7
Soil	T0	18.40	2.00	11.67	7.98	4.32	2.67	12.92
	T0	20.96	2.00	11.27	8.75	4.26	2.53	13.73
	T0	20.45	2.21	11.98	8.68	3.90	2.53	14.99
	T6	31.40	3.05	9.33	22.45	5.74	3.17	11.84
	T6	20.92	3.16	11.36	16.24	5.87	3.22	13.27
	T6	17.10	3.91	19.28	16.40	5.37	2.97	18.60
	T12	20.12	3.49	9.10	10.07	4.60	3.42	11.81
	T12	18.37	2.98	9.92	10.19	4.64	3.46	11.49
	T12	19.85	3.55	10.15	9.69	4.71	3.43	11.93
	T18	19.50		7.79				12.65
	T18	19.35		8.24				
	T18	17.99		7.95				
Worm	T0	27.64	9.42	21.92	19.92	13.51	12.10	19.92
	T0	25.77	6.21	23.36	19.13	13.68	11.98	20.84
	T0		6.99	21.60	23.26	12.91	12.93	
	T6	39.36		24.89	31.91	15.23	8.59	20.55
	T6	36.14		23.62	25.81		8.42	21.38
	T6	41.22		30.89			8.47	
	T12	51.16	21.09	29.75	27.80	21.39	16.00	30.80
	T12	48.62	20.81	28.87	27.57	29.86	15.75	29.97
	T12	53.83	21.24	28.85	27.51	21.17	16.07	30.13
	T18	50.81		26.65				46.46
	T18	50.70		25.81				45.62
	T18	49.12		26.16				45.99

(c). 2YC

2YC								
		Plot1	Plot2	Plot3	Plot4	Plot5	Plot6	Plot7
Soil	T0	11.11	3.23	6.20	9.09	8.02	2.71	8.95
	T0	12.40	3.18	6.23	7.77	7.24	2.52	9.37
	T0	10.51	3.17	7.54	7.31	7.76	2.53	11.23
	T6	11.62	3.58	9.90	9.76	8.78	3.14	10.43
	T6	8.08	3.79	11.07	8.99	8.98	3.09	11.45
	T6	9.85	4.94	13.30	8.90	7.82	2.98	15.15
	T12	13.14	3.84	8.17	6.51	7.39	3.33	10.73
	T12	11.25	3.58	9.15	3.84	7.20	3.31	11.41
	T12	11.83	4.07	9.53	6.41	6.75	3.29	11.21
	T18	12.08		8.03				8.92
	T18	12.02		7.66				9.05
	T18	11.95		8.22				8.85
Worm	T0	21.83	15.71	21.97	17.28	23.88	11.78	13.38
	T0	17.88	9.56	22.32	16.16	16.55	11.73	19.10
	T0		11.56	17.36	13.79	17.70	11.78	
	T6	18.15		16.29	13.44		8.90	18.42
	T6	18.10		18.14	14.22		8.37	17.72
	T6	23.50		17.12	7.96		8.47	
	T12	29.35	20.53	23.16	24.00	22.49	15.31	27.03
	T12	29.85	20.45	22.81	23.38	22.04	15.65	26.77
	T12	29.82	20.53	23.16	22.95	22.55	15.71	26.80
	T18	33.41		23.97				83.20
	T18	31.29		22.08				84.06
	T18	31.12		15.67				82.76

(d). 4MC

4MC								
		Plot1	Plot2	Plot3	Plot4	Plot5	Plot6	Plot7
Soil	T0	7.03	2.30	11.08	7.60	4.57	2.00	8.73
	T0	6.42	2.40	11.36	7.72	4.63	2.78	8.86
	T0	6.55	2.47	10.91	7.45	4.53	2.81	9.51
	T6	7.77	2.92	8.55	12.44	5.06	3.01	13.82
	T6	10.18	3.62	9.89	11.33	5.42	3.09	12.98
	T6	4.54	2.00	16.59	11.94	5.60	3.11	17.64
	T12	10.02	3.77	6.81	7.94	5.06	3.17	11.20
	T12	7.86	2.82	8.32	7.58	4.63	3.26	10.89
	T12	9.12	2.86	7.60	7.90	4.70	3.30	11.22
	T18	10.15		4.88				11.29
	T18	7.64		7.42				11.74
	T18	8.99		7.51				11.11
Worm	T0	18.62	16.88	30.41	20.46	16.44	12.83	28.37
	T0	16.47	9.80	19.40	21.12	9.95	12.95	28.39
	T0		11.61	13.60	21.06	11.72	12.95	
	T6	16.59		13.35	17.88		8.58	22.38
	T6	14.08		19.49	15.44		8.63	20.39
	T6			24.81	9.71		8.90	
	T12	32.65	19.61	23.07	29.67	18.38	15.40	27.38
	T12	29.84	19.91	23.72	28.45	18.43	15.43	26.97
	T12	31.60	19.94	23.86	27.14	17.96	15.72	28.04
	T18	28.07		17.33				85.87
	T18	27.76		17.59				84.46
	T18	27.30		17.83				85.44

SI Table 5-3 Observed dieldrin concentration
Unite: (μg/g d.w.)

(a). No Till

No Till								
		Plot1	Plot2	Plot3	Plot4	Plot5	Plot6	Plot7
Soil	T0	1.44	0.52	1.15	0.75	0.48	0.40	0.40
	T0	1.27	0.48	1.35	0.72	0.40	0.56	0.83
	T0	1.04	0.47	1.39	0.78	0.48	0.50	0.74
	T6	1.78	0.40	0.96	1.67	0.51	0.44	0.78
	T6	0.93	0.40	0.75	1.24	0.40	0.41	0.96
	T6	0.48	0.40	2.43 (δ)	1.27	0.37	0.55	0.67
	T12	1.02	0.33	1.25	0.64		0.41	0.62
	T12	0.81	0.23	1.16	0.54	0.29	0.41	0.57
	T12	0.70		1.25	0.68	0.43	0.41	0.58
	T18	1.00		1.18				0.42
	T18	0.90		0.75				0.47
	T18	0.94		1.10				0.44
Worm	T0	7.80	2.36	4.37	5.15	0.95	1.60	3.14
	T0	5.44	1.97	8.53	4.05	0.89	1.54	2.38
	T0		2.25	7.55	1.02	1.59	1.60	
	T6	4.05		3.64	2.72	1.06	1.01	2.14
	T6	3.94		3.96	3.38	1.11	1.01	2.10
	T6	4.90		7.52	3.64	1.01	1.01	
	T12	4.74	2.18	5.11	5.22	4.36	1.49	1.92
	T12	4.53	2.40	4.68	5.81	4.95	1.55	1.92
	T12	4.64	2.45	5.71	5.54	5.47	1.49	1.92
	T18	5.92		5.28				1.36
	T18	5.76		5.33				1.41
	T18	5.44		5.17				1.49

(b). Till

Till								
		Plot1	Plot2	Plot3	Plot4	Plot5	Plot6	Plot7
Soil	T0	1.24	0.40	0.79	0.93	0.40	0.52	0.41
	T0	1.14	0.40	0.40	1.07	0.40	0.40	0.41
	T0	1.20	0.47	0.84	0.40	0.40	0.40	0.83
	T6	1.00	0.40	0.79	1.37	0.44	0.46	0.79
	T6	0.85	0.40	0.82	1.45	0.42	0.45	0.85
	T6	0.73	0.40	2.24 (ε)	1.32	0.56	0.53	0.66
	T12	0.93		0.89	0.77	0.25	0.41	0.48
	T12	0.76	0.29	0.93	0.78	0.24	0.41	0.48
	T12	0.74	0.40	1.01	0.85	0.24	0.41	0.49
	T18	0.96		0.82				0.41
	T18	0.95		0.83				
	T18	0.88		0.78				
Worm	T0	5.29	2.30	16.69	5.04	2.01	1.76	2.92
	T0	3.46	0.48	4.95	4.01	0.74	1.65	2.80
	T0		2.66	7.01	5.97	2.17	1.76	
	T6	4.97		5.54	8.98	1.05	1.12	2.15
	T6	4.98		4.78	7.13		1.07	2.18
	T6	6.34		3.59			3.04	
	T12	4.53	2.50	4.15	4.42	6.99	1.65	1.92
	T12	5.60	2.24	4.21	4.10	7.35	1.76	1.87
	T12	5.86	2.50	4.15	4.42	7.25	1.81	1.86
	T18	4.77		4.00				1.73
	T18	5.47		3.95				2.16
	T18	5.23		4.10				1.41

(c). 2YC

2YC								
		Plot1	Plot2	Plot3	Plot4	Plot5	Plot6	Plot7
Soil	T0	1.01	0.40	0.40	0.40	0.56	0.52	0.29
	T0	1.09	0.40	0.40	0.89	0.40	0.40	0.32
	T0	0.82	0.40	0.83	0.93	0.40	0.40	0.38
	T6	0.68	0.40	0.75	1.30	0.44	0.45	0.81
	T6	0.27	0.40	0.72	0.94	0.44	0.44	0.88
	T6	0.96	0.40	0.88	0.76	0.54	0.55	0.65
	T12	0.82		0.90	0.53	0.27	0.41	0.48
	T12	0.68	0.30	0.86	0.28	0.26	0.41	0.49
	T12	0.59	0.39	0.96	0.61	0.25	0.41	0.49
	T18	0.77		0.77				0.37
	T18	0.72		0.74				0.42
	T18	0.76		0.82				0.35
Worm	T0	10.91	1.33	2.45	10.76	2.23	1.81	2.77
	T0	3.57	1.21	2.45	8.92	0.69	1.76	3.14
	T0		5.23	6.43	4.32	1.59	1.76	
	T6	2.96		3.19	3.19		1.07	2.79
	T6	2.82		3.47	4.58		1.07	2.66
	T6	5.41		5.40	2.55		1.12	
	T12	4.53	2.45	4.10	3.51	3.72	1.65	1.81
	T12	4.48	2.66	5.70	3.94	3.41	1.70	1.81
	T12	4.47	2.45	5.27	3.78	2.87	1.76	1.86
	T18	3.81		3.62				1.81
	T18	3.87		3.47				1.70
	T18	3.84		2.72				1.17

(d). **4MC**

4MC								
		Plot1	Plot2	Plot3	Plot4	Plot5	Plot6	Plot7
Soil	T0	1.11	0.43	0.88	0.78	0.61	0.40	0.46
	T0	1.06	0.53	0.95	0.86	0.40	0.57	0.84
	T0	0.97	0.46	0.99	0.82	0.51	0.54	0.55
	T6	0.71	0.40	0.74	1.24	0.42	0.42	0.72
	T6	1.27	0.40	0.73	0.96	0.61	0.43	0.89
	T6	0.40	0.40	2.13 (ζ)	0.79	0.40	0.57	0.68
	T12	0.90	0.33	0.67	0.55	0.38	0.41	0.51
	T12	0.71	0.23	0.76	0.48	0.31	0.41	0.51
	T12	0.59		0.79	0.62	0.43	0.41	0.50
	T18	1.09		0.56				0.40
	T18	0.88		0.75				0.42
	T18	1.01		0.77				0.44
Worm	T0	17.61	1.27	15.04	10.71	0.58	1.76	4.00
	T0	6.02	1.33	3.11	10.90	0.85	1.81	4.36
	T0		4.91	3.20	2.51	0.20	1.81	
	T6	3.93		3.65	3.19		1.07	3.21
	T6	3.24		4.51	3.30		2.40	2.66
	T6			3.14	0.95		1.07	
	T12	4.16	2.45	3.40	3.52	2.98	1.55	1.70
	T12	5.06	2.66	3.51	4.00	3.04	1.60	1.65
	T12	4.32	2.40	3.41	4.15	3.04	1.60	1.71
	T18	4.69		2.64				1.65
	T18	4.72		2.45				1.44
	T18	4.53		2.13				2.29

SI Figure 5-5 MCMC simulation results of μ_e. Data is from Control: Till at T6. There are 150100 runs in total, burn-in = 100, thinning = 5.

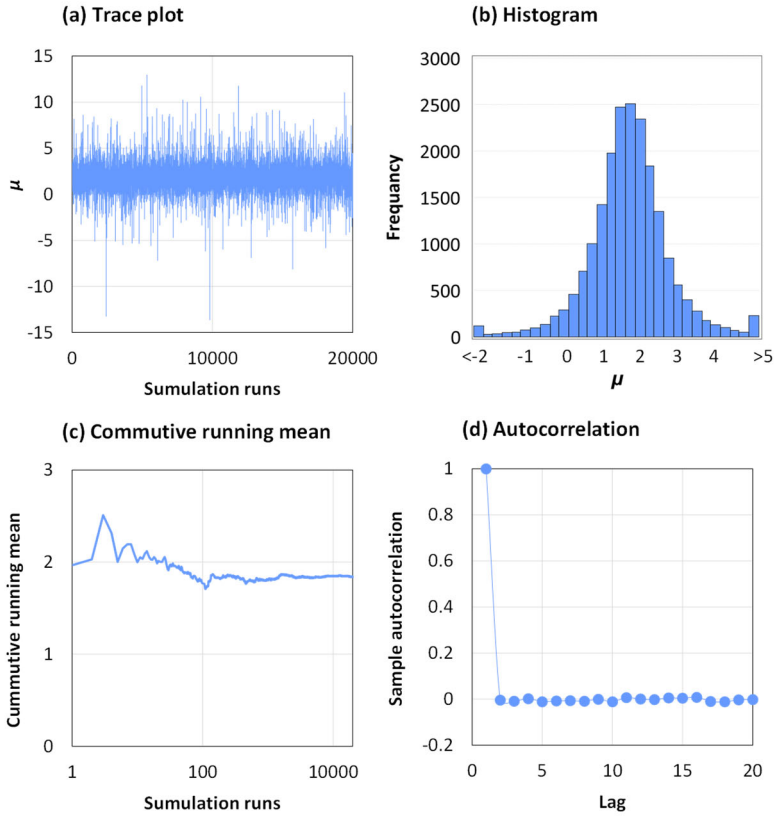

Sensitivity of the BHM to some alternative non-informative priors

The hyperprior distributions of contaminant concentration in soil and earthworm are:

$$\mu_{..} \sim N(m_{..}, s_{..}^2)$$
$$\sigma_{.j}^2 \sim IG(a_{.j}, b_{.j})$$
$$\tau_{..}^2 \sim IG(c_{..}, d_{..})$$

The hyperprior distribution for the grand mean is assumed to be normal distribution with mean, $m_{..}$, and variance, $s_{..}^2$. The hyperprior for within-plot variance and between-plot variance are inverse-gamma distributions with parameters $a_{.j}$ and $b_{.j}$, $c_{..}$ and $d_{..}$, respectively.

The *standard prior* is defined as P_0, which refers to $m_{..} = 0, s_{..}^2 = 10000$ and $a_{.j} = b_{.j} = c = d = 0.001$ and can be expressed as:

$$P_0: \begin{cases} \mu_{..} \sim N(0,10000) \\ \sigma_{.j}^2 \sim IG(0.001,0.001) \\ \tau_{..}^2 \sim IG(0.001,0.001) \end{cases}$$

This non-informative prior is usually used in BHM applications (Qian et al., 2004; Azim et al., 2011). However, if the model estimation is sensitive to different non-informative priors, the model estimations of a parameter are could be significantly different and not reliable. Therefore, sensitivity of model estimation was tested by applying different priors. Here we propose four alternative non-informative priors:

(1) $a_{.j}$, $b_{.j}$, $c_{..}$ and $d_{..}$ decreased from 0.001 to 0.0001 (10 times decrease) while $m_{..}$ and $s_{..}^2$ stay unchanged. This prior is defined as P_1, and it can be expressed as:

$$P_1: \begin{cases} \mu_{..} \sim N(0,10000) \\ \sigma_{.j}^2 \sim IG(0.0001,0.0001) \\ \tau_{..}^2 \sim IG(0.0001,0.0001) \end{cases}$$

(2) $a_{.j}$, $b_{.j}$, $c_{..}$ and $d_{..}$ increased from 0.001 to 0.01 (10 times increase) while $m_{..}$ and $s_{..}^2$ stay unchanged. This prior is defined as P_2, and it can be expressed as:

$$P_2: \begin{cases} \mu_{..} \sim N(0,10000) \\ \sigma_{.j}^2 \sim IG(0.01,0.01) \\ \tau_{..}^2 \sim IG(0.01,0.01) \end{cases}$$

(3) $m_{..}$ and $s_{..}^2$ decreased from 10000 to 1000 (10 times decrease) while $a_{.j}$, $b_{.j}$, $c_{..}$ and $d_{..}$ stay unchanged. This prior is defined as P_3, and it can be expressed as:

$$P_3: \begin{cases} \mu_{..} \sim N(0,1000) \\ \sigma_{.j}^2 \sim IG(0.001,0.001) \\ \tau_{..}^2 \sim IG(0.001,0.001) \end{cases}$$

(4) $m_{..}$ and $s_{..}^2$ increased from 10000 to 100000 (10 times increase) while $a_{.j}$, $b_{.j}$, $c_{..}$ and $d_{..}$ stay unchanged. This prior is defined as P_4, and it can be expressed as:

$$P_4: \begin{cases} \mu_{..} \sim N(0,100000) \\ \sigma_{.j}^2 \sim IG(0.001,0.001) \\ \tau_{..}^2 \sim IG(0.001,0.001) \end{cases}$$

Each parameter was estimated three times by three independent MCMC chains to evaluate convergence of the simulation. Then, three estimations of a parameter by one prior was compared with the estimations by other priors. Since group mean is the key parameter for estimation, θ_{sj} and θ_{ej} were investigated (θ_{sj} and θ_{ej} refers to group means of log-transformed soil and earthworm concentration of the j-th plot). The results of estimation of θ_{sj} and θ_{ej} by different priors are shown in **SI Figure 5-6**. It shows that:

(1) Standard deviation is very small for estimation of each parameter, so convergence was reached.

(2) The model results by the four difference priors give the similar estimation of the same parameter, so the model was not sensitive to alternative non-informative priors

SI Figure 5-6 Histogram of percent difference of different priors
Histogram was based on the whole dataset, where n = 448. P_1~P_4 are different priors defined in the text.

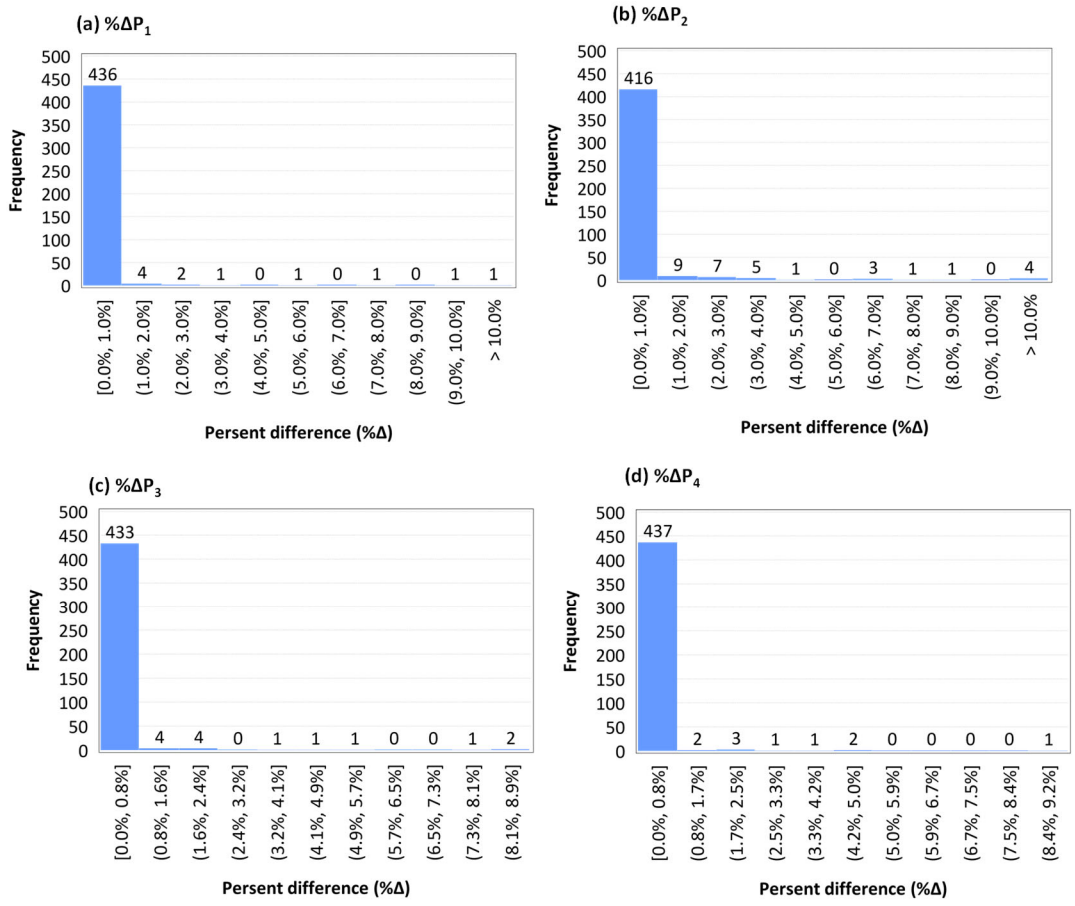

SI Table 5-4 Summary of difference of model performance. Differences of $NMSE$, $\sqrt{NMSE}$, AIC and BIC between two models were calculated by "ANOVA" minus "BHM":$\Delta NMSE = NMSE_{\text{ANOVA}} - NMSE_{\text{BHM}}$; $\Delta\sqrt{NMSE} = \sqrt{NMSE}_{\text{ANOVA}} - \sqrt{NMSE}_{\text{BHM}}$; $\Delta AIC = AIC_{\text{ANOVA}} - AIC_{\text{BHM}}$; $\Delta BIC = BIC_{\text{ANOVA}} - BIC_{\text{BHM}}$, where subscript refers to the model. According to the definitions of these statistics, if the difference is negative, then ANOVA model has better predictive accuracy; if the difference is positive, then BHM has better predictive accuracy. p values are shown in the bracket below. Significant difference was determined based on results of $\alpha = 0.05$.

	DDx		Dieldrin	
Medium	Soil	Earthworm	Soil	Earthworm
$NMSE$	0.00766 (0.311)	-0.00239 (0.417)	0.00720 (0.202)	-0.00402 (0.645)
$\sqrt{NMSE}$	0.00423 (0.401)	-0.00253 (0.470)	0.00550 (0.319)	-0.00184 (0.742)
AIC	87.30 (< 0.001)	98.67 (< 0.001)	-1.81 (0.626)	51.25 (< 0.001)
BIC	73.37 (< 0.001)	86.04 (< 0.001)	-14.66 (0.002)	52.05 (< 0.001)
Preferred model	**BHM**	**BHM**	**ANOVA**	**BHM**

SI Table 5-5 Summary of data points of high influence. C_o refers to observed concentration (μg/g d.w.); $C_{p|ANOVA}$ refers to out-of-sample ANOVA model predicted concentration (μg/g d.w.); $C_{p|BHM}$ refers to out-of-sample BHM predicted concentration (μg/g d.w.); AVG' refers to average concentration of other subplots of sub-dataset (μg/g d.w.).

Plot	Contaminant	Medium	Time	Treatment	Label	C_o	$C_{p\|OAM}$	$C_{p\|BHM}$	AVG'
3	DDx	soil	T6	No Till	α	21.48	36.83	24.62	8.90
3	DDx	soil	T6	No Till	β	16.45	39.35	29.21	8.90
3	DDx	soil	T6	No Till	γ	57.22	18.96	18.34	8.90
3	Dieldrin	soil	T6	No Till	δ	2.43	0.86	0.84	0.76
3	Dieldrin	soil	T6	No Till		0.96	1.59	1.14	0.76
3	Dieldrin	soil	T6	No Till		0.75	1.70	1.35	0.76
3	Dieldrin	soil	T6	Till	ε	2.24	0.80	0.80	0.73
3	Dieldrin	soil	T6	Till		0.79	1.53	1.17	0.73
3	Dieldrin	soil	T6	Till		0.82	1.52	1.14	0.73
3	Dieldrin	soil	T6	4M	ζ	2.13	0.74	0.74	0.65
3	Dieldrin	soil	T6	4M		0.74	1.43	1.03	0.65
3	Dieldrin	soil	T6	4M		0.73	1.44	1.04	0.65

SI Figure 5-7 Scatter plot of mean and standard deviation of coefficient of variation

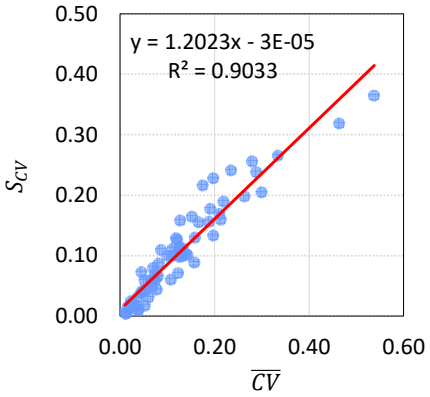

Discussion of positive correlation between mean and standard deviation of coefficient of variation

As discussion in **Section 2.7** in manuscript, for a given contaminant and given medium combination, there are 4 × 4 = 16 sub-datasets (four sampling times and four treatments). *k* was defined as the index of each sub-dataset, and *k* = 1,2,3…16. For a given sub-dataset, *k* , sub-dataset, coefficient of variation (*CV*) of the *j*-th plot is defined as:

$$CV_{kj} = \frac{\sigma_{kj}}{\mu_{kj}}$$

where μ_{kj} and σ_{kj} are the mean and standard deviation of the *j*-th subplot (*j* = 1,2,3,4,5,6,7) of the *k*-th sub-dataset. Then, for a given sub-dataset, the average CV_j's of the seven plots is calculated, which represents the average relative observational error of the sub-dataset. The average CV of the *k*-th sub-dataset, noted as $\overline{CV}_k$, is calculated by:

$$\overline{CV}_k = \frac{1}{J}\sum_{j=1}^{J} CV_{kj}$$

where *J* is the total number of subplots, and *J* = 7 for current experiment.

Standard deviation of CV, noted as S_{CV}, is the standard deviation of the CV_j values, which is defined by:

$$S_{CV_k} = \sqrt{\frac{\sum_{j=1}^{J}\left(CV_{kj} - \overline{CV}_k\right)^2}{J-1}}$$

Then, the relation between $\overline{CV}_k$ and S_{CV_k} (*k* = 1, 2, 3…16) is investigated.

Define $\bar{X}$ as mean, S as standard deviation, and n as sample size. We have:

$$S_{CV_k} = \sqrt{\frac{\sum_{j=1}^{J}\left(CV_{kj} - \overline{CV}_k\right)^2}{J-1}}$$

$$\Rightarrow (J-1){S_{CV_k}}^2 = \sum_{j=1}^{J}\left(CV_{kj} - \overline{CV}_k\right)^2$$

$$= \sum_{j=1}^{J}\left(CV_{kj} + {\overline{CV}_k}^2 - 2CV_{kj}\overline{CV}_k\right)$$

$$= \sum_{j=1}^{J} CV_{kj}^2 + J{\overline{CV}_k}^2 - 2\overline{CV}_k\sum_{j=1}^{J} CV_{kj} \qquad \because \left(\sum_{j=1}^{J} CV_{kj} = J\overline{CV}_k\right)$$

$$\Rightarrow (J-1){S_{CV_k}}^2 = J{\overline{CV}_k}^2 - 2J{\overline{CV}_k}^2 + \sum_{j=1}^{J} CV_{kj}^2$$

$$\Rightarrow (J-1){S_{CV_k}}^2 = -J{\overline{CV}_k}^2 + \sum_{j=1}^{J} CV_{kj}^2 \qquad \text{Eqn. A}$$

$$\because \left(\sum_{j=1}^{J} CV_{kj}\right)^2 = \sum_{j=1}^{J} CV_{kj}^2 + 2\sum_{j=1}^{J}\sum_{i=1}^{j-1} CV_{ki}CV_{kj}$$

$$\Rightarrow \left(\frac{1}{J}\sum_{j=1}^{J} CV_{kj}\right)^2 = \frac{1}{J^2}\left(\sum_{j=1}^{J} CV_{kj}^2 + 2\sum_{j=1}^{J}\sum_{i=1}^{j-1} CV_{ki}CV_{kj}\right)$$

$$\Rightarrow \overline{CV}_k{}^2 = \frac{1}{J^2}\sum_{j=1}^{J} CV_{kj}^2 + \frac{2}{J^2}2\sum_{j=1}^{J}\sum_{i=1}^{j-1} CV_{ki}CV_{kj}$$

$$\Rightarrow \sum_{j=1}^{J} CV_{kj}^2 = J^2\overline{CV}_k{}^2 - 2\sum_{j=1}^{J}\sum_{i=1}^{j-1} CV_{ki}CV_{kj} \qquad \text{Eqn. B}$$

Then, combine **Eqn. A** and **Eqn. B**, we have:

$$(J-1)S_{CV_k}{}^2 = -J\overline{CV}_k{}^2 + J^2\overline{CV}_k{}^2 - 2\sum_{j=1}^{J}\sum_{i=1}^{j-1} CV_{ki}CV_{kj}$$

$$= J(J-1)\overline{CV}_k{}^2 - 2\sum_{j=1}^{J}\sum_{i=1}^{j-1} CV_{ki}CV_{kj}$$

$$\Rightarrow S_{CV_k}{}^2 = J\overline{CV}_k{}^2 - \frac{2}{J-1}\sum_{j=1}^{J}\sum_{i=1}^{j-1} CV_{ki}CV_{kj}$$

$$\Rightarrow S_{CV_k} = \sqrt{J\overline{CV}_k{}^2 - \frac{2}{J-1}\sum_{j=1}^{J}\sum_{i=1}^{j-1} CV_{ki}CV_{kj}}$$

$$\therefore S_{CV_k}(\overline{CV}_k) = \sqrt{J\overline{CV}_k{}^2 - \frac{2}{J-1}\sum_{j=1}^{J}\sum_{i=1}^{j-1} CV_{ki}CV_{kj}}$$

$$\Rightarrow \frac{\partial S_{CV_k}}{\partial \overline{CV}_k} = \frac{J\overline{CV}_k}{\sqrt{J\overline{CV}_k{}^2 - \frac{2}{J-1}\sum_{j=1}^{J}\sum_{i=1}^{j-1} CV_{ki}CV_{kj}}}$$

$\therefore \overline{CV}_k$ and S_{CV_k} are mean and standard of deviation of coefficient of variance of concentration data

$\Rightarrow \overline{CV}_k > 0$, and $J > 1$

$$\Rightarrow \frac{\partial S_{CV_k}}{\partial \overline{CV}_k} > 0$$

$\Rightarrow S_{CV_k}(\overline{CV}_k)$ increases with $\overline{CV}_k$

Therefore, S_{CV_k} and $\overline{CV}_k$ of CV_{kj} are positively correlated.

Discussion of average CV versus model performance statistics

For DDx concentration in soil, $NMSE$ and $\sqrt{NMSE}$ increased with $\overline{CV}$ (**SI Figure 5-7a, 5-7b**), which indicates that predictive accuracy decreases with decreased precision of data. In addition, regression lines of the two models are indistinguishable, which is consistent with **SI Table 5-4**. *AIC* and *BIC* of both models increase with $\overline{CV}$ (**SI Figure 5-7c and 5-7d**), which indicates that predictive error increases with observational uncertainty. Furthermore, the slopes of the BHM regression line are smaller than the slopes of regression lines of the ANOVA model, which shows that the variability of data has a greater negative impact on the ANOVA model while the BHM are relatively robust. In addition, for both *AIC* and *BIC*, the regression lines of the ANOVA model are consistently above the regression lines of the BHM, which indicates that the BHM has smaller predictive errors. In terms of the difference, the slopes of regression lines of $\Delta NMSE$ and $\Delta\sqrt{NMSE}$ are significantly greater than zero (**SI Figure 5-8a and 5-8b**), which suggest that as observational uncertainty increases, the BHM is the preferred model for increasing predictive accuracy. The slopes and intercept of ΔAIC and ΔBIC are both significantly greater than zero (**SI Figure 5-8c and 5-8d**), which also suggests such advantage increases with lowered precision of the data.

In terms of DDx concentration in earthworm, the patterns of $NMSE$, $\sqrt{NMSE}$, *AIC* and *BIC* versus $\overline{CV}$ appear to be similar as DDx concentration in soil (**SI Figure 5-9**). However, the differences show different patterns. None of the regression parameters of $\Delta NMSE$ or $\Delta\sqrt{NMSE}$ are significantly different from zero (**SI Figure 5-10a** and **5-10b**), which suggests that the two models are indistinguishable. The slopes of ΔAIC and ΔBIC are not significantly different from zero, but intercepts are significantly greater than zero (**SI Figure 5-10c** and **5-10d**), which suggests that ΔAIC and ΔBIC of the BHM are consistently smaller, and the BHM is the preferred model (**SI Table 5-4)**.

For dieldrin concentration in soil, the patterns of $NMSE$, $\sqrt{NMSE}$ are the same as DDx concentration in soil (**SI Figure 5-11a** and **5-11b**). For AIC (**SI Figure 5-11c**), it shows that as $\overline{CV} > 0.17$, *AIC* of the BHM is smaller while as $\overline{CV} < 0.17$, *AIC* of the ANOVA model is smaller. This result suggests that for data with better precision, the ANOVA model appears to have smaller predictive error while for data with lower precision, the BHM appears to have smaller predictive error instead. For *BIC* (**SI Figure 5-11d**), it has similar pattern with *AIC*, but the intersection becomes $\overline{CV} = 0.37$, showing that for data with larger observational uncertainty, the BHM is more likely to have smaller predictive errors. In terms of the differences, $\Delta NMSE$ shows *increasingly* better performance of the BHM (**SI Figure 5-12a**) while ΔBIC shows *consistently* better performance of the BHM (**SI Figure 5-12d**). On the other hand, none of the regression parameters of $\Delta NMSE$ or ΔAIC is significantly different from zero, which indicates identical performance (**SI Figure 5-12a** and **5-12b**).

For dieldrin concentration in earthworm, the patterns of $NMSE$, $\sqrt{NMSE}$ are the same as DDx concentration in soil (**SI Figure 5-13a** and **5-13b**). For AIC (**SI Figure 5-13c**), it shows that the regression line of AIC of the BHM is consistently below the regression line of the ANOVA model, which indicates that BHM has smaller predictive errors. In addition, the slope of regression line of *AIC* of the BHM is smaller, which suggests that variability of the data has smaller negative impact on the BHM. For BIC (**SI Figure 5-13d**), it shows that the *BIC* of the BHM is smaller when $\overline{CV} < 0.45$ while *BIC* of the ANOVA model is smaller when $\overline{CV} > 0.45$. However, the scatter plot (**SI Figure 5-13d**) shows that the points of the ANOVA model may not be linearly correlated. Thus, for either small $\overline{CV}$

($\overline{CV} < 0.22$) or large $\overline{CV}$ ($\overline{CV} > 0.41$), BHM appears to have smaller predictive errors. More data are needed to confirm this relation. The corresponding regression parameters of $\Delta NMSE$ and $\Delta\sqrt{NMSE}$ are all not significantly different from zero (**SI Figure 5-14a** and **5-14b**), showing identical performance. On the other hand, the intercepts of ΔAIC and ΔBIC are significantly greater than zero with slope that is not significantly different from zero, showing that the BHM is preferred.

SI Figure 5-8 Scatter plot of $\overline{CV}$ versus $NMSE$, $\sqrt{NMSE}$, AIC and BIC of DDx concentration in soil. Solid lines are linear regression lines. The underlined numbers are not significantly different from zero ($p > 0.05$).

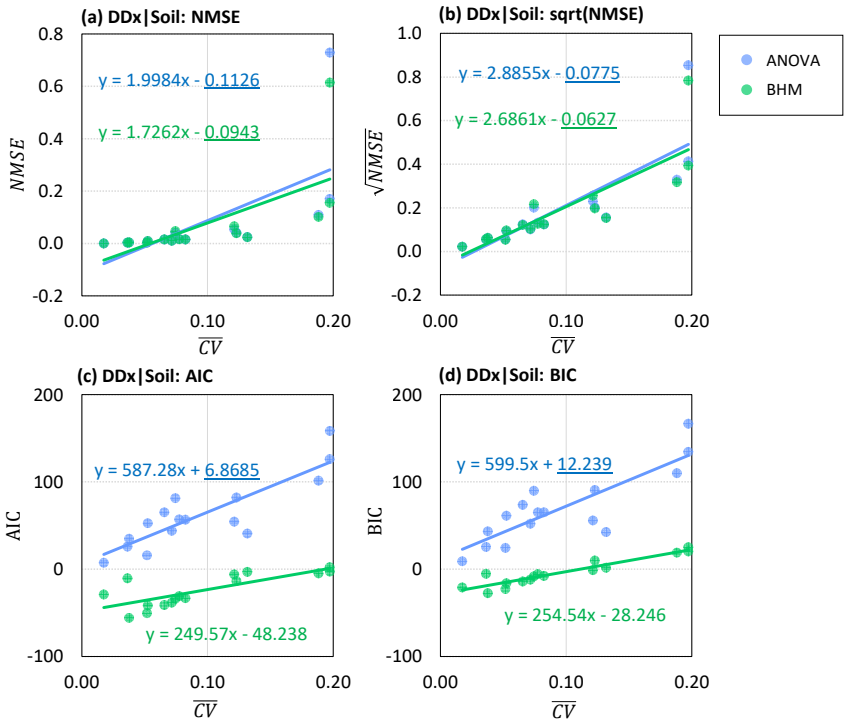

SI Figure 5-9 Scatter plot of $\overline{CV}$ versus $\Delta NMSE$ and $\Delta\sqrt{NMSE}$, ΔAIC and ΔBIC of DDx concentration in soil. Solid lines are linear regression lines. The underlined numbers are not significantly different from zero ($p > 0.05$).

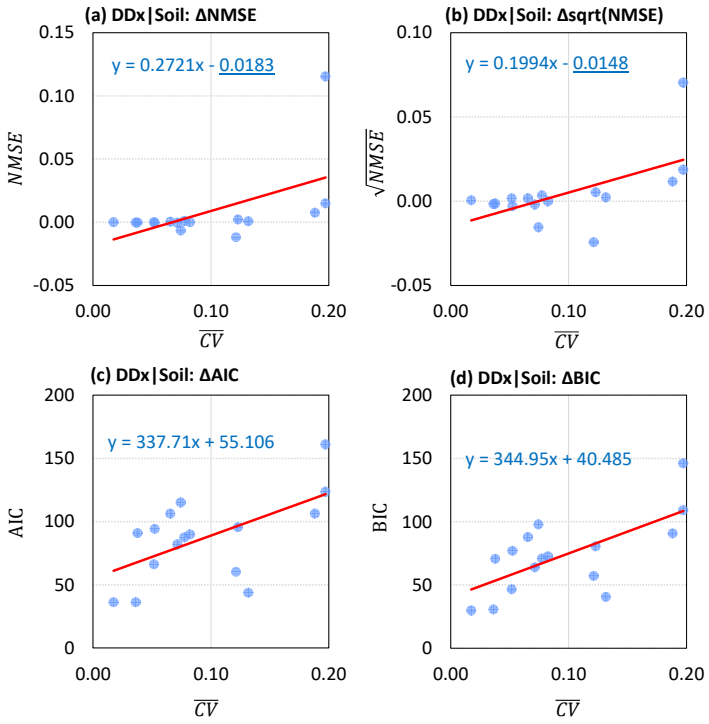

SI Figure 5-10 Scatter plot of $\overline{CV}$ versus $NMSE$, $\sqrt{NMSE}$, AIC and BIC of DDx concentration in earthworm. Solid lines are linear regression lines. The underlined numbers are not significantly different from zero ($p > 0.05$).

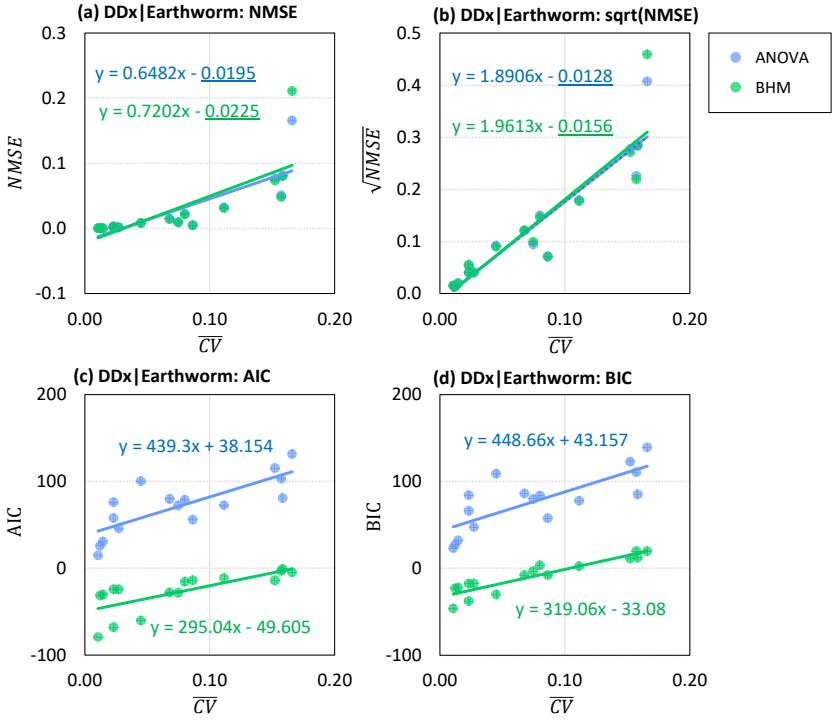

SI Figure 5-11 Scatter plot of $\overline{CV}$ versus $\Delta NMSE$ and $\Delta\sqrt{NMSE}$, ΔAIC and ΔBIC of DDx concentration in earthworm.
Solid lines are linear regression lines. The underlined numbers are not significantly different from zero ($p > 0.05$).

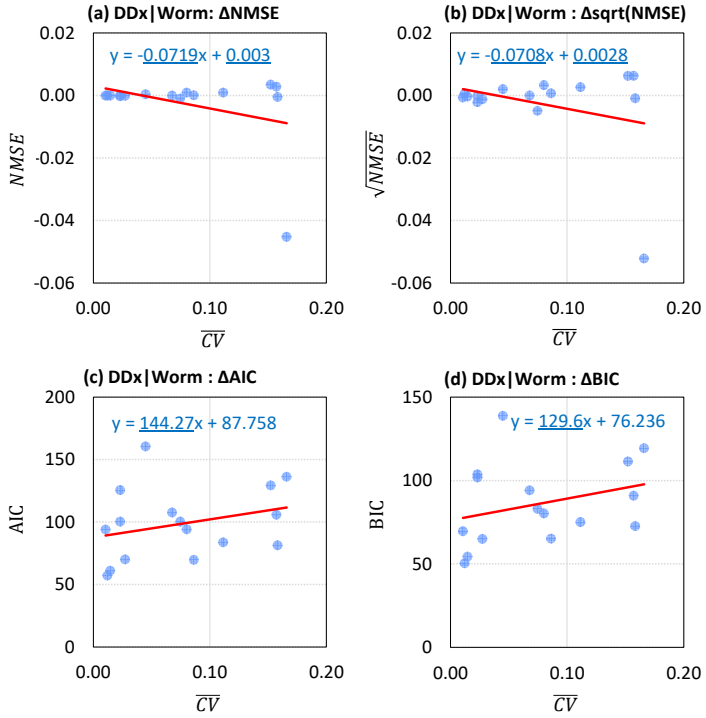

SI Figure 5-12 Scatter plot of $\overline{CV}$ versus $NMSE$, $\sqrt{NMSE}$, AIC and BIC of dieldrin concentration in soil. Solid lines are linear regression lines. The underlined numbers are not significantly different from zero ($p > 0.05$).

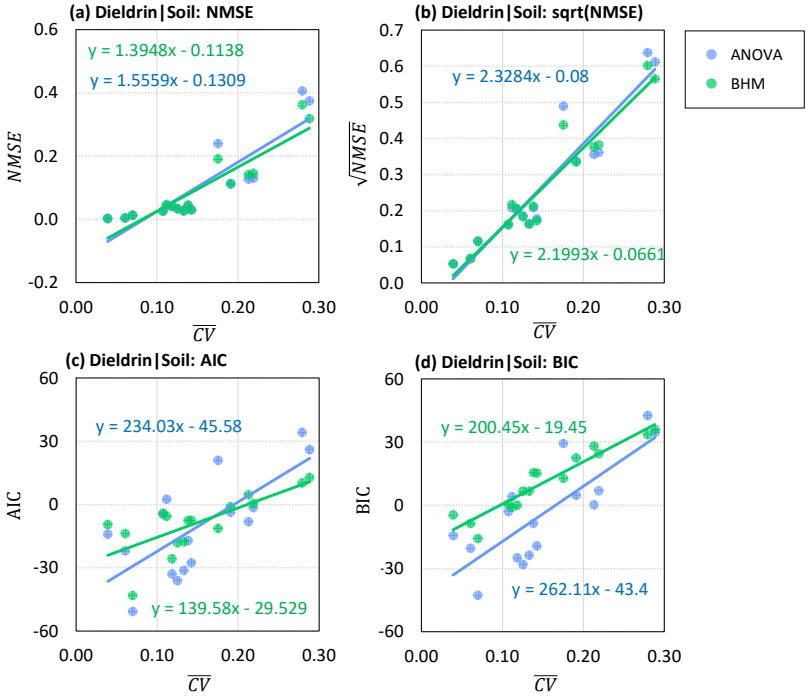

SI Figure 5-13 Scatter plot of $\overline{CV}$ versus $\Delta NMSE$ and $\Delta\sqrt{NMSE}$, ΔAIC and ΔBIC of dieldrin concentration in soil. Solid lines are linear regression lines. The underlined numbers are not significantly different from zero ($p > 0.05$).

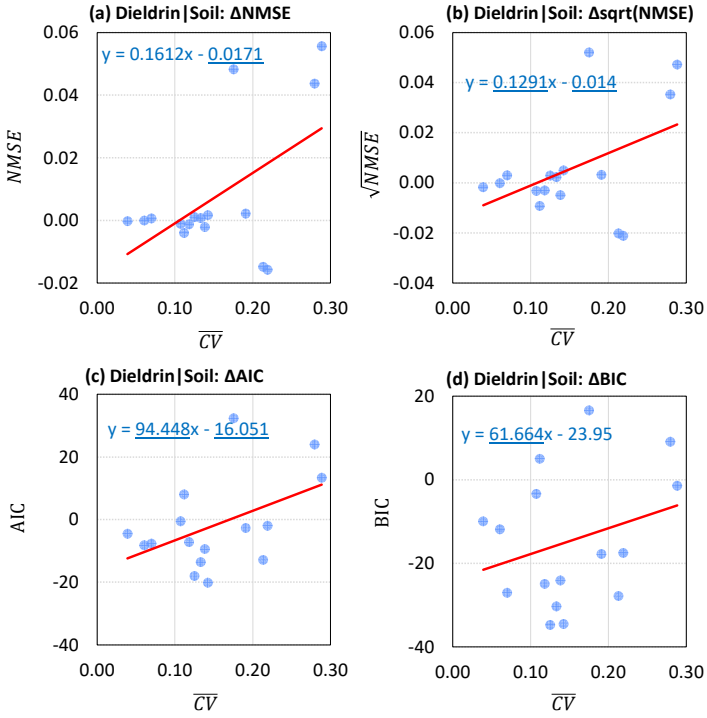

SI Figure 5-14 Scatter plot of $\overline{CV}$ versus $NMSE$, $\sqrt{NMSE}$, AIC and BIC of dieldrin concentration in earthworm. Solid lines are linear regression lines. The underlined numbers are not significantly different from zero ($p > 0.05$).

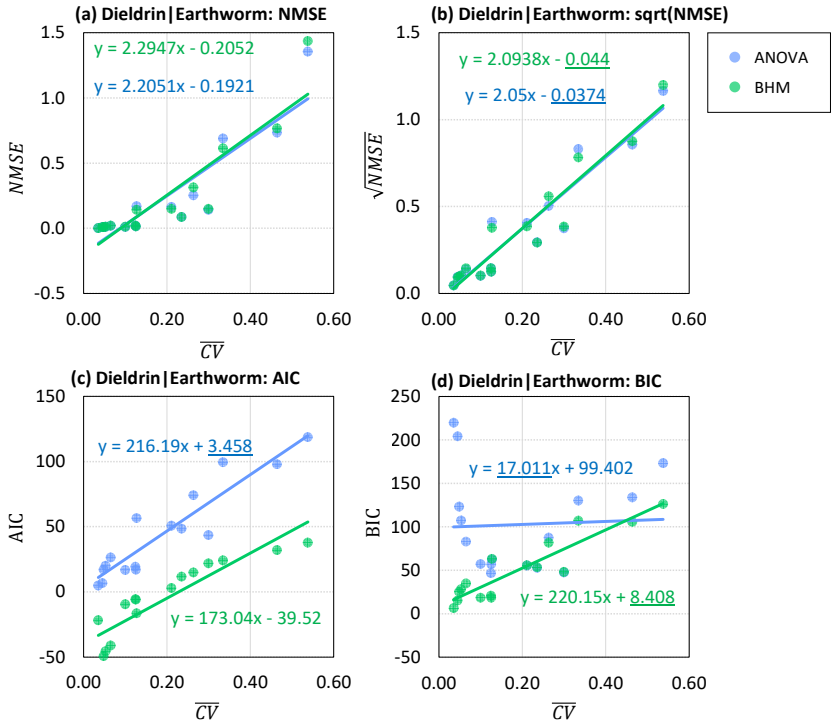

SI Figure 5-15 Scatter plot of $\overline{CV}$ versus $\Delta NMSE$ and $\Delta\sqrt{NMSE}$, ΔAIC and ΔBIC of dieldrin concentration in earthworm. Solid lines are linear regression lines. The underlined numbers are not significantly different from zero ($p > 0.05$).

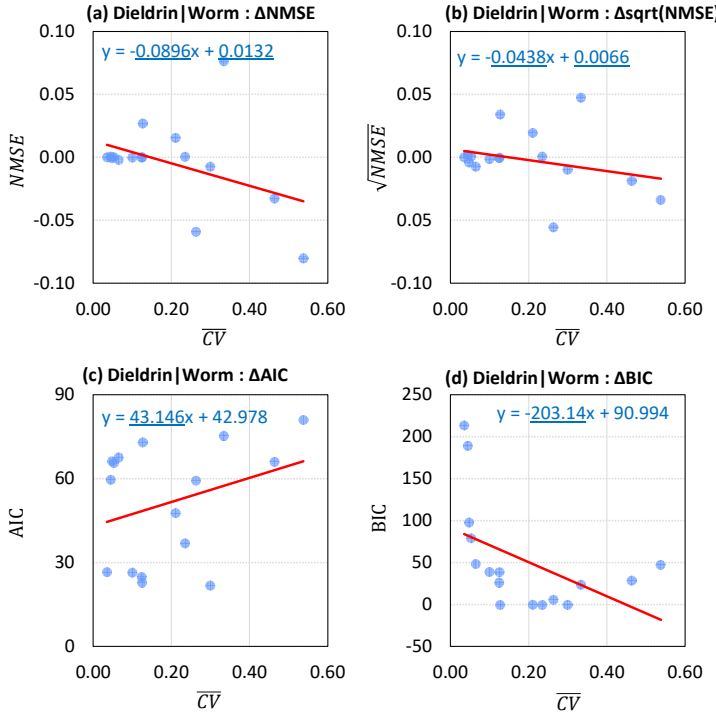

SI Figure 5-16 Plots of normalized log-transformed *BAF* of DDx. Error bar refers to upper and lower end of 95% highest posterior density (HPD). Different letters refer to statistical difference ($p < 0.05$)

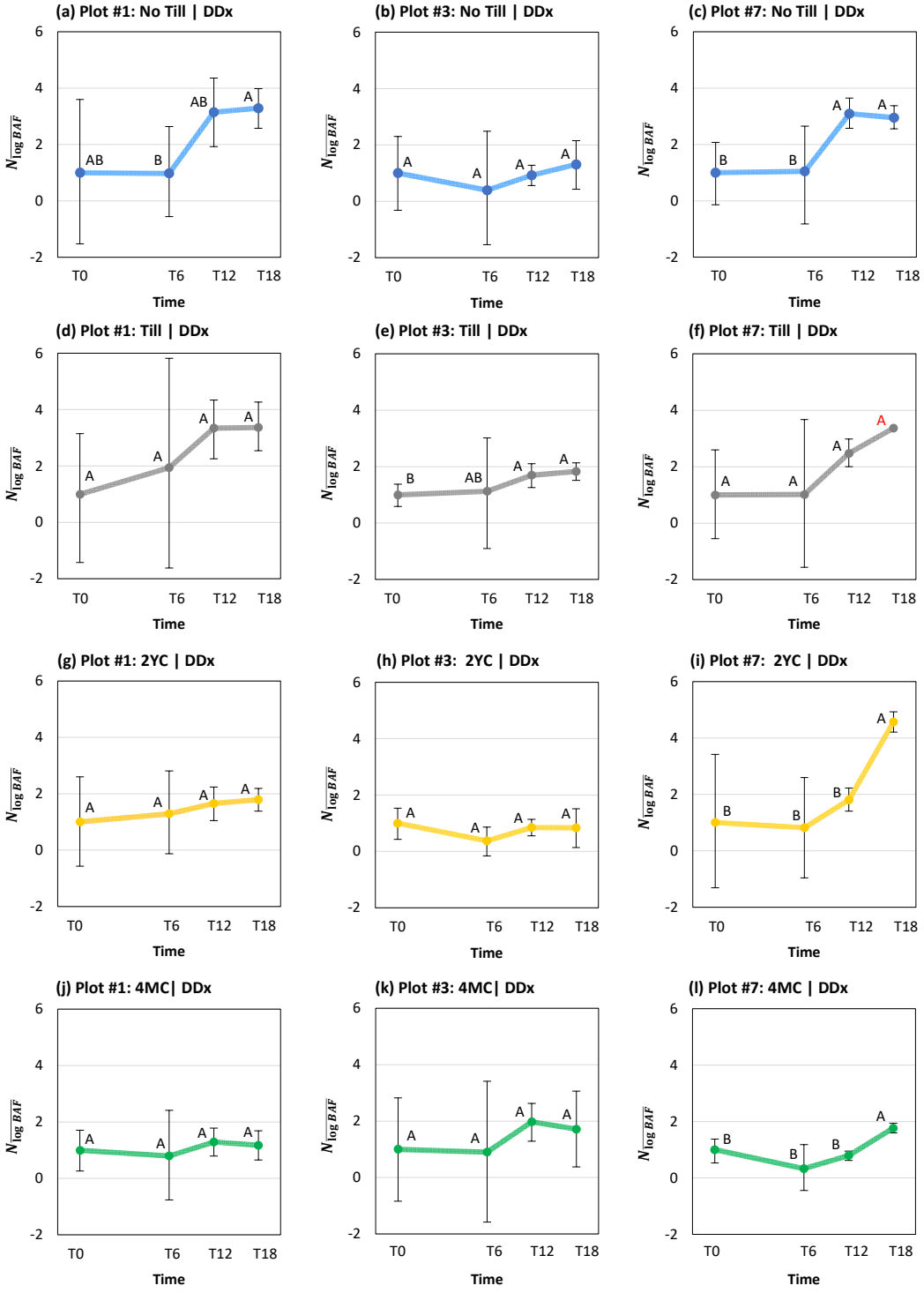

SI Figure 5-17 Plots of normalized log-transformed *BAF* of dieldrin. Error bar refers to upper and lower end of 95% highest posterior density (HPD). Different letters refer to statistical difference ($p < 0.05$)

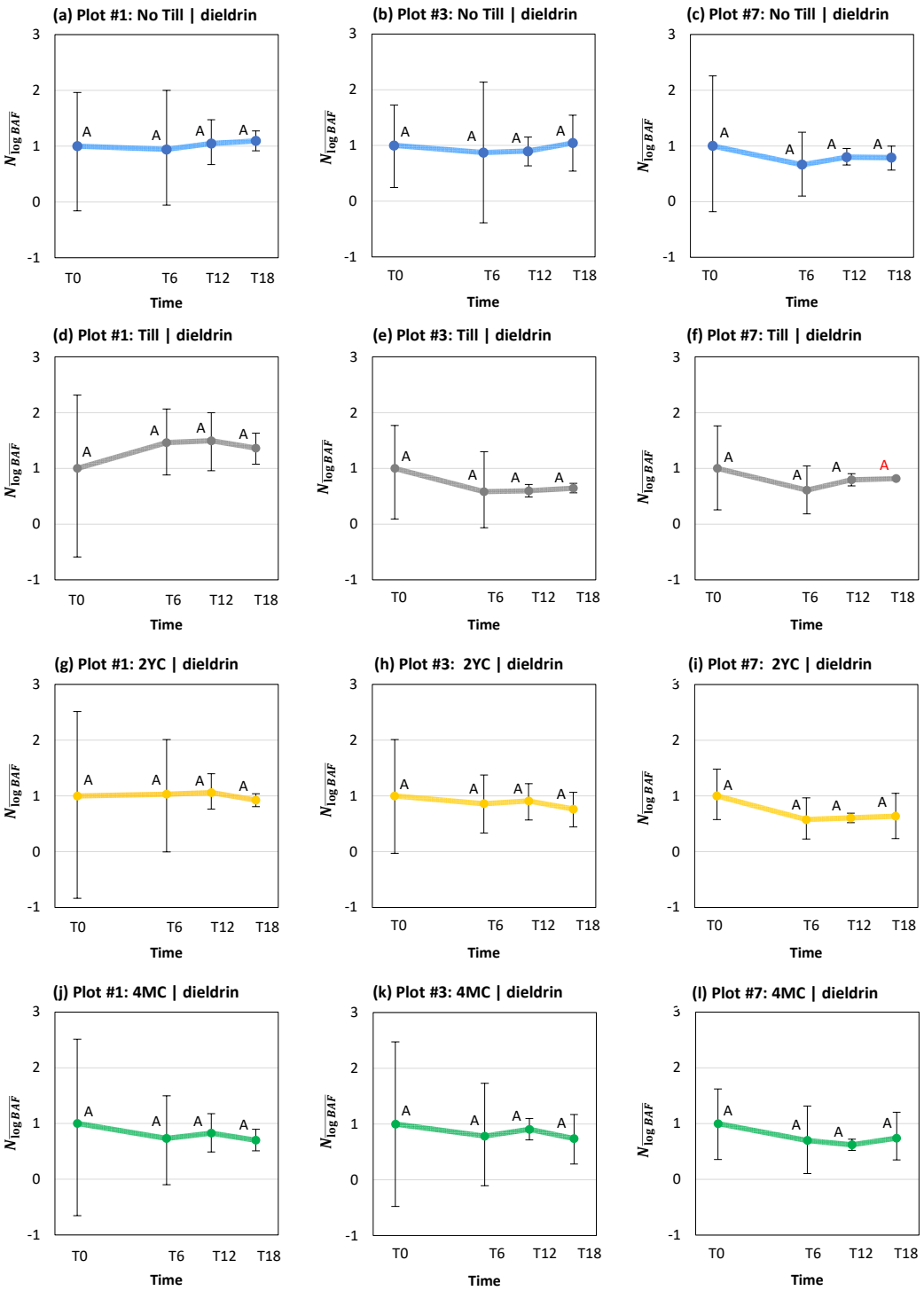

SI Figure 5-18 Plots of change in normalized log-transformed *BAF* of DDx. Error bar refers to upper and lower end of 95% highest posterior density (HPD). N refers to no significant difference, I refers to significant increase, and R refers to significant reduce ($p < 0.05$).

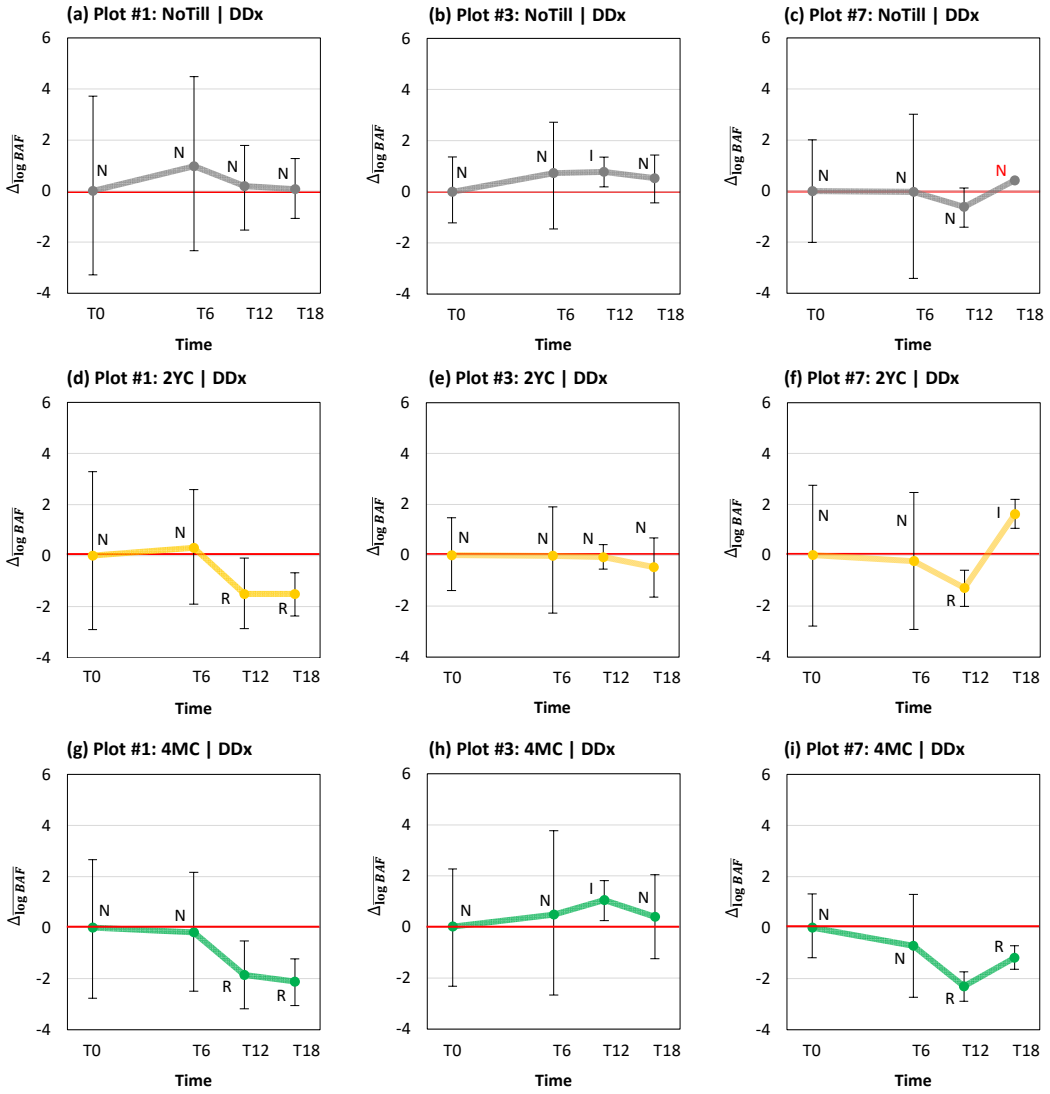

SI Figure 5-19 Plots of change in normalized log-transformed *BAF* of dieldrin.
Error bar refers to upper and lower end of 95% highest posterior density (HPD). N refers to no significant difference, I refers to significant increase, and R refers to significant reduce ($p < 0.05$).

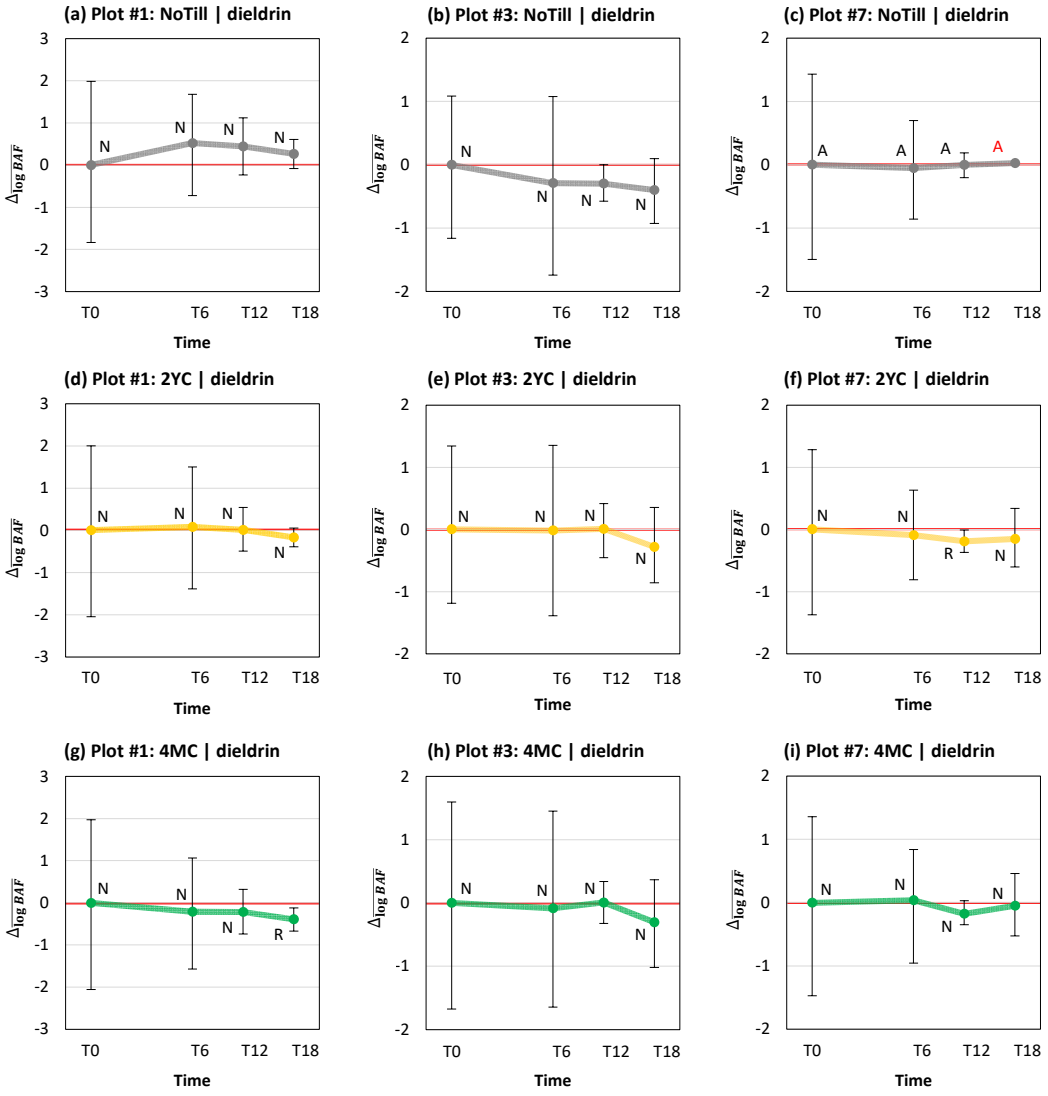

Bibliography

Abdel-Rahman, A.A., 2008. On the atmospheric dispersion and Gaussian plume model. In Proceedings of the 2nd International Conference on Waste Management, Water Pollution, Air Pollution, Indoor Climate. Mastrorakis, N.E., Poulos, M., Mladenov, V., Bojkovic, Z., Simian, D., Kartalopoulos, S., Varonides, A., Udriste, C., Eds. World Scientific and Engineering Academy Press, World Scientific and Engineering Academy and Society, pp. 31-39.

Adrizal, A., Paul H. Patterson, Ralph Michael Hulet, Ricky M. Bates, C. A. B. Myers, G. P. Martin, R. L. Shockey, M. Van der Grinten, D. A. Anderson, and Janette R. Thompson., 2008. Vegetative buffers for fan emissions from poultry farms: 2. ammonia, dust and foliar nitrogen. Journal of Environmental Science and Health, Part B 43, no. 1 (2008): 96-103.

Aelion, C.M., Davis, H.T., Liu, Y., Lawson, A.B. and McDermott, S., 2009. Validation of Bayesian kriging of arsenic, chromium, lead, and mercury surface soil concentrations based on internode sampling. Environmental science & technology, 43(12), pp.4432-4438.

Agassi, M., Hadas, A., Benyamini, Y., Levy, G.J., Kautsky, L., Avrahamov, L. and Zhevelev, H., 1998. Mulching effects of composted MSW on water percolation and compost degradation rate. Compost Science & Utilization, 6(3), pp.34-41.

Allen, R.G., Walter, I.A., Elliot, R.L., Howell, T.A., Itenfisu, D., Jensen, M.E., Synder, R.L., Eds., 2005. The ASCE Standardized Reference Evapotranspiration Equation. Technical Committee on Standardization of Reference Evapotranspiration. American Society of Civil Engineers, Reston, Virginia, USA. 59 pp.

Anderson, J. D., Wendt, J., 1995. Computational Fluid Dynamics (Vol. 206). New York: McGraw-Hill.

Anderson, O. M., Yang, Z., Hapeman, C. J., Torrents, A., Green, C., Jackson, D. Bioavailability Assessment of Historical Organochlorine Pesticide Residues: Feasibility of Carbon Amendments as Remediation Techniques Under Field Conditions. Environmental pollution **(Under preparation)**

Aneja, V.P., Schlesinger, W.H., Erisman, J.W., 2008. Farming pollution. Nat. Geosci. 1(7):409.

Akaike, H.,1974. A new look at the statistical model identification. IEEE transactions on automatic control, 19(6), 716-723.

Alexander, M., 2000. Aging, Bioavailability, and Overestimation of Risk from Environmental Pollutants. Environ. Sci. Technol. 34, 4259–4265.

Arhonditsis, G.B., Qian, S.S., Stow, C.A., Lamon, E.C. and Reckhow, K.H., 2007. Eutrophication risk assessment using Bayesian calibration of process-based models: application to a mesotrophic lake. ecological modelling, 208(2-4), pp.215-229.

Arystanbekova, N.K., 2004. Application of Gaussian plume models for air pollution simulation at instantaneous emissions. Math. Comput. Simul. 67(4):451-458.

Asman, W.A., 2001. Modelling the atmospheric transport and deposition of ammonia and ammonium: an overview with special reference to Denmark. Atmos. Environ. 35(11):1969-1983.

Atteia, O., Estrada, E.D.C. and Bertin, H., 2013. Soil flushing: a review of the origin of efficiency variability. Reviews in Environmental Science and Bio/Technology, 12(4), pp.379-389.

Azarov, A. V., Zhukova, N. S., & Antonov, F. G., 2017. Water-spray systems reducing negative effects of fine-dispersion dust at operator's workplaces of machine-building industries. Procedia Engineering, 206, 1407-1414.

Azim, M.E., Kumarappah, A., Bhavsar, S.P., Backus, S.M. and Arhonditsis, G., 2011. Detection of the spatiotemporal trends of mercury in Lake Erie fish communities: a Bayesian approach. Environmental science & technology, 45(6), pp.2217-2226.

Banerjee, S., Carlin, B.P. and Gelfand, A.E., 2014. Hierarchical modeling and analysis for spatial data. CRC press.

Bairy, J., 2013. Modeling of Particulate Matter Emissions from Agricultural Operations (Doctoral dissertation).

Begon, M., Townsend, C.R. and Harper, J.L., 2006. Ecology: from individuals to ecosystem*s* (No. Sirsi) i9781405111171).

Behera, S.N., Sharma, M., Aneja, V.P., Balasubramanian, R., 2013. Ammonia in the atmosphere: a review on emission sources, atmospheric chemistry and deposition on terrestrial bodies. Environ. Sci. Pollut. Res. 20(11):8092-8131.

Belt, S.V., 2015. Plants tolerant of poultry farm emissions in the Chesapeake Bay watershed; Maryland Plant Materials Final Report; USDA-NRCS Norman A. Berg National Plant Materials Center: Beltsville, MD. Available at https://www.nrcs.usda.gov/Internet/FSE_PLANTMATERIALS/publications/mdpmcsr12671.pdf (Accessed March 20, 2020).

Beyer, W. N., Gale, R. W., 2013. Persistence and changes in bioavailability of dieldrin, DDE, and heptachlor epoxide in earthworms over 45 years. Ambio, 42(1), 83-89.

Billoir, E., Delignette-Muller, M.L., Péry, A.R. and Charles, S., 2008. A Bayesian approach to analyzing ecotoxicological data. Environmental science & technology, 42(23), pp.8978-8984.

Bonifacio, H. F., Maghirang, R. G., Razote, E. B., Trabue, S. L., Prueger, J. H., 2013. Comparison of AERMOD and WindTrax dispersion models in determining PM10 emission rates from a beef cattle feedlot. Journal of the Air & Waste Management Association, 63(5), 545-556.

Bowers, Teresa S., Neil S. Shifrin, and Brian L. Murphy., 1996. Statistical approach to meeting soil cleanup goals. Environmental science & technology 30, no. 5 (1996): 1437-1444.

Boykin, J. C., Buser, M. D., Whitelock, D. P., Holt, G. A., 2013a. Combined mote system PM2. 5 emission factors and rates for cotton gins: Method 201A combination PM10 and PM2. 5 sizing cyclones. Journal of Cotton Science, 17(4), 447-456.

Boykin, J. C., Buser, M. D., Whitelock, D. P., Holt, G. A., 2013b. Second stage seed-cotton cleaning system PM2. 5 emission factors and rates for cotton gins: Method 201A combination PM10 and PM2. 5 sizing cyclones. Journal of Cotton Science, 17(4), 333-345.

Brown, J. S., Gordon, T., Price, O., Asgharian, B., 2013. Thoracic and respirable particle definitions for human health risk assessment. Particle and fibre toxicology, 10(1), 12.

Breeze, 2020, U.S. EPA's Preferred Regulatory Model, https://www.breeze-software.com/software/AERMOD, Access date: 15/06/2020

Brugge, D., Durant, J. L., Rioux, C., 2007. Near-highway pollutants in motor vehicle exhaust: a review of epidemiologic evidence of cardiac and pulmonary health risks. Environmental health, 6(1), 23.

Bulut, S., Akkaya, L., Gök, V. and Konuk, M., 2011. Organochlorine pesticide (OCP) residues in cow's, buffalo's, and sheep's milk from Afyonkarahisar region, Turkey. Environmental monitoring and assessment, 181(1-4), pp.555-562.

Burkhardt, J., Flechard, C.R., Mattsson, M., Gresens, F., Jongejan, P.A., Erisman, J.W., Weidinger, T., Meszaros. R., Nemitz, E., Sutton, M.A., 2009. Modelling the dynamic chemical interactions of atmospheric ammonia with leaf surface wetness in a managed grassland canopy. Biogeosci. 6(1):67-84.

Buser, M. D., Parnell, C. B., Shaw, B. W., Lacey, R. E., 2007a. Particulate matter sampler errors due to the interaction of particle size and sampler performance characteristics: background and theory. Transactions of the ASABE, 50(1), 221-228.

Buser, M. D., Parnell, C. B., Shaw, B. W., Lacey, R. E., 2007b. Particulate matter sampler errors due to the interaction of particle size and sampler performance characteristics: ambient $PM_{2.5}$ samplers. Transactions of the ASABE, 50(1), 241-254.

Buser, M. D., Parnell, C. B., Shaw, B. W., Lacey, R. E., 2007c. Particulate matter sampler errors due to the interaction of particle size and sampler performance characteristics: ambient PM_{10} samplers. Transactions of the ASABE, 50(1), 229-240.

Buser, M. D., Whitelock, D. P., Park, M., Boykin, N. J. C., 2009. Characterization of cotton gin particulate matter emissions–project plan. Journal of Cotton Science 16:105–116.

Buser, M. D., Whitelock, D. P., Boykin, J. C., & Holt, G. A., 2013a. Unloading system $PM_{2.5}$ emission factors and rates for cotton gins: Method 201A combination PM_{10} and $PM_{2.5}$ sizing cyclones. Journal of Cotton Science, 17(4), 309-319.

Buser, M. D., Moore, T. W., & Whitelock, D. P., 2013b. Mote Trash System $PM_{2.5}$, PM_{10} and Total PM Emission Factors for Cotton Gin B using Method 201a with a $PM_{2.5}$ Cyclone. Journal of Cotton Science, 17(4), 479-488.

Buser, M. D., Whitelock, D. P., Boykin, J. C., Holt, G. A., 2013c. Combined lint cleaning system $PM_{2.5}$ emission factors and rates for cotton gins: Method 201A combination PM_{10} and $PM_{2.5}$ sizing cyclones. Journal of Cotton Science, 17(4), 391-401.

Buser, M. D., Whitelock, D. P., Boykin, J. C., Holt, G. A., 2013d. Third stage seed-cotton cleaning system $PM_{2.5}$ emission factors and rates for cotton gins: Method 201A combination PM_{10} and $PM_{2.5}$ sizing cyclones. Journal of Cotton Science, 17(4), 346-356.

Byon, J., Park, S.J. and Ahn, S., 2018. Preliminary surface soil derived concentration guideline levels derivation for Kori Unit 1 by RESRAD probabilistic analysis. *Nucl. Eng. Technol*, *50*, pp.1289-1297.

Cambra-López, M., Aarnink, A. J., Zhao, Y., Calvet, S., & Torres, A. G., 2010. Airborne particulate matter from livestock production systems: A review of an air pollution problem. Environmental pollution, 158(1), 1-17.

Cambra-López, M., Torres, A.G., Aarnink, A.J., Ogink N.W., 2011. Source analysis of fine and coarse particulate matter from livestock houses. Atmospheric Environment 45(3):694-707.

Cao, G., Zhang, X., Wang, Y., Zheng, F., 2008. Estimation of emissions from field burning of crop straw in China. Chinese Science Bulletin, 53(5), 784-790.

Capowiez, Y., Renault, P., & Belzunces, L. , 2001. Three-dimensional trajectories of 60Co-labelled earthworms in artificial cores of soil. European journal of soil science, 52(3), 365-375.

Carey, J.B., Lacey, R.E., Mukhtar, S., 2004. A review of literature concerning odors, ammonia, and dust from broiler production facilities: 2. Flock and house management factors. J. Appl. Poultr. Res. 13(3), 509-513.

Casella, G. and Berger, R.L., 2002. Statistical inference (Vol. 2). Pacific Grove, CA: Duxbury

Centofanti, T., McConnell, L.L., Chaney, R.L., Beyer, W.N., Andrade, N.A., Hapeman, C.J., Torrents, A., Nguyen, A., Anderson, M.O., Novak, J.M., Jackson, D., 2016. Organic amendments for risk mitigation of organochlorine pesticide residues in old orchard soils. Environ. Pollut. 210, 182–191. https://doi.org/10.1016/j.envpol.2015.11.039

Chai, M., Lu, M., Keener, T., Khang, S.J., Chaiwatpongsakorn, C., Tisch, J., 2009. Using an improved electrostatic precipitator for poultry dust removal. J. Electrostat. 67(6), 870-875.

Chang, J.C., Hanna, S.R., 2004. Air quality model performance evaluation. Meteorol. Atmos. Phys. 87(1):167-196.

Chen, H., Bai, S., Eisinger, D., Niemeier, D., Claggett, M., 2009. Predicting near-road $PM_{2.5}$ concentrations: comparative assessment of CALINE4, CAL3QHC, and AERMOD. Transportation research record, 2123(1), 26-37.

Choi, I.H., Moore Jr, P.A., 2008. Effects of liquid aluminum chloride additions to poultry litter on broiler performance, ammonia emissions, soluble phosphorus, total volatile fatty acids, and nitrogen contents of litter. Poultr. Sci. 87(10), 1955-1963.

Chow, T. E., Gaines, K. F., Hodgson, M. E., Wilson, M. D., 2005. Habitat and exposure modelling for ecological risk assessment: A case study for the raccoon on the Savannah River Site. Ecological Modelling, 189(1-2), 151-167.

Cimorelli, A.J., Perry, S.G., Venkatram, A., Weil, J.C., Paine, R.J., Peters, W.D., 1998. AERMOD–Description of Model Formulation. U.S. Environmental Protection Agency, EPA Rep. 454/R-03-002d, 85 pp.

Clostre, F., Letourmy, P., Turpin, B., Carles, C. and Lesueur-Jannoyer, M., 2014. Soil type and growing conditions influence uptake and translocation of organochlorine (chlordecone) by Cucurbitaceae species. Water, Air, & Soil Pollution, 225(10), p.2153.

Cocchi, D., Greco, F. and Trivisano, C., 2007. Hierarchical space-time modelling of PM10 pollution. Atmospheric environment, 41(3), pp.532-542.

Cortez, J., 1998. Field decomposition of leaf litters: relationships between decomposition rates and soil moisture, soil temperature and earthworm activity. Soil Biology and Biochemistry, 30(6), pp.783-793.

Cousineau, D., Chartier, S., 2010. Outliers detection and treatment: a review. International Journal of Psychological Research, 3(1), 58-67.

Cunningham, Scott D., William R. Berti, and Jianwei W. Huang. "Phytoremediation of contaminated soils." Trends in biotechnology 13.9 (1995): 393-397.

Dai, P., Shen, D., Tang, Q., Huang, K. Li, C., 2020. $PM_{2.5}$ from a broiler breeding production system: The characteristics and microbial community analysis. Environmental Pollution, 256, p.113368.

Darko, G., & Acquaah, S. O. (2008). Levels of organochlorine pesticides residues in dairy products in Kumasi, Ghana. Chemosphere, 71, 294–298.

Darko, G., Akoto, O., & Oppong, C. (2008). Persistent organochlorine pesticide residues in fish, sediments and water from Lake Bosomtwi, Ghana. Chemosphere, 72, 21–24.

Davison, A.C. and Hinkley, D.V., 1997. Bootstrap methods and their application (Vol. 1). Cambridge university press.

Davidson, C. I., Phalen, R. F., &Solomon, P. A., 2005. Airborne particulate matter and human health: a review. Aerosol Science and Technology, 39(8), 737-749.

Delignette-Muller, M.L., Ruiz, P. and Veber, P., 2017. Robust Fit of Toxicokinetic–Toxicodynamic Models Using Prior Knowledge Contained in the Design of Survival Toxicity Tests. Environmental science & technology, 51(7), pp.4038-4045.

Department of Natural Resources, 2020, Maryland Birds. dnr.maryland.gov/wildlife/Pages/plants_wildlife/woodcock.aspx. Accessed 2020/02/05

Díez, M., Simón, M., Dorronsoro, C., García, I. and Martín, F., 2007. Background arsenic concentrations in Southeastern Spanish soils. Science of the total environment, *378*(1-2), pp.5-12.

Ding, L., Zhu, D., Peng, D., Zhao, Y., 2017. Air pollution and asthma attacks in children: A case–crossover analysis in the city of Chongqing, China. Environmental Pollution, 220, 348-353.

Donham, K.J., Wing, S., Osterberg, D., Flora, J.L., Hodne, C., Thu, K.M., Thorne, P.S., 2007. Community health and socioeconomic issues surrounding concentrated animal feeding operations. Environ. Health Perspect. 115(2):317-320.

Du, Y., Xu, X., Chu, M., Guo, Y., & Wang, J., 2016. Air particulate matter and cardiovascular disease: the epidemiological, biomedical and clinical evidence. Journal of thoracic disease, 8(1), E8.

Elminir, H. K., 2005. Dependence of urban air pollutants on meteorology. Science of the Total Environment, 350(1-3), 225-237.

Endalew, A.M., Debaer, C., Rutten, N., Vercammen, J., Delele, M.A., Ramon, H., Nicolaï, B.M., Verboven, P., 2010. A new integrated CFD modelling approach towards air-assisted orchard spraying. Part I. Model development and effect of wind speed and direction on sprayer airflow. Comput. Electron. Agric. 71(2):128-136.

Esmen, N.A. and Hammad, Y.Y., 1977. Log-normality of environmental sampling data. Journal of Environmental Science & Health Part A, 12(1-2), pp.29-41.

Farrance, I. and Frenkel, R., 2012. Uncertainty of measurement: a review of the rules for calculating uncertainty components through functional relationships. The Clinical Biochemist Reviews, 33(2), p.49.

Federal Register., 2013. National ambient air quality standards for particulate matter; final rule. Federal Register 78(10), 3086-3287.

Federal Remediation Technologies Roundtable, 2015. 4.25 Thermal Desorption, Ex. Situ Soil Remediation Technology. http://www.frtr.gov/matrix2/section4/4-26. html [accessed 14.06.15].

Feng, K., Yu, B.Y., Ge, D.M., Wong, M.H., Wang, X.C. and Cao, Z.H., 2003. Organo-chlorine pesticide (DDT and HCH) residues in the Taihu Lake Region and its movement in soil–water system: I. Field survey of DDT and HCH residues in ecosystem of the region. Chemosphere, 50(6), pp.683-687.

Firestone, M., Fenner-Crisp, P., Barry, T., Bennett, D., Chang, S., Callahan, M., ... & Barnes, D., 1997. Guiding principles for Monte Carlo analysis. Washington, DC: US Environmental Protection Agency.

Flagan, R. C., Seinfeld, J. H., 2012. Fundamentals of air pollution engineering. Courier Corporation.

Fordham, C.L., 1985. Effects of composted sewage sludge on the earthworm, Lumbricus terrestris (Doctoral dissertation, Colorado State University)

Fritz, B. K., 2003. Dispersion modeling of particulate emissions from low-level point sources.

Gautam, S., Prasad, N., Patra, A. K., Prusty, B. K., Singh, P., Pipal, A. S., Saini, R., 2016. Characterization of PM2. 5 generated from opencast coal mining operations: A case study of Sonepur Bazari Opencast Project of India. Environmental technology & innovation, 6, 1-10.

Gavrilescu, Maria. "Fate of pesticides in the environment and its bioremediation." Engineering in life sciences 5, no. 6 (2005): 497-526.

Gaylor, M.O., Harvey, E. and Hale, R.C., 2013. Polybrominated diphenyl ether (PBDE) accumulation by earthworms (Eisenia fetida) exposed to biosolids-, polyurethane foam microparticle-, and Penta-BDE-amended soils. Environmental science & technology, 47(23), pp.13831-13839.

Gaylord J. Remediation of petroleum contaminated soils: biological, physical, and chemical processes. CRC press; 1998 May 13.

Gehrig, R., Buchmann, B., 2003. Characterising seasonal variations and spatial distribution of ambient PM_{10} and $PM_{2.5}$ concentrations based on long-term Swiss monitoring data. Atmospheric Environment, 37(19), 2571-2580.

Gelman, A. and Hill, J., 2006. Data analysis using regression and multilevel/hierarchical models. Cambridge university press.

Gelman, A., Carlin, J. B., Stern, H. S., Dunson, D. B., Vehtari, A., & Rubin, D. B., 2013. Bayesian data analysis. CRC press.

Gelman, A., Hwang, J., Vehtari, A., 2014. Understanding predictive information criteria for Bayesian models. Statistics and computing, 24(6), 997-1016.

Gibson, M. D., Kundu, S., Satish, M., 2013. Dispersion model evaluation of $PM_{2.5}$, NO_x and SO_2 from point and major line sources in Nova Scotia, Canada using AERMOD Gaussian plume air dispersion model. Atmospheric Pollution Research, 4(2), 157-167.

Gish, C. D., Hughes, D. L., 1982. Residues of DDT, dieldrin, and heptachlor in earthworms during two years following application (No. 241). US Department of the Interior, Fish and Wildlife Service

Gish, D., 1970. Organochlorine insecticide residues in soils and soil invertebrates from agricultural lands. Pesticide Monitoring Journal, 3, 241-252.

Givens, G. H., Hoeting. J. A., 2013. Computational Statistics. Wiley & Sons. Inc.

Glasserman, P., 2013. Monte Carlo methods in financial engineering (Vol. 53). Springer Science & Business Media.

Gneiting, T., 2011. Making and evaluating point forecasts. Journal of the American Statistical Association, 106(494), 746-762.

Gonzalez-Rodriguez, J., Fierrez-Aguilar, J., Ramos-Castro, D., Ortega-Garcia, J., 2005. Bayesian analysis of fingerprint, face and signature evidences with automatic biometric systems. Forensic science international, 155(2-3), 126-140.

Görlitz, L., Gao, Z. and Schmitt, W., 2011. Statistical analysis of chemical transformation kinetics using Markov-chain Monte Carlo methods. Environmental science & technology, 45(10), pp.4429-4437.

Goyal, A., Small, M.J., von Stackelberg, K., Burmistrov, D. and Jones, N., 2005. Estimation of fugitive lead emission rates from secondary lead facilities using hierarchical Bayesian models. Environmental science & technology, 39(13), pp.4929-4937.

Grantz, D.A., Garner, J.H., Johnson, D.W., 2003. Ecological effects of particulate matter. Environ. Int. 29(2):213-239.

Grimmond, C.S.B., Blackett, M., Best, M.J., Barlow, J., Baik, J.-J., Belcher, S.E., Bohnenstengel, S.I., Calmet, I., Chen, F., Dandou, A., Fortuniak, K., Gouvea, M.L., Hamdi, R., Hendry, M., Kawai, T., Kawamoto, Y., Kondo, H., Krayenhoff, E.S., Lee, S.-H., Loridan, T., Martilli, A., Masson, V., Miao, S., Oleson, K., Pigeon, G., Porson, A., Ryu, Y.-H., Salamanca, F., Shashua-Bar, L., Steeneveld, G.-J., Tombrou, M., Voogt, J., Young, D., Zhang, N.2010. The international urban energy balance models comparison project: first results from phase 1. J. Appl. Meteorol. Climatol. 49(6), 1268-1292.

Hadlocon, L.S., Zhao, L.Y., Bohrer, G., Kenny, W., Garrity, S.R., Wang, J., Wyslouzil, B., Upadhyay, J., 2015. Modeling of particulate matter dispersion from a poultry facility using AERMOD. J. Air Waste Manage. Assoc. 65(2):206-217.

Hanna, S.R., Briggs, G.A., Hosker Jr, R.P., 1982. Handbook on Atmospheric Diffusion. National Oceanic and Atmospheric Administration, Oak Ridge, TN (USA). Atmospheric Turbulence and Diffusion Lab No. DOE/TIC-11223, 102 pp. doi:10.2172/5591108.

Hanna, S., Chang, J., 2012. Acceptance criteria for urban dispersion model evaluation. Meteorology and Atmospheric Physics, 116(3-4), 133-146.

Hanna, S.R., Hansen, O.R., Dharmavaram, S., 2004. FLACS CFD air quality model performance evaluation with Kit Fox, MUST, Prairie Grass, and EMU observations. Atmos. Environ. 38(28):4675-4687.

Hasan, I., Horvath, R., Mares, J., 2018. What type of finance matters for growth? Bayesian model averaging evidence. The World Bank Economic Review, 32(2), 383-409.

Hayes, E. H., Landis, W. G., 2004. Regional ecological risk assessment of a near shore marine environment: Cherry Point, WA. Human and Ecological Risk Assessment, 10(2), 299-325.

Hayya, J., Armstrong, D. and Gressis, N., 1975. A note on the ratio of two normally distributed variables. Management Science, 21(11), pp.1338-1341.

Hensen, A., Loubet, B., Mosquera, J., Van Den Bulk, W.C., Erisman, J.W., Dämmgen, U., Milford, C., Löpmeier, F.J., Cellier, P., Mikuška, P., Sutton, M.A., 2009. Estimation of NH_3 emissions from a naturally ventilated livestock farm using local-scale atmospheric dispersion modelling. Biogeosci. 6(12):2847-2860.

Hilber, I., Wyss, G.S., Mäder, P., Bucheli, T.D., Meier, I., Vogt, L., Schulin, R., 2009. Influence of activated charcoal amendment to contaminated soil on dieldrin and nutrient uptake by cucumbers. Environ. Pollut. 157, 2224–2230. https://doi.org/10.1016/j.envpol.2009.04.009

Hood, E. (2006). The apple bites back: claiming old orchards for residential development. Environmental health perspectives, 114(8), A470.

Hong T, Gurian PL. Updating a B. anthracis risk model with field data from a bioterrorism incident. Environmental Science & Technology. 2015 May 22;49(11):6701-11.

Hooten, M. B., & Hobbs, N. T., 2015. A guide to Bayesian model selection for ecologists. Ecological Monographs, 85(1), 3-28.

Hua, X.M. and Shan, Z.J., 1996. The production and application of pesticides and factor analysis of their pollution in environment in China. *Adv Environ Sci*, *4*(2), pp.33-45.

Isakov, V., Sax, T., Venkatram, A., Pankratz, D., Heumann, J., & Fitz, D., 2004. Near-field dispersion modeling for regulatory applications. Journal of the Air & Waste Management Association, 54(4), 473-482

Jackman, S., 2004. Bayesian analysis for political research. Annu. Rev. Polit. Sci., 7, 483-505.

Jacobson, M.Z., 2005. Fundamentals of Atmospheric Modeling. 2nd Edition. Cambridge University Press, Cambridge, UK. 828 pp.

Jeong, S., Murayama, M., Yamamoto, K., 2005. Efficient optimization design method using kriging model. J. Aircraft 42(2):413-420.

Jensen, S. "DDT and PCB in marine animals from Swedish waters." Nature 224 (1969): 247-250.

Jones, L., Nizam, M.S., Reynolds, B., Bareham, S., Oxley, E.R., 2013. Upwind impacts of ammonia from an intensive poultry unit. Environ. Pollut. 180:221-8.

Kakosimos, K.E., Assael, M.J., Katsarou, A.S., 2011. Application and evaluation of AERMOD on the assessment of particulate matter pollution caused by industrial activities in the Greater Thessaloniki area. Environ. Technol. 32(6):593-608.

Kelsey, J.W., Colino, A., White, J.C., 2005. EFFECT OF SPECIES DIFFERENCES, POLLUTANT CONCENTRATION, AND RESIDENCE TIME IN SOIL ON THE BIOACCUMULATION OF 2,2-BIS (p-CHLOROPHENYL)-1,1-DICHLOROETHYLENE BY THREE EARTHWORM SPECIES. Environ. Toxicol. Chem. 24, 703. https://doi.org/10.1897/04-293R.1

Kim, D., Miranda, M. L., Tootoo, J., Bradley, P., & Gelfand, A. E., 2011. Spatial modeling for groundwater arsenic levels in North Carolina. Environmental science & technology, 45(11), 4824-4831.

Kim, K.H., Kabir E., Kabir S., 2015. A review on the human health impact of airborne particulate matter. Environ. Int. 74:136-143.

Kołtowski, M., Hilber, I., Bucheli, T.D. and Oleszczuk, P., 2016. Effect of activated carbon and biochars on the bioavailability of polycyclic aromatic hydrocarbons in different industrially contaminated soils. Environmental Science and Pollution Research, *23*(11), pp.11058-11068.

Kruschke, J.K., 2013. Bayesian estimation supersedes the t test. Journal of Experimental Psychology: General, 142(2), p.573.

Lake Environmental, 2020. AERMOD View™ Gaussian Plume Air Dispersion Model, https://www.weblakes.com/products/aermod/index.html, Access date: 15/06/2020

Lam, R., Poloczek, M., Frazier, P., Willcox, K. E., 2018. Advances in bayesian optimization with applications in aerospace engineering. In 2018 AIAA Non-Deterministic Approaches Conference (p. 1656).

Lammel, G., Klánová, J., Erić, L., Ilić, P., Kohoutek, J. and Kovacić, I., 2011. Sources of organochlorine pesticides in air in an urban Mediterranean environment: volatilisation from soil. Journal of Environmental Monitoring, 13(12), pp.3358-3364.

Landau, D. P., Binder, K., 2014. A guide to Monte Carlo simulations in statistical physics. Cambridge university press.

Langlois, V.S., Rutter, A., Zeeb, B.A., 2011. Activated Carbon Immobilizes Residual Polychlorinated Biphenyls in Weathered Contaminated Soil. J. Environ. Qual. 40, 1130. https://doi.org/10.2134/jeq2010.0481

Lavelle, P., 1988. Earthworm activities and the soil system. Biology and fertility of soils, 6(3), pp.237-251

Lee, I.B., Bitog, J.P., Hong, S.W., Seo, I.H., Kwon, K.S., Bartzanas, T., Kacira, M., 2013. The past, present and future of CFD for agro-environmental applications. Comput. Electron. Agric. 93:168-183.

Levy, R., Mislevy, R. J., 2016. Bayesian psychometric modeling. CRC Press.

Link, W. A., & Sauer, J. R., 2016. Bayesian cross-validation for model evaluation and selection, with application to the North American Breeding Bird Survey. Ecology, 97(7), 1746-1758.

Liu, L., Bai, L., Man, C., Liang, W., Li, F. and Meng, X., 2015. DDT vertical migration and formation of accumulation layer in pesticide-producing sites. Environmental science & technology, 49(15), pp.9084-9091.

Löndahl, J., Massling, A., Pagels, J., Swietlicki, E., Vaclavik, E., Loft, S., 2007. Size-resolved respiratory-tract deposition of fine and ultrafine hydrophobic and hygroscopic aerosol particles during rest and exercise. Inhalation Toxicolo. 19(2):109-116.

Loos M, Krauss M, Fenner K. Pesticide nonextractable residue formation in soil: Insights from inverse modeling of degradation time series. Environmental science & technology. 2012 Sep 5;46(18):9830-7.

Luo, X., Deng, F., 2018. Nanomaterials for the Removal of Pollutants and Resource Reutilization. Elsevier.

Lu, H. C., Fang, G. C., 2002. Estimating the frequency distributions of PM_{10} and $PM_{2.5}$ by the statistics of wind speed at Sha-Lu, Taiwan. Science of the total environment, 298(1-3), 119-130.

Lushi, E., Stockie, J. M., 2010. An inverse Gaussian plume approach for estimating atmospheric pollutant emissions from multiple point sources. Atmospheric Environment, 44(8), 1097-1107.

Ma, J., Yi, H., Tang, X., Zhang, Y., Xiang, Y., Pu, L., 2013. Application of AERMOD on near future air quality simulation under the latest national emission control policy of China: A case study on an industrial city. J. Environ. Sci. 25(8):1608-1617.

Malone, G., Windsor, J., Abbott, D., Collier, S., 2006. Establishment of vegetative environmental buffers around poultry farms. Proc. Workshop Agric. Air Qual. Washington, D.C. 879-880. http://www.nrem.iastate.edu/research/veb/pub.poultryestab.pdf (Accessed March 20, 2020).

Manly, B. F., 2006. Randomization, bootstrap and Monte Carlo methods in biology (Vol. 70). CRC press.

Mansouri, A., Cregut, M., Abbes, C., Durand, M.-J., Landoulsi, A., Thouand, G., 2017. The Environmental Issues of DDT Pollution and Bioremediation: a Multidisciplinary Review. Appl. Biochem. Biotechnol. 181, 309–339. https://doi.org/10.1007/s12010-016-2214-5

Marsaglia, G., 1965. Ratios of normal variables and ratios of sums of uniform variables. Journal of the American Statistical Association, 60(309), pp.193-204.

Marsaglia, G., 2006. Ratios of normal variables. Journal of Statistical Software, *16*(4), pp.1-10

Martinez, W. L., & Martinez, A. R., 2015. Computational statistics handbook with MATLAB. Chapman and Hall/CRC

Matsumoto, E., Kawanaka, Y., Yun, S.-J., Oyaizu, H., 2009. Bioremediation of the organochlorine pesticides, dieldrin and endrin, and their occurrence in the environment. Appl. Microbiol. Biotechnol. 84, 205–216. https://doi.org/10.1007/s00253-009-2094-5

McLeese, D. W., Metcalfe, C. D., Pezzack, D. S., 1980. Uptake of PCBs from sediment byNereis virens andCrangon septemspinosa. Archives of environmental contamination and toxicology, 9(5), 507-518.

Megharaj, Mallavarapu, et al. "Bioremediation approaches for organic pollutants: a critical perspective." Environment international 37.8 (2011): 1362-1375

Melse, R.W., Ogink, N.W.M., 2005. Air scrubbing techniques for ammonia and odor reduction at livestock operations: Review of on-farm research in the Netherlands. Trans. ASAE. 48(6), 2303-2313.

Molinaro, A. M., Simon, R., Pfeiffer, R. M., 2005. Prediction error estimation: a comparison of resampling methods. Bioinformatics, 21(15), 3301-3307.

Mordechai, S., 2011. Applications of Monte Carlo method in science and engineering.

Morillo, E., Villaverde, J., 2017. Advanced technologies for the remediation of pesticide-contaminated soils. Sci. Total Environ. 586, 576–597. https://doi.org/10.1016/j.scitotenv.2017.02.020

Morrison, D.E., Robertson, B.K., Alexander, M., 2000. Bioavailability to Earthworms of Aged DDT, DDE, DDD, and Dieldrin in Soil. Environ. Sci. Technol. 34, 709–713. https://doi.org/10.1021/es9909879

Muijs, B. and Jonker, M.T., 2009. Temperature-dependent bioaccumulation of polycyclic aromatic hydrocarbons. Environmental science & technology, 43(12), pp.4517-4523

Nagendra, S., Khare, M., Gulia, S., Vijay, P., Chithra, V.S., Bell, M., Namdeo, A., 2012. Application of ADMS and AERMOD models to study the dispersion of vehicular pollutants in urban areas of India and the United Kingdom. WIT Trans. Ecol. Environ. 157:3-12.

National Chicken Council, 2017. Broiler Chicken Industry Key Facts 2019. http://www.nationalchickencouncil.org/about-the-industry/statistics/broiler-chicken-industry-key-facts/ (Accessed October 15, 2019)

National Oceanic and Atmospheric Administration, 2018. Pasquill Stability Classes https://www.ready.noaa.gov/READYpgclass.php (Accessed October 15, 2019)

Nemitz, E., Hargreaves, K.J., Neftel, A., Loubet, B., Cellier, P., Dorsey, J.R., Flynn, M., Hensen, A., Weidinger, T., Meszaros, R., Horvath, L., 2009. Intercomparison and assessment of turbulent and physiological exchange parameters of grassland. Biogeosci. 6(8):1445-1466.

Nowak, D. J., Hirabayashi, S., Bodine, A., Hoehn, R., 2013. Modeled $PM_{2.5}$ removal by trees in ten US cities and associated health effects. Environmental pollution, 178, 395-402.

Niazi, N. K., Bishop, T. F., Singh, B., 2011. Evaluation of spatial variability of soil arsenic adjacent to a disused cattle-dip site, using model-based geostatistics. Environmental science & technology, 45(24), 10463-10470.

Nightingale, M. P., Umrigar, C. J. (Eds.)., 1998. Quantum Monte Carlo methods in physics and chemistry (No. 525). Springer Science & Business Media.

Okamoto, Y., 2017. Applying bayesian approach to combinatorial problem in chemistry. The Journal of Physical Chemistry A, 121(17), 3299-3304.

Oldenkamp R, Hendriks HW, van de Meent D, Ragas AM., 2015. Hierarchical bayesian approach to reduce uncertainty in the aquatic effect assessment of realistic chemical mixtures. Environmental science & technology. 2015 Aug 17;49(17):10457-65.

Oleszczuk, P., Rakowska, M., Bucheli, T.D., Godlewska, P. and Reible, D.D., 2019. Combined effects of plant cultivation and sorbing carbon amendments on freely dissolved PAHs in contaminated soil. Environmental science & technology, *53*(9), pp.4860-4868.

Ortíz, I., Velasco, A., Le Borgne, S., Revah, S., 2013. Biodegradation of DDT by stimulation of indigenous microbial populations in soil with cosubstrates. Biodegradation 24, 215–225. https://doi.org/10.1007/s10532-012-9578-1

Ott, W. R., 1990. A physical explanation of the lognormality of pollutant concentrations. Journal of the Air & Waste Management Association, 40(10), 1378-1383.

Ounis, H., & Ahmadi, G., 1990. A comparison of Brownian and turbulent diffusion. Aerosol Science and Technology, 13(1), 47-53.

Øverjordet, I.B., Nepstad, R., Hansen, B.H., Jager, T., Farkas, J., Altin, D., Brönner, U. and Nordtug, T., 2018. Toxicokinetics of crude oil components in Arctic copepods. Environmental science & technology.

Ozono, S., Miyagi, H. and Wada, K., 2007. Turbulence generated in active grid mode using a multi-fan wind tunnel. Journal of Fluid Science and Technology, *2*(3), pp.643-654.

Pagnanelli, F., Petrangeli Papini, M., Trifoni, M., Vegliò, F., 2000. Biosorption of Metal Ions on Arthrobacter sp. : Biomass Characterization and Biosorption Modeling. Environ. Sci. Technol. 34, 2773–2778. https://doi.org/10.1021/es991271g

Ratcliffe, D. A. "Changes attributable to pesticides in egg breakage frequency and eggshell thickness in some British birds." Journal of Applied Ecology (1970): 67-115.

Paul, P., Ghosh, U., 2011. Influence of activated carbon amendment on the accumulation and elimination of PCBs in the earthworm Eisenia fetida. Environ. Pollut. 159, 3763–3768. https://doi.org/10.1016/j.envpol.2011.07.025

Pearson, J. F., Bachireddy, C., Shyamprasad, S., Goldfine, A. B., Brownstein, J. S., 2010. Association between fine particulate matter and diabetes prevalence in the US. Diabetes care, 33(10), 2196-2201.

Pescatore, A.J., Casey, K.D., Gates, R.S., 2005. Ammonia emissions from broiler houses. J. Appl. Poultr. Res. 14(3):635-637.

Pérez, N., Pey, J., Cusack, M., Reche, C., Querol, X., Alastuey, A., Viana, M., 2010. Variability of particle number, black carbon, and PM_{10}, $PM_{2.5}$, and PM1 levels and speciation: influence of road traffic emissions on urban air quality. Aerosol Science and Technology, 44(7), 487-499.

Perry, S.G., Cimorelli, A.J., Paine, R.J., Brode, R.W., Weil, J.C., Venkatram, A., Wilson, R.B., Lee, R.F. and Peters, W.D., 2005. AERMOD: A dispersion model for industrial source applications. Part II: Model performance against 17 field study databases. Journal of applied meteorology, 44(5), pp.694-708.

Petersen, R. L., Guerra, S. A., & Bova, A. S., 2017. Critical review of the building downwash algorithms in AERMOD. Journal of the Air & Waste Management Association, 67(8), 826-835.

Pignatello, J.J. Xing, B., 1995. Mechanisms of slow sorption of organic chemicals to natural particles. Environmental science & technology, 30(1), pp.1-11.

Piwowar, A. and Dzikuć, M., 2019. Development of renewable energy sources in the context of threats resulting from low-altitude emissions in rural areas in Poland: a review. Energies, 12(18), p.3558.

Powell, J. J., Parnell, C. B., Wanjura, J. D., Shaw, B. , 2006. A Comparison of Predicted Property Line Particulate Concentrations using ISCST3, AERMOD, WindTrax, and AUSTAL View.

Press, S.J., 1969. The t-ratio distribution. Journal of the American Statistical Association, 64(325), pp.242-252.

Purnomo, A.S., Nawfa, R., Martak, F., Shimizu, K., Kamei, I., 2017. Biodegradation of Aldrin and Dieldrin by the White-Rot Fungus Pleurotus ostreatus. Curr. Microbiol. 74, 320–324. https://doi.org/10.1007/s00284-016-1184-8

Qian, S. S., Schulman, A., Koplos, J., Kotros, A., & Kellar, P., 2004. A hierarchical modeling approach for estimating national distributions of chemicals in public drinking water systems. Environmental science & technology, 38(4), 1176-1182.

Rabl, A., 1999. Air pollution and buildings: an estimation of damage costs in France. Environmental Impact Assessment Review, 19(4), 361-385.

Radiello, 2019. User Manual. https://www.restek.com/pdfs/radiello-manual.pdf (accessed October 15, 2019).

Reid, B.J., Jones, K.C., Semple, K.T., 2000. Bioavailability of persistent organic pollutants in soils and sedimentsÐa perspective on mechanisms, consequences and assessment. Environ. Pollut. 10.

Rice, C. P., & Shigaev, V. V., 1997. Spatial distribution of hexachlorocyclohexane isomers in the Bering and Chukchi Sea shelf ecosystem. Environmental science & technology, 31(7), 2092-2097.

Rich, C. D., Blaine, A. C., Hundal, L., Higgins, C. P., 2015. Bioaccumulation of perfluoroalkyl acids by earthworms (Eisenia fetida) exposed to contaminated soils. Environmental science & technology, 49(2), 881-888.

Riddle, A., Carruthers, D., Sharpe, A., McHugh, C., Stocker, J., 2004. Comparisons between FLUENT and ADMS for atmospheric dispersion modelling. Atmos. Environ. 38(7):1029-1038.

Rieckermann J, Anta J, Scheidegger A, Ort C., 2011. Assessing wastewater micropollutant loads with approximate Bayesian computations. Environmental science & technology. 2011 Apr 19;45(10):4399-406.

Ritz, C.W., Fairchild, B.D., Lacy, M.P., 2004. Implications of ammonia production and emissions from commercial poultry facilities: A review J. Appl. Poultr. Res. 13(4):684-692.

Ro, K., Li, H., Hapeman, C.J., Harper, L.A., Flesch, T.K., Downey, P.M., McConnell, L.L., Torrents, A., Yao, Q., 2018. Enhanced dispersion and removal of ammonia emitted from a poultry house using a vegetative environmental buffer. Agriculture 8:46. DOI:10.3390/agriculture8040046

Rodrıguez, S., Querol, X., Alastuey, A., Viana, M. M., Alarcon, M., Mantilla, E., Ruiz, C. R., 2004. Comparative PM_{10}–$PM_{2.5}$ source contribution study at rural, urban and industrial sites during PM episodes in Eastern Spain. Science of the Total Environment, 328(1-3), 95-113.

Romijn, C.A.F.M., Luttik, R. and Canton, J.H., 1994. Presentation of a general algorithm to include effect assessment on secondary poisoning in the derivation of environmental quality criteria.: 2. Terrestrial food chains. Ecotoxicology and environmental safety, 27(2), pp.107-127.

Safe, S., 1992. Development, validation and limitations of toxic equivalency factors. Chemosphere, 25(1-2), pp.61-64.

Sample, B.E., Suter, G.W., Beauchamp, J.J. and Efroymson, R.A., 1999. Literature-derived bioaccumulation models for earthworms: Development and validation. Environmental Toxicology and Chemistry: An International Journal, 18(9), pp.2110-2120.

Saito, H. and Goovaerts, P., 2000. Geostatistical interpolation of positively skewed and censored data in a dioxin-contaminated site. Environmental Science & Technology, 34(19), pp.4228-4235.

Saito, T., Otani, T., Seike, N., Murano, H., Okazaki, M., 2011. Suppressive effect of soil application of carbonaceous adsorbents on dieldrin uptake by cucumber fruits. Soil Sci. Plant Nutr. 57, 157–166. https://doi.org/10.1080/00380768.2010.551281

Semple, K. T., Riding, M. J., McAllister, L. E., Sopena-Vazquez, F., & Bending, G. D. (2013). Impact of black carbon on the bioaccessibility of organic contaminants in soil. Journal of hazardous materials, 261, 808-816.

Sariwati, A., Purnomo, A.S., Kamei, I., 2017. Abilities of Co-cultures of Brown-Rot Fungus Fomitopsis pinicola and Bacillus subtilis on Biodegradation of DDT. Curr. Microbiol. 74, 1068–1075. https://doi.org/10.1007/s00284-017-1286-y

Schnoor, J.L., 1996. Environmental modeling: fate and transport of pollutants in water, air, and soil. John Wiley and Sons.

Schwarz, G.,1978. Estimating the dimension of a model. The annals of statistics, 6(2), 461-464.

Shoari, N. and Dubé, J.S., 2018. Toward improved analysis of concentration data: Embracing nondetects. Environmental toxicology and chemistry, 37(3), pp.643-656.

Shi, Y., Meng, F., Guo, F., Lu, Y., Wang, T. and Zhang, H., 2005. Residues of organic chlorinated pesticides in agricultural soils of Beijing, China. Archives of environmental contamination and toxicology, 49(1), pp.37-44.

Sparks, D. L., 2003. Environmental soil chemistry. Elsevier.

Stow, C.A., Lamon, E.C., Qian, S.S. and Schrank, C.S., 2004. Will Lake Michigan lake trout meet the Great Lakes strategy 2002 PCB reduction goal?. Environmental science & technology. 38, 2, 359-363

Šmídová, K., Hofman, J., 2014. Uptake kinetics of five hydrophobic organic pollutants in the earthworm Eisenia fetida in six different soils. Journal of hazardous materials, 267, 175-182.

Siefert, R. L., Scudlark, J. R., 2008. Determination of ammonia emission rates from a tunnel ventilated chicken house using passive samplers and a Gaussian dispersion model. Journal of atmospheric chemistry, 59(2), 99-115.

Siefert, R. L., Scudlark, J. R., Potter, A. G., Simonsen, K. A., Savidge, K. B., 2004. Characterization of atmospheric ammonia emissions from a commercial chicken house on the Delmarva Peninsula. Environmental science & technology, 38(10), 2769-2778.

Spiegelhalter, D. J., Best, N. G., Carlin, B. P., & Van Der Linde, A., 2002) Bayesian measures of model complexity and fit. Journal of the royal statistical society: Series b (statistical methodology), 64(4), 583-639.

Stevens, C.J., Tilman, D., 2010. Point source ammonia emissions are having a detrimental impact on prairie vegetation. Water Air Soil Pollut. 211(1-4):435-441.

Stockie, J.M., 2011. The mathematics of atmospheric dispersion modeling. SIAM Rev. 53(2):349-372.

Sudharshan, S., Naidu, R., Mallavarapu, M. and Bolan, N., 2012. DDT remediation in contaminated soils: a review of recent studies. Biodegradation, 23(6), pp.851-863.

Suter II, Glenn W., 2016. Ecological risk assessment. CRC press.

Sutton, M.A, Nemitz, E., Theobald, M.R., Milford, C., Dorsey, J.R., Gallagher, M.W., Hensen, A., Jongejan, P.A., Erisman, J.W., Mattsson, M., Schjørring, J.K., 2009. Dynamics of ammonia exchange with cut grassland: strategy and implementation of the GRAMINAE Integrated Experiment. Biogeosci. 6(3):309-31.

Sze-To, G. N., Wu, C. L., Chao, C. Y., Wan, M. P., & Chan, T. C., 2012. Exposure and cancer risk toward cooking-generated ultrafine and coarse particles in Hong Kong homes. HVAC&R Research, 18(1-2), 204-216.

Tan, Q.G., Zhou, W. and Wang, W.X., 2017. Modeling the Toxicokinetics of Multiple Metals in the Oyster Crassostrea hongkongensis in a Dynamic Estuarine Environment. Environmental science & technology, 52(2), pp.484-492.

Tanabe, S., Iwata, H., & Tatsukawa, R. (1994). Global contamination by persistent organochlorine and their ecotoxicological impact on marine mammals. The Science of the Total Environmental, 154, 163–177.

Tao, S., Liu, W., Li, Y., Yang, Y., Zuo, Q., Li, B., & Cao, J., 2008. Organochlorine pesticides contaminated surface soil as reemission source in the Haihe Plain, China. Environmental science & technology, 42(22), 8395-8400.

Thompson, J.M.T. and Stewart, H.B., 2002. Nonlinear dynamics and chaos. John Wiley & Sons.

Tieyu, W., Yonglong, L., Yajuan, S. and Hong, Z., 2005. Spatial distribution of organochlorine pesticide residues in soils surrounding Guanting reservoir, People's Republic of China. Bulletin of environmental contamination and toxicology, 74(4), pp.623-630.

Tominaga, Y., Stathopoulos, T., 2013. CFD simulation of near-field pollutant dispersion in the urban environment: A review of current modeling techniques. Atmos. Environ. 79:716-730.

Ullman, J.L., Mukhtar, S., Lacey, R.E., Carey, J. B., 2004. A review of literature concerning odors, ammonia, and dust from broiler production facilities: 4. Remedial management practices. J. Appl. Poultr. Res. 13(3), 521-531.

US Code of Federal Regulations (CFR), 2006. National ambient air quality standards for particulate matter; final rule. 40 CFR, Part 50. U.S. Government Printing Office, Washington, D.C.

USDA, 2009. Biological Availability Study Report: BARC 4/19. Document Accession Number: F-24e0454. Beltsville Agricultural Research Center Information Repository. http://www.ars.usda.gov/superfund [accessed14.06.15]

USDA, Economic Research Service (USDA ERS), 2019a. Broiler production continues its long-term expansion. https://www.ers.usda.gov/data-products/chart-gallery/gallery/chart-detail/?chartId=58338, Access date: 15/06/2020

USDA, Economic Research Service (USDA ERS), 2019b. More U.S. cotton is exported than milled domestically. https://www.ers.usda.gov/data-products/chart-gallery/gallery/chart-detail/?chartId=58352, Access date: 15/06/2020

USDA, Economic Research Service (USDA ERS), 2019c. Cotton Sector at a Glance. https://www.ers.usda.gov/topics/crops/cotton-wool/cotton-sector-at-a-glance/. (Accessed 2019/12/08)

USDA, Economic Research Service (USDA ERS), 2020a. What is agriculture's share of the overall U.S. economy?. https://www.ers.usda.gov/data-products/chart-gallery/gallery/chart-detail/?chartId=58270, Access date: 15/06/2020

USDA, Economic Research Service (USDA ERS), 2020b. Agriculture and its related industries provide 11 percent of U.S. employment. https://www.ers.usda.gov/data-products/chart-gallery/gallery/chart-detail/?chartId=58282, Access date: 15/06/2020

USDA, Economic Research Service (USDA ERS), 2020c. Meat and poultry plants employ about a third of U.S. food and beverage manufacturing employees. https://www.ers.usda.gov/data-products/chart-gallery/gallery/chart-detail/?chartId=58286, Access date: 15/06/2020

USDA, Natural Resource Conservation Service (USDA-NRCS), 2007. VEB TOOL-KIT: A Guide to Vegetative Environmental Buffers for Tunnel-Ventilated Poultry Houses. https://www.nrcs.usda.gov/Internet/FSE_DOCUMENTS/nrcs144p2_027434.pdf (Accessed March 20, 2020)

US EPA, 1992. A framework for ecological risk assessment at the EPA

US EPA, 1997. Ecological Risk Assessment Guidance for Superfund: Process for Designing and Conducting Ecological Risk Assessments. Interim Final. U.S. Environmental Protection Agency, Environmental Response Team (Edison, NJ). June 5, 1997

US EPA, 1998a, Guidelines for Ecological Risk Assessment, Washington, DC, EPA/630/R-95/002F

US EPA, 1998b. Status of Pesticides in Registration, Reregistration, and Special Review (Rainbow Report). Washington, DC, 462, pp.

US EPA, 1999. Ecological Risk Assessment and Risk Management Principles for Superfund Sites. Office of Emergency and Remedial Response, Washington, DC. OSWER Directive 9285.7-28.P.

US EPA, 2000a. Guidance for data quality assessment: Practical methods for data analysis. Washington, DC.

US EPA, 2000b. Meteorological Monitoring Guidance for Regulatory Modeling Applications.

US EPA, 2005. Bayesian Methods for Characterizing Complex Multivariate Exposures. https://cfpub.epa.gov/ncer_abstracts/index.cfm/fuseaction/display.abstractDetail/abstract/7565, Access date: 17/06/2020

US EPA, 2007a. Ecological Soil Screening Levels for DDT and Metabolites. U.S. Environmental Protection Agency.

US EPA, 2007b. Ecological Soil Screening Levels for Dieldrin. U.S. Environmental Protection Agency.

US EPA, 2007c. Ecological Soil Screening Levels Attachment 4-1. U.S. Environmental Protection Agency.

US EPA, 2014. SAMPLING AND ANALYSIS PLAN GUIDANCE AND TEMPLATE. VERSION 4, General Projects. R9QA/009.

US EPA, 2015. DDT e a Brief History and Status. http://www2.epa.gov/ingredientsused-pesticide-products/ddt-brief-history-and-status [accessed 2019.3.15]

US EPA, 2016. Air Quality Models. https://www.epa.gov/scram/air-quality-models, Access date: 15/06/2020

US EPA, 2017. Superfund Site: BELTSVILLE AGRICULTURAL RESEARCH CENTER (USDA) Site Profile." US EPA, Environmental Protection Agency, 20 Oct. 2017, https://cumulis.epa.gov/supercpad/SiteProfiles/index.cfm?fuseaction=second.schedule&id=0300415 [accessed 2019.3.15]

US EPA, 2018a. Table of Historical Particulate Matter (PM) National Ambient Air Quality Standards (NAAQS). https://www.epa.gov/pm-pollution/table-historical-particulate-matter-pm-national-ambient-air-quality-standards-naaqs (Accessed 2019/12/08)

US EPA, 2018b. Summary of the Comprehensive Environmental Response, Compensation, and Liability Act (Superfund). US EPA, Environmental Protection Agency, 15 Aug. 2018, https://www.epa.gov/laws-regulations/summary-comprehensive-environmental-response-compensation-and-liability-act [accessed 2019.3.15]

US EPA, 2019. Air Quality Dispersion Modeling - Preferred and Recommended Models. https://www.epa.gov/scram/air-quality-dispersion-modeling-preferred-and-recommended-models. (Accessed 2019/12/08)

US EPA, 2020a. Agriculture and Air Quality. https://www.epa.gov/agriculture/agriculture-and-air-quality, Access date: 15/06/2020

US EPA, 2020b. Air Quality Dispersion Modeling - Preferred and Recommended Models. https://www.epa.gov/scram/air-quality-dispersion-modeling-preferred-and-recommended-models#aermod, Access date: 15/06/2020

Venkatram, A., 2015. Lectures on Air Pollution Modeling. Springer. 389 pp.

Venkatram, A., Isakov, V., Yuan, J. Pankratz, D., 2004. Modeling dispersion at distances of meters from urban sources. Atmospheric Environment, 38(28), pp.4633-4641.

Venkataraman, C., Brauer, M., Tibrewal, K., Sadavarte, P., Ma, Q., Cohen, A., Chaliyakunnel, S., Frostad, J., Klimont, Z., Martin, R.V. and Millet, D.B., 2018. Source influence on emission pathways and ambient $PM_{2.5}$ pollution over India (2015–2050). Atmospheric Chemistry and Physics Discussions, 18, pp.8017-8039.

Vermeulen, F., Covaci, A., D'Havé, H., Van den Brink, N.W., Blust, R., De Coen, W. and Bervoets, L., 2010. Accumulation of background levels of persistent organochlorine and organobromine pollutants through the soil–earthworm–hedgehog food chain. Environment international, 36(7), pp.721-727

Von Toussaint, U., 2011. Bayesian inference in physics. Reviews of Modern Physics, 83(3), 943.

Webster, R. and Oliver, M.A., 2007. Geostatistics for environmental scientists. John Wiley & Sons.

Weijs L, Yang RS, Das K, Covaci A, Blust R., 2013. Application of Bayesian population physiologically based pharmacokinetic (PBPK) modeling and Markov chain Monte Carlo simulations to pesticide kinetics studies in protected marine mammals: DDT, DDE, and DDD in harbor porpoises. Environmental science & technology. 2013 Apr 18;47(9):4365-74.

Whitelock, D. P., Buser, M. D., Boykin, J. C., Holt, G. A., 2013a. Battery condenser system $PM_{2.5}$ emission factors and rates for cotton gins: Method 201A combination PM_{10} and $PM_{2.5}$ sizing cyclones. Journal of Cotton Science, 17(4), 402-413.

Whitelock, D. P., Buser, M. D., Boykin, J. C., & Holt, G. A., 2013b. First stage seed-cotton cleaning system $PM_{2.5}$ emission factors and rates for cotton gins: Method 201A combination PM_{10} and $PM_{2.5}$ sizing cyclones. Journal of Cotton Science, 17(4), 320-332.

Whitelock, D. P., Buser, M. D., Boykin, J. C., Holt, G. A., 2013c. Master trash system $PM_{2.5}$ emission factors and rates for cotton gins: Method 201A combination PM_{10} and $PM_{2.5}$ sizing cyclones. Journal of Cotton Science, 17(4), 489-499.

Whitelock, D. P., Buser, M. D., Armijo, C. B., Hughs, S. E., 2019. The Impact of Historical Gin Stand Technologies on Cotton Fiber and Seed Quality. Applied Engineering in Agriculture, 35(5), 775-785.

Wu, H., Shapiro, J. L., 2006. Does overfitting affect performance in estimation of distribution algorithms. In Proceedings of the 8th annual conference on Genetic and evolutionary computation (pp. 433-434).

Walker, K. C., M. B. Goette, and G. S. Batchelor. "Pesticide Residues in Foods, Dichlorodiphenyltrichloroethane and Dichlorodiphenyldichloroethylene Content in Prepared Foods." Journal of Agricultural and Food Chemistry 2.20 (1954): 1034-1037.

Wanjura, J.D., Parnell, C.B., Shaw, B.W., Lacey, R.E., 2005. Design and evaluation of a low-volume total suspended particulate sampler. Trans. ASAE 48(4):1547–1552.

Warton, D.I., Wright, I.J., Falster, D.S., Westo,by, M., 2006. Bivariate line-fitting methods for allometry. Biol. Rev. 81(2),259-291.

Willis, W.B., Eichinger, W.E., Prueger J.H., Hapeman, C.J., Li, H., Buser, M.D., Hatfield, J.L., Wanjura, J.D., Holt, G.A., Torrents, A., Plenner, S.J., Clarida, W., Browne, S.D., Downey, P.M., Yao, Q., 2017a. Particulate capture efficiency of a vegetative environmental buffer surrounding an animal feeding operation. Agric. Ecosyst. Environ. 240:101-108.

Willis, W.B., Eichinger, W.E., Prueger, J.H., Hapeman, C.J., Li, H., Buser, M.D., Hatfield, J.L., Wanjura, J.D., Holt, G.A., Torrents, A., Plenner, S.J., Clarida, W., Browne, S.D., Downey,

P.M., Yao, Q, 2017b. Lidar method to estimate emission rates from extended sources. J. Atmos. Oceanic Technol. 34:335-345.World Health Organization, 2018. Ambient (Outdoor) air quality and health." https://www.who.int/mediacentre/factsheets/fs313/en/ (Accessed October 25, 2019)

World Health Organization, 2018. Ambient (Outdoor) air quality and health." https://www.who.int/mediacentre/factsheets/fs313/en/ (Accessed October 25, 2019)

World Meteorological Organization., 2008. Guide to meteorological instruments and methods of observation. Secretariat of the World Meteorological Organization.

Yang, Z., Yao, Q., Buser, M.D., Alfieri, J.G., Li, H., Torrents, A., McConnell, L.L., Downey, P.M. and Hapeman, C.J., 2020. Modification and validation of the Gaussian plume model (GPM) to predict ammonia and particulate matter dispersion. Atmospheric Pollution Research.

Yamartino, R. J., 1984. A comparison of several "single-pass" estimators of the standard deviation of wind direction. Journal of Climate and Applied Meteorology, 23(9), 1362-1366.

Yang, X.-B., Ying, G.-G., Peng, P.-A., Wang, L., Zhao, J.-L., Zhang, L.-J., Yuan, P., He, H.-P., 2010. Influence of Biochars on Plant Uptake and Dissipation of Two Pesticides in an Agricultural Soil. J. Agric. Food Chem. 58, 7915–7921. https://doi.org/10.1021/jf1011352

Yao, Q., Torrents, A., Li, H., Buser, M.D., McConnell, L.L., Downey, P.M. and Hapeman, C.J., 2018a. Using a vegetative environmental buffer to reduce the concentrations of volatile organic compounds in poultry-house atmospheric emissions. Journal of agricultural and food chemistry, *66*(31), pp.8231-8236.

Yao, Q., Yang, Z., Li, H., Buser, M.D., Wanjura, J.D., Downey, P.M., Zhang, C., Craige, C., Torrents, A., McConnell, L.L., Holt, G.A., Hapeman, C.J., 2018b. Assessment of particulate matter and ammonia emission concentrations and respective plume profiles from a commercial poultry house. Environ. Pollut. 238:10-16.

Zhan, H., Li, Q., Zhao, K., Zhang, L., Zhang, Z., Zhang, C., Xiao, L., 2015. Evaluating $PM_{2.5}$ at a construction site using terahertz radiation. IEEE Transactions on Terahertz Science and Technology, 5(6), 1028-1034.

Zhang, A., Liu, W., Yuan, H., Zhou, S., Su, Y., Li, Y. F., 2011. Spatial distribution of hexachlorocyclohexanes in agricultural soils in Zhejiang Province, China, and correlations with elevation and temperature. Environmental science & technology, 45(15), 6303-6308.

Zeng, Q., Ni, Y., Jiang, G., Li, G., Pan, X., 2017. The short term burden of ambient particulate matters on non-accidental mortality and years of life lost: A ten-year multi-district study in Tianjin, China. Environmental Pollution, 220, 713-719.

Zwicke, G. W., 1998. The dispersion modeling of particulate for point and multiple point sources in agriculture (Doctoral dissertation, Texas A & M University).